Low Adhesion in the Wheel-Rail Contact

Investigations towards a better understanding of the problem and its possible countermeasures

Oscar Arias-Cuevas

Low Adhesion in the Wheel-Rail Contact

Investigations towards a better understanding of the problem and its possible countermeasures

Proefschrift

ter verkrijging van de graad van doctor
aan de Technische Universiteit Delft,
op gezag van de Rector Magnificus Prof.ir. K.C.A.M. Luyben,
voorzitter van het College voor Promoties,
in het openbaar te verdedigen op woensdag 8 september 2010 om 10:00 uur

door

Oscar ARIAS-CUEVAS

Ingeniero Superior Industrial, Universidad Carlos III de Madrid

geboren te Madrid (Spanje)

Dit proefschrift is goedgekeurd door de promotor:

Prof.dr.ir. A.A.A. Molenaar

Copromotor:

Dr.ir. Z. Li

Samenstelling promotiecommissie:

Rector Magnificus,	Technische Univestiteit Delft, voorzitter
Prof.dr.ir. A.A.A. Molenaar,	Technische Universiteit Delft, promotor
Dr.ir. Z. Li,	Technische Universiteit Delft, copromotor
Prof.dr.ir. L.J. Sluys,	Technische Universiteit Delft
Prof.dr. U. Olofsson,	KTH Royal Institute of Technology
Prof.dr. X.S. Jin,	Southwest Jiantong University
Dr. R. Lewis,	The University of Sheffield
Ir. F. Verheij,	ProRail
Prof.ir. A.Q.C. van der Horst,	Technische Universiteit Delft, reservelid

Published and distributed by:

O. Arias-Cuevas
E-mail: o.ariascuevas@tudelft.nl, oscar.arias.cuevas@gmail.com

Section of Road and Railway Engineering
Faculty of Civil Engineering and Geosciences
Delft University of Technnology
P.O. Box 5048, 2600 GA Delft, the Netherlands

ISBN 978-90-8570-588-8

Keywords: wheel-rail contact; low adhesion; friction modifiers; sand; lubrication; leaves; magnetic track brakes; field tests; traction control; multi-body dynamics.

Cover design: Margot Nieuwstad

Printing: Wohrmann Print Service, Zutphen, the Netherlands

© 2010 by Oscar Arias-Cuevas. All rights reserved. No part of the material protected by this copyright notice may be reproduced or utilized in any form or by any means, electronic or mechanical, including photocopying, recording or by any information storage and retrieval system, without written permission from the author.

To everyone who has (directly or indirectly) supported me

Summary

Adhesion, or adhesion coefficient, is given by the ratio of the longitudinal tangential (i.e., braking or traction) force over the normal force at the wheel-rail contact. The tangential force that a braking or tractive railway wheel can exert on a rail is limited by the friction coefficient available between the surfaces in contact for a given normal load. In clean steel-on-steel contacts, the friction coefficient is known to be mostly higher than the adhesion requirements for normal traction and braking operations of existing rolling stock. However, contaminations, such as leaves, grease and water, can easily be present at the wheel-rail contact and reduce the friction level, leading to low adhesion problems. In recent decades, some railways, such as in the Netherlands, the United Kingdom, Sweden and Germany, have particularly been affected in autumn due to the presence of moisture and fallen leaves, among other contaminants.

When low adhesion occurs, delays in the train service may be the clearest consequence to the railway commuters. However, many other negative effects may arise, such as damages to wheels and rails, signals passed at danger, station platform overruns and even collisions. Therefore, not only the reliability but also the safety and costs of railway transportation may be compromised. Extreme low adhesion conditions in the Netherlands on October 27, 2002 forced the major train operating company (NS) and the infrastructure manager (ProRail) to stop the services on most of the sections of the network during that day and considerable disruptions continued the days after.

In order to mitigate the low adhesion problem, the affected infrastructure managers and train operating companies have taken a variety of countermeasures. However, the problems still persist. This may partly be attributed to insufficient understanding of the problem and its possible countermeasures. The investigations presented in this dissertation, which have been commissioned by ProRail and NS within a research project called AdRem, have aimed at improving this understanding towards an effective solution to the problem. Four existing countermeasures have been investigated in this dissertation, namely friction modifiers, sanding, magnetic track brakes and traction control.

Friction modifiers, sanding and magnetic track brakes are countermeasures that can be taken to improve the adhesion by conditioning the surfaces of rails, wheels, or both. Some friction modifiers may rely upon sand, or other solid particles, but they are normally engineered to deliver a better performance than just sand. Both friction modifiers and sand may be applied to the wheel-rail contact either by trackside or trainborne installations.

Magnetic track brakes operate trainborne sliding over the rails, which may contribute to an increase in the train braking performance and some contamination removal. Traction control (as well as braking control, not explicitly treated in this dissertation) can be employed to make optimal use of the adhesion available by adjusting the right amount of wheel slip, or to improve the adhesion by operating at high slip. Moreover, traction control may be combined in practice with any of the other three countermeasures, depending on the railway, the track and the type of railway vehicle.

In this research, an improved insight into the low adhesion problem and the effectiveness of the four countermeasures is obtained by means of experimental and numerical approaches. The experimental investigations have been carried out in the laboratory and in field. In the laboratory a twin-disk roller rig has been employed, in which the actual wheel-rail contact is simulated by two disks in rolling-sliding motion. The influence of different types of contamination on the wheel-rail adhesion, as well as the effectiveness of friction modifiers and sanding, has been studied.

Furthermore, two field investigations have been carried out: one is on sanding using the sanders of an electrical locomotive to obtain quantitative insight in actual wheel-rail adhesion and to validate some of the laboratory findings. The other is with the magnetic track brakes of an electrical multiple unit towards their effectiveness and possible side effects to overcome low adhesion. Numerical modeling has also been employed to examine the effectiveness of an existing traction control system on one hand, and to investigate the wheel-rail adhesion during curve negotiation in typically contaminated contacts on the other.

The research has shown that none of the investigated friction modifiers was entirely optimal for the tested conditions. It is also proven that sanding may be an effective method to improve the wheel-rail adhesion in leaf contaminated contacts, but some of the sanding parameters currently employed by some railways may still need improvement. Magnetic track brakes have been found to be effective against low adhesion, but less effective than one of the friction modifiers under certain tested conditions. Furthermore, the investigated traction control has shown to lead to excessive wheel slip under low adhesion conditions. Based on the findings of the investigations, conclusions have been drawn and recommendations have been made to outline possible interesting future lines of research, as well as promising lines of development and application for rolling stock operators and railway network managers dealing with low adhesion problems.

Samenvatting

De adhesie, of adhesiecoëfficiënt, wordt weergegeven door de verhouding van de longitudinale tangentiële rem- of tractiekracht en de normaalkracht in het wiel-rail contactvlak. De tangentiële kracht, die een remmend of aanzettend treinwiel op de rail kan uitoefenen, is gelimiteerd door de beschikbare wrijvingscoëfficiënt tussen wiel en rail bij een gegeven normaalkracht. De wrijvingscoëfficiënt in schone staal-op-staal contacten is meestal hoger dan vereist voor normale rem- en tractie-operaties van het huidige rollend materieel. Vervuiling door bladeren, vet en water kan echter gemakkelijk optreden in het wiel-rail contact en het wrijvingniveau reduceren, waardoor problemen t.g.v. lage adhesie kunnen vóórkomen. In de afgelopen jaren zijn er in sommige landen, zoals in Nederland, Groot Brittannië, Zweden en Duitsland problemen in de herfst geweest t.g.v. de aanwezigheid van vocht en bladeren en nog andere vervuiling op de rails.

Als gevolg van lage adhesie op de rails kunnen vertragingen voor treinreizigers optreden. Er kunnen echter ook veel andere negatieve effecten vóórkomen, zoals wiel- en railschade, het negeren van seinen, het niet tijdig kunnen stopen op stations en zelfs botsingen. Daarom kunnen door adhesieproblemen niet alleen de betrouwbaarheid, maar ook de veiligheid van het railtransport in gevaar gebracht worden. Door een enorme herfststorm op zondag 27 oktober 2002 kwamen er veel bladeren tegelijkertijd op de rails, wat leidde tot veel adhesieproblemen. Dit dwong de grootste vervoerder (NS) en de infrabeheerder (ProRail) het railtransport in het land op die dag grotendeels te stoppen. Ook in de hierop volgende dagen traden nog veel storingen op als gevolg van bladeren op de rails.

Vervoerders en infrabeheerders hebben een aantal maatregelen genomen om de adhesieproblematiek te verminderen. De problemen zijn echter nog niet voorbij. Dit zou gedeeltelijk een gevolg kunnen zijn van nog onvoldoende begrip van de problematiek en daarmee onvoldoende inzicht in het effect van mogelijke maatregelen. Dit promotieonderzoek, dat in het kader van het project AdRem in opdracht van ProRail en NS is uitgevoerd, had tot doel het inzicht in de adhesieproblematiek te vergroten. Vier bestaande maatregelen zijn binnen dit onderzoek bestudeerd: adhesieverbeteraars, zandstrooien, magneetremmen en tractiecontrole.

Adhesieverbeteraars, zandstrooien en magneetremmen zijn maatregelen, die bedoeld zijn om de adhesie te verbeteren door middel van het conditioneren van het oppervlak van de rails, de wielen, of beide. Sommige adhesieverbeteraars zouden op zand, of ander korrelmateriaal, gebaseerd kunnen zijn, maar meestal zijn ze verder ontwikkeld om betere prestaties te leveren dan zand. Adhesieverbeteraars en strooizand kunnen op de rails toegepast worden met behulp van spoor- of materieel-gebonden installaties.

Magneetremmen zijn materieel gebonden en ze glijden over de rails om de remprestaties van de trein te verbeteren. Ze kunnen ook enige vervuiling verwijderen. Tractiecontrole (alsook remcontrole die in dit proefschrift niet onderzocht is) kan toegepast worden om optimaal gebruik te maken van de beschikbare adhesie door de juiste wielslip te selecteren, of om de adhesie te verbeteren door een hoge slip te selecteren. Tractiecontrole kan in de praktijk gecombineerd worden met elk van de drie

andere maatregelen, afhankelijk van de spoorwegmaatschappij, het spoor en het rollend materieel.

In dit proefschrift is met behulp van experimentele en numerieke methoden nieuw inzicht verkregen in de adhesieproblematiek in het algemeen en de effectiviteit van de vier maatregelen in het bijzonder. Het experimentele onderzoek is in het laboratorium en in de praktijk uitgevoerd. In het laboratorium is een tweeschijven machine gebruikt, waarbij het wiel-rail contact wordt gesimuleerd door middel van twee schijven die tegen elkaar rollen en glijden. Met deze proeven is het effect bestudeerd van verschillende typen vervuiling op de wiel-rail adhesie, evenals de effectiviteit van adhesieverbeteraars en het zandstrooien.

Daarnaast zijn er twee testen in de praktijk uitgevoerd. Een met de zandstrooiers van een elektrische locomotief om een kwantitatief inzicht in de daadwerkelijke adhesie te kunnen krijgen en om enkele laboratoriumresultaten te valideren. In de andere test is de effectiviteit van magneetremmen van een elektrisch treinstel ter bestrijding van lage adhesie bestudeerd alsmede enige mogelijke bijwerkingen. Bovendien is een numeriek model gemaakt om het tractiecontrolesysteem te bestuderen evenals de adhesie als het voertuig door een boog rijdt bij aanwezigheid van vervuiling in het wiel-rail contact.

Het onderzoek toont aan dat geen van de onderzochte adhesieverbeteraars helemaal optimaal is geweest onder de testcondities. Het is ook bewezen dat zand in een wiel-rail contact, dat vervuld is met blad, effectief kan zijn om de adhesie te verbeteren, maar ook dat bij sommige spoorwegmaatschappijen een aantal parameters van het zandstrooien verbeterd kunnen worden. Magneetremmen zijn effectief tegen adhesieproblemen maar onder bepaalde testcondities minder effectief dan één van de onderzochte adhesieverbeteraars. Het bestudeerde tractiecontrolesysteem leidt tot veel wielslip bij lage adhesie. De bevindingen van het onderzoek hebben een aantal conclusies opgeleverd. Eveneens zijn er aanbevelingen gedaan, die mogelijk interessante werkrichtingen beschrijven voor vervoerders en infrabeheerders die geconfronteerd worden met de lage adhesie problematiek.

Acknowledgements

It is well-known (and perhaps scientifically proven) that before or after reading the propositions, people always approach this Section prior to further browsing the dissertation. Such human behaviour is entirely justified in this particular dissertation because of the enormous support of colleagues, friends and family. Therefore, this Section is a must to be read, which aims at giving the deserved credit to everyone that was (directly or indirectly) involved in my research.

My PhD story started one day at the beginning of 2006, when my initial promoter Coenraad Esveld gave me the chance of demonstrating my capabilities to conduct (independent) research. Coen, bedankt daarvoor! After Coen left the university, André Molenaar became my promoter. André, I owe you big time because despite the already huge amount of work load on your shoulders, you still made room for a new PhD candidate, whose research had not much to do with roads. Dank je wel, André, dat je er voor mij bent geweest! The last, but for sure not the least of my “coaches” to be thanked is Zili Li, who since day one till the end has been my supervisor and co-promoter. Zili, thank you very very very much for those amazing years of hard work and continuous challenge! I am truly grateful to the trust you put in me, letting me follow my own path in the course of the research; this is something that a PhD candidate should never take for granted.

More people from Delft University of Technology deserve a special place in this Section. First, I will start with my direct colleagues from the Section of Road and Railway Engineering. Marco Poot, Jan Moraal, Jan-Willem Bientjes, Radjan Khedoe, Dirk Doedens, Abdol Miradi, and Paul Vermeulen, always offered me a hand when I needed, whether it was something regarding the laboratory, the budget, or just a chat, dank jullie wel! Marco, onze frequente avondetentjes hebben niet alleen mijn werk geholpen, maar hebben mij ook een vriend opgeleverd, daarvoor kan ik jou niet genoeg bedanken. Jan, Paul en Jan-Willem hadden altijd voor mij de deur open zowel voor een vraagje, alsook een uitnodiging om naar aula te gaan lunchen, bedankt jullie daarvoor! Abdol, bedankt voor jouw adviezen en vele handtekeningen! Our wonderful secretaries: Jacqueline Barnhoorn and Sonja van den Bos, whose assistance, friendlyness and patience made a difference, dank jullie wel! My colleagues from Road Engineering: Lambert Houben, Martin van de Ven and Ad Pronk, die mij hebben geholpen toen ik het nodig had, bedankt daarvoor! My colleague from Railway Engineering: Valeri Markine, who is always available for discussions either related to railways or life, bedankt voor jouw vriendschap! My fellow PhD candidates, who could understand my suffering and help me accordingly when most needed, thank you all! Xin Zhao, Marija Molodova, Milliyon Woldekidan, Sadegh Akbarnejad, Liantong Mo, Alemgena Araya, Gang Liu, Mohamad Mohajeri, Jian Qiu, Mingliang Li, Yue Xiao, Dongxing Xuan, I will never forget our time together collecting leaves in the (“special”) forests of Delft, thanks for that! Xin, my roomie and most qualified leaf hunter, thank you for sharing your time with me in the last years; hopefully, it was for you as much fun and useful as it was for me! Ivan Shetvsov and Michael Steenbergen, bedankt voor jullie ondersteuning en wijze adviezen! 1e6, thanks for sharing your skills in Excel! Dongxing, thank you very much indeed for your help in the field tests! Also Marija and Xin deserve credit for their help in those tests. I also owe my gratitude to Edi Montaluri for her support with the interferometer. There are two gentlemen from the 3ME faculty to whom I owe big time for their great kindness: Erik Peekstok and Ton Riemslag. Erik, Ton, hartelijk bedankt voor jullie hulp in het lab!

All my research work has been part of an industry project (AdRem), which gave me the privilege to meet and work with colleagues from companies and universities of different countries. I start thanking our AdRem managers: Frank Koster (ProRail), Marco Sala (NS) and Marcel Vos (NS). Frank, bedankt voor het vertrouwen in mijn initiatieven en ideeën! Marco and Marcel, bedankt voor jullie ondersteuning! My AdRem colleagues: Peter-Paul Mittrertreiner, Radu Popovici, Niels van Steenis, Sander van der Krol, Felix Chang, Erik Sikma, and Robert van Ommeren, with whom I shared (mostly) nice times. P-P, je bent een goede collega geweest en ook een vriend geworden; die week van hard werk en gezelligheid in Weert en de vake e-mails en telefoontjes, dank je wel voor alles! Radu, you were always willing to help, thanks for always making a bit of free time for me! Niels, bedankt voor altijd daar te zijn! Sander, bedankt voor jouw adviezen over blaadjes! Felix, Erik en Robert, jullie zijn altijd voor mij (en de anderen) beschikbaar en behulpzaam geweest, daarvoor dank jullie wel!

During my research I have also had the great opportunity to work (or collaborate) with people outside the AdRem group that need to be acknowledged. I start with some colleagues from ProRail: Rolf Dollevoet, Ivan Shevtsov, Steven de Sterke, Coen Valkenburg, Arjan Rijnaard, dank jullie wel voor jullie vriendelijkheid en adviezen! Several employees of LRRE have also played a role in my research: Max Winterling, Gert Liefting, Dennis de Jong, Roger van Mil, dank jullie wel voor het delen van data! Ook wil ik Yulie van Doorne en Frank Stijnen voor hun inzet tijdens de emplacementbeproevingen bedanken. A few people in DeltaRail have also been very helpful, particularly Babette Dirks and Jaap Horst, bedankt voor jullie hulp! Four gentlemen from NedTrain have also been very helpful in some parts of my work: Adri Kalis, Luc de Rond, Fred Derks and Bert Beentjes, dank jullie wel voor de geleende materialen en prettige samenwerking! I also want to thank Donald Eadie and John Cotter, from Kelsan Technologies, for the collaboration project with friction modifiers. During my stays in Sheffield, a few people showed their most sincere kindness: Roger Lewis, Rob Dwyer-Joyce, Mike Frolish (R.I.P.), Beto Gallardo-Hernandez and Steve Lewis; thank you all very much for making me feel like at my own work place! A major goal of attending conferences is to make good acquaintances: Barys Shyrokau, Sam Richardson, Bill Poole, Luis Baeza, Oldrich Polach, Ernesto García-Vadillo y Javier Santamaría, are some good examples of that. I also have some nice words for the person who first introduced me to the wonderful world of railways: Julio Alvarez. Julio, muchas gracias por tu apoyo, tus consejos y tu amistad en estos últimos años!

My friends in Holland have always been very supportive: Nakul, Jelan, Aylin, Richard, Youri, Neel, Sadek, Evan and Thijs; dank jullie wel voor jullie gezelligheid en vriendschap! I also want to thank my good friend, Hai, for being there when most needed. My (team)mates from DSTV Obvius: Thomas, David, Frank, o.a.; dank jullie wel voor de gezelligheid en sportiviteit! A mis amigos en Madrid no se les puede olvidar, ya que siempre han están ahí cada vez que vuelvo a casa: Ángel Luis, Maxi, Oscar y Javi, gracias chavales por vuestra presencia!

Mi familia siempre ha estado ahí para apoyarme. No creo que pueda olvidar esas llamadas de teléfono para darme compañía a un par de miles de kilómetros de distancia, ya sea para saber que tipo de medicamento he de tomar para los dolores o para charlar de los palos y alegrías que da la vida. Mamá, Papá, Carol, Gema, Sergio, Iñaki, Eneko y Daniela, no os podéis imaginar la ilusión que me hace poder contar con vosotros a mi lado; muchííííííííííííííííííííííííííííísimas gracias por estar siempre ahí. In general, family members are associated with a blood connection, but my best friend Luis Miguel, whom I can always count on, is a clear exception to that rule. Gracias Luis por no tener que llamarte a menudo para seguir siendo mi mejor amigo! Andere nieuwe “familie” leden te bedanken voor hun ondersteuning zijn: Jeannette, Jan, Wouter, Nina en Oma. The last to be thanked, but just to give her the importance that she really deserves, is someone special that I met probably in the most ill-timed moment of my life when work had to be given complete priority. Margot, ik kan jou niet genoeg bedanken voor jouw liefde, zorg en geduld. Zonder twijfel zeg ik dat die vrijdagavond date van ons in het lab om zand te zeven de beste date is die ik ooit heb gehad.

Colleagues, friends and family, THANK YOU ALL VERY MUCH!!!

List of abbreviations

TOC = Train Operating Company
NS = *Nederlandse Spoorwegen*
VIRM = *Verlengd Interregio Materieel*
EMU = Electrical Multiple Unit
UK = United Kingdom
TC = Traction Control
SPAD = Signal Passed At Danger
WSP = Wheel Slide Protection
LAWS = Low Adhesion Warning System
FM = Friction Modifier
FMA = Friction Modifier A
FMB = Friction Modifier B
MTB = Magnetic Track Brake
TCU = Traction Control Unit
AdRem = Adhesion Remedy
ADAMS = Advanced Dynamic Analysis of Mechanical Systems
MATLAB = MATrix LABoratory
SUROS = Sheffield University ROlling Sliding
RSSB = Rail Safety and Standards Board
FTIR = Fourier Transform Infra-Red
M sand = Medium sand
S sand = Small sand
L sand = Large sand
R sand = (Dutch) Railway sand
PVC = PolyVinyl chloride
HV = Hardness Vickers
HM = Hardness Martens
HVT = Hardness Vickers from depth measurement
FR = Feed Rate
DGPS = Differential Global Positioning System
IRJ = Insulated Rail Joint
COF = Coefficient Of Friction
AoA = Angle of Attack

Table of contents

Prologue

Friction and Adhesion

ABSTRACT

In this prologue the definitions of friction and adhesion[I] are presented, as understood by the railway engineer. Furthermore, the ambiguity between the coefficients of adhesion and traction, which can sometimes be found in the railway literature, is also outlined and clarified.

[I] In this dissertation the adhesion has a different meaning in comparison with other engineering areas.

Friction

Friction is defined as the resisting force tangential to the common boundary between two bodies when, under the action of an external force, one body moves or tends to move relative to the surface of the other [p.1]. Friction is normally represented by the friction coefficient (f), which is defined as the ratio between the friction force (F_f) and the normal force (F_N) in the contact between the two bodies, as shown in Eq. p.1.

$$f = \frac{F_f}{F_N} \tag{p.1}$$

Fig. p.1 depicts a rectangular solid body of mass m that rests on a horizontal plane. If a force (F), parallel to the plane and increasing in time, is applied at the centre of mass, as displayed in Fig. p.1, where k is an arbitrary positive constant and the t is time, there will exist an instant t_1 at which the body starts sliding over the plane. The friction opposing the start of movement is referred to as static friction. The coefficient of static friction (f_s) is given in Eq. p.2, where g is the acceleration due to gravity. From that instant onwards the body slides with an acceleration a, and the force opposing the sliding movement of the body is referred to as kinetic (or dynamic) friction. The kinetic friction coefficient (f_k) at an instant t_2 is given by Eq. p.3, where a_2 is the body acceleration at the instant t_2.

$$f_s = f(t = t_1) = \frac{k \cdot t_1}{m \cdot g} \tag{p.2}$$

$$f_k = f(t = t_2) = \frac{k \cdot t_2 - m \cdot a_2}{m \cdot g} \tag{p.3}$$

In most tribological pairs, the static friction is higher than the kinetic friction, being the difference dependent on the materials and contact conditions [p.1]. In the case of the steel employed for railway wheels and rails, laboratory investigations have shown that the static friction coefficient can be up to almost twice of the kinetic friction coefficient [p.2].

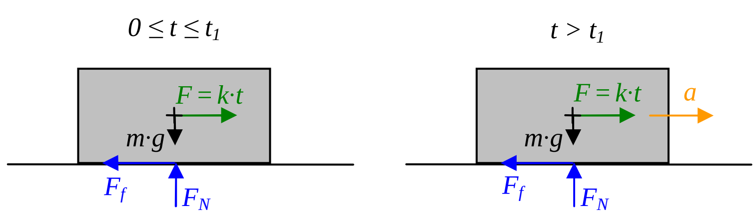

Fig. p.1. Rectangular solid body on a horizontal plane (forces applied on the body).

Adhesion

Let us consider the railway wheel as a solid cylinder of mass m, and the rail as a horizontal plane, as shown in Fig. p.2. According to the theory of Hertz described in [p.3], the contact area formed between the cylinder and the plane has a rectangular shape of width equal to the length of the cylinder. If a tractive torque (T) increasing in time is applied at the center of mass of the cylinder around its axis of rotation, the wheel starts moving with a certain angular velocity (*w*) and linear velocity (*v*), as displayed in Fig. p.2.

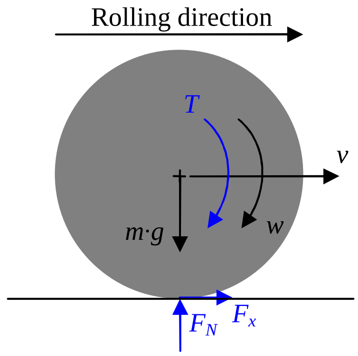

Fig. p.2. Schematic lateral view of the cylinder on the horizontal plane (forces applied on the cylinder).

The application of the tractive torque causes a reactive longitudinal tangential force at the contact interface with the plane, which is known as the traction force (F_x) (see Fig. p.2). The ratio between the traction force and the normal contact load is normally named the adhesion or adhesion coefficient (μ), as given in Eq. p.4.

$$\mu = \frac{F_x}{F_N} \tag{p.4}$$

Due to the tractive effort, the circumferential velocity of the cylinder as a rigid body is higher than its linear velocity, causing the so-called creepage or slip (s). In general, the slip can be expressed as the quotient between the relative velocity (v^{rel}) and the mean velocity (v^{mean}) of the cylinder along the plane, as shown in Eq. p.5, where r is the radius of the cylinder.

$$s = \frac{v^{rel}}{v^{mean}} = \frac{w \cdot r - v}{0.5 \cdot (w \cdot r + v)} \tag{p.5}$$

In 1926, Carter presented the first relationship between the traction force and the slip [p.4]. The representation of this relationship is known as the traction curve. Fig. p.3 depicts the theoretical traction curve of Carter, together with the contact area and the traction distribution along it (in blue color) for three representative points of the traction curve, namely A, B, and C. Point A represents the situation of null traction, i.e. μ = 0, which is known as the free rolling condition, where the whole contact patch is in stick.

As the traction force increases, an increasing part in the rear of the contact patch becomes in slip. The surface traction (q_x) distribution for point B increases in the stick area until reaching the slip area, where the surface traction is given by the product of the friction coefficient (f) and the contact pressure (p), as shown in Fig. p.3.

As the point C of the traction curve is reached, the whole contact patch becomes in slip, and the adhesion coefficient is equal to the friction coefficient. From point C onwards, the contact is said to be in full sliding conditions, and the slip may be referred to as macro-slip. On the other hand, between points A and C the contact is in partial slip conditions, and the slip may be referred to as micro-slip.

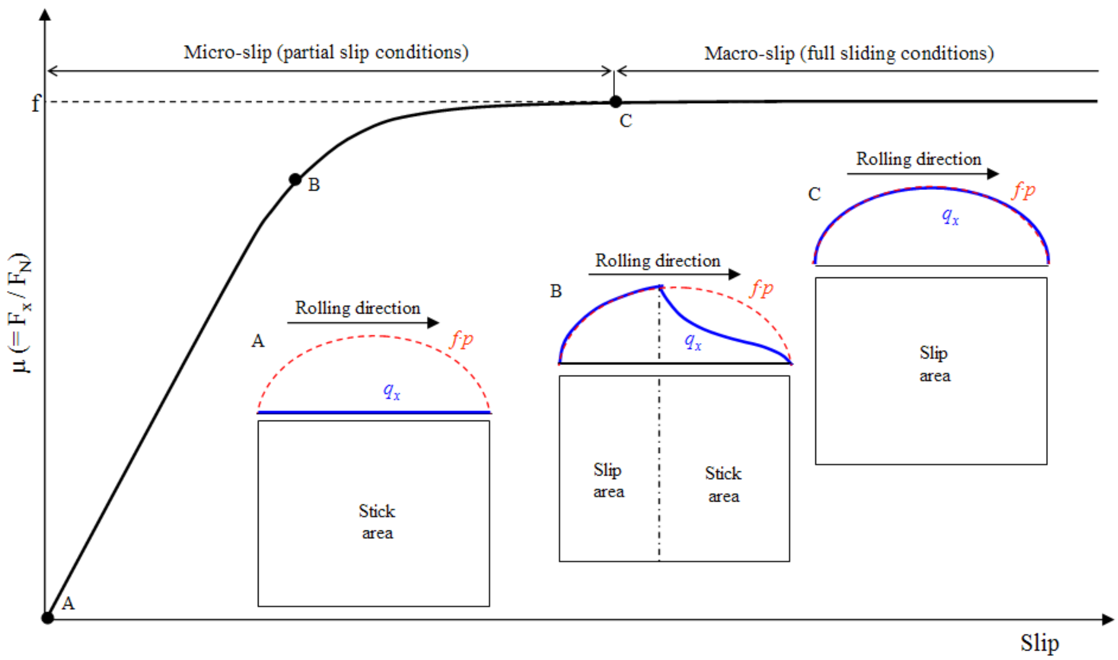

Fig. p.3. Representation of the theoretical traction curve of Carter.

Although the explanation of adhesion has been given to traction, the same holds for braking. The major difference is that the braking torque causes the circumferential velocity of the cylinder to be lower than its linear velocity, and Eq. p.5 changes to Eq. p.6. In addition, the wheel slip in full sliding conditions during braking is normally referred to as wheel slide.

$$s = \frac{v^{rel}}{v^{mean}} = \frac{v - w \cdot r}{0.5 \cdot (w \cdot r + v)} \tag{p.6}$$

Ambiguity with traction coefficient

In some literature, the term traction coefficient is employed instead of adhesion coefficient, presumably due to the fact that the investigations are mostly performed in traction conditions, i.e. wheel(s) accelerating over rail(s). In principle, both adhesion and traction coefficient may equally be used without loosing correctness, but it may sound odd to describe the braking performance of a railway vehicle based on the traction coefficient. For this reason, some authors have used the term adhesion coefficient in their braking investigations. In order to avoid confusion, while keeping a uniform definition, the term adhesion coefficient is employed in this dissertation referring to both traction and braking operations.

References

[p.1] ASM Handbook, Volume 18: Friction, Lubrication, and Wear Technology. ASM International (1992).
[p.2] T. Ohyama: Some Basic Studies on the Influence of Surface Contamination on Adhesion Force between Wheel and Rail at Higher Speeds. Quarterly Report of Railway Technical Research Institute 30 (1989) 127-135.
[p.3] K.L. Johnson: Contact Mechanics. Cambridge University Press, Cambridge (1985).
[p.4] F.W. Carter: On the Action of a Locomotive Driving Wheel. Proceedings of the Royal Society of London A112 (1926) 151-157.

Chapter 1

Introduction

ABSTRACT

Adhesion has been limiting the traction and braking capabilities of rail vehicles since the beginning of the railway transportation. In recent decades, some railways have particularly been affected by low adhesion, especially due to the presence of contamination in the wheel-rail contact. The clearest consequence of low adhesion problems is delays for the daily train commuters, which may particularly occur in autumn. Although some countermeasures have been adopted by affected railways, the adhesion related problems have to a large extent not been solved yet. In this chapter the problem of low adhesion in the wheel-rail contact is introduced, outlining its associated causes and consequences. The existing countermeasures are also described. The research motivation and approach of the dissertation are presented. Finally, the outline of the dissertation is given.

1.1. Low adhesion problem

Since the beginning of railway transportation, wheel-rail adhesion has been limiting the acceleration and deceleration capabilities of rolling stock. Locomotive designers have had to consider the optimal weight distribution for the maximum exploitation of adhesion, leading to changes in wheel arrangements in the course of time, as indicated in Fig. 1.1. In recent decades, special attention has been paid to the limitations in adhesion due to the quest for a more rapid, reliable, and denser railway transportation that can satisfy the increasing demands on public transportation. Although advances in technology have facilitated the increase of the tractive and braking capacities of the rolling stock, railway transportation is still characterized by steel wheels and steel rails operating in an open system. Thus, the wheel-rail contact remains easily contaminated by water, leaves or grease (among others), causing many railways worldwide to suffer from low adhesion problems, especially in autumn.

Low adhesion exists when an insufficient adhesion (or friction) is available in the wheel-rail contact to satisfy a certain requirement. The adhesion requirements in railway transportation are ultimately imposed by the driver, who may operate the train under the influence of pressure exerted by the timetable or the operational conditions on the track. The adhesion available in the wheel-rail contact is limited by the friction, which is dependent on the contact conditions. Under low adhesion conditions, the acceleration and deceleration capabilities of the rolling stock are diminished, compromising traction and braking performance. In countries like the Netherlands, the term "slippery tracks" (*gladde sporen* in Dutch) is commonly employed to refer to low adhesion conditions. Nevertheless, it must be emphasized that laboratory and field tests presented in this dissertation will show that not only the rails, but also wheels may be held responsible for low adhesion in the wheel-rail contact.

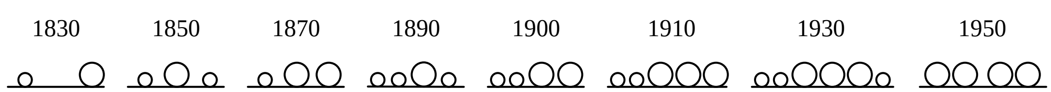

Fig. 1.1. Wheel arrangements of typical express locomotives at different times [1.1].

1.1.1. Adhesion requirements in railway transportation

In railway transportation there are normally three different types of adhesion requirements, namely given by tractive/braking capacity of the rolling stock, timetable regulations, and safety during operation. This is displayed in Fig. 1.2, where the length of the bars is given in proportion to (maximum) adhesion requirements in the Netherlands.

The first requirement corresponds to the adhesion needed to accelerate or brake the rolling stock at a given full capacity, which may be employed by the driver under certain circumstances. This adhesion requirement varies per rolling stock type, depending mostly on the characteristics of the traction and braking systems, the number of driven/braked wheel axles, the diameter of the wheels, and the axle load. For the sake of illustration, in the fleet of the major train operating company (TOC) in the Netherlands, i.e. *Nederlandse Spoorwegen* (NS), the maximum adhesion required in traction by electrical multiple units (EMUs) of the VIRM double-decker series is around 0.23, while electrical locomotives of the series 1700 may require up to 0.24. Furthermore, the tractive/braking capacity of rolling stock can vary with the travelling velocity due to limitations in motor power. For example, in traction operation VIRM trains may require a maximum adhesion of 0.23 upon start, whereas it does not require more than 0.09 at 100 km/h. Moreover, the adhesion requirement largely differs for traction and braking operations mainly due to the fact that a considerably lower number of wheel axles is employed to accelerate a train than to brake it, e.g. only 25 % of the wheel axles are used for traction in the VIRM trains. In the passenger rolling stock of NS, the maximum adhesion requirements are up to 0.25 in traction and 0.14 in braking.

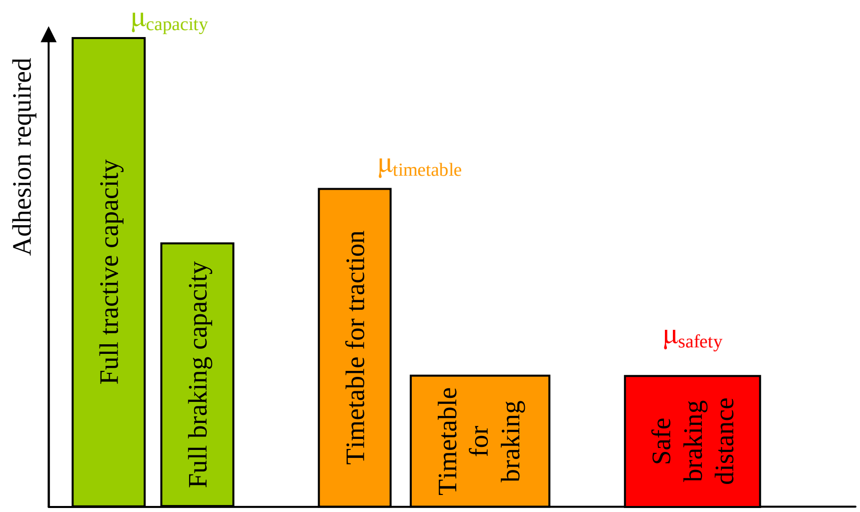

Fig. 1.2. Schematic representation of the common types of adhesion requirement in railway transportation (length of the bars is in proportion to the maximum requirements in the Netherlands).

The second adhesion requirement is given by the timetable that strongly influences the traction and braking behaviour of the drivers. In the Netherlands, an average adhesion value of 0.07 is employed for braking operation to establish the timetable of commuter trains. For traction operation, different values of adhesion are employed depending on the rolling stock, 0.17 being the maximum value employed.

The third type of adhesion requirement is indispensable to guarantee the safety in the railway transportation and is only applicable to braking operation. In most countries the railway track is divided into blocks, in which the trains are allocated for a safe control of the traffic flow. Railway signaling aims at giving instructions to the drivers to avoid that a train enters a block already occupied by another train so that no collisions can occur. The minimum distance between fixed signals or blocks is normally determined based on braking tables at the disposal of railway network managers. Note that the braking tables have been calculated by considering the characteristics of the rolling stock and the track. Table 1 shows the braking tables for a horizontal track employed by the Dutch railway infrastructure manager, ProRail, where v_i^{max} is the maximum travelling velocity allowed on the track section that the train has upon the start of a braking maneuver, s is the distance necessary to bring the train to standstill, a is the calculated average train deceleration, and μ is the calculated average adhesion coefficient at the wheel-rail contacts under the assumption that all wheels of the train exert the same braking effort. Hence, it may be said that the values given in Table 1.1 represent the minimum adhesion that is needed to ensure safe braking distances.

Table 1.1. Braking tables employed by the Dutch railways to establish the distance between signals on horizontal track sections at different operational velocities [1.2].

v_i^{max} (km/h)	40	60	80	130	140[II]
s (m)	400	475	750	950	1100
a (m/s^2)	0.15	0.29	0.33	0.69	0.69
μ (-)	0.02	0.03	0.03	0.07	0.07

1.1.2. Adhesion available in the wheel-rail contact

The adhesion available between railway wheels and rails is limited by the friction of a steel-on-steel contact. The mechanism of metallic friction has been investigated by several authors. Bowden and Tabor [1.3] attributed the friction between a hard metal slider on a soft metal surface to a combination of shearing and plowing, i.e. the sum of the force required to shear the metallic junctions formed at the points of contact and the force needed to displace the softer metal in front of the slider. Suh and Sin [1.4] proposed a theory of metallic friction based on three different mechanisms: deformation of the surface asperities, plowing by wear particles and hard asperities, and adhesion[III] of the sliding surfaces. In a compilation of findings reported by different authors in [1.5], four mechanisms of metallic friction are given: adhesion of the sliding surfaces, plastic deformation and plowing of one surface by hard asperities of the other surface, elastic deformation of the material below the plastically deformed surface, and plowing by wear particles.

The findings of laboratory and field investigations of this dissertation (see Chapters 2-4), as well as other investigations available in the literature [1.6-1.9], corroborate that the friction in dry clean wheel-rail contacts is sufficient to bear the typical adhesion requirements of rolling stock presented in Section 1.1.1. However, railway transportation occurs in an open system, which cannot impede the entrance of different contaminants in the wheel-rail contact. In the presence of contamination, the friction level can greatly be reduced from that one of clean dry conditions. The amount of adhesion reduction is strongly dependent on the type of contamination, being also influenced by the ambient conditions. Leaves, water and grease/oil have been reported to be the most common contaminants affecting railways worldwide [1.10-1.14].

1.1.2.1. Leaves

Leaves have been reported to be the major adhesion reducer in many railways, especially when combined with moisture [1.8, 1.10-1.14]. Leaves can fall on the tracks from trees and bushes located along railway lines. In the UK, it has been identified that leaves have been affecting the railway transportation since the demise of extensive lineside vegetation

[II] Note that the braking table actually indicates 160 km/h, but the maximum travelling velocity for passenger rolling stock in the Netherlands is currently limited to 140 km/h.
[III] This adhesion refers to the attractive force between adjacent surfaces.

maintenance by track gangs after the stoppage of steam locomotive operation [1.12]. Fallen leaves can be swept up by train's slipstream or be blown by cross wind to get onto the rails where passing wheels crush them to form a well compacted leaf layer on the surfaces of rails, wheels or both.

Fig. 1.3 illustrates the different steps leading to the formation of leaf layers on the top of a rail, as observed during field investigations presented in this dissertation (see Chapters 3-4). Fig. 1.3a displays the leaves resting on the top of a rail prior to the train passage. Fig. 1.3b shows the passage of the first wheel of the train over the leaf contaminated rail. It can be seen that most leaves were compacted onto the rail and wheels, whereas a few of them were blown off the top of the rail. A photograph of the top of the contaminated rail after 16 wheel passages is shown in Fig. 1.3c, in which compacted leaf mulch and some black leaf layers appear to be formed. Fig. 1.3d displays the top of the contaminated rail after 80 wheel passages, in which all adhered leaf mulch had transformed in numerous leaf layer patches of black coloration. The black coloration of the leaf layers has been attributed to a chemical reaction of pectin with the iron rather than charring of the leaf organic material [1.15]. It needs to be understood that low adhesion problems related to leaf contamination are caused by these (black) leaf layers. Leaf layers are very difficult to be removed from the rail, in contrast with the original leaves that can easily be blown or wiped away.

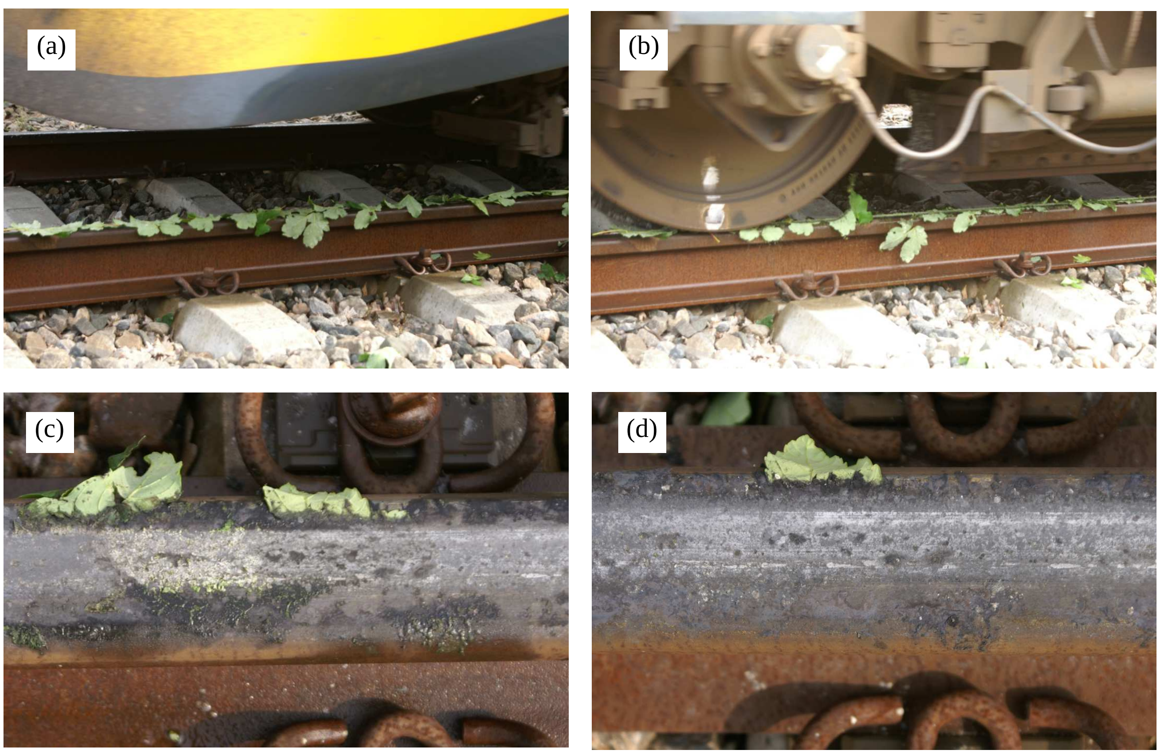

Fig. 1.3. Photograph of a leaf contaminated rail during different stages in the process of leaf layers formation: a) prior to train passage; b) upon first wheel passage; c) after 16 wheel passages; d) after 80 wheel passages.

Chemical analysis of black leaf layers in the UK has revealed a mixture of iron and iron oxide, water, leaf debris and oil [1.16]. The thickness of leaf layers created in a full scale test set-up has been determined to vary in thickness from 10 µm to 100 µm [1.17], implying that they may hinder the contact between the surface asperities of wheels and rails. In this regard, leaf layers have also been reported to cause train detection problems due to their insulating effect [1.12]. Laboratory investigations have shown that dry leaf layers are harder than wet ones [1.9]. Moreover, the shear strength of the leaf layers has been found to be inversely proportional to the moisture level, reaching the lowest friction values when the leaf layers are saturated with water [1.17].

1.1.2.2. Water

Water can appear on the top of the rails in different quantities by different means. Heavy rain leads to large amounts of water on the rails, whereas dew, fog, melted ice/snow and drizzle cause moisture formation or small amounts of water on the rails. When it is present in small amounts, water may reduce the wheel-rail adhesion to insufficient levels for both braking and traction operations in combination with other contaminants such as leaves, rust, wear debris or other solid particulates. On the other hand, large amounts of water in contaminated wheel-rail contacts are believed to contribute to wash contaminants off the rails. Additionally, wet leaves are more difficult to be lifted onto the rails than dry ones.

Investigations with water lubricated wheel-rail contacts under clean conditions have shown that friction reduction may compromise the adhesion requirements of rolling stock especially in traction [1.7, 1.18-1.20]. In those studies, the adhesion reduction given by water has been found to be dependent on the travelling velocity, the axle load, the surface roughness of wheels and rails, and the water temperature.

1.1.2.3. Grease/oil

Grease is employed by most railways on curves to lubricate the contact between the wheel flange and the gauge face of the high rail to reduce wear, noise and energy consumption [1.21-1.27]. The grease is often applied to the rails by means of trackside applicators. In case of malfunction, excessive amounts of grease may be applied, or perhaps the target location may be missed, which can lead to migration of the grease to the top of the high rail, causing an undesired reduction of the wheel-rail adhesion. Fig. 1.4a displays a photograph of the top of a rail, which has been contaminated on purpose with a grease that is widely used in the Netherlands for flange lubrication.

Oily contamination can appear on rails due to drips from rolling stock (e.g. lubricating oil), track machines (e.g. hydraulic oil) or planes (e.g. aviation fuel) [1.12]. Some laboratory investigations on adhesion of oil contaminated wheel-rail contacts can be found in the literature [1.6, 1.7, 1.9, 1.28, 1.29]. In those investigations, it was found that oil reduces the adhesion more than water in the absence of other contaminants, leading to friction levels that fall below the adhesion requirements for adequate traction and braking operations. On the other hand, it was shown that adhesion in oily contacts is higher than in leaf contaminated contacts [1.9].

1.1.2.4. Other adhesion reducing factors

Wear debris and rust can also reduce the wheel-rail adhesion, especially in combination with critical amounts of water and oil [1.30-1.32]. Personal experience of the author in a stabling yard showed that the friction level of "shiny" locomotive wheels on rusty rails under dry conditions can be lower than 0.2. Fig. 1.4b shows a photograph of the rail in the stabling yard, where the passage of the locomotive wheels can clearly be recognized by the partial appearance of metallic surface on the running band.

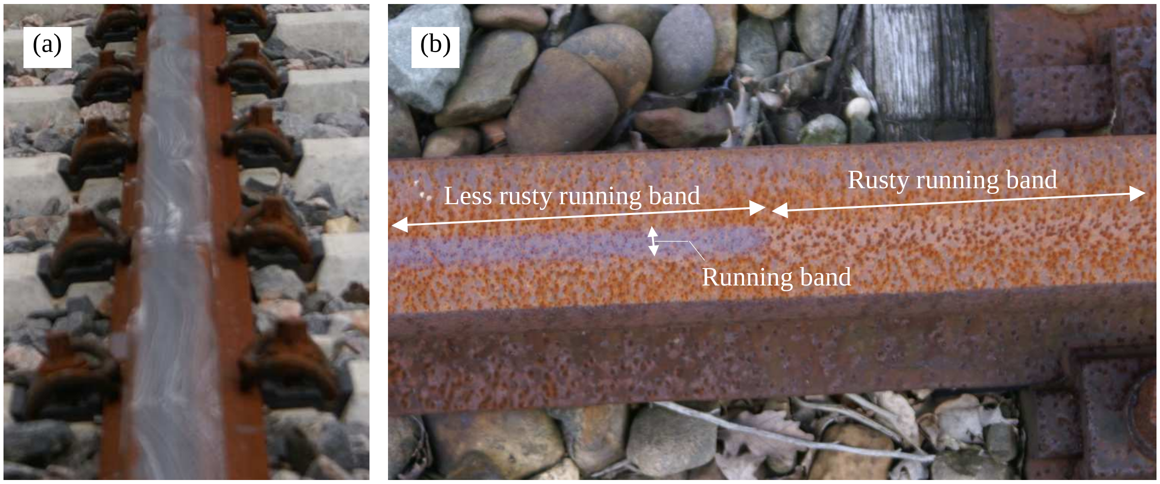

Fig. 1.4. Photograph of the top of a rail: (a) being contaminated on purpose with a grease commonly used as flange lubricant in the Netherlands; (b) with rusty running band.

Relative humidity is another important factor that can affect the wheel-rail adhesion. Laboratory investigations have shown that a high relative humidity can reduce the friction level in oily contacts [1.28] and in dry clean contacts [1.8]. The latter has been attributed to the formation of an oxygen layer on the contact surface, which is easily sheared and cannot be seen by the naked eye [1.33].

In the Netherlands, toilet paper and newspapers have been observed on the track at the stations, leading to the formation of slippery layers of composition (cellulose) similar to the leaf layers. Other possible forms of contamination suspected of affecting the wheel-rail adhesion are the sea spray originated in coastal routes and the industrial pollution from factories located near the railway tracks [1.11-1.12].

1.1.3. Consequences of low adhesion

The consequences of low adhesion differ depending on whether they are encountered during traction or braking. It is generally said that low adhesion in traction operation affects punctuality, whereas it can threaten the safety during braking. But, there may be some other consequences due to low adhesion, as presented below in more details.

1.1.3.1. During traction

Low adhesion during traction may affect the railway track capacity, reduce the punctuality of the railway transportation, and in some extreme cases damage the rails and more rarely the wheels. The track capacity can be a limiting factor to satisfy the increasing demand on railway transportation in densely populated countries like the Netherlands, in which 5400 passenger trains (around 1.2 million travelers) and 300 freight trains (around 100,000 tons of cargo) travel on a daily basis on the 4875 km of main tracks [1.27]. Reduced accelerations in rolling stock lead to longer occupation of the track, which could ultimately force the construction of new infrastructure to accommodate the increase of freight and passenger transportation [1.34].

The punctuality of passenger transportation in past years in the Netherlands is given in Table 1.2. Note that the calculation of delays in the Netherlands only considers trains that arrive at least three minutes later than scheduled. It can be seen that the average punctuality greatly decreases in autumn, which can be attributed to the likelihood of the presence of contaminants, such as leaves and water. The loss of punctuality generates a double cost to the TOCs. On one hand, the TOCs may need to pay the government as compensation for inadequate performance. The payment is normally in proportion to the percentage of punctuality loss, e.g. the costs of each punctuality loss percentage were around 3 m€ in 2004 for NS [1.35]. On the other hand, delays in commuter service generally cause dissatisfaction to the passengers, which may promote in some cases the preference of commuters to use other forms of transportation. This situation may not only increase the costs of TOCs, but also have an indirect negative impact on the environment.

Table 1.2. Average punctuality of the railway transportation in the Netherlands between 1999 and 2003 [1.35].

	1999	2000	2001	2002	2003
Whole year	86.8 %	84.7 %	79.9 %	81.2 %	83.1 %
Autumn	82.5 %	78.6 %	76.4 %	76.5 %	77.5 %

Furthermore, slipping wheels could occasionally cause damage to rails and wheels, especially in the particular case of rolling stock unequipped with an adequate traction control (TC) system. Low adhesion upon start of traction can imply spinning wheels (i.e. slipping wheels that do not move forward), which can generate high temperatures on the rail surface, leading the formation of the so-called rail burns [IV] (see Fig. 1.5a). Additionally, spalling of the brittle material formed on the surface of the rail may also occur, as pointed out in [1.37]. Moreover, the high level of wheel slip at low rolling velocities could cause fatigue crack growth on the wheel tread [1.38], as shown in Fig. 1.5b. On the other hand, at high rolling velocities thermal effects due to large wheel slip could lead to martensite formation on the tread following to spalling of the martensite in the worst cases [1.38].

1.1.3.2. During braking

Low adhesion conditions during braking can affect track capacity and punctuality (equal to the case of low adhesion during traction), threaten the safety of the railway transportation, and cause significant damage to wheels. If a train is requested to stop at a signal, the adhesion at the wheel-rail contacts is critical to the rate at which the train can decelerate. Signals passed at danger (SPADs) can occur due to low adhesion conditions, e.g. nine low adhesion related SPADs were registered in 2005 in the UK [1.39]. In the most detrimental cases, a SPAD may lead to a collision if the “invaded” track is occupied by another train. This type of incident was presumably encountered in the accident that recently occurred in the metro system of Amsterdam in the Netherlands [1.40].

[IV] In some literature the term wheel burns is employed instead of rail burns.

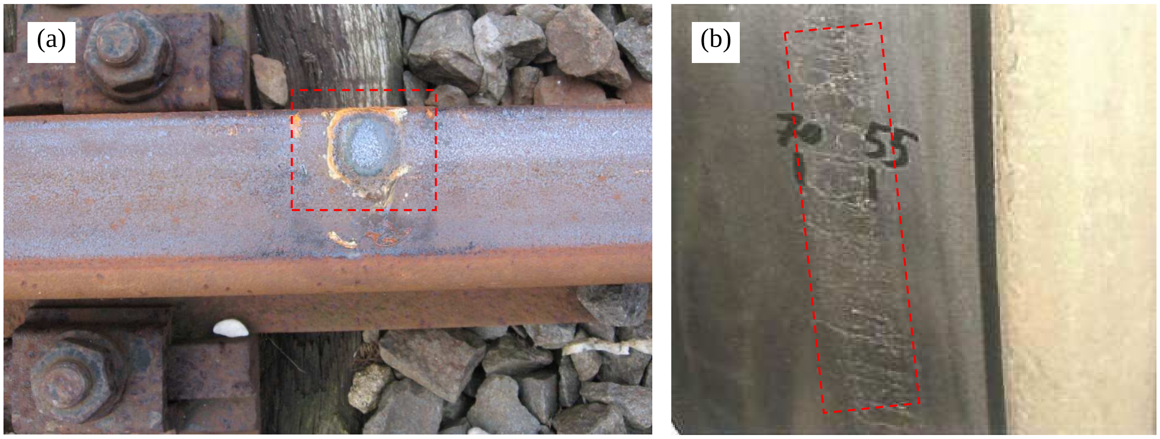

Fig. 1.5. Photograph of: (a) a rail burn [1.36]; (b) cracks on the wheel tread due to large slip [1.38].

Furthermore, damage to wheels due to braking under low adhesion conditions can often occur, particularly in rolling stock not equipped with an adequate wheel slide protection (WSP) system. The blockage or partial blockage of a wheelset during a braking maneuver leads to a high level of slide, causing part of the wheel tread to wear off forming a wheel flat (see Fig. 1.6a). The high temperature in the contact patch, exceeding 800-850 °C due to the dissipated energy, transforms the pearlitic wheel steel into austenite [1.38]. The subsequent rapid cooling of the thermally affected zone as the wheel starts rotating again causes a transformation of the austenitic phase into martensite. Furthermore, the initial wheel flat with sharp edges transforms into a longer flat with rounded edges due to the plastic deformation of the wheel material upon subsequent impacts with the rail [1.41]. Crack formation may take place in the martensite due to the repeated mechanical loading, leading to the spalling of the martensitic steel [1.38], as shown in Fig. 1.6b.

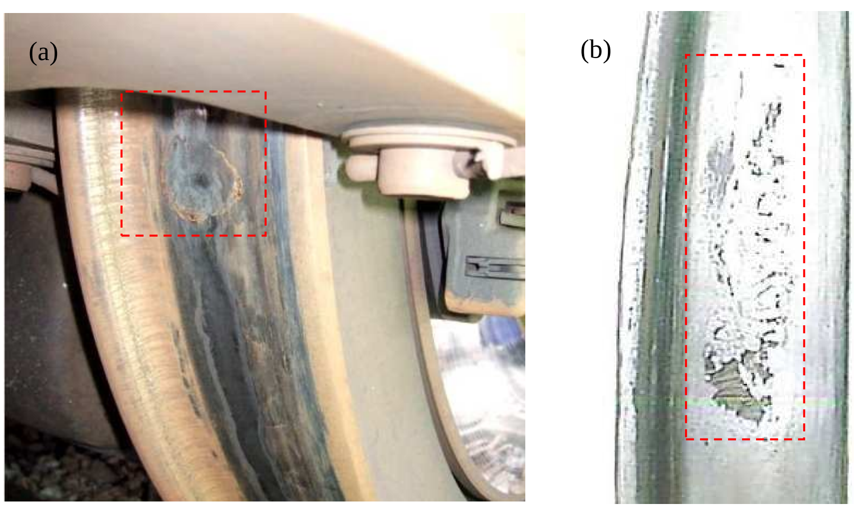

Fig. 1.6. Photograph of: (a) a wheel flat due to excessive slide [1.36]; (b) a severe wheel flat with spalling [1.38].

The high impact forces in the wheel-rail contact associated with wheel flats may lead to damage on the rail, concrete sleepers and some parts of the wheelset [1.42]. They can also produce excessive noise and vibration levels, affecting the passenger comfort. In order to remove the wheel flats, the wheels are normally reprofiled, which increases the maintenance costs of the TOCs. In the Netherlands, annual re-profiling costs associated with low adhesion were on average 1 m€ between 1997 and 2002 [1.35, 1.43].

1.1.4. Existing countermeasures against low adhesion

The oldest countermeasure against low adhesion in the history of railway transportation is sanding, which consists of the application of sand into the wheel-rail contact to improve the adhesion. Sanders are often employed to apply the sand. Most locomotives are fitted with sanders, being employed for the first time in the UK back in 1836 [1.1]. In Fig. 1.7 a photograph of the sander in an old and new locomotive is given. In the last decades, affected railways have adopted other countermeasures to overcome, or reduce, low adhesion problems [1.11, 1.12, 1.14, 1.44]. The countermeasures may be classified in: operational, track related, and rolling stock related measures.

1.1.4.1. Operational

The TOCs and railway infrastructure managers in affected countries have applied some of the following operational countermeasures:

- staff awareness by means of internal communications;
- warning systems of the adhesion conditions found on the network, e.g. LAWS™ [1.12];
- specific training and instructions to drivers on how to operate trains under low adhesion conditions;
- weather forecast to determine the likelihood of leaf fall and moisture formation on rails;
- adaptation of the timetable.

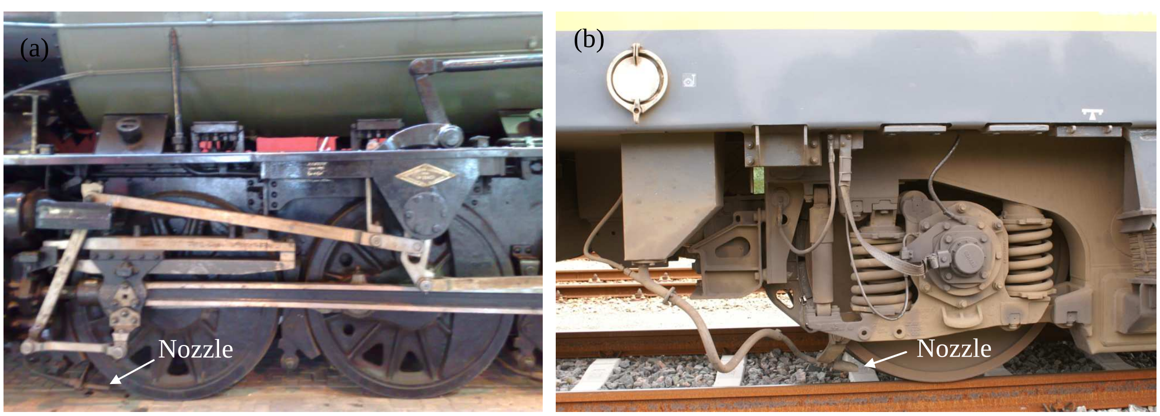

Fig. 1.7. Photograph of a sander in: (a) an old steam locomotive exhibited at the Railway Museum in Utrecht, the Netherlands; (b) an electrical locomotive (series 1700) currently available in the NS fleet.

1.1.4.2. Track related

Railway infrastructure managers may undertake some countermeasures to prevent the presence of contamination on the rails or reduce its impact on the wheel-rail adhesion, such as:

- vegetation management to ensure that there exists a minimum distance between the track and the nearest lineside vegetation, as shown in Fig. 1.8a;
- leaf fences adjacent to the track to avoid the entrance of leaves onto the track (see Fig. 1.8b);
- leaf guards, as the ones given in Fig. 1.8c, which reduce the amount of leaves that are brought onto the rails by train's slipstream or cross wind;
- trackside applicators of Sandite, which is a sand-based friction modifier (FM) designed to improve the wheel-rail adhesion. The trackside applicators are normally located close to stations (see Fig. 1.8d), signals or level crossings that can be susceptible to low adhesion incidents, so that adequate braking and traction operations can be guaranteed. Hereinafter Sandite will be referred to as FMB;
- multi-purpose vehicles, which are employed to clean the rails of certain areas of the network by means of water jetting (i.e. blasting the rails with water at very high pressure), sanding, FMB or a combination of them [1.12];
- rail grinding aimed at overcoming the low adhesion problem by roughening the rails so that steel-on-steel contact is promoted [1.12].

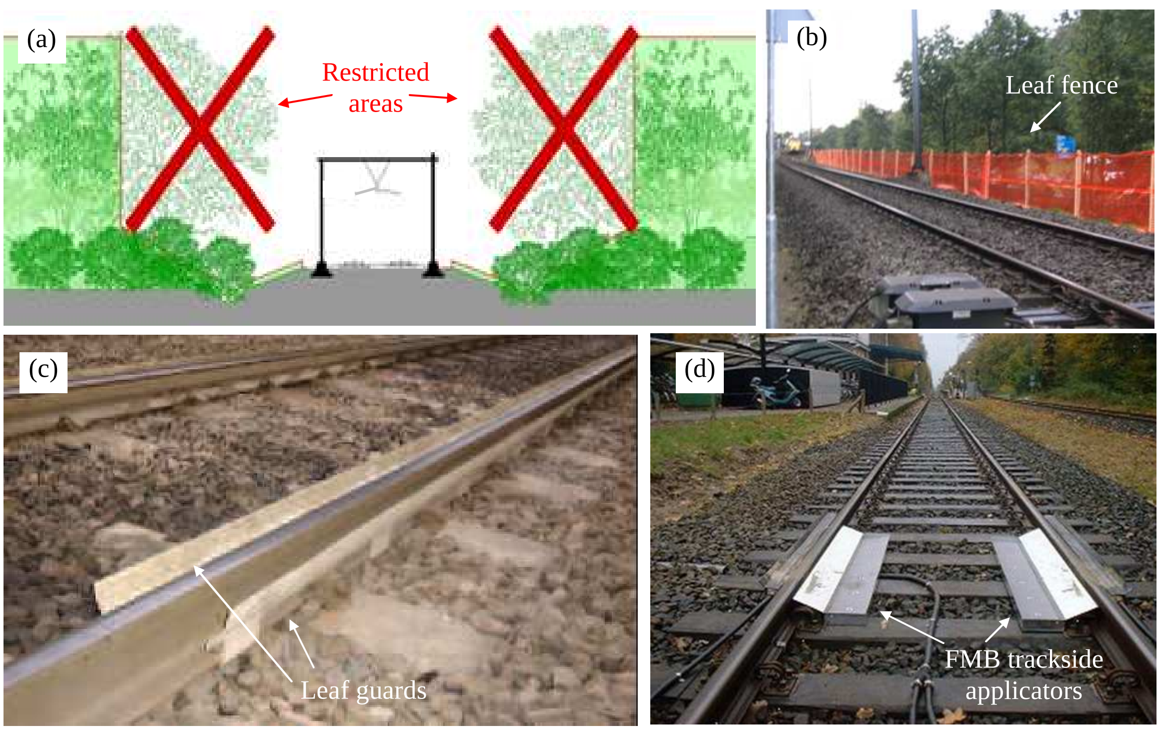

Fig. 1.8. Photograph of: (a) vegetation management [1.44]; (b) leaf fence [1.44]; (c) leaf guards [1.12]; (d) FMB trackside applicators [1.44].

1.1.4.3. Rolling stock related

Some of the TOCs operating in affected countries, sometimes together with the infrastructure managers, have adopted the following trainborne countermeasures:

- besides locomotive sanding, sanding practice has been extended in recent years to some EMUs in countries like Germany and the UK [1.14, 1.45];
- trainborne application of FMB (see Fig. 1.9a), which is widely employed in the Netherlands and the UK;
- ceramic particle jetting, which is employed in Japan in a similar way to sanding but reported to be more effective at higher travelling velocities (up to 300 km/h) thanks to the jet [1.46];
- incorporation of TC/WSP systems in existing and new rolling stock to maximize the use of the existing adhesion under low adhesion conditions;
- magnetic track brakes (MTBs), which have been fitted to trailing bogies of some EMUs to increase the braking performance mostly (or only) during emergency braking. A photograph of an active MTB is given in Fig. 1.9b.

Fig. 1.9. Photograph of: (a) trainborne application of FMB in the Netherlands [1.44]; (b) MTB in active position of the VIRM train of NS.

1.2. Research motivation

The problems related to low adhesion have to a large extent not been solved yet, despite the countermeasures adopted by the affected railways. It is noteworthy that two recent SPADs in the UK involved rolling stock equipped with WSP systems and sanders [1.47-1.48]. Investigations on the punctuality in the Dutch railways in the period 2006-2008 have revealed reductions of up to 11 % in the autumn months compared to the yearly average [1.36]. To a great extent, the persistence of low adhesion problems may be attributed to the following main reasons:

- insufficient grasp of the low adhesion phenomenon;
- poor understanding on the effectiveness, optimal use and side effects of existing countermeasures;
- need for proper detection and identification of the causes of low adhesion in service;
- lack of information on the adhesion level available in service.

In order to tackle the low adhesion problem, NS and ProRail have commissioned a research project called AdRem to investigate the abovementioned points [1.49]. As part of the AdRem project, this dissertation has investigated the first two points, while the other points have been examined by AdRem colleagues [1.36, 1.50, 1.51]. Regarding the understanding on existing countermeasures, four of them have been investigated in this dissertation, namely FMs, sanding, MTBs, and TC.

The relationship between the investigated countermeasures and the low adhesion problem is depicted in Fig. 1.10. FMs, sanding and MTBs are countermeasures that can be taken to improve the adhesion by conditioning the surfaces of rails, wheels, or both. There may be an additional relationship between FMs and sanding when sand is the main constituent of the FM, as it occurs in FMB. Furthermore, TC may be employed to make better use of the adhesion available or to improve the adhesion by operating at high slip. This dissertation has primarily focused on the former aspect. In many situations, TC may be used in combination with any of the other three countermeasures.

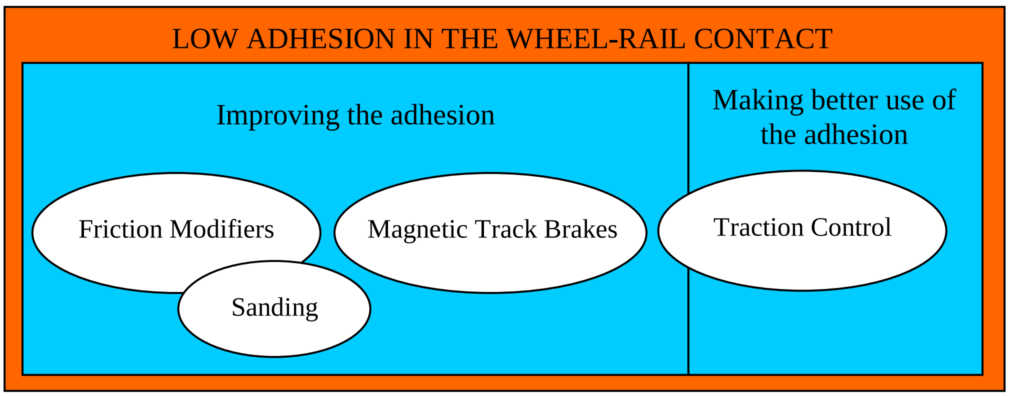

Fig. 1.10. Relationship between investigated countermeasures and low adhesion problem.

1.2.1. Understanding the low adhesion phenomenon

The most common types of contamination causing low adhesion incidents have already been reported by the affected railways, i.e. leaves, water and grease (see Section 1.1.2). Furthermore, some investigations have been performed with these contaminants, as indicated in Section 1.1.2. However, those investigations have not given answer yet to all aspects of low adhesion, as will be explained in detail in Chapters 2-5. Some of the remaining questions that this dissertation aims at answering are:

- How much is the wheel-rail adhesion available in typically contaminated contacts?
- What is the influence of the number and the slip level of wheel passages on the wheel-rail adhesion in typically contaminated contacts?
- How much is the wheel-rail adhesion during curve negotiation in typically contaminated contacts?

1.2.2. Understanding the effectiveness and side effects of friction modifiers

Although FMB has widely been used for more than ten years in countries like the Netherlands and the UK, no fundamental understanding has been pursued on its effectiveness and possible side effects, especially under controlled conditions. In recent years, another FM, referred to as FMA in this dissertation, was tested successfully against water contamination in a train depot in Japan. In order to examine possible improvements in the FM design, the performance of the two FMs has been compared in this dissertation. The main questions to be answered are the following:

- How much is the adhesion improvement by using the FMs in typically contaminated contacts?
- What is the influence of the number and the slip level of wheel passages on the effectiveness of the FMs?
- What are the possible side effects of using FMs?
- What can be improved in the FM design?

1.2.3. Understanding the effectiveness, side effects and optimal use of sanding

Literature has shown that different standards on sanding practice appear to be used by different railways. In particular, different particle size distributions are employed, e.g. 0.2-1.2 mm in the Netherlands, 0.7-2.8 mm in the UK [1.45], 0.1-0.6 mm in France [1.52], and 0.63-2 mm in Germany [1.53]. In addition, different application rates may also be used depending on the railways and the characteristics of the sanders. To the surprise of the author, not much research seems to have been done towards the influence of the particle size and feed rate, as well as other sanding parameters, on the effectiveness of sanding. Furthermore, in a recent document found in the literature, the benefit of sanding on adhesion improvement appears to be brought into question [1.54].

On the other hand, railways may be reluctant to employ sand because it may cause two important side effects: a) insulation of the wheel-rail contact leading to train detection problems [1.52, 1.55]; b) acceleration of the wear of wheels and rails [1.6, 1.56]. In addition, sand may act as a solid lubricant under certain conditions, reducing the wheel-rail adhesion from that of dry contacts [1.6, 1.9, 1.57]. Nevertheless, the effect of the sanding parameters on those side effects is not well understood.

Suffice it to say that this lack of fundamental understanding of the effect of sanding parameters on its effectiveness and side effects hinders any possible optimization in the use of sand not only for sanding, but also in part for sand-based FMs (e.g. FMB). Hence, the major questions that this dissertation aims to address are the following:

- Is sand an effective method to improve the wheel-rail adhesion in typically contaminated contacts?
- What is the influence of some sanding parameters (e.g. particle size, wheel slip, feed rate and number of sanding axles) on the adhesion improvement in typically contaminated contacts?
- What is the influence of some sanding parameters (e.g. particle size, wheel slip, feed rate) on the side effects caused by sanding?
- What can be improved in some current uses of sand?

1.2.4. Understanding the effectiveness and side effects of magnetic track brakes

MTBs are nowadays employed only during emergency braking in the Dutch railways. In recent years, interest has grown in the Netherlands and the UK towards the possible frequent use of MTBs against slippery tracks [1.58, 1.59], while in other railways MTBs may already be employed [1.14]. However, there seems to be a lack of knowledge on the major benefits and possible side effects of using MTBs to overcome low adhesion problems. This impedes any possible cost-benefit analysis in the use of MTBs as an efficient countermeasure against low adhesion. Thus, the main questions that this dissertation addresses are the following:

- Are MTBs an effective method to improve wheel-rail adhesion in typically contaminated contacts?
- Can safe braking distances be guaranteed by means of MTBs?
- What are the possible side effects on the track and the maintenance of rolling stock due to the frequent use of MTBs?

1.2.5. Understanding the effectiveness of traction control

The TC system (as well as the WSP system) is tested by the manufacturer prior to their implementation on the rolling stock to obtain the optimal parameters for the control algorithm. However, the low adhesion conditions in the tests may often be created with a soap solution, whose rheological properties can clearly differ from the contaminants affecting railways in reality. In this dissertation, the effectiveness of the existing TC system of a Dutch railway vehicle will be investigated with actual low adhesion data to answer the question:

- Is the existing TC effective in typically contaminated contacts?

1.3. Research approach

In order to find answers to the questions presented in the research motivations, experimental and numerical investigations have been performed. The experimental investigations have been carried out in the laboratory and in field. In the laboratory investigations the wheel-rail adhesion has been examined with a twin-disk roller rig, in which the actual wheel-rail contact is simulated by two disks in rolling-sliding motion. The influence of different types of contamination on the wheel-rail adhesion, as well as the effectiveness of FMs and sanding, has been investigated by means of displacement controlled tests, i.e. fixed slip ratio and rolling velocity.

The laboratory test approach has been chosen for two main reasons. On one hand, investigations in the laboratory can be much more economical than performing field tests, particularly when it comes to parametric studies. On the other hand, tests in the laboratory can be performed under closely controlled conditions, offering the possibility to investigate the effect of an isolated parameter. The major trade-off when testing in the laboratory is that the results may not be extrapolated directly to the actual wheel-rail contact mainly due to differences in geometry, and sometimes in operational conditions. Therefore, laboratory testing can provide a qualitative indication of what happens in the actual wheel-rail to identify influencing parameters on adhesion. Afterwards, field tests can be employed to quantify their effect under actual conditions.

Two series of field investigations are presented in this dissertation, one with an electrical locomotive of the series 1700, and one with an EMU of the series VIRM. E-loc 1700 and VIRM have been selected because they are the major type of rolling stock in the NS fleet fitted with sanders and MTBs, respectively. One of the aims of the field investigations has been to quantify the impact of typically contaminated contacts on the wheel-rail adhesion. Furthermore, the field tests with E-loc 1700 have aimed at validating one of the trends observed in the laboratory investigations with sand, namely the effect of the particle size on the wheel-rail adhesion. The field tests with VIRM have focused on quantifying the effectiveness of MTBs. The wheel-rail adhesion has been measured by means of readings from the motors in the tests with VIRM, or derived from acceleration measurements in the tests with E-loc 1700.

In this dissertation, numerical modeling has been employed to investigate the wheel-rail adhesion during curve negotiation in typically contaminated contacts on one hand, and to examine the effectiveness of an existing TC system on the other. Numerical modeling has been preferred over field or laboratory tests because it has lower costs and it facilitates more in-depth investigations of multiple parameters. VIRM has been the train type selected for the calculations for several reasons: a) available technical data; b) available measured data to validate the numerical model; c) VIRM is the major train type in the NS fleet. The numerical calculations have been performed with two types of commercial software. On one hand, the multi-body dynamics software ADAMS/VI-Rail has been employed to model the leading coach of VIRM for the vehicle-track interaction. On the other hand, the TC system of VIRM has been simulated by means of MATLAB/Simulink to examine the suitability of the control algorithm. Additionally, a friction model, which has been developed and validated at the University of Twente to characterize lubricated contacts [1.51], has been coupled to the vehicle and TC models to simulate the curving behaviour under low adhesion conditions caused by improper flange lubrication.

1.4. Outline of the dissertation

The logic development of this dissertation is schematically represented in Fig. 1.11. The investigations have been grouped into four chapters (or clusters) that have been entitled according to the main countermeasure investigated. Each chapter also contributes to a better understanding on the low adhesion phenomenon, as shown in Fig. 1.11.

Chapter 2 presents the laboratory investigations on two FMs (FMA and FMB), in which the tests have been performed in dry, wet and leaf contaminated contacts. In Chapter 2, as well as in others chapters, a baseline of the untreated situation has also been obtained. The baseline has had a double purpose: on one hand, it has facilitated the derivation of the relative effect of FMs (or sanding or MTBs in other chapters); on the other hand, it has provided information on the low adhesion phenomenon.

The findings of Chapter 2 pointed out the relevant effect of FM particle size on the adhesion recovery. In Chapter 3, the influence of the particle size, as well as other important parameters, is investigated on the effectiveness and side effects of sanding practice towards a possible optimization. Table 1.3 shows the sanding parameters and effects that have been examined in laboratory and field tests in dry and leaf contaminated contacts. In these investigations, comparisons with a baseline have also been made.

The field investigations with MTBs are presented in Chapter 4. In these investigations, the wheel-rail adhesion improvement, the braking force, and the side effects of using MTBs have been examined. The tests have been carried out in dry, wet, grease and leaf contaminated contacts. The performance of the MTBs has been compared to a baseline, and also to FMB in leaf contaminated contacts.

Table 1.3. Sanding parameters and effects investigated in lab or field tests as treated in Chapter 3.

	Adhesion	Train detection	Damage to wheels and rails
Sand particle size	lab/field	lab	lab
Wheel slip	lab	lab	lab
Feed rate	lab	lab	-
Number of sanders	lab/field	-	-

In Chapter 5, the models, which have been developed for the numerical analysis of low adhesion and traction control, are introduced. The validation of the VIRM vehicle model is presented. The investigations on the curving behaviour of the VIRM vehicle during traction under low adhesion conditions are also given.

Chapter 6 presents the conclusions and recommendations. In comparison with the more detailed conclusions given in Chapters 2-5, the conclusions of Chapter 6 are rather general in an attempt to answer the questions presented in the research motivation. The recommendations outline interesting lines of scientific research on the one hand, and possible prosperous investments for rolling stock operators and railway network managers dealing with low adhesion problems on the other.

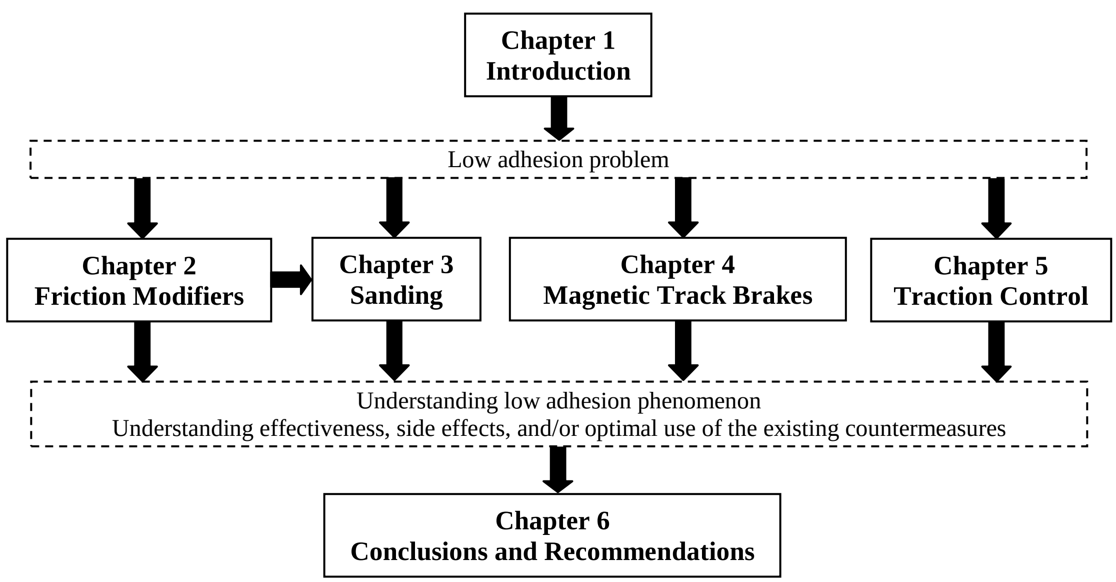

Fig. 1.11. Schematic representation of the outline of the dissertation.

References

[1.1] H.I. Andrews: Railway Traction—the Principles of Mechanical and Electrical Railway Traction. Elsevier (1986).
[1.2] ProRail: Algemeen Voorschrift, Seinstelsel en seingeving remafstanden bij de seingeving, AV 132 (April 2005) in Dutch.
[1.3] F.P. Bowden and D. Tabor: The Friction and Lubrication of Solids. Clarendon Press, Oxford (1956).
[1.4] N.P. Suh and H.C. Sin: The Genesis of Friction. Wear 69 (1981) 91-114.
[1.5] ASM Handbook, Volume 18: Friction, Lubrication, and Wear Technology. ASM International (1992).
[1.6] S. Kumar, K. Krishnamoorthy, D.L. Prasanna Rao: Wheel-Rail Wear and Adhesion With and Without Sand for a North American locomotive. Journal of Engineering for Industry 108 (1986) 141-148.
[1.7] W. Zhang, J. Chen, X. Wu, X. Jin: Wheel/rail adhesion and analysis by using full scale roller rig. Wear 253 (2002) 82–88.
[1.8] U. Olofsson, K. Sundvall: Influence of Leaf, Humidity and Applied Lubrication on Friction in the Wheel-Rail Contact: Pin-on-Disc Experiments. Journal of Rail and Rapid Transit 218 (2004) 235-242.
[1.9] E.A. Gallardo-Hernandez, R. Lewis: Twin disc assessment of wheel/rail adhesion. Wear 265 (2008) 1309–1316.
[1.10] C.W. Jenks: Improved Methods for Increasing Wheel/Rail Adhesion in the Presence of Natural Contaminants. Transit Cooperative Research Program Sponsored by the Federal Transit Administration, Transportation Research Board National Research Council (May 1997).
[1.11] J. Eleveld: Gladde Sporen, Oplossingsrichtingen voor Adhesieproblemen. Report published by the Dutch Railways Technical Research (NSTO) in Dutch (March 1999).
[1.12] Managing Low Adhesion. Report published by the Adhesion Working Group, UK (September 2001).
[1.13] N. Tanabe, Y. Hirota, T. Omichi, J. Hirama, K. Nagase: Study on the Factors Which Cause the Wheel Skidding of JR Ltd. Express EMUs. JSME International Journal 47 (2004) 488-495.
[1.14] W. Voges, P. Spiess: Optimising Services with EMU ET42x in Autumn 2004 and 2005. In the Proceedings of 7th World Congress on Railway Research, Canada (2006).
[1.15] P.M. Cann: The ‘‘leaves on the line’’ problem—a study of leaf residue film formation and lubricity under laboratory test conditions. Tribology Letters 24 (2006) 151-158.
[1.16] C.R. Fulford, Review of Low Adhesion Research, Report published by the Rail Safety and Standards Board, UK (2004)
[1.17] W. Poole: Characteristics of Railhead Leaf Contamination. Summary Report published by Rail Safety and Standards Board (May 2007).
[1.18] T. Ohyama: Tribological studies on adhesion phenomena between wheel and rail at high speeds. Wear, 144 (1991) 263-275.
[1.19] H. Chen, T. Ban, M. Ishida, T. Nakahara: Adhesion between rail/wheel under water lubricated contact. Wear 253 (2002) 75–81.

[1.20] H. Chen, T. Ban, M. Ishida, T. Nakahara: Experimental investigation of influential factors on adhesion between wheel and rail under wet conditions. Wear 265 (2008) 1504–1511.
[1.21] P. Scroba, M. Roney, R. Dashko, E. Magel: Canadian Pacific Railway's 100% Effective Lubrication Initiative. AREMA 2001, Conference and Exhibition, Chicago, Illinois (2001).
[1.22] R. Fröhling, J. de Koker, M. Amade: Rail Lubrication and its Impact on the Wheel/Rail System. Journal of Rail and Rapid Transit 223 (2009) 173.
[1.23] P.O. Larsson-Kraik: Managing the wheel-rail interface: Railway infrastructure maintenance in a severe environment: The Swedish experience. In Wheel-Rail Interface Handbook, Woodhead Publishing Limited (2009).
[1.24] J. Tunna: Managing the wheel-rail interface: the US experience. In Wheel-Rail Interface Handbook, Woodhead Publishing Limited (2009).
[1.25] M. Ishida: Managing the wheel-rail interface: the Japanese experience. In Wheel-Rail Interface Handbook, Woodhead Publishing Limited (2009).
[1.26] S. Marich: Managing the wheel-rail interface: the Australian experience. In Wheel-Rail Interface Handbook, Woodhead Publishing Limited (2009).
[1.27] A. Zoeteman, R. Dollevoet, R. Fischer, J.W. Lammers: Managing the wheel-rail interface: the Dutch experience. In Wheel-Rail Interface Handbook, Woodhead Publishing Limited (2009).
[1.28] T.M. Beagley, I.J. McEwen, C. Pritchard: Wheel/rail adhesion - Boundary lubrication by oily fluids. Wear 31 (1975) 77-88.
[1.29] R. Lewis, E.A. Gallardo-Hernandez, T. Hilton, T. Armitage: Effect of oil and water mixtures on adhesion in the wheel/rail contact. Journal of Rail and Rapid Transit 223 (2009) 275-283.
[1.30] M. Broster, C. Pritchard, D.A. Smith: Wheel/rail adhesion - Its relation to rail contamination on British railways. Wear 29 (1974) 309-321.
[1.31] T.M. Beagley, I.J. McEwen, C. Pritchard: Wheel/rail adhesion - The influence of railhead debris. Wear 33 (1975) 141-152.
[1.32] T.M. Beagley, C. Pritchard: Wheel/rail adhesion - The overriding influence of water. Wear 35 (1975) 299-313.
[1.33] U. Olofsson: A multi-layer model of low adhesion between railway wheel and rail. Journal of Rail and Rapid Transit 221 (2007) 385-389.
[1.34] Ministerie van Verkeer en Waterstaat, Personenvervoer: Landelijke Markt- en Capaciteitsanalyse Spoor. Eindrapport, 19 november 2007 (in Dutch).
[1.35] Y. Post, R. Mennens, J. R. van der Voort, R.B. Rookhuiszen: Basisplan Zandstrooiers ICMIV. Report produced by Nedtrain Consulting (2004) in Dutch.
[1.36] N. van Steenis: Monitoring train performance in case of low adhesion. PhD Thesis, University of Twente, Enschede, the Netherlands (2010).
[1.37] A. Kapoor, D.I. Fletcher, F. Schmid, K.J. Sawley, M. Ishida: Tribology of Rail Transport. In Modern Tribology Handbook. Boca Raton, CRC Press (2001).
[1.38] R. Deuce: Wheel Tread Damage. Bombardier Inc (2007).
[1.39] Rail Accident Investigation Branch (RAIB): Autumn Adhesion Investigation Part 3: Review of adhesion-related incidents Autumn 2005. Report 25 (Part3)/2006 (2007).

[1.40] Press release by NOS on the metro accident in Amsterdam on February 20th, 2010. Available online at http://nos.nl/artikel/138434-31-gewonden-bij-metrobotsing-amsterdam.html.
[1.41] J. Nielsen: Out-of-round railway wheels. In Wheel-Rail Interface Handbook. Woodhead Publishing Limited (2009).
[1.42] M.J.M.M. Steenbergen: Wheel-Rail Interaction at Short-Wave Irregularities. PhD Thesis, Delft University of Technology, Delft, the Netherlands (2008).
[1.43] T. Oosterom: Gladde sporen - Probleeminventarisatie. Report produced by NedTrain Consulting (2001) in Dutch.
[1.44] A. Rijnaard: ProRail autumn campaign. Presentation given at the Adhesion Working Group (AWG) Conference (2008).
[1.45] Sanding Equipment Fitted to Multiple Units and On-track Machines. Railway Group Standard GM/RT 2461 (2001).
[1.46] K. Ono: Adhesion-Increasing-Agent Jetting System “Cerajet”. Railway Technology Avalanche 2 (2003) 13.
[1.47] Rail Accident Investigation Branch (RAIB): Autumn Adhesion Investigation Part 1: Signals WK338 and WK336 Passed at Danger at Esher 25 November 2005. Report 25 (Part1)/2006 (2007).
[1.48] Rail Accident Investigation Branch (RAIB): Autumn Adhesion Investigation Part 2: Signal LW9 Passed at Danger at Lewes 30 November 2005. Report 25 (Part2)/2006 (2007).
[1.49] AdRem Management Rapport voor NSR en ProRail (January 29, 2010) in Dutch.
[1.50] S. van der Krol: ADREM Rail VIR en NIR Spectrum Analyse. Report produced by Wageningen University (April 2009) in Dutch.
[1.51] R.I. Popovici: Friction in the Wheel-Rail Contacts. PhD Thesis, University of Twente, Enschede, the Netherlands (2010).
[1.52] Mesures a Prendre Pour Ameliorer la Sensibilite au Shuntage des Circuits de Voie. UIC737-2 in French (1980).
[1.53] G. Gfatter, D. Lang, H. Kalbas, G. Krause, W. Rychli: Sanding Systems. Handbook published by Knorr-Bremse GmbH (2002).
[1.54] Department of Transportation, Federal Railroad Administration: Locomotive Safety Standards; Sanders. Federal Register 72 (2007) 59216-59224.
[1.55] R. Lewis, R.S. Dwyer-Joyce, J. Lewis: Disc Machine Study of Contact Isolation During Railway Sanding. Journal of Rail and Rapid Transit 217 (2003) 11-24.
[1.56] R. Lewis, R.S. Dwyer-Joyce: Wear at the Wheel-Rail Interface when Sanding is Used to Increase Adhesion. Journal of Rail and Rapid Transit 220 (2006) 29-41.
[1.57] Boiteux, Cadier, J. Kling, W. Kunnes: Summary of Theoretical and Practical Knowledge of Poor Adhesion Conditions Acquired since Publication of B 164/RP 2. Report DT 257 (B 164) published by the Office for Research and Experiments of the International Union of Railways (1992).
[1.58] N. van Steenis: Voorstudie Magneetrem op Gladde Sporen. Report produced by NedTrain Consulting (2003) in Dutch.
[1.59] D. Shipley: Outline Feasibility of Fitting Magnetic Track Brakes to UK Rolling Stock. Report produced by Interfleet Technology Ltd. (2006).

Chapter 2

Friction modifiers

ABSTRACT

Chapter 2 presents some laboratory investigations carried out with two "commercial" FMs (FMA and FMB), which have been used or tested by several railways to improve the adhesion in contaminated contacts. The chapter is divided into two parts. Part A shows the investigations performed in dry and wet contacts, which examine not only the adhesion characteristics of the FMs, but also their possible side effects on wheels and rails. In Part B, the adhesion recovery when using the FMs in leaf contaminated contacts is investigated, and the solid components of the FMs are analyzed. In both Part A and Part B, baselines of the untreated situations (i.e. no FMs) are also presented, which are employed for two purposes: on one hand, they facilitate the derivation of the relative effect of the FMs; on the other hand, they provide information on the low adhesion phenomenon.

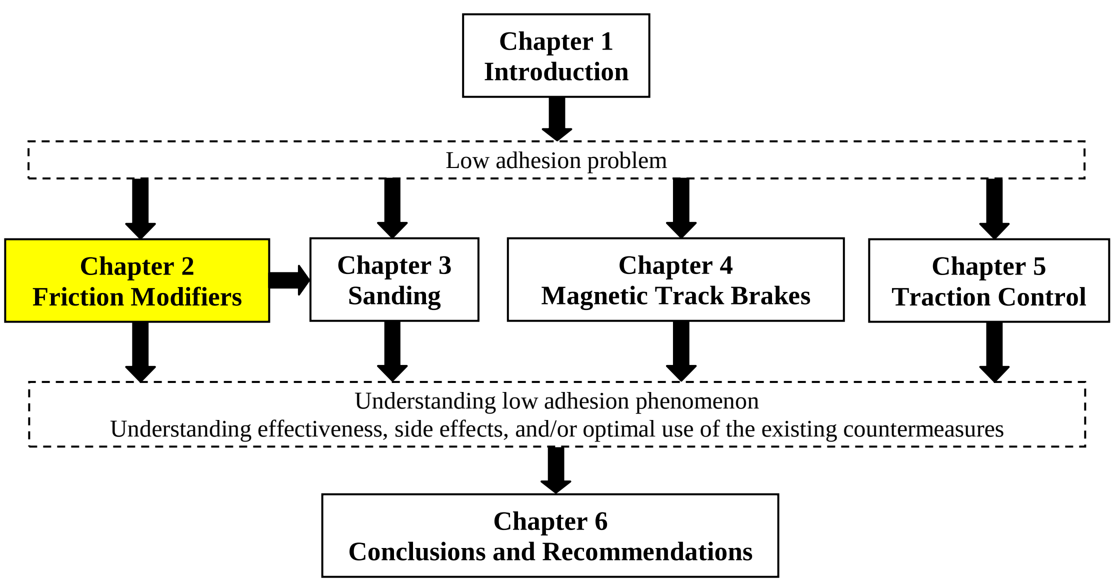

Chapter 2, Part A

Laboratory tests in dry and wet contacts[V]

ABSTRACT

Friction management has been carried out extensively in the majority of railway networks in the last few years. A popular practice is the application of friction modifiers to increase the adhesion level in contaminated wheel-rail contacts. Two friction modifiers have particularly been used or tested on several railway networks as adhesion enhancers to facilitate the traction and braking operation under poor adhesion conditions. However, for assessment of the performance the railway operators and infrastructure managers mostly rely on practical observations that do not elucidate completely the effectiveness and side effects of these adhesion enhancers. In this paper, the constituents of the two friction modifiers are identified and the solid components are analyzed. A twin-disk roller rig has been used to study their performance in dry and wet contacts under closely controlled laboratory conditions. The adhesion characteristics of both friction modifiers are examined for different slip ratios. Furthermore, the wheel and rail disks are examined after a series of dry tests to analyze the mass loss, the surface damage, the change in surface hardness and roughness, and the subsurface deformation caused by the friction modifiers compared to dry clean contacts.

[V] This chapter has been published as: O. Arias-Cuevas, Z. Li, R. Lewis, E.A. Gallardo-Hernandez: Rolling-Sliding Laboratory Tests of Friction Modifiers in Dry and Wet Wheel-Rail Contacts. Wear 268 (2010) 543–551.

2A.1. Introduction

In the railway industry, the friction utilized between wheel and rail during braking and traction operations is known as wheel-rail adhesion. The adhesion, or the adhesion coefficient, is defined as the ratio of the tangential (i.e. braking or traction) force over the normal force at the wheel-rail contact. Adhesion is influenced by vehicle speed, wheel slip, contact pressure, environment conditions, and many other factors. Whilst too high friction in the wheel-rail contact is undesired because it leads to more wear and rolling contact fatigue (among other problems), it must be sufficient to ensure an adequate adhesion level for the traction and braking operation of the rail vehicles. Many studies on wheel-rail adhesion have already been conducted in both laboratory and field tests. Beagley et al. presented pioneering work in 1975 about the influence of water on adhesion [2A.1]. They also investigated the influence of other factors on adhesion, such as railhead debris and oil contamination [2A.2, 2A.3]. More recently, laboratory studies on adhesion for dry and wet wheel-rail contacts have also been carried out with a twin-disk roller rig [2A.4-2A.6] and with a full-scale roller rig [2A.7].

In recent years, friction management has been carried out extensively in the majority of railway networks with different purposes. Some friction modifiers (FMs) have been designed to eliminate the negative slope of the traction curve that is responsible of the stick-slip oscillations, thus overcoming the squealing noise and corrugation phenomena that can especially occur in small-radius curves [2A.8, 2A.9]. FMs have also been aimed at reducing the occurrence rolling contact fatigue (e.g., head checks) and the rates of wear [2A.10]. This paper deals with another popular practice of friction management, in which FMs are used to increase the adhesion between wheel and rail facilitating the traction and braking operation under poor adhesion conditions. Such FMs are also known as adhesion enhancers. Sanding from the train or locomotive is used on railway networks world wide [2A.11]. Laboratory studies on sanding to investigate its effect on adhesion and its damage to wheel and rail have been published [2A.4, 2A.12]. Besides sanding, other adhesion enhancers have been used or tested on several railway networks. In countries such as the United Kingdom and the Netherlands, a commercial adhesion enhancer has been used since the late 90’s to overcome poor adhesion conditions, especially due to leaf layer contamination combined with small amounts of water during the autumn season [2A.13]. Nevertheless, there exists a lack of research on this adhesion enhancer to understand both its adhesion characteristics and its possible damage to wheels and rails. Therefore, the railway operators and infrastructure managers mostly rely on practical observations that do not elucidate completely the effectiveness of the adhesion enhancer used on their network. In this paper, a laboratory study of this widely used adhesion enhancer is presented together with another adhesion enhancer designed for wet wheel-rail contacts due to rainfall.

The aim of this work is to investigate the performance of the two adhesion enhancers in dry and wet contact conditions. A study of these adhesion enhancers in leaf contaminated contacts has also been carried out [2A.14]. The two adhesion enhancers are named FMs throughout this paper. Both FMs are water-based and have been designed to increase the adhesion in different conditions. Friction modifier A (FMA) has been tested successfully in a train depot in Japan to overcome adhesion problems related to rainfall. FMA is to be applied to the top of both rails in a very thin layer. Friction modifier B (FMB) has extensively been used in autumn on the Dutch and British railways networks to mitigate adhesion problems mostly due to leaves and small amounts of water. In The Netherlands, FMB is primarily trainborne applied to top of both rails by means of a speed dependent pumping system, which delivers 4 cc/m per rail. In this work, a twin-disk roller rig has been used to simulate the wheel-rail contact in controlled laboratory conditions. The adhesion characteristics of the two FMs have been studied in dry and wet conditions for up to four different slip ratios: 0.5, 1, 2 and 3%. The damage caused to the wheel and rail disks by the FMs has also been analyzed. The constituents of the FMs have been examined and their influence on adhesion and disk damage has been assessed.

2A.2. Test set-up

2A.2.1. Test roller rig

The rolling-sliding tests were conducted on the SUROS (Sheffield University ROlling Sliding) roller rig, shown in Fig. 2A.1. A detailed description of the roller rig is given in [2A.15]. The test disks were mounted on independent shafts. By means of a hydraulic jack, a controlled contact pressure was achieved during the test. The slip ratio between the disks was prescribed by setting different rotational speed of the shafts and maintained constant throughout each test with a controller. The slip ratio is defined in Eq. 2A.1, where w and r are the rotational speed and rolling radius of the disks, respectively. The adhesion coefficient was calculated with the readings of the torque transducer and the load cell, as given in Eq. 2A.2, by T and F_N, respectively. A personal computer was used to acquire the data and to control both the speed and the load.

$$Slip = \frac{w_{wheel} \cdot r_{wheel} - w_{rail} \cdot r_{rail}}{w_{wheel} \cdot r_{wheel} + w_{rail} \cdot r_{rail}} \cdot 200\% \qquad (2A.1)$$

$$\mu_{adhesion} = \frac{T}{F_N \cdot r_{rail}} \qquad (2A.2)$$

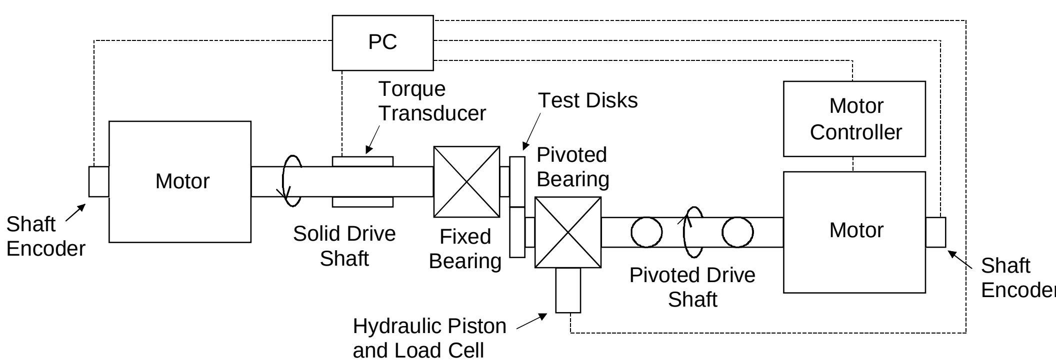

Fig. 2A.1. Schematic representation of the SUROS roller rig.

2A.2.2. Test disks

The test disks were cut from rails and wheel tires retired from service in the Dutch railway network; R260Mn and B5T steel for the rail and wheel, respectively. The disks were machined with their axes perpendicular to the longitudinal axis of both wheel and rail (see Fig. 2A.2). The Vickers macro-hardness of the wheel and the rail steel used in the tests was measured as 267 HV_{20kg} and 281 HV_{20kg} on average, respectively. Prior to testing, the disks were cleaned in a bath of ethanol by means of ultrasonic vibration. The roughness of the new disks was measured as 1±0.2 μm on average with a profilometer. Before assembling the disks into the roller rig, their diameter was measured with a vernier calliper as necessary for the calculations of slip and adhesion coefficient.

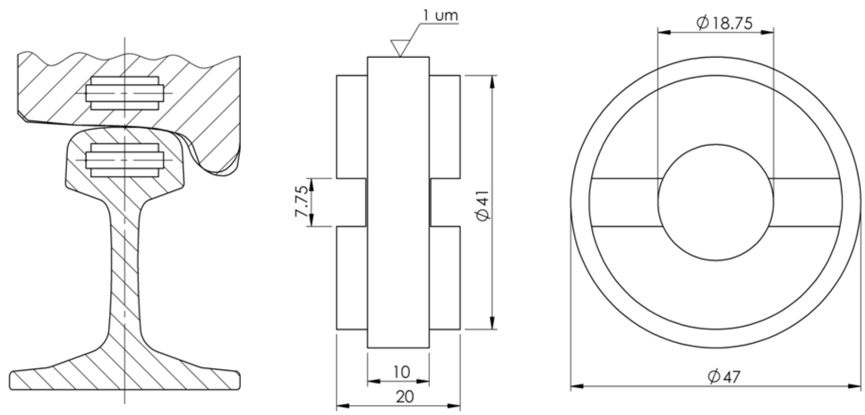

Fig. 2A.2. Orientation and dimensions of the wheel and rail disks specimens.

2A.2.3. Tested friction modifiers

Two top-of-the-rail water-based FMs have been tested in this work. Microscope photographs of the dried samples are given in Fig. 2A.3. The particle size distribution of both FMs was measured by means of a laser particle analyzer, as shown in Fig. 2A.4. FMA contains several types of solid components, which have different physical and tribological characteristics that provide the final product with varied functionalities such as friction enhancement and film transfer between wheel and rail. Two size ranges of solid particles are predominant in the mix; the small particles (≈10 μm) surround the large ones (≈ 100 μm) providing them support. Furthermore, there are several polymeric components in FMA, all of which assist in promoting adherence to the wheel and rail steel surfaces. In Fig. 2A.3, it can be seen that the particles agglomerate after drying in the oven. FMB is a mixture composed of an inorganic gelling agent, stabilizer, water, sand grains and stainless steel particles. The gelling agent promotes the adherence of the mix to the wheel and rail surfaces, while the stabilizer provides a reasonable storage life. The stainless steel particles guarantee appropriate electrical properties of the mix, which are necessary due to the trainborne application of FMB on the rails. It can be seen from Fig. 2A.3 that the sand grains vary in size and type, most probably coming from different types of rocks. The black coloured particles correspond to the stainless steel, as pointed in Fig. 2A.3.

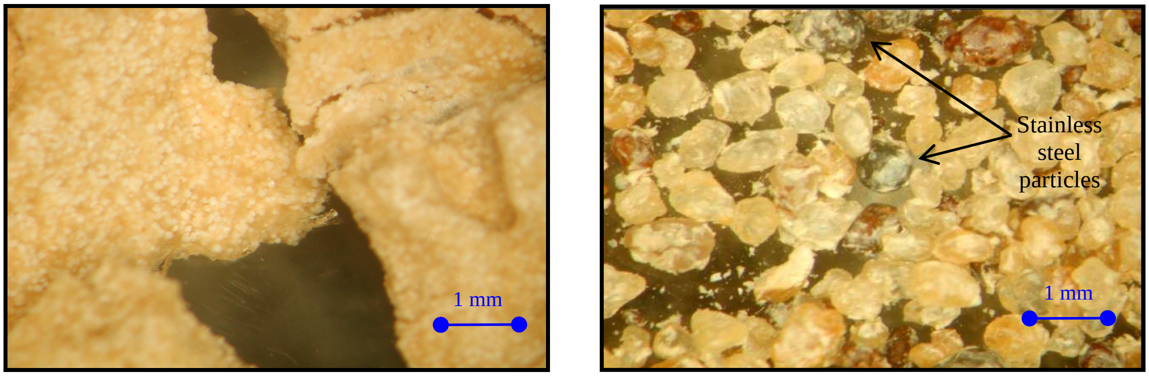

Fig. 2A.3. Microscope photographs of FMA (left) and FMB (right).

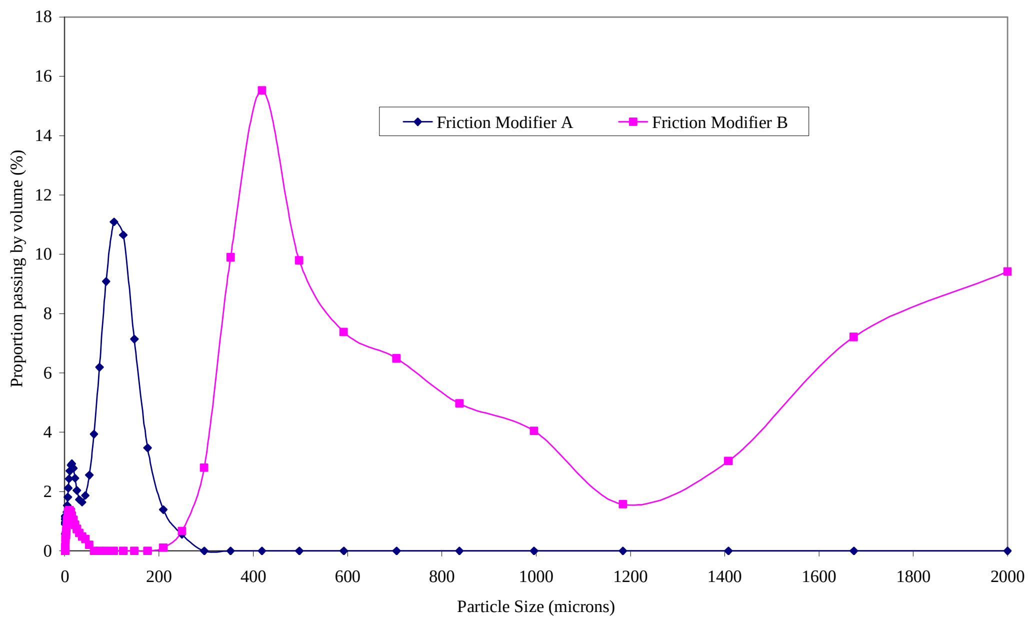

Fig. 2A.4. Particle size distribution of FMA and FMB.

2A.2.4. Test procedure

In the tests the wheel disk rotated faster than the rail disk; the rotational speed of the rail was maintained at 400 rpm, equivalent to 1 m/s of rolling speed. Since cylindrical disks were used in the experiments, a line contact of 10 mm width was present in the tests. A load of 4.7 kN was applied on the disks producing a maximum Hertzian pressure of 1.2 GPa in the contact zone, which is representative of the contact between wheel tread and top of rail for passenger trains in the Netherlands. When testing the performance of the two FMs, they were painted onto the rail disk surface prior to the start of the test, as shown in Fig. 2A.5. Due to the different solid contents of the FMs, completely covering the rail disk with the FMs yielded different masses: 0.4-0.5 g for FMA and 0.7-0.8 g for FMB. In the wet tests, the water was applied to the rail disk surface once the disks were running in order to simulate rainfall conditions, as depicted in Fig. 2A.5. For each test conducted with the FMs in both dry and wet conditions a baseline was first obtained so as to compare the performance of FMs with the untreated conditions. The dry tests were run for 2000 cycles at 0.5, 1, 2 and 3% slip; on the other hand, the wet tests were run for 1000 cycles at 0.5, 1 and 2% slip. The number of cycles in wet conditions was halved because of the enhanced removal of FMs in presence of water. The slip ratios used in this work correspond to typical values that can be found in the contact between wheel tread and top of the rail. A run-in conditioning test of 4000 cycles in dry conditions at 0.5% slip was run for each new pair of disks.

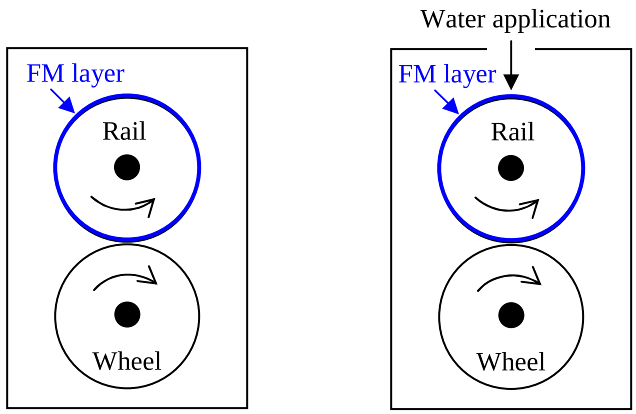

Fig. 2A.5. Test procedure for dry tests (left) and wet tests (right).

2A.3. Results

2A.3.1. Dry tests

The adhesion results of the two FMs together with the baseline for 0.5, 1, 2 and 3% slip in dry conditions are given in Figs. 2A.6-2A.9. The baseline gave the largest adhesion, with adhesion coefficients between 0.30 and 0.60 for the slip range considered. The maximum adhesion coefficient was observed at 2% slip—this is in good agreement with previous research carried out with this roller rig [2A.4, 2A.16]. Furthermore, FMA led to moderate adhesion coefficients before starvation occurred and metal-metal contact was reached. The adhesion coefficients for dry contacts with FMA could be estimated to be between 0.15 and 0.35 depending on the slip ratio. On the other hand, FMB led to an adhesion range between 0.25 and 0.55 before starvation.

The traction curve, which presents the change of the adhesion coefficient with the slip, is given in Fig. 2A.10 for the dry tests with baseline and FMs. It must be noted that the adhesion coefficients used for the traction curve have been taken from those registered at 80 cycles in the tests depicted in Figs. 2A.6-2A.9. This number of cycles was selected as the best compromise between two restrictions. On one hand, the number of cycles could not be too low because the roller rig required around 20-50 cycles to increase the slip from null (beginning of the test) to the set value. On the other hand, the selected number of cycles could not be too high to ensure that the friction modifier had not been removed from the disks surfaces. The data points have been connected by straight lines in Fig. 2A.10. It can be seen that the adhesion coefficient in baseline conditions saturates at around 2% slip followed by a decreasing slope. This decreasing slope may excite stick-slip oscillations leading to the occurrence of squeal noise and corrugation, as indicated in the introduction. Both FMA and FMB appeared to remove the decreasing slope, at least for the slip regime considered in this investigation.

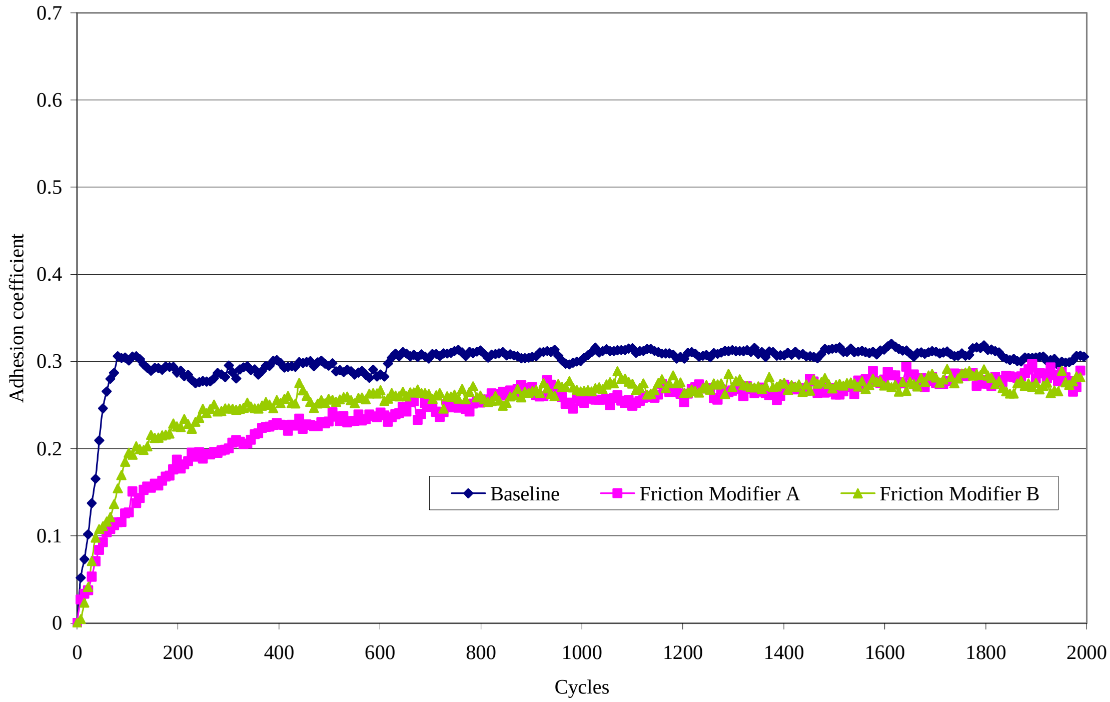

Fig. 2A.6. Adhesion tests in dry conditions at 0.5% slip.

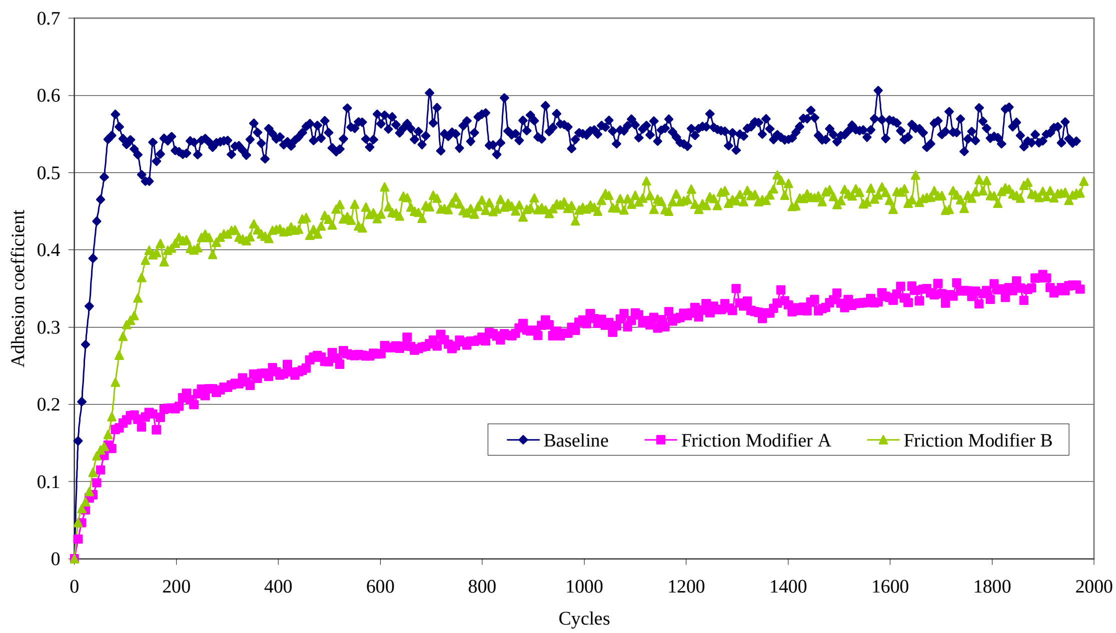

Fig. 2A.7. Adhesion tests in dry conditions at 1% slip.

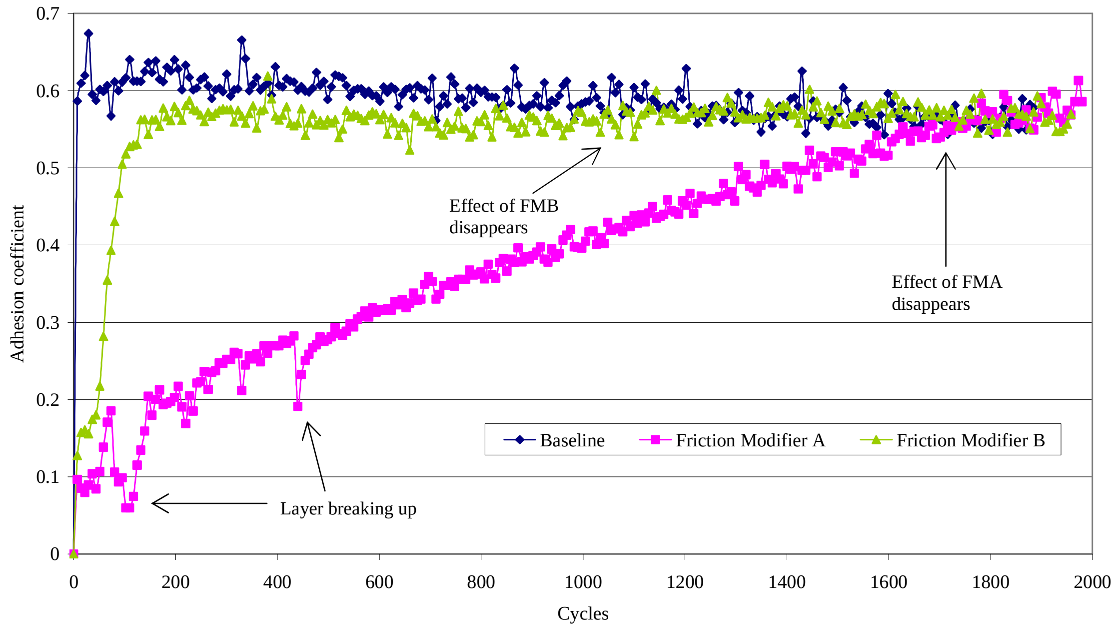

Fig. 2A.8. Adhesion tests in dry conditions at 2% slip.

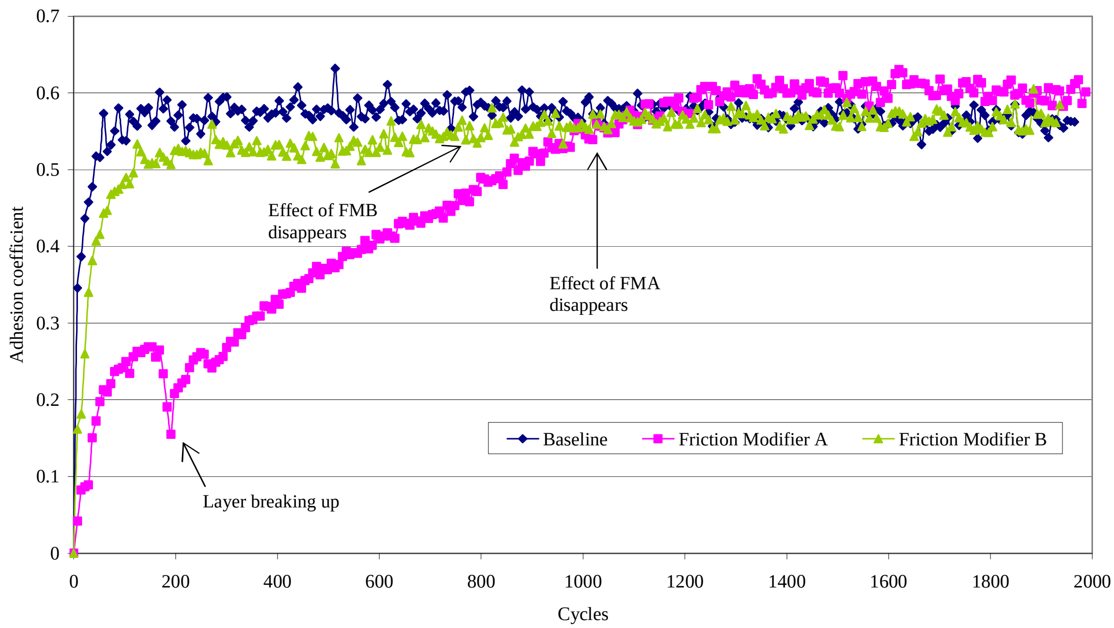

Fig. 2A.9. Adhesion tests in dry conditions at 3% slip.

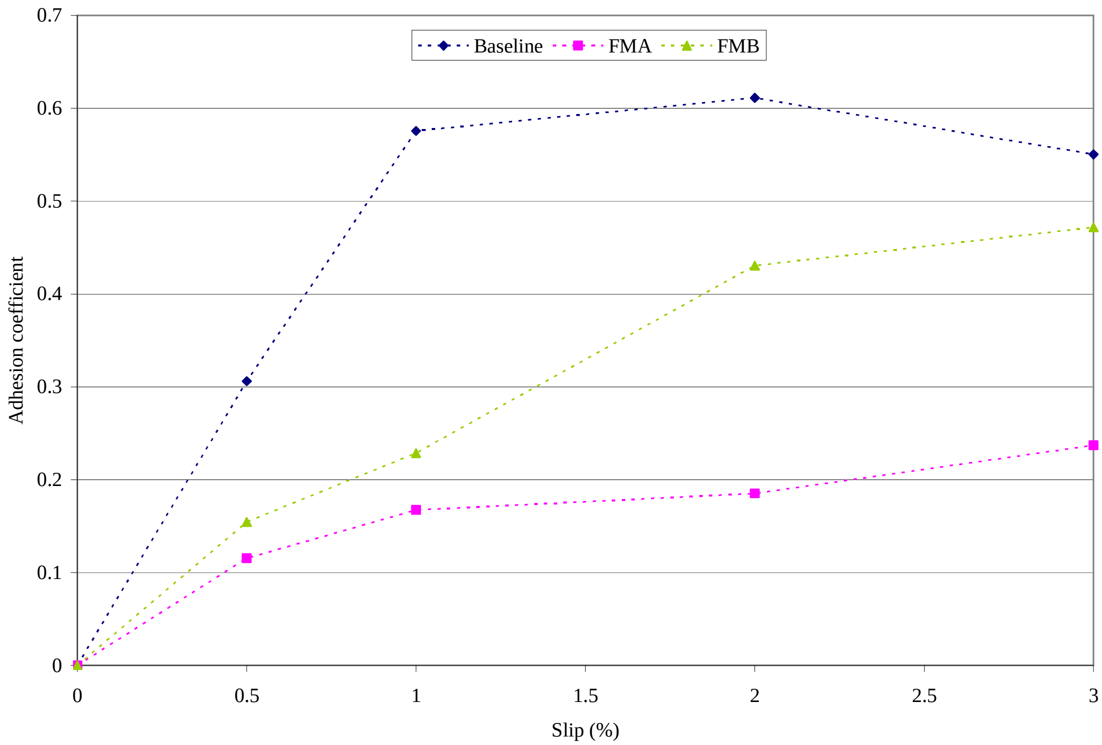

Fig. 2A.10. Traction curve of baseline, FMA, and FMB in dry conditions.

The lasting effect of the FMs was examined in dry conditions. It can be seen that the effect of both FMs on adhesion remained throughout the test for slip values up to 1%. At higher values of slip, metal-metal contact was eventually reached and the adhesion level equalled that one of the baseline. This gives evidence that the higher the slip the faster the FM is removed from the disk surfaces. Furthermore, FMA showed a longer lasting effect than FMB at 2 and 3% slip, as shown in Figs. 2A.8 and 2A.9. This could be attributed to their different composition, because it seems that FMA has a stronger structure that retains the product in contact with the disk surfaces. In addition, some sudden drops in the adhesion coefficient could be observed in the initial part of the adhesion curves for FMA at 2 and 3% slip, which could be attributed to the breaking up of the third body layer present in the contact.

Due to the slip between the disks, there exists a mass transfer of the FM from the surface of the rail disk to the wheel disk. Such phenomenon has already been investigated by other researchers [2A.17, 2A.18]. The mass transfer could be observed in the laboratory during each test. Due to this mass transfer the rail disk was predominantly clean at the end of each test; whereas the wheel disk normally had a layer composed of broken FM and oxides.

In order to assess the damage that the FMs may cause to wheel and rail, three pairs of disks used for a complete set of dry tests were examined. Each pair was used to run 12000 dry cycles, which consisted of 4000 initial run-in cycles at 0.5% slip and 2000 cycles at each slip ratio: 0.5, 1, 2 and 3%. Firstly, the surfaces of the three pairs of disks were examined by means of optical microscopy, as shown in Figs. 2A.11-2A.13. Note that due to the radial curvature of the disks, the left and right edges are darker than the centred area. A substantial difference in surface morphology could be observed between wheel and rail for all contact conditions. For the baseline tests, the rail disk presented surface corrugation, surface cracks and small pits that are associated with ratchetting wear. This type of wear had also been observed in previous work [2A.12, 2A.19]. On the other hand, oxidative wear was observed on the wheel disk surface, and a brown reddish oxide layer was seen on the surface together with exposed steel material. When using FMA, only a little ratchetting wear seemed to take place with several small pits on both wheel and rail disk surfaces, but in far less extent than in the baseline. Moreover, indentations and scratches were observed when using FMB (see Fig. 2A.13) that are attributed to the interaction with the solid particles. The size of these indentations was around 1 mm in characteristic diameter and they were present on both wheel and rail disks. These indentations were caused by sand particles indenting the wheel and rail steel material. Besides abrasive wear, oxidative wear could also be seen on the wheel surface. On the other hand, ratchetting wear was predominant on the rail disk surface with the presence of small pits.

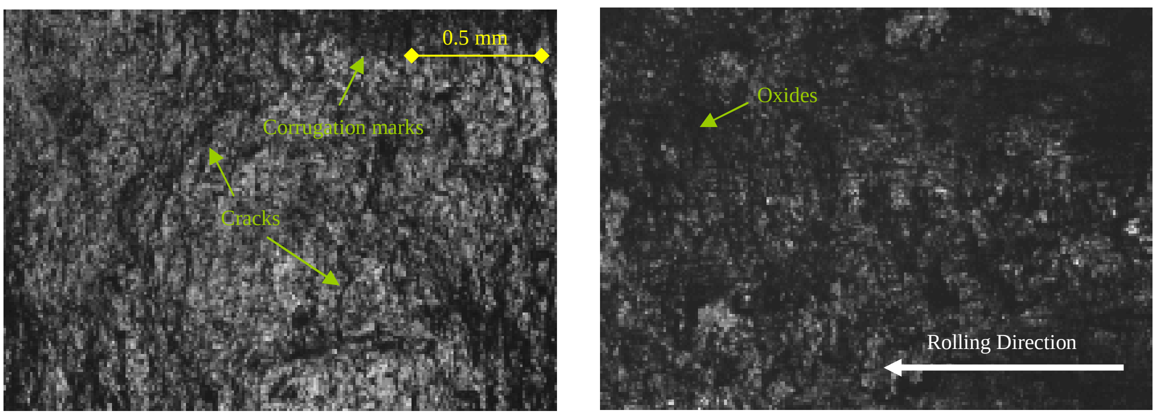

Fig. 2A.11. Micro-photographs of the rail (left) and wheel (right) disks surfaces after 12000 cycles in dry conditions with baseline.

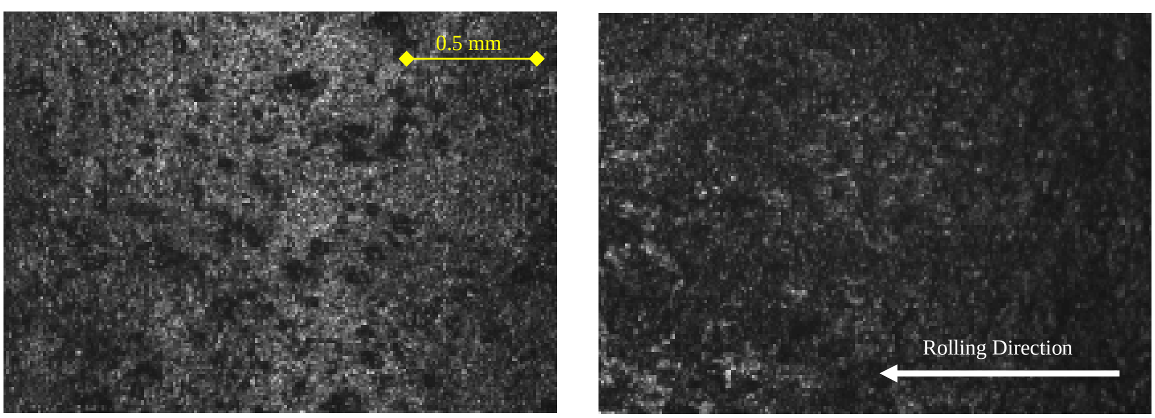

Fig. 2A.12. Micro-photographs of the rail (left) and wheel (right) disks surfaces after 12000 cycles in dry conditions with FMA.

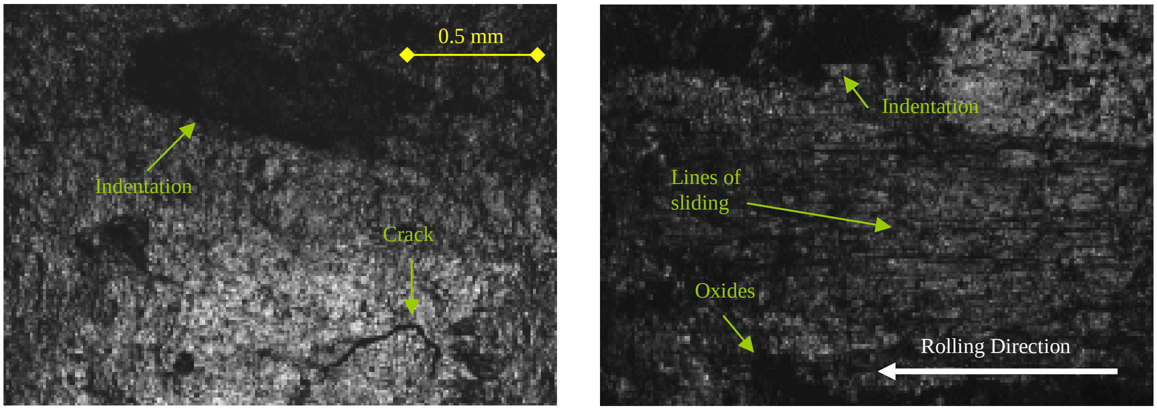

Fig. 2A.13. Micro-photographs of the rail (left) and wheel (right) disks surfaces after 12000 cycles in dry conditions with FMB.

The surface roughness was measured after the complete set of tests, as given in Table 2A.1. The large roughness measured in the wheel disk of the baseline tests is attributed to the presence of oxide layers of different thickness in relation to the bulk steel material. A similar effect, although in less degree, was observed in the FMB tests. The rail disk presented almost unaltered roughness values in the tests with FMA and FMB. However, there was an increase in roughness of the rail disk for the baseline test due to the corrugation marks.

Table 2A.1. Average surface roughness of wheel and rail disks after 12000 cycles in dry conditions.

	Initial	Baseline	Friction Modifier A	Friction Modifier B
Wheel disk	1±0.2 µm	7±3 µm	2.75±0.65 µm	4±1 µm
Rail disk	1±0.2 µm	2.7±1 µm	0.9±0.3 µm	1.1±0.3 µm

The subsurface of the three pairs of disks was examined under a microscope in cross and longitudinal sections, as shown in Figs. 2A.14-2A.15. The differences in the contrast of Figs. 2A.14-2A.15 are due to the different amounts of etching during metallographic preparation. The deepest subsurface deformation seemed to be observed for the baseline; whereas, FMA led to the shallowest subsurface plastic deformation (see Fig. 2A.14). The plastic deformation depth is in agreement with the adhesion results presented above, the higher the tangential load the deeper the plastic deformation. For all contact conditions, the rail presented deeper plastic deformation layer than the wheel, which could be attributed to the different microstructure of the two steels. Both steels were composed of ferrite and pearlite; however, more pearlite was observed in the rail steel. Furthermore, smaller pearlite grain size was observed in the wheel steel. Due to the high adhesion coefficient values in the tests, the maximum shear stress occurred at the surface, which caused a highly strained layer, as noticeable in Figs. 2A.14-2A.15.

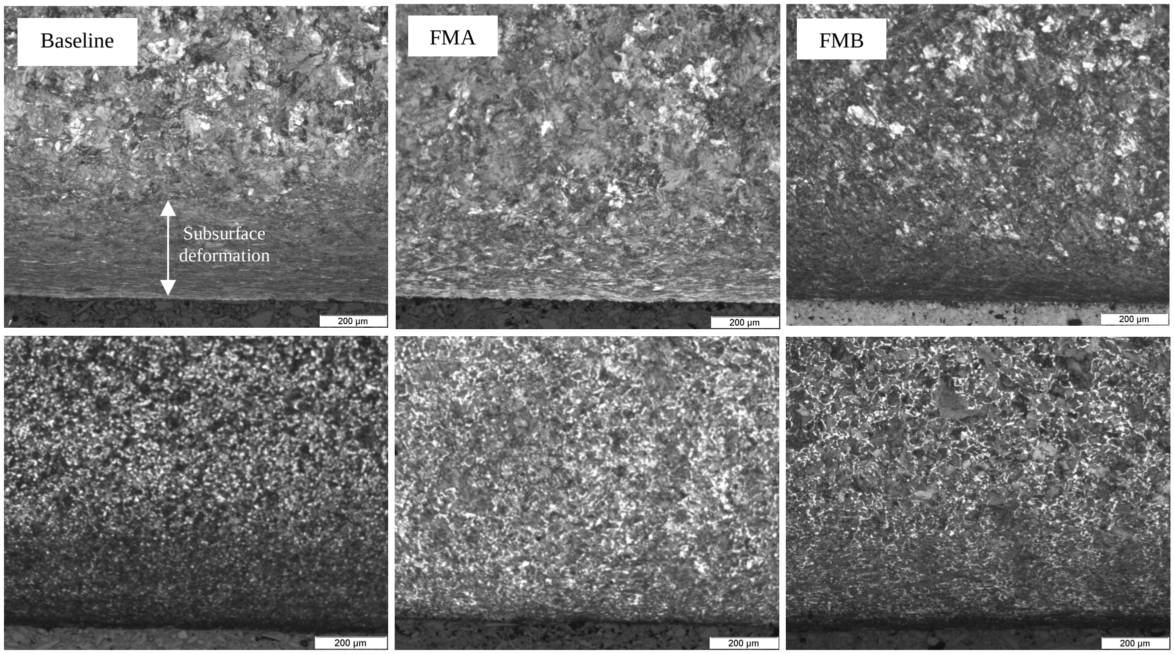

Fig. 2A.14. Sub-surface micro-photographs of the cross section of the rail (top) and wheel (bottom) disks after 12000 cycles in dry conditions with baseline, FMA, and FMB.

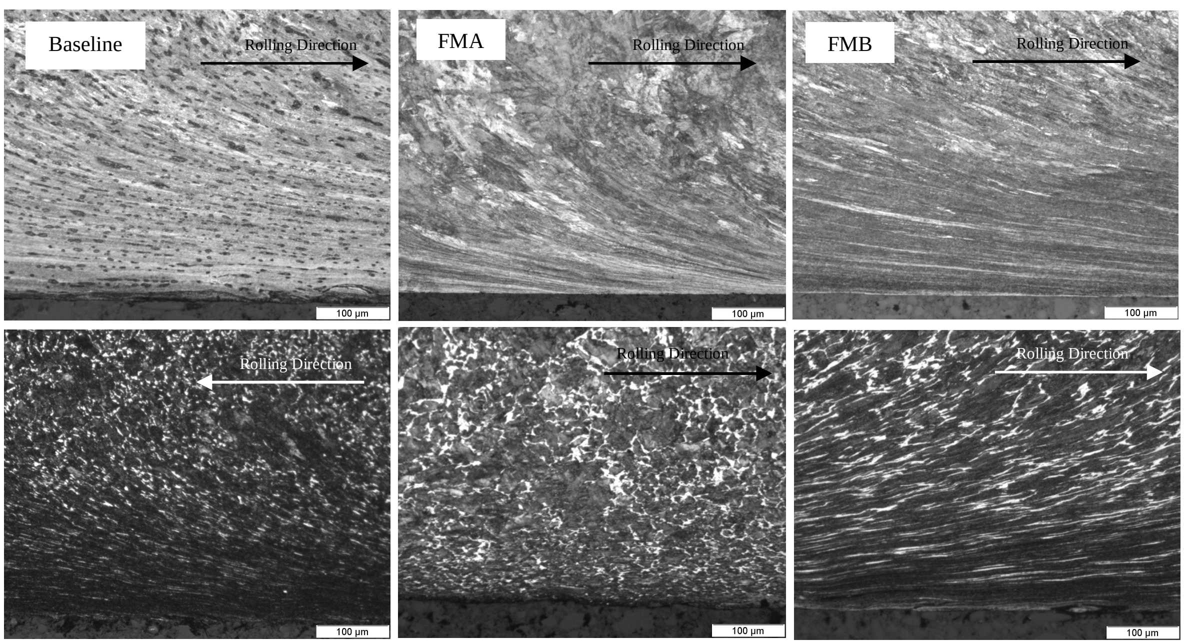

Fig. 2A.15. Sub-surface micro-photographs of the longitudinal section of the rail (top) and wheel (bottom) disks after 12000 cycles in dry conditions with baseline, FMA, FMB.

The hardness of the surface of the three pairs of disks was measured using Vickers macro-indentation technique with a 20 kg load (see results in Table 2A.2). The largest hardening effect was observed for both the baseline and the FMB. This can be explained by examination of the adhesion history during the tests (Figs. 2A.6-2A.9). The lower adhesion coefficients obtained with FMA led to the lowest work-hardening effect of the surface. Furthermore, the rail work hardened more than the wheel, which could be attributed to the different steel microstructure. In the tests with FMs, it may be possible that the firm adherence of the third body layer on the wheel disk (rather than on both disks) could also have influenced the different work-hardening between wheel and rail. Berthier et al. [2A.20] showed that a third body layer present between wheel and rail surfaces can accommodate their relative displacement (or slip) so that the shearing of the near-surface grains of wheel and rail surfaces is decreased, thus reducing the work-hardening effect. Since the third body layer appeared to be firmly adhered to the wheel disk in these tests, the extent of grain deformation in the near-surface of wheel disk could have been reduced compared to the rail because of a different shear stress distribution across the depth in the wheel and rail disks. However, further investigation would be required to validate this last hypothesis.

Table 2A.2. Average hardness of the surface of wheel and rail disks after 12000 cycles in dry conditions.

	Initial	Baseline	Friction Modifier A	Friction Modifier B
Wheel disk	267 HV_{20kg}	420 HV_{20kg}	290 HV_{20kg}	420 HV_{20kg}
Rail disk	281 HV_{20kg}	490 HV_{20kg}	390 HV_{20kg}	470 HV_{20kg}

The accumulated wear of the three pairs of disks was determined by means of mass loss measurements using electronic scales with ±0.05 mg accuracy (see Table 2A.3). Note that the wheel disks ran 150 cycles more than the rail disks due to the slip; however, it only represents ~1% of the total cycles so that the extra wear amount may be neglected. The largest accumulated wear corresponded to the wheel for all contact conditions, which is attributed to the softer wheel steel material. Similar findings have been reported in previous work [2A.12]. The baseline showed the largest wear rates, while the lowest were found when using FMA. This is found in good agreement with the adhesion results presented in Figs. 2A.6-2A.9.

Table 2A.3. Mass loss of the disks after 12000 cycles in dry conditions with baseline, FMA and FMB.

	Baseline		FMA		FMB	
	Wheel	Rail	Wheel	Rail	Wheel	Rail
m_{loss} (mg)	114.9	90.1	30.3	28.4	109.6	70.5

2A.3.2. Wet tests

In order to simulate the wet wheel-rail contact, water was applied to the rail disk once the disks were running, as previously depicted in Fig. 2A.5. In this way, rainfall conditions with pre-application of the FMs were simulated with these tests. Two different application methods of water were first tested (at 0.5% slip) to verify their suitability in reducing the adhesion in a uniform and consistent way. Water was applied by means of a pipette and a spray bottle. Furthermore, different amounts were also tested with both methods. It was concluded that the effect of water on adhesion could be controlled better with drops of water from the pipette than with the spray bottle. Mass measurements of water applied with the pipette showed good repeatability only for the first drop. Therefore, only one drop of water was used for the tests with a mass content of 0.04 g. One of the goals in the wet tests was to assess the recovery time, which is defined as the number of cycles necessary to recover to the dry adhesion level prior to water application (see Fig. 2A.16). Therefore, the recovery time determined the number of cycles in which the applied water exerted an influence on adhesion.

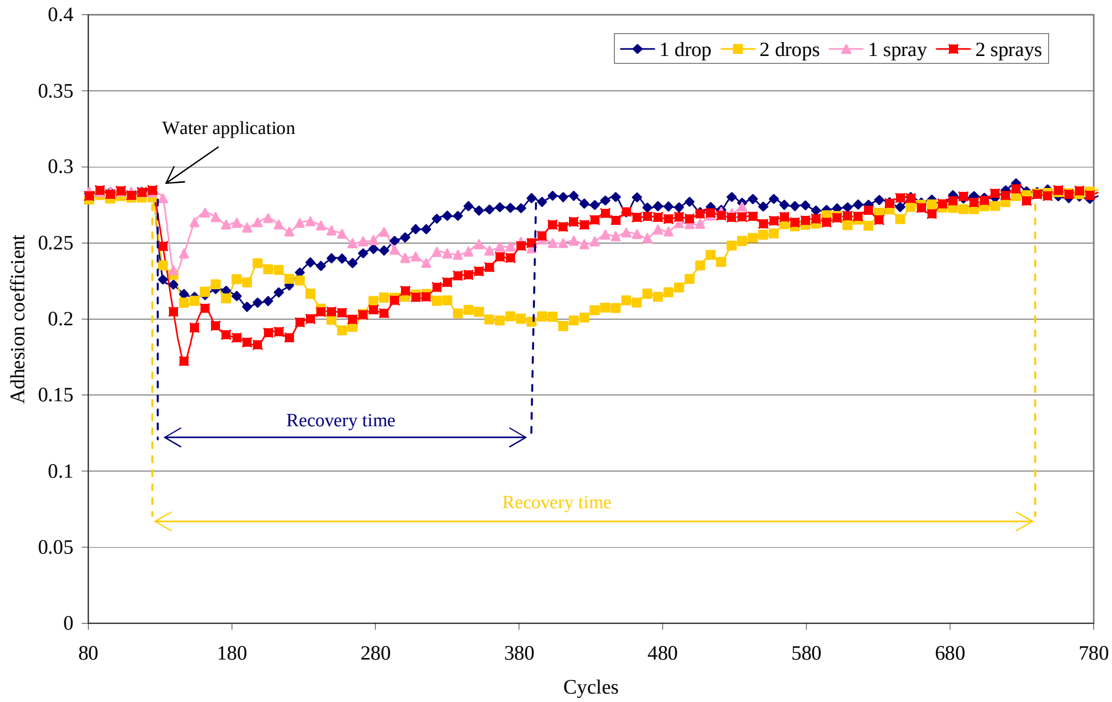

Fig. 2A.16. Water application method tests at 0.5% slip.

Figs. 2A.17-2A.19 show the adhesion results obtained for the tests with water. In these tests, a single drop of water was applied not before the initial 20-50 cycles to ensure that the set slip had been reached. Care was taken that the water was applied before the friction modifier was entirely removed from the disk surfaces, which was established by examination of the results previously obtained in dry conditions tests. In addition, in the tests with FMs the drop of water was applied at around the same number of cycles for each slip tested to enable the comparison between them. As soon as water was entrained in the contact, the adhesion coefficient decreased. In wet conditions, the adhesion decreased to 0.2 for the baseline, and similarly for FMB. The lowest value in adhesion coefficient was observed with FMA and water, close to 0.07. The drop was smaller for FMA compared to baseline and FMB. Furthermore, the water applied seemed to interact with FMA forming a layer that remained throughout the tests at 0.5 and 1% slip. The shearing of that layer yielded an adhesion coefficient of 0.18-0.19. At 2% slip the layer was removed and starvation was reached at the end of the test. Special attention has to be paid to the sudden drop in adhesion in the initial part of the adhesion curve for FMA at 2%, which was due to the break-up of the layer as pointed out previously for the dry tests. Furthermore, in the presence of water the lasting effect of FMB was shortened. The water seemed to help to remove FMB faster in comparison with the dry conditions.

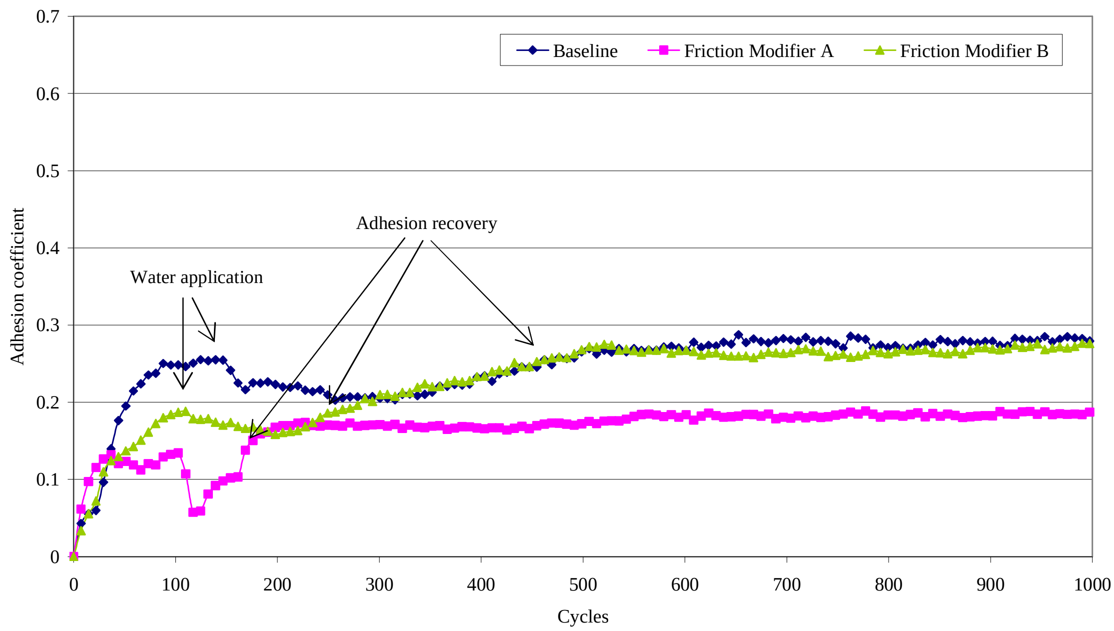

Fig. 2A.17. Adhesion tests with one drop of water at 0.5% slip.

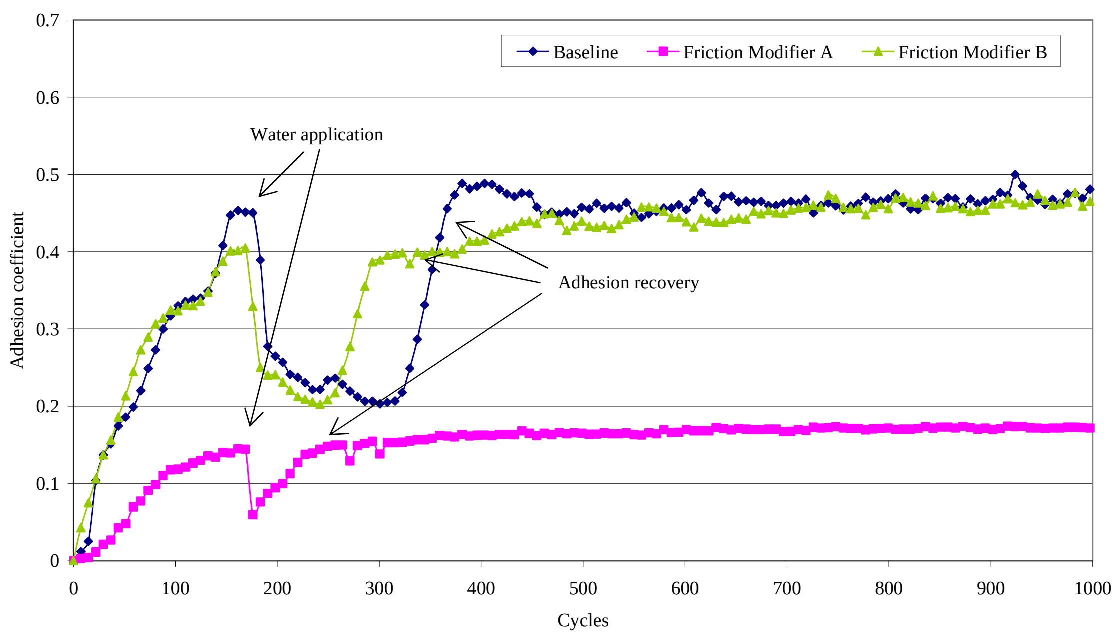

Fig. 2A.18. Adhesion tests with one drop of water at 1% slip.

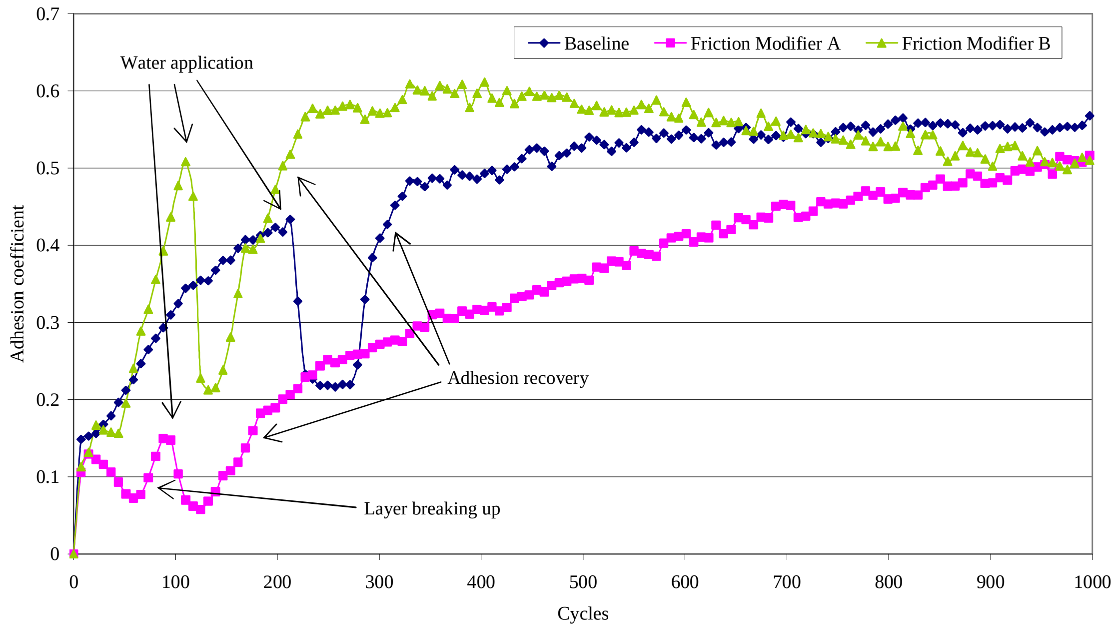

Fig. 2A.19. Adhesion tests with one drop of water at 2% slip.

The recovery time observed in the tests is given in Table 2A.4. FMA showed the shortest recovery times in comparison with FMB and baseline for all the slip ratios tested. The increase in slip led to shorter recovery times for the baseline, as it is expected due to the removal of the water by higher differential speeds. The recovery time for the FMs is influenced by the amount of product present on the disks surfaces once water is applied. It has already been pointed out that the increase in slip leads to a faster removal of the FMs from the disk surfaces. If an insufficient amount of FM is available, the recovery time will be similar to that of the baseline. This was observed for FMB at 1 and 2% slips. On the other hand, the slip seemed to have negligible influence on the recovery time of FMA, which could be attributed to its long lasting effect.

Table 2A.4. Recovery time (cycles) with a drop of water for baseline, FMA and FMB at 0.5, 1 and 2% slip.

	0.5% slip	1% slip	2% slip
Baseline	316 cycles	190 cycles	103 cycles
Friction Modifier A	66 cycles	73 cycles	80 cycles
Friction Modifier B	147 cycles	183 cycles	103 cycles

2A.4. Discussion

In dry conditions the highest adhesion levels are obtained with the baseline, which are 0.30-0.60 for the slip ratios considered. FMA shows moderate adhesion with values between 0.15 and 0.35 before starvation conditions are reached. FMB leads to adhesion values of 0.25-0.55. If water is applied to the disks contact, the adhesion coefficient drops between 30 and 65% depending on the slip and the FM used. The largest drop in adhesion is seen with both FMB and baseline. The lowest adhesion values are observed with FMA, which are around 0.07 in the presence of water. On the other hand, baseline and FMB have an adhesion coefficient around 0.2 in the same conditions. Furthermore, the water applied seems to interact with FMA forming a layer that was not removed during the tests at 0.5 and 1% slip. The shearing of that layer yielded an adhesion coefficient of 0.18-0.19. The adhesion requirements differ for traction and braking operations, and they also depend on the type of vehicle under consideration. An adequate braking performance demands an adhesion up to 0.09, whereas in traction this can be up to 0.20 [2A.13]. Based on this, the low level of adhesion found with FMA in the presence of water may primarily lead to traction problems. On the other hand, the moderate adhesion level reached with FMA in dry contacts would be advantageous for reducing wear and the occurrence of rolling contact fatigue defects (e.g., squats [2A.21]) in rails subject to high tangential forces, like track sections where traction or braking is frequent and curves of small radius. However, it has to be acknowledged that the adhesion coefficients obtained in this testing may not be completely in agreement with the actual wheel-rail adhesion, because of the differences between actual and laboratory testing conditions as already pointed out in [2A.22]. Therefore, the results presented in this work can only be taken as qualitative representations of the actual wheel-rail situation to be used for comparisons between the products tested and the baseline.

In the presence of water the recovery time is one of the most important factors to consider, as it will determine the number of cycles in which the applied water exerts an influence on adhesion. The tests show that FMA has the shortest recovery times compared with FMB and baseline for the whole slip range studied. The increase in slip leads to shorter recovery times for the baseline, as it is expected due to the removal of the water by higher differential speeds. This removal effect also contributes to a faster removal of the FMs from the disk surfaces; therefore, the recovery time will approach the baseline if insufficient FM is available on the disk surfaces. This tendency was observed for FMB at 1 and 2% slips. On the other hand, the slip seemed to have negligible influence on the recovery time of FMA, which could be attributed to its long lasting effect.

The lasting effect of the FMs is a crucial parameter to take into account during the development stage of a FM because it has an economical impact on the costs of the railway network operators. The lasting effect of the FM will determine the frequency in which the FM has to be applied. In this study, it is shown that FMA has the longest lasting effect, which could be attributed to the strong matrix that is formed between the solid particles and the polymeric components. The adherence on the disk surfaces seems to be enhanced by the polymeric components. On the contrary, it seems that the solid particles in FMB tend to be removed from the disk surfaces once they are crushed due to the weak bond between particles and gelling agent. Furthermore, the lasting effect of FMB is reduced to a large extent in the presence of water.

The side effects in terms of damage to wheels and rails are a major concern when using FMs on a railway network. Rolling stock operators and infrastructure managers demand the damage to be as low as possible. In this work, it can be observed that the large particle size and hardness of the solid particles contained in FMB led to indentations on the disk surfaces. The hard large solid particles of FMB are necessary to be able to cut through the leaf layers that are formed in autumn on railheads, which is a design purpose of this FM. On the contrary, no indentations are observed with FMA. In order to reduce surface damage, the toughness, hardness and size of the solid particles of the FM should be optimized. Indentations were also observed when simple sanding was used to increase adhesion [2A.12]. It was reported that sand particles embedded the softer wheel disk and scored the harder rail disk, due to the large difference in hardness between the steel materials. In our work, however, indentations are present in both wheel and rail disks, which can be attributed to the small difference in hardness of the wheel and rail steels.

Furthermore, the moderate adhesion coefficients obtained with FMA in dry conditions led to less plastic deformation on the disks compared to the baseline and FMB. The wear rates were also reduced by a factor of 3 in the tests with FMA compared to baseline and FMB. These facts would make FMA more beneficial from the railway maintenance point of view if the FMs are applied on sections where the rails experience high tangential forces as indicated above. Nevertheless, in these laboratory tests the disks have been scaled down, whereas the FMs have been used in real size; therefore, the results in wear and damage presented in this paper can only be taken as a reference of what happens in the actual wheel-rail contact, as already indicated in [2A.12].

2A.5. Conclusions

A twin-disk roller rig is used to simulate the wheel-rail contact in controlled laboratory conditions so as to study the performance of two water-based friction modifiers (FMs) in dry and wet contacts. These two FMs have been used or tested in several railway networks as adhesion enhancers. In this work, tests with the FMs and the baseline are carried out in dry and wet conditions at different slip ratios. Surface and subsurface examination of the disks is undertaken in order to assess the damage caused when using the FMs. The following conclusions are drawn:

a) In dry conditions the highest adhesion coefficients are obtained with the baseline. FMA seems to form a durable third body layer that yields moderate adhesion coefficients in dry conditions, which could be beneficial from the point of view of railway maintenance.
b) In the presence of water the adhesion coefficient is reduced to 0.2 for baseline and FMB, whereas 0.07 is reached for FMA. The latter may primarily lead to traction problems for the majority of the rail vehicles.
c) FMA leads to a faster recovery time than both baseline and FMB for all the slip ratios considered. The increase in slip leads to shorter recovery time for the baseline, whereas it shows negligible influence on FMA. For FMB, the increase in slip leads to recovery times closer to the baseline due to the removal of FMB from the disk surfaces. Therefore, the use of adequate additives could enhance the adhesion recovery in wet contacts.
d) FMA has longer lasting effect than FMB, which is attributed to its stronger matrix of solid particles and polymeric components. In the presence of water, the lasting effect of FMB is clearly reduced. Considering its impact on the costs of the railway network operator, improvements in the lasting effect of the FM are of importance.

e) The lowest wear is obtained with FMA, while FMB shows similar wear rates with the baseline. The amount of plastic deformation follows the same pattern of the wear, as determined by the adhesion history.
f) Severe surface damage is observed when using FMB due to its large hard solid particles, which cause indentations and scratches on both disks. No indentations are observed with FMA. In order to reduce surface damage, the toughness, hardness and size of the solid particles of the FM should be optimized.

References

[2A.1] T.M. Beagley, C. Pritchard, Wheel/Rail Adhesion — The Overriding Influence of Water, Wear 35 (1975) 299-313.

[2A.2] T.M. Beagley, I.J. McEwen, C. Pritchard, Wheel/Rail Adhesion — The Influence of Railhead Debris, Wear 33 (1975) 141-152.

[2A.3] T.M. Beagley, I.J. McEwen, C. Pritchard, Wheel/Rail Adhesion—Boundary Lubrication by Oily Fluids, Wear 31 (1975) 77-88.

[2A.4] E.A. Gallardo-Hernandez, R. Lewis, Twin Disc Assessment of Wheel/Rail Adhesion, Wear 265 (2008) 1309-1316.

[2A.5] H. Chen, T. Ban, M. Ishida, T. Nakahara, Experimental Investigation on Influential Factors on Adhesion between Wheel and Rail under Wet Conditions, Wear 265 (2008) 1504-1511.

[2A.6] L. Deters, M. Proksch, Friction and Wear Testing of Rail and Wheel Material, Wear 258 (2005) 981-991.

[2A.7] W. Zhang, J. Chen, X. Wu, X. Jin, Wheel/Rail Adhesion and Analysis by Using Full Scale Roller Rig, Wear 253 (2002) 82-88.

[2A.8] D.T. Eadie, J. Kalousek, K.C. Chiddick, The Role of High Positive Friction (HPF) Modifier in the Control of Short Pitch Corrugations and Related Phenomena, Wear 253 (2002) 185-192.

[2A.9] D.T. Eadie, M. Santoro, J. Kalousek, Railway Noise and the Effect of Top of Rail Liquid Friction Modifiers: Changes in Sound and Vibration Spectral Distributions in Curves, Wear 258 (2005) 1148-1155.

[2A.10] D.T. Eadie, D. Elvidge, K. Oldknow, R. Stock, P. Pointner, J. Kalousek, P. Klauser, The Effects of Top of Rail Friction Modifier on Wear and Rolling Contact Fatigue: Full Scale Rail-Wheel Test Rig Evaluation, Analysis, and Modelling, Wear 265 (2008) 1222-1230.

[2A.11] U. Olofsson, R. Lewis, Tribology of the Wheel-Rail Contact, in: S. Iwnicki (Ed.), Handbook of railway vehicle dynamics, Taylor & Francis Group, Boca Raton, pp, 121-141, 2006.

[2A.12] R. Lewis, R.S. Dwyer-Joyce, Wear at the Wheel-Rail Interface when Sanding is Used to Increase Adhesion, Journal of Rail and Rapid Transit 220 (2006) 29-41.

[2A.13] C.R. Fulford, Review of low adhesion research, Report published by the Rail Safety and Standards Board, UK, 2004.

[2A.14] O. Arias-Cuevas, Z. Li, R. Lewis, E.A. Gallardo-Hernandez, Rolling-Sliding Laboratory Tests of Friction Modifiers in Leaf Contaminated Wheel-Rail Contacts, 2008 International Joint Tribology Conference, Miami, Florida, USA, October 20-22, 2008.

[2A.15] D.I. Fletcher, J.H. Beynon, Development of a Machine for Closely Controlled Rolling Contact Fatigue and Wear Testing, Journal of Testing and Evaluation, 28 (2000) 267-275.
[2A.16] E.A. Gallardo-Hernandez, R. Lewis, R.S. Dwyer-Joyce, Temperature in a Twin-disk Wheel/rail Contact Simulation, Tribology International 39 (2006) 1653-1663.
[2A.17] P.H. Dawson, M.B. Coyle, Metal Transfer During Rolling with Sliding—A Challenge, Wear 12 (1969) 385-386.
[2A.18] X. Lu, K.C. Wong, P.C. Wong, K.A.R. Mitchell, J. Cotter, D.T. Eadie, Surface Characterization of Polytetrafluoroethylene (PTFE) Transfer Films During Rolling-Sliding Tribology Tests Using X-ray Photoelectron Spectroscopy, Wear 261 (2006) 1155-1162.
[2A.19] W.R. Tyfour, J.H. Beynon, A. Kapoor, The Steady State Wear Behaviour of Pearlitic Rail Steel under Dry Rolling-sliding Contact Conditions, Wear 180 (1995) 79-89.
[2A.20] Y. Berthier, S. Descartes, M. Busquet, E. Niccolini, C. Desrayaud, L. Baillet, M.C. Baietto-Dubourg, The Role and Effects of the Third Body in the Wheel-Rail Interaction, Fatigue & Fracture of Engineering Materials & Structures 27 (2004) 423-436.
[2A.21] Z. Li, X. Zhao, C. Esveld, R. Dollevoet, M. Molodova, An Investigation into the Causes of Squats—Correlation Analysis and Numerical Modeling, Wear 265 (2008) 1349-1355.
[2A.22] H. Harrison, T. McCanney, J. Cotter, Recent Developments in Coefficient of Friction Measurements at the Wheel-Rail Interface, Wear 253 (2002) 114–123.

.

Chapter 2, Part B

Laboratory tests in leaf contaminated contacts[VI]

ABSTRACT

Leaf-related adhesion problems have been present in many railway networks all over the world in the last few decades. Since the early 1970's many measures have been undertaken in order to mitigate the problem. One of the measures adopted by many railway networks is the use of friction modifiers. However, the low adhesion problem still persists. Furthermore, the effectiveness of these friction modifiers has not well proven yet due to the lack of research in controlled conditions. Consequently, the rolling stock operators and infrastructure managers do not clearly understand the performance and side effects of the friction modifiers used on their networks. In this paper, an investigation of the performance of two existent friction modifiers in controlled laboratory conditions is presented. These friction modifiers have been used or tested in several railway networks. A twin-disk roller rig has been used to study their performance in leaf contaminated contacts. The adhesion characteristics of both friction modifiers are examined for different slip ratios. The constituents of the friction modifiers are identified and the solid components are analyzed. In addition, damage that these friction modifiers may cause to wheel and rail is also discussed.

[VI] This chapter has been published as: Z. Li, O. Arias-Cuevas, R. Lewis, E.A. Gallardo-Hernandez: Rolling-sliding Laboratory Tests of Friction Modifiers in Leaf Contaminated Wheel-Rail Contacts. Tribology Letters 33 (2009) 97–109.

2B.1. Introduction

The friction available between wheel and rail during braking and traction operation is known in the railway terminology as adhesion. It is a crucial factor for the railway industry as a minimum level of adhesion is required for an appropriate braking and traction performance of the rail vehicles. Adhesion is influenced by many factors such as vehicle speed, wheel slip, contact pressure, environmental conditions and natural contaminants. The major cause of decreasing adhesion is the natural contamination; water, rust, oil, and leaves, have been identified as being mainly responsible [2B.1-2B.5]. The combination of leaves and a small amount of water has been reported to bring the lowest adhesion levels, as it occurs during the autumn season [2B.6]. The leaves are normally swept up onto the rails by wind or the train's slipstream, where they are crushed under the high wheel-rail contact pressure. Consequently, a Teflon-like leaf layer is formed, which has black colouration and is hard to remove. This layer is known to have low shear strength and high electrical resistance, which may bring about two negative consequences: low adhesion and electrical isolation [2B.6]. When low adhesion occurs, delays in the train service are the clearest consequence to the railway commuters. However, many other negative effects can arise, such as damages to wheels and rails, signals passed at danger, station platform overruns and, even, collisions. Flat wheels and rail burns caused by low adhesion may also lead to rolling contact fatigue defects such as squats [2B.7]. Therefore, not only the punctuality, but also the safety of the passengers can be threatened if low adhesion situations are encountered. Moreover, the annual costs of low adhesion to the railway industry were reported to be £50 million in United Kingdom [2B.6] and 100 million SEK in Sweden [2B.8]. In the Netherlands, extreme low adhesion conditions on a day in the autumn of 2002 caused wheel defects to increase up to 20% percent of the railway fleet, forcing the train operator to stop the services on most of the sections of the network during that day [2B.9].

Several studies on wheel-rail adhesion in leafy contacts have already been conducted in both laboratory and field tests. A report on low adhesion published by the Rail Safety and Standards Board (RSSB) gives a good overview of the research and findings on leaf related adhesion problems in the last decades [2B.5]. Recently, a study into the characteristics of the leaf layer contamination was carried out by AEA Technology Rail (DeltaRail Group) in UK [2B.10]. They used a full scale wheel-on-rail test rig to produce leaf layer samples, whose mechanical and chemical properties were examined. The shear strength of the leaf layer was found to be inversely proportional to the moisture level; the thickness of the generated layer ranged from 10 to 100 μm, which implies that the metal surface asperities of wheel and rail will not touch each other in the presence of a leaf layer. The samples were analyzed using Fourier Transform Infra-Red (FTIR) spectroscopy; lignin, cellulose and pectin were found as the major constituents contributing to the adherence of leaf to the rail. Validation of the laboratory test results was undertaken by comparison with those of samples taken from the British railway network. Laboratory tests to investigate the friction behaviour in leaf contaminated contacts have also been carried out with pin-on-disk [2B.8], ball-on-disk [2B.11], and twin-disk [2B.12] tribometers. Olofsson and Sundvall [2B.8] showed in their pioneering laboratory work the influence of leaf contamination and humidity on sliding friction. In the presence of leaf contamination, the friction was significantly decreased compared to dry contacts; furthermore, the increase in relative humidity led to a decrease in sliding friction. Cann [2B.11] investigated the friction properties of the leaf layers under different rolling speeds and slip ratios. In her work, she also analyzed the post-test contamination leaf layer using FTIR micro-spectroscopy; pectin and cellulose were found in the samples. She suggests that the water-soluble pectin reacts chemically with the metal to form iron pectate, which causes the black colouration of the leaf layers that has been extensively reported. Gallardo-Hernandez and Lewis [2B.12] obtained the traction curves (up to 5% slip) in dry and wet leafy contacts. The dry leaf layers gave the lowest adhesion values and the micro-hardness measurements showed that dry leaf layers were harder than wet ones. They also carried out tests with sand and leaves, in which an increase in adhesion using sand was observed. Besides, Lewis and Dwyer-Joyce published a study on the wear caused by sanding [2B.13].

In order to fight low adhesion, some practical measures have already been applied in the abovementioned countries, such as vegetation management, rail cleaning methods and friction modifiers (FMs) [2B.5, 2B.6, 2B.14]. Simple sanding from the train or locomotive is used on railway networks world wide to overcome adhesion problems [2B.15]. In countries such as The United Kingdom and The Netherlands, other FMs have been used and tested in field during the last years [2B.5, 2B.14]. However, the low adhesion problem still persists. Furthermore, the effectiveness of these FMs has not been well proven yet due to the lack of research in controlled conditions. Consequently, the rolling stock operators and infrastructure managers do not clearly understand the performance and side effects of the FMs used on their networks. In this paper, a laboratory study of a widely used FM is presented together with another FM designed for wet wheel-rail contacts due to rainfall.

The aim of this work was to examine the performance of two FMs in leaf contaminated contacts. A study of these FMs in dry and wet contacts has already been carried out [2B.16]. Both FMs are water-based and have been designed to increase the adhesion in their respective target contamination conditions. One of the FMs—referred as FMB in this paper— has extensively been used in the autumn season on the Dutch and British railways networks to overcome adhesion problems, especially due to leaves and small amounts of water. In The Netherlands, FMB is primarily applied train-borne to top of both rails by means of a speed dependent pumping system, which delivers 4 cc/m per rail. The other FM—referred as FMA hereinafter— has been tested in a train depot in Japan to increase adhesion in the presence of water, and it was considered to be a potential adhesion enhancer for leafy contacts, although improvement may be needed. FMA is to be applied to the top of both rails in a very thin layer. In this work, a twin-disk roller rig has been used to simulate the wheel-rail contact in controlled laboratory conditions. The adhesion characteristics of the two FMs have been studied in leaf contaminated contacts for three different slip ratios: 0.5, 1, and 2%. The leaf layers obtained during testing have been analyzed by means of FTIR micro-spectroscopy in order to assess the leaf layer removal. The constituents of the FMs have been examined and their influence on adhesion improvement and disks damage has been discussed.

2B.2. Test set-up

2B.2.1. Test roller rig

The rolling-sliding tests were conducted on the SUROS (Sheffield University ROlling Sliding) roller rig, shown in Fig. 2B.1. A detailed description of the roller rig is given in [2B.17]. The test disks were mounted on independent shafts. By means of a hydraulic jack, a controlled contact pressure was achieved during the test. The slip ratio between the disks was prescribed by setting different rotational speed of the shafts and maintained constant throughout each test with a controller. The slip ratio is defined in Eq. 2B.1, where w and r are the rotational speed and rolling radius of the disks, respectively. The adhesion coefficient was calculated with the readings of the torque transducer and the load cell, as given in Eq. 2B.2 by T and F_N, respectively. A personal computer was used to acquire the data and to control both the speed and the load.

$$Slip = \frac{w_{wheel} \cdot r_{wheel} - w_{rail} \cdot r_{rail}}{w_{wheel} \cdot r_{wheel} + w_{rail} \cdot r_{rail}} \cdot 200\% \tag{2B.1}$$

$$\mu_{adhesion} = \frac{T}{F_N \cdot r_{rail}} \tag{2B.2}$$

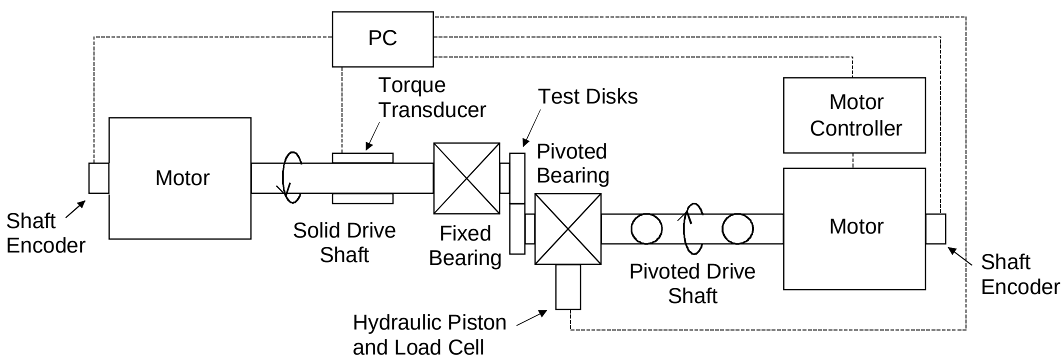

Fig. 2B.1. Schematic representation of the SUROS roller rig.

2B.2.2. Test disks

The test disks were cut from rails and wheel tires retired from service in the Dutch railway network; R260Mn and B5T steel for the rail and wheel, respectively. The disks were machined with their axes perpendicular to the longitudinal axis of both wheel and rail (see Fig. 2B.2). The Vickers macro-hardness of the wheel and the rail steel used in the tests was measured as 267 HV_{20kg} and 281 HV_{20kg} on average, respectively. Prior to testing, the disks were cleaned in a bath of Ethanol by means of ultrasonic vibration. The roughness of the new disks was measured as 1±0.2 µm on average with a profilometer. Before assembling the disks into the roller rig, their diameter was measured with a vernier calliper as necessary for the calculations of slip and adhesion coefficient.

2B.2.3. Tested products

The two water-based FMs tested in this work are applied to the top of the rail in order to increase the wheel-rail adhesion. Microscope photographs of the dried samples are given in Fig. 2B.3. Friction Modifier A (FMA) contains several types of solid components, which have different physical and tribological characteristics that provide the final product with varied functionalities such as friction enhancement and film transfer between wheel and rail. Furthermore, there are several polymeric components in FMA, all of which assist in promoting adherence to the wheel and rail steel surfaces. In Fig. 2B.3, it can be seen that the particles agglomerate after drying in an oven.

Friction Modifier B (FMB) is a mixture of an inorganic gelling agent, stabilizer, water, sand grains and stainless steel particles. The gelling agent promotes the adherence of the mix to the wheel and rail surfaces, while the stabilizer provides a reasonable storage life. The stainless steel particles guarantee adequate electrical conductivity of the mix, which is necessary for train detection. As FMB is applied from train mounted actuators directly into the wheel/rail contact, the lack of electrically conductive particles could lead to track circuit failure along the network. It can be seen from Fig. 2B.3 that the sand grains vary in size and type, as most probably come from different types of rocks. The black coloured particles correspond to the stainless steel, as pointed in Fig. 2B.3.

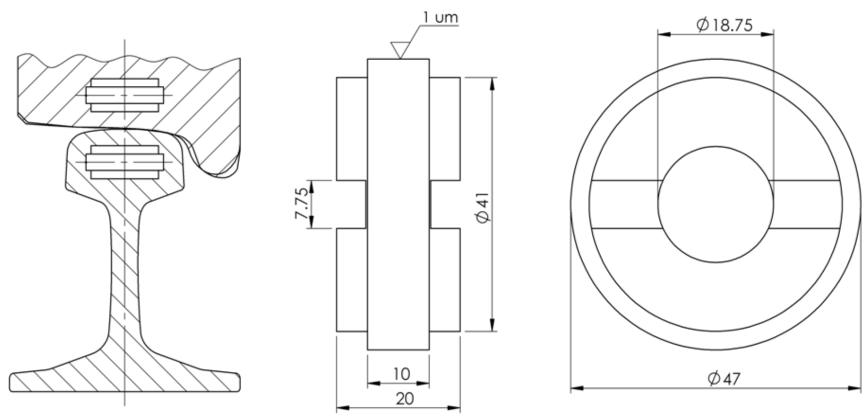

Fig. 2B.2. Orientation and dimensions of the wheel and rail disks specimens.

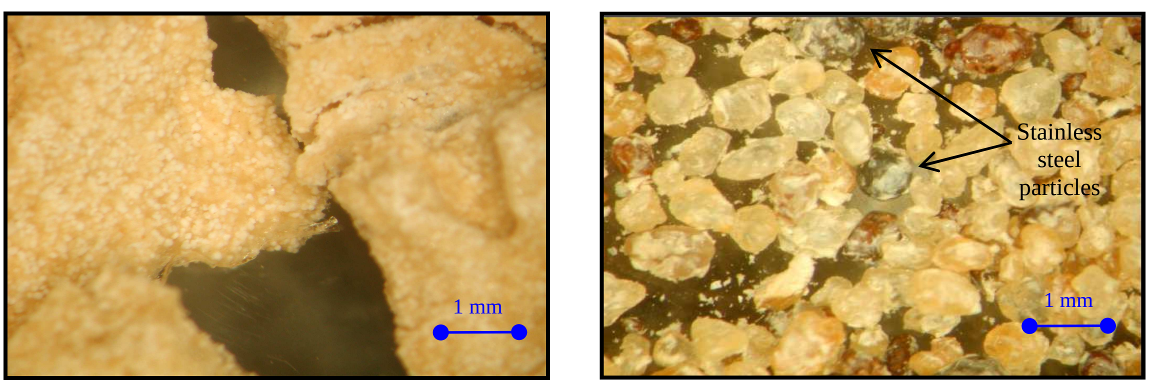

Fig. 2B.3. Microscope photographs of FMA (left) and FMB (right).

The leaves used in the experiments were from the sycamore tree. This type of tree is present along the Dutch railroads. The fallen leaves were collected in autumn 2006 in Utrecht, the Netherlands (see Fig. 2B.4). Once they were picked up, they were rinsed in water and frozen at -80 ºC to preserve there properties for the subsequent testing. Leaves were still partially green, but the petiole was dead. In comparison with fully dead leaves, they should contain more soluble organic compounds.

2B.2.4. Test procedure

In the tests the wheel disk rotated faster than the rail disk; the rotational speed of the rail was maintained at 400 rpm, equivalent to 1 m/s of rolling speed. Since cylindrical disks were used in the experiments, a line contact of 10 mm width was present. A load of 4.7 kN was applied on the disks producing a maximum Hertzian pressure of 1.2 GPa in the contact zone, which is representative of that between wheel tread and railhead for passenger trains in The Netherlands. Prior to application, the leaves were defrosted and cut into pieces smaller than the disk contact width to ease their entrapment into the disks interface. The small pieces of leaf were dried out before application. They were manually fed through a chute to the disks interface and being drawn through by a suction system located on the other side of the disks, as depicted in Fig. 2B.4. Initial trials demonstrated that 25 g of dry leaves were enough to create a relatively hard, durable leaf layer on the disks surface; subsequently, this amount was used for each test.

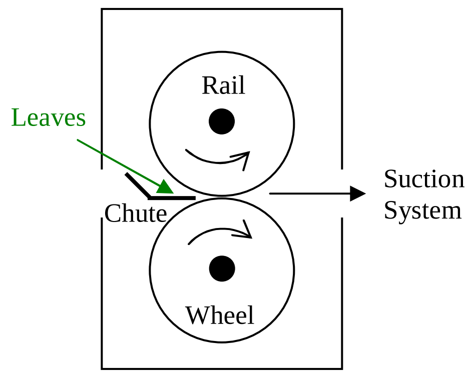

Fig. 2B.4. Dutch sycamore leaves used in the tests (left) and experimental set-up (right).

Fig. 2B.5 depicts a typical complete test with all the stages. At the beginning of each test, the disks were run for 4000 cycles at 0.5% slip to condition the surfaces before the leaves were fed in; then 300-400 cycles were required to apply the necessary amount of leaves. Thus, the leaf layer generation simulated what happens in the real situation, in which repeated wheel passages compact and shear leaves on the top of the rail. Next, the test was stopped to apply the FM and/or to change the slip. The FM was painted onto the rail surface with a brush; care was taken that no leaf layer was removed in this procedure. In Fig. 2B.6, pictures of the disks with leaf layer on their surfaces can be seen as well as the FMs when these were applied. Finally, the test was run for 3000 cycles to examine the removal of the leaf layer in different contact conditions. For each test conducted with the FMs, a baseline (i.e., no FM applied) was first obtained so as to compare the performance of FMs with the untreated situation. The tests were carried out at 0.5, 1, and 2% slip, which represent typical values that can be found in the contact between wheel tread and top of the rail. Furthermore, a thermometer and a hygrometer were next to the twin-disk rig. The ambient temperature recorded ranged from 24 to 28 °C and the relative humidity between 30 and 45%.

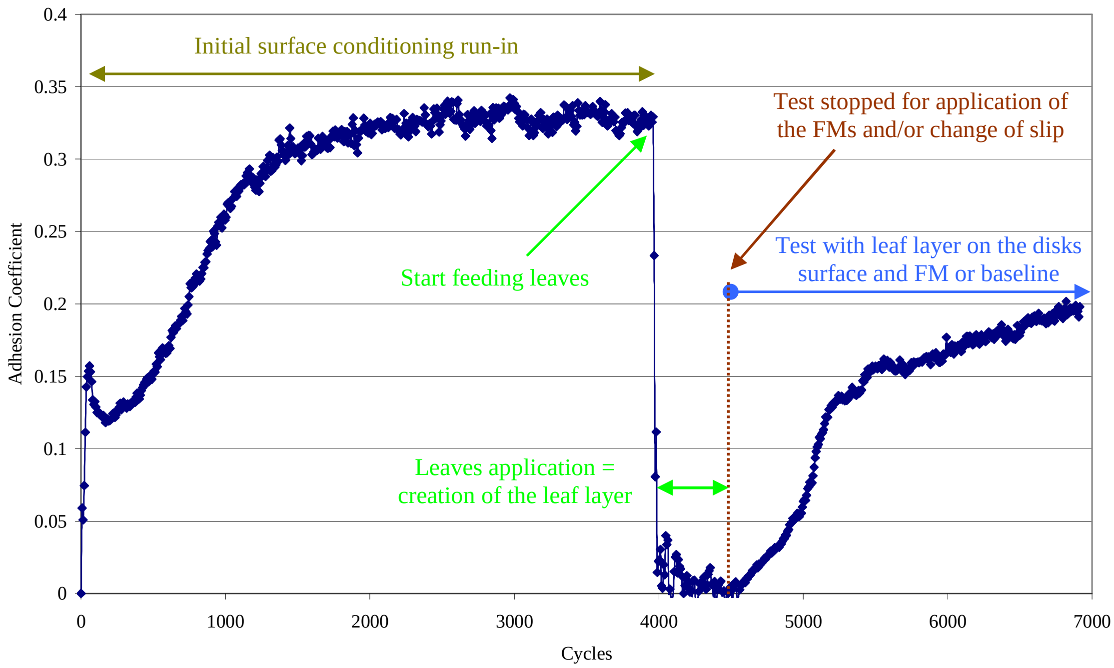

Fig. 2B.5. Typical complete adhesion test with run-in, leaf layer formation, and test with leaf layer on disks surface.

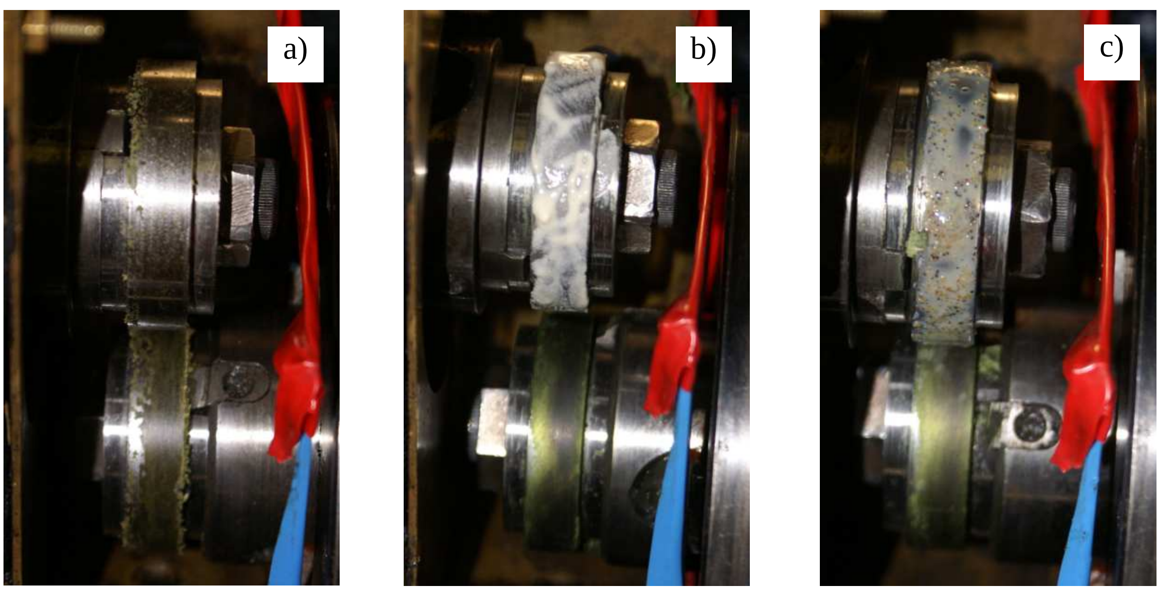

Fig. 2B.6. Disks surfaces after leaf layer has been created and ready to test with: a) baseline; b) FMA; c) FMB.

2B.3. Results

2B.3.1. Adhesion tests

The adhesion performance of the two FMs and the baseline for a leaf contaminated contacts was investigated. During the feed of leaves, the adhesion coefficients registered were 0.01-0.04 for 0.5% slip, which is in agreement with previous work on the same roller rig [2B.12]. Note that on this roller rig an adhesion coefficient of 0.30 is typical of dry uncontaminated contacts for 0.5% slip [2B.12, 2B.16]. Once the feed of leaves was stopped and the test started again with the selected slip ratio, the leaf layer was gradually broken and removed from the disks surface with the increasing number of cycles; eventually metal-to-metal contact was reached either partially or completely.

The tests were run at 0.5, 1, and 2% slip, as shown in Figs. 2B.7-2B.9; a baseline data for a dry uncontaminated contact is also included (named baseline-dry) for the sake of comparison. In all the tests, FMB showed the best performance in breaking up the layer and, therefore, bringing the adhesion to that of uncontaminated dry contacts. On the contrary, tests with baseline and FMA did not reach the adhesion levels of the baseline-dry contact after 3000 cycles for the slip ratios considered (see Figs. 2B.7-2B.9). Moreover, the influence of the leaf layer did not disappear at 0.5% slip for any of the three cases after 3000 cycles, indicating that higher slip or more cycles are necessary to deplete the leaf layer completely. However, much steeper initial slope was observed in the adhesion curves with both FMs at 0.5% slip, which led to faster recovery in adhesion compared to the baseline.

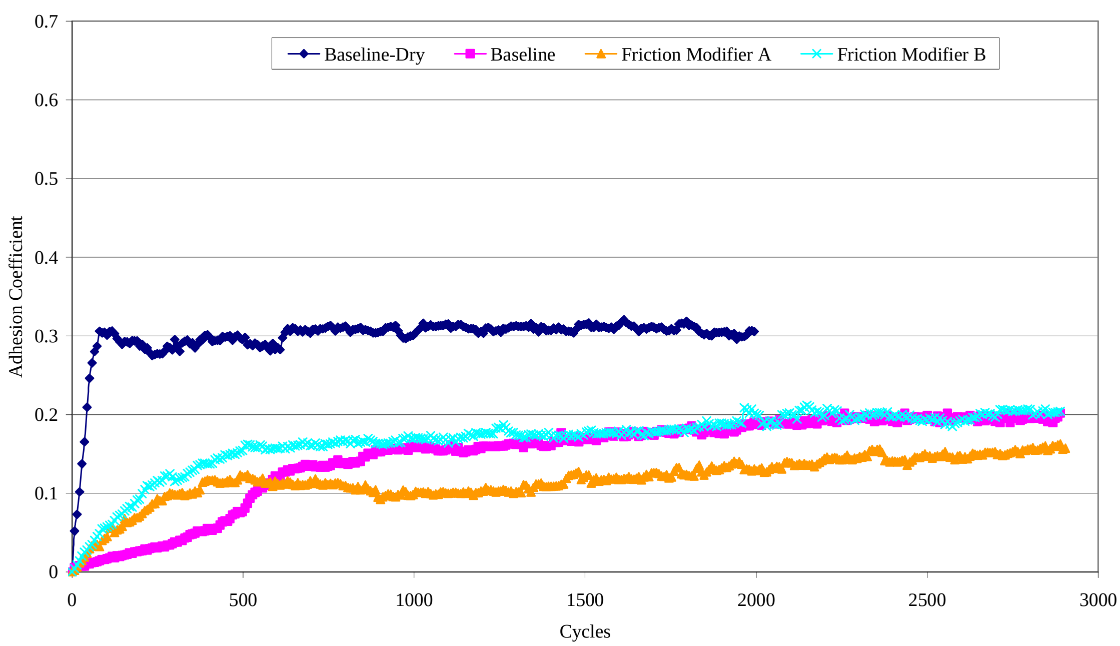

Fig. 2B.7. Leaf contaminated tests at 0.5% slip (and reference baseline-dry without contamination).

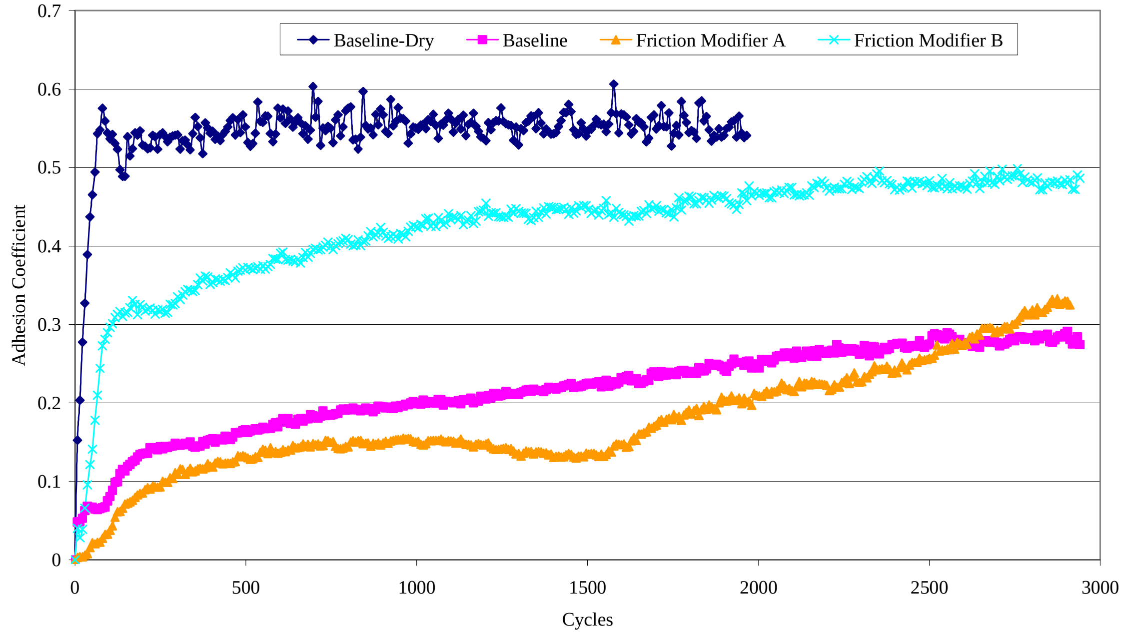

Fig. 2B.8. Leaf contaminated tests at 1% slip (and reference baseline-dry without contamination).

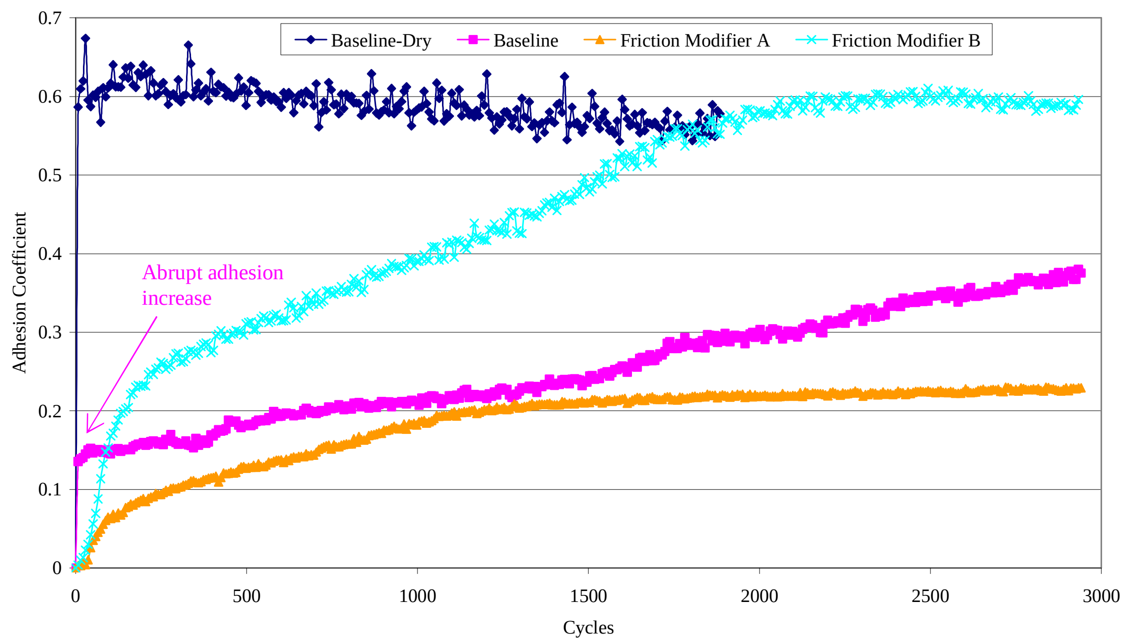

Fig. 2B.9. Leaf contaminated tests at 2% slip (and reference baseline-dry without contamination).

Furthermore, a moderate adhesion characteristic of FMA was observed in these tests; a third body layer was formed at the disks surface that yields lower adhesion coefficients than the baseline. This moderate adhesion behaviour was already observed in a previous work with FMA in dry and wet contacts [2B.16]. In the baseline test at 2% slip, it seemed that the abrupt increase in slip when the disks are brought into contact could have caused the leaf layer to be depleted, yielding an instantaneous increase of 0.14 in the adhesion coefficient, as indicated in Fig. 2B.9. The abrupt increase in adhesion did not occur for the tests at 2% with FMs, which may be attributed to their water and solid contents that accommodate the slip.

The level of adhesion necessary for an adequate braking and traction performance depends on the train type, composition, and the traction and braking systems. It is well-known that the adhesion required for braking is lower than for traction. As an example, one of the most adhesion demanding electrical multiple-units running on the Dutch railway network requires 0.14 for braking and 0.24 for traction. In this work, we took as reference the adhesion requirements given in [2B.5], which are 0.09 in braking and 0.2 in traction. Table 2B.1 gives an overview of the number of cycles required for the tests with FMs and the baseline tests to reach those requirements for each slip considered. It can be seen that FMB always reached adequate adhesion levels first for all slip ratios. There seemed to be an optimum slip of 1% for FMB in both traction and braking, which may be due to the balance in the removal of the leaf layer and FMB from the disks surfaces. This optimum slip was observed with FMA only for braking; the moderate adhesion characteristic of FMA breaks the tendency for traction, as shown in Table 2B.1. In addition, for the baseline it was found that the higher the slip the better the performance, as it could be expected due to the associated higher rate of removal of the leaf layer.

Table 2B.1. Number of cycles required to reach the adhesion for adequate braking and traction performance.

	Braking (μ=0.09)			Traction (μ=0.2)		
	0.5% slip	1% slip	2% slip	0.5% slip	1% slip	2% slip
Baseline	515	115	0	2255	982	667
FMA	245	207	220	not reached	1884	1151
FMB	187	35	70	1965	65	145

2B.3.2. IR spectroscopy analysis

After running each adhesion test, the remaining layers were analyzed using FTIR microspectroscopy. By looking at the organic components of those layers, it was possible to determine whether the leaf layer had been removed from the disk surface. In order to establish a reference, IR micro-reflection spectra of the sycamore leaf and the FMs were taken.

In Fig. 2B.10 the spectra of the remaining layers in the adhesion tests with FMA are depicted; the leaf and FMA samples used in those tests are also included together with the leaf layer resulting from the preliminary feeding stage before FMA is applied. Similar spectra can be observed for the leaf sample and the created leaf layer. There was a broad reflection peak from 3100-3700 cm^{-1} that is presumably due to water OH stretch vibrations. The two characteristic peaks at 2920 and 2850 cm^{-1} could be related to lignin present in the leaf sample, while the absorption profile from 1800-800 cm^{-1} is from other compounds present in leaves thoroughly explained in [2B.11]. It is worthwhile to mention that the peak at 1600cm^{-1} could be attributed to lignin because the riblets of our leaf samples were not removed. Furthermore, FMA showed a high moisture content (peak at 3100-3700 cm^{-1}), a characteristic peak at 1640 cm^{-1} and a rise in absorbance below 900 cm^{-1}. Moreover, the spectra of the remaining layer in the test at 2% slip showed the most similar pattern with the leaf layer. It can also be seen that there was some FMA in that layer, which caused the rise in absorbance below 860 cm^{-1}. Hence, FMA seemed to mix with the leaf layer in that test forming a layer that led to a reduction of 60% in the adhesion coefficient compared to the dry uncontaminated contact at 2% slip (see Fig. 2B.9). Similar findings applied to the post-test layer at 1% slip, in which the reduction of the adhesion coefficient was 42%.

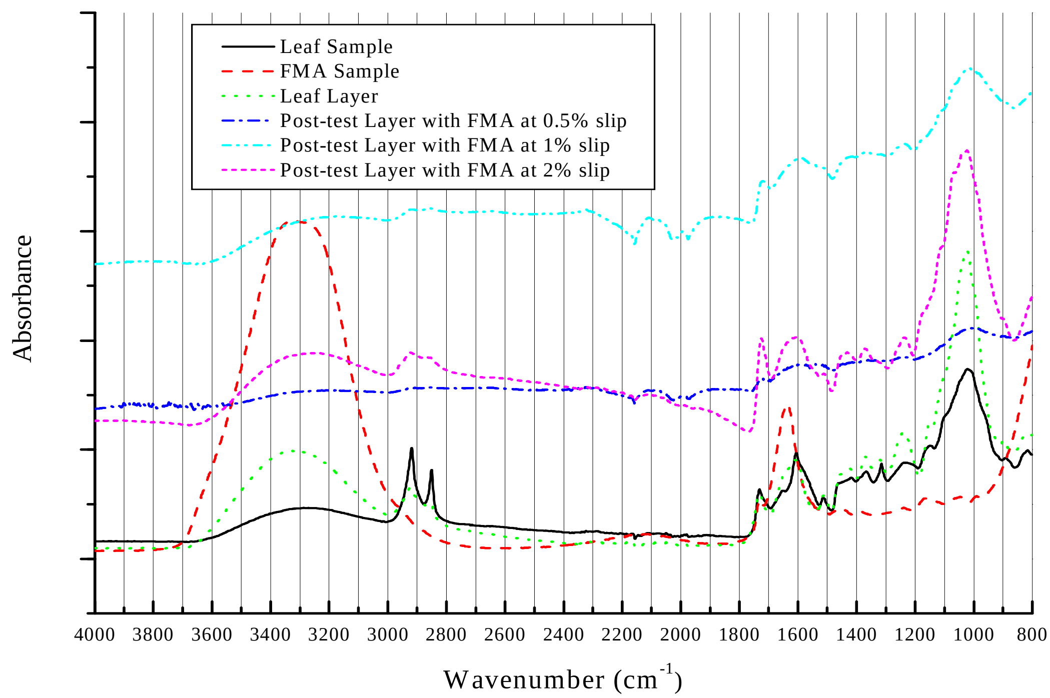

Fig. 2B.10. IR micro-reflection spectra of initial samples, leaf layer and post-test layers with FMA.

FMB showed mainly the same characteristic peaks in spectra as FMA (see Fig. 2B.11); however, different spectra peaks were observed in the range of 1500-1000 cm^{-1}. In the tests with FMB, post-test layers were only found at 0.5% slip. This remaining layer seemed to have some FMB left as shown by the rise in absorbance below 820cm^{-1}. Some of the characteristic peaks of the leaf layer spectra were also observed, e.g. at wavelengths 1600cm^{-1} and 1020 cm^{-1} on the post-test layer spectra, which would indicate that the leaf layer was not completely removed in the test. Thus, the adhesion did not fully recover with 30% decrease compared to the dry uncontaminated contact, as shown in Fig. 2B.7.

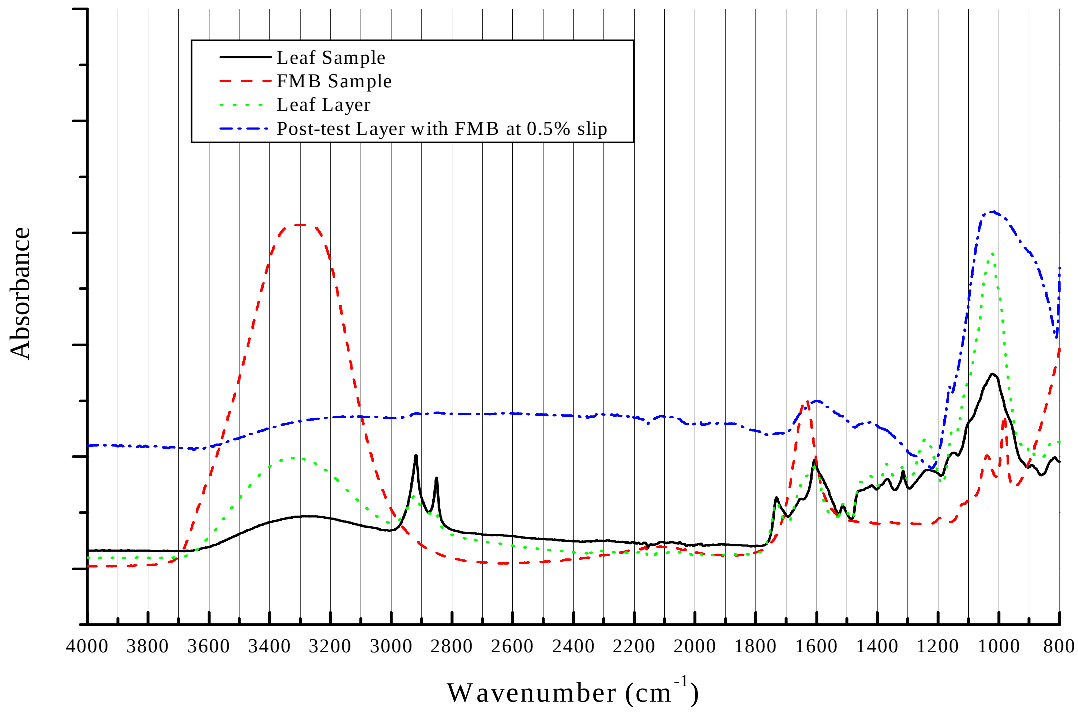

Fig. 2B.11. IR micro-reflection spectra of initial samples, leaf layer and post-test layer with FMB.

2B.3.3. Leaf layer and friction modifiers solid particles analysis

Fig. 2B.12 (left) shows an example of the leaf layer generated after 4000 cycles of run-in and 300-400 cycles of leaves application. Different coloration is observed on the layers present on the disks surface. Some light greenish layers correspond to adhered leaf mulch; whereas the majority of the layers present a black coloration and are firmly adhered on the disks surfaces. The latter layers have been identified in this paper as the black leaf layer that is equivalent to that found on the railway track. In Fig. 2B.12 (right) the remaining layer on the disks surfaces after 3000 cycles of removal test is shown. The previously generated black leaf layer is not fully removed from the disks surface after 3000 cycles in baseline conditions at 0.5% slip, as some patches still adhere to the disk surface. This proves that the generated black leaf layer is very durable as it has also been reported from observations on the track [2B.5, 2B.6].

The particle size of the FMs determines whether the particles could prevail over the leaf layer to interact with wheel and rail in a metal-particle-metal contact, as compared to the thickness of the leaf layer. The particle size distribution of both FMs was measured by means of a laser particle analyzer; the results are depicted in Fig. 2B.13. In FMA two size ranges of solid particles were predominant in the mix: 10 and 100 µm. The solid particles of FMB had a larger size, which ranged from 300 to 2000 µm. The thickness of the post-test leaf layer (i.e., after 3000 cycles of removal test) was measured with an optical 3D profiling system WykoNT3300 (Veeco Metrology Group, USA). The values of thickness ranged 3-13 µm.

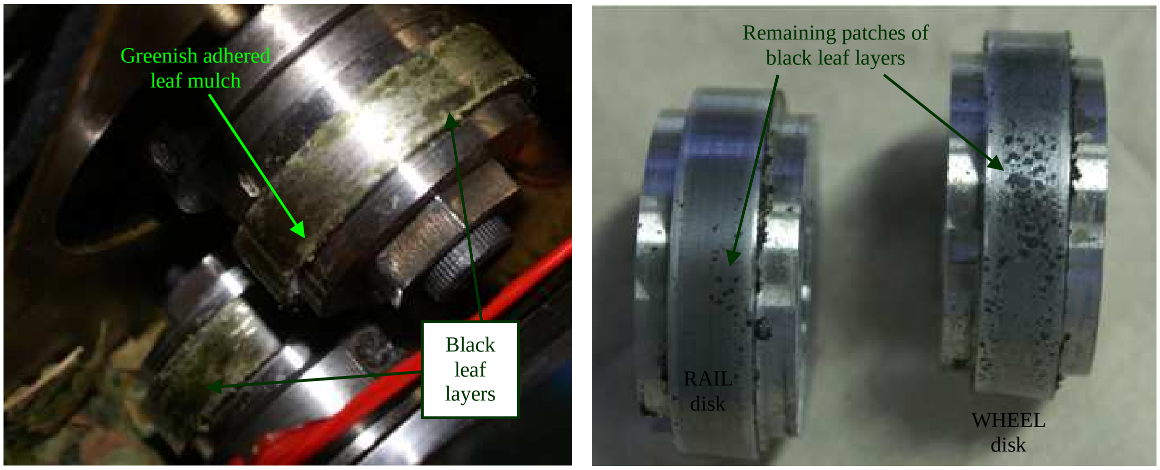

Fig. 2B.12. Leaf layers on the disks surface after generation test (left) and after removal test (right).

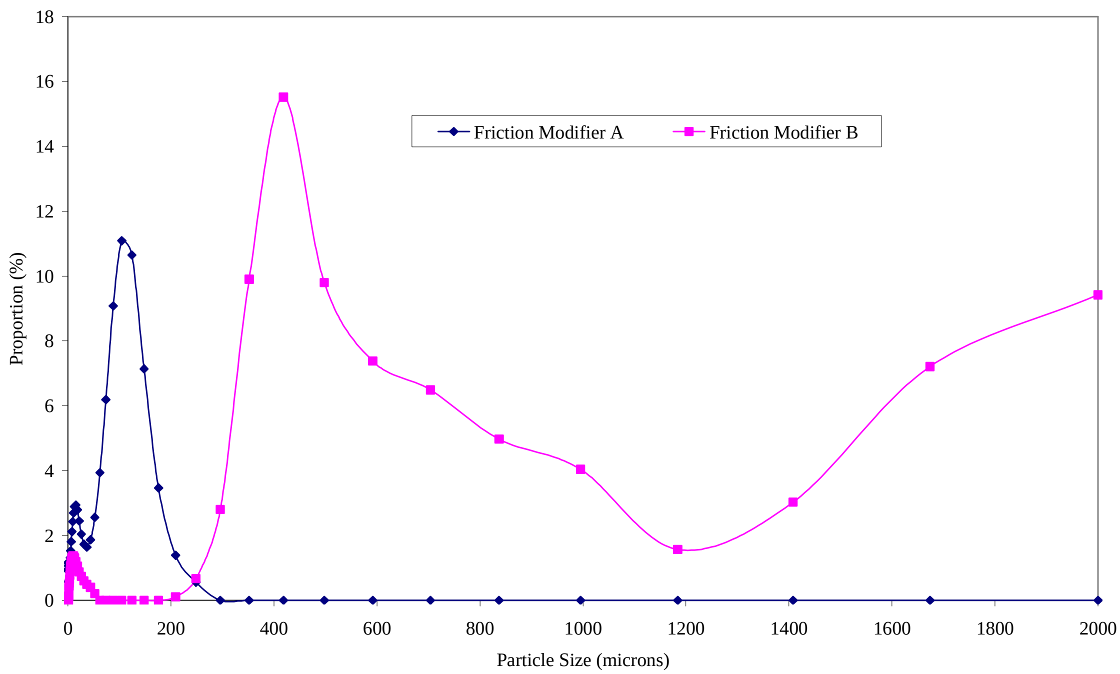

Fig. 2B.13. Particle size distribution of FMA and FMB (proportion given in volume).

In order to study the rupture strength and associated particle size change, particle strength analyses of the FMs were carried out by means of a high precision press in the laboratory. An individual particle of each FM was put between two metal plates and subject to normal load in a displacement controlled process. Fig. 2B.14 depicts the most representative tests. The difference in stiffness of the particles contained in FMB (i.e., stainless steel and sand) was observed in terms of different initial load-deflection slope. The sand particles had a steeper slope and presented a brittle behaviour. They could be either crushed for a few times into dust (as shown with particle FMB_S2) or be embedded in the softer steel material (see particle FMB_S1). If the sand particles were crushed, smaller particles were formed that could bear the load until dust was finally formed. The reduction in size in the tests ranged from 50 to 400 µm, until no more load could be born by the particles. On the other hand, the stainless steel particles underwent plastic deformation owing to their ductility; some particles just flattened and remained unbroken throughout the test (as seen in FMB_SS2), some broke and were further deformed (as observed in FMB_SS1). There was a slight change in slope between FMB_SS1 and FMB_SS2, which can be attributed to the amorphous shape of the particles that leads to a different contact area. The solid particles contained in FMA broke up at smaller loads (around 0.5 N) due to its small size compared to FMB. The decrease in size ranged from 20 to 80 µm before dust was fomed.

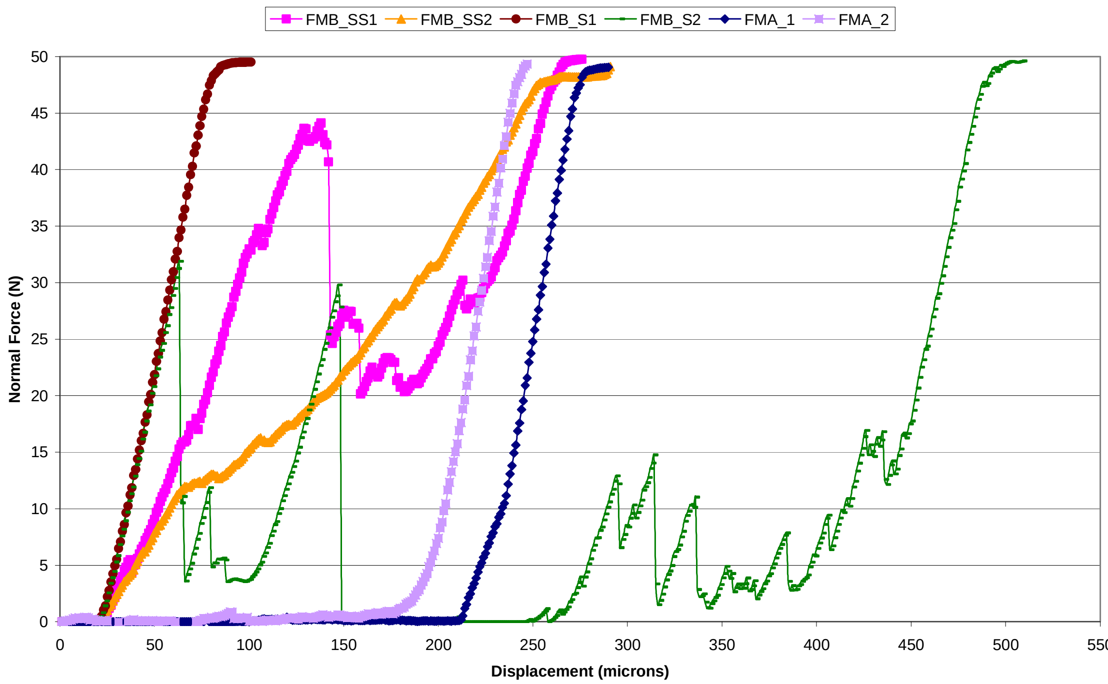

Fig. 2B.14. Particle strength tests of FMB (SS = Stainless Steel, S = Sand) and FMA solid particles.

In addition, the hardness of the solid particles contained in the FMs will determine the effectiveness of cutting through the leaf layer. The hardness of the leaf layer remaining after each test was measured by means of Vickers micro-indentation technique; average values between 47 HV_{10g} and 68 HV_{10g} were obtained depending on the degree of compaction of the layer. This is in line with previous work carried out with leaves on the same roller rig [2B.12]. The hardness of the solid particles of both FMs was also measured using the same technique. The stainless steel particles of FMB gave an average 320 HV_{10g}, while an average of 1500 HV_{10g} was obtained for the sand particles. Despite many attempts, the hardness measurements of the particles contained in FMA were not successful due to their small size.

2B.3.4. Disk surface analysis

After completion of the tests, the surface of the disks was examined. No surface damage was found in the baseline tests. In the tests with FMB, the hard solid particles, which were responsible for cutting through the leaf layer, caused indentations on the surface of both wheel and rail disks. The indentations varied in size from 0.8 to 2 mm in equivalent diameter and with 50 µm depth on average. A picture of an indented rail disk together with a microphotograph of the indentation is given in Fig. 2B.15. Similar findings for different solid contaminants have been presented by other researchers [2B.13, 2B.18], and also in a previous work carried out with FMB in dry and wet contacts [2B.16]. On the contrary, no surface damage was observed when using FMA.

2B.4. Discussion

The adhesion coefficient during the feed of leaves ranged from 0.01 and 0.04 for 0.5% slip. Once the feed of leaves was stopped, the adhesion increased with the cycles as the leaf layer was removed from the disks surfaces. FMB showed the fastest recovery in adhesion for both braking and traction. It was up to 70% faster in braking and up to 93% faster in traction compared to the baseline. Hence, when using FMB in real wheel-rail systems the number of wheel passages needed to restore adhesion to an adequate level for traction could be reduced by a factor of up to 15; whereas in braking the improvement factor could reach up to 3. However, these results can only be taken as a qualitative indication of the actual wheel-rail situation because of the differences with the twin-disk setup, as already outlined in [2B.15]. On the other hand, the moderate adhesion characteristics of FMA brought about slower recoveries in adhesion for traction requirements when compared to the baseline for all slips considered. In addition, it is worth to notice that in this work we have tested the traction operation, in which the wheel slips over the rail; however, we have also used our results for comparisons with the braking requirements. In braking operation, the rail would be represented by the faster disk and the wheel by the slower one. Nevertheless, previous research has shown that there exists a negligible influence on the adhesion results when changing the direction of the slip [2B.19]; therefore, our adhesion results can be used for both traction and braking.

By means of these tests, the optimum slip ratio for the best adhesion recovery in the different contact conditions could be investigated. For the baseline, it was found that faster adhesion recovery was achieved at higher slips, as it could be expected due to the increased removal effect. An interesting direction of research would be to study which optimum slip is necessary to remove the leaf layer without much additional damage to wheels and rails. If trainborne leaf layer detection techniques were developed, the wheels could be set to a certain slip in order to remove the leaf layer from the rails for the subsequent wheels. In the tests with FMB, an optimum was observed at 1% slip in reaching both braking and traction adhesion requirements. This optimum can be explained as a balance between the amount of FMB and leaf layer that is removed from the disks surface. When using FMA, the optimum could also be observed at 1% slip, but only from the point of view of braking. For traction, it seems that FMA cannot bring the adhesion to what is required, unless FMA is removed from the disks surface. This finding is in good agreement with observations from previous work with FMA in dry contacts, in which it was found that FMA decreased adhesion compared to the baseline to moderate values in uncontaminated dry conditions [2B.16].

When compared to the thickness and hardness of the leaf layer, the size and hardness of the solid particles contained in the FM will primarily determine the capacity to break up the leaf layer and restore the adhesion back to acceptable levels. Measurements of the leaf layer thickness in both field and laboratory scale have been performed in the United Kingdom [2B.5, 2B.10]. The thickness ranged from 10 to 100 µm depending on the compaction to which the leaves had been subjected. Samples of leaf layer taken from the Dutch railways network in autumn 2006 have been measured with thickness 20-30 µm. In our laboratory tests, the thickness of the post-test leaf layer ranged 3-13 µm. This layer thickness is larger than the wheel and rail disks roughness; therefore, the layer may inhibit the metal-metal contact. The particle size of the FM determines whether the solid particles will interact with the wheel and the rail in a metal-particle-metal contact. The solid particles of FMB could prevail over the leaf layer due to its large size; while the initial particle size of FMA is in the same range as the leaf layer thickness. Nevertheless, one must bear in mind that the majority of the particles will break up due to the high wheel-rail contact pressure. This phenomenon was investigated for sand particles [2B.13] and for crushed granite ballast [2B.18]. Broken-up particles will have smaller size and may be entrapped within the third-body leaf layer; thus, losing its effectiveness. The strength analysis tests showed a reduction of 20-80 µm in size for the solid particles of FMA and 50-400 µm for the sand particles contained in FMB. The stainless steel particles of FMB either deformed due to their ductility or broke with a maximum reduction in size of 200 µm. Hence, the broken-up FMA particles may be entrapped within the third-body leaf layer; whereas the solid particles of FMB would still have larger dimensions than the leaf layer thickness. Moreover, considerations on the feasibility of small particles to get entrained in the wheel-rail contact must be taken into account, as it was already mentioned in [2B.13]. Observations during the testing showed that a great number of particles of FMB were expelled due to their large particle size. Therefore, the size of the solid particles of a FM should be optimized towards adequate particle entrapment and efficacy against leaf layer thickness.

In addition, the hardness of the solid particles of the FM will determine the effectiveness of cutting through the leaf layer. The hardness of the leaf layer mainly depends on the degree of compaction (given by the contact load and wheel slip) and the water content. It was shown in previous laboratory tests that dry leaf layers are harder than wet ones [2B.12]. In fact, the softening effect of water can help in the removal of the leaf layer, as already mentioned in the literature [2B.5, 2B.10]. In this paper, only dry leaf layers have been tested, as they represent the hardest to be removed from the wheel and rail surfaces. In field and full-scale tests carried out in The United Kingdom, leaf layers have been reported to have a hardness of 1-4 in Mohs scale [2B.10]. In previous work with dry and wet leaves on the SUROS roller rig, micro-hardness of the layer was reported to range from 15 to 60 HV_{1g} [2B.12]. In this paper, the micro-hardness of the layers ranged 47-68 HV_{10g} depending on the degree of compaction of the layer. The solid particles of FMB are harder than the leaf layer. Accordingly, the solid particles could effectively cut through the leaf layer, leading to a fast recovery in adhesion as shown in this paper. Conversely, they caused indentations on the surface of both wheel and rail disks. FMA did not show as effective break-up of the leaf layer as FMB; however, no indentations were observed in the tests with FMA. Hence, it can be concluded that the hardness of the solid particles of a FM should be optimized to a compromise between effective leaf layer removal and minimized surface damage to wheel and rail.

Moreover, it is worthwhile to emphasize that the study here presented corresponds to the post-application of the FMs, i.e. application of the FM once the leaf layer is already present on the disks surfaces. An interesting possibility and still open question is whether the pre-application of the FM would be effective in hindering the formation of the leaf layer. Some trials were carried out by the authors, in which the rail disk was coated with FM before leaves were applied. Unfortunately, those trials did not lead to clear results due to stability problems of the roller rig that yielded wrong measurements in the torque transducer.

2B.5. Conclusions

The leaf contaminated wheel-rail contact has been simulated in rolling-sliding conditions with a twin-disk roller rig in closely controlled laboratory tests. The leaf layer has been generated in similar conditions to the actual wheel-rail contact. Two water-based FMs have been tested in order to evaluate their performance to overcome low adhesion problems associated with leaves. FMB has been extensively used in the Dutch and British railways networks for the last years to overcome adhesion problems, especially leaf-related ones during autumn. FMA was tested successfully in wet contacts and its performance in leafy contacts was of much interest. In order to compare the results of the FMs with the untreated conditions (i.e., without FM), a baseline has also been tested. This work yields the following conclusions:

(a) In the presence of leaf layer the adhesion coefficient is between 0.01 and 0.04. As the leaf layer is removed after some necessary cycles, adhesion recovers to a certain degree. FMB shows the largest adhesion recovery as its large hard solid particles effectively break up the leaf layer.

(b) FMB leads to the fastest adhesion improvement in both traction and braking requirements with a reduction in cycles of up to 93 and 70%, respectively, when compared to the baseline. FMA seems to be slower than the baseline due to its moderate adhesion characteristics.

(c) An optimum in adhesion recovery is found at 1% slip for FMB due to the balance between leaf layer and FMB removal. For FMA the optimum is also at 1% for braking, while for traction the higher the slip the better the performance due to its moderate adhesion characteristics. In baseline conditions, higher slip leads to better performance in both traction and braking because of the increased removal effect.

(d) FTIR microspectroscopy showed that FMA seems to mix up with the leaf layer forming a layer that reduces the adhesion coefficient between 42 and 60% in the tests with FMA at 1 and 2% slip, respectively, as compared to the clean dry conditions.

(e) Two parameters of a FM play the main role in adhesion recovery: the hardness of the solid particles and the particle size. These two parameters need to be designed in accordance with the hardness and thickness of the leaf layer so as to optimize the removal of leaf layer.

(f) The large hard particles of FMB cause indentations to the wheel and rail disk surfaces; whereas, no indentations are observed as caused by the small particles of FMA. Therefore, a compromise needs to be found for the hardness and size of the solid particles when a FM is developed in order to cut through the leaf layer and not cause severe surface damage on wheel and rail.

References

[2B.1] T.M. Beagley, I.J. McEwen, C. Pritchard: Wheel-Rail Adhesion Boundary Lubrication by Oily Fluids. Wear 31, 77-88 (1975).
[2B.2] T.M. Beagley, I.J. McEwen, C. Pritchard: Wheel/Rail Adhesion — The Influence of Railhead Debris. Wear 33, 141-152 (1975).
[2B.3] T.M. Beagley, C. Pritchard: Wheel/Rail Adhesion — The Overriding Influence of Water. Wear 35, 299-313 (1975).
[2B.4] T.M. Beagley: The Rheological Properties of Solid Rail Contaminants and Their Effect on Wheel/Rail Adhesion. Proc. of the Inst. of Mech. Eng. 190, 419-428 (1976).
[2B.5] C.R. Fulford: Engineering Review of Low Adhesion Research. Report published by Rail Safety and Standards Board, UK (2004).
[2B.6] Managing Low Adhesion. Report published by the Adhesion Working Group, UK (September 2001).
[2B.7] Z. Li, X. Zhao, C. Esveld, R. Dollevoet, M. Molodova: An Investigation into the Causes of Squats—Correlation Analysis and Numerical Modeling, Wear (in press 2008).
[2B.8] U. Olofsson, K. Sundvall: Influence of Leaf, Humidity and Applied Lubrication on Friction in the Wheel-Rail Contact: Pin-on-Disc Experiments. Journal of Rail and Rapid Transit 218, 235-242 (2004).
[2B.9] Press release by the Dutch Railways in Dutch, www.ns.nl (October/November 2002).
[2B.10] W. Poole: Characteristics of Railhead Leaf Contamination. Summary Report published by Rail Safety and Standards Board (May 2007).
[2B.11] P.M. Cann: The 'Leaves on the Line'—a Study of Leaf Residue Film Formation and Lubricity under Laboratory Test Conditions. Tribology Letters 24, 151-158 (2006).
[2B.12] E.A. Gallardo-Hernandez, R. Lewis: Twin Disk Assessment of Wheel/Rail Adhesion. Wear (in press 2008).
[2B.13] R. Lewis, R.S. Dwyer-Joyce: Wear at the Wheel/Rail Interface when Sanding is Used to Increase Adhesion. Journal of Rail and Rapid Transit 220, 29-41 (2006).
[2B.14] Gladde Sporen, Oplossingsrichtingen voor Adhesieproblemen. Report published by the Dutch Railways Technical Research (NSTO) in Dutch (1999).
[2B.15] U. Olofsson, R. Lewis: Tribology of the Wheel-Rail Contact. In Iwnicki, S. (ed.), Handbook of railway vehicle dynamics, Taylor & Francis Group, Boca Raton, pp. 121-141 (2006).
[2B.16] O. Arias-Cuevas, Z. Li, R. Lewis, E.A. Gallardo-Hernandez: Rolling-Sliding Laboratory Tests of Friction Modifiers in Dry and Wet Wheel-Rail Contacts (to be published).
[2B.17] D.I. Fletcher, J.H. Beynon: Development of a Machine for Consely Controlled Rolling Contact Fatigue and Wear Testing. Journal of Testing and Evaluation 28, 267-275 (2000).
[2B.18] D.G. Grieve, R.S. Dwyer-Joyce, J.H. Beynon: Abrasive Wear of Railway Track by Solid Contaminants. Journal of Rail and Rapid Transit 215, 193-205 (2001).
[2B.19] L. Deters, M. Proksch: Friction and Wear Testing of Rail and Wheel Material. Wear 258, 981-991 (2005).

Chapter 3

Sanding

ABSTRACT

Chapter 3 presents laboratory and field investigations on sanding. These investigations have been partially motivated by some findings in Chapter 2 that have shown the importance of the particle size for the suitability of a FM. In addition to the sand size, other sanding parameters, such as feed rate, number of sanding axles and wheel slip are also investigated. The chapter is divided into four parts. Part A presents some laboratory tests in initially leaf contaminated contacts, in which the influence of the particle size and wheel slip on adhesion and wheel/rail wear is examined. Part B shows the results of laboratory tests in dry contacts aimed at analyzing the effect of particle size, feed rate and wheel slip on adhesion and electrical insulation during sanding. Part C studies with laboratory tests the effect of particle size, number of sanding axles and wheel slip on the adhesion recovery in leaf contaminated contacts. Part D, as a first step towards the validation of some laboratory findings, examines the influence of particle size and number of sanding axles on the adhesion recovery in leaf contaminated contacts by means of field tests. Moreover, baselines (i.e. no sand applied) have also been obtained in Parts A-D to quantify the relative effect of sanding and contribute to a better understanding on the low adhesion phenomenon.

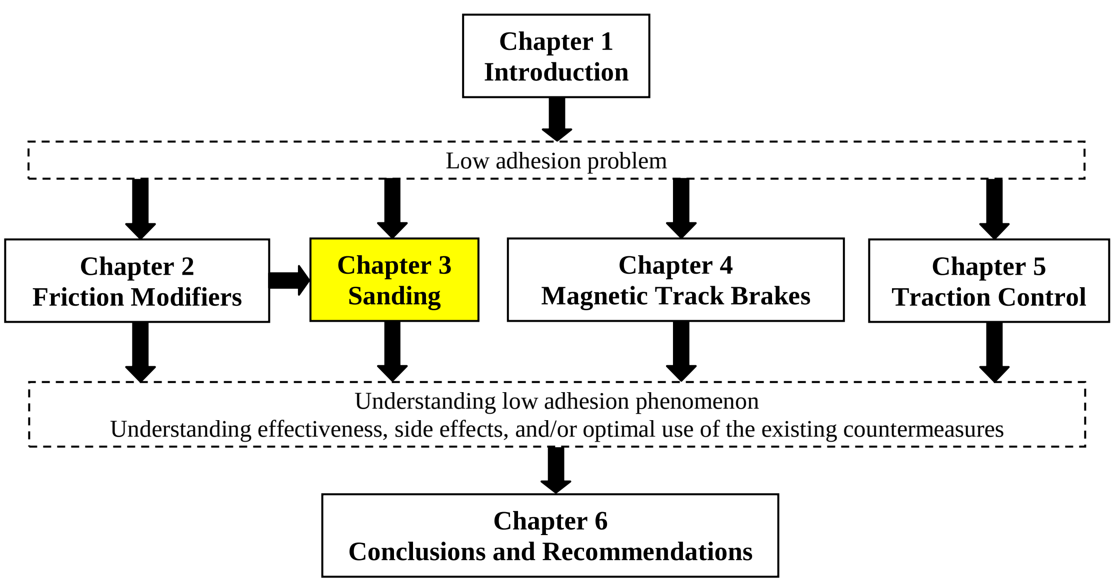

Chapter 3, Part A

Laboratory tests on adhesion and wear[VII]

ABSTRACT

The adhesion (or utilized friction) in the wheel-rail contact is the most important parameter in braking and traction operation of rail vehicles. Since the beginning of railway transportation, sanding from the locomotive has been a common practice to enhance the wheel-rail adhesion in most of the railway networks. In recent years, sanding has also been used in electrical multiple units in some countries. Sand-based friction modifiers are another practical measure that some railway organizations have been using to overcome low adhesion incidents caused by contamination like autumn leaves. Although sand has widely been accepted as an effective adhesion improver in most of the contamination conditions, there seems to be a lack of understanding on the influence of the sand particle size. This hinders not only a possible optimum sanding practice, but also the development of suitable sand-based friction modifiers. Furthermore, the wheel slip at which sanding is activated is another relevant parameter that may help optimize sanding practice. In this paper, a laboratory investigation on the influence of particle size and slip on the adhesion and wear obtained during railway sanding is presented. The wheel-rail contact has been simulated by means of a twin-disk roller rig in rolling-sliding motion. Three different slips representative of actual traction and braking operations have been considered in the testing. Four different sands have been used to account for the influence of the particle size. The results show that a large particle size of sand yields a higher adhesion coefficient, but it may bring about more wear depending on the slip. The increase in slip leads to higher adhesion coefficients, but it also brings along higher wear rates of wheel and rail disks.

[VII] This chapter has been submitted in 2009 for publication to Journal of Wear as: O. Arias-Cuevas, Z. Li, R. Lewis: A Laboratory Investigation on the Influence of the Particle Size and Slip During Sanding on the Adhesion and Wear in the Wheel-Rail Contact.

3A.1. Introduction

The adhesion between wheel and rail is a crucial factor in railway transportation, as it determines the acceleration and braking capabilities of a train. The increasing demands in railway transportation have led to faster trains with higher accelerations and decelerations; however, the adhesion still remains limited by the available friction between the steel wheels and rails. Consequently, low adhesion problems have been present in many railway networks in recent decades, especially those related to leaf contamination in autumn [3A.1-3A.4]. Since the beginning of railways, sanding has been a common practice to increase the adhesion of locomotives [3A.5]. In some countries like Germany and the UK, sanding has also become a common practice to overcome low adhesion conditions experienced by Electrical Multiple Units (EMUs) [3A.6, 3A.7]. Besides sanding, many railway organizations have opted for using friction modifiers (FMs), some of which may contain sand or other solid particles to increase the adhesion level under certain contamination conditions [3A.1, 3A.4, 3A.8].

Several investigations on sanding have been carried out [3A.5, 3A.9-3A.12]. Andrews [3A.5] investigated the adhesion values given by some mineral powders (silica sand among them). He proposed an empirical relationship in which the adhesion increased proportionally with the product of particle hardness and size of the mineral powders. However, only one particle size was used for each mineral tested, and his empirical relationship is restricted to particle sizes smaller than 0.4 mm. Astle-Fletcher [3A.9] stated that the working principle of sanding was mainly achieved by mechanical interlocking of sand particles with the roughness of the wheel and rail surfaces. He also presented an investigation of the most important parameters in the sand applicators, such as proximity to the contact interface and velocity. Kumar et al. [3A.10] carried out laboratory investigations to analyze the wear and adhesion experienced by sanding on locomotive wheels and they compared it to dry steel-on-steel contacts. The wear rates were shown to increase by an order of 1 to 2 due to the application of sand. The sand increased the adhesion in oily contacts. An increase in the adhesion coefficient with slip on dry contacts during sanding was shown. Nevertheless, slip only up to 1% was used in their work, which is below those found in practice under low adhesion conditions. More recently, Lewis et al. [3A.11, 3A.12] showed that sanding can help to overcome low adhesion caused by leaves and water, but wear was increased by factors between 2 and 10 during sanding.

Although sand has widely been accepted as an effective adhesion improver in most of the contamination conditions, there seems to be a lack of understanding on how sand particle size affects adhesion, electrical insulation and wear in the wheel-rail contact. This hinders not only a possible optimum sanding practice, but also the development of suitable sand-based FMs. There exist several standards on sanding, in which specifications on different requirements in the particle size distribution of the sand can be found. The particle size distribution is given in the standards as 0.7-2.8 mm in the UK [3A.6], 0.63-2 mm in Germany [3A.13], and 0.1-0.6 mm in France [3A.14]. Furthermore, sanding can be activated manually by the driver or automatically by the Wheel Slide Protection (WSP) and Traction Control (TC) systems. The activation by the WSP/TC systems is triggered with a certain wheel slip (or slide) threshold. Nevertheless, there is no grasp on how relevant the wheel slip can be on the performance of sanding, not only in terms of adhesion, but also its impact on wear and electrical insulation. All these facts encouraged the authors to investigate the influence of the particle size, feed rate, and wheel slip during sanding on adhesion, electrical insulation, and wear of wheels and rails. This paper describes the influence of particle size and wheel slip on adhesion and wear. Another paper will be published by the authors to present the influence of the particle size, feed rate, and wheel slip on adhesion and electrical insulation [3A.15].

In this work, the wheel-rail contact is simulated by means of a twin-disk roller rig under closely controlled laboratory conditions. The adhesion coefficient during sanding in initially leaf contaminated contacts at three different slips and four sand particle size distributions has been analyzed. The wheel and rail disks have also been examined after each test to analyze the wear, not only in terms of mass loss, but also the surface damage, surface work-hardening, and subsurface deformation caused by sanding at different sizes and slips.

3A.2. Test description

3A.2.1. Test set-up

The SUROS (Sheffield University ROlling Sliding) roller rig was used to simulate the wheel-rail contact in rolling-sliding conditions. The SUROS roller rig, which is shown in Fig. 3A.1, is described in detail in the literature [3A.16]. The test disks were mounted on independent shafts. By means of a hydraulic jack, a controlled load of 4.7 kN was applied on the disks producing a maximum Hertzian pressure of 1.2 GPa in the contact zone, which is representative of the contact between wheel tread and railhead for passenger trains in the Netherlands. Since cylindrical disks were used in the experiments, a line contact of 10 mm width was present (see Fig. 3A.2). In the tests, the wheel disk rotated faster than the rail disk to realize the slip; the rotational speed of the rail was maintained at 400 rpm, equivalent to 0.98 m/s of rolling speed. The slip is defined in Eq. 3A.1, where w and r are the rotational speed and rolling radius of the disks, respectively. The adhesion coefficient was calculated with the readings of the torque transducer and the load cell, as indicated in Eq. 3A.2, where represents the torque and is the normal contact force. A personal computer was used to acquire the data and to control both the speed and the load during each test.

$$Slip = \frac{w_{wheel} \cdot r_{wheel} - w_{rail} \cdot r_{rail}}{w_{wheel} \cdot r_{wheel} + w_{rail} \cdot r_{rail}} \cdot 200\% \tag{3A.1}$$

$$\mu_{adhesion} = \frac{T}{F_N \cdot r_{rail}} \tag{3A.2}$$

The test disks were cut from rails and wheel tires retired from service on the Dutch railway network; R260Mn and B5T steel for the rail and wheel disks, respectively. The disks were machined with their axes perpendicular to the longitudinal axis of both wheel and rail, as shown in Fig. 3A.2. The Vickers macro-hardness of the wheel and the rail steel used in the tests was measured as 267 HV_{20kg} and 281 HV_{20kg} on average, respectively. The roughness of the disks was measured with a profilometer, with an average value of Ra = 1.3±0.2 µm. Note that this value is close to values of roughness measured with a Hommel tester on the running band of rails of a traction/braking section. In addition, the European standard for the manufacturing of wheels specifies that the initial surface roughness must be lower than 6.3 μm on the tread on average [3A.17]. But, laboratory investigations have shown that rough wheels tend to approach a roughness level close to the one of the smoother rails [3A.18-3A.19].

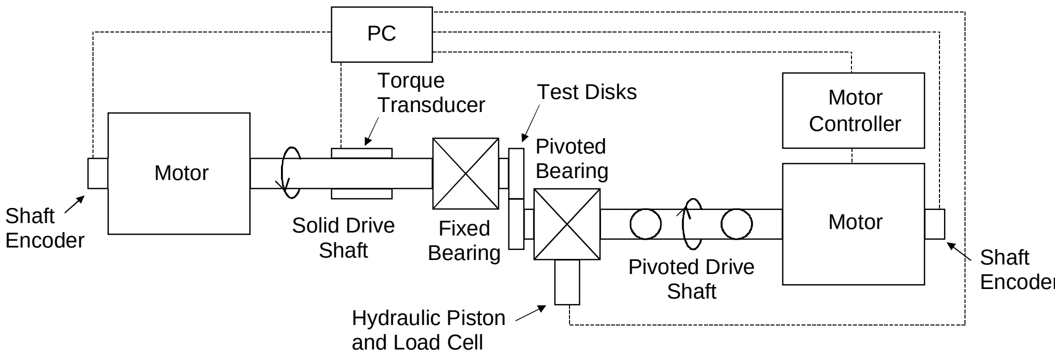

Fig. 3A.1. Schematic representation of the SUROS roller rig.

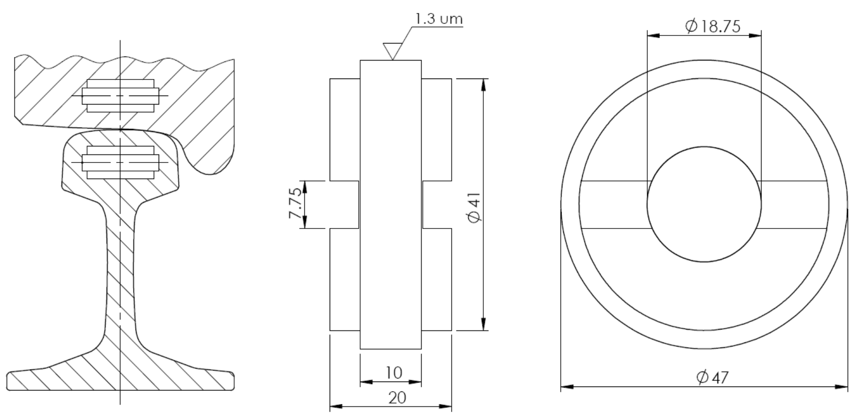

Fig. 3A.2. Orientation and dimensions of the wheel and rail disks specimens.

3A.2.2. Tested sands

Two types of commercial sand were used in this work: silica sand and filter sand. The silica sand had been extracted from a pit in south Germany, whereas the filter sand had been collected from a river in the Netherlands. A photograph of the sands is given in Fig. 3A.3. The particle size distribution of the sands was measured with a laser particle analyzer and is given Fig. 3A.4. The filter sand is used in the Netherlands to increase the adhesion in railways; thus, it is hereinafter referred to as railway sand, R sand for short. Although different rocks can be seen in the sample, the weight content in SiO_2 is around 96% as given by the supplier. The particle size distribution of R sand ranged from 0.25 to 1.4 mm with a wide peak at 0.6-1 mm, as shown in Fig. 3A.4. The silica sand had a SiO_2 content around 99% according to the supplier. It was sieved in the laboratory to three different particle size ranges: small (0.06-0.3 mm, with peak at 0.15 mm), medium (0.3-0.6 mm, with peak at 0.35 mm), and large (0.85-1.6 mm, with peak at 1.2 mm). These three sands are referred in this paper as S sand, M sand and L sand, for short. Moreover, due to the similar composition, shape, and hardness of the four tested sands the particle size distribution could be considered as the only study parameter for this work.

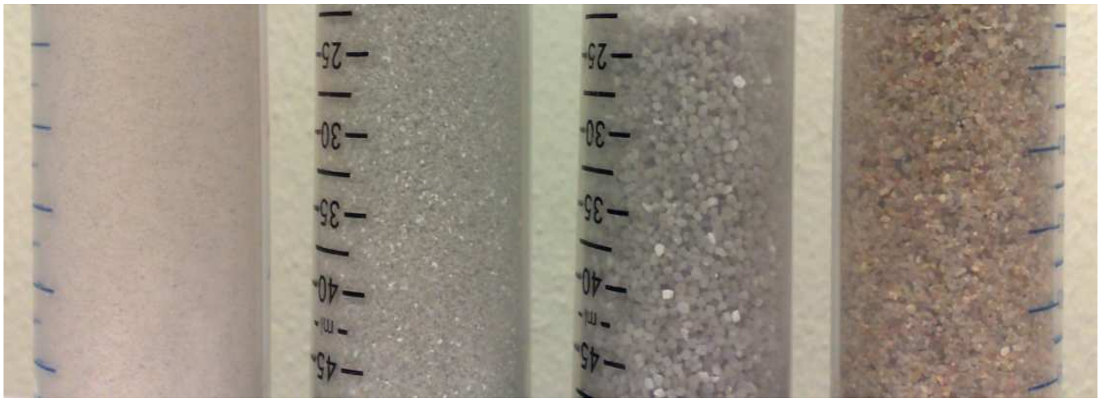

Fig. 3A.3. Photograph of the tested sands: S sand, M sand, L sand, R sand.

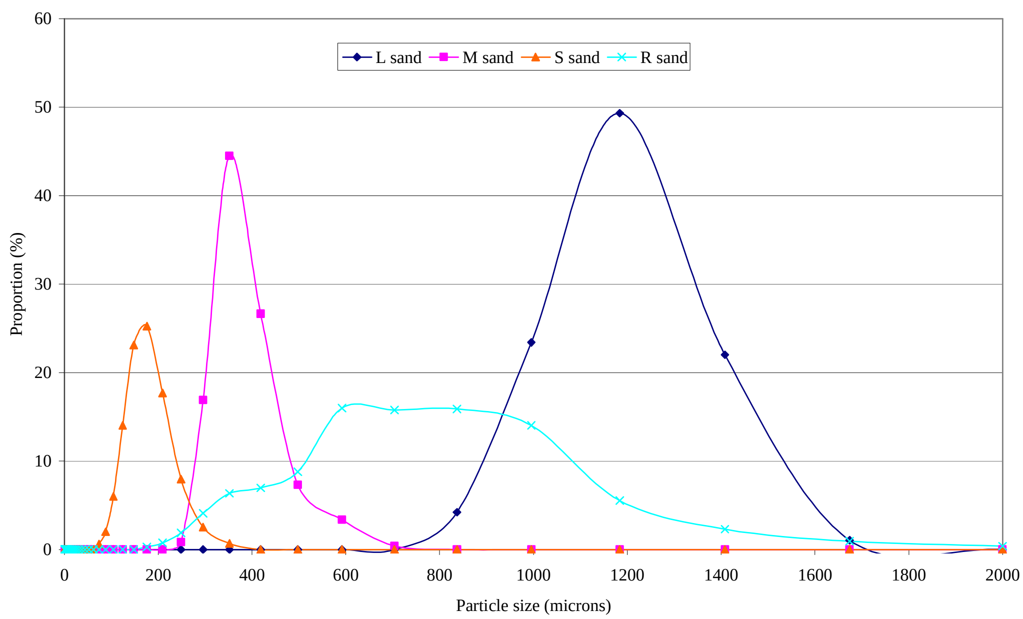

Fig. 3A.4. Particle size distribution of the tested sands obtained with the laser particle analyzer.

The sand was fed to the disk interface by means of gravity, as shown in Fig. 3A.5. After exiting the valve, the sand passed through a PVC pipe and was oriented to the disk interface with a chute. A vacuum cleaner placed behind the disks sucked the sand into the wheel-rail contact, which simulated the compressed air system used in reality. In order to regulate the sand feed rate, plastic syringes were used as valves. The orifice had to be modified to achieve the desired feed rate. The different particle size distribution of the four sand types required different orifice sizes because of their different bulk density. In this work, the sand feed rate used was around 7.35 g/s, which equates to 7.5 g/m taking the distance and rolling speed of the rail as reference. This feed rate was taken as representative of the ones used in practice [3A.12].

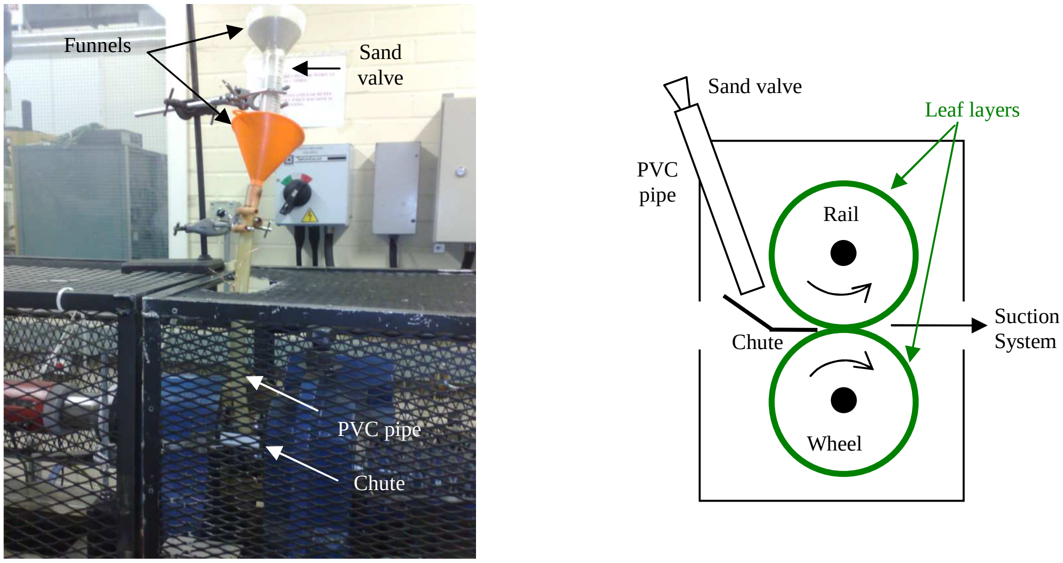

Fig. 3A.5. Application of sand in the tests: photograph (left) and schematic representation (right).

3A.2.3. Test procedure

In this work, the disks were intended to have black leaf layer contamination upon the start of the test. In order to form the black leaf layer onto the disk surfaces, the same preparation procedure used in previous work [3A.4] was followed. Note that an analysis of the created leaf layers can be found in [3A.4] along with a comparison with leaf layers found in field. The disks were allowed to run in for 2000 cycles to condition the surfaces at 0.5% slip followed by 300 cycles of leaves fed onto the contact. At the end of the preparation test the surfaces of the rail and wheel disks were covered with black leaf layers and, therefore, ready for the leaf contaminated test. It must be noted that a new pair of disks was used for each test.

Each leaf contaminated test was run for 1000 cycles, in which the sand was continuously fed from the start of the test. The tests were conducted at three slips: 1, 5 and 10%, which are typical values found during traction and braking operations in practice. Besides the tests with the four sands, a baseline (i.e. without sand applied at the disk interface) for leaf contaminated contacts was also carried out so that the effectiveness of sand as an adhesion improver could be assessed. Before and after running each test, the rail and wheel disks were placed in a bath of ethanol with ultrasonic vibration. An electronic scale of ± 0.05 mg accuracy was used to measure the mass loss of the disks. The surfaces of the disks were examined under a microscope for damage and wear features. The roughness of the surfaces was measured with a profilometer, and the macro-hardness of the surfaces was also determined. In order to observe the subsurface of some of the disks in the rolling direction under an optical microscope, the disks were sectioned, mounted in Bakelite, polished, and etched with Nital 0.5%.

3A.3. Results

3A.3.1. Adhesion

The adhesion results of the leaf contaminated tests with all sands and baseline at three slips are shown in Figs. 3A.6-3A.8. Additionally, a baseline for dry clean contacts is given to compare the adhesion coefficients to those under uncontaminated steel-on-steel conditions. Comparing the baseline-dry with the baseline it can be seen that the adhesion coefficient is greatly reduced in the presence of leaf layers, which was outlined in a previous work [3A.4]. The layers were removed from the disk surfaces progressively with cycles, and consequently the adhesion increased. At higher slips, faster adhesion recoveries were observed with the baseline, which keeps in line with the previous findings [3A.4].

When sand was applied to the wheel-rail interface, the leaf layer was effectively removed in the first few cycles due to the abrasive action of the sand (see Figs. 3A.6-3A.8). Note that the sand particles are more than 10 times harder than the leaf layers [3A.4]. Once the leaf layers had been removed, the test contact conditions corresponded to those of sanding under dry clean conditions. This can be corroborated by comparing the adhesion coefficients obtained in these leaf contaminated tests after the initial cycles with the ones achieved during sanding in dry contacts [3A.15].

After the initial cycles the adhesion coefficient exhibited a steady pattern for the tests with S and M sands, which was not observed in the tests with R and L sands, as seen in Fig. 3A.7. Since R sand incorporated a broad particle size distribution, the load borne by the particles may not be held constant as particles travel through the disk interface. The largest particles bear the contact load first, and break up accordingly until sufficient number of particles can withstand the contact load. Hence, the fluctuations observed in the adhesion coefficient results may be caused by the break-up of the particles as they travel through the contact. The range of the particle size distribution of S, M, and L sands was much narrower, so that all the particles that entered the contact may roughly bear the same contact load. However, due to its large particle size L sand experienced more break-up than smaller sands and, therefore, more oscillations in the adhesion coefficient occurred (see Fig. 3A.7). Oscillations in the adhesion coefficient caused by particle break-up in three-body abrasion tests were also observed by other researchers [3A.20].

Furthermore, the steady pattern of the adhesion coefficient could also be attributed partly to the formation of a coating on the disk surfaces of compacted crushed sand. At higher slips and larger particle sizes the abrasive removal of the coating was increased, causing more oscillations on the adhesion coefficient (see Figs. 3A.6-3A.8). Moreover, the coating may have been responsible for the sudden decrease in the adhesion coefficient of the test with M sand at 10% slip, as pointed in Fig. 3A.8. That coating was observed to be broken at the end of the test. Finally, it can be observed that oscillations in the adhesion coefficient occurred in the baseline-dry tests, which could be attributed to variations on the surfaces of the disks as wear particles formed.

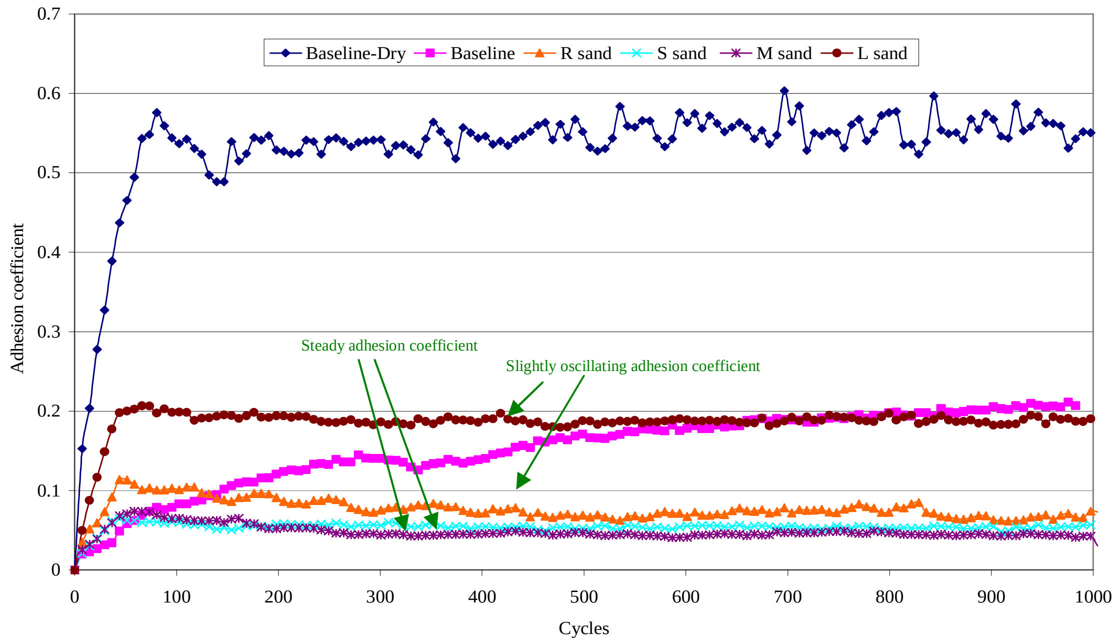

Fig. 3A.6. Leaf contaminated tests at 1% slip (and reference baseline-dry without contamination).

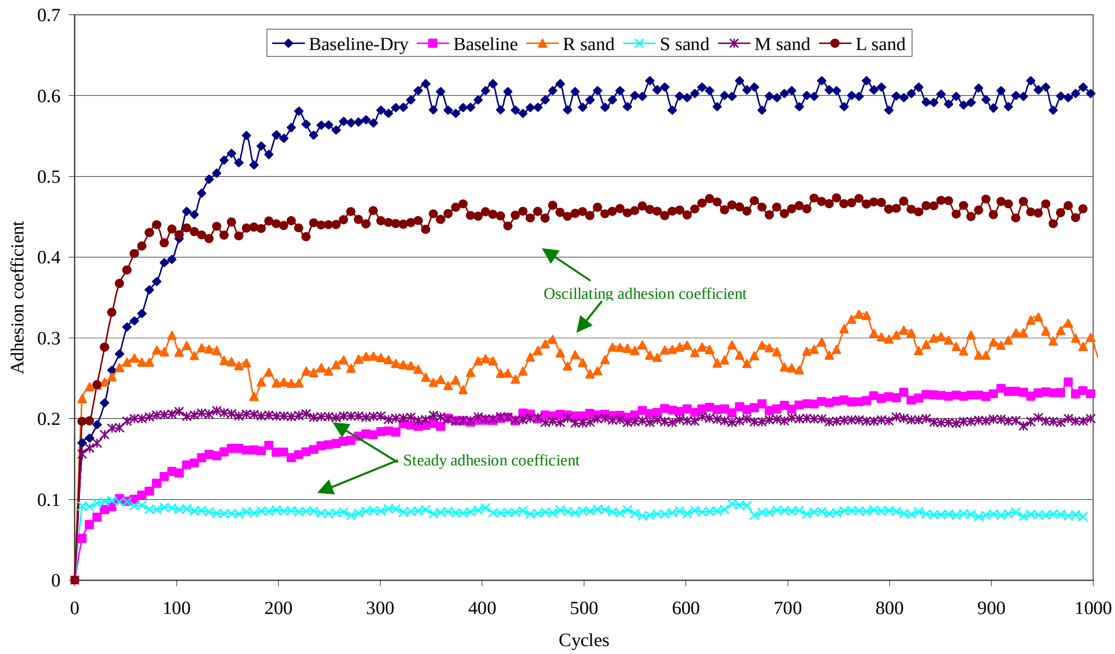

Fig. 3A.7. Leaf contaminated tests at 5% slip (and reference baseline-dry without contamination).

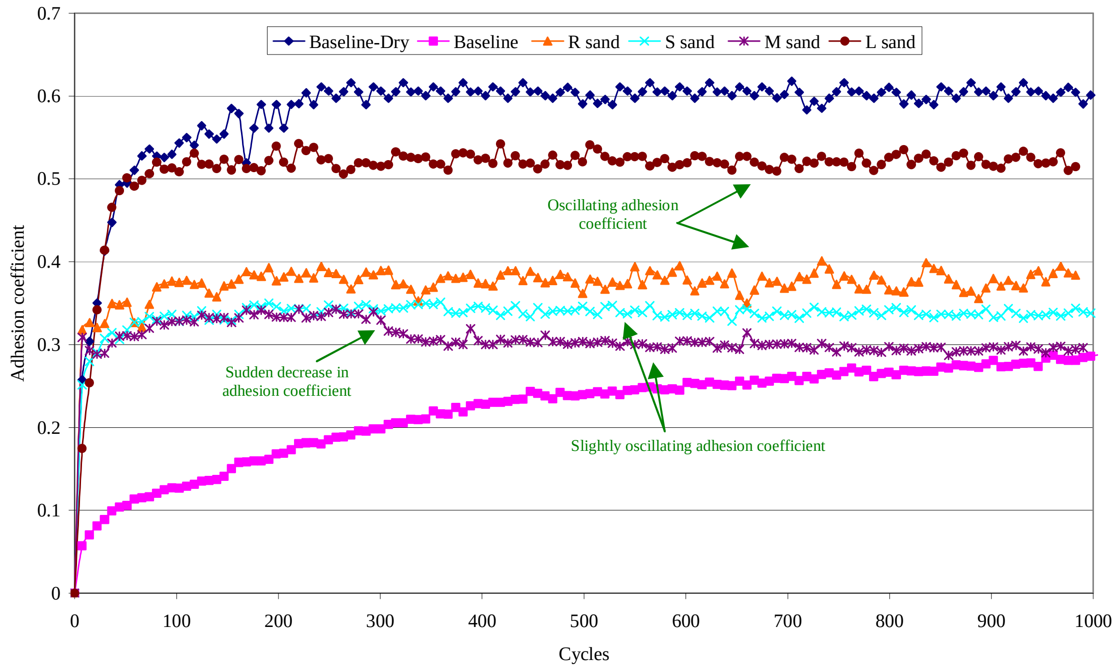

Fig. 3A.8. Leaf contaminated tests at 10% slip (reference baseline-dry without contamination).

3A.3.2. Surface microscopy

After completion of the leaf contaminated tests, the surfaces of the disks were examined under an optical microscope. The surface morphology presented considerable differences with respect to the slip applied and the sand used. At 1% slip the wheel and rail disk surfaces were covered with a coating that resembled the typical appearance of a sand-blasted surface. During sanding it is obvious that (crushed) sand particles embedded in the softer steel surfaces. These particles were repeatedly compressed under contact load, while new particles entered the contact and experienced the same situation. This process led to the formation of a coating of compacted crushed sand embedded on the disk surfaces.

It was seen that the formation of the coating was dependent on the particle size and the slip. At higher slips more metal surface was seen on the disks at the end of the test, as shown for the tests with R sand in Fig. 3A.9. Since embedded (crushed) sand particles abrade the surface of the opposite disk due to the relative motion, increased sliding distance of higher slips could reduce the possibility of coating formation and, additionally, lead to surface damage. Furthermore, less coating formation was observed to occur with larger particle sizes for the same slip. This may be caused by two facts. On one hand, larger sand particles may cause deeper abrasion and remove more coating. On the other hand, less sand particles will be entrained in the disk interface at larger particle sizes [3A.15], reducing the extent of coating formation. Therefore, there seemed to be a threshold dependent on both sand particle size and slip above which no coating would be formed.

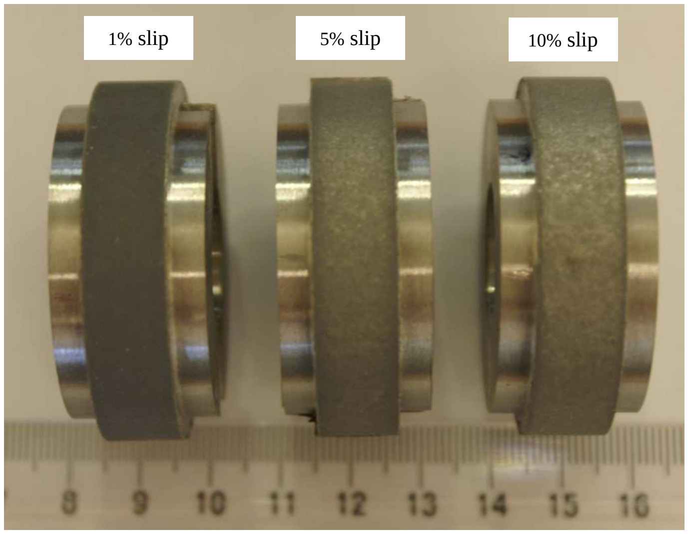

Fig. 3A.9. Photograph of the wheel disk surfaces of tests with R sand at 1, 5 and 10% slip.

In addition, surface cracks were also observed on the disk surfaces of tests at 5 and 10% slips with R and L sands. Indentations caused by the entrapped sand particles were also seen on the disk surfaces.

3A.3.3. Subsurface microscopy

The disks used in the leaf contaminated test were cut in sections in the rolling direction to examine their subsurface morphology under an optical microscope. In order to illustrate the influence of the sand particle size and slip, Fig. 3A.10 shows the subsurface micro-photographs resulting from tests with R sand at different slips, while Fig. 3A.11 corresponds to the tests with S, M, and L sands at 5% slip. Note that some scratches generated during sample preparation were not totally removed after polishing, being still visible in the micro-photographs.

The slip had a clear influence on the subsurface deformation, as shown in Fig. 3A.10. In the disks tested at 1% slip the grains were not largely deformed compared to the disks tested at 5 and 10% slip. These results correlate well with the adhesion coefficient obtained in those tests, which was higher at higher slips (see Figs. 3A.6-3A.8). At 10% slip a highly strained layer was observed near the surface of the rail and wheel disks, as indicated in Fig. 3A.10. Crack initiation was also observed at 10% slip with R sand, which may cause break-off as a flake. Such (micro-) fracture contributes to the mass loss as a result of wear due to fatigue.

Using different sand particles sizes led to distinct microstructural changes of the subsurface. It can be seen that larger particle sizes of sand caused deeper plastic deformation on the wheel and rail disks at 5% slip (see Fig. 3A.11). This agrees well with the adhesion coefficients observed at 5% slip, shown in Fig. 3A.7. In addition, higher strains near the disk surfaces were observed with larger particle sizes. These strains, if high enough, may lead to the formation of cracks, as shown in Fig. 3A.11 for the test with L sand.

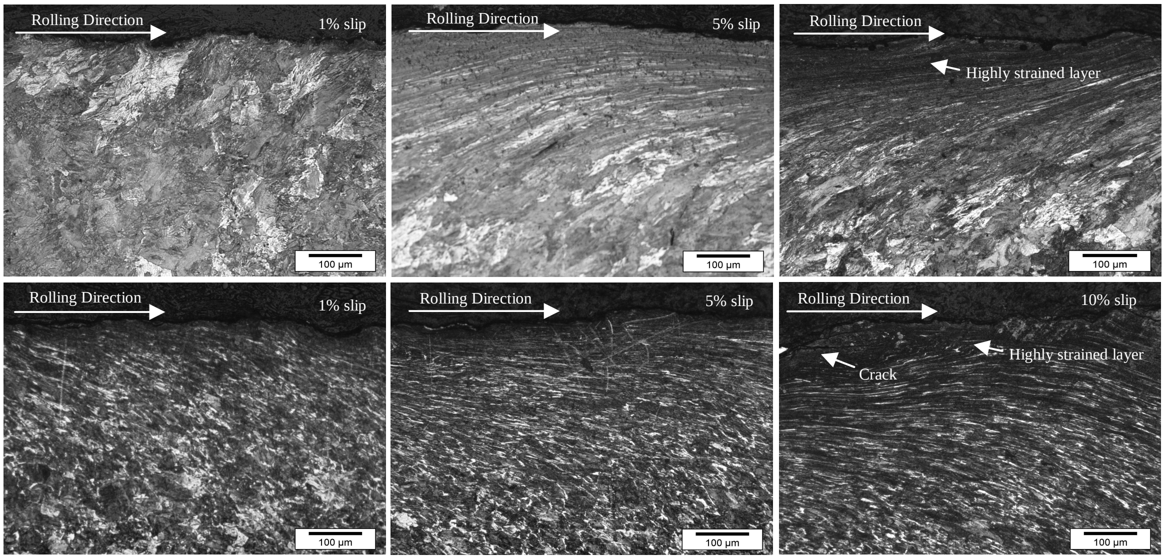

Fig. 3A.10. Subsurface micro-photographs of the longitudinal section of rail (top) and wheel (bottom) after tests with R sand at 1, 5 and 10% slip.

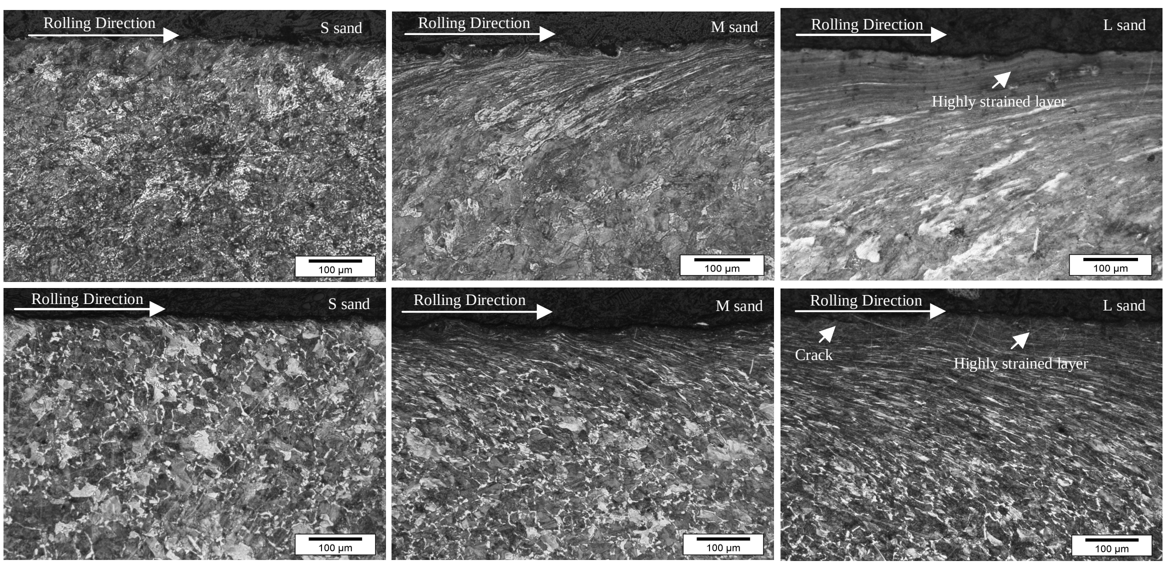

Fig. 3A.11. Subsurface micro-photographs of the longitudinal section of rail (top) and wheel (bottom) after tests with S, M, and L sand at 5% slip.

An interesting comparison is between the tests with S sand at 5% slip and R sand at 1% slip, whose adhesion history were similar (see Figs. 3A.6-3A.7). The subsurface of the disks used in those tests greatly differed, as shown in Figs. 3A.10-3A.11. The wheel disk of the test at 1% slip with R sand presented a subsurface microstructure with a certain degree of deformation in the rolling direction, whereas the wheel disk with S sand at 5% slip had an almost unaltered microstructure looking equal to the bulk. This could be explained by the presence of a third-body layer of (crushed) sand particles travelling through the disk interface in the test with S sand at 5% slip, which acted as a solid lubricant protecting the disk surfaces. The protective action of third body layers was previously outlined by other researchers [3A.21]. Thus, the relative motion (i.e. slip) between the wheel and rail disks could have been accommodated by that third-body layer of sand. Electrical insulation measurements, which were carried out in another work of the authors, corroborated that the wheel-rail contact was completely insulated in tests with S sand [3A.15], leading to a full solid lubrication in which the steel surfaces were separated. On the other hand, similar measurements showed that some steel-on-steel contact existed in tests with R sand. This may explain the deformation in the rolling direction observed in the microstructure. Moreover, differences in the subsurface were found between wheel and rail disks that can be attributed to their different microstructure, as it was described in a previous work [3A.8].

3A.3.4. Surface roughness and hardness

The surface roughness of each disk was measured at four sections, from which the initial value of average roughness (1.3 μm) was subtracted to show directly the roughening effect. The average, maximum and minimum values are given in Fig. 3A.12. It must be mentioned that some compacted coating, which could not be removed with ultrasonic vibration in a bath of ethanol, was present in several disks upon measurement. In this way, the roughness of the resultant surface after completion of a test was measured.

The surface of all disks appeared to have been roughened up during sanding. In general, the wheel presented a rougher surface than the rail, which could be attributed to the differences in hardness as sand particles would be more likely to indent the softer wheel surface. Furthermore, a tendency of having rougher surfaces at higher slips for most of the sands seemed to exist. This can be attributed to the increased abrasive effect of sand particles with the slip. It must be noted that although the surface roughness was measured at four different sections of the disks to obtain a reasonable consistency, large scatter (i.e. difference between the average value and the max and min values) was obtained in the measurements mostly due to the non-uniform presence of indentations on the surfaces.

In Fig. 3A.12 it can be seen that S sand led to the least rough surfaces and minimum scatter, which could be attributed to its small particle size. The extraordinary high roughness measured for the test with M sand at 10% slip was due to the existence of a broken coating of compacted crushed sand. Moreover, L sand seemed to cause less rough surfaces than M and R sand. This could be related to the balance existing between the number of particles entering the disk interface and their effective abrasive size. It has been shown in another work that with larger particle sizes, less number of particles enters the disk interface [3A.15] and, therefore, the abrasion could be reduced. On the other hand, larger particles cause deeper abrasion.

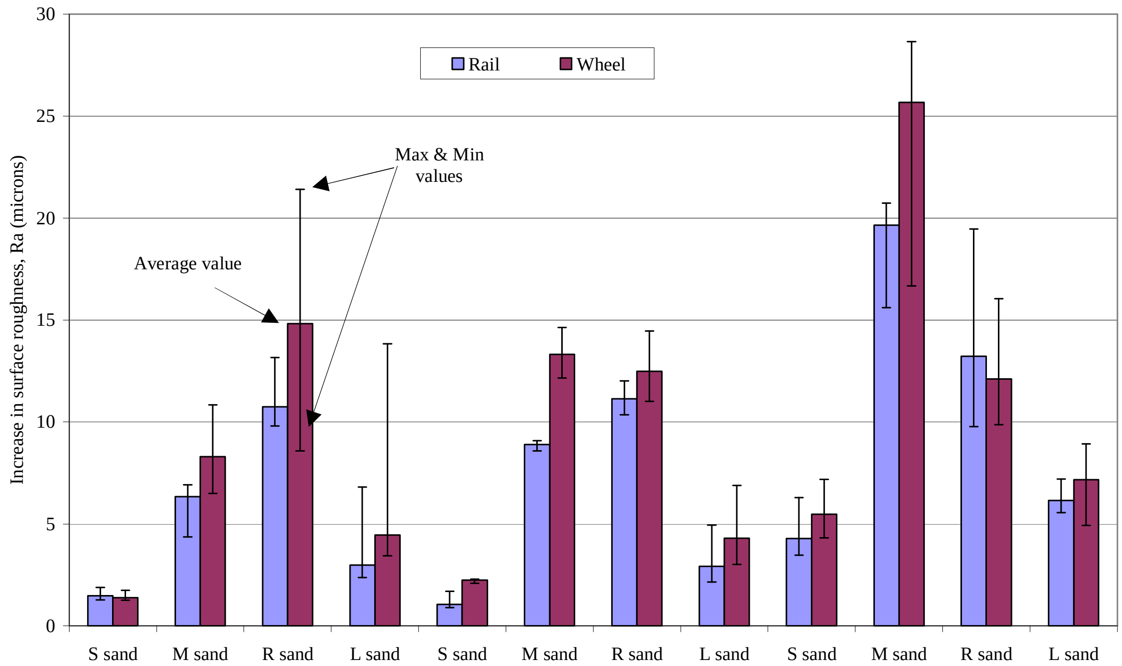

Fig. 3A.12. Average, maximum and minimum values of the increase in surface roughness of rail and wheel disk surfaces after tests with all sands at different slips (from left to right, 1% to 10% slip).

The surface macro-hardness of the disks was measured with a Hardness Testing Machine ZHV20/Z2.5 (Zwick Roell Group) by using a Vickers indenter at 20 kg. Besides the remaining plastic deformation, this machine can continuously measure the indentation depth as the load increases, so not only plastic, but also elastic deformation was considered in the measurement. Due to the opaque surface of some test disks after sanding, it was not possible to measure the Vickers hardness directly as the diagonals of the indentation were not entirely clear. Hence, the Martens Hardness (HM), also known as universal hardness, was employed. By means of Eq. 3A.3, the modified method to Vickers (HVT) could be obtained.

$$HVT = 0.102 \cdot HM \qquad (3A.3)$$

Fig. 3A.13 depicts the average HVT of the wheel and rail disks after tests with S, M and L sands at 1% and 10% slip. Note that the hardness value of the bulk material was subtracted for the results given in Fig. 3A.13 to show the increase in hardness after each test. It can be seen that bigger particle sizes caused more work-hardening of the disk surface for both wheel and rail at all slips. This is in good agreement with the subsurface micro-photographs, which showed that the grain deformation in the near-surface region was increased when using larger particle sizes (see Fig. 3A.11). Furthermore, the surface work-hardening was increased with the slip, which can be attributed to the higher tangential stresses occurring at higher slips that could have led to more grain deformation (see Fig. 3A.10). Moreover, comparing the right and left plots of Fig. 3A.13 it can be seen that the rail work-hardened more than the wheel. This may be a consequence of the different steel microstructure as it was also observed in a previous work [3A.8].

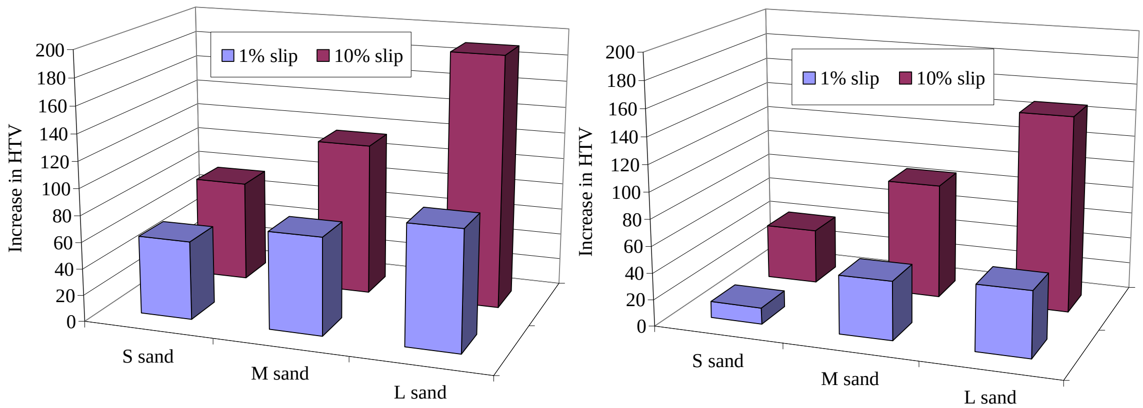

Fig. 3A.13. Increase in average HVT of rail (left) and wheel (right) disks after tests with S, M, and L sand at 1 and 10% slip.

3A.3.5. Mass loss and wear mechanisms

The mass loss of the wheel and rail disks was measured to get an indication of the wear rates. The results are depicted in Figs. 3A.14-3A.15. Comparing the two figures it can be seen that the softer wheel disk wore more than the harder rail disk under all test conditions. Note that in most of the tests the difference was not large, except for the case of the R sand test at 10% slip. The higher wheel wear rates are found in contradiction with observations on three-body abrasion tests made by other researchers who showed that the harder surface experienced higher wear rates [3A.22, 3A.23]. A possible explanation could be given by the fact that sand particles may indent and abrade deeper in the softer wheel disk than in the rail disk. Furthermore, the coating, which could not be removed with ultrasonic vibration in a bath of ethanol, may have influenced the results by increasing the apparent mass of the disks. This could explain the low mass loss observed at low slips in Figs. 3A.14-3A.15, particularly with L sand. Mass increase of the specimens at the initial stage of three-body abrasion tests was previously observed by other researchers [3A.24].

In addition, cracks have been observed in several tests, particularly in tests with larger sands and higher slips. This may indicate that a (micro-) fracture process is also occurring (see Figs. 3A.10-3A.11). The cracks may be attributed to low cycle fatigue due to repeated ploughing, but they could also be a result of subsurface cracking initiated at indentations as observed in previous work carried out with UK railway sand [3A.12].

The influence of the particle size on wear rates seemed to be dependent on the slip. At 10% slip the mass loss seemed to follow the trend of the adhesion coefficient (see Fig. 3A.14-3A.15). In general, wear caused by abrasion is promoted by the particle size. In this work, this tendency is broken by the test with M sand. This could be attributed to the existence of a broken coating on the disk surfaces of M sand test observed upon post-test examination. In addition to abrasion, the similar trends of the mass loss and adhesion could have been caused by an increase in crack formation due to higher strain accumulation. On the other hand, the tendency seemed to be reversed at 1% slip (see Figs.

3A.14-3A.15. Since no cracks were observed, abrasion may have been the only cause of wear at 1% slip. The amount of abrasion for a given slip is mainly determined by the size and amount of particles travelling through the disk interface. Electrical insulation measurements of the disk interface showed that decreasing the particle size promotes particle entrapment and that complete insulation was achieved with M and S sands [3A.15]. This may explain the fact that M sand caused the largest mass loss at 1% slip because the abrasion caused by M sand could have been maximized by a balance between particle size and number of particles entrapped in the contact.

Moreover, higher wear rates of wheel and rail disks were experienced at higher slips for all sands tested. At higher slips the (crushed) sand particles slide longer distances when travelling through the disk interface, which causes more abrasion and, therefore, higher wear rates. Besides, material removal due to crack formation is promoted by higher slips because of the higher adhesion coefficient that leads to higher strains.

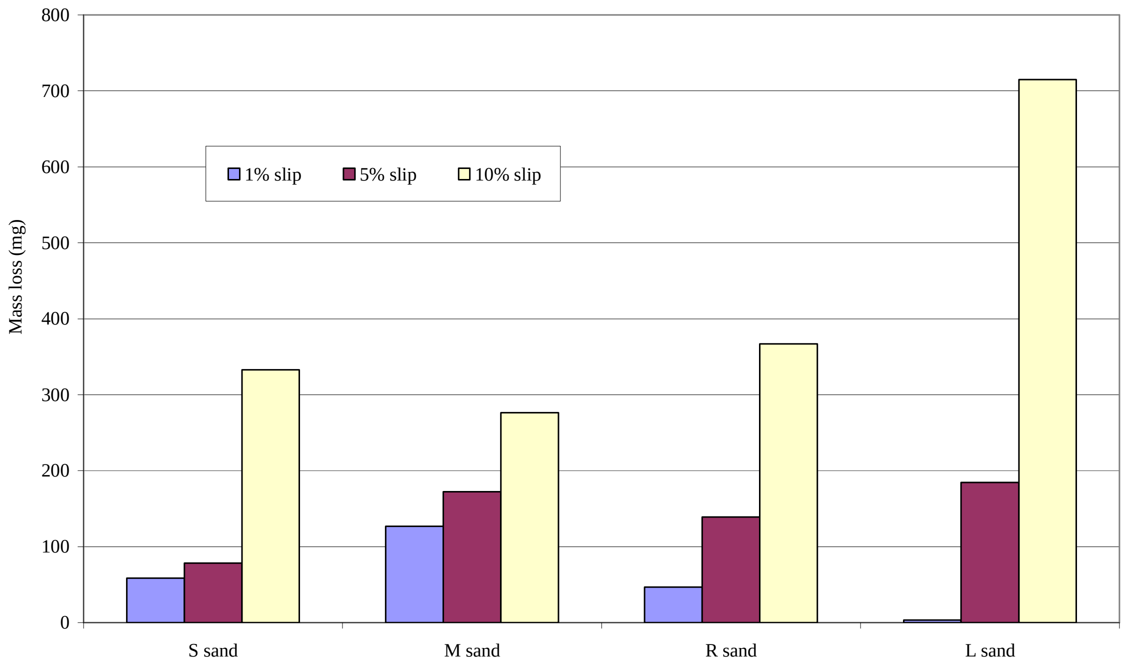

Fig. 3A.14. Mass loss of rail disk after tests with all sands at 1, 5 and 10% slip.

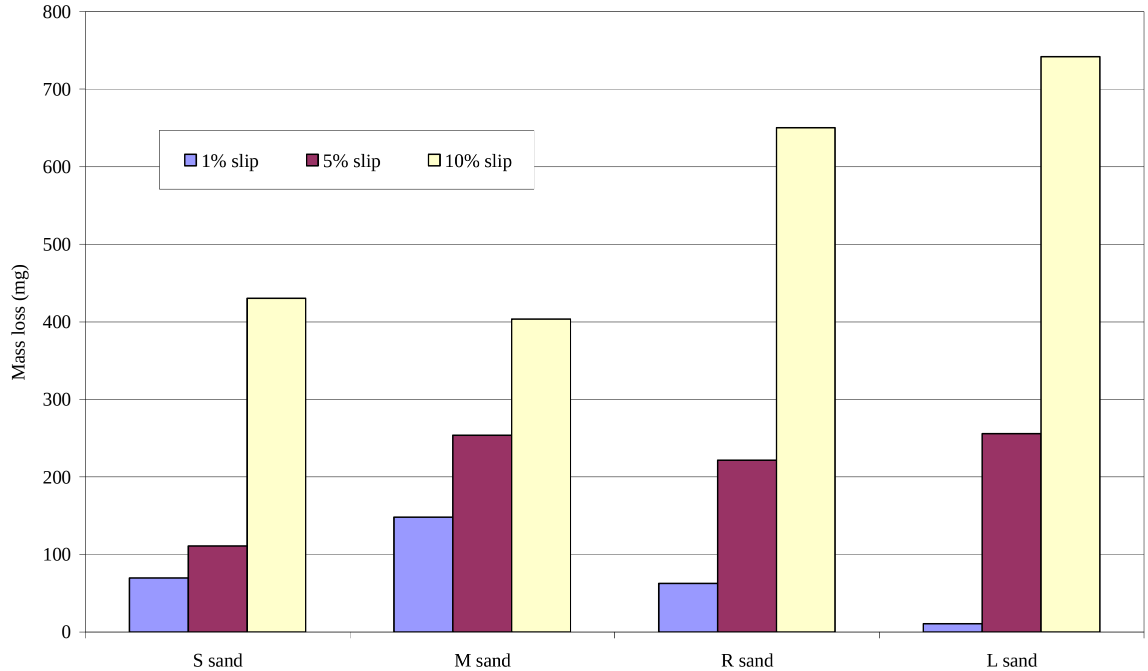

Fig. 3A.15. Mass loss of wheel disk after tests with all sands at 1, 5 and 10% slip.

3A.4. Discussion

Previous investigations on FMs highlighted the importance of the particle size on the removal of leaf layer contamination [3A.4]. Once hard abrasive particles have penetrated through the contamination layers, if they are large enough, they will prevail in the wheel-rail contact and help in removing the contamination gradually with the wheel passages. In these tests, the continuous application of sand rapidly led to dry contact conditions as leaf layers were removed. Thus, a clear influence of the sand particle size on the adhesion recovery could not be seen. The authors will separately publish an investigation in leaf contaminated wheel-rail contacts on the adhesion recovery enhanced by sand applied in less amount to show the influence of the number of sanding axles of rolling stock together with sand particle size and wheel slip [3A.25].

In many sanding systems the sand is automatically applied on the rails once the WSP/TC systems of the train detect a wheel slip (or slide) above a given slip threshold. Investigations on the leaf layer removal by sanding have shown that the adhesion recovery can be enhanced with the increase in slip [3A.25]. However, this paper has shown that higher wear rates are obtained as the slip is increased for all sands tested. Therefore, the optimum slip for sanding at which adhesion recovery can be maximized should also guarantee that admissible wear rates of wheels and rails are not compromised.

In this work, a coating of compacted (crushed) sand has formed on the disk surfaces, particularly at low slips and small particle sizes. This coating is the consequence of the continuous application of sand to a wheel-rail contact simulated by the same two disks in constant contact. In recent field tests, it has been observed that some (crushed) sand particles may remain on the top of the rail after four wheel locomotive passages over a sanded track [3A.26], as shown in Fig. 3A.16. But, in practice sand is only applied locally as low adhesion conditions are encountered and only a few axles are equipped with sanders, decreasing the likelihood of a continuous sanded wheel-rail contact that could lead to the coating formation as in the laboratory.

Fig. 3A.16. Photograph of the top of a rail after four locomotive wheel passages over a sanded track.

In this work, the same feed rate has been employed for all tested sands in order to reproduce what happens in practice among railways using similar feed rates but different sized sands, as explained in Section 1. Laboratory investigations have shown that the feed rate can greatly influence the adhesion coefficient obtained during sanding [3A.15]. In future investigations the effect of feed rate on damage to wheels and rails for a given particle size could be treated in a similar approach to the one presented in this work.

Furthermore, it needs to be mentioned that the results of this work correspond to the low speed regime. In this regime and also up to 11-17 m/s, the adhesion requirements for most types of (conventional) rolling stock (at least for the Dutch railways) are at their maximum. In future works, it may be interesting to investigate the adhesion and wear caused by sanding at higher rolling velocities than the one used in this work, especially up to 17 m/s. In such investigations, the effect of the train's slipstream may also need to be taken into account.

It is necessary to emphasize that there were several limitations in this testing that impede a quantitative comparison with the actual situation in railway sanding, as already explained in previous works [3A.12, 3A.27]. The contact geometry of the disks was clearly different from reality, as the typical wheel diameter (between 860 mm and 1250 mm for most rolling stock using sanders) was reduced to 47 mm in the tests, and the rail was modeled by an Ø47 mm rail disk. Since both disks are in complete rotational motion, sand could not rest on the rail as it happens in practice. The length of the contact area in the rolling direction was 0.5 mm in these tests. Although most of the particles could break up into much smaller sizes, some of the (crushed) sand particles travelling through the disk interface may be larger than the contact length. This could have led to a behavior different from the actual situation. In future studies, it is may be wise to investigate the change in size of sand particles travelling through the contact, possibly with a similar approach as presented in [3A.23]. Moreover, in this testing more sand could have been entrained than in practice because the sand was directly applied to the disks contact in the absence of cross wind and/or train's slipstream. Therefore, field tests should be undertaken in future works to examine the applicability of the laboratory results to the actual wheel-rail contact and to determine to what extent the scaled twin-disk test can approximate the reality under different operating conditions. A first attempt in this direction has recently been undertaken by the authors [3A.26].

3A.5. Conclusions

A laboratory investigation on the influence of the particle size and slip during sanding on the adhesion and wear in the wheel-rail contact has been presented in this paper. The wheel-rail contact has been simulated by means of a twin-disk roller rig in rolling-sliding motion under closely controlled conditions. Three different slips have been considered in the testing that are representative of traction and braking operations. Four different sands have been used to investigate the influence of the particle size. Based on the results, the following conclusions can be drawn:

a) Leaf layers are rapidly removed from the disks surfaces by continuous application of the abrasive sand particles. Leaf layer removal needs to be investigated in tests with less amount of sand applied to obtain better grasp of the adhesion recovery brought by sanding.
b) Large particle sizes and high slips lead to a higher adhesion coefficient. This in turn leads to deep plastic deformation in the wheel and rail disks.
c) Large particle sizes and high slips increase the work-hardening caused on the surfaces of both wheel and rail disks.
d) The particle size has a strong influence on wear that is dependent on the slip. At high slips the wear trend seems to follow the adhesion coefficient, whereas at low slips this trend seems to be precisely reversed.

References

[3A.1] Rail Safety and Standards Board, Review of low adhesion research, 2004.
[3A.2] U. Olofsson and K. Sundvall: Influence of Leaf, Humidity and Applied Lubrication on Friction in the Wheel-Rail Contact: Pin-on-Disc Experiments. Proc. Inst. Mech. Eng. Part F, 2004, vol. 218, pp 235-242.
[3A.3] P.M. Cann: The 'Leaves on the Line'—a Study of Leaf Residue Film Formation and Lubricity under Laboratory Test Conditions. Tribology Letters, 2006, vol. 24, pp 151-158.
[3A.4] Z. Li, O. Arias-Cuevas, R. Lewis, and E.A. Gallardo-Hernandez: Rolling-Sliding Laboratory Tests of Friction Modifiers in Leaf Contaminated Wheel-Rail Contacts. Tribology Letters, 2009, vol. 33, pp 97-109. Available online for public access at http://www.springerlink.com/content/y812p16340215p67/.
[3A.5] H.I. Andrews: Railway Traction—the Principles of Mechanical and Electrical Railway Traction, Elsevier, 1986, pp 33-62.
[3A.6] Railway Group Standard GM/RT 2461, Sanding Equipment Fitted to Multiple Units and On-track Machines, 2001.

[3A.7] W. Voges, and P. Spiess: Optimizing Services with EMU ET42x in Autumn 2004 and 2005. Proc. 7th World Congress on Railways Research, Montreal, Canada, 4-8 June, 2006.
[3A.8] O. Arias-Cuevas, Z. Li, R. Lewis, and E.A. Gallardo-Hernandez: Rolling-Sliding Laboratory Tests of Friction Modifiers in Dry and Wet Wheel-Rail Contacts. In press, Wear, 2009.
[3A.9] M.W. Astle-Fletcher: Mechanical Methods of Improving Rail Adhesion. Proc. Inst. Mech. Eng., 1963-64, vol. 178, pp 185-205.
[3A.10] S. Kumar, P.K. Krishnamoorthy, and D.L. Prasanna Rao: Wheel-Rail Wear and Adhesion With and Without Sand for a North American Locomotive. J. Eng. for Industry, Trans. ASME, 1986, vol. 108, pp 141-147.
[3A.11] E.A. Gallardo-Hernandez, and R. Lewis: Twin Disc Assessment of Wheel/Rail Adhesion. Wear, 2008, vol. 265, pp 1309-1316.
[3A.12] R. Lewis, and R.S. Dwyer-Joyce: Wear at the Wheel-Rail Interface when Sanding is Used to Increase Adhesion. Proc. Inst. Mech. Eng. Part F, 2006, vol. 220(1), pp 29-41.
[3A.13] G. Gfatter, D. Lang, H. Kalbas, G. Krause, W. Rychli: Sanding Systems, 2nd ed., Knorr-Bremse GmbH, 2002, pp 21.
[3A.14] UIC737-2, Mesures a Prendre Pour Ameliorer la Sensibilite au Shuntage des Circuits de Voie, 1980.
[3A.15] O. Arias-Cuevas, Z. Li, and R. Lewis: Investigating the Lubricity and Electrical Insulation Caused by Sanding in Dry Wheel-Rail Contacts. Submitted for publication, 2009.
[3A.16] D.I. Fletcher, J.H. Beynon: Development of a Machine for Closely Controlled Rolling Contact Fatigue and Wear Testing. J. Testing and Evaluation, 2000, vol. 28, pp 267-275.
[3A.17] European Standard EN13262: Railway Applications – Wheelsets and Bogies – Wheels – Product requirement (2004).
[3A.18] H. Chen, T. Ban, M. Ishida, T. Nakahara: Experimental Investigation of Influential Factors on Adhesion between Wheel and Rail under Wet Conditions. Wear 265 (2008) 1504-1511.
[3A.19] R. Lewis, E.A. Gallardo-Hernandez, T. Hilton, T. Armitage: Effect of oil and water mixtures on adhesion in the wheel/rail contact. Journal of Rail and Rapid Transit 223 (2009) 275-283.[3A.17] L. Fang, X.L. Kong, J.Y. Su, Q.D. Zhou: Movement Patterns of Abrasive Particles in Three-body Abrasion. Wear, 1993, vol. 162-164, pp 782-789.
[3A.20] L. Fang, X.L. Kong, J.Y. Su, Q.D. Zhou: Movement Patterns of Abrasive Particles in Three-body Abrasion. Wear, 1993, vol. 162-164, pp 782-789.
[3A.21] Y. Berthier, S. Descartes, M. Busquet, E. Niccolini, C. Desrayaud, L. Baillet, M.C. Baietto-Dubourg: The Role and Effects of the Third Body in the Wheel-Rail Interaction. Fatigue & Fracture of Engineering Materials & Structures, 2004, vol. 27, pp 423-436.
[3A.22] L. Fang, Q.D. Zhou, Y.J. Li: Movement Patterns of Abrasive Particles in Three-body Abrasion. Wear, 1991, vol. 151, pp 313-321.
[3A.23] D.G. Grieve, R.S. Dwyer-Joyce, and J.H. Beynon: Abrasive Wear of Railway Track by Solid Contaminants. Proc. Inst. Mech. Eng. Part F, 2001, vol. 215, pp 193-205.

[3A.24] A. Misra, and I. Finnie: An Experimental Study of Three-body Abrasive Wear. Wear, 1983, vol. 85, pp 57-68.
[3A.25] O. Arias-Cuevas, Z. Li, R. Lewis, and E.A. Gallardo-Hernandez: Laboratory Investigation of Sanding Parameters to Improve Adhesion in Leaf Contaminated Wheel-Rail Contacts. Submitted for publication, 2009.
[3A.26] O. Arias-Cuevas, Z. Li: Field Investigations on Rolling Stock Components Designed to Overcome Low Adhesion Related Problems. Proceedings of the 2010 Joint Rail Conference, April 27-29, 2010, Urbana-Champaign, Illinois (USA).
[3A.27] R. Lewis, R.S. Dwyer-Joyce, J. Lewis: Disc Machine Study of Contact Isolation During Railway Sanding. Journal of Rail and Rapid Transit 217 (2003) 11-24.

Chapter 3, Part B

Laboratory tests on adhesion and electrical insulation[VIII]

ABSTRACT

The adhesion (or available friction) in the wheel-rail contact is the most important parameter for the braking and traction operation of rail vehicles. Since the beginning of railway transportation, sanding from the locomotive has been a common practice to enhance the wheel-rail adhesion. In recent years, sanding from electrical multiple units and sand-based friction modifiers have been adopted in some railway networks to overcome low adhesion incidents caused by contamination like autumn leaves. Although sanding has been proven to improve the adhesion under most of the typical contamination conditions, laboratory and field investigations have shown that sand may act as a solid lubricant in dry wheel-rail contacts. Nevertheless, the influence of the current sanding parameters on the solid lubrication effect has not been entirely investigated. Depending on the resulting adhesion coefficient, the traction and braking operations of rail vehicles could be affected. Furthermore, the influence of those parameters on the electrical insulation is also of special importance because it may affect the train detection. This paper presents a laboratory investigation of the influence of three sanding parameters (i.e., feed rate, particle size, and slip) on the adhesion and electrical insulation in dry wheel-rail contacts. The tests have been carried out with a twin-disk roller rig in rolling-sliding motion under closely controlled conditions. Three different slips representative of the actual traction and braking operations have been considered. Sands of four different sizes and up to five feed rates of sand have been used. The results show that using smaller particle sizes and higher feed rates promotes the lubrication and causes more electrical insulation in the wheel-rail contact. Furthermore, the increase in slip is found to reduce the lubrication, leading to a higher adhesion coefficient.

[VIII] This chapter has been published as: O. Arias-Cuevas, Z. Li, R. Lewis: Investigating the Lubricity and Electrical Insulation Caused by Sanding in Dry Wheel-Rail Contacts. Tribology Letters 37 (2010) 623-635.

3B.1. Introduction

The friction between wheel and rail is a crucial factor in railway transportation, as it may limit the acceleration and braking capabilities of a train. The increasing demands in railway transportation have led to faster trains with higher accelerations and decelerations; however, the wheel-rail adhesion still remains limited by the available friction between the steel wheels and rails. Consequently, low adhesion problems have been present in many railway networks in recent decades, especially those related to leaf contamination in autumn [3B.1-3B.4]. Recent field investigations have demonstrated that leaf layers in dry conditions can lead to low adhesion incidents as well as in humid conditions [3B.5]. Since the beginning of railways, sanding from the locomotive has been a common practice to enhance the wheel-rail adhesion [3B.6]. In recent years, sanding from electrical multiple units (EMUs) has also been adopted in some railways to overcome low adhesion conditions [3B.1, 3B.7-3B.8]. Besides sanding, many railways have opted for using friction modifiers (FMs), some of which may contain sand or other solid particles to increase the adhesion level under certain contamination conditions [3B.1, 3B.4, 3B.9].

Although railway sanding has been proven to improve the adhesion under most of the typical contamination conditions, laboratory and field investigations have shown that sand may act as a solid lubricant in dry wheel-rail contacts [3B.6, 3B.10-3B.12]. Lubricity is in the scope of this paper identified with the reduction of the adhesion coefficient caused by sanding. Depending on the resulting adhesion coefficient, the traction and braking operations of rail vehicles could be affected. Andrews [3B.6] investigated the adhesion values given by some mineral powders (silica sand among them) with a full-scale test bogie. He proposed an empirical relationship in which the adhesion coefficient increased proportionally with the product of particle hardness and size of the mineral powders. However, only one particle size was used for each mineral tested, and his empirical relationship was restricted to particle sizes smaller than 0.4 mm. Kumar et al. [3B.10] investigated in the laboratory the adhesion experienced by locomotive wheels during sanding and compared it to adhesion levels of dry clean contacts. They showed that the lubricant effect may only occur above a certain feed rate, but the feed rates of their study were below those used in current practice. They also showed that the adhesion coefficient increased with slip; however, only slip up to 1% was used in their work, which is below those found in braking and traction practice under low adhesion conditions. Boiteux et al. [3B.11] presented the results of some braking tests performed in field under different contact conditions, in which the adhesion and wheel (gross-) slip were measured with two measuring wheelsets. They showed that sanding on rails covered by fallen leaves improved the adhesion, while sanding slightly reduced the adhesion on clean rails. Gallardo-Hernandez et al. [3B.12] showed that sanding can help to overcome low adhesion caused by leaves and water, but it can decrease the adhesion in clean contacts. The findings of all those studies lead to the conclusion that feed rate, particle size, and wheel slip are the most influencing parameters on the solid lubrication effect of railway sanding. However, the influence of all those parameters was not investigated in a single study, and most of the investigations considered a range of parameter variation that does not correspond to the current sanding practice.

Furthermore, the most negative side effect of railway sanding is that it may insulate the electrical conductivity of the wheel-rail contact, depending on the amount of sand entrapped in the contact. The increase in electrical insulation is identified by the increase in the voltage across the wheel-rail contact due to sanding. In practice, if the voltage surpasses a certain threshold value, the functioning of the railway track circuits that are used for the detection of trains can be affected. Thus, the railway traffic signaling would be impaired, causing traffic disruption and perhaps, in the worst case, even collisions of trains. This has led railway organizations to establish standards on railway sanding that guarantee correct functioning of track circuits [3B.13]. Lewis et al. [3B.14, 3B.15] investigated the electrical insulation of the wheel-rail contact caused by sanding in both static and dynamic tests. Their results showed that the electrical insulation of the wheel-rail contact varied with the sand feed rate, and complete electrical insulation may occur above a certain sand feed rate. Nevertheless, no study is found in the literature that considers the influence of the particle size and the wheel slip on the electrical insulation of the wheel-rail contact caused by sanding. This understanding becomes essential for an optimization of the sanding practice as correct train detection is of prime importance in railway transportation.

This paper presents a laboratory investigation on the influence of the sand particle size, feed rate, and wheel slip on the lubricity and electrical insulation caused by railway sanding in dry contact conditions. The wheel-rail contact has been simulated in rolling-sliding conditions by means of a twin-disk roller rig under closely controlled laboratory conditions. During each test the adhesion coefficient and the electrical voltage across the wheel-rail contact have been recorded. Four different sands have been used to account for the influence of the particle size. Three different slips representative of the actual traction and braking operations have been considered, and up to five feed rates have been applied in this work.

3B.2. Test description

3B.2.1. Test set-up

The SUROS (Sheffield University ROlling Sliding) roller rig was used to simulate the wheel-rail contact in rolling-sliding conditions. The SUROS roller rig is shown in Fig. 3B.1 and described in detail in [3B.16]. The test disks were mounted on independent shafts. By means of a hydraulic jack, a controlled load of 4.7 kN was applied on the disks producing a maximum Hertzian pressure of 1.2 GPa in the contact zone, which is representative of the contact between wheel tread and railhead for passenger trains in the Netherlands. Since cylindrical disks were used in the experiments, a line contact of 10 mm width was present (see Fig. 3B.2).

In the tests the rotational speed of the rail was maintained at 400 rpm, equivalent to 0.98 m/s of rolling speed. The wheel disk rotated faster than the rail disk to realize the slip. The slip is defined in Eq. 3B.1, where w and r are the rotational speed and rolling radius of the disks, respectively. Tests were carried out at three different wheel slips, namely 1, 5 and 10%, which are typical values found in actual traction and braking operations. Considering the range of wheel slip used in the tests and the rolling speed of the rail disk, the mean rolling speed in the contact was between 0.99 and 1.07 m/s in the tests. This low speed regime is especially critical for those vehicles fitted with sanders that apply sand at a fixed rate in kg/min as more sand is laid per length of rail. A personal computer was used to acquire the data and to control both the speed and the load during each test. The adhesion coefficient was calculated with the readings of the torque transducer and the load cell, as indicated in Eq. 3B.2, where T represents the torque and F_N is the normal contact force. During calibration of the test rig, the uncertainty of the contact pressure was reported to be less than ± 2%, while the standard error of the torque was found to be 0.30 Nm [3B.16]. Considering the values of the torque in this work, the maximum uncertainty in the torque readings was ± 2.72%. Moreover, a hygrometer and a thermometer were placed next to the roller rig to monitor the ambient relative humidity and temperature in the tests. Measured values varied between 22 °C and 23.6 °C in temperature, and between 30% and 43% in relative humidity, which are values close to typical conditions of dry days.

$$Slip = \frac{w_{wheel} \cdot r_{wheel} - w_{rail} \cdot r_{rail}}{\frac{(w_{wheel} \cdot r_{wheel} + w_{rail} \cdot r_{rail})}{2}} \cdot 100\% \tag{3B.1}$$

$$\mu_{adhesion} = \frac{T}{F_N \cdot r_{rail}} \tag{3B.2}$$

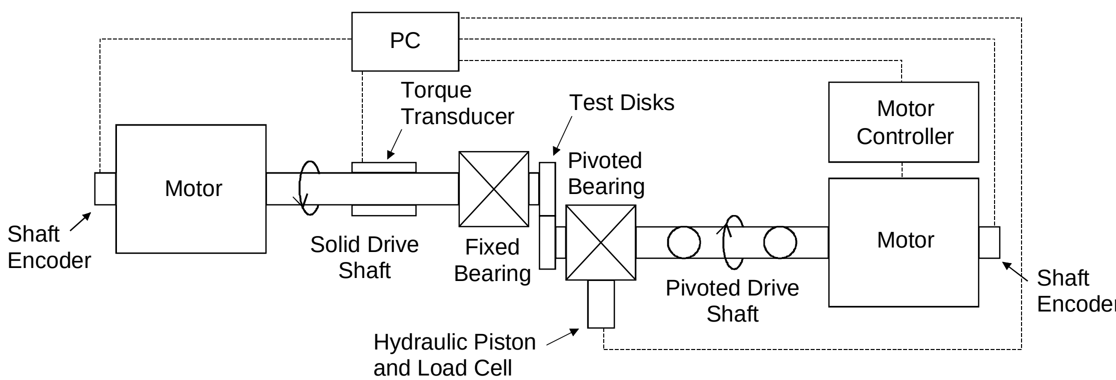

Fig. 3B.1. Schematic representation of the SUROS roller rig set-up employed in the tests.

The test disks were cut from rails and wheel tires retired from service on the Dutch railway network; R260Mn and B5T steel for the rail and wheel disks, respectively. The disks were machined with their axes perpendicular to the longitudinal axis of both wheel and rail, as shown in Fig. 3B.2. The Vickers macro-hardness of the wheel and the rail steel used in the tests was measured as $267HV_{20kg}$ and $281HV_{20kg}$ on average, respectively. The roughness of the disks was measured with a profilometer, with an average value 1.3±0.2 µm. This value is close to values of roughness measured with a Hommel tester on the running band of rails in field. Furthermore, the European standard for the manufacturing of wheels specifies that the initial surface roughness must be lower than 6.3 µm on the running band on average [3B.17]. However, laboratory investigations have shown that rough wheels tend to approach a roughness level close to the one of the smoother rails [3B.18, 3B.19].

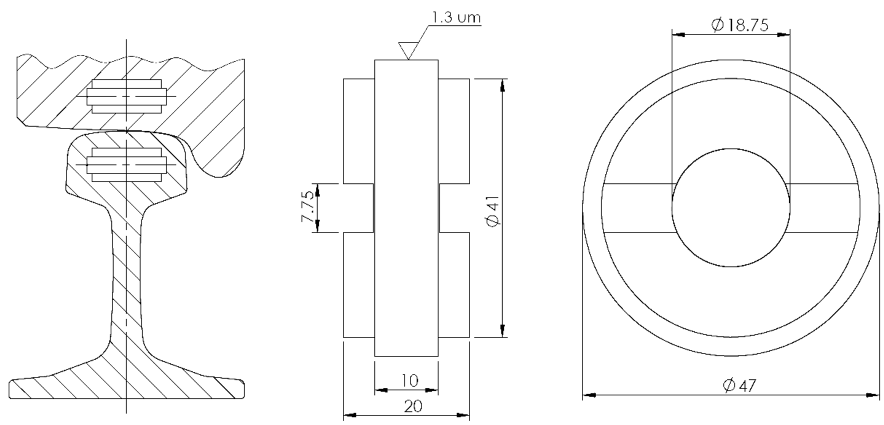

Fig. 3B.2. Orientation and dimension of the disks.

In order to monitor the electrical voltage across the disks contact area, an electrical circuit was installed on the roller rig so that voltage readings together with adhesion data could be obtained in the course of each test. Fig. 3B.3 depicts the electrical circuit, which had also been used for insulation studies on wheel-rail contacts in previous work [3B.14]. In these tests a nominal input voltage of 2 V was taken, but note that previous work demonstrated the negligible influence of the input voltage on the electrical insulation of the wheel-rail contact [3B.14]. The accuracy of the voltmeter used to monitor Vout was ± 0.5 mV, which corresponds to a maximum uncertainty of ± 0.5% for Vout ≥ 0.1 V. Due to the position of the voltmeter in the set-up, a so-called bearing resistance had to be included in the Vout readings, as indicated in Fig. 3B.3. This resistance accounted for the lubricant circulating inside the bearing, but it could be neglected once sand was entrained into the disk interface as sand dominated the Vout readings. The Vout was recorded at a sampling frequency of 2 kHz, i.e. every 0.5 mm of travel distance of the rail disk, which corresponded to the length of the contact area in the rolling direction. The readings were further averaged to have one Vout reading per rail revolution (or cycle).

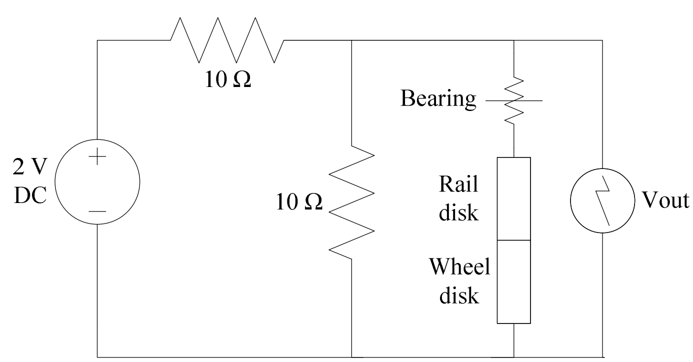

Fig. 3B.3. Schematic representation of the electrical circuit.

In the presence of an insulating contamination at the disk interface, the electrical resistance may become too high so that open circuit conditions occur, in which Vout = 1 V. If the contact is not totally insulated, the voltage readings (in Volts) correspond to Eq. 3B.3, in which *Rc* and *Rb* are the disks contact resistance and bearing resistance (in

Ohms), respectively. Additionally, a combined resistance of the total resistance seen by Vout, which is given by $Rt = Rc + Rb$, could be used to simplify the formula.

$$Vout = \frac{10\cdot(Rc+Rb)}{10+Rc+Rb}\cdot\frac{2}{10+\frac{10\cdot(Rc+Rb)}{10+Rc+Rb}} = \frac{10\cdot(Rt)}{10+Rt}\cdot\frac{2}{10+\frac{10\cdot(Rt)}{10+Rt}} \qquad (3B.3)$$

3B.2.2. Tested sands

Two types of commercial sand were used in this work: silica sand and filter sand. The silica sand had been extracted from a pit in south Germany, whereas the filter sand had been collected from a river in the Netherlands. A photograph of the sands is given in Fig. 3B.4. The particle size distribution of the sands was measured with a laser particle analyzer and is given Fig. 3B.5. The filter sand is the standard type used in the Netherlands to increase the adhesion in railways; thus, it is hereinafter referred to as Railway sand, R sand for short. Although different rocks can be seen in the sample, the weight content in SiO_2 is around 96% as given by the supplier. The particle size distribution of R sand ranged from 0.25 to 1.4 mm with a wide peak at 0.6-1 mm, as shown in Fig. 3B.5. The silica sand had a SiO_2 content around 99% according to the supplier. It was sieved in the laboratory to three different particle size ranges: small (0.06-0.3 mm, with peak at 0.15 mm), medium (0.3-0.6 mm, with peak at 0.35 mm), and large (0.85-1.6 mm, with peak at 1.2 mm). These three sands are referred in this paper as S sand, M sand and L sand, for short. Moreover, due to the similar composition and hardness of the four tested sands the particle size distribution could be considered as the only study parameter for this work.

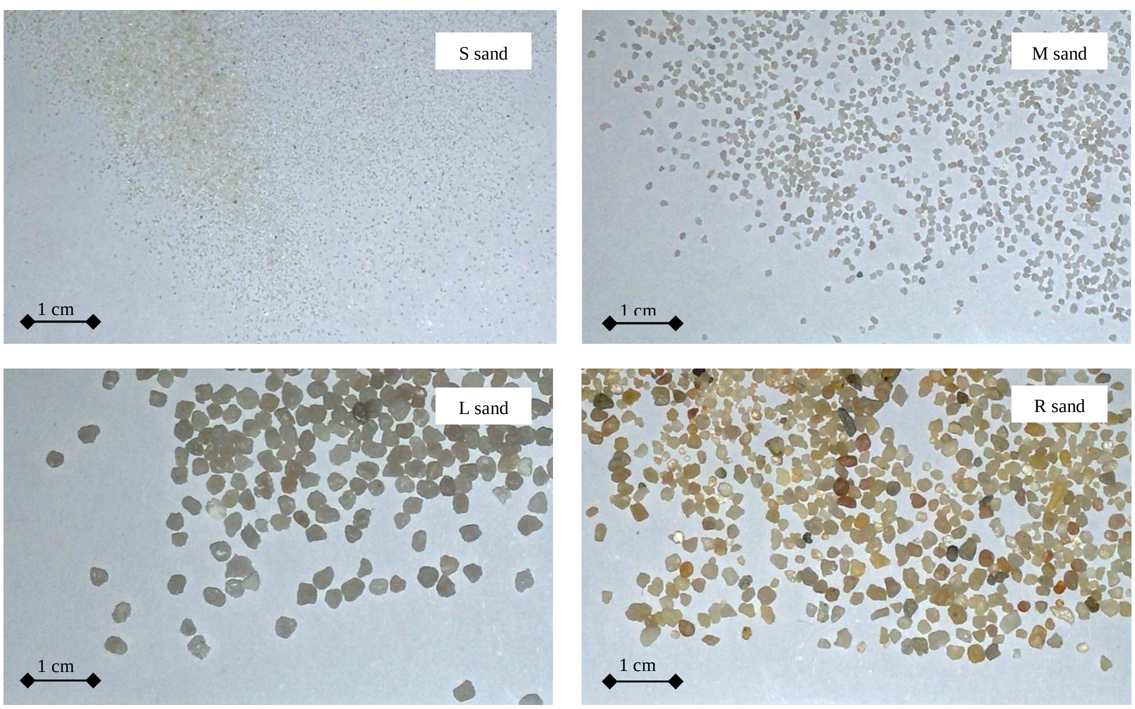

Fig. 3B.4. Photograph of the tested sands: S sand, M sand, L sand, R sand.

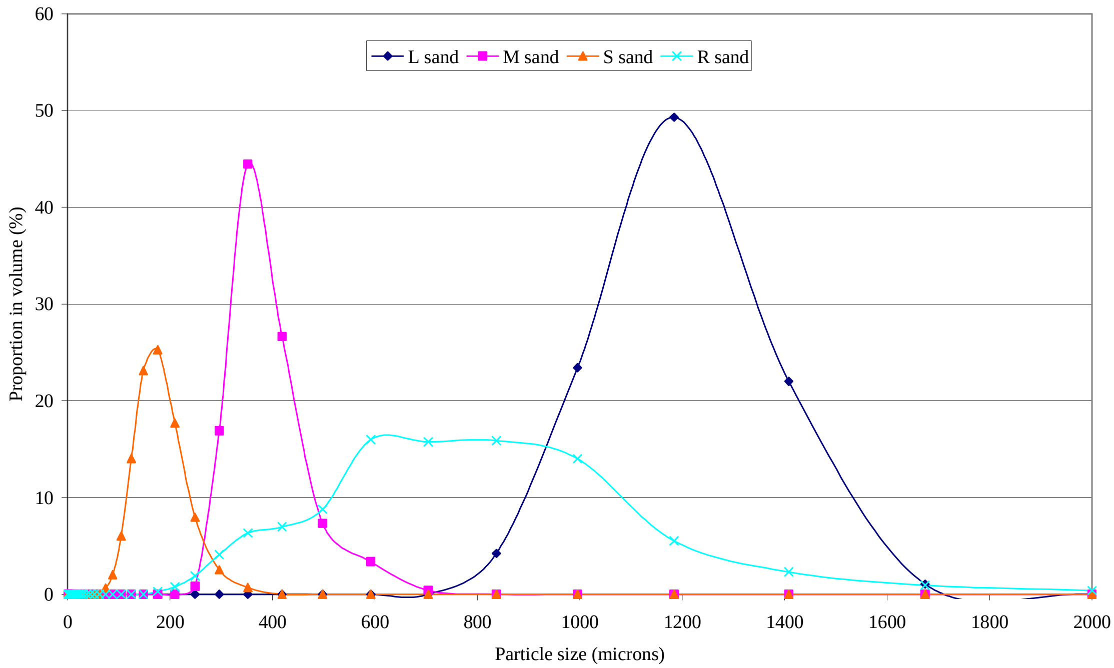

Fig. 3B.5. Particle size distribution of the tested sands obtained with the laser particle analyzer.

3B.2.3. Test procedure

In the tests the sand was fed to the disk interface by means of gravity, as shown in Fig. 3B.6. After exiting the valve, the sand passed through a PVC pipe and was oriented to the disk interface with a chute. A vacuum cleaner placed behind the disks sucked the sand into the wheel-rail contact, which simulated the compressed air system used in reality. Two funnels helped the sand feed to the PVC pipe. In order to regulate the sand feed rate, plastic syringes were used as valves. The orifice had to be modified to achieve the desired feed rate. The different particle size distribution of the four sand types required different orifice sizes because of their different bulk density. Up to five sand feed rates were used in the testing, namely FR1 = 0.75 g/m, FR2 = 1.5 g/m, FR3 = 3 g/m, FR4 = 4.5 g/m, FR5 = 7.5 g/m. In the calculation of these feed rates the rolling speed and travelled length of the rail disk are taken as reference. Note that FR5 is representative of some feed rates used in practice [3B.20].

Fig. 3B.7 depicts a generic test with two outputs: adhesion coefficient and Vout. Each single test was run with a new pair of disks and a fixed slip. Several sand applications were undertaken within one test to reduce the total number of separate tests. Each sand application lasted for around 60 cycles and some cycles between each sanding were left to account for the run-in of the disk surfaces, as shown in Fig. 3B.7. Thus, the adhesion coefficient (and correspondingly the condition of the surfaces) was always around the same level at the start of each sand application so that the results of different sand applications were comparable in one test.

Based on the Vout readings two regimes of lubrication could be identified during sanding, which are designated in this work as partial lubrication and full lubrication. In partial lubrication regime, there existed some metal-metal contact between asperities leading to readings of Vout below 1 V, but due to the presence of sand particles the Vout readings were higher than those of pure metal-metal contact, as shown in Fig. 3B.7. In the full lubrication regime, enough sand entrained the contact to separate the surfaces of wheel and rail disks, leading to open circuit conditions. Therefore, increasing the amount of sand entrained in the contact resulted in a transition from partial lubrication to full lubrication regime.

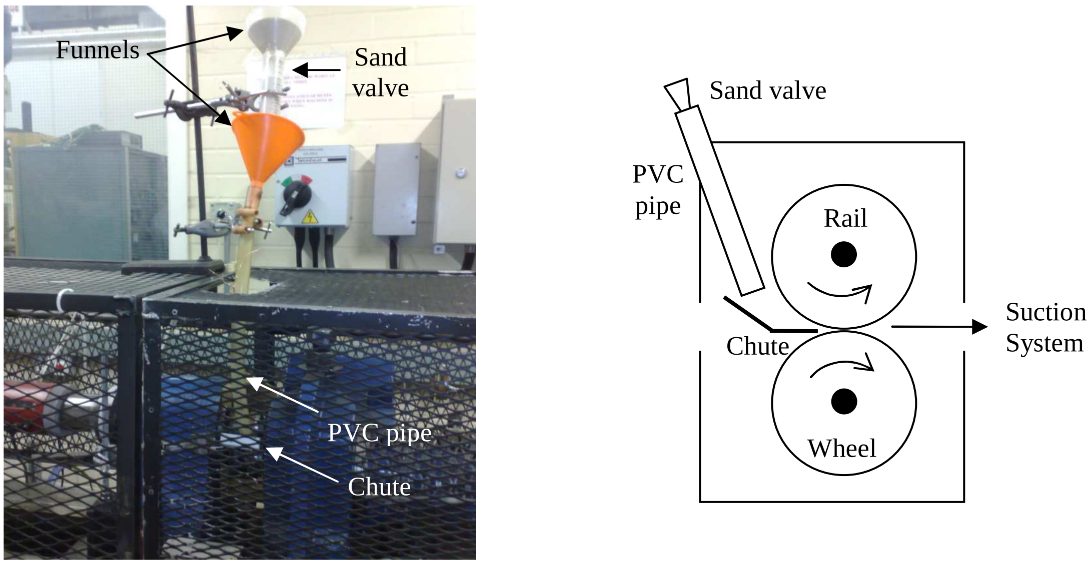

Fig. 3B.6. Sand application method in the test set-up: photograph (left) and schematic (right).

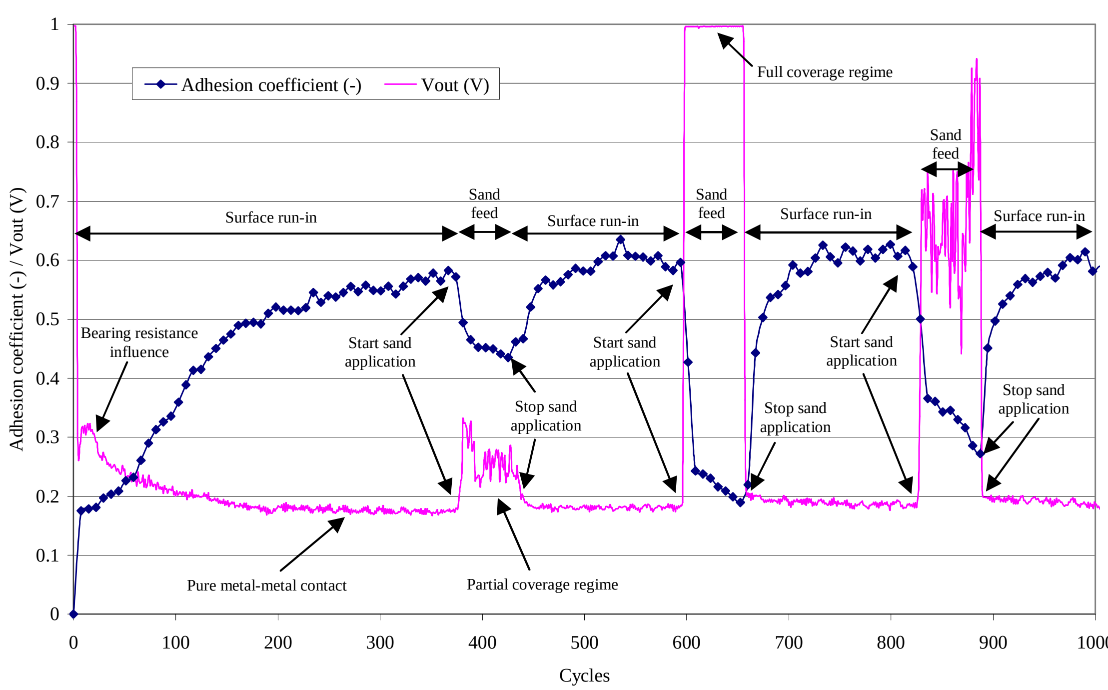

Fig. 3B.7. Representation of a generic test with several sand applications in one test.

The tests were aimed at investigating the influence of the feed rate and the particle size on both adhesion and electrical insulation at different slips. In order to analyze the influence of the feed rate, S sand was applied at five different feed rates, i.e. from FR1 to FR5 in increasing order. S sand was chosen due to its small particle size that allowed for low feed rates before clogging. On the other hand, the influence of the particle size was investigated by applying each of the tested sands at FR5 in the following order: L, M, R, and S sand. Furthermore, all tests were repeated at 1, 5 and 10% slip, so that the influence of the wheel slip on lubricity and electrical insulation could also be analyzed.

3B.3. Results

3B.3.1. Feed rate tests

The adhesion and electrical insulation results of the feed rate tests are given in Figs. 3B.8-3B.10 (note that the order of application was from FR1 to FR5 in the tests). As it was expected, the entrapment of sand in the disk interface caused an increase in the electrical insulation of the wheel-rail contact. In the tests the transition from partial lubrication to full lubrication could be observed as the feed rate increased. Open circuit conditions, and thus full lubrication regime, were reached for the highest feed rate, as indicated in Fig. 3B.8. Furthermore, once sand particles were entrained into the disk interface the adhesion instantly dropped for all slips and feed rates tested, corroborating the solid lubrication caused by S sand in dry contacts. One striking phenomenon was observed during the sand feed. Besides the instantaneous reduction of adhesion due to the initial sand entrapment, the adhesion coefficient continued to decrease as the sand feed progressed, as shown in Fig. 3B.8. This second adhesion reduction phenomenon could be attributed to the formation of a coating of compacted embedded crushed sand on the wheel and rail disk surfaces. The coating formation during continuous sanding was also observed in another work of the authors [3B.21]. In order to distinguish between these two phenomena, we refer to them hereinafter as initial and continuous adhesion reduction.

The continuous adhesion reduction phenomenon was particularly noticeable at low slips (see Fig. 3B.8), whereas it occurred to a lesser extent at higher slips (see Fig. 3B.10). This can be explained by the increased abrasion caused at higher slips, which may have hindered the coating formation. This is in agreement with observations in other work [3B.21]. On the other hand, the feed rate showed some influence on this phenomenon, which was particularly visible in the tests at 5% slip. Higher feed rates were found to promote the continuous adhesion reduction, which could be attributed to the increased flooding of particles through the contact that may effectively reduce the abrasion, promoting the coating formation. Moreover, it can be observed that less number of cycles was needed to complete the tests at high slips. This was expected because the increase in slip can enhance the run-in of the disks surfaces so that fewer cycles between sand applications were necessary at higher slip.

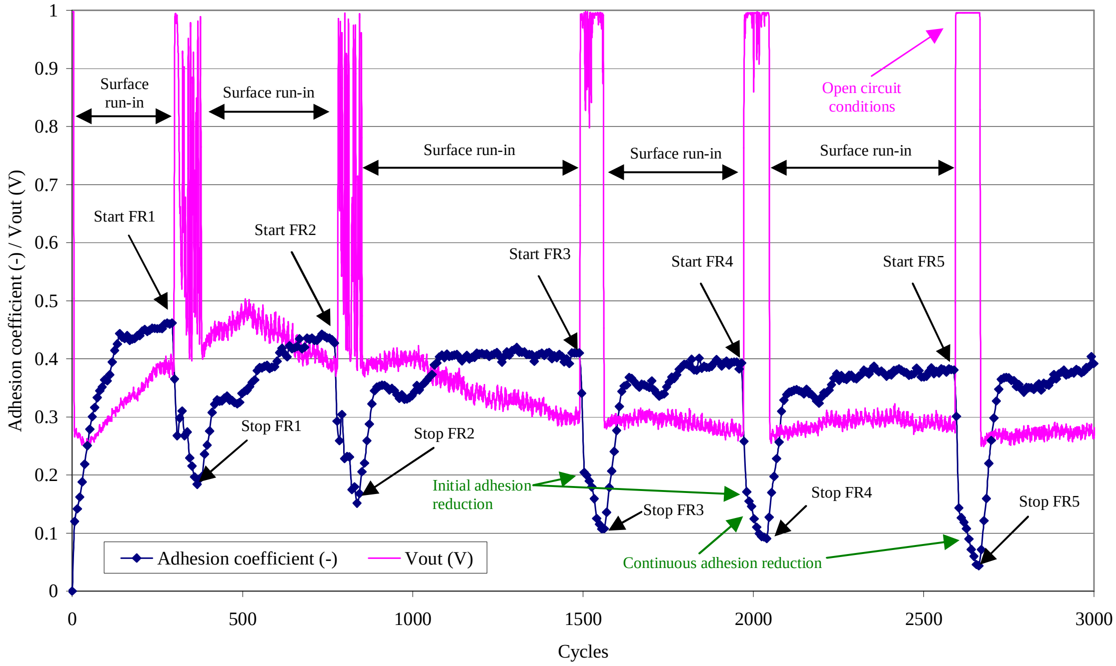

Fig. 3B.8. Adhesion and conductivity results during feed rate test with S sand at 1% slip (order: from FR1 to FR5).

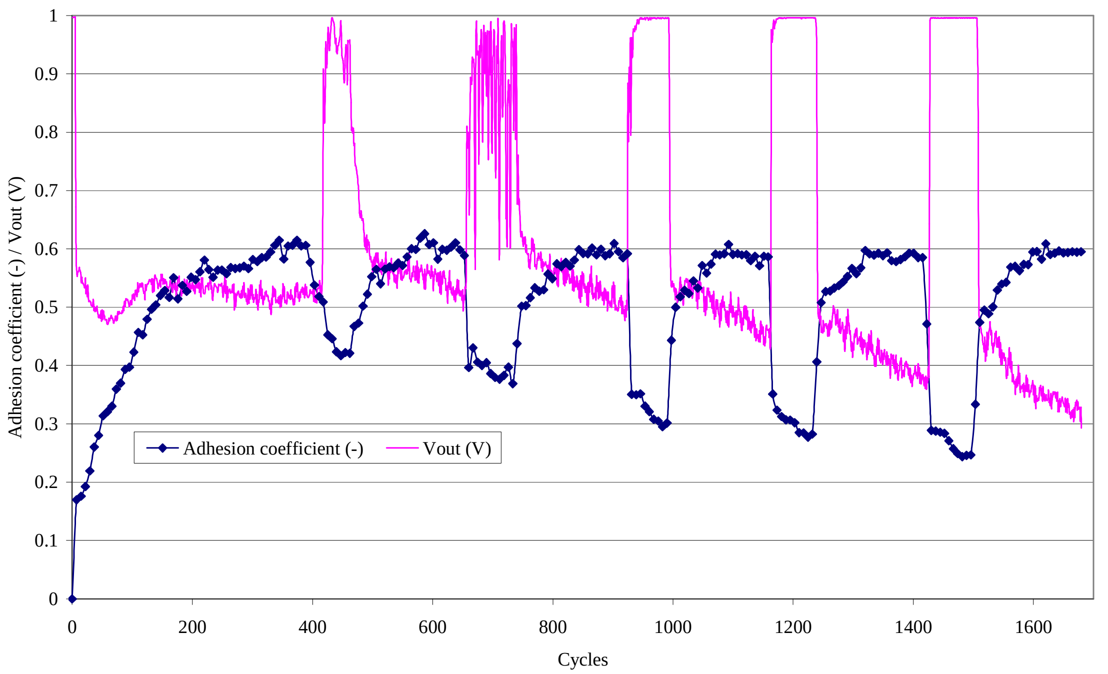

Fig. 3B.9. Adhesion and conductivity results during feed rate test with S sand at 5% slip (order: from FR1 to FR5).

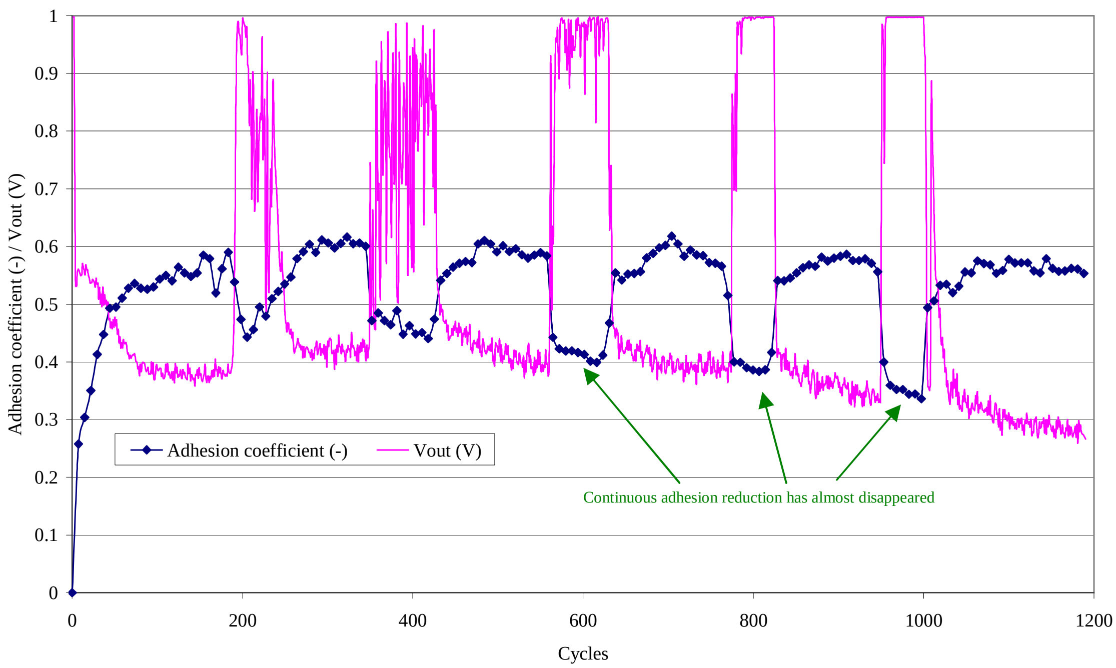

Fig. 3B.10. Adhesion and conductivity results during feed rate test with S sand at 10% slip (order: from FR1 to FR5).

In Fig. 3B.11 the average adhesion coefficient registered during the sand feed is given as a function of the feed rate, in which the data points have been connected by straight lines. Note that the values at null feed rate correspond to those of the dry metal-metal contacts, which correspond to a traction curve in dry contacts. It can be observed that the adhesion coefficient decreased with the increase of feed rate for all slips tested. The increase in feed rate led to more particles in the contact, which could partly bear the contact load and accommodate some of the slip, leading to an increase in the lubricating effect in the partial lubrication regime. Above a certain feed rate, full lubrication regime was reached, which could be identified with the open circuit conditions. Further increase in the feed rate from this point on could have led to more particles free to move relative to each other, promoting the decrease in the adhesion coefficient. In addition, it can be seen in Fig. 3B.11 that the increase in slip resulted in higher adhesion coefficients for all feed rates applied. This means that the longer sliding distances travelled by the (crushed) sand particles over the disk surfaces may have enhanced the interlocking action between the disk surfaces. This interlocking mechanism has been identified as responsible of the friction force obtained in the wheel-rail contact during sanding [3B.22].

The increase in the wheel-rail electrical insulation (in average) during the sand feed at different feed rates and slips is displayed in Fig. 3B.12. The feed rate was found to have an important effect on the electrical insulation, where higher feed rates led to more electrical insulation. This was expected as increasing the number of particles present at the disk interface can lead to the transition from partial lubrication to full lubrication regime. In general, the particles may agglomerate at the disk interface to form a third-body layer, whose electrical insulating properties increase the voltage across the disk contact area. Furthermore, the slip seemed to cause an increase in the Vout at low feed rates. This could indicate that the particle entrapment at the disk interface was somewhat promoted by higher slips at those feed rates.

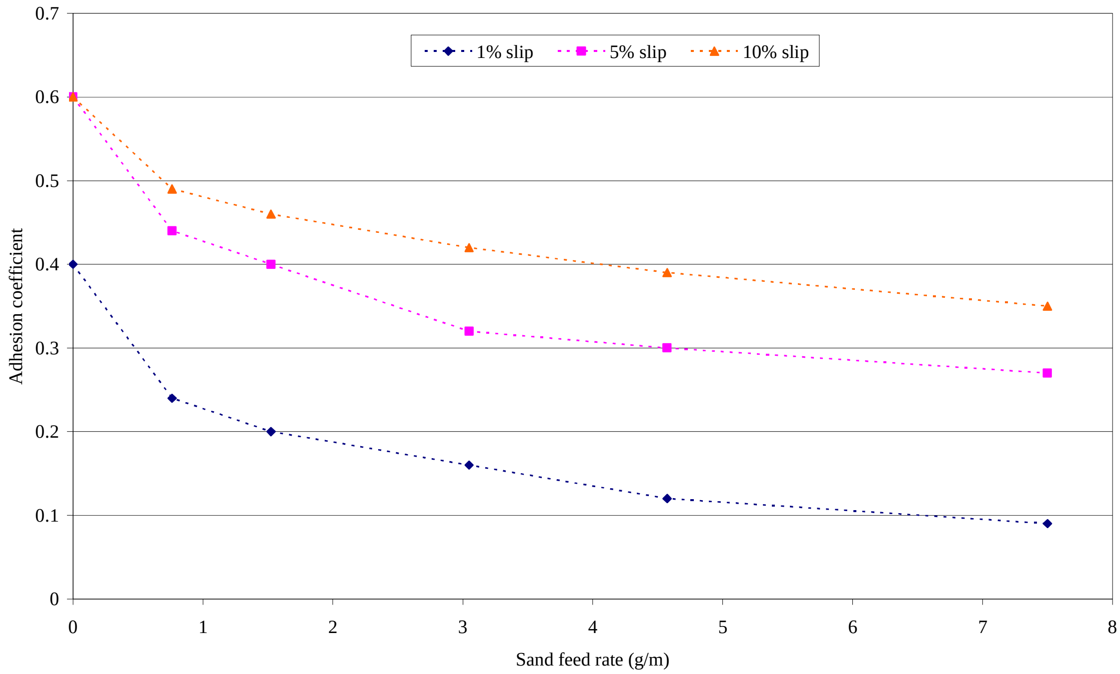

Fig. 3B.11. Average adhesion coefficient during feed of S sand at different slips and feed rates in dry contacts.

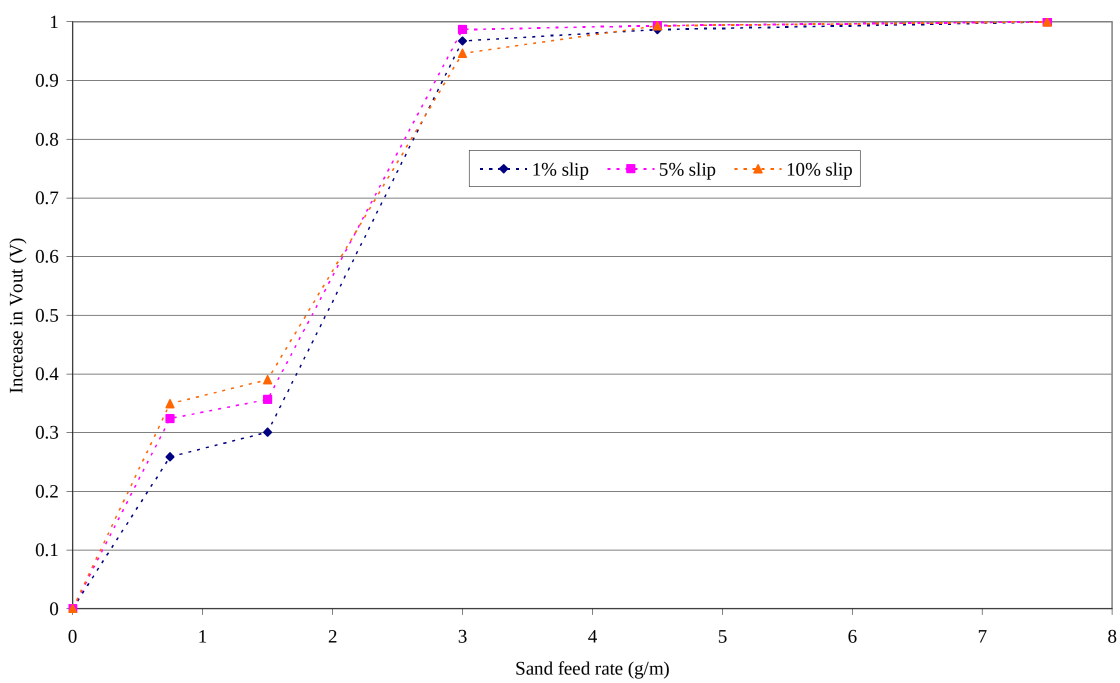

Fig. 3B.12. Increase in average Vout during feed of S sand at different slips and feed rates in dry contacts.

3B.3.2. Particle size tests

The adhesion and electrical insulation results of the particle size tests are given in Figs. 3B.13-3B.15. In these tests the sand was fed at rate FR5, as representative of rates used in practice. Note that the order of sand application was arbitrarily chosen as: L, M, R and S sand. It can be seen that the electrical insulation of the wheel-rail contact increased due to the sand entrapment for all sands tested, but open circuit conditions were only experienced with S and M sand as shown in Fig. 3B.13. On the other hand, the solid lubrication effect of sanding was observed with all sands and slips used. Furthermore, the continuous adhesion reduction as the sand feed progressed (previously outlined in the feed rate tests) also occurred in these tests, especially at low slips (see Fig. 3B.13).

In Figs. 3B.13-3B.15 it can be seen that the adhesion reduction was dependent on the particle size and the particle size distribution. By comparing the results of the three sands of similar particle size distribution but different size (i.e., S, M, and L sand), it could be seen that increasing the particle size could hinder the continuous adhesion reduction effect. This could have two possible explanations: firstly, less volume of sand travelling through the contact when using larger particle sizes, leading to less lubrication; secondly, deeper abrasion could be expected with larger particles. Moreover, the continuous adhesion reduction was especially noticeable with R sand, which could be caused by its broad particle size distribution. In another work [3B.21] the authors observed notable oscillations of the adhesion coefficient in tests with R sand, which seemed to be partly caused by the continuous process of formation and break-up of the coating on the disk surfaces. Hence, the authors would expect that if the sanding of these tests was continued further than 60 cycles, the adhesion coefficient may have increased again and continue to oscillate. This was, however, not examined in this work. Finally, it is worthwhile to mention that the adhesion coefficient and Vout results obtained with S sand at FR5 in Figs. 3B.8-3B.10 and Figs. 3B.13-3B.15 matched very well, which demonstrated the consistency of the test results.

Fig. 3B.16 depicts the average value (together with the maximum and minimum values) of the adhesion coefficient during the sand feed of all tested sands at the three slips applied. It can be seen clearly that the influence of the sand particle size on the adhesion coefficient had a consistent tendency for all slips, which appeared to be curvilinear with a trough at M sand as indicated by the trendlines of Fig. 3B.16. Hence, higher adhesion coefficients were obtained when using larger particle sizes for the range M-L sands. On the other hand, the tendency of increasing adhesion coefficient with particle size distribution was reversed in the smaller particle size range S-M sands. No explanation has been found for this result, and further investigation with more sand sizes in the small particle size range should be performed to draw solid conclusions. Moreover, it can be seen that the increase in slip led to an increase in the adhesion coefficient for all sands tested, which is in line with the observations on the feed rate tests with S sand (see Fig. 3B.11).

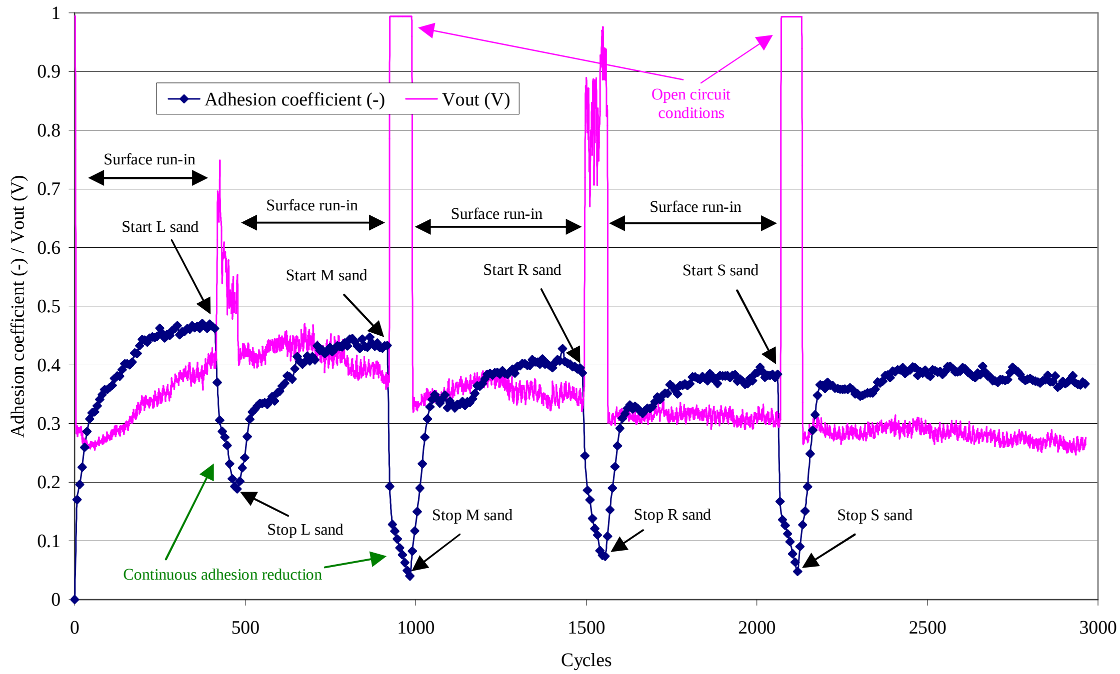

Fig. 3B.13. Adhesion and conductivity results during particle size test at 1% slip (order of application: L, M, R and S).

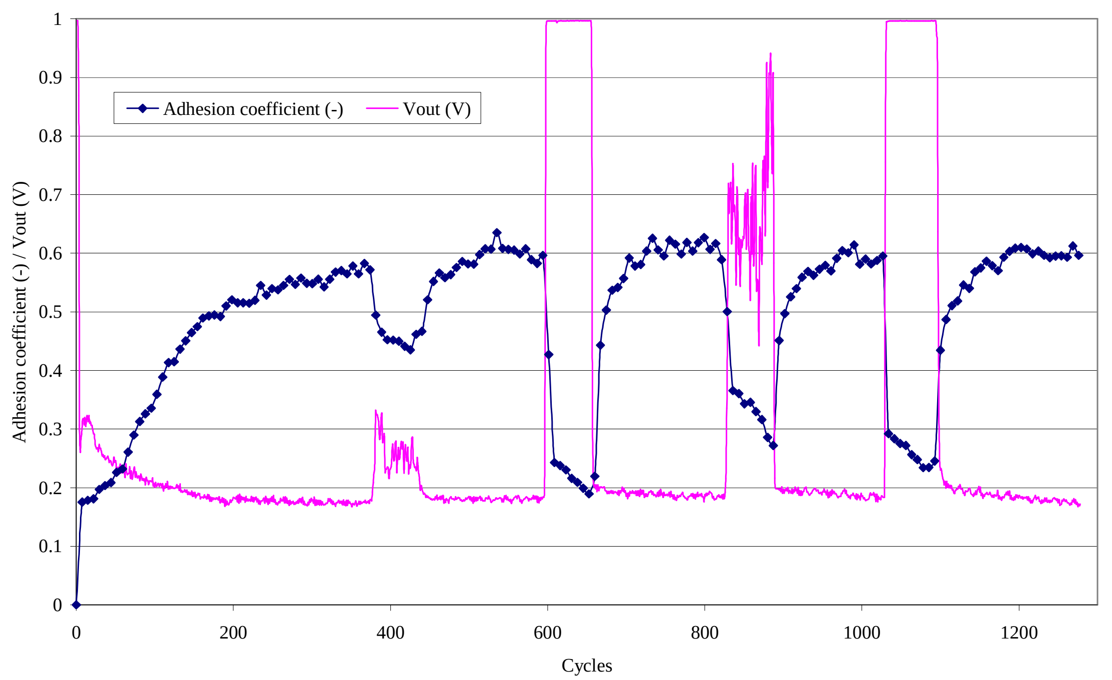

Fig. 3B.14. Adhesion and conductivity results during particle size test at 5% slip (order of application: L, M, R and S).

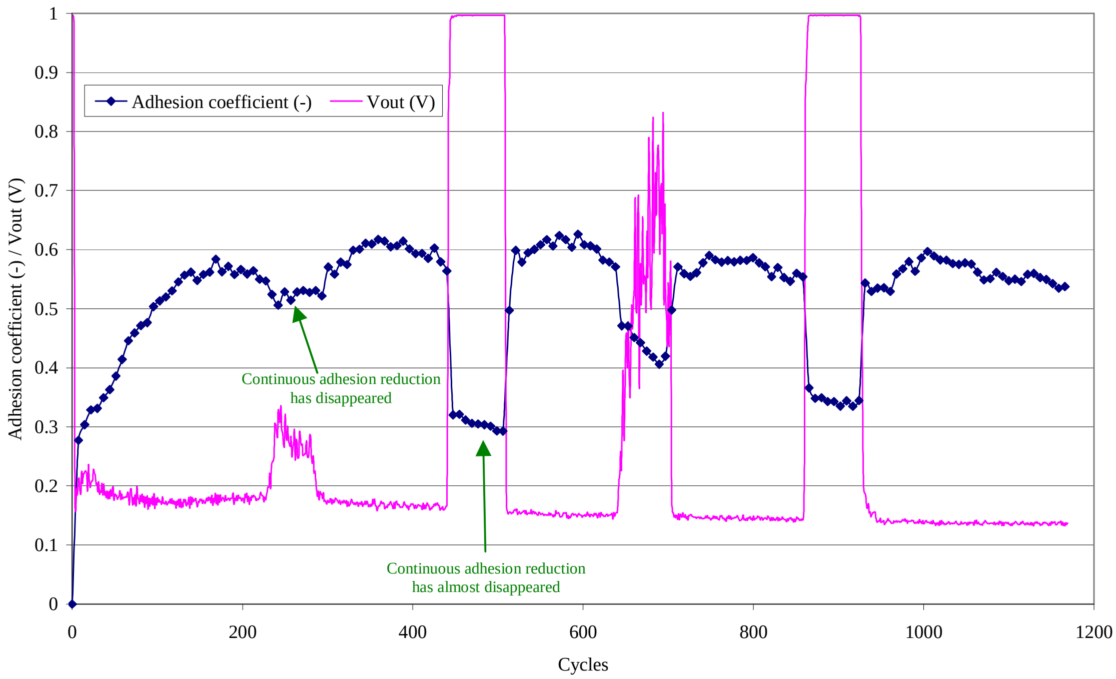

Fig. 3B.15. Adhesion and conductivity results during particle size test at 10% slip (order of application: L, M, R and S).

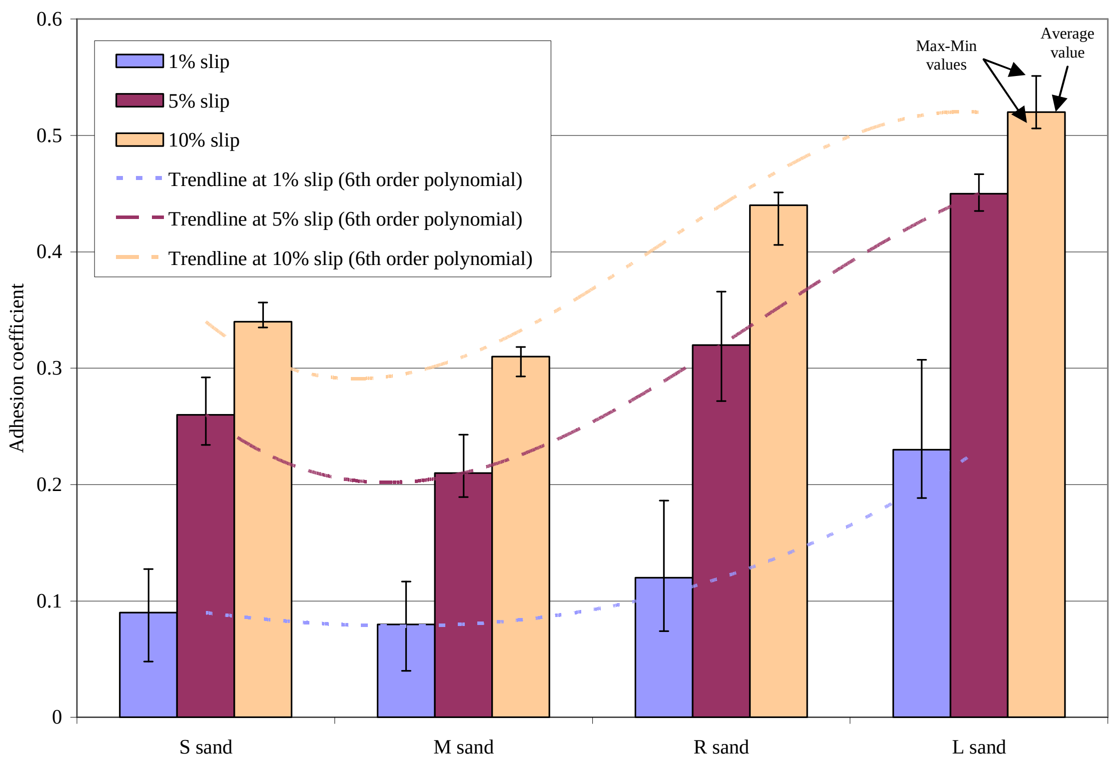

Fig. 3B.16. Average adhesion coefficient (together with max and min values) during feed of different sands at different slips in dry contacts.

The electrical insulation was found to be largely dependent on the particle size of the sand used, as shown in Fig. 3B.17. Smaller particle sizes of sand caused more electrical insulation than larger sands, leading to open circuit conditions with M and S sands. In the tests with R and L sands, Vout increased compared to the clean contact conditions, but no open circuit conditions were reached. However, R sand caused more electrical insulation than L sand, which is ascribed to its smaller particle size. Fig. 3B.18 depicts a schematic representation of the particle entrapment experienced by sands of different particle size. In general, the largest particles present in the contact break up first to form a sufficient number of particles that can bear the contact load. Some broken particles enter the disk interface, while some are ejected. When using smaller sized sand, more particles can enter the contact without being broken up. Therefore, the electrical insulation threshold in sanding is not only dependent on the feed rate but also on the particle size. Although it has been shown that the insulation threshold is to be found at lower feed rates when using smaller particles (see Figs. 3B.12 and 3B.17), no detailed quantitative study has been carried out in this work.

Moreover, a different influence of the slip on the electrical insulation was observed in these tests compared to the feed rate tests with S sand. It can be seen in Fig. 3B.17 that the increase in slip seem to cause less electrical insulation in the wheel-rail contact for R and L sands, which may be attributed to the less coating formation occurring at higher slips. This can be examined by looking at the continuous adhesion reduction phenomenon pointed in Figs. 3B.13-3B.15. Hence, the possible enhancement of particle entrapment with the slip could not be observed in these tests.

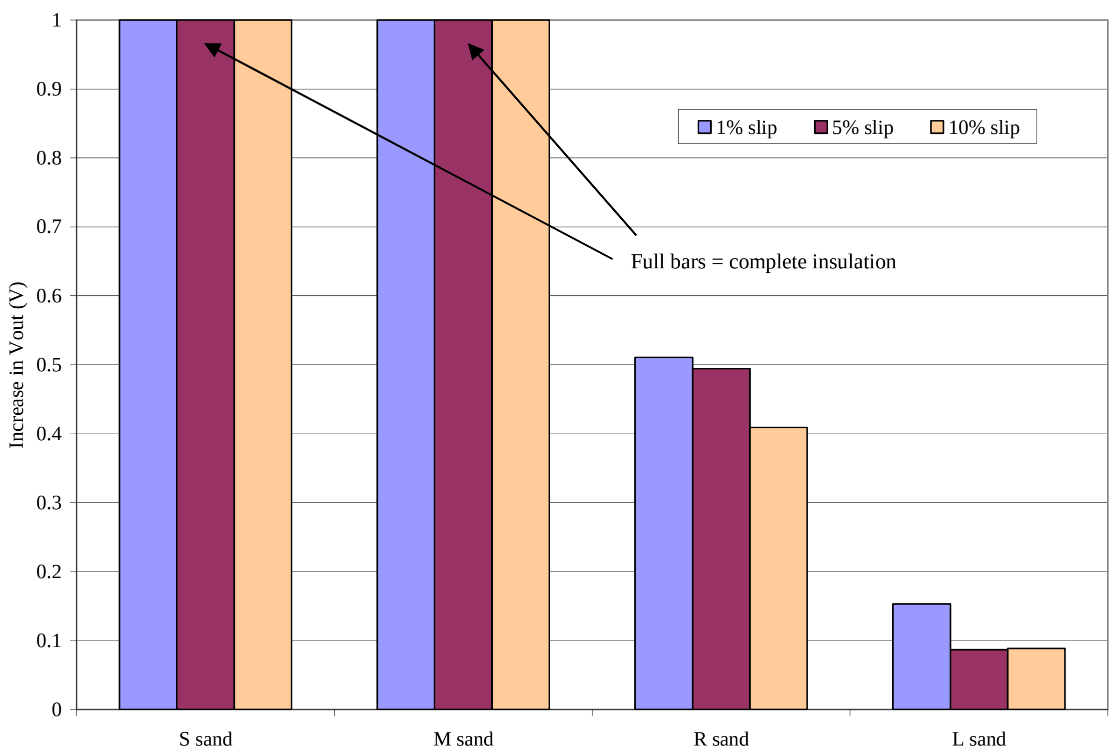

Fig. 3B.17. Increase in Vout (in average) during feed of different sands at different slips in dry contacts.

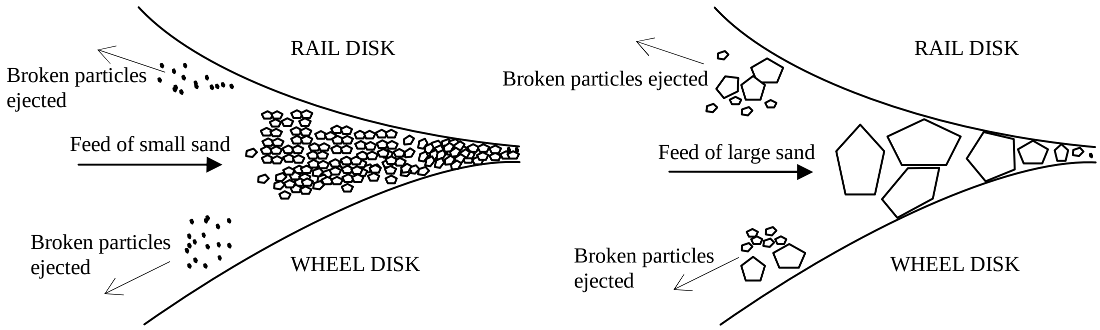

Fig. 3B.18. Schematic representation of the possible sand entrapment with different particle sizes.

3B.4. Discussion

The results of this work showed that for all particle sizes, feed rates, and slips, sand acted as a solid lubricant in dry wheel-rail contacts. Kumar et al. [3B.10] showed that the lubrication effect of sanding was not observed below a transition feed rate identified as around 0.75 oz/min in their set-up. If one considers the differences in contact geometry and rolling speed between their set-up and the one used for this work, their transition feed rate can be calculated to be between 0.167 and 0.33 g/m, depending on the evolution of their contact area width. Therefore, in our work we could never have seen that effect of higher adhesion with sand than in dry steel-on-steel contact because our minimum feed rate tested was 0.75 g/m. Note that there are other differences in both test set-ups that complicate a quantitative comparison such as the sand particle size, the contact area dimensions, the roller rig characteristics, and the contact pressure.

In both locomotives and EMUs, railway sanding is often activated automatically by the wheel slide protection and traction control systems, which trigger the sand application once the wheel slip is found to have passed a certain threshold according to existent specifications [3B.7]. The present work has shown that there is a strong influence of the wheel slip on the adhesion coefficient yielded by sanding, which shows that higher adhesion coefficients are obtained at higher slips for all sand particle sizes of the these tests. In another work, the authors have shown that the slip greatly affects the wear rates of wheels and rails during sanding, with higher wear rates at higher slips [3B.21]. Hence, further investigations in field may be encouraged to find the optimum slip that can yield an adhesion coefficient suitable for traction and braking operation, without compromising admissible wear rates of wheels and rails.

Sand-based FMs and railway sanding are used in some railway networks to guarantee an adhesion level suitable for traction or braking operation. On the other hand, if not properly applied, they may also cause very high friction, leading to excessive wear or rolling contact fatigue (among others). The results of this work indicate that an appropriate combination of particle size, feed rate and slip could be found to yield an optimal adhesion level. In particular, it has been shown that by decreasing the particle size of the sand, lower feed rates are necessary to obtain the same adhesion level than with larger particles. This may increase the interval required to re-fill the sand boxes, reducing the costs of sanding operation. In order to examine the possible optimization of sanding practice, the authors have also carried out an investigation on wear and adhesion recovery in leaf contaminated contacts [3B.21, 3B.23].

In this work, the feed rate and particle size have been found as the main parameters affecting electrical insulation during sanding. Higher feed rates and smaller sand particles have been shown to insulate more the electrical conductivity of the wheel-rail contact. Since this electrical conductivity is used in practice for the track circuits of the train detection system, special importance must be given to the identification of the critical sand feed rate for a chosen particle size distribution so that the train operation is not disturbed during sanding.

In practice, the sanders are not fitted on all the axles of a train consist so that the amount of sand laid on the rails is firstly used by the wheels of sanding axles, while the following wheels roll over the remaining crushed sand. Hence, the results obtained in this work are related to the wheels of sanding axles, and in particular to the first sanding wheelset in the travelling direction. One of the limitations of this testing is that the infinite rail has been simulated with a disk so that every cycle the wheel surface comes in contact with an already sand-treated rail surface. This circumstance may have been responsible for the continuous adhesion reduction effect, which was especially observed at low slips. At higher slips the removal of crushed sand from the rail surface is increased, so that the effect of the rail surface treatment is diminished.

In wet contacts the behavior of sand entrapment may be different from what is described in this work. Previous work showed higher adhesion coefficient when sanding is carried out in wet contacts compared to sanding under dry conditions [3B.20]. This could be explained by the capillary action of a water film, which can promote the particles entrapment, particularly with the larger particles where fractured bits of sand are pulled into the contact as they adhere to the disk surfaces. This different entrapment mechanism can thus affect the electrical insulation and adhesion. Since sand is more likely to be applied in wet conditions, the possible influence of water on the results presented in this paper may be interesting for further studies.

Furthermore, there are several differences that impede a direct comparison of the results of this testing with the actual situation in railway sanding. There exists a considerable geometrical scaling between the test set-up and the actual wheel-rail contact. In particular, the wheel and rail disks used in the testing had a finite rolling radius of 23.5 mm, while actual wheels and rails have a rolling radius of 460 mm and infinity, respectively. This geometrical difference could have led to a different particle entrapment compared to the actual situation. In addition, the length of the contact area in the rolling direction was 0.5 mm in these tests, which may be smaller than some of the (crushed) sand particles travelling through the disk interface, leading to a different behavior. Moreover, more sand could have been entrained than in practice because in this testing the sand was directly applied to the disks contact in the absence of cross wind and train’s slipstream. Therefore, the results given in this article can only be taken so far as indicative of what happens in the actual wheel-rail contact. Future work should aim at determining the scaling factors so that quantitative relationships between the twin-disk testing and actual operation conditions can be established.

3B.5. Conclusions

A laboratory investigation on the influence of three railway sanding parameters (i.e., feed rate, particle size and wheel slip) on the adhesion and electrical insulation has been presented in this paper. The wheel-rail contact has been simulated by means of a twin-disk roller rig in rolling-sliding conditions. Three different slips have been considered in the testing that are representative of actual traction and braking operations of railways. Four different sizes of sand have been used to investigate the influence of the particle size. Up to five different feed rates have applied in the testing to analyze their effects. Based on the results obtained in this work, the following conclusions can be drawn:

a) Sand acts as a solid lubricant for all tested particle sizes, slips and feed rates in dry wheel-rail contacts.
b) Using larger particle size of sand generally yields higher adhesion coefficient and causes less electrical insulation in the wheel-rail contact.
c) Higher feed rates lead to lower adhesion coefficient and more electrical insulation.
d) The increase in slip enhances the interlocking action of sand so that higher adhesion coefficients are obtained.
e) An optimal adhesion coefficient may be achieved with a suitable combination of particle size, feed rate and wheel slip.

References

[3B.1] C.R. Fulford: Review of low adhesion research. Report published by the Rail Safety and Standards Board, UK (2004).
[3B.2] U. Olofsson, K. Sundvall: Influence of Leaf, Humidity and Applied Lubrication on Friction in the Wheel-Rail Contact: Pin-on-Disc Experiments. Journal of Rail and Rapid Transit 218 (2004) 235-242.
[3B.3] P.M. Cann: The 'Leaves on the Line'—a Study of Leaf Residue Film Formation and Lubricity under Laboratory Test Conditions. Tribology Letters 24 (2006) 151-158.
[3B.4] Z. Li, O. Arias-Cuevas, R. Lewis, E.A. Gallardo-Hernandez: Rolling-Sliding Laboratory Tests of Friction Modifiers in Leaf Contaminated Wheel-Rail Contacts. Tribology Letters 33 (2009) 97-109.
[3B.5] O. Arias-Cuevas, Z. Li: Field investigations in the adhesion improvement by locomotive sanders with different sand particle sizes in dry and wet leaf contaminated wheel-rail contacts. To be submitted for publication (2009).
[3B.6] H.I. Andrews: Railway Traction—the Principles of Mechanical and Electrical Railway Traction. Elsevier (1986).
[3B.7] Sanding Equipment Fitted to Multiple Units and On-track Machines. Railway Group Standard GM/RT 2461 (2001).
[3B.8] W. Voges, P. Spiess: Optimizing Services with EMU ET42x in Autumn 2004 and 2005. Proceedings of 7th World Congress on Railway Research, Canada (2006).
[3B.9] O. Arias-Cuevas, Z. Li, R. Lewis, E.A. Gallardo-Hernandez: Rolling-Sliding Laboratory Tests of Friction Modifiers in Dry and Wet Wheel-Rail Contacts. Wear (2009) doi:10.1016/j.wear.2009.09.015.
[3B.10] S. Kumar, P.K. Krishnamoorthy, D.L. Prasanna Rao: Wheel-Rail Wear and Adhesion With and Without Sand for a North American Locomotive. Journal of Engineering for Industry 108 (1986) 141-147.

[3B.11] Boiteux, Cadier, J. Kling, W. Kunnes: Summary of Theoretical and Practical Knowledge of Poor Adhesion Conditions Acquired since Publication of B 164/RP 2. Report DT 257 (B 164) published by the Office for Research and Experiments of the International Union of Railways (1992).
[3B.12] E.A. Gallardo-Hernandez, R. Lewis: Twin Disc Assessment of Wheel/Rail Adhesion. Wear 265 (2008) 1309-1316.
[3B.13] Mesures a Prendre Pour Ameliorer la Sensibilite au Shuntage des Circuits de Voie. UIC737-2 in French (1980).
[3B.14] R. Lewis, R.S. Dwyer-Joyce, J. Lewis: Disc Machine Study of Contact Isolation During Railway Sanding. Journal of Rail and Rapid Transit 217 (2003) 11-24.
[3B.15] R. Lewis, J. Masing: Static Wheel/Rail Contact Isolation due to Track Contamination. Journal of Rail and Rapid Transit 220 (2006) 43-53.
[3B.16] D.I. Fletcher, J.H. Beynon: Development of a Machine for Closely Controlled Rolling Contact Fatigue and Wear Testing. Journal of Testing and Evaluation, 28 (2000) 267-275.
[3B.17] European Standard EN13262: Railway Applications – Wheelsets and Bogies – Wheels – Product requirement (2004).
[3B.18] H. Chen, T. Ban, M. Ishida, T. Nakahara: Experimental Investigation of Influential Factors on Adhesion between Wheel and Rail under Wet Conditions. Wear 265 (2008) 1504-1511.
[3B.19] R. Lewis, E.A. Gallardo-Hernandez, T. Hilton, T. Armitage: Effect of oil and water mixtures on adhesion in the wheel/rail contact. Journal of Rail and Rapid Transit 223 (2009) 275-283.
[3B.20] Lewis, R., Dwyer-Joyce, R.S.: Wear at the Wheel-Rail Interface when Sanding is Used to Increase Adhesion. Journal of Rail and Rapid Transit 220 (2006) 29-41.
[3B.21] O. Arias-Cuevas, Z. Li, R. Lewis: A Laboratory Investigation on the Influence of the Particle Size and Slip During Sanding on the Adhesion and Wear in the Wheel-Rail Contact. Paper to be presented at 8th International Conference on Contact Mechanics and Wear of Rail/Wheel Systems, Firenze, Italy, September 15-18 (2009).
[3B.22] M.W. Astle-Fletcher: Mechanical Methods of Improving Rail Adhesion. Proc. Inst. Mech. Eng., 178 (1963-64) 185-205.
[3B.23] O. Arias-Cuevas, Z. Li, R. Lewis, E.A. Gallardo-Hernandez: Laboratory Investigation of some Sanding Parameters to Improve the Adhesion in Leaf Contaminated Wheel-Rail Contacts. Submitted for publication (2009).

Chapter 3, Part C

Laboratory tests on adhesion recovery[IX]

ABSTRACT

Leaf contamination has been identified as the major cause of low adhesion incidents occurring on some railway networks in the last few decades. In the presence of leaf layers, the trains cannot have the required adhesion at the wheel-rail contact for adequate traction and braking operation. Under these circumstances not only the punctuality can be threatened, but also the safety of the railway transportation. In order to mitigate low adhesion problems, railway organizations have opted for different measures, particularly in autumn. The most employed measure consists of bringing sand to the wheel-rail interface, which can be performed by means of air-pumped sanders or in the form of sand-based friction modifiers. Although sand has widely been accepted as an effective adhesion improver, the effect of some sanding parameters on the adhesion improvement in leaf contaminated contacts seems to be unclear. This hinders the possible optimized use of sand on the railway networks. In this paper the influence of the number of sanding axles, particle size of sand, and wheel slip on the adhesion recovery in leaf contaminated wheel-rail contacts is presented. Rolling-sliding tests under closely controlled conditions have been performed on a twin-disk roller rig. An electrical circuit has been connected to the rig for monitoring the effect of the contamination on the electrical conductivity across the wheel-rail contact. The results show that the application of sand contributes to removing the leaf layers from the disks surfaces, which leads to a higher adhesion coefficient in comparison with the untreated (baseline) situation. Accordingly, the electrical conductivity across the wheel-rail contact is also improved. Furthermore, the adhesion recovery is shown to become larger and faster with the increase of sanding axles and wheel slip. Among the particle sizes tested in this work, medium particles are found to yield the most effective adhesion recovery.

[IX] This chapter has been published as: O. Arias-Cuevas, Z. Li, R. Lewis, E.A. Gallardo-Hernandez: Investigation of some Sanding Parameters to Improve the Adhesion in Leaf Contaminated Wheel-Rail Contacts. Proc. IMechE, Part F: J. Rail and Rapid Transit 224 (2010) 139-157.

3C.1. Introduction

The friction available between wheel and rail during braking and traction operation is The adhesion, or the adhesion coefficient (also known as the traction coefficient), is given by the ratio between the traction or braking force and the normal force at the wheel-rail contact. If the adhesion at the wheel-rail contact is below certain requirements, not only the punctuality, but also the safety of the railway transportation may be compromised. Additionally, low adhesion incidents may lead to the damage of wheels (e.g., wheel flats) and rails (e.g., rail burns) increasing the maintenance costs of the infrastructure and the rolling-stock. Although many factors can influence the wheel-rail adhesion, leaf contamination has been identified to cause most of the low adhesion incidents on some railway networks in the last few decades [3C.1-3C.7]. The leaf related problems mostly occur in autumn, when large amounts of fallen leaves cover the railway tracks. Once these leaves come to the top of the rails, passing wheels compact and shear them to form Teflon-like layers [3C.6]. These slippery layers adopt a black colouration and become very hard to be removed from the wheel and rail surfaces. Besides problems related to adhesion, the leaf layers may also affect train detection because of their electrical insulating properties.

In recent years, railway organizations have taken different measures to fight the low adhesion problems [3C.1, 3C.2, 3C.5]. Operational measures, such as warning systems and training for drivers to operate under low adhesion conditions, and infrastructure remedial measures, such as vegetation management and the use of dedicated vehicles to clean the rails, have been adopted. The most used measure to improve the adhesion conditions has been the application of sand to the wheel-rail contact. Two major practices of bringing sand particles to the wheel-rail interface are employed, namely sanders and sand-based friction modifiers (FMs). The sanders eject the sand from on-board storage hoppers by means of compressed air through a nozzle oriented towards the wheel-rail interface. Locomotive sanders have existed since the earliest days of the railway transportation [3C.8]. In recent years, sanders have also been fitted to some of the electrical multiple units (EMUs) in countries like Germany and the UK [3C.2, 3C.5, 3C.9]. Field and laboratory tests have corroborated that using sanders can enhance the adhesion in the presence of leaves at the wheel-rail contact [3C.10, 3C.11].

On the other hand, dry sand may easily be blown off the rail surfaces in the presence of wind or train’s slipstream leading to a short lasting effect. This shortcoming has led countries like the Netherlands and the UK to opt for a commercial sand-based FM, which incorporates a gelling agent that promotes the adherence of the mix to the wheel and rail surfaces [3C.2, 3C.7, 3C.12]. The commercial sand-based FM can be applied train-borne or with trackside installations. The adhesion improvement given by this FM in leaf contaminated contacts was corroborated in laboratory tests against a baseline representing the untreated conditions [3C.7]. It was shown that the number of cycles (i.e. wheel passages) needed to reach an adequate adhesion for braking and traction could be reduced up to 70 and 93%, respectively, when using the FM compared to the baseline.

Although positive in adhesion improvement, the use of sand in the wheel-rail contact can have some undesired side effects. The abrasive action of sand particles can cause an increase in the wear rates of both wheels and rails, leading to higher maintenance costs [3C.13, 3C.14]. Furthermore, sand particles may electrically insulate the wheel-rail contact, leading to a failure in the train detection [3C.15, 3C.16]. This situation may lead to traffic disruption, and sometimes even collisions.

Recently, the authors investigated in the laboratory the influence of some sanding parameters on the electrical insulation and wheel and rail damage caused by sanding [3C.17, 3C.18]. It was found that the wear rates caused by sanding are dependent on the particle size and wheel slip, and that electrical insulation caused by sanding is dependent not only on the feed rate, but also on the particle size and in a minor degree on the wheel slip. These studies indicated that some of the parameters could be optimized to reduce the negative impact of sanding on both wear and electrical insulation. Nevertheless, the effect of the sanding parameters on the adhesion recovery in leaf contaminated contacts still seems to be unclear. This hinders the possible optimized use of sand in the wheel-rail contact.

This paper presents a laboratory investigation on the influence of three sanding parameters (i.e. number of sanding axles, wheel slip, and particle size) on the adhesion recovery in leaf contaminated wheel-rail contacts. The tests have been performed on a twin-disk roller rig under rolling-sliding conditions. Three different slips have been applied in this work to study the influence of the wheel slip. Four sands have been used in the testing to account for the influence of the particle size. Three amounts of sand have been fed with a fixed feed rate to analyze the importance of the number of sanding axles on the adhesion recovery. Besides adhesion, the electrical conductivity across the wheel-rail contact has been monitored during the tests to help understanding the impact of contamination on the electrical insulation.

3C.2. Test description

3C.2.1. Test set-up

The wheel-rail contact was simulated in rolling-sliding conditions on the SUROS (Sheffield University ROlling Sliding) roller rig, which is shown in Fig. 3C.1 and described in detail in [3C.19]. The test disks were mounted on independent shafts. By means of a hydraulic jack, a controlled load of 4.7 kN was applied on the disks producing a maximum Hertzian pressure of 1.2 GPa in the contact zone, which is representative of the contact between wheel tread and railhead for passenger trains in the Netherlands. Since cylindrical disks were used in the experiments, a line contact of 10 mm width was present (see Fig. 3C.2).

In the tests the rotational speed of the rail was maintained at 400 rpm, equivalent to 0.98 m/s of rolling speed. In order to apply the wheel slip, the rotational speed of the wheel disk was maintained higher than the one of the rail disk. The definition of slip is given in Eq. 3C.1, where w and r are the rotational speed and rolling radius of the disks, respectively. To obtain an indication of the adhesion in the wheel-rail contact, the adhesion coefficient was recorded throughout the test. It was calculated with the readings of the torque transducer and the load cell, as indicated in Eq. 3C.2, where T represents the torque and F_N is the normal contact force. A personal computer was used to acquire the data and to control both the speed and the load during each test.

$$slip = \frac{w_{wheel} \cdot r_{wheel} - w_{rail} \cdot r_{rail}}{w_{wheel} \cdot r_{wheel} + w_{rail} \cdot r_{rail}} \cdot 200\% \quad (3C.1)$$

$$\mu_{adhesion} = \frac{T}{F_N \cdot r_{rail}} \quad (3C.2)$$

The test disks were cut from rails and wheel tyres retired from service on the Dutch railway network; R260Mn and B5T steel was used for the rail and wheel disks, respectively. The disks were machined with their axes perpendicular to the longitudinal axis of both wheel and rail, as shown in Fig. 3C.2. The Vickers macro-hardness of the wheel and the rail steel used in the tests was measured as $267HV_{20kg}$ and $281HV_{20kg}$ on average, respectively. The roughness of the disks was measured with a profilometer, with an average value 1.3±0.2 µm.

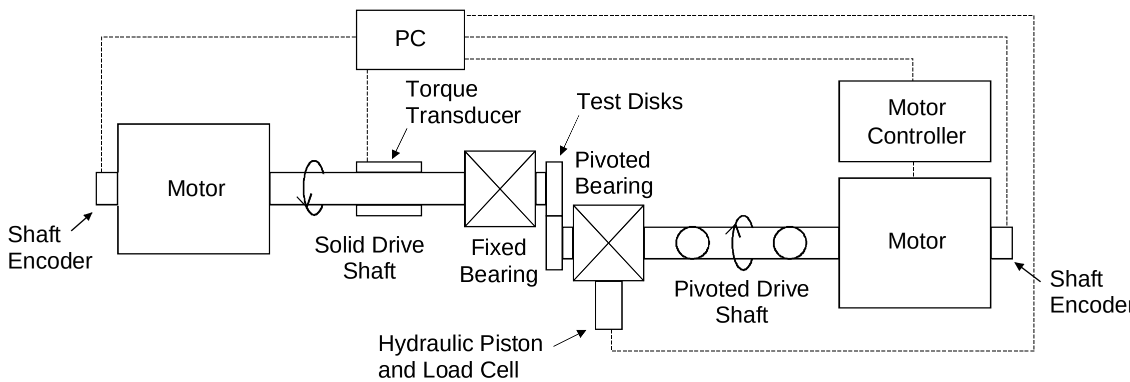

Fig. 3C.1. Schematic representation of the SUROS roller rig setup.

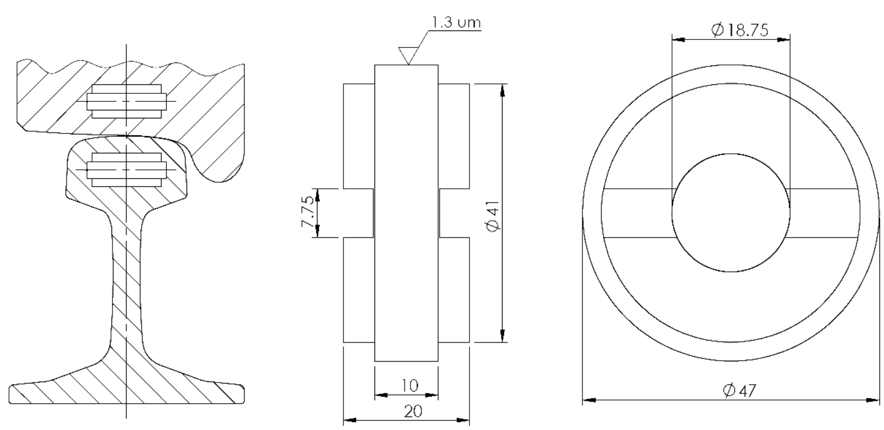

Fig. 3C.2. Orientation and dimension of the disks.

In order to monitor the electrical voltage across the disks contact area in the course of each test together with the adhesion data, an electrical circuit was installed on the roller rig. Fig. 3C.3 depicts the electrical circuit, which had also been used in previous investigations of insulation at the wheel-rail contact [3C.16]. Due to the position of the voltmeter in the set-up a so-called bearing resistance, which accounted for the lubricant circulating inside the bearing, had to be included in the *Vout* readings, as indicated in Fig.

3C.3. Nevertheless, the bearing resistance could be neglected once sand and leaves were entrained into the disk interface because of its smaller influence on the *Vout* readings compared to the contamination present at the wheel-rail contact. The *Vout* was recorded at a frequency of 2 kHz, i.e. every 0.5 mm of travelled distance of the rail, which corresponded to the length of the contact area in the rolling direction. The readings were further averaged to have one *Vout* reading per rail revolution (or cycle).

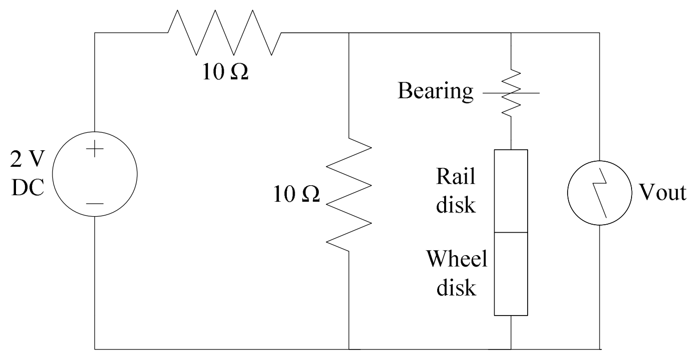

Fig. 3C.3. Schematic representation of the electrical circuit.

In the presence of insulating contamination at the disk interface, the electrical resistance can increase until open circuit conditions are reached, in which case *Vout* = 1 V. If the contact is not totally insulated, the voltage readings (in Volts) correspond to Eq. 3C.3, in which *Rc* and *Rb* are the resistance (in Ohms) of the disk contact and the bearing, respectively. Additionally, a combined resistance of the total resistance seen by *Vout*, which is given by $Rt = Rc + Rb$, can be used to simplify the formula.

$$Vout = \frac{10 \cdot (Rc + Rb)}{10 + Rc + Rb} \cdot \frac{2}{10 + \frac{10 \cdot (Rc + Rb)}{10 + Rc + Rb}} = \frac{10 \cdot (Rt)}{10 + Rt} \cdot \frac{2}{10 + \frac{10 \cdot (Rt)}{10 + Rt}} \qquad (3C.3)$$

3C.2.2. Tested sands

Two types of commercial sand were used in this work: silica sand and filter sand. The silica sand had been extracted from a pit in south Germany, whereas the filter sand had been collected from a river in the Netherlands. A photograph of the sands is given in Fig. 3C.4. The particle size distribution of the sands, which is given in Fig. 3C.5, was measured with a laser particle analyzer. The filter sand is used by the Dutch railways to increase the adhesion of the locomotives; thus, it is hereinafter referred to as railway sand, R sand for short. Although different rocks can be seen in the sample, the weight content in SiO_2 is around 96% as given by the supplier. The particle size distribution of R sand ranged from 0.25 to 1.4 mm with a wide peak at 0.6-1 mm, as shown in Fig. 3C.5. The silica sand had a SiO_2 content around 99% according to the supplier. It was sieved in the laboratory to three different particle size ranges: small (0.06-0.3 mm, with peak at 0.15 mm), medium (0.3-0.6 mm, with peak at 0.35 mm), and large (0.85-1.6 mm, with peak at 1.2 mm). These three sands are referred in this paper as S sand, M sand and L sand, for short. Moreover, due to the similar composition, form, and hardness of the four tested sands the particle size distribution could be considered as the only parameter of study for this work.

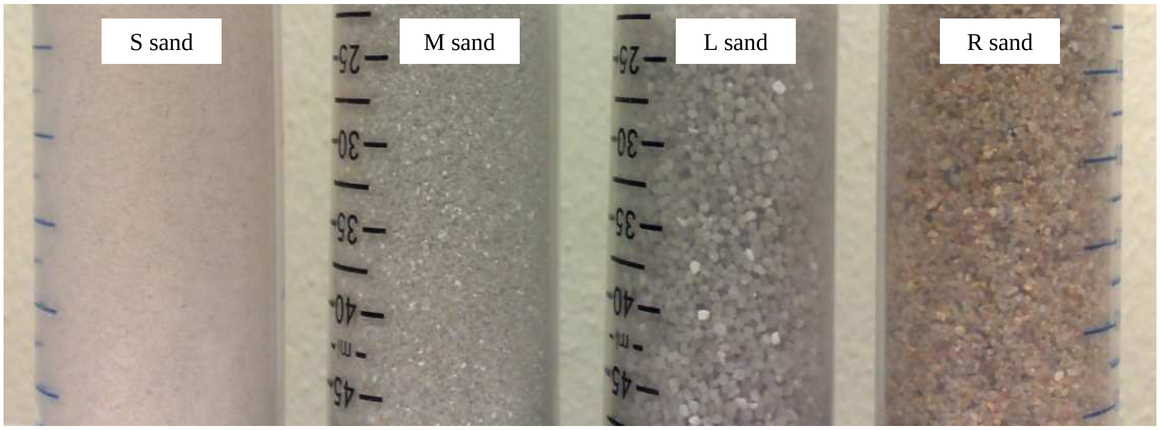

Fig. 3C.4. Photograph of the tested sands: S sand, M sand, L sand, R sand.

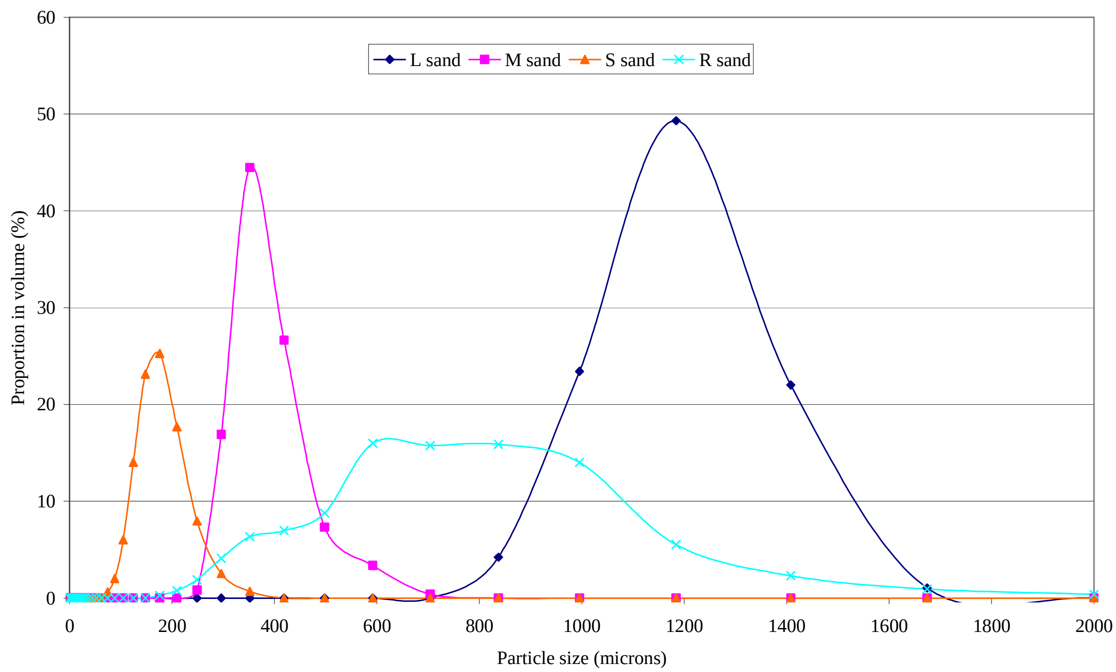

Fig. 3C.5. Particle size distribution of the tested sands obtained with the laser particle analyzer.

3C.2.3. Test procedure

In order to form the black leaf layers onto the disks that are representative of those causing low adhesion incidents in practice, the same preparation procedure used in previous work was followed [3C.7]. In a single test at 0.5% slip, the disks were let run in for 2000 cycles to condition the surfaces followed by 300 cycles of leaves feed. Around 20 g of autumn sycamore leaves were fed in each test, which had been cut into small pieces to ease their entrapment into the disks interface. Sycamore is one of the tree types present along the Dutch railway network. Fig. 3C.6 depicts the adhesion and voltage output of a generic preparation test. The adhesion coefficient is seen to increase rapidly from 0.05 to around 0.13, which accounts for the initial adjustment of the slip set for the test and the contact load. Thus, this initial transition occurs every time a test is started and it normally lasts between 20 and 50 cycles. The further increase of the adhesion coefficient until a steady value of 0.32 is attributed to the conditioning of the disk surfaces, which is observed particularly when using new disks.

Due to the re-circulation of the lubricant inside the bearing and the change in surface roughness of the disks, some variation in *Vout* can be observed in the initial 2000 cycles. Once the leaves started to be fed into the contact, the adhesion dramatically went down to values around 0.02 and *Vout* increased accordingly with the cycles as insulating leaf layers formed onto the disks. At the end of the preparation test, the contaminated rail and wheel disks were separated and the test was stopped. Then, the slip and/or sand applicator were adjusted for the leaf contaminated test. It must be noted that besides the black leaf layers, patches of leaf mulch of a few hundreds microns thick were adhered onto the disks at the end of the preparation test. It can be expected that if those leaf mulch patches were not removed from the disk surfaces, they may have transformed into the black leaf layers in the progress of a leaf contaminated test.

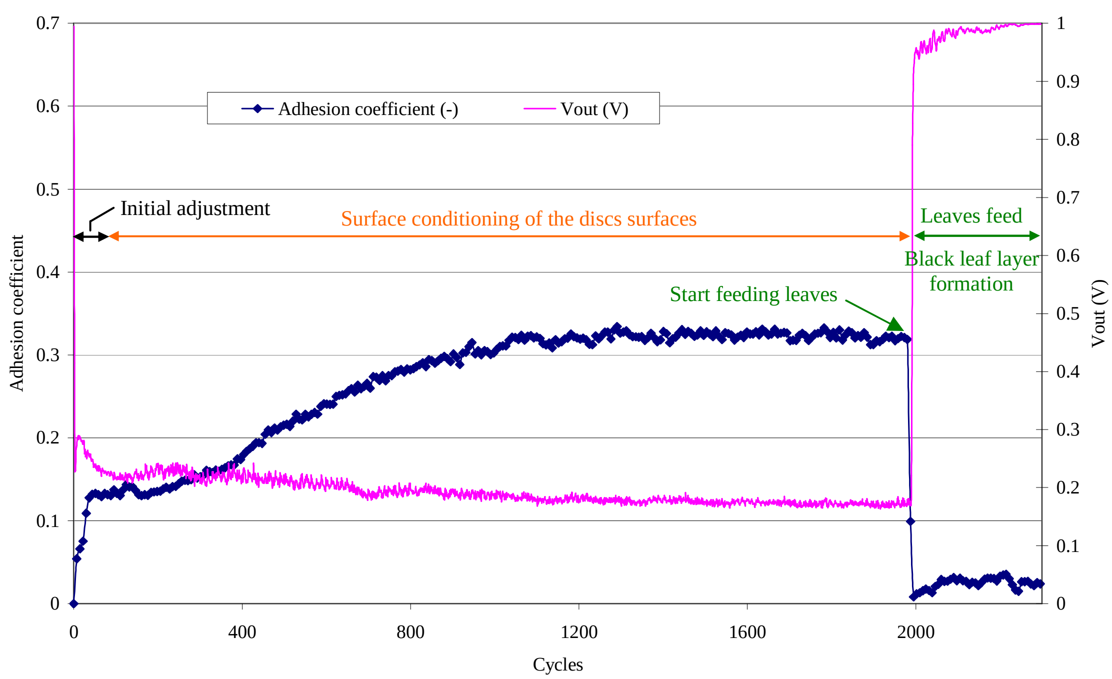

Fig. 3C.6. Adhesion and conductivity results during the leaf contaminated test preparation at 0.5% slip.

Each leaf contaminated test was run for 1000 cycles. The tests were conducted at three slips: 1, 5 and 10%, which represent typical values found during actual traction and braking operations. The sand was applied after some cycles for the initial adjustment. In the results presented in Section 3C.3 the cycles used for initial adjustment and sand application will not be shown to illustrate better the adhesion available after sand application. The sand was fed by means of gravity, as shown in Fig. 3C.7. After exiting the valve, the sand passed through a PVC pipe and was oriented to the wheel-rail interface with a chute. A vacuum cleaner placed behind the disks sucked the sand into the wheel-rail contact so that the compressed air system used in actual sanders could be simulated. Besides, two funnels helped feeding the sand to the PVC pipe.

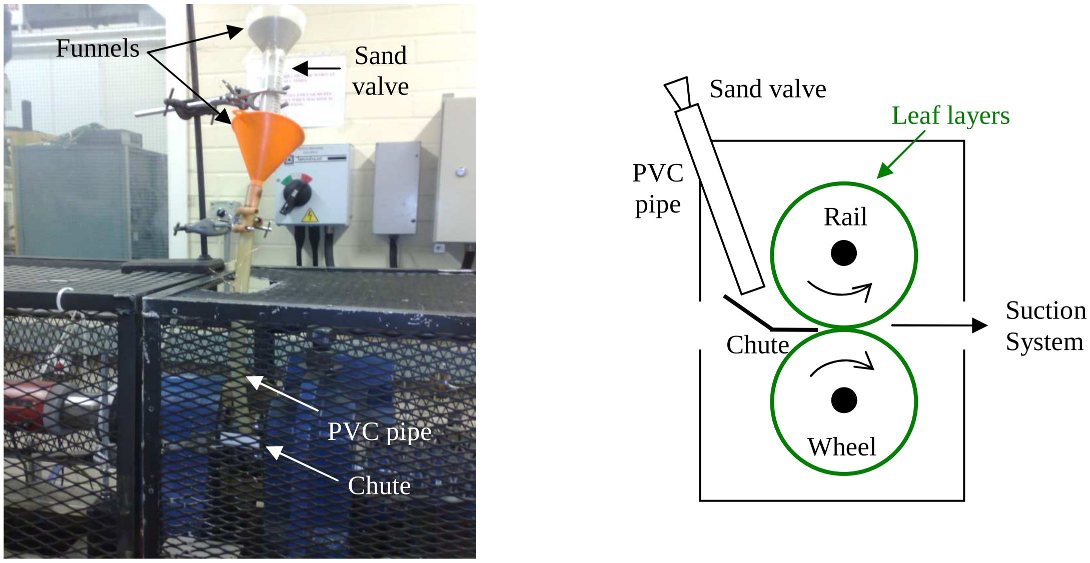

Fig. 3C.7. Sand application method in the test set-up: photograph (left) and schematic (right).

In order to regulate the sand feed rate, plastic syringes were used as valves. The orifice of the syringe was adapted to achieve the nominal feed rate, which was 7.5 g/m in every test taking as reference the travelling distance and rolling speed of the rail disk. Note that this feed rate is representative of the ones used in practice [3C.14]. The different particle size distribution of the four sands required different orifice sizes because of their different bulk density. Moreover, three amounts of sand were employed in the tests: m1 = 1.108 g, m2 = 2.216 g, and m3 = 4.432 g. In this way, the tests simulated the equivalent situation of a passing rail vehicle over a contaminated section of length equal to the rail disk circumference (= 47π mm), which had sanders fitted to one, two, and four wheelsets, respectively. Thus, the residual effect on adhesion and electrical insulation left to the subsequent non-sanding wheel passages could be investigated for all sand particle sizes and for the different slips.

In addition to the tests with sand, two baselines were conducted. A baseline for dry clean contacts (named baseline-dry in this paper) was performed to examine the impact of leaf contamination on wheel-rail adhesion. Moreover, a baseline without any sand application on leaf contaminated contacts (named baseline in this paper) was also carried out so that the improvement in adhesion given by sand could be shown. The baseline tests were carried out at five different slips (i.e., 0.5, 1, 5, 10, and 15%) to additionally investigate the effect of wheel slip on the adhesion recovery. Finally, the surfaces of the disks were examined after each leaf contaminated test with both sand and in baseline conditions. The thickness of the remaining layers was measured with an optical 3D profiling system WykoNT3300 (Veeco Metrology Group, USA). Micro-hardness measurements of the layers were undertaken with a Vickers indenter with a 10 g load.

Finally, the remaining contamination was scraped off the disk surfaces to be analyzed using Fourier Transform Infra-Red (FTIR) micro-spectroscopy.

3C.3. Results

3C.3.1. Influence of the number of sanding axles

The importance of the number of sanding axles was investigated for all types of sand. In the tests with R sand three slips were tested (Figs. 3C.8-3C.10), while for S, M and L sands only 5% slip was considered (Figs. 3C.14-3C.16). The two baseline tests, which were performed without sand on leafy and clean contacts, are also given for each figure. It can be seen that the initial adhesion coefficient was always higher in the tests with sand than in the baseline (with leaf layers and no sand application), see Fig. 3C.8 as example. This adhesion improvement can be attributed to the enhanced removal of the black leaf layers by the entrapped (crushed) sand particles, which leads to a higher initial adhesion for all tests with sands compared to the baseline. The amount of adhesion improvement due to the sand application is depicted in Fig. 3C.8 by means of arrows. Furthermore, the highest initial adhesion coefficient was mostly observed in the baseline-dry tests (no leaf layers and no sand application), which was expected due to the absence of contamination. In order to illustrate the initial adhesion improvement due to sanding quantitatively, the adhesion coefficient at 65 cycles of baseline and sand tests is displayed in Table 3C.1. After sand application the adhesion coefficient was always higher than 0.10, which is above the maximum adhesion requirements of the majority of the rolling stock for braking. Nevertheless, the adhesion coefficient was not always above the required values for traction operation, especially when using insufficient number of sanding axles. This will be further discussed in Section 3C.3.4.

Table 3C.1. Adhesion coefficient at 65 cycles (after initial adjustment and sand application).

	1% slip	5% slip				10% slip
Baseline	0.07	0.11				0.12
	R sand	R sand	S sand	M sand	L sand	R sand
m1	0.11	0.15	0.19	0.20	0.14	0.15
m2	0.15	0.17	0.21	0.26	0.15	0.18
m3	0.17	0.22	0.30	0.35	0.18	0.36

Increasing the number of sanding axles caused a higher initial adhesion coefficient for the four sands used in the testing. In most of the tests the increase in sanding axles not only led to a larger initial adhesion recovery, but also to a higher value in the maximum adhesion coefficient reached. The only exception to this tendency was observed in the m1 and m2 tests with R sand at 5% slip and in the m2 and m3 tests with L sand at 5% slip, as pointed out in Fig. 3C.9 and Fig. 3C.16, respectively. It can be seen in those tests that after a large number of cycles, when the sand could have been removed entirely from the surfaces, a higher adhesion coefficient was reached for the test with fewer sanding axles. These results could be explained by the non-uniform distribution and evolution of the leaf layers on the disks surfaces.

In the R sand tests the importance of having enough sanding axles was particularly reflected at 10% slip. In Fig. 3C.10 it can be seen that a peak in the adhesion coefficient around 0.37 was reached around six times faster with m3 compared to m2, while that peak value was not reached with m1. Once the adhesion coefficient reached the peak, it unexpectedly decayed with the increasing number of cycles. The explanation for this odd behaviour was found upon post-test examination of the disks, which demonstrated the presence of remaining contamination on the wheel disk in the form of powder that could easily be rubbed away with the finger. FTIR analysis of that powder revealed a mix of sand and leaves (see Section 3C.3.5). A photograph of a wheel disk with this powder on its surface is given in Fig. 3C.11. The height of that powder on the disk surface was measured to be up to 33 µm (see Fig. 3C.12). It must be mentioned that in all tests with sand the rail disk presented a complete clean shiny surface that can be attributed to the material transfer characteristic of this type of rolling-sliding tests, which was previously outlined in [3C.12].

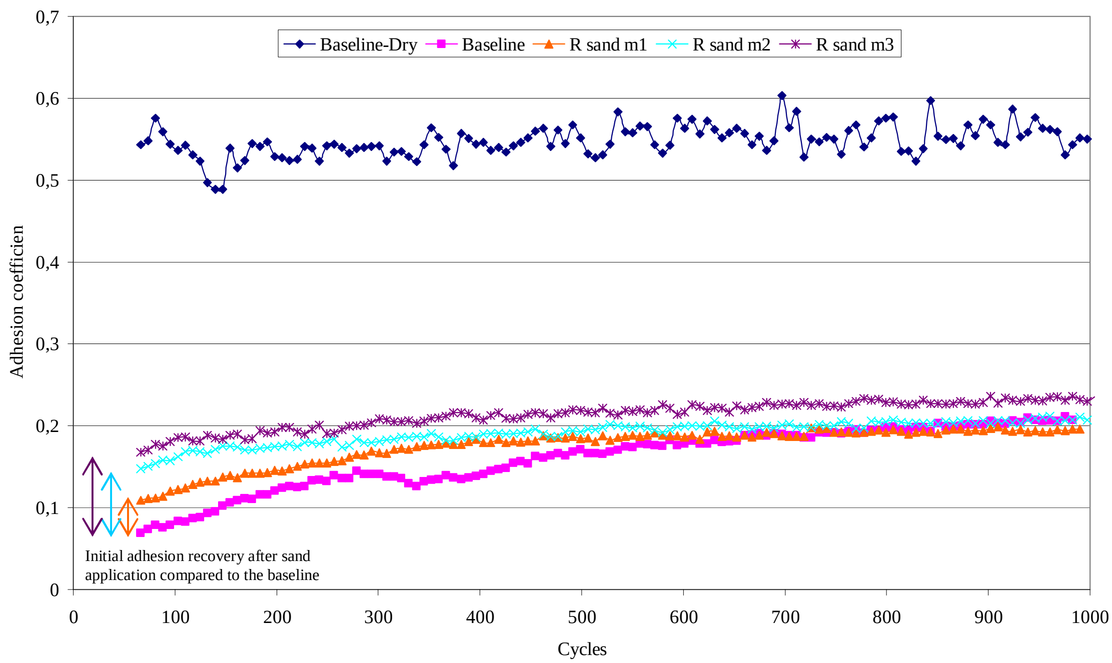

Fig. 3C.8. Adhesion results in leaf contaminated tests with R sand at 1% slip at different number of sanding axles (references: baseline-dry without any contamination and baseline without sand).

Since no solid leaf layer, but powder, was found on the wheel disk surface of the R sand m3 test at 10% slip, it could be assumed that in general the leaf layer started to break apart once the peak in the adhesion coefficient was reached. The subsequent transformation into powder may have caused the continuous reduction in the adhesion coefficient observed in Fig. 3C.10, i.e. the powder may have acted as a solid lubricant. Once the leaf layer was mostly converted into powder the minimum adhesion coefficient could have been reached, which was around 0.25 for both m2 and m3 tests with R sand at 10% slip. This last assumption was validated upon post-test examination of the wheel disk surface used in the m2 test, which had just reached the minimum adhesion coefficient at the end of the test. With further increase in cycles the powder may have gradually been removed from the disk surfaces leading to the steady increase in the adhesion coefficient, as observed in the m3 test of Fig. 3C.10.

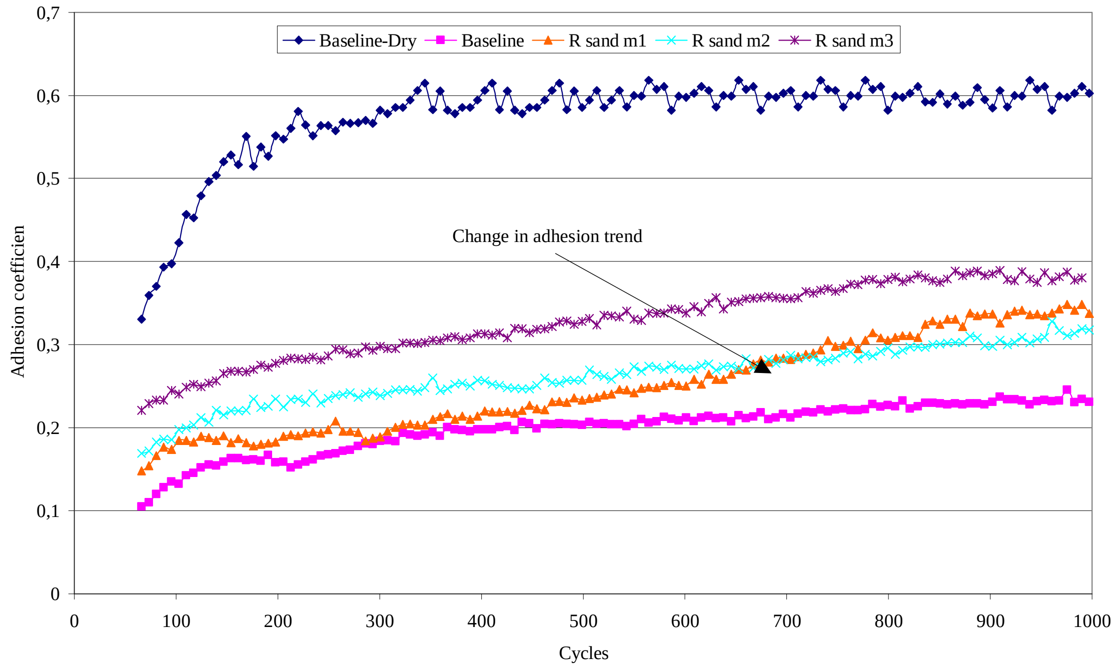

Fig. 3C.9. Adhesion results in leaf contaminated tests with R sand at 5% slip at different number of sanding axles (references: baseline-dry without any contamination and baseline without sand).

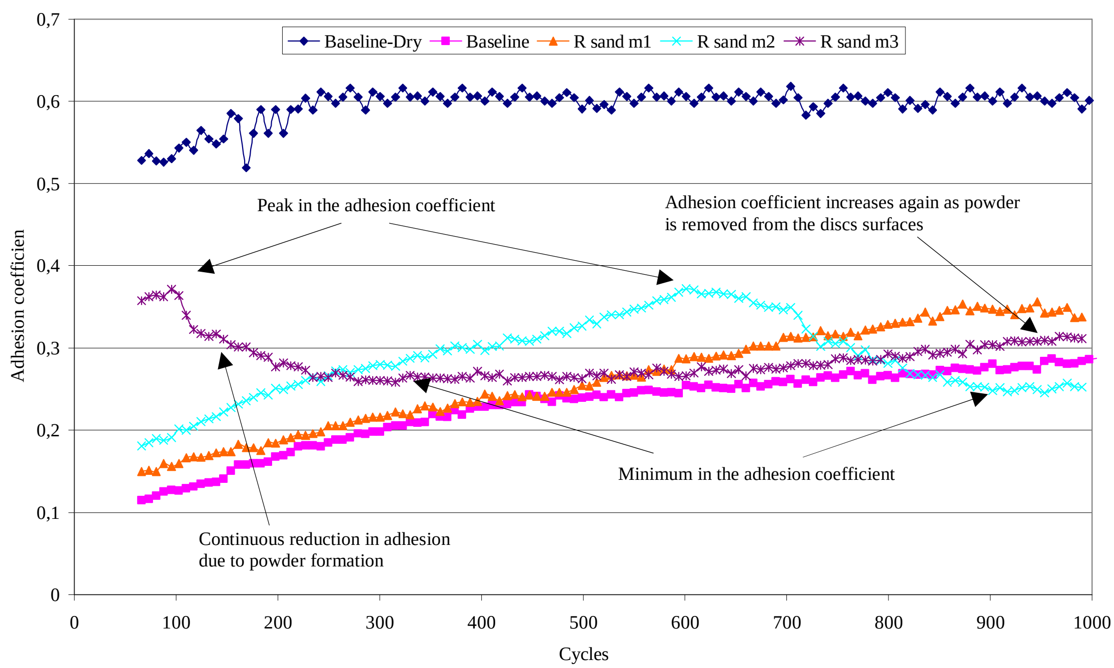

Fig. 3C.10. Adhesion results in leaf contaminated tests with R sand at 10% slip at different number of sanding axles (references: baseline-dry without any contamination and baseline without sand).

Increasing the number of sanding axles did not lead to the formation of powder in the R sand tests at 1 and 5% slip, which indicated that a certain slip and amount of sand was required to break up the leaf layers. Nevertheless, an improvement in the adhesion recovery in both tests was observed (see Figs. 3C.8-3C.9). The wheel disks of those tests had remaining solid layers like the one displayed on Fig. 3C.11. The Vickers micro-hardness of those layers ranged between 59 and 67 HV_{10g}, and the thickness between 4 and 12 μm. In order to illustrate the solid and powder forms of post-test contamination, photographs and 3D optical pictures of two wheel disks are given in Figs. 3C.11-3C.12. Note that the curvature of the disks has been corrected in Fig. 3C.12 to show flat surfaces. Besides the solid layers and the powder, indentations on the disks surfaces could be seen in Fig. 3C.12, which were caused by sand particles.

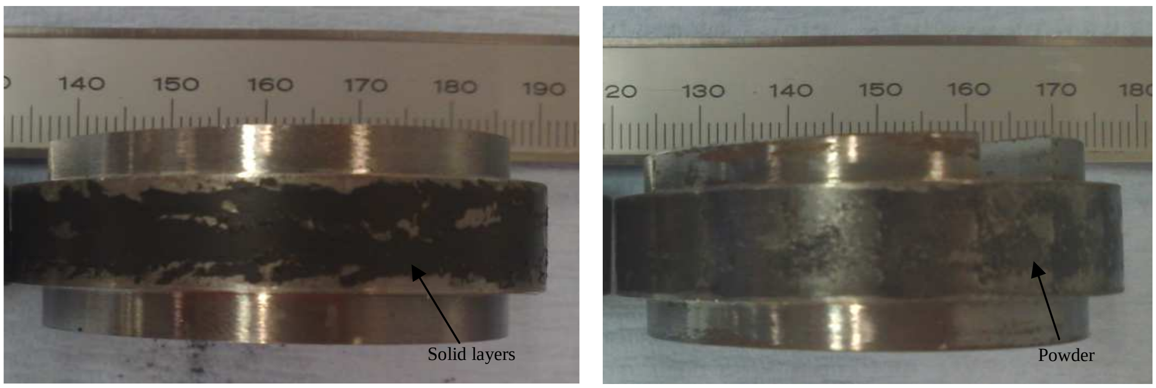

Fig. 3C.11. Photographs of wheel discs during post-test examination with: (left) remaining solid layer; (right) powder of broken layer.

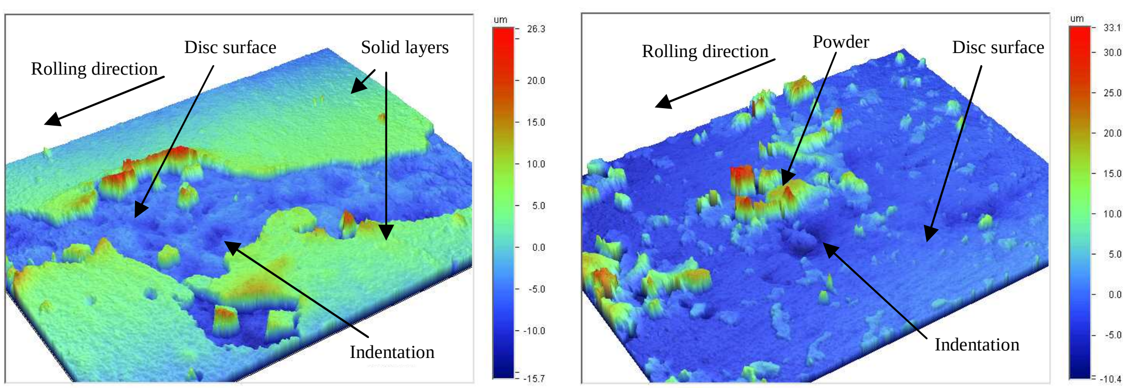

Fig. 3C.12. Pictures taken with an optical 3D profiling system of the wheel disc surface with: (left) remaining solid layer; (right) powder of broken layer.

Fig. 3C.13 depicts the electrical insulation results of the tests with R sand at 10% slip, whose adhesion history was given in Fig. 3C.10. The *Vout* readings could be identified as a three-phase process. During the initial cycles of the test the leaf layers, which had adhered to the disk surfaces during test preparation, could insulate the wheel-rail contact, e.g. baseline test in Fig. 3C.13. It can be seen that the application of sand had a positive effect on improving the wheel-rail conductivity by removing the insulating leaf layers, which led to a lower initial *Vout* compared to the baseline, as pointed out in Fig. 3C.13. Furthermore, the increase in the number of sanding axles gave a faster improvement of the electrical conductivity, which was particularly noticeable in the m3 test. As expected, the lowest *Vout* corresponded to the baseline-dry test due to the absence of contamination. The second phase corresponded to a steep decreasing slope of *Vout* in some tests, e.g. baseline and R sand m1 and m2 tests. This could indicate a substantial removal of the leaf layers, or the fact that their thickness reduced to facilitate more metal-metal contact between asperities. The third phase was represented by variations of the *Vout* with a decreasing tendency towards the *Vout* of the baseline-dry test. Those variations in *Vout* could partly be due to the influence of the bearing resistance, which cannot be neglected in Eq. 3C.3 in the absence of contamination in the wheel-rail contact (i.e. low values of *Rc*). In the m3 test an increase in *Vout* is observed between 300 and 800 cycles, which could have been caused by a possible increase in *Rb* on the one hand, and by the powder transformation leading to a higher *Rc*, on the other. After 1000 cycles the baseline test registered a considerably higher *Vout* than the tests with sand, which was found to be in good agreement with the findings on the remaining contamination during the post-test examination. Particularly, the wheel disk used in the baseline test had a larger coverage of solid layers compared to the tests with sand. Some patches of solid layers were also present on the rail disk of the baseline test, whereas the rail disks of all tests with R sand were clean.

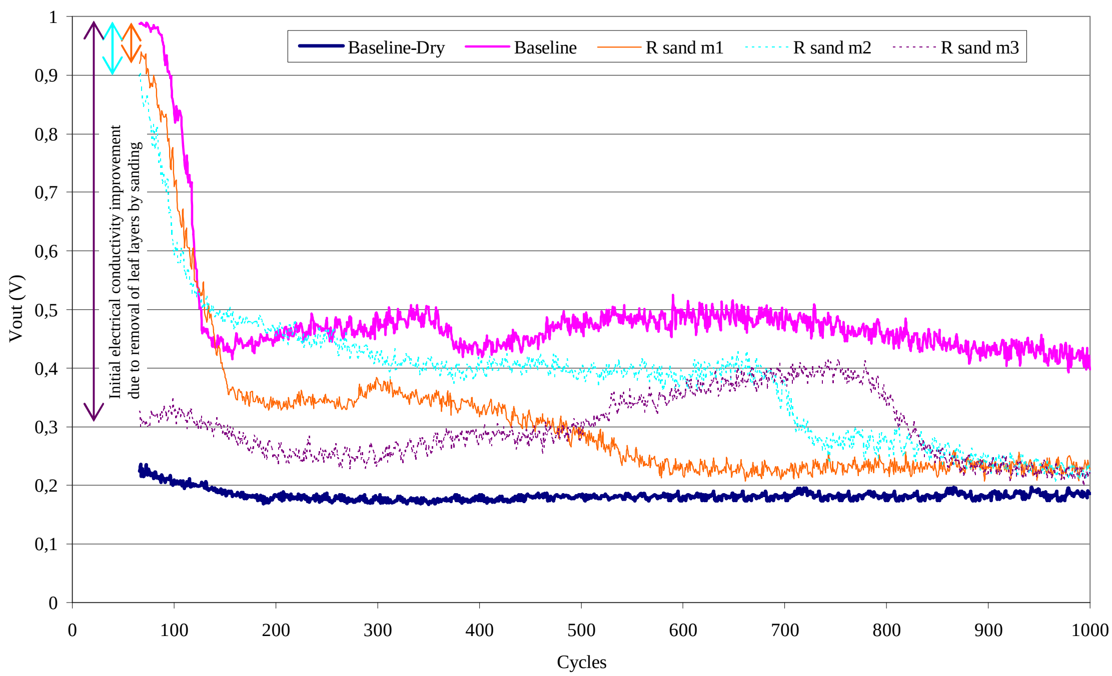

Fig. 3C.13. Electrical insulation results in leaf contaminated tests with R sand at 10% slip at different number of sanding axles (references: baseline-dry without any contamination and baseline without sand).

In Fig. 3C.14 the results with S sand at 5% slip are depicted. It can be seen that the increase in the number of sanding axles led to a larger initial adhesion improvement.

Furthermore, in the m3 test the adhesion coefficient reached a peak value of 0.45 after around 300 cycles, and then the adhesion decreased. The adhesion coefficient decreased to 0.35 at 700 cycles and then the adhesion started to increase again. Powder was observed on the wheel disk surface so this could explain the variations in adhesion similarly to the tests with R sand at 10% slip. Similar results in adhesion appeared in the m1 and m2 tests with S sand compared to the m3 test; however, a phase lag was present as slower leaf layer removal occurred with a lower number of sanding axles. Another difference found among the tests with S sand was on the peak in the adhesion coefficient, which was 0.39 for both m1 and m2 tests compared to 0.45 in the m3 test. Hence, the increase in number of sanding axles not only gave a faster adhesion recovery, but also led to a higher peak in the adhesion coefficient. The explanation for the different value of the peaks was found upon post-test examination of the disks. In the m1 and m2 tests, the wheel disk surfaces had some patches of remaining solid layers, which were not observed in the wheel disk of the m3 test. Additionally, no powder formation had occurred in the m1 test.

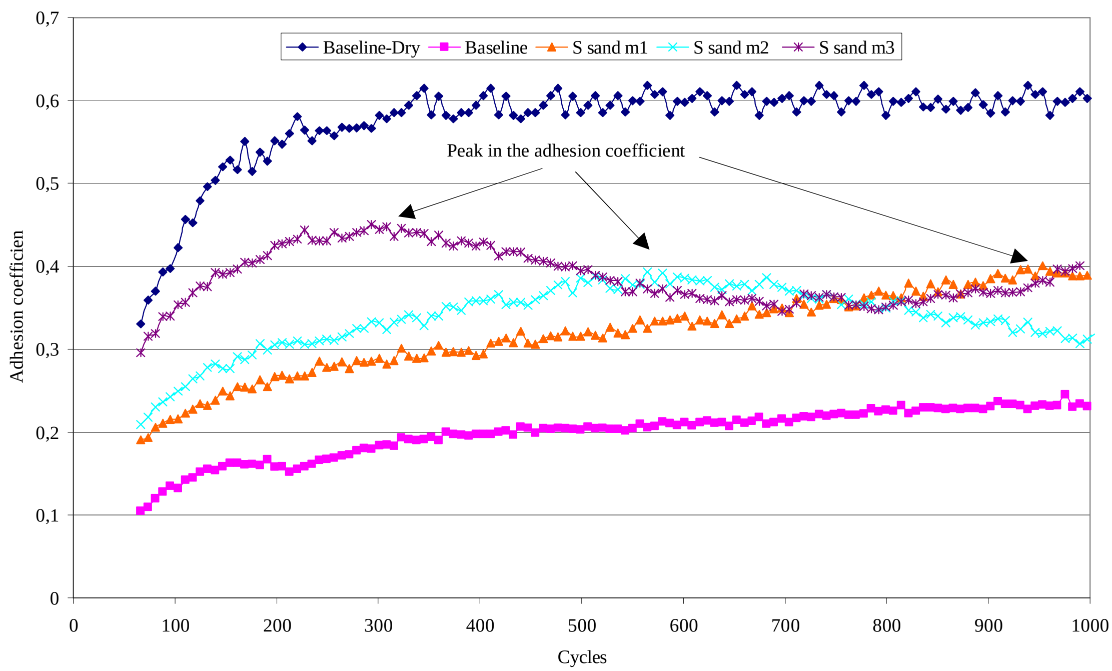

Fig. 3C.14. Adhesion results in leaf contaminated tests with S sand at 5% slip at different number of sanding axles (references: baseline-dry without any contamination and baseline without sand).

In the tests with M sand at 5% slip the increase of sanding axles showed a considerable improvement on the adhesion recovery, as shown in Fig. 3C.15. The peak in the adhesion coefficient was obtained as 0.39 after 100, 380 and 990 cycles, for m3, m2 and m1 tests, respectively. The phenomenon of powder formation after layer break-up was only observed in the m2 and m3 tests. Additionally, clean adhesion conditions were reached in the m3 test after 750 cycles, as pointed out in Fig. 3C.15. It can be seen that the initial adhesion coefficient is larger in the m3 test with M sand than in the baseline-dry test.

This is due to the initial surface run-in of the disks used in the baseline-dry test, which lasted for the first 300 cycles.

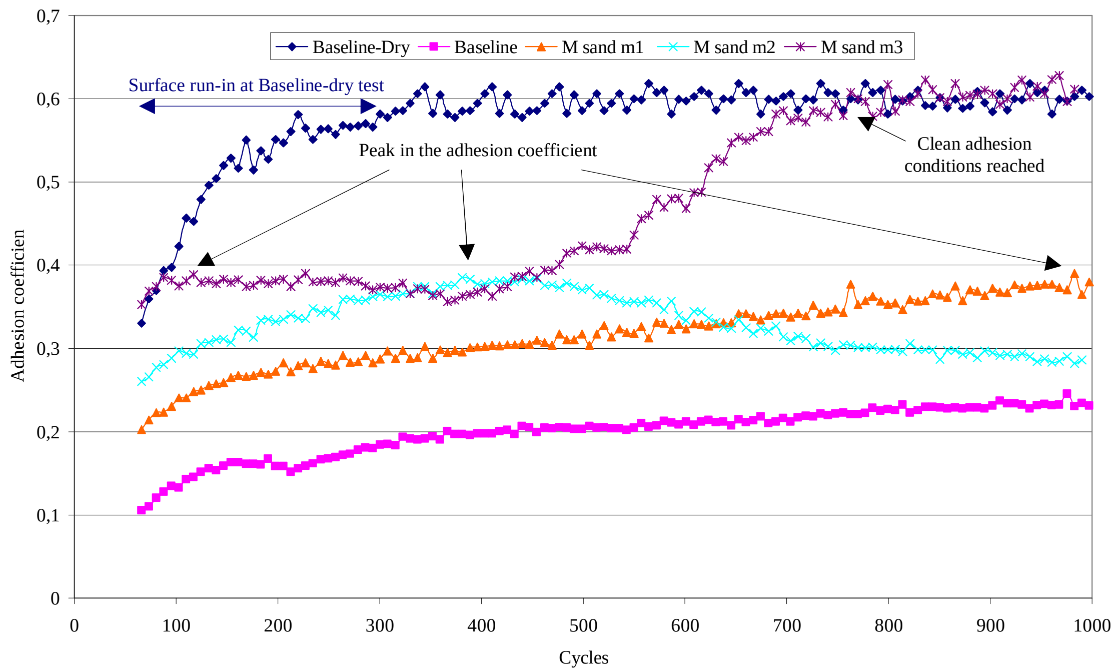

Fig. 3C.15. Adhesion results in leaf contaminated tests with M sand at 5% slip with different number of sanding axles (references: baseline-dry without any contamination and baseline without sand).

Furthermore, the application of L sand slightly increased the initial adhesion coefficient compared to the baseline, as shown in Fig. 3C.16. Nevertheless, this adhesion improvement was considerably lower than with the other sands, which could be attributed to the poor entrapment of large particles. The most effective initial adhesion recovery was achieved in the test with m3, which clearly showed a considerably better performance than the baseline. However, increasing the number of sanding axles did not lead to powder formation. Remaining layers could be seen on the wheel disk of all tests performed with L sand. Vickers micro-hardness tests on those layers yielded a value between 50 and 69 HV_{10g}, and their thickness was measured between 6 and 18 µm.

3C.3.2. Influence of the wheel slip

In order to investigate the influence of the wheel slip on the adhesion recovery during sanding, tests with R sand were carried out in different number of sanding axles at three different slips: 1, 5 and 10% (see Figs. 3C.17-3C.19). It can be seen that the influence of the wheel slip became weaker when using fewer number of sanding axles. In the m1 tests, 5 and 10% slip yielded similar adhesion recovery with a slight higher adhesion coefficient reached at 10% slip (see Fig. 3C.17). On the other hand, 1% slip led to the lowest initial adhesion coefficient and the slowest adhesion recovery. Some remaining solid layers were observed on the wheel disks for the three slips tested. However, less contamination was found on the wheel disk surfaces of tests with higher slip. For example, the remaining leaf layer of the test at 10% slip had begun to break up and did not cover the whole surface. Vickers micro-hardness measurements on that layer led to erroneous values because the indenter penetrated through the layer. On the other hand, the remaining layer of the test at 1% slip, which almost covered the entire wheel disk surface, was between 59 and 67 HV_{10g} in Vickers micro-hardness.

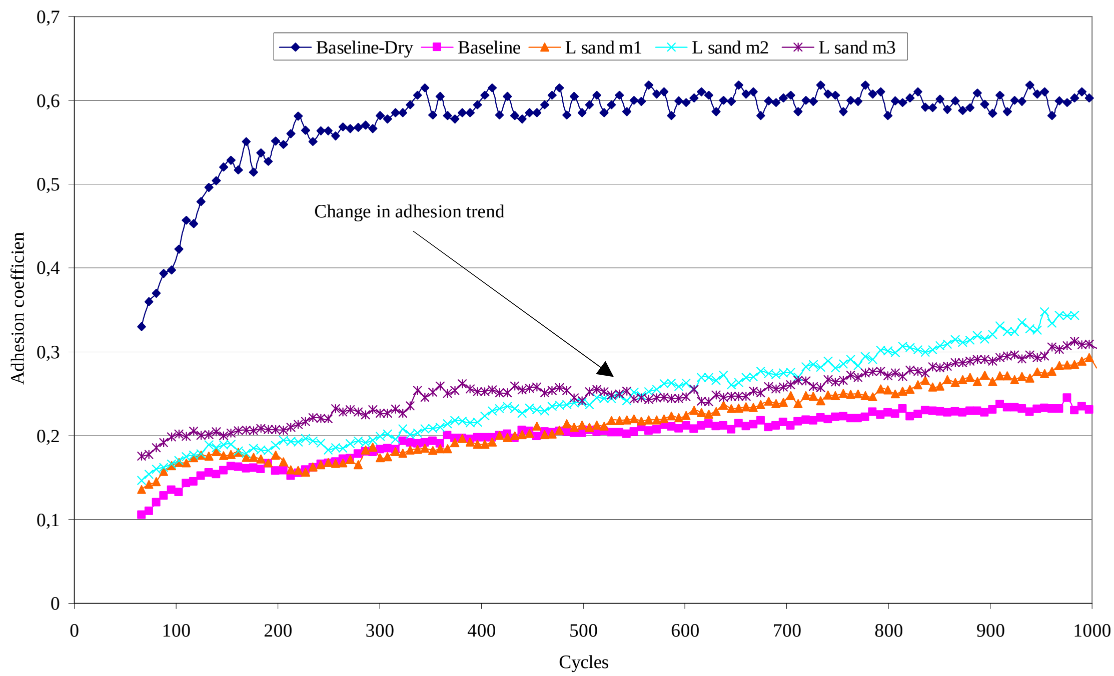

Fig. 3C.16. Adhesion results in leaf contaminated tests with L sand at 5% slip at different number of sanding axles (reference baseline-dry without any contamination and baseline without sand).

The increase in wheel slip clearly promoted a faster adhesion recovery in the m2 and m3 tests, as shown in Figs. 3C.18-3C.19. It can be seen that the basic difference between Fig. 3C.18 and Fig. 3C.19 is a phase lag, which accounted for the faster adhesion recovery experienced with higher number of sanding axles. At 10% slip the peak in the adhesion coefficient was reached at 0.37 as the leaf layers were breaking up. Then, the adhesion decreased as a consequence of the formation of powder, and after reaching a minimum in the adhesion coefficient around 0.25, the adhesion started to increase again. Some remaining powder was observed on the wheel disk surfaces after completion of those tests. In tests at 5% slip no powder formation was observed and the peak in adhesion reached was lower than in tests at 10% slip. This was due to the presence of some patches of remaining solid layers that were found on the wheel disk surfaces. The slowest adhesion recovery was observed at 1% slip, which was attributed to remaining contamination layers on the wheel disk surfaces. Vickers micro-hardness of those layers ranged between 59 and 67 HV_{10g}, and their thickness was measured between 8 and 12 μm. Moreover, a higher initial adhesion coefficient with higher wheel slip was clearly observed in the m3 tests. The initial adhesion coefficient was around 0.17 with 1% slip, whereas it was around 0.36 for 10% slip (see Fig. 3C.19 and Table 3C.1).

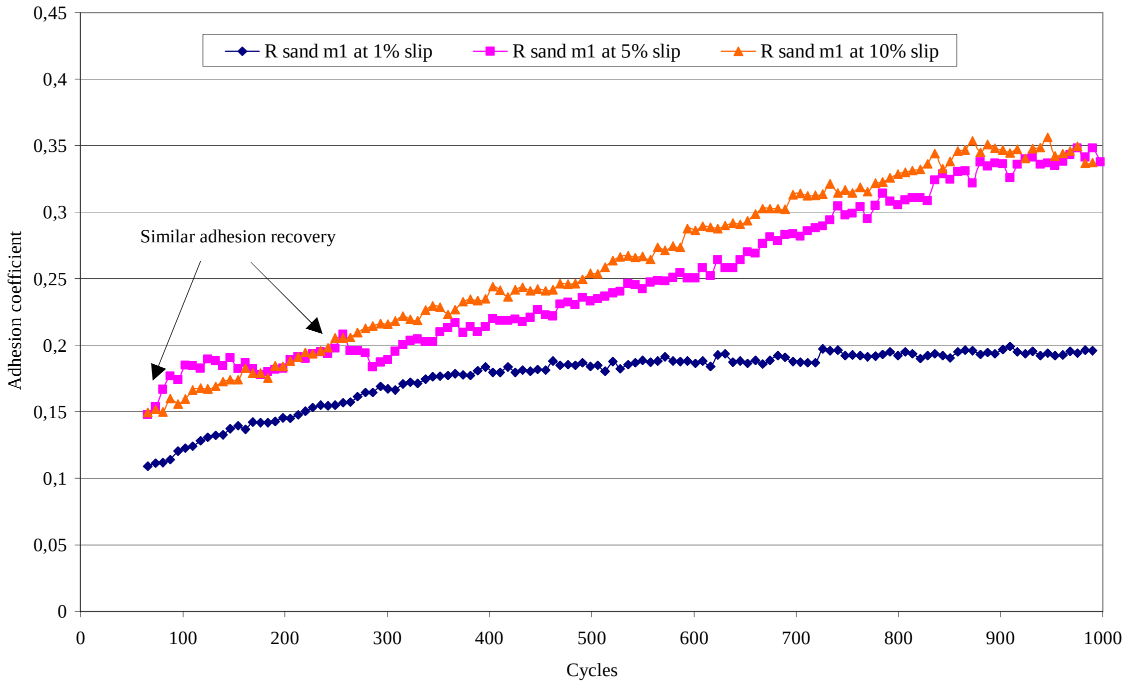

Fig. 3C.17. Adhesion results in leaf contaminated tests with R sand at different slips for m1 application.

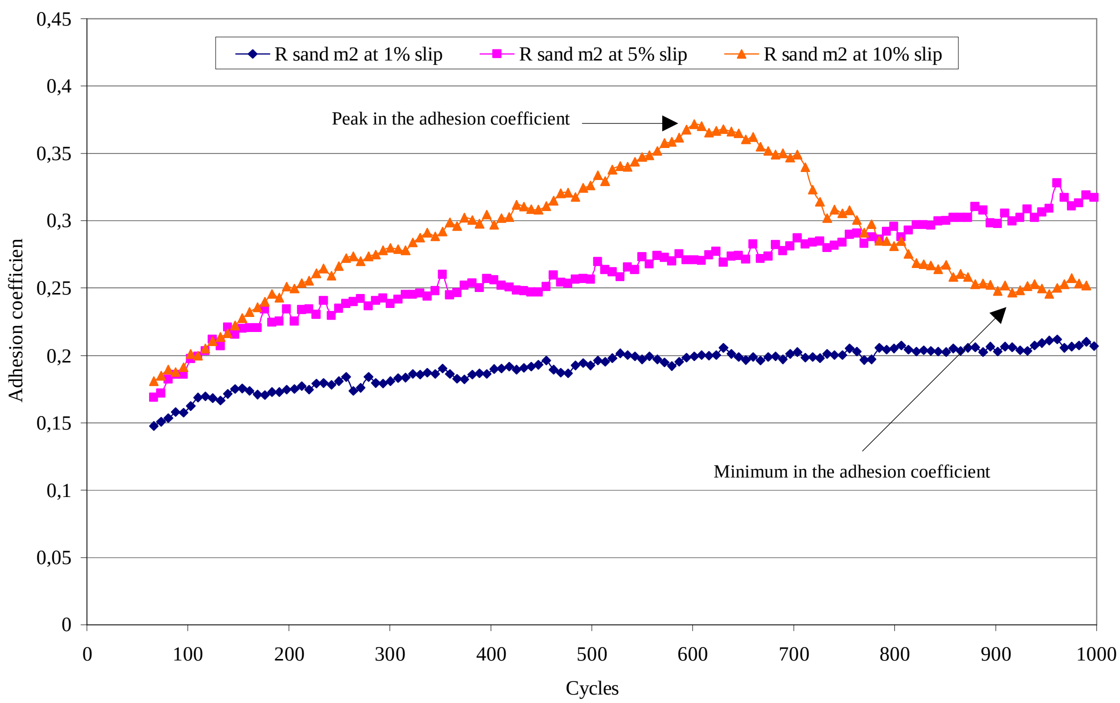

Fig. 3C.18. Adhesion results in leaf contaminated tests with R sand at different slips for m2 application.

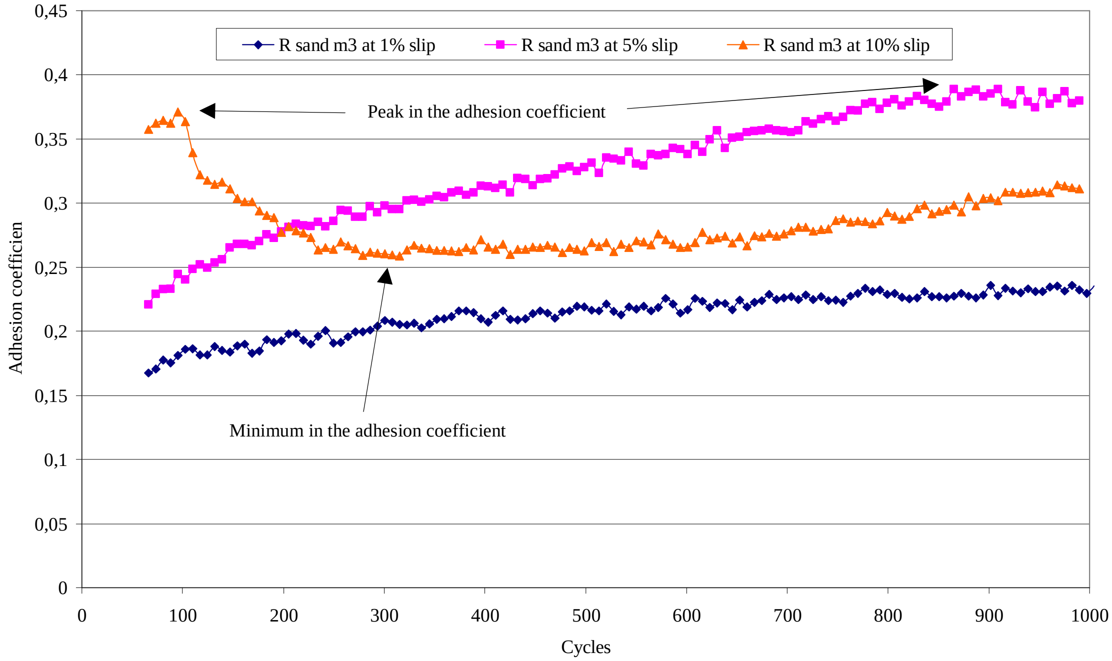

Fig. 3C.19. Adhesion results in leaf contaminated tests with R sand at different slips for m3 application.

Furthermore, the influence of the wheel slip on the adhesion recovery was also investigated for the baseline situation at 5 different slips. It can be seen in Fig. 3C.20 that a higher adhesion coefficient was initially obtained at higher values of wheel slip until 5% slip. No significant difference in the initial adhesion recovery (i.e. up to 300 cycles) was observed between tests at 5 and 15% slip, which may indicate saturation on the layer removal by wheel slip. In most of the tests, the evolution of the adhesion followed a trend on which higher adhesion coefficient was reached at the end of the test with higher wheel slip. There was, however, an odd result obtained at 15% slip that broke this tendency. Post-test examination showed that the wheel and rail disks used in that test presented some remaining contamination in the form of powder as well as few tiny patches of solid layer. This means that 15% slip was high enough to break up some of the leaf layer patches leading to the powder formation. The presence of that powder may have been responsible for decelerating the increase of the adhesion coefficient. On the other hand, no powder formation was observed in tests with wheel slips between 0.5 and 10%. Furthermore, less coverage of remaining leaf layers was observed on the disk surfaces used in tests with higher slip, which corresponded well with the adhesion results. Those layers had a thickness between 3 and 13 μm, and Vickers micro-hardness of 47-68 HV_{10g}.

Moreover, there was one striking difference between the baseline and the sanding tests. In the baseline tests, the rail disk was not completely free of contamination, which suggests that sanding may have enhanced the material transfer from the rail to the wheel disk due to the abrasive action of entrapped sand particles. The wheel steel is softer than the rail steel and, thus, more particles may indent and remain in the wheel disk surface and then abrade the rail disk surface along the sliding distance of the contact patch. In baseline conditions, this material transfer must be fulfilled by the asperities. If one considers that the average roughness of the disks was around one tenth of the thickness of the leaf layers and at most one hundredth of the initial size of the smallest particles of sands tested, it can be understood that the mechanical transfer of the contamination is expected to be considerably less effective in the baseline tests than in tests with sand.

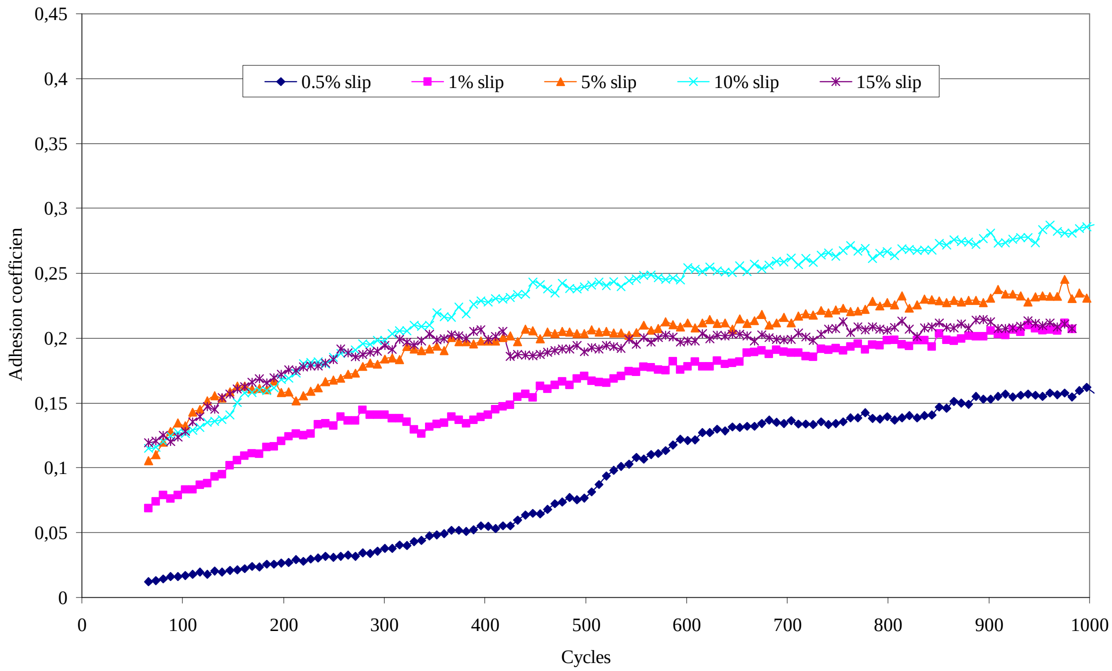

Fig. 3C.20. Adhesion results in leaf contaminated tests with baseline at different slips.

3C.3.3. Influence of the particle size

The influence of the particle size was investigated at 5% slip for the three numbers of sanding axles (m1, m2, and m3), as shown in Figs. 3C.21-3C.23. Note that the two baselines are also given in the figures. It can be observed that the highest initial adhesion improvement was obtained with M sand, with an initial adhesion coefficient between 0.20 and 0.35 depending on the number of sanding axles used. Note that the initial adhesion coefficient of the baseline was around 0.11. Furthermore, the fastest adhesion recovery was also achieved with M sand. The peak in the adhesion coefficient was reached in fewer cycles compared to tests with other sands, as shown in Figs. 3C.22-3C.23, and the adhesion even recovered to that of clean dry conditions in the m3 test, as pointed in Fig. 3C.23. The S sand presented a similar good performance with a phase lag of 100-200 cycles with respect to M sand, but clean adhesion conditions were not reached in those tests. On the other hand, L and R sands rendered a slightly faster adhesion recovery compared to the baseline, which was particularly poor in the m1 tests. In all tests with L sand, remaining layers were found on the wheel disk, which ranged 51-69 HV_{10g} in Vickers micro-hardness and with thickness between 6 and 18 μm. In the tests with R sand the layers, which remained on the wheel disk surface, had a Vickers micro-hardness between 59 and 67 HV_{10g} and 8-12 μm in thickness.

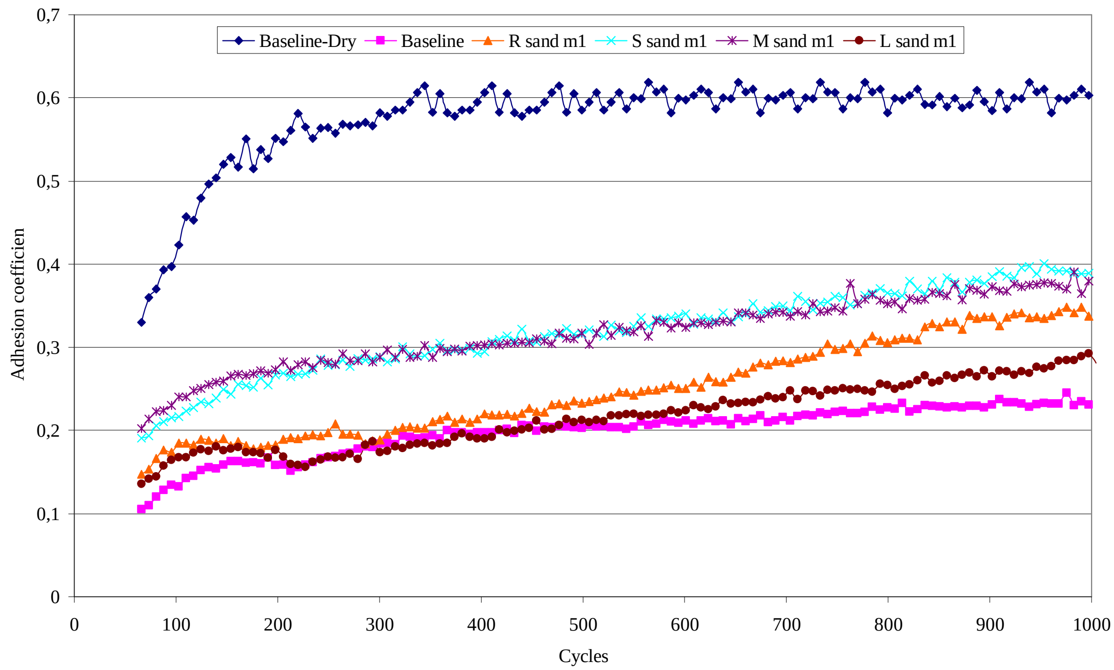

Fig. 3C.21. Adhesion results in leaf contaminated tests with different sands at 5% slip for m1 application (reference baseline-dry without contamination).

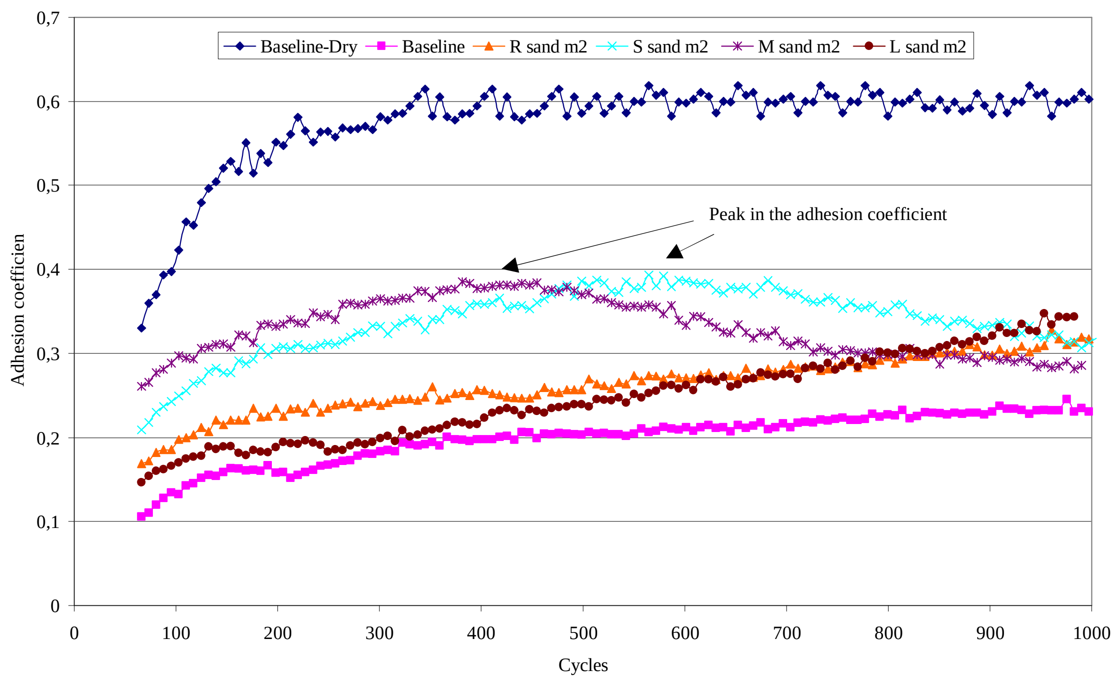

Fig. 3C.22. Adhesion results in leaf contaminated tests with different sands at 5% slip for m2 application (reference baseline-dry without contamination).

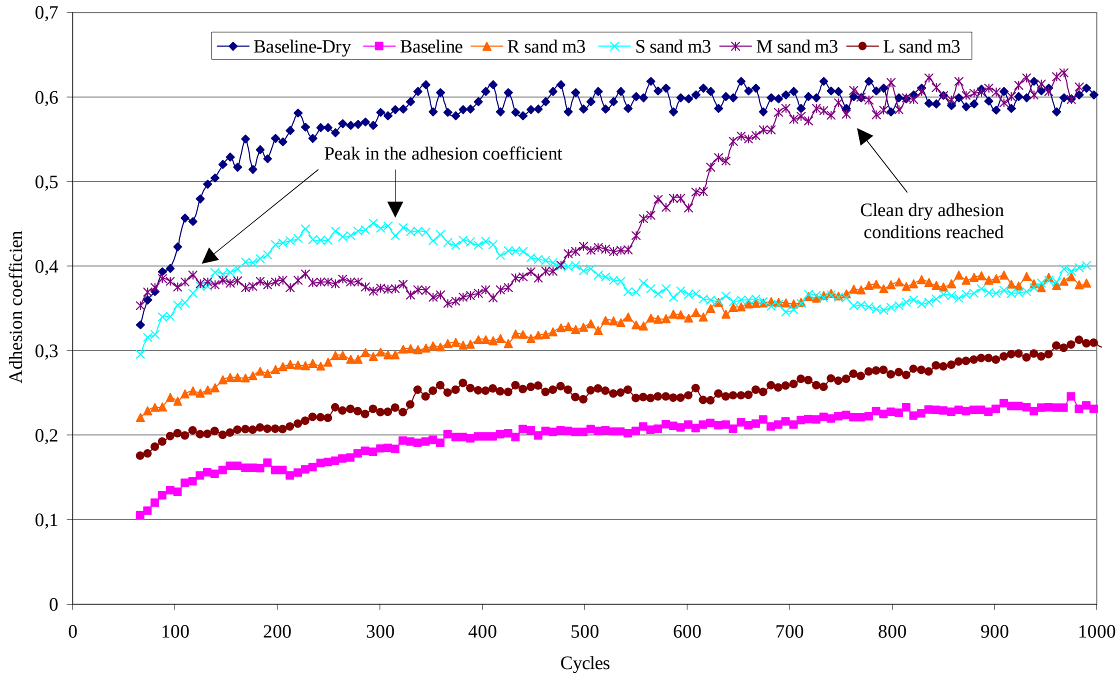

Fig. 3C.23. Adhesion results in leaf contaminated tests with different sands at 5% slip for m3 application (reference baseline-dry without contamination).

The best performance of M sand can be explained by considering the balance between the better particle entrapment in the wheel-rail contact of smaller sands, and the more effective layer removal of particles the size of which is larger than the thickness of the contamination layer. In another work, in which the sands were applied continuously in a dry uncontaminated wheel-rail contact, it was shown that S and M sands entirely insulated the wheel-rail contact, whereas R and L sands only increased the electrical resistance with respect to the steel-on-steel contact [3C.18]. In other words, the decrease in particle size promoted the entrapment in the wheel-rail contact, causing more insulation. In general, it is expected that having more particles travelling through the wheel-rail contact would help in removing the contamination to a greater extent, leading to a better adhesion recovery. Hence, this may indicate that smaller sized sand could be more effective than larger sands. Nevertheless, M sand had better performance than S sand, which may be attributed to its slightly larger particle size, which is small enough to promote good particle entrapment, but large enough to prevail over the leaf layers. The small size of S sand may have caused some of the particles to get entrained in the leaf layers, or even the leaf mulch patches, reducing the possibility of abrasion. Therefore, M sand appears to be the optimum size for enhancing the poor adhesion caused by leaf layers in this test set-up.

In order to illustrate the influence of the particle size on the evolution of the electrical insulation of the wheel-rail contact, the *Vout* readings of the m3 tests at 5% slip are given in Fig. 3C.24. The *Vout* of the baseline test is not given because it was not measured. Note that the corresponding adhesion results were given in Fig. 3C.23. It can be seen that the electrical insulation correlated well with the adhesion results. The application of M sand led to the lowest initial *Vout*, followed by S sand, R sand and L sand. On the other hand, open circuit conditions can be observed in the test with L sand up to 100 cycles due to the presence of remaining leaf layers. In all sand tests, the *Vout* showed a decreasing tendency with the increasing number of cycles. However, some variations in that tendency were observed in the tests with M and S sand, which may have been caused by the transformation of the layers into powder.

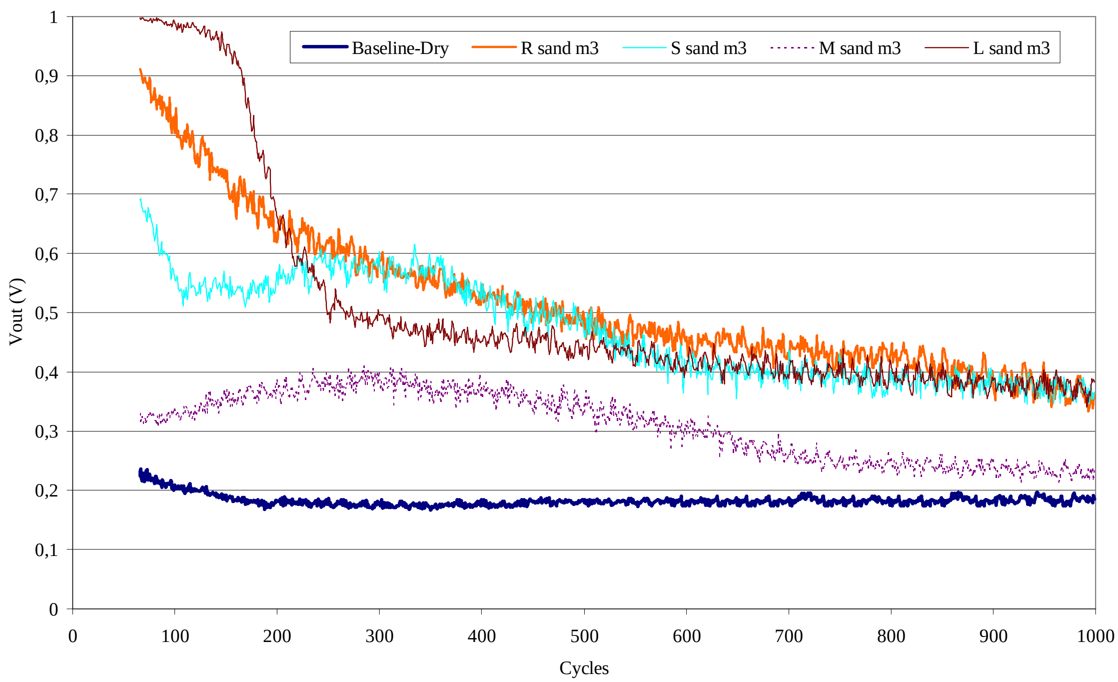

Fig. 3C.24. Electrical insulation results in leaf contaminated tests with different sands at 5% slip for m3 application (reference baseline-dry without contamination).

3C.3.4. Necessary wheel passages for adequate traction

Adhesion measurements carried out on the Dutch railway network in autumn 2008 with an on-board system on five passenger trains showed that low adhesion incidents occurred during traction operation much more frequently than in braking [3C.20]. This was expected due to the different adhesion requirements of the measuring train, which were around 0.22 and 0.10 for traction and braking, respectively. In practice, the adhesion required by traction can be up to three times of that by braking, depending mostly on the type of rolling-stock, but also on the driver's behaviour. Table 3C.2 gives an overview of the number of cycles (similar to the wheel passages) that were required in each test to reach an adhesion coefficient of 0.2, which can be taken as a general threshold for adequate traction operation [3C.7]. It can clearly be seen that the application of sand leads to fewer necessary wheel passages compared to the baseline. It can be seen in Table 3C.2 that in some tests with sand an adhesion coefficient higher than 0.2 was obtained before the 65 cycles due to the immediate adhesion improvement of sand. The reduction in wheel passages brought about by sanding was dependent on the number of sanding axles, the particle size, and the wheel slip. The increase of sanding axles reduced the required wheel passages between 27% and 95%, depending on the particle size. The influence of the number of sanding axles was predominant in sands of larger particle size, which could be attributed to their poor entrapment. Decreasing the particle size with respect to R sand, which is the standard used in the Netherlands, reduced the required wheel passages by 50-80%, depending on the particle size. On the other hand, increasing the particle size was proven to be ineffective. Finally, increasing the wheel slip led to a reduction in the required wheel passages of 50-95% in tests with R sand and 50-70% in the baseline.

Table 3C.2. Number of cycles (similar to wheel passages) required to reach the needed adhesion for adequate traction performance.

	1% slip	5% slip				10% slip
Baseline	880	418				308
	R sand	R sand	S sand	M sand	L sand	R sand
m1	1000	315	80	66	440	249
m2	528	117	<65	<65	308	117
m3	286	<65	<65	<65	117	<65

3C.3.5. FTIR micro-spectroscopy analysis

The remaining contamination found on the disks was analyzed by FTIR micro-spectroscopy. Fig. 3C.25 gives the spectra of three tests that represent different patterns observed in the adhesion recovery: a baseline test, in which solid leaf layers remained; a test with sand, in which some solid layers remained in spite of the sand application; a test with sand, in which the sand application caused the transformation of the solid layers into powder. For comparison, the FTIR spectra of leaf material and crushed sand are also given in Fig. 3C.25. Note that only one sand is given because all sands showed similar spectra in the measurements.

It can be observed that the generated leaf layer had a broad absorbance peak between 3700 and 3100 cm^{-1} that may be attributed to the water OH stretch vibrations. The two characteristic peaks at 2920 and 2850 cm^{-1} could be related to lignin present in the leaf sample, while the absorption profile from 1800 to 600 cm^{-1} is from other compounds present in leaf layers, such as pectin and cellulose, thoroughly explained in [3C.4]. Note that laboratory and field studies concluded that lignin is one of the major compounds responsible for the bonding of the leaf layers to the railhead [3C.6]. Furthermore, the spectrum of sand was clearly distinguished from the one of generated leaf layers with a null absorbance range above 1300 cm^{-1}, and some characteristic peaks at 1160 cm^{-1}, 1050 cm^{-1}, 800 cm^{-1}, 775 cm^{-1}, 690 cm^{-1}.

The spectra of the solid layer A (from the baseline test) corresponded closely to the one of the generated leaf layer, as shown in Fig. 3C.25. This indicates that the increase in adhesion observed in that test may be attributed to the reduction in coverage and thickness of the leaf layers rather than to any transformation of the layers. In the tests with sand, various characteristic peaks of sand could be seen in the spectra measurements of solid layer B and powder, e.g. 800 cm^{-1} and 775 cm^{-1}, indicating that sand had mixed up with the leaf layers and remained in the mixed layer even after transformation into powder. Moreover, some of the characteristic peaks related to the generated leaf layer were no longer distinctly present in the spectra of solid layer B and especially powder (e.g. peaks in the range 1200-1600 cm^{-1}). This change could be due to chemical modification of the leaf material, but it is more likely to be caused by altered light trapping properties of the leaf/sand mixture.

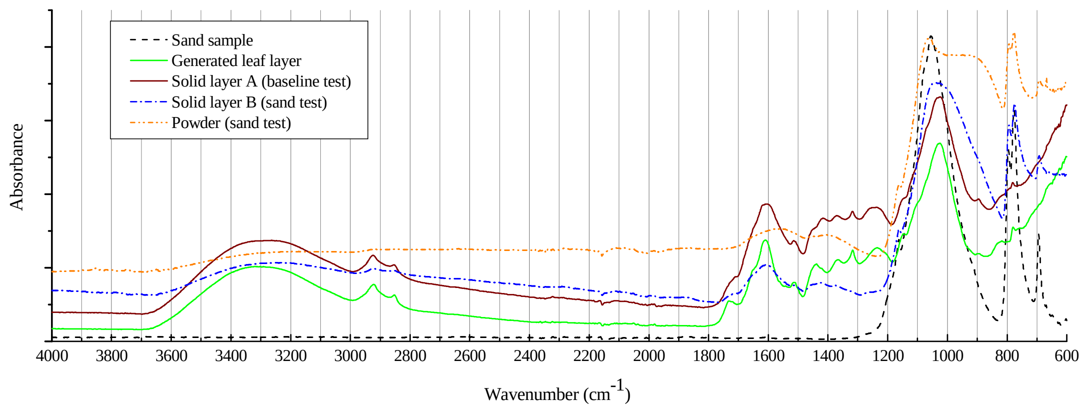

Fig. 3C.25. IR micro-reflection spectra of the initial samples (leaf and sands), leaf layer, and the remaining contamination of three representative leaf tests.

3C.4. Discussion

There are mostly three possible approaches to remove leaf contamination from the wheel and rail surfaces, i.e. mechanical, thermal, and chemical. In this paper, we have presented the mechanical removal by means of hard particulate material (i.e. sand) applied between the wheel and rail. The sand particles, which penetrate through the softer contamination layers and indent the steel surfaces, can abrade the layers, and sometimes even the wheel and rail surfaces, when travelling through the wheel-rail contact. It has been shown that sanding is much more effective than the baseline in recovering the wheel-rail adhesion. In baseline conditions the mechanical removal of the leaf layer relies on the surface asperities, which fail to be effective because the surfaces are usually too smooth for the asperities to prevail over the thickness of the leaf layers. A possible interesting line of investigation may be finding a suitable surface roughness of the top of the rail that can prevail over the leaf contamination, reducing the adhesion problems. Such roughness could be applied to sections of the track that are identified to be affected by low adhesion problems, e.g. zones with a substantial presence of lineside vegetation. However, considerations on the duration of the optimal roughness and its possible side effects should also be addressed.

In practice, not all the axles of a train formation are equipped with sanders. Locomotives, which can haul a substantial number of passenger coaches or freight wagons, normally have sanders on every axle; on the other hand, EMUs normally have less than half of the bogies fitted with sanders. The tests of this work simulated the passage of a train with a variable number of sanding axles (1, 2 or 4) over a contaminated section of track (of length equivalent to the circumference of the rail disk) followed by almost 1000 non-sanded wheel passages. The results have shown that increasing the number of sanding axles considerably promotes a larger and faster adhesion recovery for the same slip and particle size. This indicates that there may be an optimal number of passages of sanding axles, which can condition the railhead for an adequate adhesion so that subsequent trains would not be affected, or less affected, by leaf contamination. Efforts to find this optimum in practice could be justified especially for those railway networks on which dedicated vehicles employ sand (perhaps together with other means) to clean the rails from contamination.

Nowadays most of the trains are fitted with traction control (TC) and/or wheel slide protection (WSP) systems, which are adjusted to prevent the wheel slip surpassing a certain threshold value. If poor adhesion conditions are present, the wheels will suffer from (gross-) slip that triggers the TC/WSP systems. There has been some discussion within the research community on whether letting the wheels slide with a higher slip could enhance the removal of the contamination. It is believed that the leaf layer may be burned off if the thermal input is above a certain value. Research carried out by the German Railways (DB) indicated that the optimum wheel slip under leaf contamination conditions must be low to achieve the best possible use of the adhesion [3C.5]. The results of the baseline tests in this work may be in agreement with this finding as saturation of slip seemed to be observed when the slip was higher than 5% slip. On the other hand, it was not reported on the work of DB about the residual effect of an optimized wheel slip on adhesion for subsequent wheels. The baseline tests of this work have shown that the leaf layers were only transformed into powder for 15% slip, which was the highest slip tested. Further work seems necessary to determine whether there is a value of wheel slip, which causes a beneficial residual effect on the adhesion for subsequent wheel passages.

Furthermore, on trains equipped with sanders the WSP and/or TC systems can trigger the application of sand on the rails once the registered wheel slip surpasses the threshold. In the sand tests of this work, the increase of wheel slip has shown to promote a faster adhesion recovery, which can be attributed to an enhanced abrasion that promotes the mechanical removal of the leaf layers. On the other hand, sanding at higher wheel slip leads to increased wear rates [3C.17]. Hence, further investigations on a possible optimization of this parameter should take into consideration its possible side effects.

In the literature several standards can be found that specify the requirements in particle size distribution of the sand to be used. The standard in the UK specifies 0.7-2.8 mm [3C.9], while 0.1-0.6 mm in France [3C.15], and 0.63-2 mm in Germany [3C.21]. Laboratory investigations have shown that using larger sized particles led to higher wear rates of wheels and rails in tests at 10% slip [3C.17]. In this work, the use of medium particles of sand has led to the fastest adhesion recoveries under leaf contamination conditions. Hence, it could be possible to find a particle size distribution of sand that promotes a faster adhesion recovery, while reducing the damage caused to wheels and rails compared to some existing standards. Nevertheless, care has to be taken that the feed rates used do not compromise the train detection. This has shown to be of particular importance when using small particle sizes of sand due to their effective entrapment [3C.18]. Furthermore, the possible clogging of pipes and applicators when using small particles is another practical concern that requires attention, especially if moisture may be present.

In a number of tests, the adhesion coefficient unexpectedly decayed with the increasing number of cycles once it reached a peak value. The explanation to this odd behaviour was found upon post-test examination of the disks, which demonstrated the presence of remaining contamination in the form of powder that could easily be rubbed away with the finger. It can be expected that this situation is rather intrinsic to this type of tests than possible to be encountered in practice. In our test conditions the same wheel is rolling over the same length of rail that is given by the circumference of the rail disk. In practice, the formed powder could be carried away by new wheel passages, or perhaps be blown away by the train's slipstream.

Moreover, there are several differences that impede a quantitative comparison of this testing with the actual situation in railway sanding. The length of the contact area (i.e. in the rolling direction) was 0.5 mm in these tests, which may be smaller than some of the (crushed) sand particles travelling through the disk interface so that it may lead to a behaviour different from the actual wheel-rail contact. Additionally, more sand could have been entrained in these tests than in practice because the sand was directly applied to the wheel-rail interface in the absence of cross wind and train's slipstream. Furthermore, it must be mentioned that the results of this work are valid for the low velocity regime. It may be interesting to investigate the adhesion improvement of sanding at higher rolling velocities than the one used in this work. In such investigations, the effect of the train's slipstream should also be taken into account.

3C.5. Conclusions

This paper presents a laboratory investigation on the influence of the number of sanding axles, particle size of sand, and wheel slip on the adhesion recovery in leaf contaminated wheel-rail contacts. Baseline tests have also been performed with two goals: on one hand, to demonstrate the benefit of sanding in rendering an effective adhesion recovery; and on the other hand, to analyze the possible positive effect of an increase in the wheel slip in baseline conditions. Additionally, tests in dry conditions have been conducted to show the impact of leaf contamination on the wheel-rail adhesion. These rolling-sliding tests have been performed on a twin-disk roller rig under closely controlled conditions. An electrical circuit has been connected to the rig for monitoring the effect of contamination on the electrical insulation across the wheel-rail contact. Based on the results obtained in this work, the following conclusions can be drawn:

a) Sanding is an effective method to enhance the wheel-rail adhesion in leaf contaminated contacts. The removal effect provided by sanding also contributes to overcome the electrical insulation of the wheel-rail contact caused by leaf layers.
b) Increasing the number of sanding axles considerably promotes a faster adhesion recovery for the same slip and particle size. If the first train, which encounters leaf contamination, is equipped with a sufficient number of sanding axles, the railhead could be conditioned so that subsequent trains would not experience low adhesion problems.
c) The positive effect of sanding can be improved further with higher wheel slip, but possible adjustments on the optimum wheel slip should consider that wear rates of wheels and rails are increased with wheel slip during sanding.
d) Medium sized sand particles are identified as the most effective in the adhesion recovery, indicating that some standards on sand particle size may lead to inefficiency of the sand use. If the use of smaller sand particles is to be

investigated in practice on available systems, the possible effect on train detection and clogging must be examined.

e) In the absence of sand, increasing the wheel slip leads to a faster recovery of the wheel-rail adhesion. The evolution of the adhesion with the cycles indicates higher adhesion coefficient in tests at higher wheel slip until 10% slip under these test conditions, but the leaf layers appeared to be broken only with 15% slip. There could be a value of wheel slip that causes a beneficial residual effect on the adhesion for subsequent wheel passages.

References

[3C.1] J. Eleveld: Gladde Sporen, Oplossingsrichtingen voor Adhesieproblemen. Report published by the Dutch Railways Technical Research (NSTO) in Dutch (March 1999).

[3C.2] C.R. Fulford: Review of low adhesion research. Report published by the Rail Safety and Standards Board, UK (2004).

[3C.3] U. Olofsson, K. Sundvall: Influence of Leaf, Humidity and Applied Lubrication on Friction in the Wheel-Rail Contact: Pin-on-Disk Experiments. Journal of Rail and Rapid Transit 218 (2004) 235-242.

[3C.4] P.M. Cann: The 'Leaves on the Line'—a Study of Leaf Residue Film Formation and Lubricity under Laboratory Test Conditions. Tribology Letters 24 (2006) 151-158.

[3C.5] W. Voges, P. Spiess: Optimizing Services with EMU ET42x in Autumn 2004 and 2005. In proceedings of 7th World Congress on Railway Research, Canada (2006).

[3C.6] W. Poole: Characteristics of Railhead Leaf Contamination. Summary Report published by Rail Safety and Standards Board (May 2007).

[3C.7] Z. Li, O. Arias-Cuevas, R. Lewis, E.A. Gallardo-Hernandez: Rolling-Sliding Laboratory Tests of Friction Modifiers in Leaf Contaminated Wheel-Rail Contacts. Tribology Letters 33 (2009) 97-109.

[3C.8] H.I. Andrews: Railway Traction—the Principles of Mechanical and Electrical Railway Traction. Elsevier (1986).

[3C.9] Sanding Equipment Fitted to Multiple Units and On-track Machines. Railway Group Standard GM/RT 2461 (2001).

[3C.10] Boiteux, Cadier, J. Kling, W. Kunnes: Summary of Theoretical and Practical Knowledge of Poor Adhesion Conditions Acquired since Publication of B 164/RP 2. Report DT 257 (B 164) published by the Office for Research and Experiments of the International Union of Railways (1992).

[3C.11] E.A. Gallardo-Hernandez, R. Lewis: Twin Disk Assessment of Wheel/Rail Adhesion. Wear 265 (2008) 1309-1316.

[3C.12] O. Arias-Cuevas, Z. Li, R. Lewis, E.A. Gallardo-Hernandez: Rolling-Sliding Laboratory Tests of Friction Modifiers in Dry and Wet Wheel-Rail Contacts. Wear 268 (2010) 543–551.

[3C.13] S. Kumar, P.K. Krishnamoorthy, D.L. Prasanna Rao: Wheel-Rail Wear and Adhesion With and Without Sand for a North American Locomotive. Journal of Engineering for Industry 108 (1986) 141-147.

[3C.14] R. Lewis, R.S. Dwyer-Joyce: Wear at the Wheel-Rail Interface when Sanding is Used to Increase Adhesion. Journal of Rail and Rapid Transit 220 (2006) 29-41.

[3C.15] Mesures a Prendre Pour Ameliorer la Sensibilite au Shuntage des Circuits de Voie. UIC737-2 in French (1980).

[3C.16] R. Lewis, R.S. Dwyer-Joyce, J. Lewis: Disk Machine Study of Contact Isolation During Railway Sanding. Journal of Rail and Rapid Transit 217 (2003) 11-24.
[3C.17] O. Arias-Cuevas, Z. Li, R. Lewis: A Laboratory Investigation on the Influence of the Particle Size and Slip During Sanding on the Adhesion and Wear in the Wheel-Rail Contact. In proceedings of the 8th International Conference on Contact Mechanics and Wear of Rail/Wheel Systems, Firenze, Italy, September 15-18 (2009).
[3C.18] O. Arias-Cuevas, Z. Li, R. Lewis: Investigating the Lubricity and Electrical Insulation Caused by Sanding in Dry Wheel-Rail Contacts. In press, Tribology Letters (2009) DOI 10.1007/s11249-009-9560-1.
[3C.19] D.I. Fletcher, J.H. Beynon: Development of a Machine for Closely Controlled Rolling Contact Fatigue and Wear Testing. Journal of Testing and Evaluation, 28 (2000) 267-275.
[3C.20] N. van Steenis: Monitoren Treinprestaties bij Gladheid; Verkrijgen van Kennis ten Behoeve van Ontwikkeling van Gladheidmaatregelen. Ph.D. Thesis, University of Twente, Enschede, the Netherlands (2010).
[3C.21] G. Gfatter, D. Lang, H. Kalbas, G. Krause, W. Rychli: Sanding Systems. Handbook published by Knorr-Bremse GmbH (2002).

Chapter 3, Part D

Field tests on adhesion recovery[X]

ABSTRACT

Locomotives of railways worldwide have been using sand since 1838 to improve the wheel-rail adhesion during traction and braking operations. In more recent years, sanders have also been fitted to electrical multiple units in some railways to fight (often in combination with traction control or wheel slide protection systems) the low adhesion conditions, especially encountered in autumn due to leaf contamination. In spite of the worldwide broad use of sand, different standards on sanding practice appear to be used by different railways, while there is a lack of fundamental understanding on the influence of sanding parameters, such as particle size distribution, feed rate, and number of sanding axles (among others), on the adhesion recovery, wear, and train detection. In order to gain a better understanding on these interrelationships, the authors have carried out laboratory investigations in recent years. As a continuation of that work, the influence of the sand particle size on the adhesion recovery in leaf contaminated contacts is investigated in this paper by means of traction tests of an electrical locomotive in a stabling yard. Three differently sized silica sands are used in the testing. In addition to the particle size investigations, the standard sand currently used in the Dutch railways is also tested to quantify its effectiveness against leaf contamination. Besides the immediate adhesion improvement upon sanding, the remaining friction level left for subsequent tractive wheel passages is also investigated for all sands tested. Furthermore, baseline tests (i.e. without application of sand) are also performed to obtain some quantitative insight in the impact of leaf contamination on the wheel-rail adhesion in field.

[X] This chapter has been submitted for publication to Proc. IMechE, Part F: J. Rail and Rapid Transit as: O. Arias-Cuevas, Z. Li: Field Investigations on the Adhesion Recovery in Leaf Contaminated Wheel-Rail Contacts with Locomotive Sanders.

3D.1. Introduction

The adhesion, or the adhesion coefficient (by some authors also referred as traction coefficient), is given by the ratio of the longitudinal tangential (i.e., braking or traction) force over the normal force at the wheel-rail contact. The tangential force that a braking or tractive wheel can exert on a rail is limited by the friction coefficient available at the surfaces in contact for a given normal load. In clean steel-on-steel contacts the friction coefficient is known to be higher than the adhesion requirements of the majority of the existent rolling stock. However, in the presence of contamination (e.g. leaves, grease, and others) the friction level can decrease to values far below the adhesion required for normal traction and braking operations. In particular, the combination of leaves and small amounts of water has been identified by many railways to cause considerable low adhesion problems [3D.1-3D.7]. The leaf related problems mostly occur in autumn, when large amounts of leaves can fall on the railway tracks. Once these leaves come to the top of the rails, passing wheels can compact and shear them to form Teflon-like layers [3D.2]. These slippery layers normally adopt a black coloration and become very hard to be removed from the wheel and rail surfaces.

Sand has been used in locomotives of railways worldwide since 1838 to improve the wheel-rail adhesion [3D.8]. In more recent years, sanders have also been fitted to electrical multiple units (EMUs) in some railways [3D.5, 3D.9]. The literature known to the authors shows that different standards on sanding practice appear to be used by different railways; in particular different particle sizes are employed. The particle size distribution in the Netherlands is in the range 0.2-1.2 mm, while 0.7-2.8 mm in the UK [3D.9], 0.1-0.6 mm in France [3D.10], and 0.63-2 mm in Germany [3D.11]. In addition, different application rates may also be used depending on the railways and on the characteristics of the sanders. In general, most locomotives are fitted with sanders that apply a fixed amount of sand per second independent of the train speed. In contrast with these fixed rate sanders, some railways have fitted their EMUs with sanders that apply sand at a feed rate dependent on the vehicle speed or the traction/braking effort selected by the drivers.

In spite of the different standards on sanding practice, not much research appears to have been done on the possible influence of particle size distribution, feed rate, and number of sanding axles (among others), on the adhesion coefficient, wear, adhesion recovery, and train detection during sanding. This situation hinders the possible optimization of the sanding practice. In order to gain a fundamental understanding on these interrelationships, the authors carried out laboratory investigations on a twin-disk roller rig [3D.12-3D.14]. Investigations on the adhesion recovery in leaf contaminated contacts showed that sand could effectively improve the wheel-rail adhesion, as expected; however, this adhesion improvement was dependent upon the size of the sand particles [3D.14]. Excessively large particles could improve the adhesion much less than smaller sized sands. Due to the inevitable differences in geometry and operational conditions between the laboratory and the actual wheel-rail contact, field tests are essential to validate the laboratory findings.

In this work, the influence of the particle size on the adhesion recovery in leaf contaminated contacts has been investigated by means of field tests. The tests have been performed with an electrical locomotive of the major train operating company in the

Netherlands (NS) in a stabling yard. The locomotive has fixed rate sanders. Commercial silica sand has been sieved to three different particle size distributions for the tests. Besides the immediate adhesion improvement upon sanding, the remaining friction level left for subsequent tractive wheel passages is also investigated. Hence, the number of sanding axles required for a suitable adhesion recovery can be obtained.

In addition to the investigations on the influence of sand particle size, tests have also been performed with the Dutch standard railway sand. These tests are motivated by the lack of information on the quantitative adhesion improvement by the current practice in the Netherlands, despite the widely accepted qualitative adhesion improvement reported by drivers. Moreover, the impact of leaf contamination on wheel-rail adhesion has also been investigated by means of baseline tests (i.e. no sand applied). In the baseline tests the traction performance of the locomotive under leaf contaminated conditions has been compared to that in dry “clean” contacts. The adhesion values obtained in the baseline tests contribute to the rather poor amount of data available in the literature about leaf contaminated contacts in field as well as about the variation of the adhesion conditions with the wheel passages.

3D.2. Testing description

3D.2.1. Locomotive

The electrical locomotive employed in the tests is shown in Fig. 3D.1. The locomotive has a B’B’ axle configuration with an axle load of 21.5 t. In practice, the locomotive is normally used to haul passenger vehicles. In the tests, no vehicle was coupled to the locomotive to reduce the required track length and the maneuver during testing. In Fig. 3D.2 a two-dimensional schematic representation of the locomotive is shown. The traction of the rear bogie was deactivated in the tests to ensure that the active bogie operated at full traction capacity along the whole contaminated track section before reaching the speed limitation of stabling yards (i.e. 40 km/h). Thus, the first two wheel axles were driven, whereas the last two behaved as non-driven axles in the tests. Furthermore, the motors of the locomotive are equipped with a traction control unit (TCU), which regulates the motor torque in case the limiting adhesion is reached, as will be explained in Section 3D.2.4.

Fig. 3D.1. Photograph of the electrical locomotive used in the field tests.

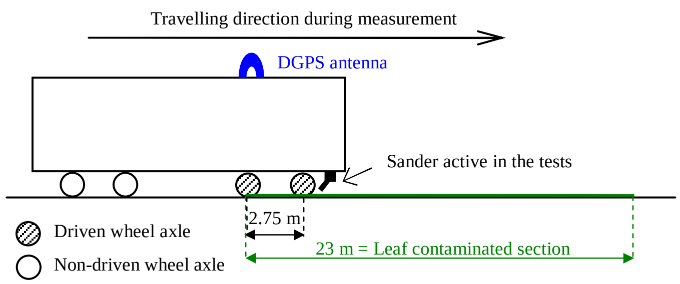

Fig. 3D.2. Two-dimensional schematic representation of the locomotive at the starting test position.

3D.2.2. Sander

There are four sanders on each side of the locomotive, having one in front and one behind each bogie. Sand is only applied by the sanders located in front of the leading wheels of each bogie for a given travelling direction. In the tests, only the sanders of the active motorized bogie applied sand, as shown in Fig. 3D.2. The main parts of a sander are shown in Fig. 3D.3. The sandbox stores the sand, which falls by gravity into the valve that controls the feed rate. The sand is pumped by air through the sandpipe and it is oriented to the wheel-rail interface by means of a nozzle, as indicated in Fig. 3D.3. In practice, sand can be applied either manually by the driver or automatically triggered by the TCU upon detection of excessive wheel slip. In the tests, the automatic sand application was deactivated to ensure that no sand was applied in the baseline tests when the wheels slipped. The feed rate was measured in the tests to be around 1 kg/min/rail on average.

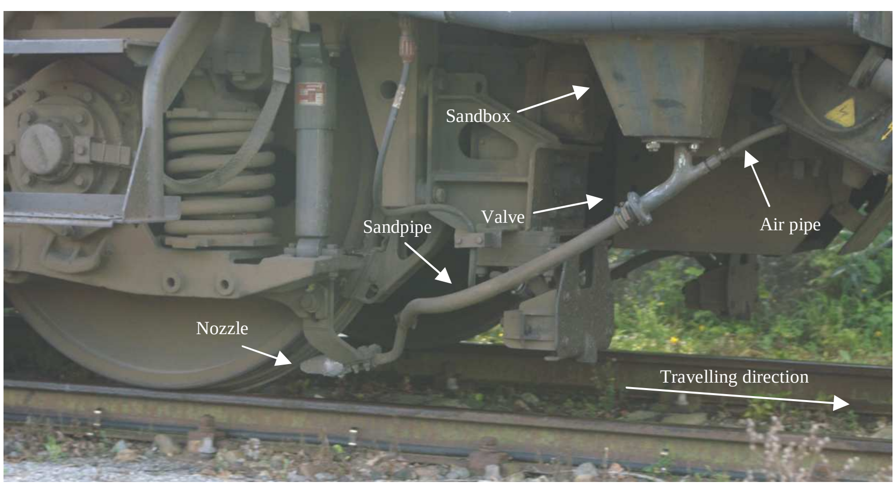

Fig. 3D.3. Photograph of the locomotive sander.

3D.2.3. Sands tested

Four different sands were employed in the testing, which are shown in Fig. 3D.4. The Dutch standard railway sand originated from a river in the south of the Netherlands and it has a SiO_2 content around 96% according to the supplier. It is named R sand in this paper for short. On the other hand, the three silica sands have a SiO_2 content higher than 99% according to the supplier, and had been collected from a pit in South Germany. The particle size distribution of the four sands was measured in the laboratory by means of a laser particle analyzer, as shown in Fig. 3D.5. It can be seen that a small percentage of particles in L sand may have surpassed the range of measurement, which was up to 2 mm for the analyzer. Moreover, all sands were chosen to have amorphous shape to obtain comparable results between them.

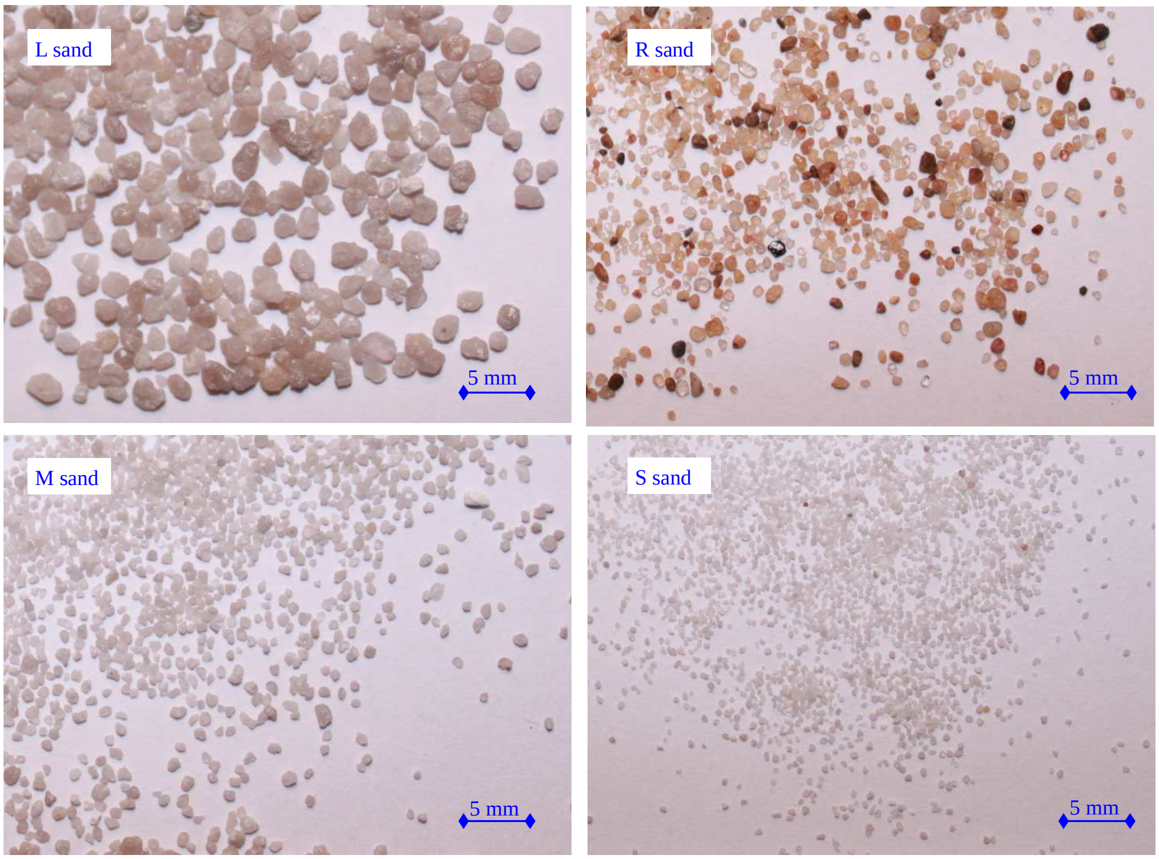

Fig. 3D.4. Photograph of the sands used in the testing.

3D.2.4. Testing preparation and procedure

During the test preparation, the leaves were first placed one by one along the two rails of a track section of 23 m length, as shown in Fig. 3D.6a. This section will be referred in this paper to as contaminated section. Small amounts of water were initially used to help adhering the leaves to the top of the rail before the first passage of the locomotive wheels so that they were not blown away. Then, the locomotive travelled over the contaminated section with no traction/braking efforts at very low speed so that most of the leaves were compacted onto the top of the rails. After six passages of the locomotive (i.e. 24 axle passages), leaf layers could be seen to be well compacted on the running band of the rails, while some leaf mulch remained at the sides of the running band (see Fig. 3D.6b). After the test preparation, the created leaf layers were mostly dry as no water had been applied to the leaves after the first locomotive passage.

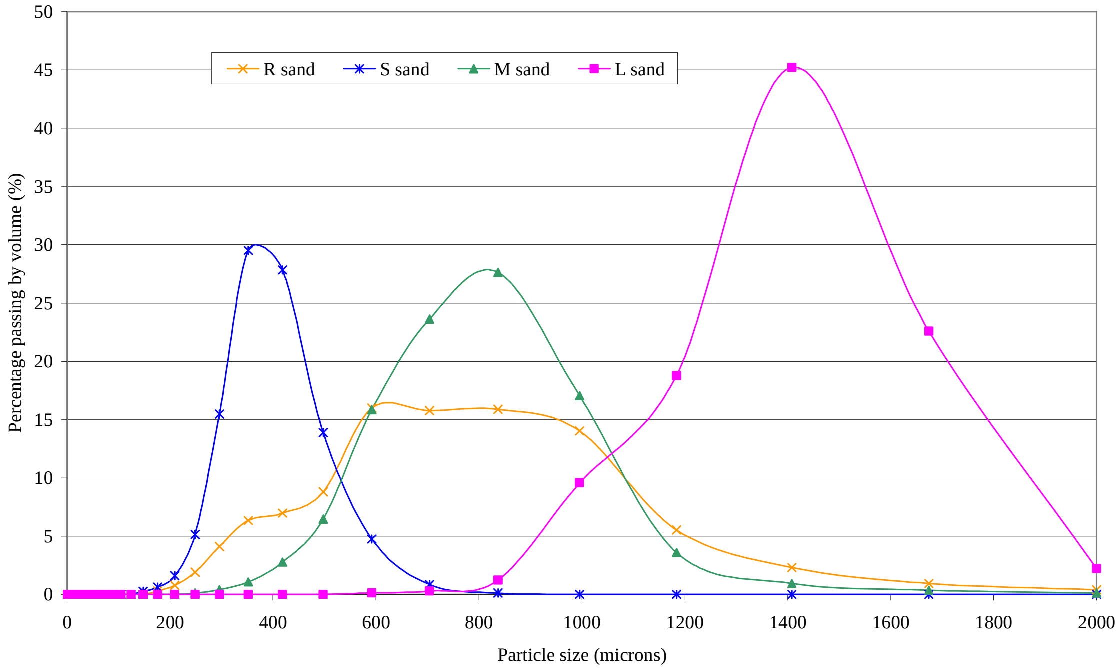

Fig. 3D.5. Particle size distribution of the sands used in the testing.

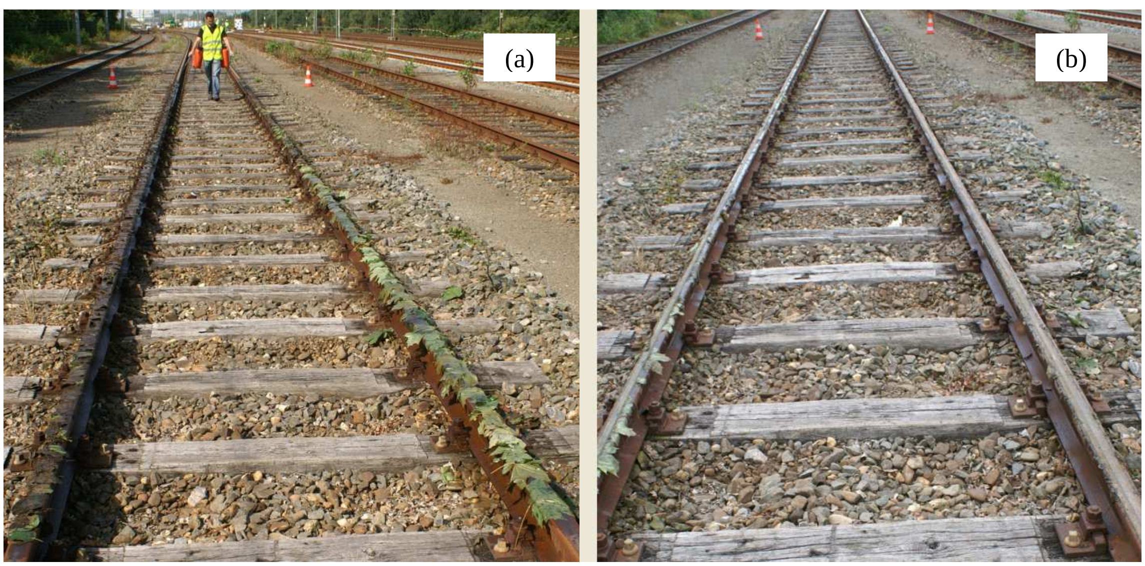

Fig. 3D.6. Photographs of the contaminated section (a) before and (b) after the six locomotive passages for creation of the leaf layers.

Each test consisted of a number of traction runs, in which repeated passages over the contaminated section were performed to examine the adhesion improvement. Upon start of a traction run, the four driven wheels were inside the contaminated section, as depicted in Fig. 3D.2. Considering that the wheel base of the bogie is 2.75 m, the driving wheels travelled over around 20 m of leaf contamination before the first driven wheel axle exited the contaminated section. The results presented in this paper only relate to the these first 20 m of the traction run, but it can be said that once the driven axles exited the contaminated section the friction level accordingly increased, as expected. Some tests runs were performed under dry leaf contaminated conditions, which may be representative of dry autumn days. Other test runs were performed under wet conditions, water being sprayed on the contaminated section prior to the start to create moisture conditions typical of dewy, foggy or drizzling autumn days.

In the tests carried out with sand, dry conditions were tested first, followed by the runs under wet conditions. A traction run without sand was always performed prior to each sand application to measure the available adhesion before sanding. In this way, the improvement in adhesion attributed to sanding could be quantified for every traction run with sand. Similarly, the remaining friction level after sanding for subsequent non-sanded tractive wheel passages could also be investigated for all sands tested.

Fig. 3D.7 gives a simplified representation of the traction performance along the distance/time in a traction run under both adequate and low (or poor) adhesion conditions. The tractive effort of the locomotive (*TE*), which was applied by the two driven axles, is given by the solid (blue) line in Fig. 3D.7. The tractive effort requested by the driver (TE_{driver}), which is represented by a dashed (blue) line, was always at the maximum since the beginning of each test. The friction, which is depicted with a dash-dot (red) line, is assumed to be constant along the distance to ease the explanation, being about twice higher in case A than in case B. Note that the same units are assumed for the tractive efforts and the friction in Fig. 3D.7 for the sake of comparison. Initially, the motor torque increased linearly until the maximum tractive effort, which is limited by the motor capacity, was reached as far as the friction level was not surpassed like in case A. In practice, this initial increase limits the jerk so that passenger comfort is not compromised.

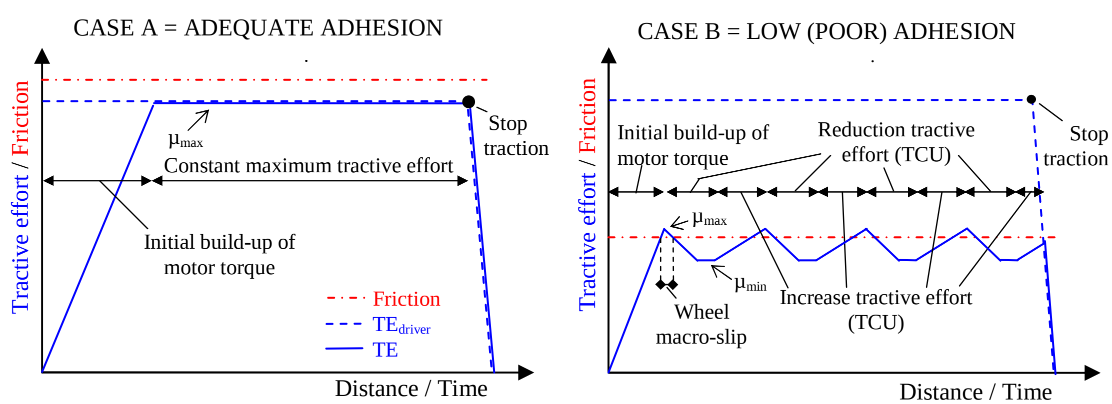

Fig. 3D.7. Simplified representation of the tractive effort variation along the distance/time under adequate and low (or poor) adhesion conditions.

If the tractive effort stayed below the friction level, a constant maximum tractive effort was present in the tests after the initial torque build-up, similarly to case A shown in Fig. 3D.7. On the other hand, when the tractive effort surpassed the friction level, like in case B of Fig. 3D.7, low adhesion conditions were encountered and the driven wheels experienced macro-slip. Once the wheel macro-slip exceeded the threshold set in the TCU, the tractive effort was reduced by the TCU until the wheel macro-slip decreased below the threshold. Then, the TCU increased the motor torque towards the tractive effort requested by the driver, as shown in Fig. 3D.7. Due to the continuous low friction assumed in case B, the TCU would keep adjusting the tractive effort close to the available friction level along the distance until the traction was stopped, which is represented by a (black) point in Fig. 3D.7.

3D.2.5. Measuring methodology

In the tests, the speed, time and distance of the locomotive during each traction run was monitored by means of a differential global positioning system (DGPS) OmniSTAR 8200HP. The DGPS was mounted on the roof of the locomotive, as indicated in Fig. 3D.2. OmniSTAR VBS GPS correction signals were used on the 8200HP to operate with sub-meter accuracy for the number of satellites available during the testing [3D.15]. The speed and location values were acquired with a sampling frequency of 10 Hz. The speed variation was further evaluated to obtain the acceleration of the locomotive. The acceleration was used to have an indirect measure of the tractive effort and, therefore, the available adhesion along the travelled distance.

The equation of motion that governs the traction operation of the locomotive in the tests is given in Eq. 3D.1, in which TE is the tractive effort, M is the total mass of the locomotive, γ is the factor of the inertia of rotating masses (γ = 1.12 for this locomotive), a is the acceleration, and R_{tot} is the total train resistance. The components of the total train resistance are given in Eq. 3D.2, where R_{air} is the air resistance, $R_{running}$ is the running resistance, R_{curve} is the curve resistance, and $R_{gradient}$ is the gradient resistance. Since the tests were performed on a horizontal straight track, the curve and gradient resistances were zero. Based on data from the manufacturer, the sum of air and running resistances was below 2.5 kN for the operational conditions in the tests so that its contribution in Eq. 3D.1 could be neglected.

Considering that the tangential and normal forces are approximately the same for each of the four driven wheels, the adhesion coefficient can be related to the tractive effort as shown in Eq. 3D.3, in which F_N is the normal contact load and μ is the coefficient of adhesion at the wheel-rail contact. Neglecting the small change in axle load due to the possible unloading conditions of the driven wheels, and assuming that the normal contact load is almost equal to the vertical load, Eq. 3D.3 is further simplified to include the total mass of the locomotive. Substituting Eq. 3D.3 into Eq. 3D.1, an explicit relationship can be found between the acceleration of the locomotive and the adhesion coefficient at the driven wheel-rail contacts, as shown in Eq. 3D.4.

$$TE = \gamma \cdot M \cdot a + R_{tot} \approx \gamma \cdot M \cdot a \tag{3D.1}$$

$$R_{tot} = R_{air} + R_{running} + R_{curve} + R_{gradient} = R_{air} + R_{running} \approx 0 \tag{3D.2}$$

$$TE \approx 4 \cdot \mu \cdot F_N \approx \frac{\mu \cdot M \cdot g}{2} \tag{3D.3}$$

$$\mu \approx \frac{2 \cdot \gamma \cdot a}{g} \tag{3D.4}$$

From the variation of the adhesion coefficient along the distance travelled by the driven axles, the minimum, maximum and average values of adhesion were derived. The minimum value corresponded to the lowest value among the local minimum adhesion coefficient obtained during the traction reductions by the TCU due to excessive wheel macro-slip, as pointed out in the case B of Fig. 3D.7. Note that in that example the local minimum was the same in every traction reduction and thus equal to the global minimum, because it was assumed that the friction level was constant. If no low adhesion conditions were encountered in a traction run, there is no minimum adhesion coefficient given in the results, e.g. case A in Fig. 3D.7. In the tests, the minimum adhesion coefficient can be taken in a conservative manner to be the maximum tractive effort to which the driven axles of the locomotive could be subjected along the contaminated section before experiencing low adhesion.

Furthermore, the maximum value of the adhesion coefficient corresponded to the highest tractive effort reached in the traction run, as indicated in Fig. 3D.7. In the runs under adequate adhesion conditions, the maximum adhesion coefficient was given by the full traction capacity of the locomotive (e.g. case A in Fig. 3D.7). In traction runs under low adhesion conditions, the maximum adhesion was constrained by the friction level available in the wheel-rail contacts (e.g. case B in Fig. 3D.7). The maximum adhesion coefficient may be taken as the minimum tractive effort at which the driven wheels could experience low adhesion. But, considering the finite sampling frequency of the TCU, it can be understood that the driven wheels were already slipping above the threshold when the TCU began to decrease the tractive effort.

Moreover, the average adhesion coefficient was calculated according to Eq. 3D.5, by assuming a uniform acceleration from the start of the traction run. Note that in Eq. 3D.5 v_f is the final locomotive speed and s is the distance travelled by the locomotive (s = 20 m in the tests). Although the acceleration of the locomotive was clearly not uniform along the section, this average value is used in this paper to provide a single value indicative of the mean level of adhesion along the whole contaminated section.

$$a_{av} = \frac{{v_f}^2}{2 \cdot s} \tag{3D.5}$$

3D.3. Results

3D.3.1. Impact of leaf contamination

Three baseline tests in leaf contaminated contacts were carried out: two under dry conditions (i.e. leaf tests 1 and 2) and one under wet conditions (leaf test 3). The values of the maximum, average and minimum adhesion coefficient during each test run are shown in Fig. 3D.8. In order to give a reference of adequate adhesion conditions, a traction run on dry “clean” rails was also performed. In this run, the locomotive could reach a final speed of around 21 km/h after 20 m of traction run, with average and maximum values of the adhesion coefficient of around 0.20 and 0.23, respectively. As expected, no low adhesion conditions were encountered in this run, indicating that the friction level in dry “clean” wheel-rail contacts was higher than 0.23. Note that no minimum adhesion coefficient is given for the reference run in Fig. 3D.8 as no low adhesion conditions were experienced. The average adhesion coefficient was below the maximum adhesion coefficient because the motor needed some time to reach the maximum torque, as schematically depicted in Fig. 3D.7.

In all runs of the baseline tests, the tractive effort had been reduced by the TCU due to low adhesion, similarly to the example case B given in Fig. 3D.7. The traction reductions suggest that the driven wheels experienced excessive wheel macro-slip. This has been indicated with red S letters on top of the bars in Fig. 3D.8. Comparing the average values of the adhesion coefficient in the baseline tests with the reference run under dry ‘clean” conditions, it can be seen that the adhesion was greatly affected by the leaf layers. In the baseline runs, the average tractive effort along the contaminated section was between 20% and 82% of that measured in dry “clean” contacts. The lowest minimum adhesion coefficient in dry leaf contaminated contacts was around 0.02, which is in line with values obtained in laboratory scale [3D.12, 3D.14, 3D.16, 3D.17]. It can also be seen in Fig. 3D.8 that the adhesion was reduced more when the leaf layers were combined with moisture. This is in agreement with laboratory and field observations [3D.1, 3D.2, 3D.17]. In the traction runs under wet conditions, the minimum adhesion reached values of as low as zero (see Fig. 3D.8).

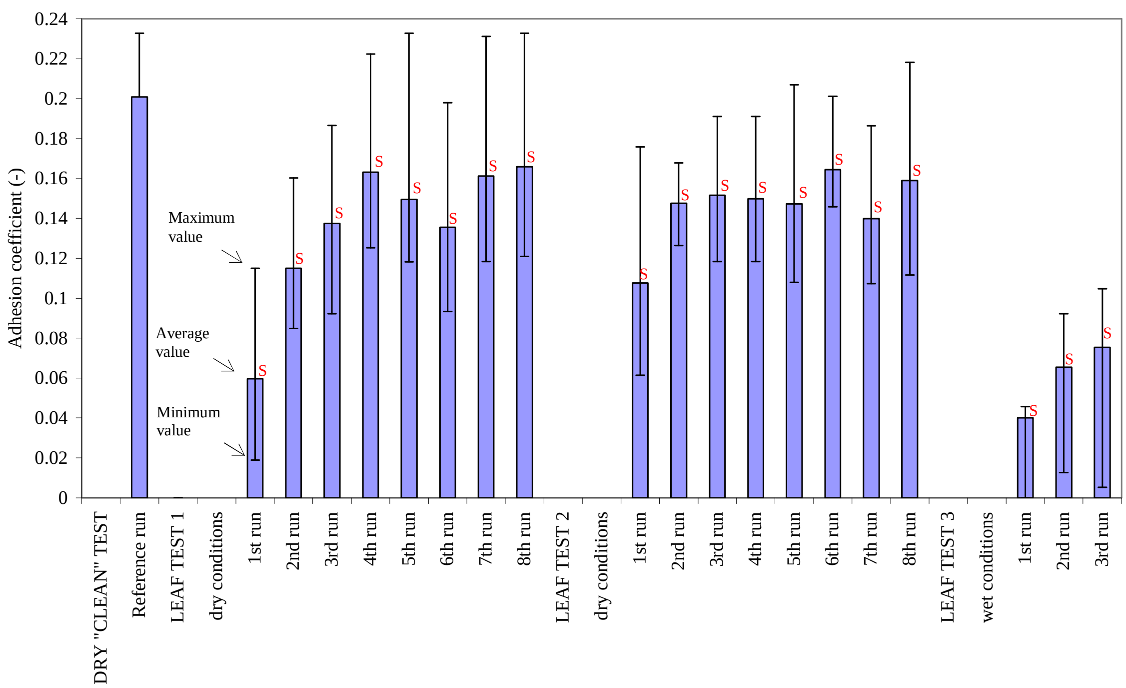

Fig. 3D.8. Adhesion coefficient values in traction runs of the baseline tests (leaf tests 1, 2 and 3) and in the dry “clean” reference run: average (given in vertical blue bars), maximum and minimum values (indicated with the “error” bars).

The adhesion was clearly found to recover with the number of passages in the first three runs for the baseline tests, leading to higher values of the average adhesion coefficient in Fig. 3D.8. This adhesion improvement could be a consequence of the leaf layer removal by slipping (driven) wheels. Laboratory investigations have shown that an increase in the wheel slip can promote the adhesion improvement in leaf contaminated wheel-rail contacts [3D.18]. The adhesion recovery seemed to slow down in the subsequent passages of the dry tests, i.e. from the 4th run onwards in Fig. 3D.8, and the adhesion coefficient could occasionally be lower with increasing runs, e.g. 5th and 6th runs of leaf test 1 and 6th and 7th runs of leaf test 2 in Fig. 3D.8. A similar slowdown of the adhesion recovery has also been observed in laboratory tests [3D.18]. The slowdown may indicate that larger layer removal occurs in the first runs (or wheel passages).

In order to illustrate the adhesion recovery with the initial traction runs along the contaminated section, Figs. 3D.9-3D.10 display the variation of the adhesion coefficient along the contaminated section in some dry and wet runs. The first sign of adhesion improvement in the 3rd run compared to the 1st run was that the first encounter of low adhesion conditions was at a higher adhesion coefficient, e.g. $\mu \approx 0.09$ in the 1st run and $\mu \approx 0.17$ in the 3rd run of test 2 (see Fig. 3D.9). This indicates that a higher friction level was present in the initial meters of the contaminated section during the 3rd run of leaf tests 1 and 2. Moreover, the adhesion coefficient in the 3rd traction run was always higher along the travelled distance for both leaf tests 1 and 2, as shown in Fig. 3D.9. This suggests that the friction level in the 3rd run was continuously higher than in the 1st run in the whole contaminated section.

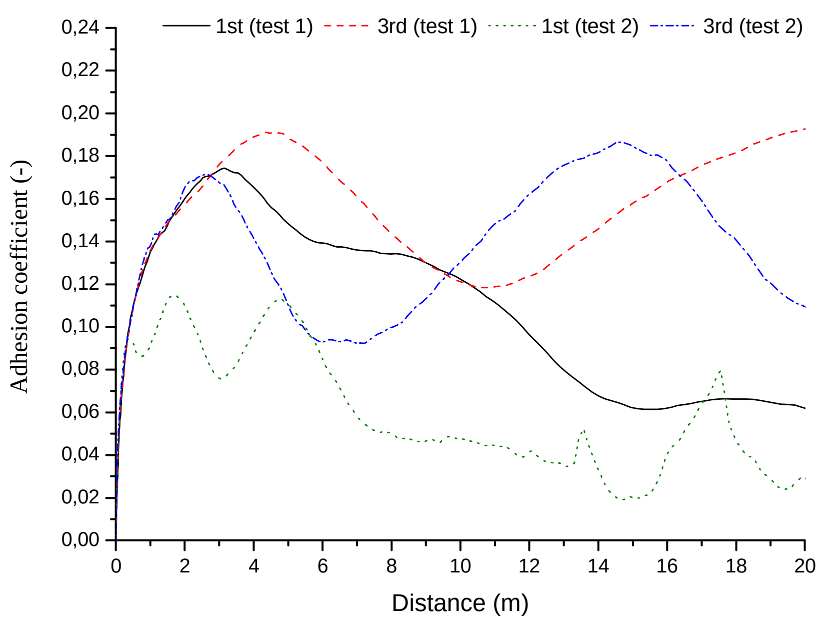

Fig. 3D.9. Variation of the adhesion coefficient along the contaminated section in the 1st and 3rd runs of the leaf tests 1 and 2 (baseline tests under dry conditions).

Fig. 3D.10 displays the variation of the adhesion coefficient along the contaminated section for the three runs of the baseline test under wet conditions. Note that the maximum and minimum values of the adhesion coefficient have been illustrated. It can be seen that the adhesion improvement with the increasing runs led to the highest adhesion coefficient in the 3rd run. The average value of the adhesion coefficient was also the highest in the 3rd run, as displayed in Fig. 3D.8. Similarly to the tests under dry conditions, the adhesion coefficient in the 3rd run under wet conditions was mostly higher along the contaminated section than the one measured in the 1st run (see Fig.

3D.10). There were, however, a few locations in which the opposite was observed, as pointed out in Fig. 3D.10. This could be attributed to large traction reductions in the 3rd run that temporarily brought the adhesion coefficient below the one measured in the 1st run at the same travelled distance.

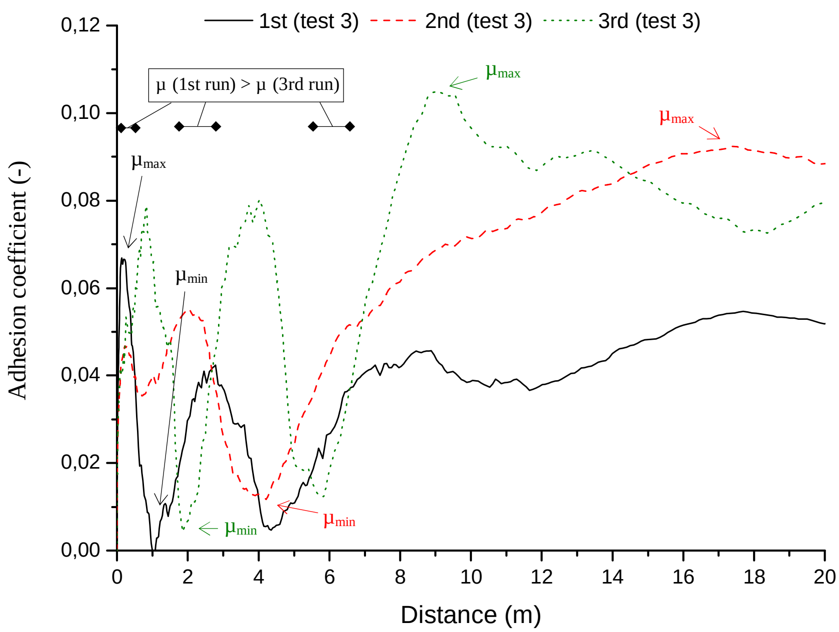

Fig. 3D.10. Variation of the adhesion coefficient along the contaminated section in the three runs of leaf test 3 (baseline test under wet conditions).

Some parts of the rails along the contaminated section were photographed after each traction run to seek a possible relationship between the adhesion improvement and the layer removal. Fig. 3D.11 shows two photographs of the top of a rail at the same location after the 1st and 8th runs of leaf test 2. It can be seen that there were significantly less leaf layers on the running band after the 8th run than after the 1st run. The presence of the still remaining leaf layers in Fig. 3D.11b is in agreement with the low adhesion conditions measured in the 8th run of leaf test 2 (see Fig. 3D.8).

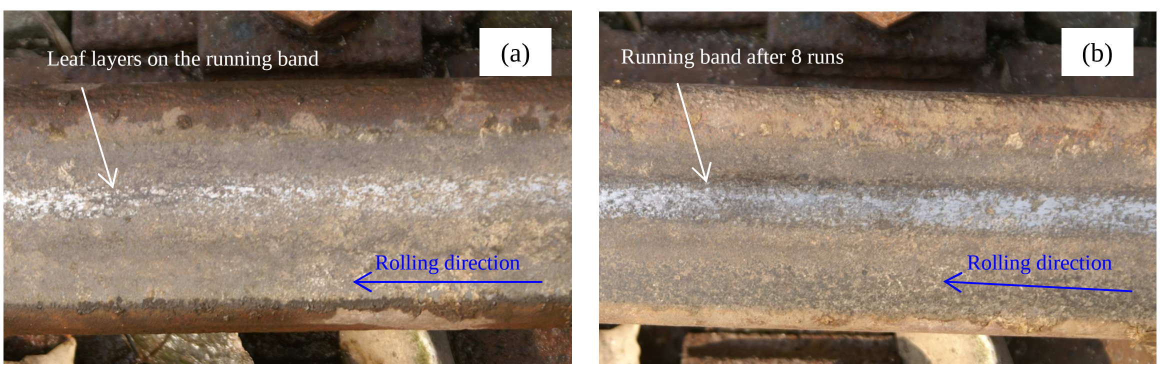

Fig. 3D.11. Photographs of the top of a rail in the leaf test 2 after: (a) 1st run and (b) 8th run.

3D.3.2. Effectiveness of Dutch standard railway sand

Two leaf tests under dry and wet conditions were performed with R sand, numbered 4 and 5, whose adhesion results are depicted in Fig. 3D.12. When sand had been applied in a traction run, it is indicated in the horizontal axis together with the ordinal number of the traction run. Under dry conditions, the first application of R sand entirely recovered the adhesion level in both tests (see 2nd runs in Fig. 3D.12). In addition, no low adhesion conditions were encountered in the 3rd runs. This could account for the conditioning effect by sanding, which is attributed to the removal of leaf layers from the surfaces of wheels and rails by the abrasive action of entrapped sand, and to the presence of some remaining (crushed) sand particles on the running band of the rails. In order to illustrate the conditioning effect, Fig. 3D.13 shows two photographs of the top of a rail at the same location before and after the traction run under dry conditions with sand application. It can be seen that some sand still remained on the rail surface, which could have contributed to the increase of the friction level for the 3rd runs. However, some leaf layers could still be observed on the top of the rails.

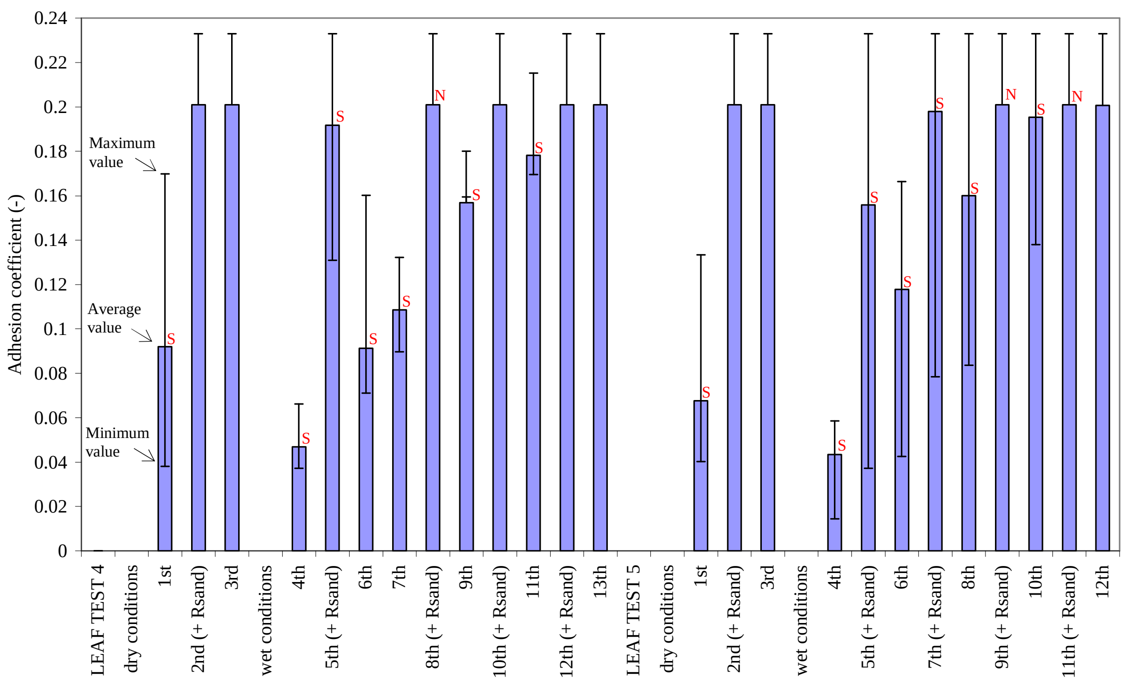

Fig. 3D.12. Adhesion coefficient values in traction runs of the tests with R sand (leaf tests 4 and 5): average (given in vertical blue bars), maximum and minimum values (indicated with the "error" bars).

Starting from the 4th run, water was sprayed on the contaminated section prior to each traction run in order to simulate moisture on the rail surface. Comparing the adhesion results of the 4th run with the 3rd run in leaf tests 4 and 5 displayed in Fig. 3D.12, it can be seen that the introduction of water in the wheel-rail contact considerably reduced the adhesion. Upon first application of R sand under wet conditions, i.e. 5th run of Fig. 3D.12, the adhesion was considerably improved compared to the 4th run, but some wheel macro-slip still arose in the 5th run. After two traction runs with sand application under wet conditions, the average adhesion coefficient had not reach 0.17 and the minimum values of the adhesion coefficient were still below 0.09, as shown in the 9th run of test 4 and the 8th run of test 5 in Fig. 3D.12. The adhesion recovery under wet conditions was found to be entirely effective only after four runs with R sand so that no low adhesion conditions were encountered when driving along the contaminated section without application of sand. This finding emphasizes the importance of having enough number of sanding axles when sanding is to be used to condition the rails to a certain friction level for subsequent train passages, as it was previously found in the laboratory [3D.14]. Moreover, it must be mentioned that in some traction runs wheel macro-slip was noticed by the driver from the cabin, whereas the DGPS readings did not show any appreciable effect on the acceleration of the locomotive and, therefore, the tractive effort. In those traction runs, a red letter N has been placed on top of the bar, as shown in Fig. 3D.12.

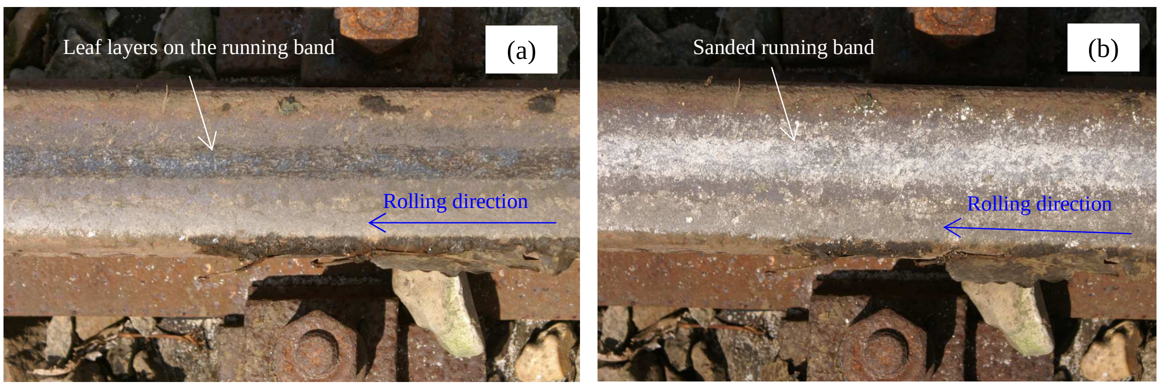

Fig. 3D.13. Photographs of the top of a rail in the leaf test 5 after: (a) 1st run and (b) 2nd run.

In Figs. 3D.14-3D.15, the variation of the adhesion coefficient along the contaminated section is displayed for some runs of the tests with R sand. It can be seen that the adhesion coefficient in the 2nd runs was always higher than the one measured in the 1st runs, indicating that the friction level had consistently increased throughout the contaminated section. The adhesion coefficient of the 5th runs in tests 4 and 5 was also higher than that of the 4th runs, as shown in Figs. 3D.14-3D.15. However, low adhesion was experienced in the 5th runs despite the sand application (see Figs. 3D.14-3D.15). In particular, two significant decreases of the tractive effort due to low adhesion conditions can be observed in the 5th run of Fig. 3D.15.

3D.3.3. Influence of the sand particle size

Five tests were performed with L, M and S sands to investigate the influence of the particle size on the adhesion recovery in leaf contaminated contacts. One leaf test under dry and wet conditions was performed with L sand (named leaf test 6), whose results are given in Fig. 3D.16. Under dry conditions, it can be seen that the application of L sand in the 2nd run led to a seemingly entire adhesion recovery, but wheel macro-slip was still noticed by the driver. In the 3rd run no low adhesion conditions were experienced, indicating that the conditioning effect had been effective. In the wet runs, a comparison between the 4th and 5th runs, as well as the 6th and 7th runs, proves that the application of L sand improved the adhesion, but this improvement did not overcome the occurrence of wheel macro-slip. Moreover, the improvement in adhesion did not seem to increase uniformly with the runs, e.g. 8th and 9th runs in Fig. 3D.16. In the 12th run low adhesion conditions were still present and the minimum adhesion coefficient was around 0.08, as shown in Fig. 3D.16.

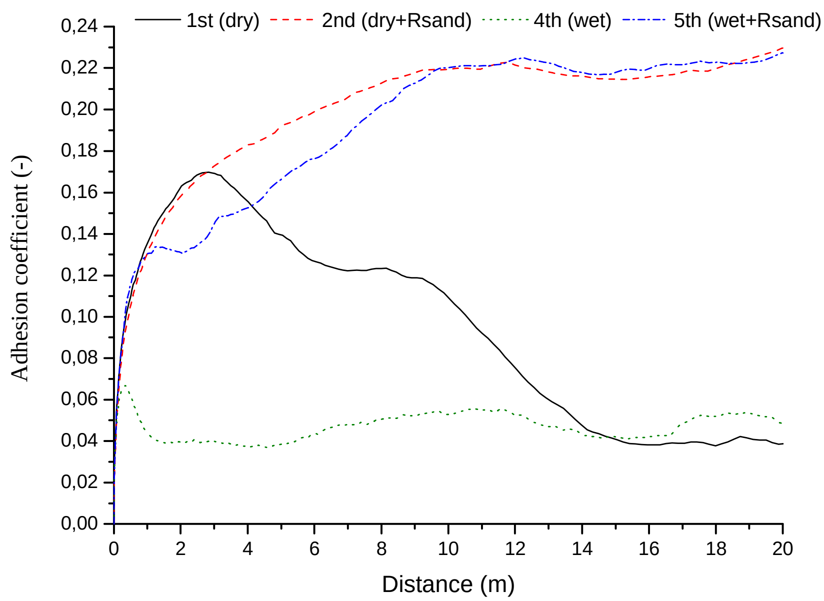

Fig. 3D.14. Variation of the adhesion coefficient of the driven wheels along the contaminated section in some runs of the leaf test 4.

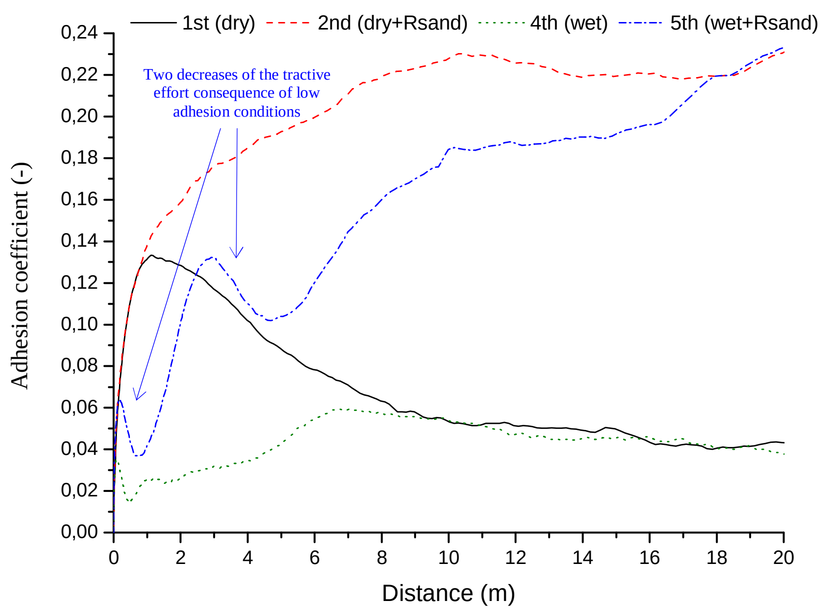

Fig. 3D.15. Variation of the adhesion coefficient of the driven wheels along the contaminated section in some runs of the leaf test 5.

Two leaf tests were carried out with M sand: one only under wet conditions due to the drizzling weather conditions during the test (leaf test 7), and one under dry and wet conditions (leaf test 8). The values of the adhesion coefficient in both tests are given in Fig. 3D.17. Under dry conditions, the application of M sand improved the adhesion in the 2nd run compared to the 1st run of leaf test 8, but not entirely as the driven wheels still experienced some wheel macro-slip yielding a minimum adhesion of around 0.11. In the 3rd run of leaf test 8, the adhesion appeared to be entirely recovered due to the conditioning effect brought about by the application of M sand in the 2nd run. In the runs under wet conditions of leaf tests 7 and 8, the adhesion was considerably improved with the application of M sand. The adhesion was entirely recovered upon second application of M sand in leaf test 7, i.e. 4th run in Fig. 3D.17. In the leaf test 8, no reduction of the tractive effort could be appreciated from the acceleration results in the 7th and 9th runs, but occurrence of wheel macro-slip had been noticed by the driver, as indicated in Fig. 3D.17. Furthermore, there was a clear trend of an increasing adhesion with the increasing runs. After three runs applying M sand under wet conditions, no low adhesion conditions were encountered in the subsequent runs, i.e. 7th run of test 7 and 10th run of test 8 (see Fig. 3D.17). Therefore, M sand was found to perform considerably better than L sand under the tested conditions.

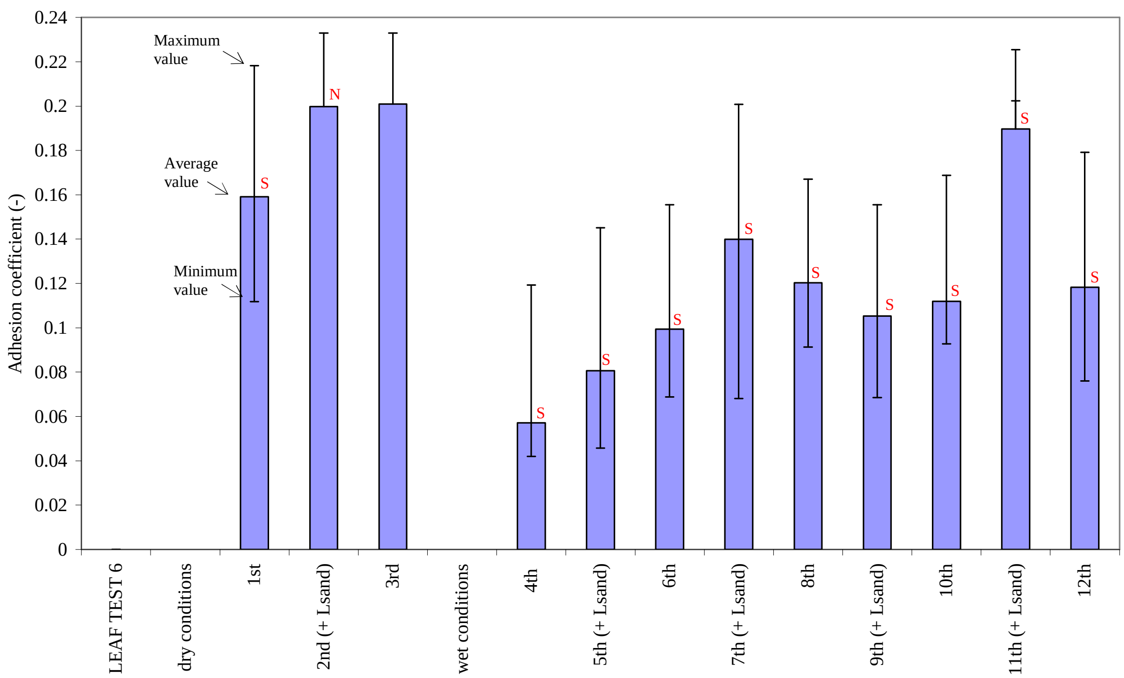

Fig. 3D.16. Adhesion coefficient values in traction runs of the test with L sand (leaf test 6): average (given in vertical blue bars), maximum and minimum values (indicated with the “error” bars).

Two leaf tests under dry and wet conditions were performed with S sand, named leaf tests 9 and 10 in this paper, whose adhesion results are depicted in Fig. 3D.18. By first looking at the results under dry conditions, it can be seen that wheel macro-slip was prevented in leaf test 9 upon application of S sand in the 2nd run, while in test 10 some wheel macro-slip was experienced yielding a minimum adhesion coefficient of around 0.11. Note that the minimum adhesion coefficient of the 1st run was around 0.03 for both leaf tests, as shown in Fig. 3D.18. In both tests, no low adhesion conditions were encountered in the 3rd runs, indicating that the conditioning effect of S sand under dry conditions had been effective. Under wet conditions, the adhesion was found to be almost recovered completely with the first application of S sand in the leaf test 10, as only a small traction reduction occurred in the 5th run at the beginning of the contaminated section. Furthermore, the average adhesion coefficient was always higher than 0.18 in each run with S sand under wet conditions, which was 10% below the one measured in the reference run in dry "clean" contacts (see Fig. 3D.8). Moreover, the conditioning effect of S sand showed to be quite effective as the average adhesion coefficient was mostly higher than 0.16 in every subsequent wet run without sand application. Four applications of S sand in wet runs were found to be necessary for an entire adhesion recovery, which was reached in the 12th run of test 9 and in the 13th run of test 10. Comparing the adhesion values of leaf tests 9 and 10 with leaf tests 7 and 8, it could be said that S sand had a slightly better performance in the adhesion recovery than M sand.

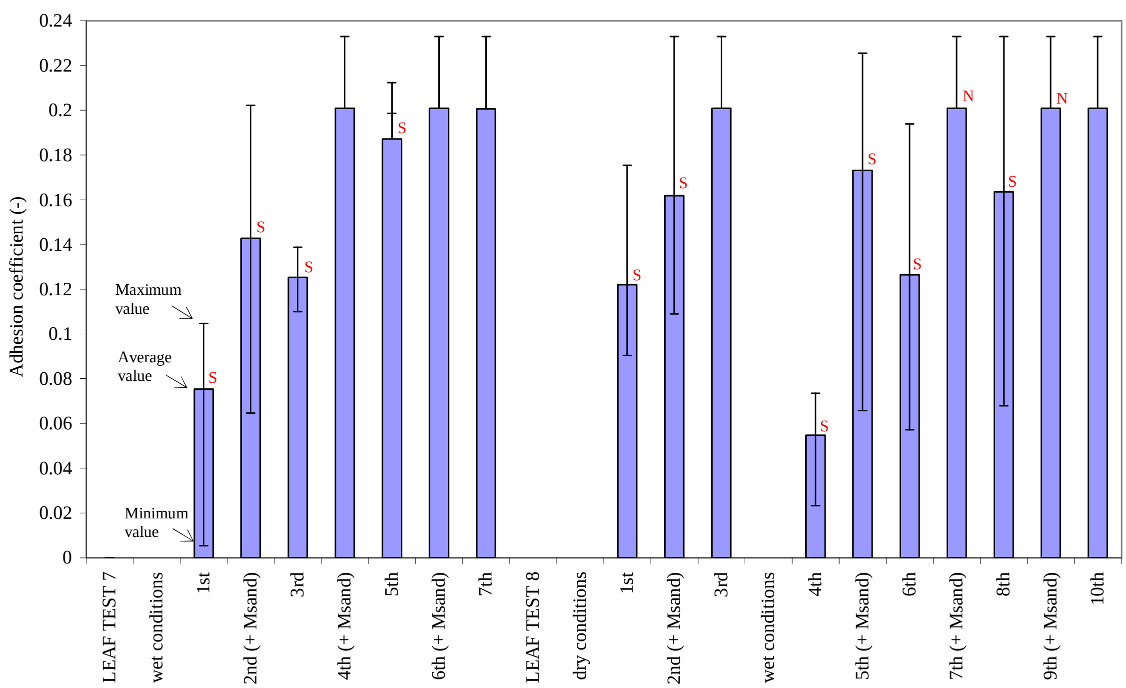

Fig. 3D.17. Adhesion coefficient values in traction runs of tests with M sand (leaf tests 7 and 8): average (given in vertical blue bars), maximum and minimum values (indicated with the "error" bars).

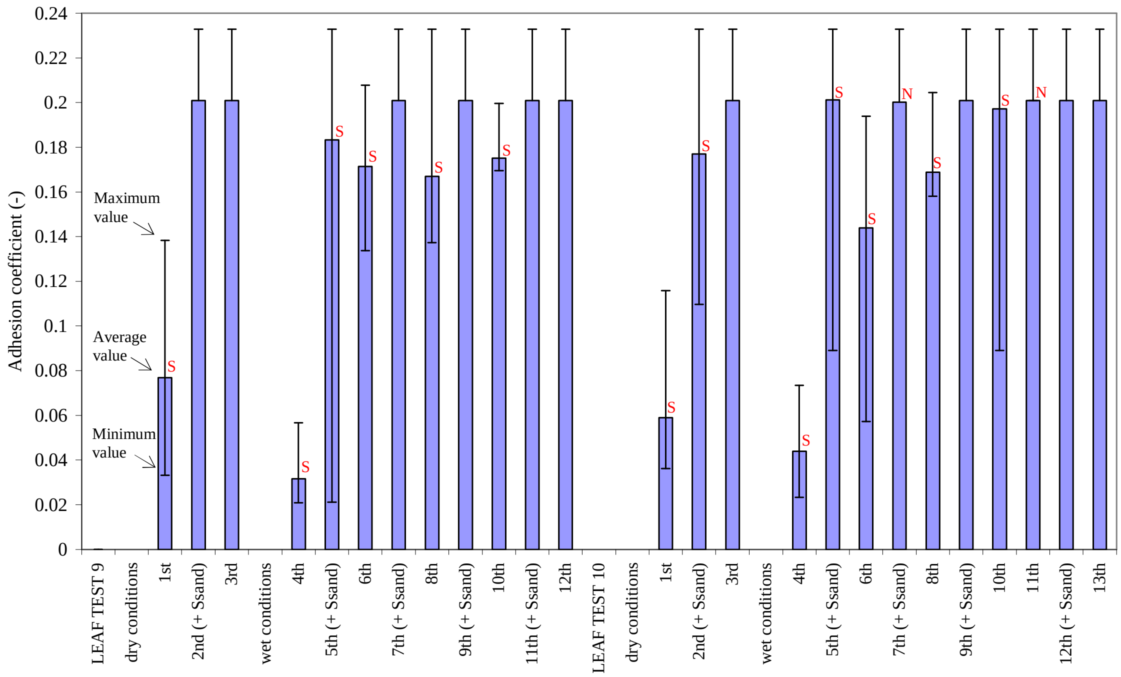

Fig. 3D.18. Adhesion coefficient values in traction runs of tests with S sand (leaf tests 9 and 10): average (given in vertical blue bars), maximum and minimum values (indicated with the "error" bars).

3D.4. Discussion

The baseline tests have shown that leaf contaminated contacts can lead to low adhesion under both dry and wet conditions. After the 1st locomotive passage over the dry leaf layers, the minimum adhesion coefficient among all traction runs was above 0.08, while under wet conditions the minimum adhesion coefficient reduced to values close to zero. Hence, tractive/braking wheels over dry leaf contaminated rails would not experience any wheel macro-slip/slide when the driver does not require an adhesion coefficient higher than 0.08, but a train can barely accelerate or brake when the leaf layers are wet. The adhesion requirements of rolling stock in the Netherlands can go up to 0.25 in traction, while in the UK values up to 0.20 and 0.09 are reported for traction and braking [3D.18]. A maximum value of 0.17 for traction is used when making the timetable of commuter trains in the Netherlands. Furthermore, the Dutch Railway Regulations (*Reglement Keuring Spoorwegen*) demand that the maximum braking distance on a descending slope of 5‰ at 140 km/h (maximum allowable line speed) should not exceed 1150 m [3D.19], which yields an average required adhesion of about 0.07 considering that all wheel axles of the train exert the same braking effort. Considering all the abovementioned adhesion requirements and the results of these field tests, it could be said that in dry autumn days countermeasures may mostly be required during traction operation so that punctuality is not compromised, while in dewy, foggy or drizzling autumn days braking can also be affected, even the safety may be at risk, if no effective countermeasures are taken.

A great part of this work has focused on the quantification of the adhesion improvement caused by sanding with the number of wheel passages. In particular, not only the immediate positive effect on wheel-rail adhesion upon sand application has been shown, but also for the following driven wheels due to the conditioning effect by sand. These results may be useful to those railways that make use of dedicated cleaning vehicles to condition the friction level of the rails by means of sanding. It has been shown that the friction level due to conditioning is dependent on the number of passages and the particle size of sand used. Hence, the results presented in this work may help those railways to estimate roughly the effectiveness of their policy according to their selected standard particle size and number of sanding axles employed.

The particle size of sand is found in the literature to be different among railways, as indicated in the introduction of this paper. It seems possible that railway engineers once adopted a certain particle size distribution without a thorough consideration into the possible effect on the adhesion improvement to be obtained. In this work, it has been shown that the particle size of sand can exert a strong influence on the adhesion coefficient upon sanding and on the conditioning effect of sanding. Smaller sands have been found to be more effective, which could be attributed to a better particle entrapment in the wheel-rail interface. This is in good agreement with previous laboratory investigations performed by the authors [3D.14]. In addition, the optimal particle size found in the field tests (i.e. S sand) also corresponds to the optimal size found in the laboratory investigations (referred to as medium sand in that work) [3D.14]. Hence, a good correlation between laboratory and field has been found.

The findings on the effect of particle size indicate that some railways could benefit from a reduction in the particle size of the sand used. Nevertheless, one of the major limitations is that some of the existent sanders operate in an open environment. When using excessively small sand particles under damp ambient conditions, clogging of the pipes may occur, limiting the particle size of sand to be used. Another important concern to bear in mind when aiming at smaller sands is that the train detection may be affected depending on the feed rate used, as shown in previous laboratory investigations [3D.13]. Since faults in the train detection may threaten the safety of the railway transportation, this should be investigated in future works.

Besides the sand particle size, laboratory investigations have shown that other factors, such as feed rate and wheel slip, played an important role in the effectiveness of sanding for adhesion recovery [3D.13-3D.14]. Due to the limitations of the locomotive sanders used in this work, the influence of those two factors could not be investigated. In particular, operating at the optimum feed rate in sanding becomes crucial because it can have an impact not only on the adhesion recovery, but also on the costs related to sanding as well as on the safety of railway transportation. Excessive feed rates could lead to an inadequate adhesion coefficient and they may affect train detection [3D.13]. When applying more sand than required, re-fill of the sandboxes is more frequently required, increasing the costs of sanding practice. Therefore, future investigations in field on the optimal feed rate for a given particle size are justified.

In some of the traction runs, wheel macro-slip was noticed by the driver from the cabin, whereas the DGPS readings did not show any appreciable change in the acceleration of the locomotive and, thus, the tractive effort. This suggests that the amount of wheel macro-slip noticed by the driver could be below the threshold of the TCU. In practice, the appreciation of a driver can influence the traction operation of rail vehicles to a large extent. Some drivers may instinctively reduce the traction effort when they notice some wheel macro-slip so that no damage on wheels and rails is caused. Nevertheless, the manual reduction of the traction effort can lead to certain inefficiency if the right amount of traction reduction is not selected. In the Netherlands, monitoring of the driving performance of five EMUs in the autumn of 2008 showed that punctuality can greatly be affected by low adhesion, especially due to a “too conservative” selection of the traction effort by the drivers [3D.20].

The adhesion results given in this paper are quite sensitive to the algorithm of torque regulation of the TCU of the locomotive used in the tests. The algorithm determines the wheel macro-slip threshold at which the tractive effort is reduced under low adhesion conditions, and it also establishes the amount and duration of the tractive effort reduction as well as the subsequent increase of tractive effort once low adhesion conditions disappear. It can be understood that a different algorithm may have led to different adhesion results under the same contact conditions. In particular, the average adhesion coefficient values may be the most affected by the algorithm. The maximum and minimum values could also vary depending mostly on the macro-slip threshold of the TCU. It is, however, needless to say that the algorithm does not affect the comparison of the traction performance between the baseline and the different sands tested, which was the main purpose of this investigation. But, care has to be taken when extrapolating the adhesion results of these tests to another type of rolling stock.

All results presented in this work correspond to the low speed regime. In general, it can be expected that the effectiveness in adhesion recovery may somewhat differ at higher train speeds due to different particle entrapment and the presence of larger train’s slipstream. The speed in the tests could not be increased above 40 km/h due to the restrictions in stabling yards in the Netherlands. However, it is well known that the maximum adhesion requirements in traction are mostly at travelling speeds up to 60 km/h for locomotives and 40 km/h for EMUs. Therefore, one part of the most adhesion demanding range has been investigated in the tests. In future investigations, it is clearly interesting to examine the sanding performance at speeds higher than the ones of this work.

3D.5. Conclusions

In this work, traction tests of a locomotive in dry and wet leaf contaminated contacts have been presented. The field tests have been performed in a stabling yard. Firstly, baseline tests have been performed to investigate the quantitative impact of leaf contamination on the wheel-rail adhesion. Secondly, tests with the Dutch standard railway sand have been carried out to assess the effectiveness of the currently used countermeasure. Thirdly, tests with three differently sized silica sands have been performed to investigate the effect of the sand particle size on the adhesion recovery. Based on the results obtained in the tests, the following conclusions can be drawn:

a) Leaf layers can lead to low adhesion incidents under both dry and wet conditions. The adhesion values measured in this work indicate that dry leaf layers may mostly affect traction operation, whereas wet leaf layers can threaten both braking and traction operations.

b) Although the adhesion tends to increase gradually with the driven wheel passages, the adhesion recovery without sanding may be more than 7 times slower than with sanding.
c) Sanding is effective in improving the adhesion in leaf contaminated wheel-rail contacts not only for the sanding axles, but also for the subsequent passing wheels due to the conditioning of the top of the rail.
d) The adhesion improvement due to conditioning is found dependent on the number of sanding axles employed. The adhesion data gathered in this work may help some railways to estimate roughly the necessary number of sanding axles according to a given particle size.
e) The adhesion improvement by sanding is strongly dependent on the particle size used. The performance of the largest particles used in this work is effective compared to the baseline (i.e. no sand application), but much less effective than smaller sized sands. This finding may encourage some railways to revise their standards on particle size towards an optimal sanding practice.
f) A good correlation has been found between these field tests and previous laboratory investigations. Not only similar trends have been observed, but also the optimal particle size for adhesion recovery has been found to be same in both investigations.

References

[3D.1] J. Eleveld: Gladde Sporen, Oplossingsrichtingen voor Adhesieproblemen. Report published by the Dutch Railways Technical Research (NSTO) in Dutch (March 1999).
[3D.2] Adhesion Working Group: Managing Low Adhesion. Report published by the Adhesion Working Group, UK (September 2001)
[3D.3] Press release by the Dutch Railways in Dutch, www.ns.nl (October/November 2002).
[3D.4] U. Olofsson, K. Sundvall: Influence of Leaf, Humidity and Applied Lubrication on Friction in the Wheel-Rail Contact: Pin-on-Disc Experiments. Journal of Rail and Rapid Transit 218 (2004) 235-242.
[3D.5] W. Voges, P. Spiess: Optimizing Services with EMU ET42x in Autumn 2004 and 2005. In proceedings of 7th World Congress on Railway Research, Canada (2006).
[3D.6] C.W. Jenks: Improved Methods for Increasing Wheel/Rail Adhesion in the Presence of Natural Contaminants. Transit Cooperative Research Program Sponsored by the Federal Transit Administration, Transportation Research Board National Research Council (May 1997).
[3D.7] N. Tanabe, Y. Hirota, T. Omichi, J. Hirama, K. Nagase: Study on the Factors Which Cause the Wheel Skidding of JR Ltd. Express EMUs. JSME International Journal 47 (2004) 488-495.
[3D.8] H.I. Andrews: Railway Traction—the Principles of Mechanical and Electrical Railway Traction. Elsevier (1986).
[3D.9] Sanding Equipment Fitted to Multiple Units and On-track Machines. Railway Group Standard GM/RT 2461 (2001).
[3D.10] Mesures a Prendre Pour Ameliorer la Sensibilite au Shuntage des Circuits de Voie. UIC737-2 in French (1980).
[3D.11] G. Gfatter, D. Lang, H. Kalbas, G. Krause, W. Rychli: Sanding Systems. Handbook published by Knorr-Bremse GmbH (2002).

[3D.12] O. Arias-Cuevas, Z. Li, R. Lewis: A Laboratory Investigation on the Influence of the Particle Size and Slip During Sanding on the Adhesion and Wear in the Wheel-Rail Contact. In proceedings of the 8th International Conference on Contact Mechanics and Wear of Rail/Wheel Systems, Firenze, Italy, September 15-18 (2009).
[3D.13] O. Arias-Cuevas, Z. Li, R. Lewis: Investigating the Lubricity and Electrical Insulation Caused by Sanding in Dry Wheel-Rail Contacts. Tribology Letters 37 (2010) 623–635.
[3D.14] O. Arias-Cuevas, Z. Li, R. Lewis, E.A. Gallardo-Hernandez: Laboratory Investigation of some Sanding Parameters to Improve the Adhesion in Leaf Contaminated Wheel-Rail Contacts. In press, Journal of Rail and Rapid Transit (2010).
[3D.15] OmniSTAR 8200HP User Manual, Issue 1.05 (April 2007).
[3D.16] Z. Li, O. Arias-Cuevas, R. Lewis, E.A. Gallardo-Hernandez: Rolling-sliding laboratory tests of friction modifiers in leaf contaminated wheel-rail contacts. Tribology Letters 33 (2009) 97–109.
[3D.17] E.A. Gallardo-Hernandez, R. Lewis: Twin disc assessment of wheel/rail adhesion. Wear 265 (2008) 1309–1316.
[3D.18] C.R. Fulford: Review of low adhesion research. Report published by the Rail Safety and Standards Board, UK (2004).
[3D.19] Regeling Spoorverkeer, Article 8, Chapter 3: Maximumsnelheid Treinen. Available online in Dutch at http://wetten.overheid.nl/BWBR0017707 (accessed on February 3rd, 2010).
[3D.20] N. van Steenis: Monitoring train performance in case of low adhesion; acquiring knowledge for the development of low adhesion measures. PhD Thesis, University of Twente, Enschede, the Netherlands (2010).

Chapter 4

Magnetic Track Brakes

ABSTRACT

Chapter 4 presents some field investigations on the effectiveness and possible side effects of using MTBs to overcome the low adhesion problems. The tests have been performed in grease, water and leaf contaminated contacts as well as under dry conditions. The chapter is divided into two parts. In Part A, emphasis is put on the adhesion recovery attributed to each MTB passage along a track section contaminated with leaf layers, water and grease. Additionally, the performance of the MTBs is compared to baselines (i.e. no use of MTBs) in water and leaf contaminated contacts, and to FMB in leaf contaminated contacts. Part B firstly presents the investigations on the MTB braking force in clean and contaminated contacts, including calculations of the train deceleration under different operational conditions. Furthermore, Part B examines some possible side effects of using MTBs, such as damage to rails, effect on insulated rail joints and wear of the MTB brake shoes.

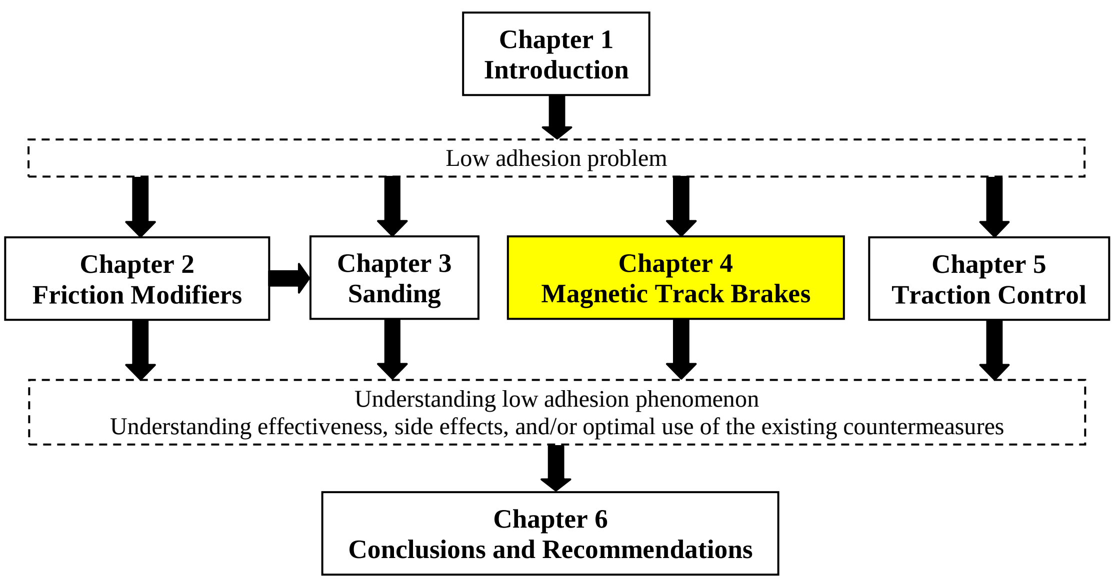

Chapter 4, Part A

Field tests on adhesion recovery[XI]

ABSTRACT

Some rolling stock designed for conventional and high speed railway operation has magnetic track brakes to have a brake independent of the wheel-rail adhesion to be mostly activated in emergency situations. In recent years, interest has grown in some railways towards the possible use of magnetic track brakes against slippery tracks. However, there seems to be a lack of knowledge on the major benefits and possible side effects of using magnetic track brakes to overcome low adhesion conditions. This hinders the realization of a cost-benefit analysis to look at possible implementations. In order to contribute to a better understanding, field tests have been performed with the permanent magnetic track brake of an electrical multiple unit in a stabling yard. Low adhesion conditions have been created by three types of contamination representative of slippery tracks, i.e. leaves, water, and grease. The entire work has been divided in two parts. In this Part A, emphasis is put on the adhesion recovery, in particular the benefit for subsequent wheel (or train) passages. Baseline tests (i.e. no use of magnetic track brake) have also been performed with water and leaves. Additionally, an adhesion improver widely used in the Dutch and British railways has also been tested with leaves to allow for a comparison in effectiveness with magnetic track brake under similar operating conditions. In each test, the wheel-rail adhesion conditions along the initially contaminated track have been measured to evaluate the adhesion improvement under the different testing conditions.

[XI] This chapter has been submitted in 2010 for publication to Proc. IMechE, Part F: J. Rail and Rapid Transit as: O. Arias-Cuevas, Z. Li: Field Investigations on the Performance of Magnetic Track Brakes of an Electrical Multiple Unit against Slippery Tracks. Part I: Adhesion Improvement.

4A.1. Introduction

Magnetic track brakes (MTBs) have been fitted to some rolling stock since the beginning of the 20th century [4A.1]. Currently, one of the major applications of MTBs is found in trams, in which sufficient braking power is indispensable as the space designated for tramways may temporarily be shared with different forms of transportations (e.g., bus, bicycle, car and motorbike) and pedestrians. In rolling stock designed for conventional and high speed railway operation, MTBs are sometimes fitted to have a brake independent of the wheel-rail adhesion to be mostly activated in emergency situations. Around half of the passenger rolling stock in the Netherlands is currently fitted with MTBs, which are activated in case of a rapid braking, the driver's fatality, or the activation of the passenger's emergency brake.

In recent years, interest has arisen in the Dutch and other railways towards a more frequent use of MTBs to fight slippery tracks. In the United Kingdom, an assessment of fitting the rolling stock with MTBs has been undertaken [4A.2]. In Germany, some electrical multiple units (EMUs) have recently been retrofitted with MTBs to improve the braking performance in autumn [4A.3]. In the Netherlands, the use of existing MTBs during normal braking operation has been evaluated [4A.4]. A conceptual approach of MTB use against slippery tracks has been proposed by the authors to the Dutch railways, in which one (or more) MTB of a train consist is activated upon detection of low adhesion conditions at a given location along the track, and it is deactivated once the low adhesion conditions have disappeared. In this way, the brake shoes of the MTB would only slide over the contaminated rails, leading to an increase of the braking performance of the train along the slippery track section and to the (partial or complete) removal of the cause of low adhesion for subsequent passing trains, while minimizing unnecessary wear to brake shoes and rails. Nevertheless, there exist a number of concerns that have been discussed with the major train operating company (NS) and the railway infrastructure manager (ProRail), which need to be investigated to allow for a cost-benefit analysis. On one hand, the benefit of MTB use against slippery tracks needs to be clearly quantified in both the increase of the braking force and the adhesion improvement for subsequent wheel passages. On the other hand, possible side effects, such as increased maintenance of MTB brake shoes, compatibility with insulated rail joints (IRJs) and switches, and possible damage to the rails (among others), must be examined. As a first step to investigate these concerns to some extent, the authors have carried out field tests with a permanent MTB of an EMU of NS. The results obtained in the tests are presented in two parts. Part A, which is shown in this paper, gives the results on the adhesion recovery, while Part B focuses on the braking force and some possible side effects [4A.5]. The main objective of Part A is to quantify the adhesion improvement attributed to each MTB passage along a slippery track under different types of contamination.

A few investigations on the performance of MTBs under low adhesion conditions can be found in the literature [4A.6, 4A.7]. In the late 80s, some field tests were undertaken in the Netherlands to test the braking performance of electro MTBs along rails that had been contaminated with a soap solution and a break-free oil [4A.6]. An increase in the train deceleration was reported in contaminated and clean contacts when using MTBs. In addition, measurements of the rotational velocity of the wheel axles during braking showed that less wheel slide occurred in the rear axles, which suggested that the wheel-rail adhesion had been improved after the passage of the MTB brake shoes along the contaminated rails. Boiteux et al. [4A.7] presented the results of some braking tests performed in field with electro MTBs on clean and leaf contaminated rails. Measuring wheelsets were employed to assess the level of adhesion after the passage of different number of MTBs. They showed that using MTBs on rails covered by fallen leaves improved the adhesion for subsequent wheel passages to a level that appeared to be dependent on the number of MTBs employed.

In this work, field tests have been performed in traction operation with or without MTB depending on the test. Low adhesion conditions have been created with leaves, water, and grease. In the tests with leaves and water, baseline tests have also been performed. Additionally, an adhesion improver, which is widely used in the Dutch and British railways, has also been tested with leaves to allow for a comparison in effectiveness with MTB under similar operating conditions. The wheel-rail adhesion in each test run has been measured by means of the traction control unit (TCU) of a motorized bogie. The position of the driven wheels and the MTB on the track has been monitored and synchronized with the TCU data to determine the location of the measurements. By comparison of the traction performance between different passages along the contaminated rails, the adhesion improvement has been determined.

4A.2. Testing description

4A.2.1. Electrical multiple unit

The tests were performed with a double-decker EMU of NS in a stabling yard (see Fig. 4A.1). The EMU consists of four vehicles with eight bogies and sixteen wheel axles in total, as schematically shown in Fig. 4A.2. The profile of the wheels was S1002 and the profile of the rails was UIC54. Considering that tests were performed with the EMU under unloaded conditions, the axle loads were around 15 t and 17 t for non-driven and driven wheel axles, respectively.

Fig. 4A.1. Photograph of the EMU in the stabling yard during the field tests.

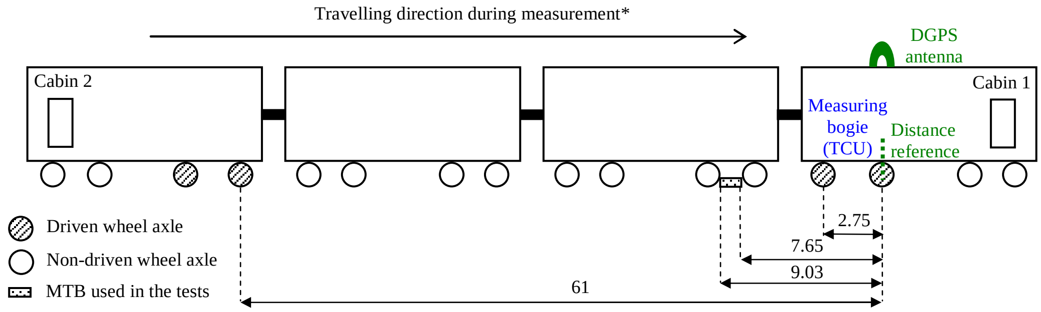

Fig. 4A.2. Two-dimensional schematic representation of the EMU employed in the tests (dimensions in meters). *Travelling direction was opposite in the wet "clean" contacts tests.

Two of the eight bogies are motorized. In each motorized bogie, an inverter supplies voltage to two motors in parallel so that each wheel axle is driven by a motor. The torque-speed characteristics of the motor are given in Fig. 4A.3. Note that the values given in Fig. 4A.3 are referred to the torque applied on the wheel axle. It can be seen that the motor torque can be at its maximum until around 40 km/h, when it starts decreasing with the speed at constant power. Hence, the low speed range between 0 km/h and 40 km/h can be identified as the most critical in terms of limiting adhesion. In the tests, the travelling speed of the EMU was limited to 40 km/h, which is also the limitation of the stabling yard. Furthermore, the torque exerted by the two motors of a bogie is regulated by means of a TCU. In case that low adhesion conditions are encountered, the TCU adjusts the torque of both motors so that the tractive effort stays below the friction level available. In the tests, the data of the TCU of one motorized bogie was recorded to measure the wheel-rail adhesion, as will be explained in Section 4A.2.5. The location of the measuring bogie is indicated in Fig. 4A.2.

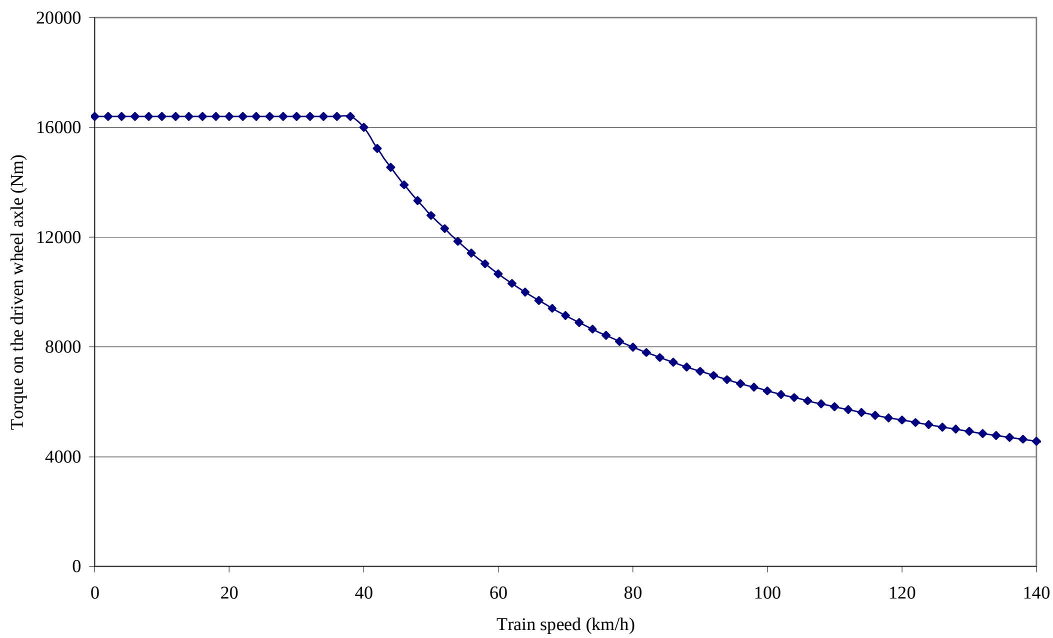

Fig. 4A.3. Torque-speed characteristics of the motor.

4A.2.2. Magnetic track brake

The EMU is equipped with a high-suspension permanent MTB in four of the six trailing bogies. In the tests only one MTB was employed, which was situated behind the measuring bogie in the travelling direction, as indicated in Fig. 4A.2. A photograph of a permanent MTB is displayed in Fig. 4A.4, where the main parts of the MTB are also pointed out. In a MTB there are two brake magnets, one for each rail, which are linked by means of two track rods. The four lift cylinders have in-built springs that support the mass of the MTB on the bogie frame in the rest position.

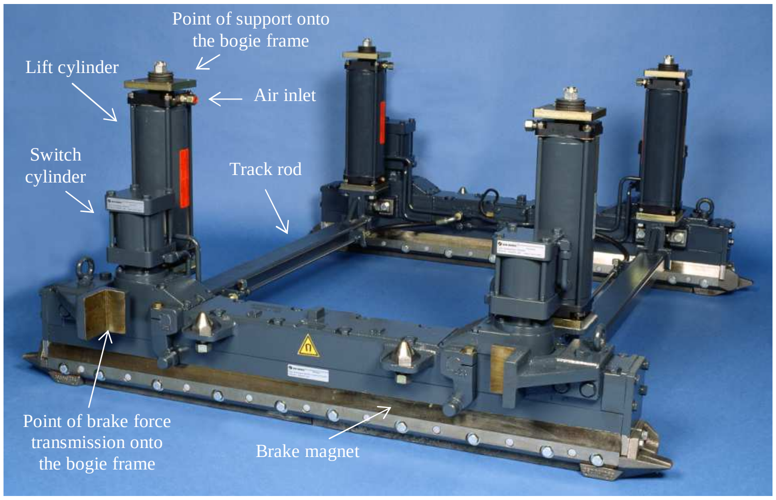

Fig. 4A.4. Photograph of a permanent magnetic track brake (Courtesy of Faiveley Transport).

In Fig. 4A.5, a simplified drawing of the cross-section of a brake magnet is given in both rest and active positions. Note that magnetic parts have been filled in with (blue) lines, whereas non-magnetic parts have been filled with (red) dots. The brake shoes of each brake magnet consist of right and left pole shoes and an insulating strip. In the rest position, there exists a distance of slightly more than 10 cm between the brake shoes and the top of the rail, and the magnetic field created by the permanent magnet is in a closed loop away from the pole shoes, as shown in Fig. 4A.5. When the MTB is to be activated, air pressure builds up in the four lift cylinders and in the four switch cylinders. The lift cylinders bring the MTB onto the rails, while the switch cylinders lower the permanent magnet to put it in contact with the pole shoes. This leads to the formation of a closed magnetic field between the rails and the pole shoes, as indicated in Fig. 4A.5. This magnetic field is responsible for the attractive force, or in other words, the normal contact load between pole shoes and rail. Since the insulating strip is mechanically constrained to the pole shoes, it is also pressed against the rail surface. The sliding motion of the brake shoes over the rails generates the MTB force, which is transmitted to the bogie frame by means of transmission pads that are positioned at the points of brake force transmission indicated in Fig. 4A.4. To deactivate the MTB, air pressure is released from the lift and switch cylinders so that the brake magnets are lifted to the rest position.

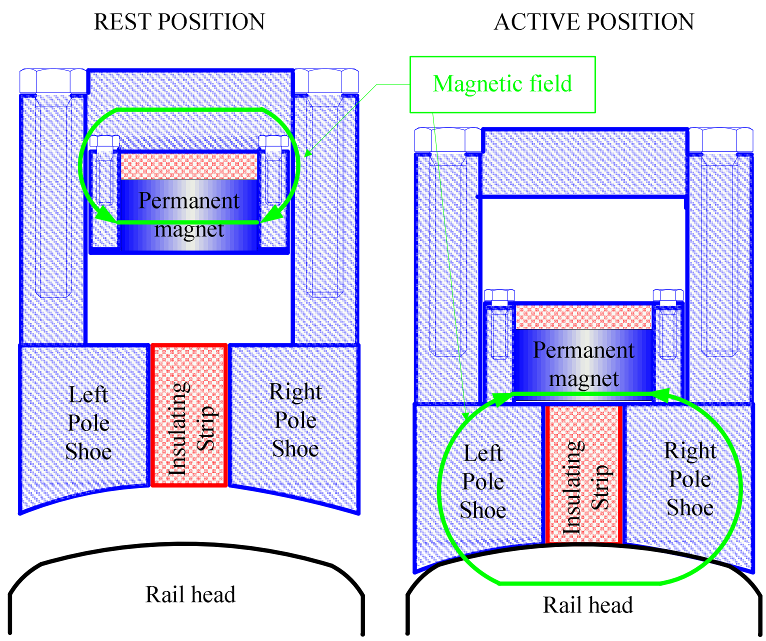

Fig. 4A.5. Simplified drawing of a cross-section of a brake magnet of the MTB in rest and active positions.

4A.2.3. Testing preparation

In the tests, the low adhesion conditions were created with three different types of contamination, i.e. leaves, water, and grease. These contaminants were selected because they have been reported to be among the most prominent responsible for slippery tracks in the Netherlands and overseas [4A.3, 4A.8-4A.12]. The contaminants were initially applied to the top of the rails along a track section, which is referred in this work to as the contaminated section. The length of the contaminated section varied depending on the type of contamination used in the tests, being 15 m in the tests with grease and 25 m in the tests with leaves and water. The temperature and relative humidity in the stabling yard was monitored in the tests by means of a thermo-hygrometer. The ambient temperature ranged between 20 °C and 30 °C, and the relative humidity changed between 20% and 40%. There was no rain during the tests.

Table 4A.1 gives a description of the field tests performed for the adhesion recovery investigations. The field tests were named alphabetically according to the order of realization. This was especially important to monitor variations in wheel-rail adhesion and MTB force due to changes in surface conditions of brake shoes, rails and wheels. It can be seen in Table 4A.1 that some tests are missing, e.g. tests A, D, E, J, K, and M. These tests were only relevant to the MTB force measurements, being presented in [4A.5]. Furthermore, in order to avoid undesired mix-up of contaminants in a test, the total available length of the stabling yard was divided into four test sections, employing a different test section for each type of contamination. The section used in each test is indicated in Table 4A.1. Note that two test sections were used for the tests with leaves. The length of a test section included a contaminated section and a distance required for the EMU to accelerate and to brake safely.

Table 4A.1. List of the tests relevant to adhesion recovery investigations.

Test B = Baseline leaf test on test section 1

RUN	Ref-B	B1	B2	B3	B4	B5	B6	B7	B8	B9	B10	B11	B12	B13	B14
COND.	dry	dry	dry	dry	dry	dry	dry	dry	dry	wet	wet	wet	wet	wet	wet

Test C = MTB leaf test on test section 1

RUN	Ref-C	C1	C2	C3	C4	C5	C6	C7	C8	C9	C10	C11
COND.	dry/wet	dry	dry	dry	dry	wet	wet	wet	wet	wet	wet	wet

Test F = Baseline leaf test on test section 1

RUN	Ref-F	F1	F2	F3	F4	F5	F6	F7	F8	F9	F10	F11	F12
COND.	dry/wet	dry	dry	dry	dry	dry	dry	dry	wet	wet	wet	wet	wet

Test G = MTB leaf test on test section 1

RUN	Ref-G	G1	G2	G3	G4	G5	G6	G7	G8	G9	G10	G11	G12	G13
COND.	dry/wet	dry	dry	dry	dry	dry	dry	dry	dry	wet	dry	wet	wet	wet

Test H = MTB leaf test on test section 1

RUN	Ref-H	H1	H2	H3	H4	H5	H6	H7	H8	H9	H10
COND.	dry/wet	dry	dry	dry	dry	dry	wet	dry	wet	dry	wet

Test I = FMB leaf test on test section 1

RUN	Ref-I	I1	I2	I3	I4	I5	I6	I7	I8
COND.	dry/wet	dry	“dry”	dry	wet	wet	wet	wet	wet

Test L = Wet “clean” test on test section 3

RUN	L1	L2	L3	L4

Test N = MTB leaf test on test section 2

RUN	Ref-N	N1	N2	N3	N4	N5	N6	N7
COND.	dry/wet	dry	dry	dry	wet	wet	wet	wet

Test O = MTB grease test on test section 4

RUN	O1	O2	O3	O4	O5	O6

4A.2.3.1. Tests with leaf contaminated rails

The leaves, which originated from different types of trees, were first placed one by one on the top of the two rails of the contaminated section, as shown in Fig. 4A.6. Small amounts of water were initially sprayed to help adhering the leaves to the top of the rails before the first passage of the EMU wheels. The EMU passed four times over the contaminated section with no traction/braking efforts and at low speed so that most of the leaves were compacted onto the rail surfaces. The resulting leaf layers were mostly dry prior to the start of the test as no water had been applied after the first passage of the EMU over the leaves. It can be seen in Table 4A.1 that runs under dry and wet conditions were performed in a leaf test. In general, runs under wet conditions were only performed after no low adhesion conditions were encountered in a run under dry conditions. Prior to the start of a test run under wet conditions, water was sprayed on the rails along the contaminated section to simulate wet leaf contaminated conditions typical of foggy, dewy or drizzling autumn days.

Fig. 4A.6. Photograph of the contaminated section prior to the EMU passages of test preparation.

When a leaf test was finished, some cleaning runs were performed in an attempt to remove remaining leaf contamination from wheel and rail surfaces so that the same section could be used for the next test in comparable conditions. The same cleaning procedure was followed after each leaf test. Firstly, sand was applied to top of the rails of the test section, and the EMU travelled four times with full traction/braking. Afterwards, brooms were employed to wipe remaining sand off the rails. Then, the EMU travelled again four times along the test section with full traction/braking. Note that the MTB was not activated in any of the cleaning runs. Before starting a new leaf test, a reference run was performed under dry and wet conditions to measure the actual initial adhesion conditions of the new test.

4A.2.3.2. Test with wet “clean” rails

Prior to the start of each test run, water was sprayed onto the top of the rails along the contaminated section. After each run the remaining moisture rapidly evaporated. Water was sprayed again along the contaminated section to perform a new test run. Note that the quotation marks as in “clean” are employed in this paper to distinguish the clean conditions in field from the more purely clean conditions typically present in laboratory testing.

4A.2.3.3. Test with grease contaminated rails

The grease used in the tests is a lubricant, which is currently applied to the flange contact along some curved sections of the Dutch railway network by means of trackside installations to reduce wear, noise and risk of derailment [4A.13]. Before the start of the test, the grease was painted on the top of the two rails along the contaminated section.

4A.2.4. Testing procedure

In every test, the measuring bogie was at a distance of around 30 m before the contaminated section at the start of a run. The driver requested the maximum tractive effort until a maximum travelled distance of 61 m, when the traction was stopped to ensure that the wheels of the second motorized bogie “freely” rolled over the contaminated section. The measuring wheels entered the contaminated section at a rolling velocity of 22 ± 2 km/h in every test. Depending on the test and the adhesion conditions, the velocity at the exit of the contaminated section varied, being 25 ± 4 km/h in tests with grease and 27 ± 2 km/h in tests with leaves and water.

In the tests with MTB, the MTB had been activated from the start of the run. The combination of traction (by the motorized bogies) and braking (by the MTB) during the measurements clearly differed from actual operation, but it was adopted in the tests for two main reasons. On one hand, the adhesion requirements in traction of this EMU are about twice larger than in braking, which allowed a wider measuring range of adhesion improvement in the tests. On the other hand, the complexity of actions needed by the driver was in this way simplified; for example, it was required in the tests that non-measuring wheels did not exert longitudinal forces on the contaminated section, and this was more complex to achieve during braking due to the higher number of active axles.

Furthermore, the wheel-rail adhesion measurement corresponded to the condition prior to the MTB passage over the contaminated section because the MTB was located behind the measuring bogie in the travelling direction (see Fig. 4A.2). By repeating runs along the contaminated section, the adhesion before and after MTB passage could be measured and, therefore, the adhesion improvement could be quantified. The only exception to this procedure was in the test runs with water, in which the direction was intentionally reversed to measure directly the wheel-rail adhesion improvement after each MTB passage. This was necessary due to the ambient conditions in the tests, which led to a rapid evaporation of the moisture before the EMU could repeat its travel along the contaminated section.

In tests with leaves and water, baseline tests were also performed with a double purpose. On one hand, the adhesion improvement measured in the baseline tests could be used to quantify the relative adhesion improvement of MTB. On the other hand, the baseline tests aimed at giving insight into the impact of leaf contamination on the wheel-rail adhesion in field conditions and the adhesion improvement by slipping (driven) wheels. It can be understood that the procedure of the baseline tests was exactly the same as in tests with

MTB, with the only exception that the MTB was not activated. Additionally, an adhesion improver used in the Dutch and British railways, which was named friction modifier B (FMB) in recent laboratory investigations by the authors [4A.14, 4A.15], was also employed in a test with leaves. A description of the constituents of FMB can be found in the literature [4A.14, 4A.15]. The leaf test with FMB intended to allow for a comparison in effectiveness with MTB under similar operating conditions. The testing procedure of this FMB test was the same as the baseline test.

4A.2.5. Measuring methodology

Data from the TCU of the measuring bogie was collected in the tests. The tractive effort exerted by the two driven wheel axles, the tractive effort requested by driver, the rotational speed of the driven wheel axles, and the travelling speed of the train were among the signals acquired. Eq. 4A.1 displays the equation of motion of a tractive wheelset under the consideration that the tractive force (F_t) and rolling radius (r_w) are the same for both wheels of the axle. Note that this assumption was acceptable in the tests because the track was straight and the contamination, if any, had been placed equally on both rails. In addition, the rolling radius of the measuring (driven) wheels was measured in the tests to be 435.4 mm on average with a maximum deviation between wheels below 0.9 mm. In Eq. 4A.1, T is the wheel axle torque, I_w is the inertia of the wheel axle around its rotation axis, and α_w is the rotational acceleration of the wheel axle. Furthermore, the tractive force can be expressed as a function of the adhesion coefficient (μ) and the normal contact force (F_N), as shown in Eq. 4A.2. Combining Eq. 4A.2 with Eq. 4A.1, an expression is found of the adhesion coefficient as a function of the readings from the TCU, which is given in Eq. 4A.3. Since the data available in the TCU applies to both motors, i.e. both driven wheel axles, it is assumed in this paper that the adhesion coefficient is the same for the four driven wheels. Note that possible errors in the torque measurement, which could affect the adhesion calculation, have been reported to be below 5% [4A.16].

The normal force in the wheel-rail contact present in the tests was calculated from a multi-body dynamics model of the leading coach of the EMU. The model was presented in [4A.13]. For the calculation, wheel and rail profiles measured in the field tests have been included in the model. Due to the rear location of the motorized bogie in the travelling direction during measurement, the axle load of the driven wheels could increase depending on the tractive effort. However, this load transfer could be neglected as it caused an error below 1.3% in the calculated adhesion coefficient under the test conditions. Because the tests were carried out on straight track, the contact point was located on the top of the rail and the lateral creep force was very small in the tests; therefore, the adhesion coefficient was limited by the coefficient of friction (*COF*), as shown in Eq. 4A.4. Introducing the measured values in Eq. 4A.3, the maximum adhesion coefficient was calculated to be around 0.22 in the tests. Hence, it can be said that traction operation at the maximum performance could only be possible in the tests if the COF at the driven wheel-rail contacts was equal to or higher than 0.22.

$$T - 2 \cdot F_t \cdot r_w = I_w \cdot \alpha_w \tag{4A.1}$$

$$F_t = \mu \cdot F_N \tag{4A.2}$$

$$\mu = \frac{T - I_w \cdot \alpha_w}{2 \cdot F_N \cdot r_w} \tag{4A.3}$$

$$\mu \leq COF \tag{4A.4}$$

In Fig. 4A.7 a simplified example of the traction operation of the measuring bogie during a test run is presented. The torque applied on the two driven axles (Tout) is given by the solid (blue) line in Fig. 4A.7, while the torque requested by the driver (Treq) is represented by a dashed (green) line. The friction, which is depicted with a dash-dot (red) line, is assumed in this example to be above the required adhesion outside the contaminated section. In Fig. 4A.7, friction, Tout and Treq are normalized in a way so that they can be plotted with the same units for the sake of comparison. The length of the contaminated section is indicated in light (blue) colour on the abscissa. The x is used because different length was used in different tests, as explained in Section 4A.2.3. Initially, the motor torque increases linearly until reaching the tractive effort requested by the driver. In practice, this initial slope limits the jerk so that passenger comfort is not compromised by an abrupt acceleration.

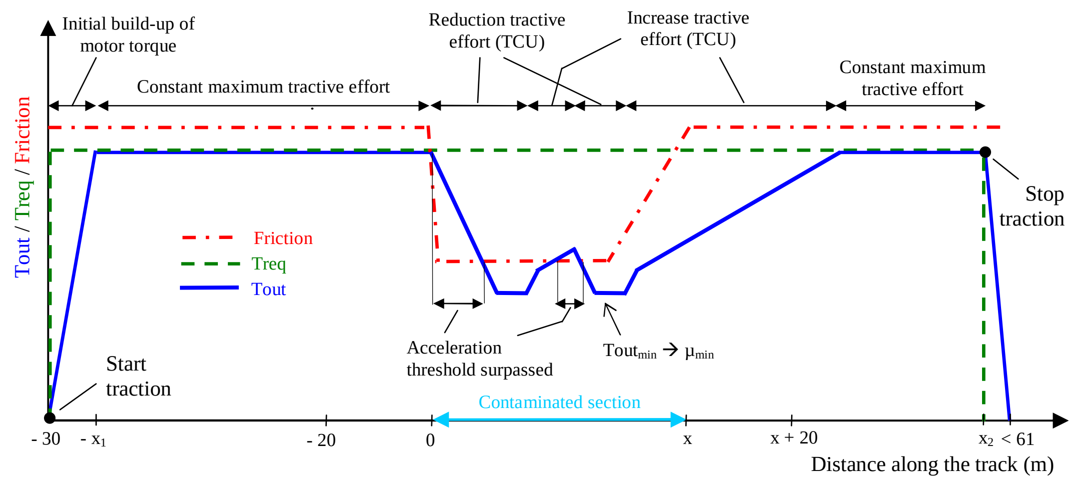

Fig. 4A.7. Representation of a simplified example of the traction operation in a test run (note that the distance travelled refers to the first driven axle of the measuring bogie).

If the friction level is higher than the requested tractive effort, a constant maximum tractive effort can be maintained in the test run after the initial torque build-up, as shown in Fig. 4A.7. When the driven wheels travel over contaminated rails, the friction level drops below the adhesion required for the maximum tractive effort and, consequently, the driven wheels start to slip. In this paper, this type of wheel slip will be referred to as macro-slip to distinguish it from the micro-slip that is always present at tractive (and braking) wheels before saturation of the friction. Since the adhesion coefficient is limited by the COF, a sudden decrease in the friction level without variation in the wheel axle torque leads to an increase in the wheel axle rotational acceleration, according to Eq. 4A.1, and macro-slip may be initiated. There exists an acceleration threshold imposed in the TCU, which is dependent on the torque that is applied on the axle, as shown in Fig. 4A.8. If the acceleration surpasses the threshold, the TCU reduces the motor torque to limit the amount of wheel slip. When the acceleration of the driven axles decreases below the threshold, the motor torque is still further reduced for a certain period and then kept constant for some time, as shown in Fig. 4A.7. After that, the TCU increases the motor torque towards the tractive effort requested by the driver. As shown in Fig. 4A.7, the friction is saturated again and the acceleration threshold is surpassed, leading to a new reduction of the motor torque. The driven axles finally exit the contaminated section and the motor torque can be increased to reach the maximum tractive effort, which is kept constant until the traction is stopped, as represented by a (black) point in Fig. 4A.7.

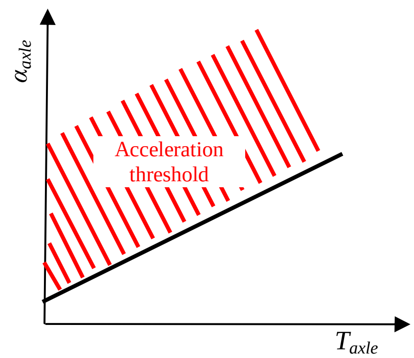

Fig. 4A.8. Schematic representation of the acceleration threshold calculation in the TCU.

In order to display the adhesion improvement with the increasing runs in a test, the minimum and average values of the adhesion coefficient in each run were calculated with the measured data according to Eq. 4A.3. The minimum adhesion coefficient corresponded to the global minimum value of Tout among the local minimums reach during each traction reduction experienced in a test, as pointed for the example in Fig. 4A.7. Note that in the simplified example presented in Fig. 4A.7, $Tout_{min}$ is the same in both reductions of the tractive effort because the friction level was assumed to remain constant, but in case of inequality the lowest of the reductions would be taken. The average value of the adhesion coefficient corresponded to the mean value of Tout in the test run along a given distance. This distance was different depending on the test. In the leaf tests the distance used to calculate the average Tout was from - 20 m until 45 m, which was identified to be prone to low adhesion as will be shown in Section 4A.3.1. In the tests with "clean" wet rails, the distance was the contaminated section where water had been sprayed (i.e. from 0 m till 25 m). In the grease tests, the distance was between -x_1 and x_2 (see Fig. 4A.7) due to the vast spread of the grease after the first wheel passages, as will be outlined in Section 4A.3.3.

The location of the driven wheel axles on the track was monitored in the tests by means of a differential global positioning system (DGPS) OmniSTAR 8200HP. The DGPS was mounted on the roof of the EMU above the measuring bogie, as indicated in Fig. 4A.2. OmniSTAR VBS GPS correction signals were used on the 8200HP to operate with sub-meter accuracy for the number of satellites available during the testing [4A.17]. A sampling frequency of 10 Hz was employed to capture the location data. In the post-processing the location was synchronized with the TCU data. In the results presented in this paper, the distance refers to the location of the first driven wheel axle of the measuring bogie, as shown in Fig. 4A.2. Note that the location of other important elements of the EMU can be deduced from the dimensions given in Fig. 4A.2.

4A.3. Results

4A.3.1. Tests with leaf contaminated rails

Seven tests with leaf contaminated rails were performed under dry and wet conditions, namely two baseline tests, four MTB tests and one FMB test (see Table 4A.1).

4A.3.1.1. Baseline

The two baseline tests have been named tests B and F. Figs. 4A.9-4A.10 depict the ratio between Tout and Treq along the distance in some dry and wet runs of test B. It can be seen in Fig. 4A.9 that low adhesion conditions were encountered before reaching the contaminated section, e.g. in run B1 low adhesion conditions were first experienced at around -12 m. This indicated that during the test preparation leaf contamination was brought outside the contaminated section by rolling wheels, and the measuring wheels could have become contaminated. Field observations have also reported that leaf contamination can be found away from the location of the source [4A.8, 4A.9].

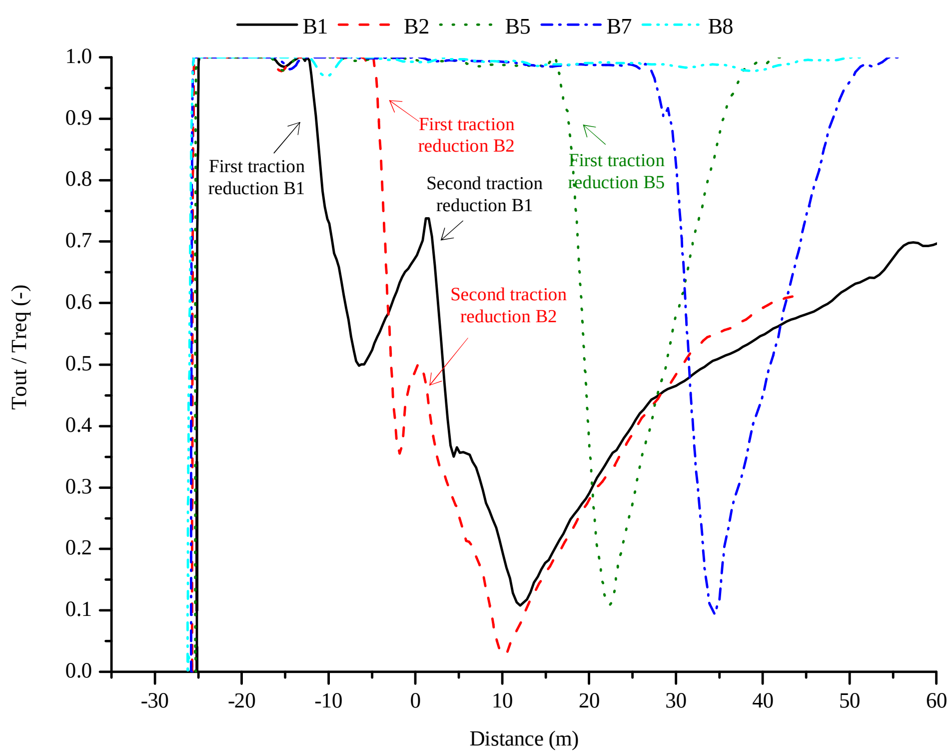

Fig. 4A.9. Ratio between Tout and Treq along the distance travelled by the first driven wheel axle in some dry runs of test B (initially contaminated section between 0 m and 25 m).

Two drops of adhesion occurred in run B1, as shown in Fig. 4A.9. In the first drop the tractive effort had to be reduced by the TCU to 50% of Treq to cease the wheel macro-slip, while the reduction was almost 10% of Treq in the second drop located at about 13

m. The large difference in the traction reduction between the two drops indicates that the friction level was much lower inside the contaminated section, as expected. In run B2, two decreases of tractive effort can also be seen in Fig. 4A.9. The first decrease started at around -4 m, while the second one started at around 2 m. Similarly to run B1, the drop inside the contaminated section was the largest in run B2.

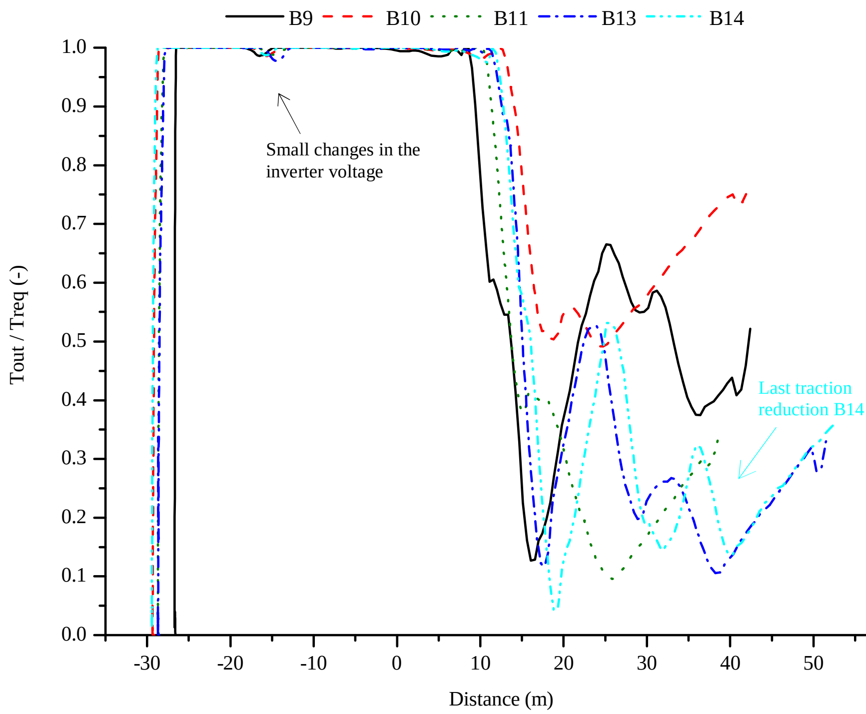

Fig. 4A.10. Ratio between Tout and Treq along the distance travelled by the first driven wheel axle in some wet runs of test B (initially contaminated section between 0 m and 25 m).

A photograph of the top of a rail after a few dry runs of test B is given in Fig. 4A.11. It can be seen that the original leaves placed along the contaminated section (see Fig. 4A.6) had transformed into leaf layers that were well adhered to the rail along its running band. The leaf layers presented a black colouration typically reported in field and laboratory observations [4A.8, 4A.9, 4A.11, 4A.14, 4A.18-4A.22]. Note that the colouration of leaf layers has been reported to be attributed to a chemical reaction of pectin with the iron rather than charring of the leaf organic material [4A.18]. Furthermore, some leaf mulch had remained at both sides of the rail running band.

In Fig. 4A.9, a trend can be observed in which the first traction reduction occurred further from the beginning of the contaminated section with the increasing number of runs. The onset of the first traction reduction went from -12 m in run B1, to -4 m in run B2 and to 16 m in run B5, as pointed out in Fig. 4A.9. This trend may be attributed to the leaf layer removal by slipping (driven) wheels. The layer removal in the tests could be due to thermal effects by high relative velocities between the contacting surfaces or mechanical effects due to the interaction between asperities of the surfaces during their relative displacement. In a laboratory work, it has been shown that an increase in the wheel slip can lead to a faster adhesion recovery in leaf contaminated wheel-rail contacts

[4A.19]. According to those results, it may be assumed that free rolling wheels can hardly contribute to the removal of leaf layers. In the present tests, the driven wheels only slipped during traction reduction and a few meters before, as explained in Section 4A.2.5. It can be seen in Fig. 4A.9 that the driven wheels did not slip in run B1 in the interval between -7 m and 0 m, because of this leaf layers remained and were responsible for the low adhesion conditions in run B2 at around -4 m. The progressive layer removal by slipping (driven) wheels in each run led to an entire adhesion recovery in run B8 so that the tractive effort could be maintained to the maximum requested by the driver.

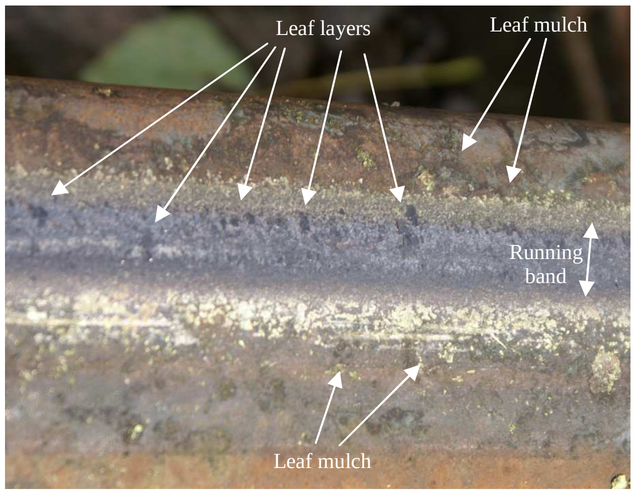

Fig. 4A.11. Photograph of the top of a rail along the contaminated section after a few dry runs.

In the runs under wet conditions, some different tendencies can be observed in Fig. 4A.10. Since water had only been applied along the contaminated section (i.e. between 0 m and 25 m), no low adhesion conditions were encountered before 0 m, as expected. It must be noted that the variations of Tout/Treq ratio at around -15 m in Fig. 4A.10 were not caused by low adhesion but by small changes in the inverter voltage, which could be due to variation in the current collected by the pantograph. Similar oscillations can also be observed in Fig. 4A.9, as well as in other figures later on, to occur mostly at around the same location. A major difference between the dry and wet runs of test B was the adhesion recovery trend. Although the earliest traction reduction occurred in the first run under wet conditions (i.e. run B9 in Fig. 4A.10), there was no clear trend of displacing the first traction reduction further from the contaminated section with the increasing runs, as it was observed in the dry runs. Furthermore, it can be seen in Fig. 4A.10 that low adhesion conditions were encountered after exiting the contaminated section. In some runs like B9 and B14, there existed a reduction of the tractive effort up to a distance of 40 m (see Fig. 4A.10). This phenomenon may be attributed to possible remaining moisture present on the wheels when they exited the contaminated section that could have mixed with some remaining leaf contamination.

Fig. 4A.12 displays the minimum and average values of the adhesion coefficient of all runs in test B. Note that these values have been extracted from the results of Figs. 4A.9-4A.10, as explained in Section 4A.2.5. During the first run under dry conditions over the leaf contaminated section the minimum adhesion coefficient was around 0.02, as shown in Fig. 4A.12. This value is in line with results obtained in the laboratory [4A.14, 4A.19-

4A.21] and in other field investigations [4A.22]. It can be seen that the average adhesion under dry conditions increases with the number of runs, while the minimum value did not follow such a trend. The explanation needs to be sought in Fig. 4A.9. On one hand, the first traction reduction was displaced in the travelling direction with the increasing runs, leading to higher average values of the adhesion. On the other hand, leaf layer removal was caused by wheel macro-slip, which did not occur continuously along the distance, resulting in some "intact" parts of the contaminated section, leading to the low values of the minimum adhesion coefficient seen in Fig. 4A.12. After seven runs the adhesion had been entirely recovered, with the average and minimum values of the adhesion coefficient in run B8 becoming equal to the maximum as in Ref-B.

The application of water to the remaining leaf contamination caused a considerable reduction of the adhesion in run B9 with a minimum value of around 0.03, as shown in Fig. 4A.12. In all the runs under wet conditions of test B, the minimum adhesion coefficient was below 0.05 with the only exception of run B10. Furthermore, no uniform tendency of increasing adhesion could be observed in the runs under wet conditions, i.e. run B9 till run B14 in Fig. 4A.12. In fact, the lowest average and minimum values of adhesion were obtained in the last run, dropping the adhesion coefficient to a minimum value around 0.01.

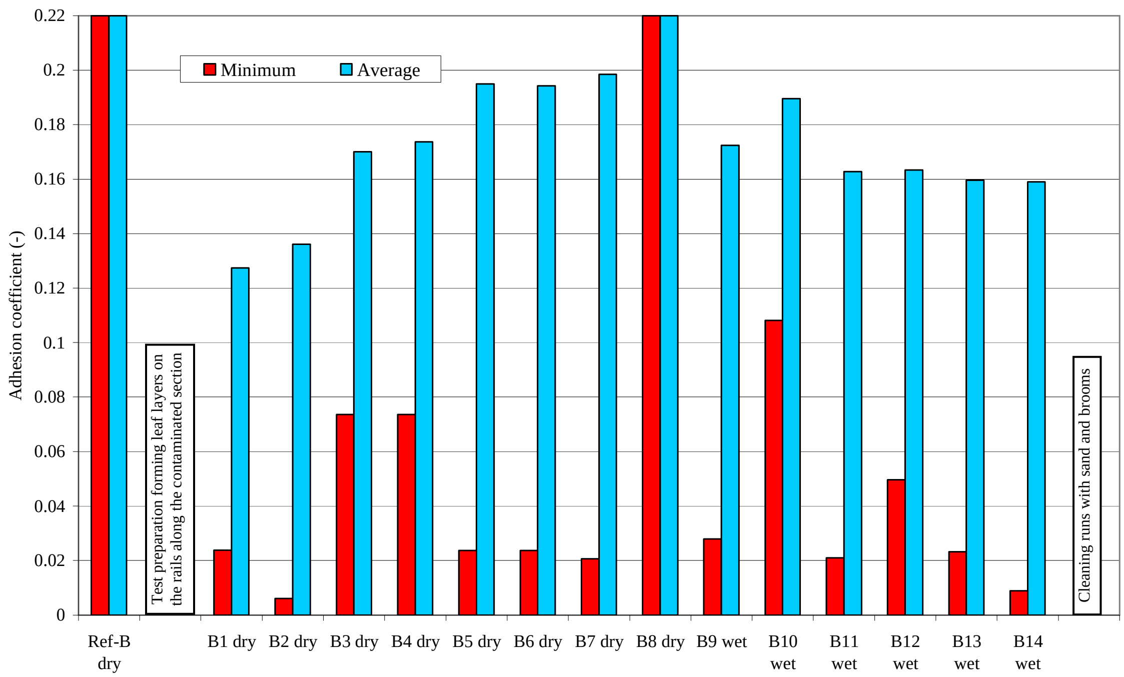

Fig. 4A.12. Minimum and average values of the adhesion coefficient in dry and wet runs of test B.

Fig. 4A.13 depicts the adhesion results of the second baseline test, named test F. It must be noted that a reference run (named Ref-F) under dry and wet conditions was performed prior to the test preparation to obtain an indication of the starting adhesion conditions along the contaminated section. In the dry runs of test F (i.e. F1 till F7), an increasing trend of the average and minimum adhesion can be seen in Fig. 4A.13. After six runs under dry conditions the adhesion was entirely recovered. In the wet runs, the average adhesion seemed to increase slightly with the runs, while the minimum adhesion coefficient did not show any clear trend. In the last run (i.e. run F12 in Fig. 4A.13) the minimum adhesion was 23% of that measured in run Ref-F under wet conditions and 14% of run Ref-F under dry conditions. Furthermore, the minimum values of adhesion were noticeably lower in the wet runs than in the dry ones. In the dry runs the minimum adhesion was always above 0.02 except for run F1, whereas the minimum adhesion was below 0.005 in all wet runs except for run F12, as shown in Fig. 4A.13. Considering that some of the leaf contamination had been removed in the dry runs, it can be said that the friction level of wet leaf contaminated wheel-rail contacts was clearly lower than in the dry conditions. This is in agreement with field and laboratory findings reported in the literature [4A.8-4A.10, 4A.21-4A.23].

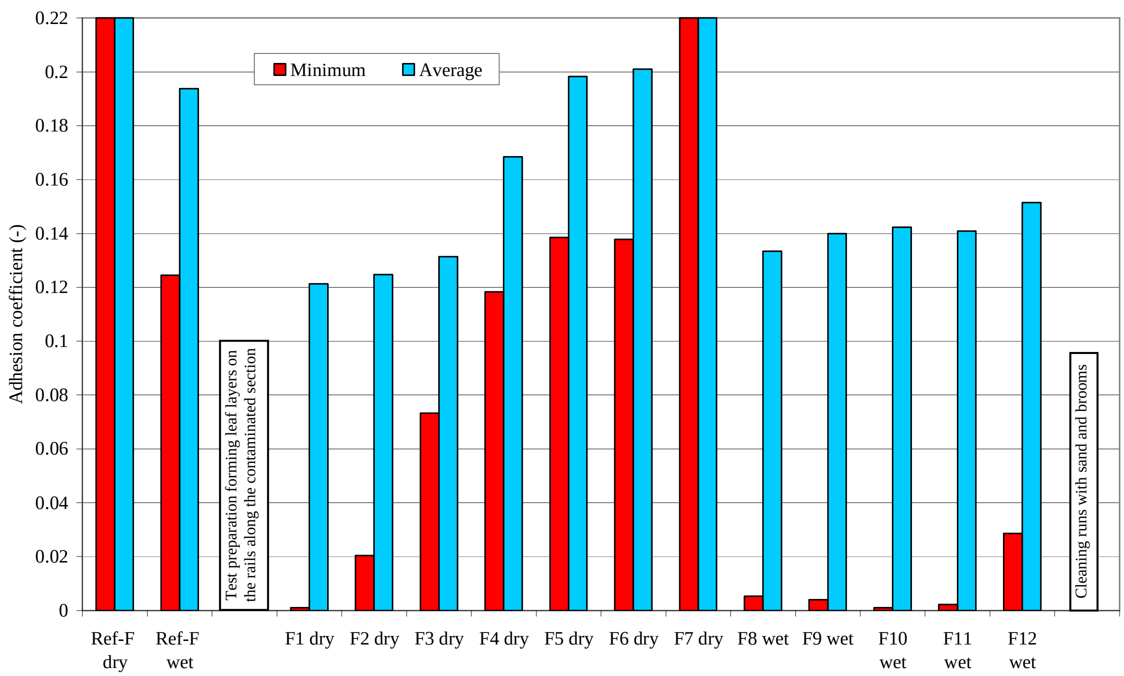

Fig. 4A.13. Minimum and average values of the adhesion coefficient in dry and wet runs of test F.

4A.3.1.2. Magnetic track brake

The four MTB tests have been named tests C, G, H and N (see Table 4A.1). It is noted that in all MTB tests, the adhesion had been measured along the contaminated rails prior to the brake shoes passage, as explained in Section 4A.2.4. Figs. 4A.14-4A.15 depict the ratio between Tout and Treq along the distance in some dry and wet runs of test C. In run C1 only one traction reduction was experienced, which occurred at the beginning of the contaminated section (see Fig. 4A.14). In run C2 three reductions in tractive effort were observed, being the first one inside the contaminated section and the last two outside it. As expected, the adhesion drop inside the contaminated section was the largest (see Fig. 4A.14). In the dry runs of test C, the first time to encounter low adhesion conditions was displaced further from the beginning of the contaminated section with the increasing runs. This trend was similar to the one observed in the baseline tests (e.g. test B in Fig. 4A.9), but at a higher rate in test C. The increase in rate can be attributed to the adhesion improvement by MTB given by leaf layer removal action of the brake shoes. After three

MTB passages, the adhesion entirely recovered and the tractive effort could be maintained to the maximum in run C4 (see Fig. 4A.14). Therefore, the required number of EMU passages for complete adhesion recovery under dry conditions using one MTB was reduced up to 57% compared to the baseline.

In the first passage of the MTB brake shoes over the leaf layers, a large amount of leaf contamination could be seen to be pushed away by the brake shoes. This leaf contamination corresponded mostly to leaf mulch that had adhered to the top of the rail during test preparation, but some leaf layers could also have been removed. Thus, the "push-effect" could partially have contributed to the adhesion improvement in dry runs of test C. On the other hand, measurements of the friction force in the contact between MTB brake shoes and rails showed a clear drop at the contaminated section [4A.5]. This indicated that the brake shoes also slid over the leaf layers, suggesting that thermal and mechanical removal effects could also have contributed to the adhesion improvement given by the MTB.

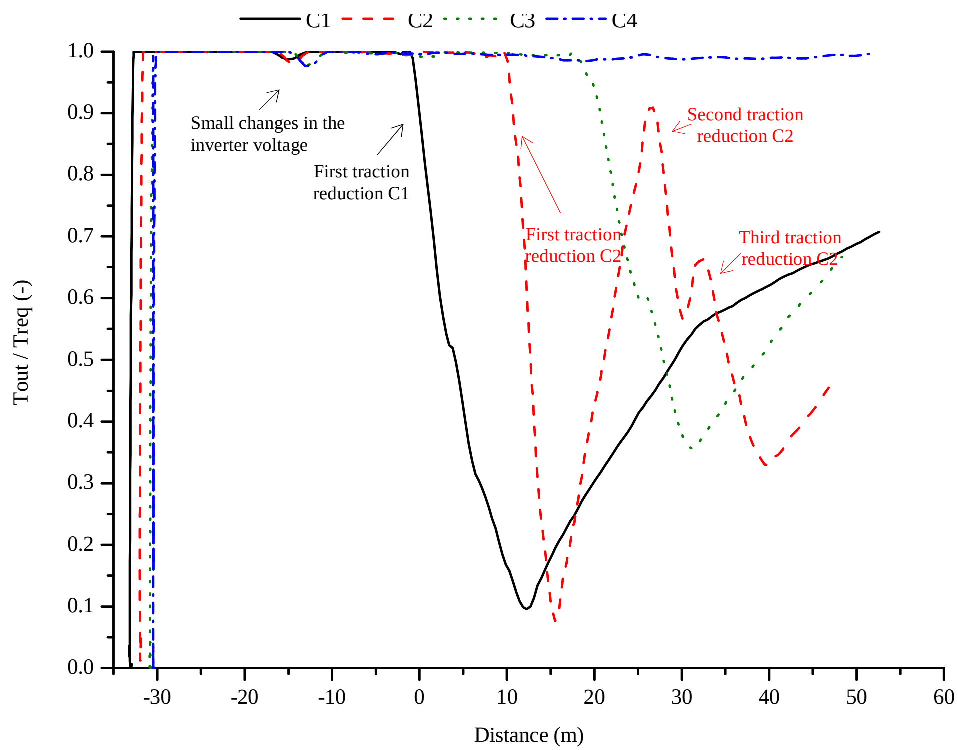

Fig. 4A.14. Ratio between Tout and Treq along the distance travelled by the first driven wheel axle in the dry runs of test C (initially contaminated section between 0 m and 25 m).

An illustration of the leaf contamination removed from the top of the rail by the MTB during run C1 can be observed in Fig. 4A.16. In Fig. 4A.16a, the rail head is shown before the MTB passage. Leaf mulch and layers can be seen on the top of the rail. Note that the photographs are taken at an IRJ, as indicated in Fig. 4A.16a. An instant when the MTB brake shoes slid over the top of the rail is shown in Fig. 4A.16b. After the MTB passage, leaf mulch and some of the leaf layers had disappeared from the top of the rail (see Fig. 4A.16c). It can also be observed in Fig. 4A.16c that some debris had fallen off the MTB brake shoe, remaining at the IRJ gap. This could deteriorate the electrical insulation performance of the IRJ and it will be examined in Part B of these investigations [4A.5].

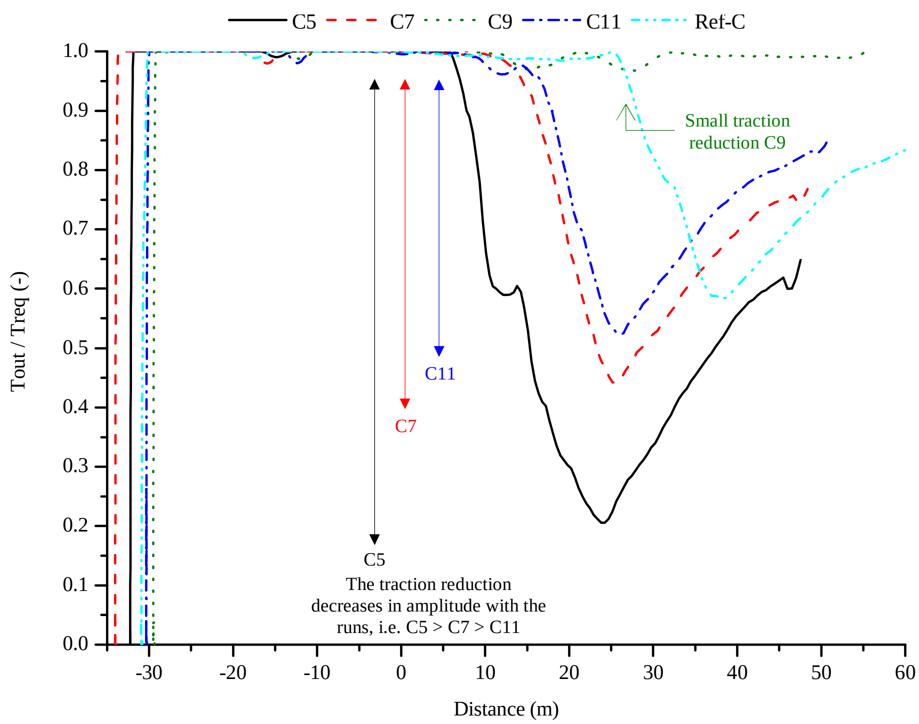

Fig. 4A.15. Ratio between Tout and Treq along the distance travelled by the first driven wheel axle in some wet runs of test C (initially contaminated section between 0 m and 25 m).

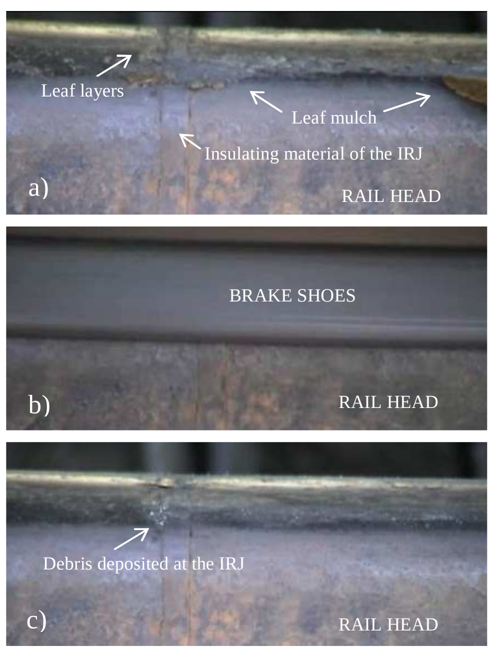

Fig. 4A.16. Photograph of a piece of rail head in run C1: a) before MTB passage, b) during MTB passage; c) after MTB passage.

In the runs under wet conditions shown in Fig. 4A.15, an improvement in adhesion with increasing runs was observed as the amplitude of the traction reduction clearly decreased. In fact, a general trend approaching the reference measurement (Ref-C) can be seen in Fig. 4A.15. There was, however, an odd result obtained in run C9, for which only a small traction reduction was observed at around 25 m of distance. Although the same procedure had been followed to spray water along the contaminated section in each test run, it could be possible that less water was effectively entrained in the wheel-rail contact in run C9, leading to higher adhesion conditions than in the other runs. The velocity measurements obtained from the TCU showed that only some small wheel macro-slip occurred in run C9.

The minimum and average values of the adhesion coefficient in the runs of test C are given in Fig. 4A.17. Similarly to test B, a minimum adhesion coefficient of around 0.02 was measured in the first run, i.e. run C1. A trend of increasing average adhesion with the runs under dry conditions can clearly be seen in Fig. 4A.17. Upon the first application of water, i.e. run C5, the adhesion went down to a minimum value of slightly below 0.05. This value was higher than in runs B9 (0.03) and run F8 (0.01) of the baseline tests, which may be owing to the more extensive leaf layer removal in the dry runs by the use of MTB. Furthermore, a comparison between the minimum adhesion values in wet runs of test C (Fig. 4A.17) with the ones of test B (Fig. 4A.12) and test F (Fig. 4A.13) points out that using MTB had clearly been effective in improving the adhesion under wet conditions. In wet runs of tests B and F, the minimum adhesion coefficient was mostly below 0.05, whereas it was mostly above 0.09 in test C. Moreover, in run C11 the average adhesion was around the same level as in run Ref-C under wet conditions, and the minimum adhesion coefficient was only about 10% lower than in Ref-C, as shown in Fig. 4A.17.

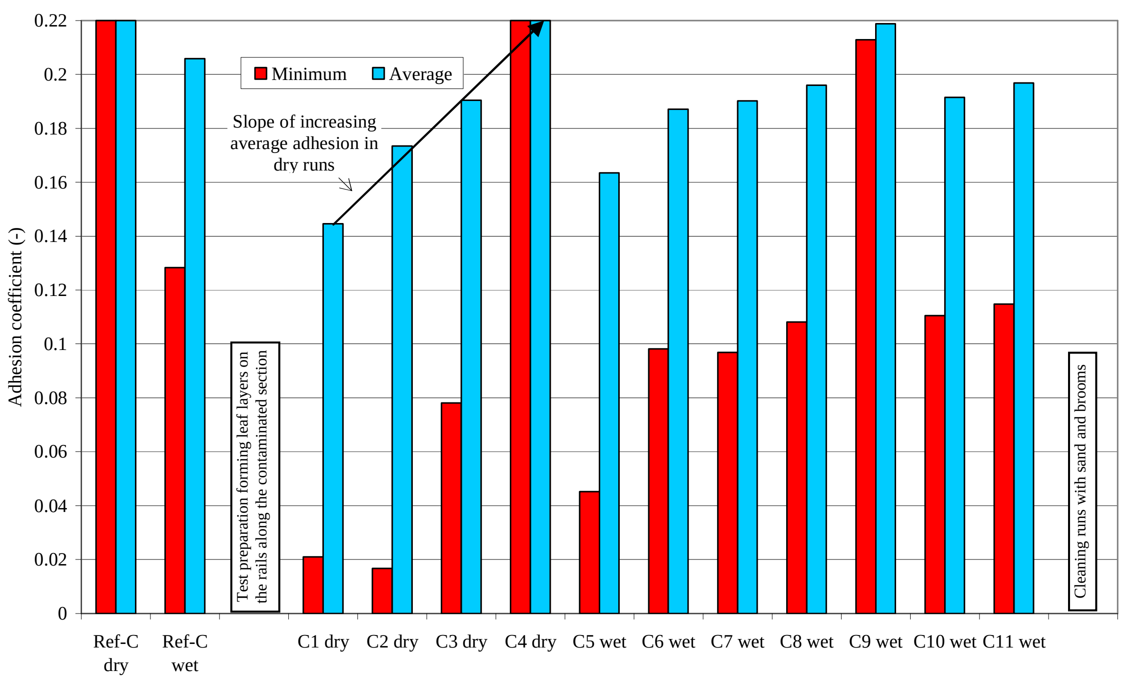

Fig. 4A.17. Minimum and average values of the adhesion coefficient in dry and wet runs of test C.

Fig. 4A.18 displays the minimum and average adhesion values measured in test G. In the dry runs G1 till G8 a clear trend can be seen of an increasing average adhesion with the runs. The minimum adhesion coefficient followed a generally similar, but locally varying, increasing trend with the runs. The rate of adhesion recovery in dry runs of test G (Fig. 4A.18) was slower than in test C (Fig. 4A.17). After seven MTB passages in dry runs of test G, the adhesion had not yet been recovered entirely. Looking at the ratio between Tout and Treq along the distance in some dry runs of test G, which is given in Fig. 4A.19, some differences with respect to the dry runs of test C can be observed. Firstly, low adhesion conditions were encountered in runs G1 and G2 between -19 m and 49 m (see Fig. 4A.19), while between 0 m and 40 m in runs C1 and C2 (see Fig. 4A.14). This indicates that the leaf contamination may have been distributed over a longer section of track in test G compared to test C, despite the fact that the leaf contamination had initially be placed equally for both tests during test preparation.

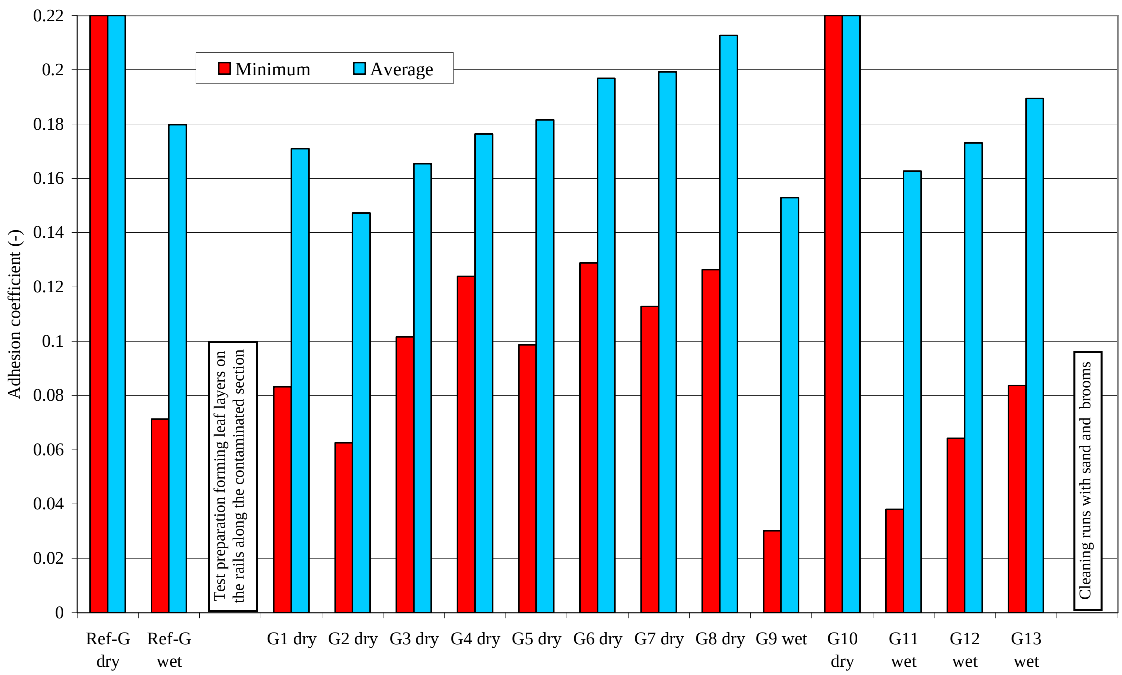

Fig. 4A.18. Minimum and average values of the adhesion coefficient in dry and wet runs of test G.

Furthermore, the first traction reduction in run G2 occurred sooner than in run G1 (see Fig. 4A.19), whereas the first reduction in run C2 occurred at a further distance in the travelling direction than in run C1 (see Fig. 4A.14). Considering that free rolling wheels hardly contributed to the transfer of leaf layer from wheels to rails or vice versa, as explained above, it may be possible that leaf layers had adhered to the surfaces of the measuring wheels during run G1. This could have promoted the drop of adhesion starting at -19 m in run G2. Furthermore, contamination on the wheel surfaces may also have been responsible for the slow adhesion recovery in dry runs of test G. In Fig. 4A.20 a driven wheel of the measuring bogie after run G5 is shown. It can clearly be seen that part of the wheel tread was contaminated with some leaf layers. Hence, leaf layers on the wheel tread of the driven wheels may have led to low adhesion conditions even if the running band of the rail had perfectly been cleaned.

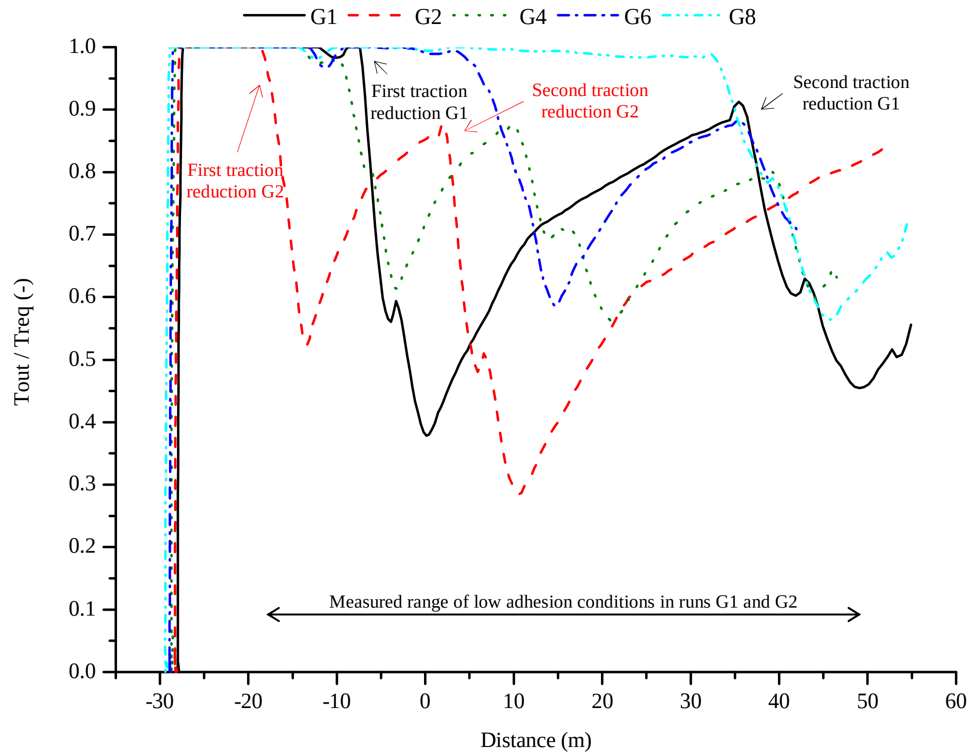

Fig. 4A.19. Ratio between Tout and Treq along the distance travelled by the first driven wheel axle in some dry runs of test G (initially contaminated section between 0 m and 25 m).

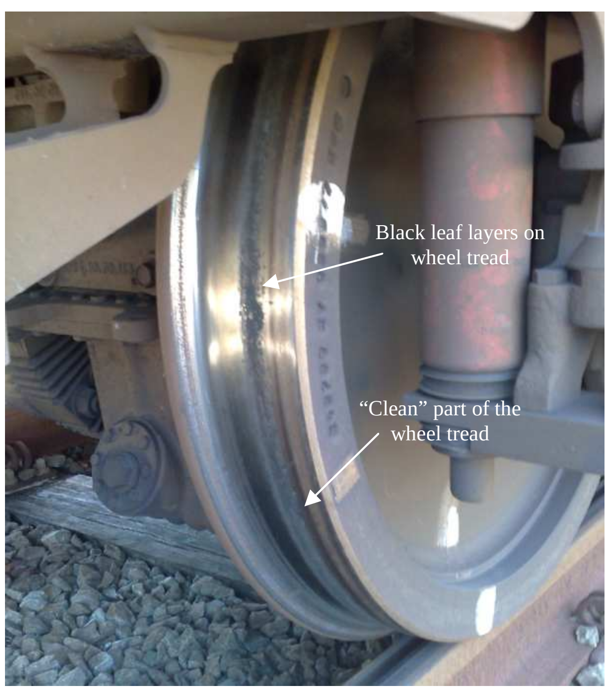

Fig. 4A.20. Photograph of the surface of one measuring wheel after the start of test G.

In run G9 wet conditions were tested, even though an entire adhesion recovery under dry conditions had not been reached in run G8 (see Fig. 4A.18). In run G10 the adhesion had been entirely recovered. In the wet runs of test G, both minimum and average values of the adhesion coefficient increased constantly with the runs. The minimum and average adhesion in run G13 surpassed the adhesion measured in Ref-G under wet conditions, suggesting that the adhesion conditions had been improved compared to the initial state. The ratio between Tout and Treq along the distance in wet runs of test G shown in Fig. 4A.21 indicates that not only the amplitude of the traction reduction decreased with the runs, but also the first occurrence of traction reduction was displaced further from the beginning of the contaminated section. Note that a similar trend was observed in the wet runs of test C (see Fig. 4A.15).

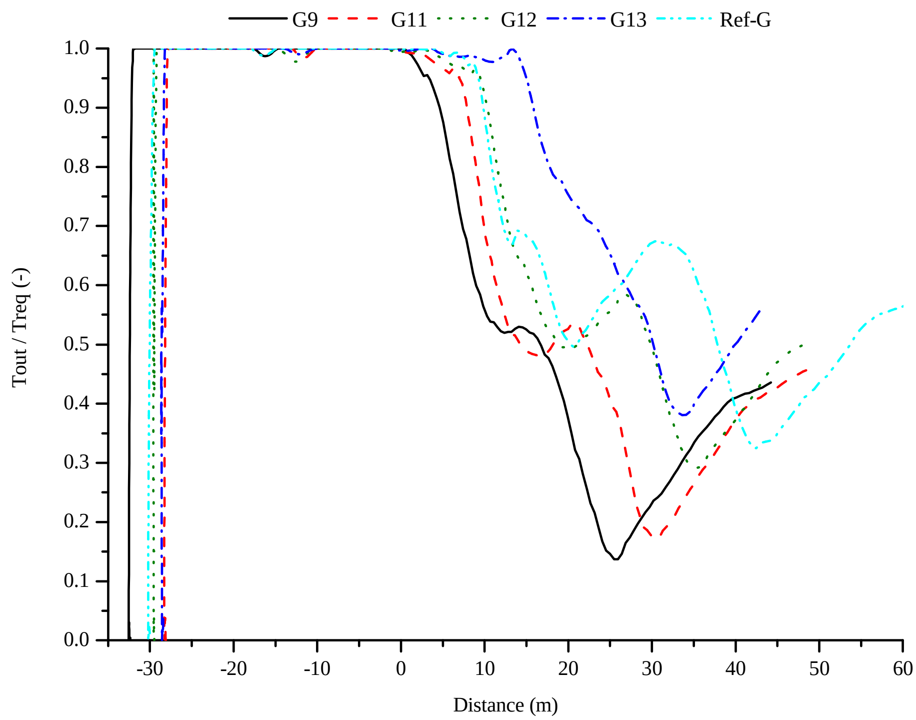

Fig. 4A.21. Ratio between Tout and Treq along the distance travelled by the first driven wheel axle in wet runs of test G (initially contaminated section between 0 m and 25 m).

Fig. 4A.22 displays the minimum and average adhesion coefficients of test H. It can be seen that after four MTB passages under dry conditions the adhesion had not entirely been recovered, being the minimum adhesion coefficient around 0.11 in run H5. Hence, as it occurred in test G, the adhesion recovery in dry runs of test H had been slower than in test C. The adhesion appeared to be entirely recovered under dry conditions in run H9, after a few runs under wet conditions had been performed (see Fig. 4A.22). Furthermore, in both dry and wet runs, there was a clear trend of an increasing average adhesion with the runs, as indicated in Fig. 4A.22. The minimum adhesion coefficient also followed a similar trend, which was particularly noticeable during runs under dry conditions.

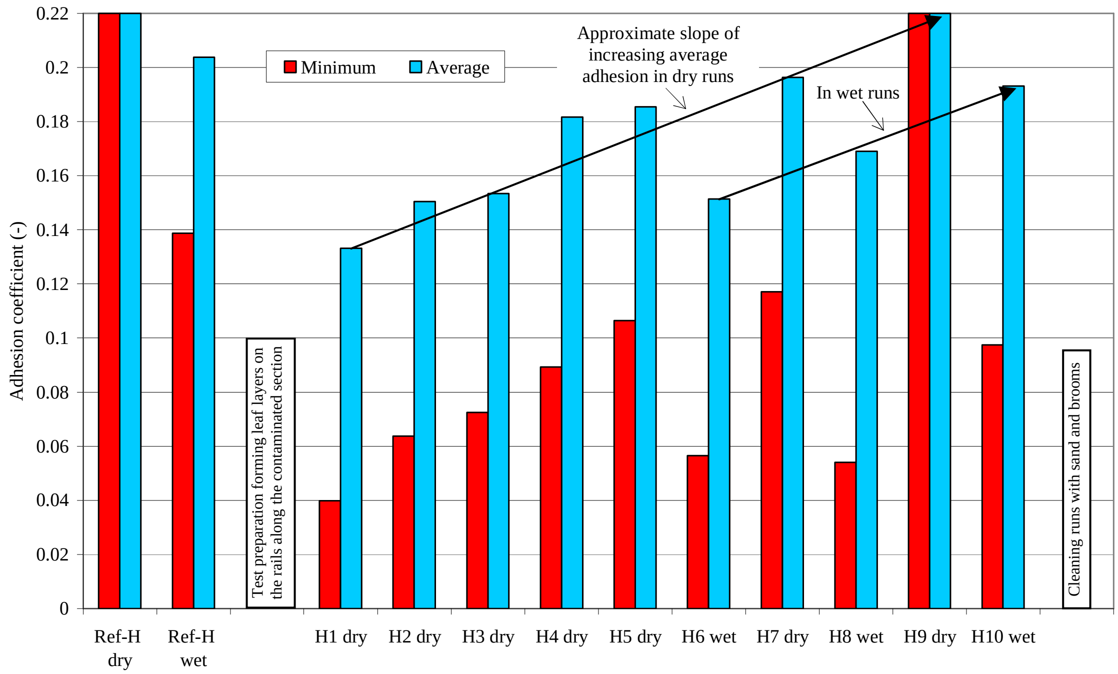

Fig. 4A.22. Minimum and average values of the adhesion coefficient in dry and wet runs of test H.

The last MTB test with leaf contamination (named test N) was performed on a different test section than the previous leaf tests (see Table 4A.1). The adhesion results of test N are given in Fig. 4A.23. It can be seen that after two MTB passages under dry conditions, the adhesion had entirely been recovered. Hence, the rate of adhesion recovery under dry conditions of test N was the highest among the MTB tests performed, and close to that obtained in test C. On the other hand, the minimum values of adhesion during runs under wet conditions of test N were among the lowest. Particularly, they were lower than those in test C, in spite of having had similar number of previous dry runs in both tests C and N. Comparing reference runs under wet conditions, it can be seen that Ref-N was around 0.08 (see Fig. 4A.23) and Ref-C was around 0.13 (see Fig. 4A.17). Therefore, it may be possible that some contamination was present on the wheels at the beginning of test N, affecting the wheel-rail adhesion under wet conditions.

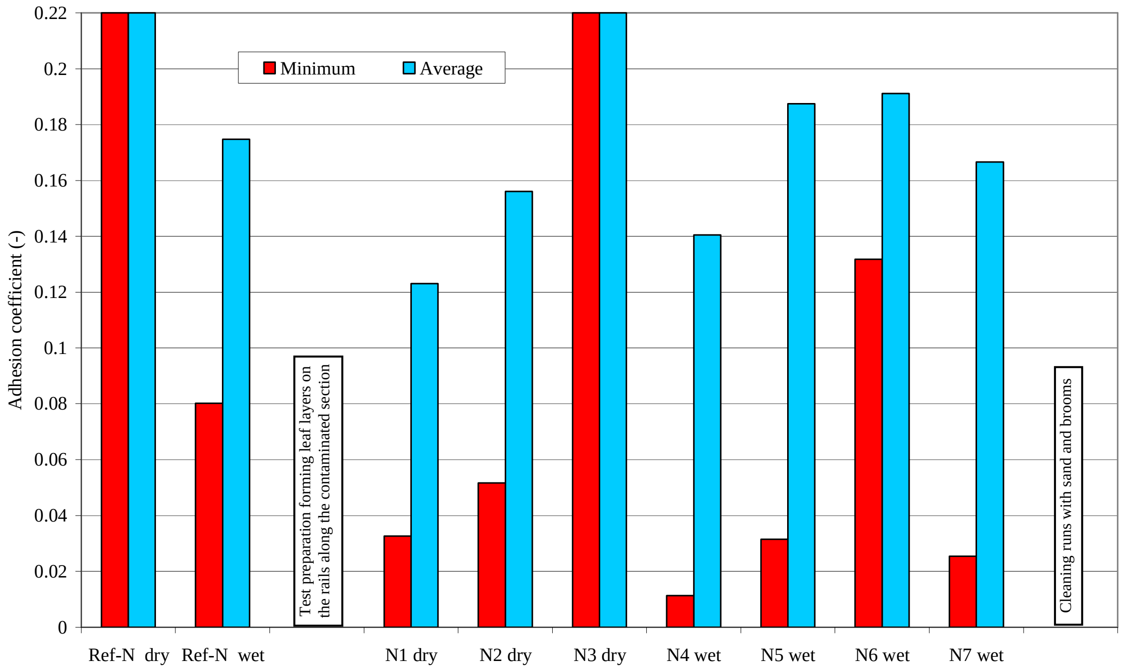

Fig. 4A.23. Minimum and average values of the adhesion coefficient in dry and wet runs of test N.

4A.3.1.3. Friction modifier B

One test was performed with leaf contaminated rails with FMB, which has been named test I (see Table 4A.1). The adhesion results of test I are given in Figs. 4A.24-4A.26. It is important to bear in mind that FMB was brought onto the rails of the contaminated section after run I1, as indicated in Fig. 4A.24. Upon first passage after FMB application (i.e. run I2) only a slight adhesion improvement was obtained compared to run I1 (see Fig. 4A.24). Although no water had been applied in run I2, it may be possible that the leaf layers were wet due to the water content of FMB. For this reason, the designation “dry” has been used in Fig. 4A.24 and Table 4A.1. In the next passage, i.e. run I3, the adhesion had been entirely recovered to the maximum level. This means that the amount of EMU passages had been reduced between 80% and 87% compared to baseline tests B and F, respectively. In previous laboratory investigations with FMB in leaf contaminated wheel-rail contacts, the reduction in passages ranged between 87% and 95% depending on the wheel slip used [4A.14]. Note that measurements of the slip of the driven wheels in tests B, F, and I reached values up to 35%. Furthermore, it can be seen in Fig. 4A.24 that the minimum adhesion coefficient constantly increased with the runs under wet conditions, whereas no clear increasing trend of the average adhesion could be observed in the wet runs.

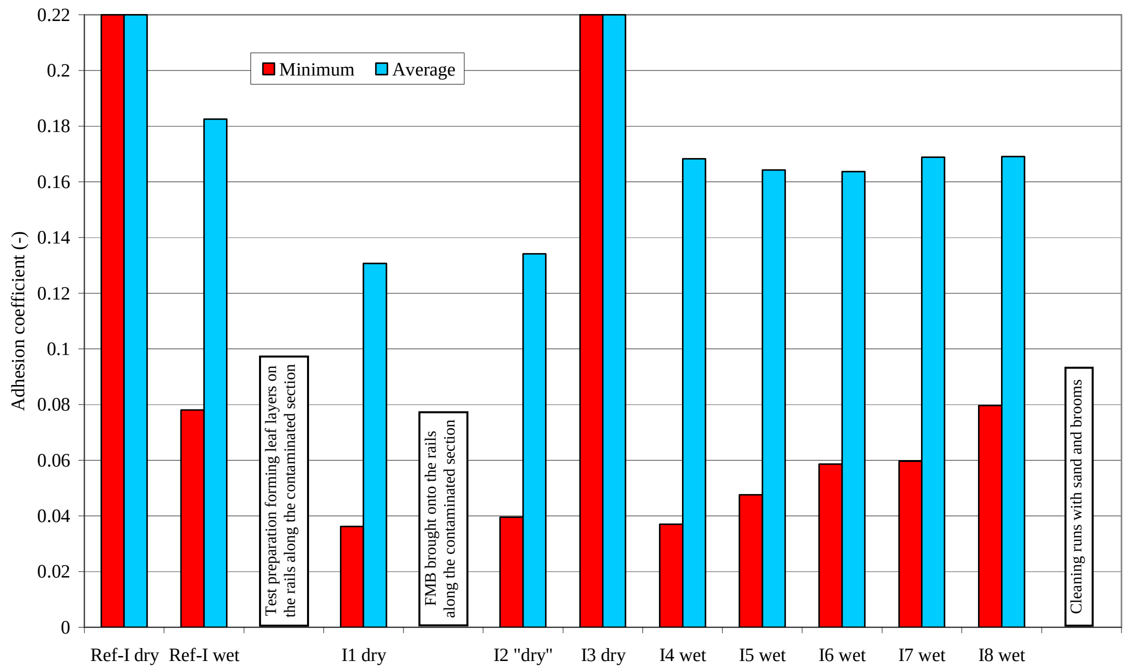

Fig. 4A.24. Minimum and average values of the adhesion coefficient in dry and wet runs of test I.

Figs. 4A.25-4A.26 depict the Tout/Treq ratio along the distance in dry and wet runs of test I. In Fig. 4A.25 it can be seen that similar evolution of the traction along the track was obtained in runs I1 and I2. In run I2, no significant improvement of the traction can be seen along the contaminated section where FMB had been applied. The improvement in adhesion was observed in run I3, in which no traction reduction occurred. In Fig. 4A.26, no trend can be seen of displacing the first traction reduction with the wet runs. This explains the lack of increasing trend of the average adhesion in the wet runs (see Fig. 4A.24). In fact, the first traction reduction occurred the soonest in the last test run, i.e. run I8 in Fig. 4A.26. Comparing the results of wet runs of test I (Fig. 4A.26) with test B (Fig. 4A.10), similar results can be seen in both tests, with the major difference being that the traction reduction was smaller in test I. The trend of adhesion improvement towards the reference run, which was observed in the tests with MTB (e.g. Figs. 4A.15 and 4A.21), was not observed in Fig. 4A.26. This may suggest that more than one application of FMB could have been necessary in test I. Furthermore, in most wet runs the largest traction reduction was experienced by the driven wheels after they exited the contaminated section, e.g. I4, I5 and I8 in Fig. 4A.26. This may be explained by considering that FMB had only been applied along the contaminated section.

An inspection of the rails along the contaminated section before and after test I showed that the top of the rail had been indented at some locations by the solid particles contained in FMB, as displayed in Fig. 4A.27. It can be seen that the indentations had a diameter between 1 mm and 2 mm. Similar indentations were also observed in laboratory tests performed with FMB [4A.14, 4A.15]. Laboratory investigations available in the literature have shown that rail discs with artificial surface indentations do not necessarily have a reduced fatigue life when operating under dry and wet conditions, but they may do so in oil contaminated contacts [4A.24].

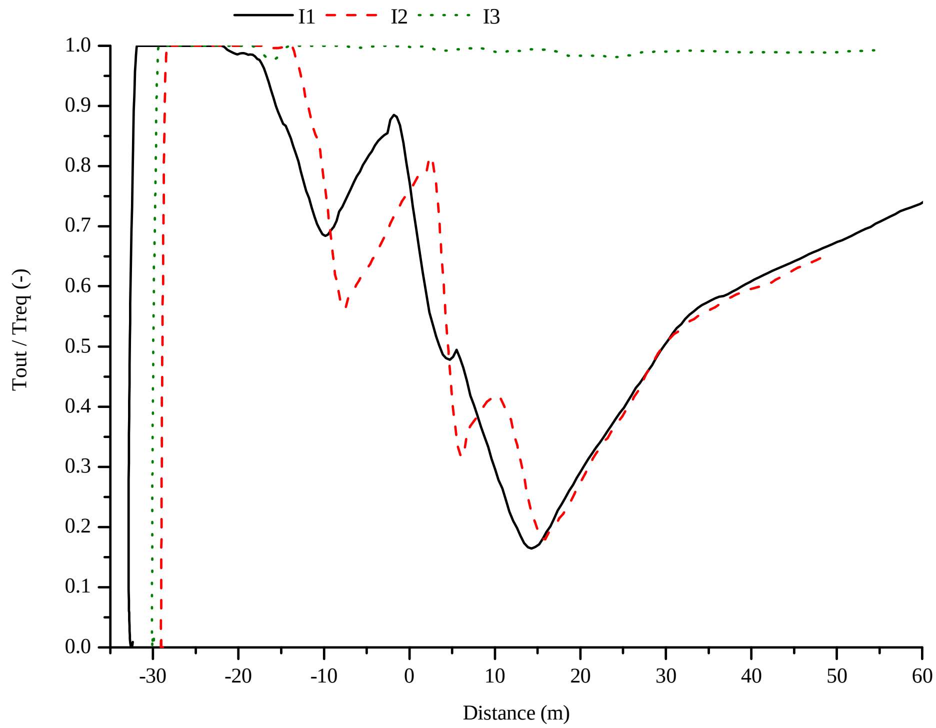

Fig. 4A.25. Ratio between Tout and Treq along the distance travelled by the first driven wheel axle in dry runs of test I (initially contaminated section between 0 m and 25 m).

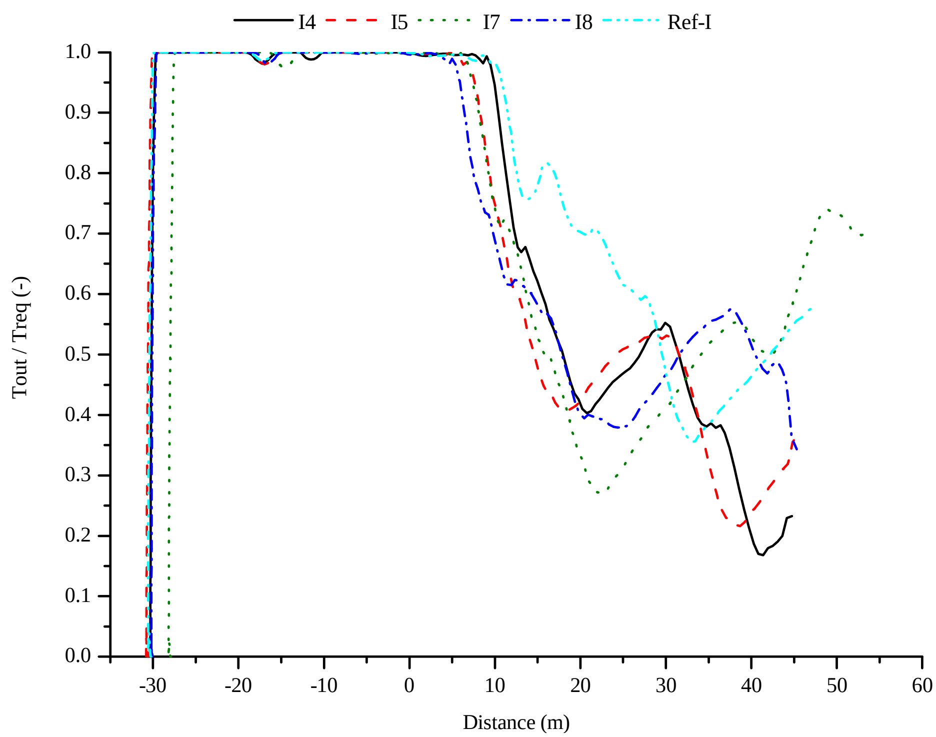

Fig. 4A.26. Ratio between Tout and Treq along the distance travelled by the first driven wheel axle in some wet runs of test I (initially contaminated section between 0 m and 25 m).

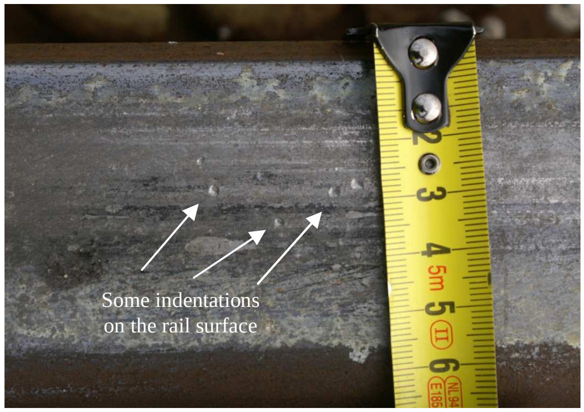

Fig. 4A.27. Photograph of the top of a piece of rail along the contaminated section after test I.

4A.3.2. Test with wet "clean" rails

The test performed with wet "clean" rails has been named L (see Table 4A.1). Four runs were performed, two with MTB and two baseline. In the baseline runs, the minimum and average values of the adhesion coefficient along the contaminated section were 0.10 and 0.15, respectively. The major aim of test L was to examine the adhesion improvement due to water removal by using one MTB ahead of the measuring wheels. The increase in the minimum and average values of the adhesion coefficient was respectively 0.014 ± 0.007 and 0.010 ± 0.008. This indicated that the adhesion conditions for the subsequent wheel passages were only slightly improved by the MTB.

4A.3.3. Test with grease contaminated rails

One test was performed with grease contaminated rails with MTB, which has been named test O (see Table 4A.1). The minimum and average adhesion values of test O are given in Fig. 4A.28. It can be seen that there existed a clear trend of increasing the minimum value of the adhesion coefficient. The lowest minimum adhesion coefficient was experienced in run O1 with a value around 0.01. The average adhesion coefficient also followed a similar continuous trend with the runs, with the only exception of the first two runs. In order to find an explanation, the ratio Tout/Treq along the distance is depicted in Fig. 4A.29. It is seen that in run O1 the traction was firstly reduced at a distance of around 10 m. According to the wheel base of the motorized bogie and the measured rolling radius of the driven wheels, it can be said that the traction was reduced after roughly three revolutions of the first wheels and two revolutions of the second wheels over the contaminated rails. With the increasing number of rotations on the greasy rails, the surfaces of the driven wheels could have become more contaminated leading to the formation of a lubricated contact at the wheel-rail contact. In run O1, after 10 m enough grease appeared to have accumulated on the measuring wheels to decrease the friction below 0.22 and force the TCU to reduce the tractive effort. Low adhesion conditions were maintained until around 20 m, i.e. 5 m after exiting the contaminated section. This suggests that the first non-driven wheels could have brought some grease onto the rails beyond the contaminated section, or that picked-up grease contamination remained on the measuring wheels for a few meters.

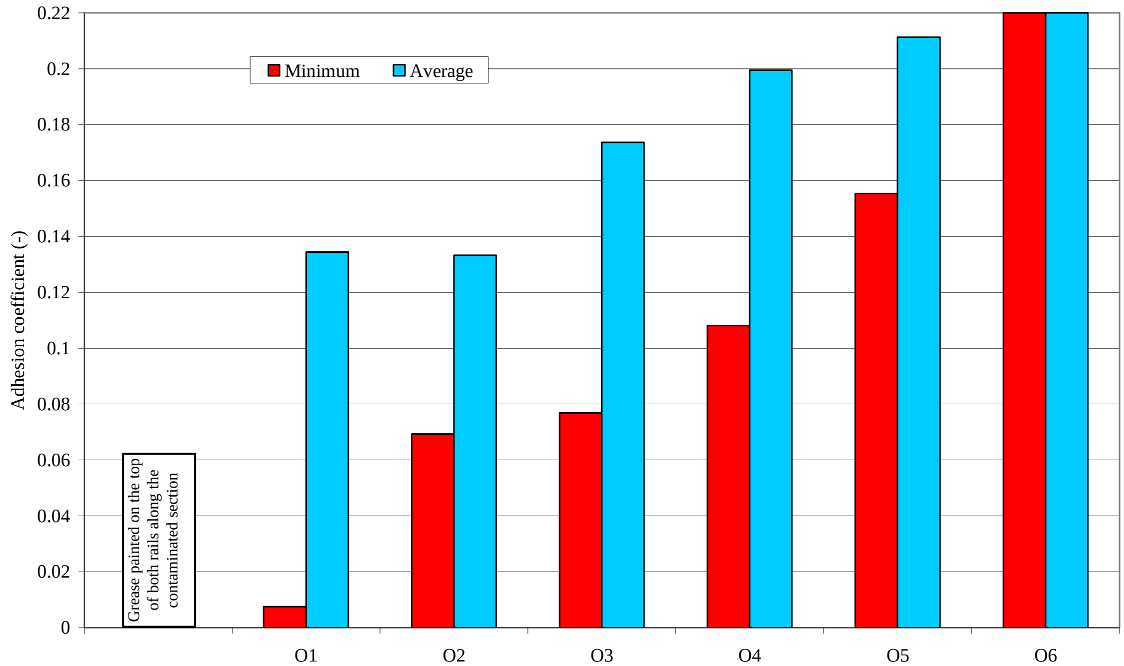

Fig. 4A.28. Minimum and average values of the adhesion coefficient in runs of test O.

In run O2, low adhesion conditions were encountered right after reaching the maximum tractive effort, as shown in Fig. 4A.29. This could have been caused by remaining grease on the driven wheels and some grease being brought outside the contaminated section by the wheels. Up to four traction reductions were experienced in run O2; however, the traction reduction was not as large as in run O1, indicating an increase in the friction level. This could possibly be due to a reduction in the thickness of the grease layer as the amount of grease painted on the rails was spread along a larger distance. Due to the large extent of low adhesion conditions in run O2, the average adhesion coefficient of run O2 was a bit lower than in run O1, in spite of the lower minimum adhesion value measured in run O1.

It can be seen in Fig. 4A.29 that the first occurrence of traction reduction occurred further along the distance with the increasing runs from O2 onwards, which explains the increase of average adhesion displayed in Fig. 4A.28. The amount of traction reduction could also be seen reducing with the runs, which may be due to the depletion of the grease layer at the driven wheel-rail contacts. One interesting observation is that the amount of traction reduction increased with the distance in every run. Since the vehicle speed continuously increased with the distance, it could be said that the friction level may have decreased with the wheel rolling velocity in the grease test runs. The adhesion was entirely recovered after five passages with MTB (see Fig. 4A.28). Unfortunately, the lack of a baseline test with grease contaminated rails hinders the quantification of the relative adhesion improvement that can be attributed to the MTB.

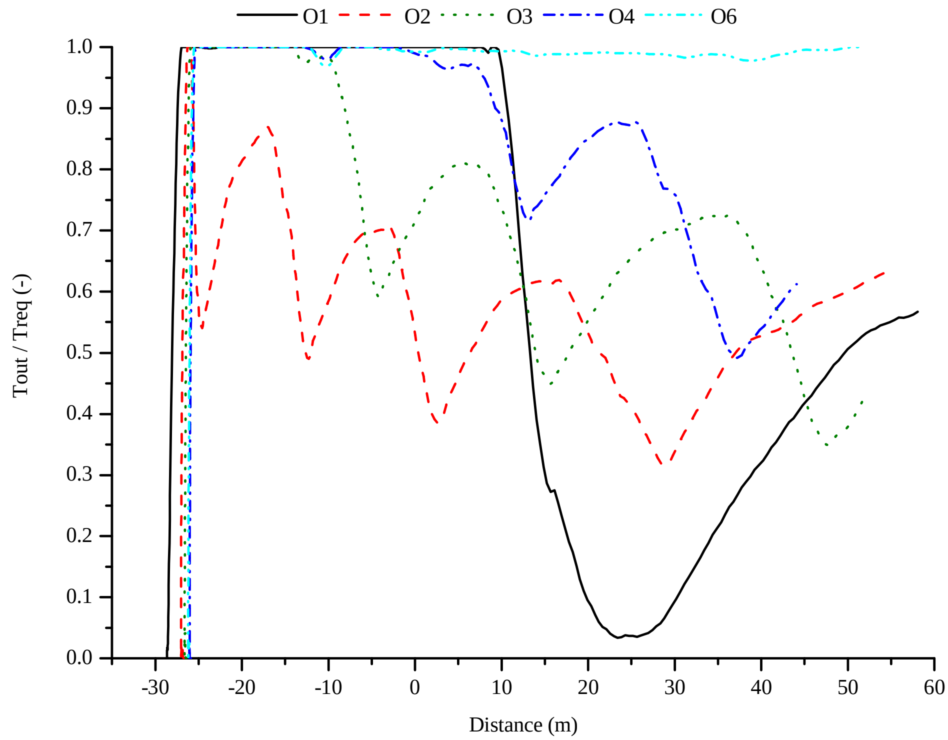

Fig. 4A.29. Ratio between Tout and Treq along the distance travelled by the first driven wheel axle in some wet runs of test O (initially contaminated section between 0 m and 15 m).

4A.4. Discussions

Depending on the level of adhesion at the wheel-rail contact, the safety (braking dependent) and punctuality (mostly traction dependent) of the railway transportation may be affected. In the Netherlands, a maximum adhesion of 0.17 is adopted in traction for calculations when making the timetable of commuter trains. On the other hand, the Dutch Railway Regulations (*Reglement Keuring Spoorwegen*) demand that the braking distance on a descending slope of 5‰ at 140 km/h (maximum allowable line speed) should not exceed 1150 m [4A.25], which yields an average required adhesion of about 0.07 considering that all wheel axles of the train exert the same braking effort. Nevertheless, demands on wheel-rail adhesion can be higher than 0.17 in traction and 0.07 in braking, depending on the driver behaviour and the rolling stock. The maximum adhesion requirements of rolling stock in the Netherlands can reach 0.25 in traction and 0.14 in braking, while in the UK values up to 0.20 and 0.09 are reported in [4A.23]. In this paper, the adhesion coefficient has been measured in wheel-rail contacts contaminated with leaf layers, water and grease, which have been reported in the literature to cause slippery tracks in different railways worldwide. Upon first passage over the contaminated section, minimum adhesion values even below 0.005 have been reached in the presence of leaf layers. Grease contamination has led to a minimum value around 0.01, whereas a minimum value around 0.10 has been measured in wet “clean” contacts. Hence, slippery tracks caused by leaf layers can be considered to be the most problematic for railway transportation, affecting both safety and punctuality. With grease contaminated rails, safety and punctuality can also be affected; however, grease contamination usually appears only on one of the rails as a consequence of migration during flange lubrication on curve. In this situation, low adhesion conditions may come to exist only in traction, braking, or both, depending on the friction available at the contact points on the other rail, as discussed in other investigations [4A.13]. The adhesion values measured in wet “clean” contacts suggest that foggy, dewy or drizzling conditions in the absence of other contaminants may only affect traction operation.

In the presence of wet leaf layers, the minimum values of adhesion were mostly higher in the MTB tests than in the baseline tests. Additionally, the minimum and average values of the adhesion coefficient increased continuously with the increasing MTB passages, while no consistent trend was observed in the baseline tests. These two facts give an indication of the effectiveness of the MTB against this type of low adhesion problems. In the presence of dry leaf layers, the adhesion recovery with MTBs was in some tests faster than in the baseline tests, while in other tests it was similar. The latter has partly been attributed to leaf layers adhered to the driven wheels, while the rails seemed mostly clean to the naked eye. Note that the train employed in the tests to measure the wheel-rail adhesion, had also been used to create the leaf layers on the rails. When using MTBs to fight slippery tracks, it needs to be understood that low adhesion conditions may not only be a consequence of contamination on the rails, but also on the tractive/braking wheels. It can be expected that another train entering the contaminated section with “clean” wheels could have led to better adhesion recoveries than the ones presented in this work. In future implementations, if MTBs are to be employed to clean the top of the rails, it may be beneficial to have a low adhesion detector that can identify the location of the contamination so that MTBs are not activated unnecessarily.

The main objective of this paper has been to quantify the adhesion improvement of each MTB passage along a slippery track under different types of contamination. In practice, more than one MTB of a train consist could be used to improve the adhesion conditions for subsequent train passages. In future implementations, train operating companies may decide upon the number of MTBs depending on the desired adhesion recovery for subsequent train passages. The adhesion results obtained in this work have shown that after two MTB passages the minimum adhesion coefficient was above 0.07 in most contamination conditions tested except with leaf layers under wet conditions. Hence, it could be said that using two MTBs along a contaminated track may normally improve the adhesion conditions so that the braking safety for the subsequent train is not compromised. In the presence of wet leaf layers, more than three MTBs have been found to be necessary.

In the leaf test with FMB, a more rapid recovery of adhesion could be seen during runs under dry conditions than in any test with MTB. This could have been expected to some extent because the application of FMB to the contaminated section could have conditioned the surfaces of both wheels and rails, while MTB could only condition the rails. However, the values and trends observed in the wet runs indicate that one application of FMB had been insufficient. Considering the broad use of FMB in the Dutch and the British railways, future investigations towards the required frequency of FMB application are justified.

The method employed in this work to measure the wheel-rail adhesion requires care when the measured values of the adhesion coefficient are extrapolated to a similar train with a different TCU. The algorithm of the TCU determines the threshold at which the motor torque is reduced under low adhesion conditions, and it establishes the amount and duration of the traction reduction as well as the subsequent increase once the acceleration falls below the threshold. Hence, different minimum and average values of the adhesion coefficient could be obtained when using a different TCU. Nevertheless, this does not affect the comparison of results in this paper between different contact conditions and countermeasures employed in the tests.

The tests presented in this work have been performed at a maximum train speed of 40 km/h due to the fact that the maximum motor torque is available in the speed range 0-40 km/h, but also due to the speed limitation of the stabling yard. The maximum speed of passenger rolling stock is 140 km/h on conventional track in the Netherlands. It can be expected that some of the adhesion results presented in this paper may be somewhat different in the range 40-140 km/h. In grease lubricated wheel-rail contacts, an increase in the wheel rolling velocity can lead to a decrease in the adhesion coefficient [4A.13]. The increase of wheel rolling velocity has also been reported to decrease the adhesion in wet clean wheel-rail contacts [4A.26]. In leaf contaminated contacts only investigations at very low rolling velocities are found in the literature [4A.18]. Furthermore, the increase in train speed can lead to a decrease in the MTB force on the one hand, but an increase in the dissipated frictional power on the other, as reported in [4A.5]. Hence, thermal removal of the leaf layers could perhaps be promoted at higher train speeds, but this still needs to be investigated. The effectiveness of FMB could also be affected as particle entrapment in the wheel-rail contact may be influenced by the wheel surface velocity. Therefore, it is advisable to perform additional tests in a speed range higher than the one treated in this work.

4A.5. Conclusions

Part A of the field investigations on the performance of MTB against slippery tracks has focused on the adhesion recovery using a MTB under low adhesion conditions. The field tests have been performed in traction operation with or without the MTB depending on the goal of the tests. Low adhesion conditions have been created by three types of contamination representative of slippery tracks, i.e. leaves, water, and grease. In the tests with leaves and water, baseline tests (i.e. no use of MTB) have also been performed. Additionally, an adhesion improver widely used in the Dutch and the British railways has also been employed in a test with leaves to allow for a comparison in effectiveness with MTB under similar operating conditions. The wheel-rail adhesion conditions of the wheels in a motorized bogie have been determined by means of the TCU. The adhesion improvement has been obtained by comparing the wheel-rail adhesion values measured in increasing passages. The position of the measuring bogie has been monitored and synchronized with the TCU data to determine the location of the measurements. Based on the adhesion results obtained in this work, the following conclusions can be drawn:

a) Leaf contaminated rails cause the largest reduction in the wheel-rail adhesion, closely followed by grease. Not only traction, but also braking may be affected in the presence of leaves or grease on the rails. Moisture in “clean” wheel-rail contacts may mostly affect traction.

b) Contamination may be dragged forward by passing wheels leading to low adhesion conditions far from the original slippery track, with grease being the most mobile of the contaminants investigated. This should be borne in mind by railway network managers when placing trackside lubricators.
c) With leaves, water and grease contaminated rails a continuous adhesion improvement is obtained with the MTB passages. The rate of the adhesion recovery depends upon the type of contamination, but in leaf tests it can also affected by the possibility of having leaf layers adhered to the driven wheels.
d) Using two MTBs may bring the adhesion level above 0.07 under most of the contamination conditions tested, guaranteeing effective braking along an initially contaminated track for the subsequent trains. The only exception was found in the presence of wet leaf layers, for which more than three MTBs can be necessary.
e) One application of FMB to the leaf contaminated rails has shown faster adhesion recoveries under dry conditions than using MTB. However, more applications of FMB are necessary to have an effective adhesion recovery on wet leaf contaminated rails.

References

[4A.1] G. Gfatter, S. Haas, G. Vohla: Track Brakes. Knorr-Bremse Handbook (2004).
[4A.2] D. Shipley: Outline Feasibility of Fitting Magnetic Track Brakes to UK Rolling Stock. Report produced by Interfleet Technology Ltd. (2006).
[4A.3] W. Voges, P. Spiess: Optimising Services with EMU ET42x in Autumn 2004 and 2005. Proceedings of 7th World Congress on Railway Research, Canada (2006).
[4A.4] N. van Steenis: Voorstudie Magneetrem op Gladde Sporen. Report produced by NedTrain Consulting (2003) in Dutch.
[4A.5] O. Arias-Cuevas, Z. Li: Field Investigations on the Performance of Magnetic Track Brakes of an Electrical Multiple Unit against Slippery Tracks. Part II: Braking Force and Side Effects. Companion paper submitted for publication (2010).
[4A.6] L. Vermeulen: Beproeving van Elektromagnetische remmen en Microprocessorgestuurde Anti-blokkeerinstallatie van DH 3219 en DH 3113. Report produced by the Centre for Technical Research (CTO) of the Dutch Railways (1988) in Dutch.
[4A.7] Boiteux, Cadier, J. Kling, W. Kunnes: Summary of Theoretical and Practical Knowledge of Poor Adhesion Conditions Acquired since Publication of B 164/RP 2. Ed. ORE (1992).
[4A.8] J. Eleveld: Gladde Sporen, Oplossingsrichtingen voor Adhesieproblemen. Report published by the Dutch Railways Technical Research (NSTO) in Dutch (March 1999).
[4A.9] Managing Low Adhesion. Report published by the Adhesion Working Group, UK (September 2001).
[4A.10] C.W. Jenks: Improved Methods for Increasing Wheel/Rail Adhesion in the Presence of Natural Contaminants. Transit Cooperative Research Program Sponsored by the Federal Transit Administration, Transportation Research Board National Research Council (May 1997).
[4A.11] U. Olofsson, K. Sundvall: Influence of Leaf, Humidity and Applied Lubrication on Friction in the Wheel-Rail Contact: Pin-on-Disc Experiments. Journal of Rail and Rapid Transit 218 (2004) 235-242.

[4A.12] N. Tanabe, Y. Hirota, T. Omichi, J. Hirama, K. Nagase: Study on the Factors Which Cause the Wheel Skidding of JR Ltd. Express EMUs. JSME International Journal 47 (2004) 488-495.
[4A.13] O. Arias-Cuevas, Z. Li, R.I. Popovici, D.J. Schipper: Simulation of Curving Behavior under High Traction in Lubricated Wheel-Rail Contacts. Under review, Journal of Vehicle System Dynamics (2010).
[4A.14] Z. Li, O. Arias-Cuevas, R. Lewis, E.A. Gallardo-Hernandez: Rolling-sliding Laboratory Tests of Friction Modifiers in Leaf Contaminated Wheel-Rail Contacts. Tribology Letters 33 (2009) 97–109.
[4A.15] O. Arias-Cuevas, Z. Li, R. Lewis, E.A. Gallardo-Hernandez: Rolling-Sliding Laboratory Tests of Friction Modifiers in Dry and Wet Wheel-Rail Contacts. Wear 268 (2010) 543–551.
[4A.16] D. Uittenbogaart: Studie VIRM als tribotrein. Report published (in Dutch) by Strukton Systems, the Netherlands (December 2006).
[4A.17] OmniSTAR 8200HP User Manual, Issue 1.05 (April 2007).
[4A.18] P.M. Cann: The ‘‘leaves on the line’’ problem—a study of leaf residue film formation and lubricity under laboratory test conditions. Tribology Letters 24 (2006) 151-158.
[4A.19] O. Arias-Cuevas, Z. Li, R. Lewis, E.A. Gallardo-Hernandez: Laboratory Investigation of some Sanding Parameters to Improve the Adhesion in Leaf Contaminated Wheel-Rail Contacts. In press, Journal of Rail and Rapid Transit (2010).
[4A.20] O. Arias-Cuevas, Z. Li, R. Lewis: A Laboratory Investigation on the Influence of the Particle Size and Slip During Sanding on the Adhesion and Wear in the Wheel-Rail Contact. In proceedings of the 8th International Conference on Contact Mechanics and Wear of Rail/Wheel Systems, Firenze, Italy, September 15-18 (2009).
[4A.21] E.A. Gallardo-Hernandez, R. Lewis: Twin disc assessment of wheel/rail adhesion. Wear 265 (2008) 1309–1316.
[4A.22] O. Arias-Cuevas, Z. Li: Field Investigations on the Adhesion Recovery in Leaf Contaminated Wheel-Rail Contacts with Locomotive Sanders. Submitted for publication in an international journal (2010).
[4A.23] C.R. Fulford: Review of low adhesion research. Report published by the Rail Safety and Standards Board, UK (2004).
[4A.24] N. Gao, R.S. Dwyer-Joyce and D.G. Grieve: Disc Machine Testing to Assess the Life of Surface Damaged Railway Track. Journal of Rail and Rapid Transit 215 (2001) 261-275.
[4A.25] Regeling Spoorverkeer, Article 8, Chapter 3: Maximumsnelheid Treinen. Available online in Dutch at http://wetten.overheid.nl/BWBR0017707 (accessed on February 3rd, 2010).
[4A.26] H. Chen, T. Ban, M. Ishida, T. Nakahara: Experimental investigation of influential factors on adhesion between wheel and rail under wet conditions. Wear 265 (2008) 1504-1511.

Chapter 4, Part B

Field tests on braking force and side effects[XII]

ABSTRACT

Part B of the field investigations focuses on the braking force and some possible side effects of the frequent use of magnetic track brakes against slippery tracks. Field tests have been performed with the permanent magnetic track brake of an electrical multiple unit in a stabling yard. Three types of contamination representative of slippery tracks have been employed, e.g. water, leaves and grease. Tests with dry “clean” rails have also been performed throughout the testing to obtain a reference of the braking force in the speed range 0-40 km/h. Furthermore, the braking performance of the electrical multiple unit in different braking modes is analyzed under the tested conditions. The surfaces of the brake shoes and the rails have been examined to analyze possible changes during the testing. The profile of rails and the mass loss of the brake shoes have also measured in the tests to quantify the wear caused in the tests. Moreover, the effect of a passing magnetic track brake on the electrical insulation of an insulated rail joint has been examined by means of electrical measurements and visual inspection.

[XII] This chapter has been submitted in 2009 for publication to Proc. IMechE, Part F: J. Rail and Rapid Transit as: O. Arias-Cuevas, Z. Li: Field Investigations on the Performance of Magnetic Track Brakes of an Electrical Multiple Unit against Slippery Tracks. Part II: Braking Force and Side Effects.

4B.1. Introduction

The complete work, which has been divided in two parts, presents field investigations in a stabling yard on the performance of magnetic track brakes (MTBs) against slippery tracks. In Part A, the investigations on the adhesion recovery in contaminated contacts were presented [4B.1]. Part B focuses on the braking force of the MTB in clean and contaminated contacts and some possible side effects of its frequent use against slippery tracks.

The low adhesion conditions at the wheel-rail contact associated with slippery tracks may affect the braking operation of railway vehicles, leading to a safety threat in the worst case. During an emergency braking, MTBs may be activated, if present in the rolling stock, in an attempt to increase the braking performance. Aiming at a possible countermeasure to fight slippery tracks, a conceptual approach of MTB use against slippery tracks has been proposed by the authors to the Dutch railways, in which one (or more) MTB of a train consist is activated upon detection of low adhesion conditions at a given location along the track, and it is deactivated once the low adhesion conditions have disappeared. In this way, the braking performance of the train along the slippery track section could be enhanced, and the adhesion conditions along that section could also be improved for subsequent trains due to the cleaning effect of MTB [4B.1]. However, there exists a lack of data on the braking force that a MTB can exert on clean and contaminated rails. The field tests in this paper have aimed at quantifying the effect of train speed and contamination conditions on the MTB force. Water, leaves and grease, which have been reported to be representative contaminants of slippery tracks in the Netherlands and overseas [4B.2-4B.7], have been applied onto the rails to measure the MTB force under different types of low adhesion conditions. In addition, tests have also been performed throughout the testing in dry “clean” contacts to establish a reference of the braking force in the absence of contamination and to study the influence of the train speed on the force.

On the other hand, a frequent use of MTBs on a railway network in typical periods of slippery tracks, e.g. autumn, could bring along some undesired side effects. Discussions with the major train operating company in the Netherlands (NS) and the railway infrastructure manager (ProRail) identified some concerns of high priority such as the effect on the rails, the maintenance of the MTB brake shoes, and the compatibility with insulated rail joints (IRJs) and switches. In the tests presented in this paper, these concerns have been investigated to some extent. The rail profile has been measured before and after the tests in some sections to evaluate whether significant rail wear had occurred. The roughness and hardness of the top of the rail has also been measured before and after the tests.

It can be expected that a more frequent use of the MTB may lead to a need for more frequent maintenance, particularly for the brake shoes. Depending on the frequency operational costs, or even the availability of the fleet, may be compromised. Hence, it is essential to determine the wear rates of the brake shoes and the effect of varying surface conditions on the MTB force. The mass loss of the brake shoes has been measured after the tests. Then, a wear rate has been calculated as a function of the total frictional power dissipation and another as a function of the total distance travelled. Additionally, the surface of the brake shoes has been examined after the tests, measuring changes in hardness and roughness.

IRJs are mostly used on tracks in which train detection is based on track circuits, requiring that the IRJ electrically insulates the adjoining rails. The magnetic field created by the MTB may attract some ferrite debris onto the pole shoes. The debris can be wear particles from rails and pole shoes, and perhaps remains produced during rail grinding. When pole shoes slide over an IRJ, debris may fall and deposit causing an electrical bridge between the two adjoining rails. Depending on the size and amount of deposited debris the insulating function of the IRJ may be deteriorated, causing extra maintenance work so that costs are increased and track availability is compromised. In this work, the possible influence of MTB on the electrical insulation of an IRJ has been examined by means of electrical measurements and visual inspection. Another possible side effect of MTB is that brake shoes may damage some of the parts of a switch. This has also been investigated in field tests and the results can be found in the literature [4B.8].

4B.2. Testing description

4B.2.1. Electrical multiple unit

The tests were performed with a double-decker electrical multiple unit (EMU) of NS in a stabling yard. The EMU consists of four vehicles with eight bogies and sixteen wheel axles in total, as schematically shown in Fig. 4B.1. Two of the eight bogies are motorized, and four trailing bogies have a high-suspension permanent MTB, as indicated in Fig. 4B.1. In the tests, only one MTB was employed (see Fig. 4B.1). The length of the MTB and its location with respect to other relevant elements of the EMU are also given in Fig. 4B.1.

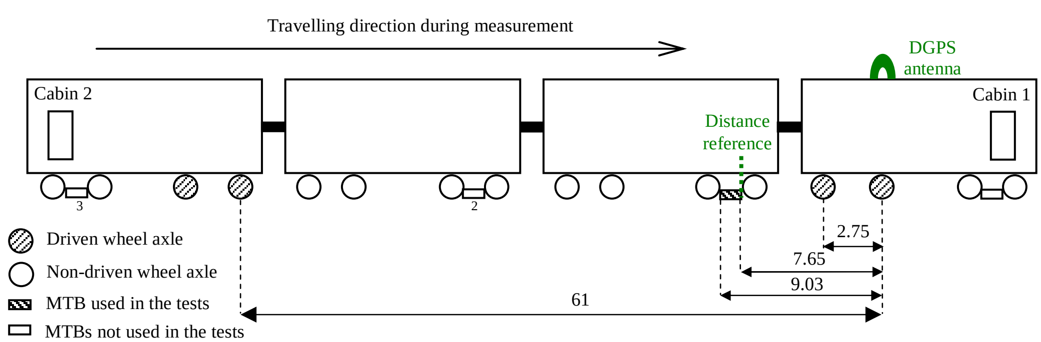

Fig. 4B.1. Schematic representation of the EMU employed in the tests (dimensions in meters).

4B.2.2. Magnetic track brake

A detailed description of the principal components of the MTB and the working principle during activation and deactivation can be found in Part A [4B.1]. An MTB counts with two brake magnets, one for each rail. The brake shoes of each brake magnet consist of four pole shoes on the right, four on the left, and four insulating strips in between. Fig. 4B.2 gives a cross section of the brake magnet in active and rest positions, in which magnetic parts have been filled with (blue) lines and non-magnetic parts with (red) dots.

In this MTB, the pole shoes are made of nodular cast iron GGG-40 (DIN 1693) and the insulating strips are made of austenitic cast iron GGG-NiCr 20 2 (DIN1694) [4B.9]. The pole shoes are responsible for the magnetic attraction to the rails, and thus the normal contact force. The initial curvature of the pole shoes, which is shown in Fig. 4B.2, aims at having a conformal contact with the top of the rail to maximize the attractive force. According to the manufacturer, the nominal attractive force for this MTB is around 70 kN per brake magnet. As the insulating strips are mechanically constrained to the pole shoes, they are also pressed against the rail surface. The sliding motion of the brake shoes over the rail generates the MTB force.

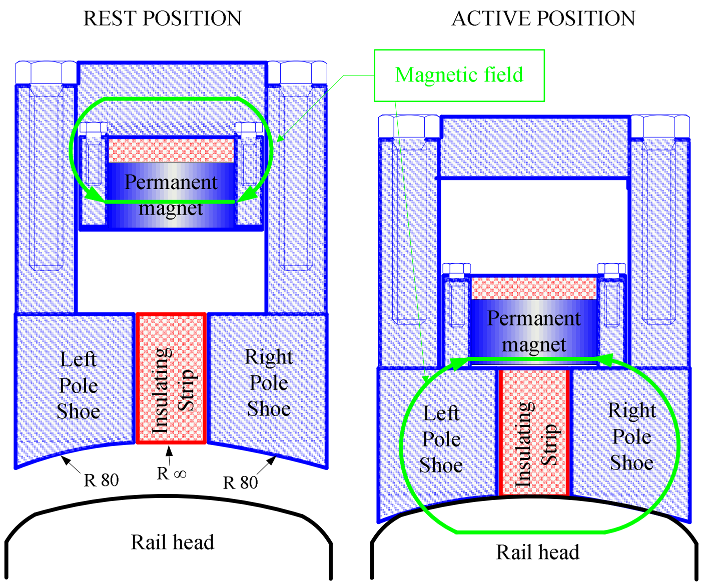

Fig. 4B.2. Simplified drawing of a cross-section of a brake magnet of the MTB in rest and active positions.

4B.2.3. Testing preparation and procedure

Table 4B.1 displays a list of the tests performed that were relevant to the MTB force measurements. Note that some field tests (i.e. tests B, F, I, and L) were only relevant to adhesion recovery measurements and they can be found in [4B.1]. Each field test has been named in alphabetic order according to the time of execution. This was especially important due to the surfaces changes of brake shoes and rails in the course of the tests, as will be explained in Section 4B.3. It can be seen in the table that each test consisted of a series of runs. In the tests with dry and wet “clean” rails the runs were simply a repetition of the measurement; whereas in the tests with leaf and grease contaminated rails the runs were used to investigate the evolution of the MTB force as contamination was progressively being removed with the runs.

Table 4B.1. List of the tests performed relevant to MTB force measurements.

<table>
<tr><th colspan="14">Test A = Dry “clean” test on test section 1</th></tr>
<tr><td>RUN</td><td colspan="6">A1</td><td colspan="7">A2</td></tr>
<tr><th colspan="14">Test C = Leaf test on test section 1</th></tr>
<tr><td>RUN</td><td>C1</td><td>C2</td><td>C3</td><td>C4</td><td>C5</td><td>C6</td><td>C7</td><td>C8</td><td>C9</td><td>C10</td><td colspan="3">C11</td></tr>
<tr><td>CONDITIONS</td><td>dry</td><td>dry</td><td>dry</td><td>dry</td><td>wet</td><td>wet</td><td>wet</td><td>wet</td><td>wet</td><td>wet</td><td colspan="3">wet</td></tr>
<tr><th colspan="14">Test D = Dry “clean” test on test section 1</th></tr>
<tr><td>RUN</td><td colspan="6">D1</td><td colspan="7">D2</td></tr>
<tr><th colspan="14">Test E = Wet “clean” test on test section 1</th></tr>
<tr><td>RUN</td><td colspan="6">E1</td><td colspan="7">E2</td></tr>
<tr><th colspan="14">Test G = Leaf test on test section 1</th></tr>
<tr><td>RUN</td><td>G1</td><td>G2</td><td>G3</td><td>G4</td><td>G5</td><td>G6</td><td>G7</td><td>G8</td><td>G9</td><td>G10</td><td>G11</td><td>G12</td><td>G13</td></tr>
<tr><td>CONDITIONS</td><td>dry</td><td>dry</td><td>dry</td><td>dry</td><td>dry</td><td>dry</td><td>dry</td><td>dry</td><td>wet</td><td>dry</td><td>wet</td><td>wet</td><td>wet</td></tr>
<tr><th colspan="14">Test H = Leaf test on test section 1</th></tr>
<tr><td>RUN</td><td>H1</td><td>H2</td><td>H3</td><td>H4</td><td>H5</td><td>H6</td><td>H7</td><td>H8</td><td>H9</td><td colspan="4">H10</td></tr>
<tr><td>CONDITIONS</td><td>dry</td><td>dry</td><td>dry</td><td>dry</td><td>dry</td><td>wet</td><td>dry</td><td>wet</td><td>dry</td><td colspan="4">wet</td></tr>
<tr><th colspan="14">Test J = Dry “clean” test on test section 1</th></tr>
<tr><td>RUN</td><td colspan="6">J1</td><td colspan="7">J2</td></tr>
<tr><th colspan="14">Test K = Wet “clean” test on test section 1</th></tr>
<tr><td>RUN</td><td colspan="6">K1</td><td colspan="7">K2</td></tr>
<tr><th colspan="14">Test M = Dry “clean” test on test section 3</th></tr>
<tr><td>RUN</td><td colspan="6">M1</td><td colspan="7">M2</td></tr>
<tr><th colspan="14">Test N = Leaf test on test section 3</th></tr>
<tr><td>RUN</td><td>N1</td><td>N2</td><td>N3</td><td>N4</td><td>N5</td><td>N6</td><td colspan="7">N7</td></tr>
<tr><td>CONDITIONS</td><td>dry</td><td>dry</td><td>dry</td><td>wet</td><td>wet</td><td>wet</td><td colspan="7">wet</td></tr>
<tr><th colspan="14">Test O = Grease test on test section 4</th></tr>
<tr><td>RUN</td><td>O1</td><td>O2</td><td>O3</td><td>O4</td><td>O5</td><td colspan="8">O6</td></tr>
</table>

In every test, each run was performed in traction operation with the MTB being actived (i.e. brake shoes in contact with the rails) from the start until the EMU had come to standstill. In the tests with leaves and grease, the contaminants were initially applied to the top of the rails along a track section, which is referred in this work to as the contaminated section. The length of the contaminated section was 25 m for the leaf tests and 15 m for the grease tests. In order to avoid undesired mix-up of contaminants in a test, the total available length of the stabling yard was divided in four test sections, employing a different test section for each type of contamination, as indicated in Table 4B.1. Note that test section 2 was only used in an adhesion recovery test presented in [4B.1]. The length of a test section included a contaminated section and a distance required for the EMU to accelerate and to brake safely.

4B.2.3.1. Tests with dry and wet “clean” rails

In these tests the MTB force was measured in the range 0-40 km/h. Two runs were performed in each test (see Table 4B.1). In the tests with wet “clean” rails, water was sprayed on the top of the rails prior to the start of a run. Note that the quotation marks as in “clean” are employed in this paper to distinguish the clean conditions in field from the more purely clean conditions typically present in laboratory testing.

4B.2.3.2. Tests with leaf contaminated rails

In the test preparation, the leaves, which originated from different types of trees, were placed one by one on the top of the two rails of the contaminated section. Small amounts of water were initially sprayed to help adhering the leaves onto the rail surfaces before the first EMU passage. The EMU passed four times over the leaf contaminated section with no traction/braking efforts and at low speed so that most of the leaves were compacted onto the rails. The resulting leaf layers were mostly dry prior to the start of the testing as no water had been applied after the first EMU passage.

After test preparation, test runs were firstly performed under dry conditions. Once the adhesion was entirely recovered under dry conditions as measured in [4B.1], test runs under wet conditions were performed. Prior to the start of a test run under wet conditions, water was sprayed on the rails along the contaminated section to simulate typical conditions of dewy, foggy or drizzling autumn days. In all test runs with leaf contaminated rails, care was taken to start approximately from the same position every time. In this way, the difference in train speed along the contaminated section between runs was minimized. In the leaf contaminated tests, the MTB entered the contaminated section with a speed of 22 ± 2 km/h and exited it with 27 ± 5 km/h.

Once a leaf test was finished, some cleaning runs were performed in an attempt to remove remaining leaf contamination from the rails so that the same test section could be employed for the next test in comparable conditions. The same cleaning procedure was followed after each leaf test. Firstly, sand was laid along most of the test section, and the EMU travelled four times with full traction/braking. Afterwards, brooms were employed to wipe remaining sand off the top of the rails. Then, the EMU travelled again four times along the test section with full traction/braking. It is important to emphasize that the MTB was not activated in any of the cleaning runs.

4B.2.3.3. Test with grease contaminated rails

The grease used in the tests is a lubricant, which is currently applied to the flange contact along some curved sections of the Dutch railway network by means of trackside installations to reduce wear, noise and risk of derailment [4A.13]. Before the start of the test, the grease was painted on the top of the two rails along the contaminated section. Similarly to the leaf tests, care was taken to start approximately from the same position to reduce the influence of the speed between runs. In the runs, the MTB entered the contaminated section at 22 ± 2 km/h and exited it at around 25 ± 4 km/h. Six runs were performed in the grease test, which has been named test O, as indicated in Table 4B.1.

4B.2.4. Measuring methodology

The MTB force was measured by means of a load cell (type LLW350, FUTEK Advanced Sensor Technology Inc.). According to the calibration data and the measurement range, the inaccuracy of the load cell was below 6% in the tests. The load cell was situated in the transmission pad, which is located between the bogie and the MTB to transmit the braking force of the MTB. Fig. 4B.3 gives a photograph of the brake magnet where the load cell was installed. In the tests one load cell was employed, but it could be assumed that the braking force was similar in both brake magnets because the tests were performed on straight track and the contamination, if any, had been applied equally to both rails. Hence, the total MTB force may be estimated to be twice of the values to be presented in this work. The sampling frequency of the load cell was 100 Hz, and the force signal was smoothened using the Savitzky-Golay filter [4B.11], which is implemented in MATLAB.

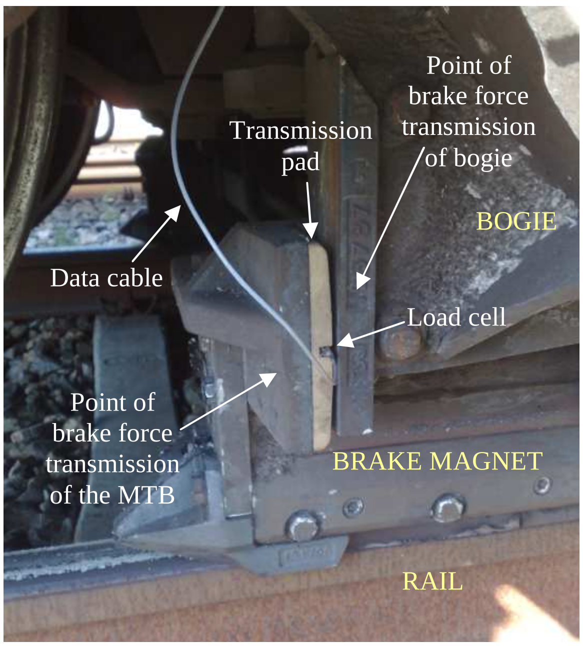

Fig. 4B.3. Photograph of the brake magnet in which the load cell was installed.

An example of the MTB force measurement in a test run is given in Fig. 4B.4. As the tractive effort built up at the start of a test run, the MTB force increased. In this first phase, the MTB force due to static friction was still larger than the tractive effort so that the EMU did not move (i.e. speed = 0). Once the tractive effort overcame the static friction force, the EMU started moving with a combination of traction effort and MTB (braking) force. With the increase of train speed the MTB force normally decreased, as will be outlined in Section 4B.3.1. In the next phase the traction was stopped, while the MTB was still braking the train, which caused a slow decrease of the speed and, correspondingly, a gradual increase in the MTB force. Afterwards, the wheels started to brake together with the MTB, causing a faster decrease of the train speed. The decreasing speed led to a further increase in the MTB force. As indicated in Fig. 4B.4, only MTB force results during traction are presented in Section 4B.3.1 to facilitate a comparison with the wheel-rail adhesion results presented in [4B.1]. Nevertheless, the other MTB force results have also been processed to obtain an indication of the total frictional energy dissipated in the testing for wear rate calculations, as will be presented in Section 4B.3.3.

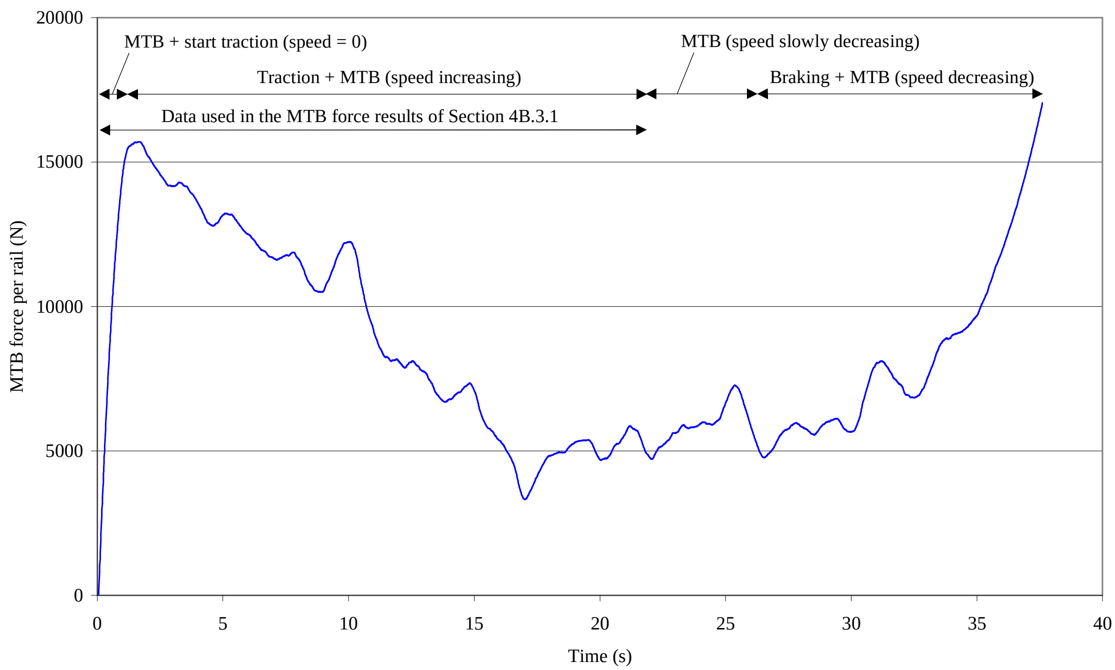

Fig. 4B.4. Example of the MTB force per rail in a test run.

The location of the MTB on the track was obtained with a differential global positioning system (DGPS) 8200HP (OmniSTAR B.V.). The DGPS antenna was mounted on the roof, as indicated in Fig. 4B.1. OmniSTAR VBS GPS correction signals were used on the 8200HP to operate with sub-meter accuracy for the number of satellites available during the testing [4B.12]. The sampling frequency of the DGPS was 10 Hz in the tests. During post-processing the location values were synchronized with the MTB force data obtained from the load cell. In the results presented in this paper, the distance is referred to the location of the initial tip of the brake shoes in the travelling direction, as indicated in Fig. 4B.1. Furthermore, the sliding speed of the MTB, equivalent to the train speed, was measured by means of a radar that was attached to the carbody of one of the vehicles.

4B.3. Results

4B.3.1. Magnetic track brake force

4B.3.1.1. Dry and wet "clean" rails

Four tests with dry "clean" rails (e.g. tests A, D, J, and M) and two tests with wet "clean" rails (e.g. tests E and K) were performed, as indicated in Table 4B.1. Fig. 4B.5 depicts the mean value and deviation of the average MTB force in the ranges 0-40 km/h and 22-27 km/h. Note that the latter speed range is only used to compare results with tests with leaf contaminated rails in Section 4B.3.1.2. It can be seen in Fig. 4B.5 that the average MTB force in the tests under dry "clean" conditions performed on section 1 followed a decreasing trend, i.e. $F_A > F_D > F_J$. This trend could have been the result of two phenomena. On one hand, contamination may have been accumulated on the surface of rails despite the cleaning procedure. In this regard, the increase of MTB force in test M compared to test J could have been due to the cleaner conditions of rail surfaces in test section 3. However, MTB force in test M was greatly lower than in test A, suggesting that another phenomenon was clearly dominant in the decrease of the MTB force under dry "clean" conditions. This phenomenon could have been related to the surface conditions of the brake shoes, which changed in the course of the testing. For example, variations in the contact area and accumulation of contamination in the surfaces of brake shoes may have affected the MTB force. The examination of the brake shoes after testing will be presented in Section 4B.3.3.

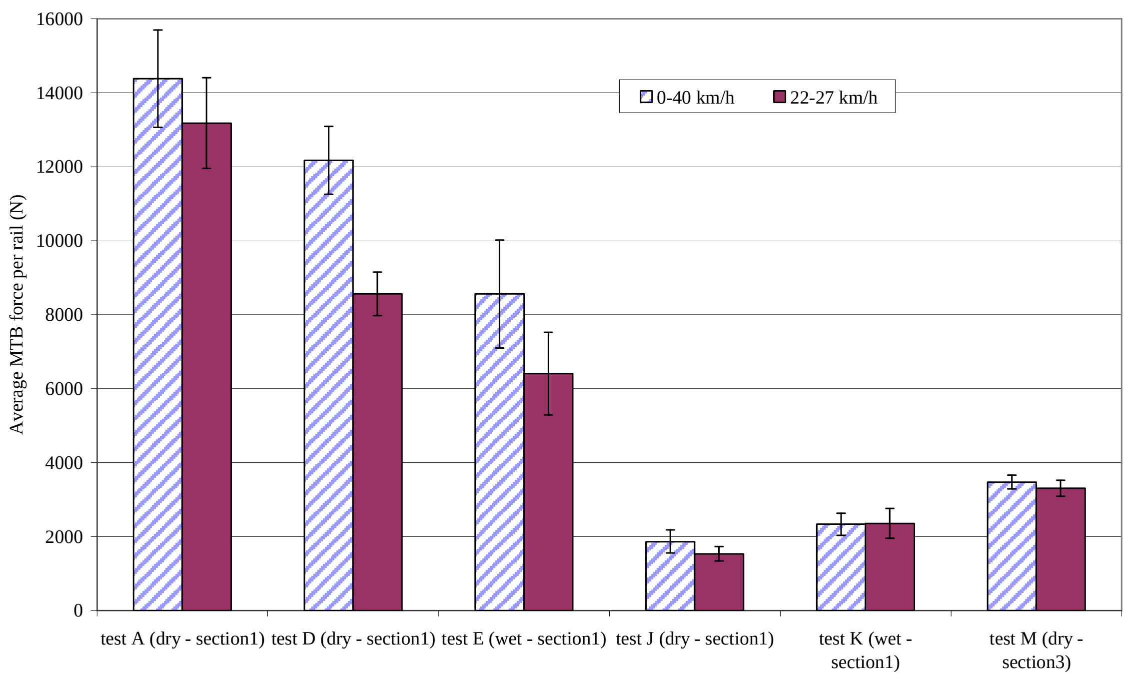

Fig. 4B.5. Mean value and deviation of the average MTB force per rail in the speed ranges 0-40 km/h and 22-27 km/h measured in tests with dry and wet "clean" rails.

In Fig. 4B.6 the variation of the MTB force with the train speed is shown for the first runs of the tests with dry “clean” rails. In general a trend of a decreasing MTB force with the speed can be seen in all runs. The decrease of the friction force with the increasing sliding speed in metal-metal contacts has been attributed by some authors to the high temperatures in the contact, which may lead to the formation of oxides that can act as solid lubricants [4B.13]. Other authors have attributed the decrease to the softening of the cast iron under high temperatures [4B.14]. In Fig. 4B.6, the slope is seen to change its magnitude in the different tests, indicating that the force-speed characteristic curve of an MTB can also be highly affected by the surface contact conditions of the brake shoes.

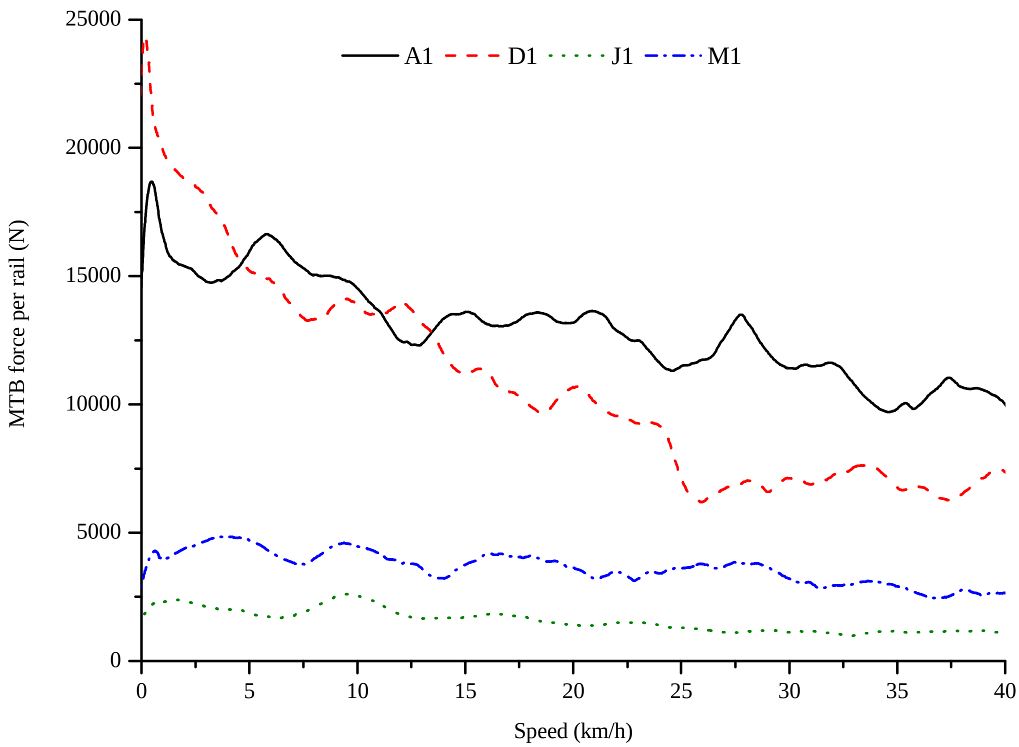

Fig. 4B.6. MTB force per rail as function of the train speed in first run of tests with dry “clean” rails.

Comparing test E with test D in Fig. 4B.5, it is seen that the MTB force was reduced 30% on average in the presence of moisture in “clean” contacts. In contrast, the MTB force in test K was higher than in test J (see Fig. 4B.5). In order to find an explanation for the latter result, the MTB force variation with the increasing train speed is given in Fig. 4B.7 for all runs of tests J and K. A trend towards higher values of the MTB force with the increasing runs can be seen, which is particularly clear in the speed range 10-40 km/h. This trend was independent of the dry or wet conditions of the test run, i.e. $F_{K2} > F_{K1} > F_{J2} > F_{J1}$. The trend could be attributed to the removal of some remaining contamination present on the brake shoes and the rails from the tests previous to test J. This contamination could also have been responsible for the large reduction in MTB force between tests D and J. Hence, in general it could be said that the MTB force decreased in the presence of moisture in a “clean” contact, while it increased if the contact was to some extent contaminated.

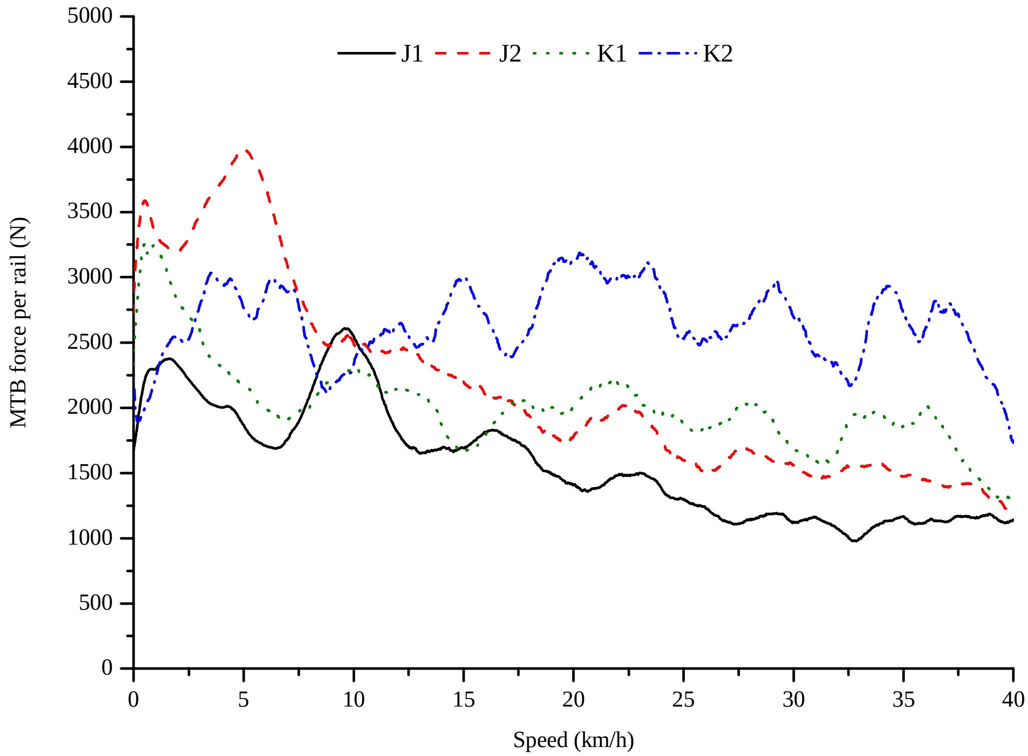

Fig. 4B.7. MTB force per rail as function of the train speed in runs of tests J and K.

4B.3.1.2. Leaf contaminated rails

Four tests were performed with leaf contaminated rails, which have been named C, G, H, and N (see Table 4B.1). Fig. 4B.8 and Fig. 4B.9 display the variation of the MTB force in the runs under dry conditions of test C as a function of the train speed and the distance, respectively. In Fig. 4B.8 it can be seen that there existed a valley in the MTB force evolution in run C1 due to leaf contamination. The initial location of this valley was about 8 m before the start of the contaminated section, indicating that leaf contamination had been spread outside the contaminated section by passing wheels during test preparation. This observation is in line with the wheel-rail adhesion results of test C reported in [4B.1]. Within the valley, a rapid decrease of the MTB force occurred between -8 m and 0 m of distance, as shown in Fig. 4B.9. This was followed by a gentler decrease of the MTB force along the contaminated section. After exiting the contaminated section, the MTB force started to increase in spite of the continuously increasing speed, suggesting that the leaf contamination was disappearing from the contact between brake shoes and rails. At a distance of around 41 m, the MTB force in run C1 seemed to have recovered the characteristic decreasing slope with the speed observed in dry “clean” contacts, as outlined in Section 4B.3.1.1.

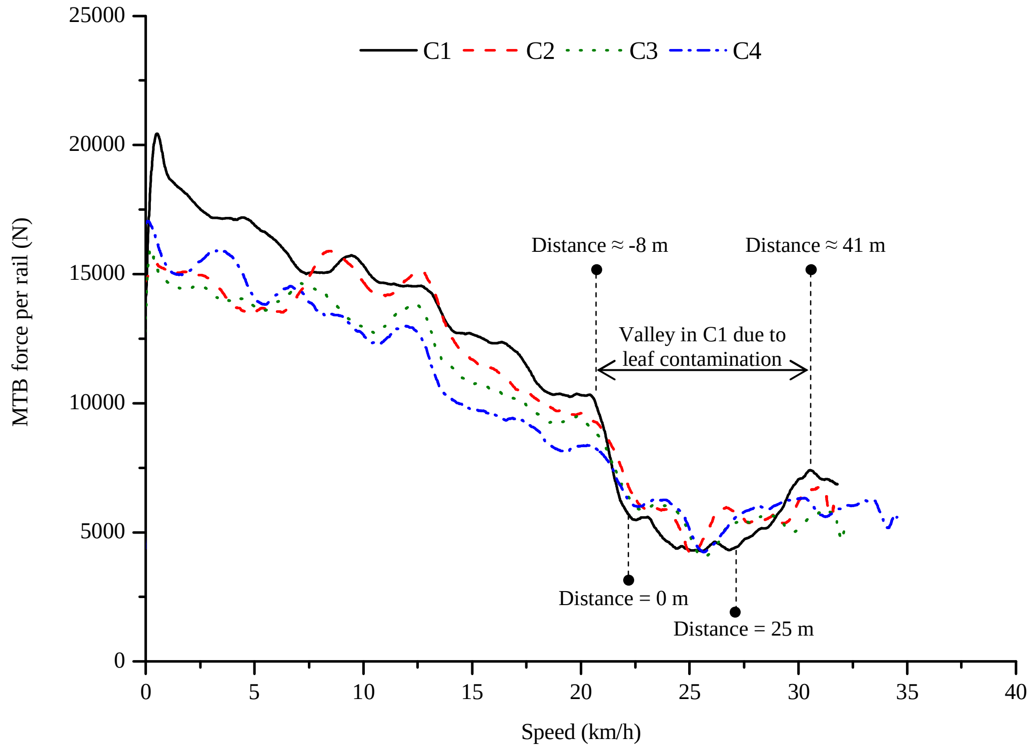

Fig. 4B.8. MTB force per rail as function of the train speed in some runs of test C (initially contaminated section between 0 m and 25 m).

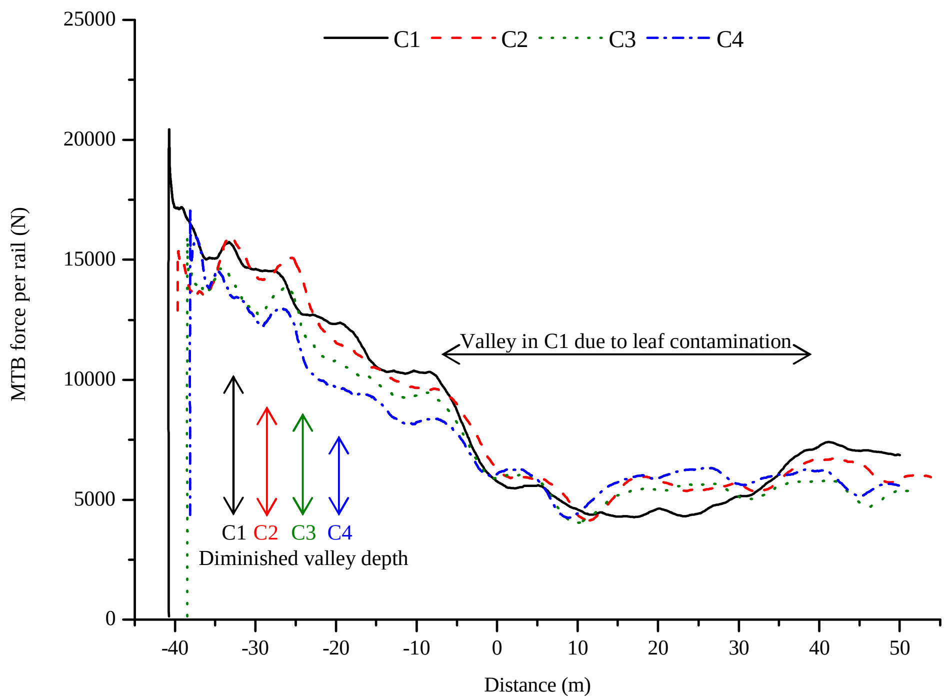

Fig. 4B.9. MTB force per rail along the distance in dry runs of test C (initially contaminated section between 0 m and 25 m).

Despite the spread of leaf contamination, it can clearly be seen in Fig. 4B.9 that the lowest value of the MTB force in run C1 was reached inside the contaminated section. This also occurred in the other runs under dry conditions, with the minimum at around 10 m of distance (see Fig. 4B.9). Looking at the evolution of the MTB force with the increasing runs under dry conditions, two different tendencies can be observed in Fig. 4B.9. On one hand, the MTB force in the intervals (-40 m, -5 m) and (35 m, 55 m) generally decreased with the increasing runs. This could have been caused by the continuous pick-up of leaf contamination by the brake shoes, leading to a lower friction force in the next runs. On the other hand, the MTB force in the interval (-5 m, 35 m) slightly increased with the runs, which suggests that the leaf layers were being removed from the rails, resulting in higher friction force in the next runs. As a consequence of the reduction in the MTB force outside the contaminated section with the runs, the depth of the valley diminished, as indicated in Fig. 4B.9.

During the first passage of the MTB over the contaminated section, leaf contamination could be seen to be pushed by the brake shoes, as shown in Fig. 4B.10. This leaf contamination consisted of both leaf layers from the rail running band and leaf mulch adhered at the sides of the running band. Thus, the push-effect contributed to the layer removal, leading to the increase of MTB force along the contaminated section, as observed in Fig. 4B.9. On the other hand, the presence of the valley in the MTB force measurements clearly indicates that some leaf contamination remained, suggesting that the brake shoes also slid over the leaf layers. Hence, thermal or mechanical mechanisms between the contacting surfaces could also have contributed to the layer removal together with the push-effect. In the thermal removal, the high temperature arising in the sliding contact between the brake shoes and the rails could have contributed to burn off the leaf layers. In the mechanical removal, the surface asperities of the brake shoes could have abraded the leaf layers off the rail surface during sliding.

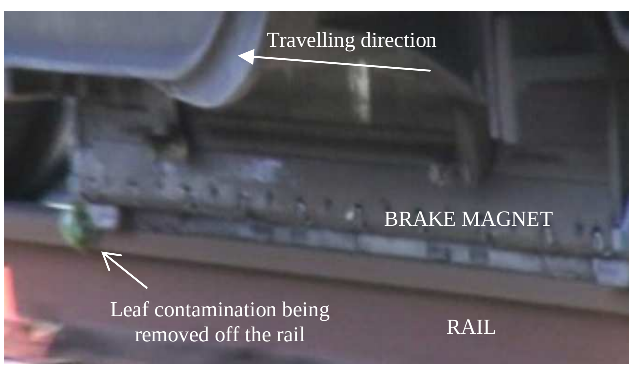

Fig. 4B.10. Photograph of the left magnet of the MTB during its motion along the contaminated section in run C1.

Fig. 4B.11 depicts the variation of the MTB force along the distance in some wet runs of test C. It can clearly be seen that the MTB force increased with the runs not only along the contaminated section, but also outside it. This may indicate that leaf contamination was being removed from both the rails and the brake shoes. Comparing the trend and values of Fig. 4B.11 with Fig. 4B.9, it could be said that the introduction of water in the contact between brake shoes and rails may have promoted the cleaning effect. It has previously been reported that water can help softening leaf layers [4B.15, 4B.16]. The lowest value of the MTB force was located at around 10 m of distance in all wet runs, as shown in Fig. 4B.11. The lowest MTB force value in the dry runs was also observed around the same distance (see Fig. 4B.9), indicating that leaf layers had predominantly remained around that location throughout test C. It is noteworthy that the location of the lowest MTB force was in close agreement with the initial traction reduction in the wet runs of test C as presented in [4B.1]. This indicates that the low friction conditions in the contact between brake shoes and rails were in agreement with those in wheel-rail contacts.

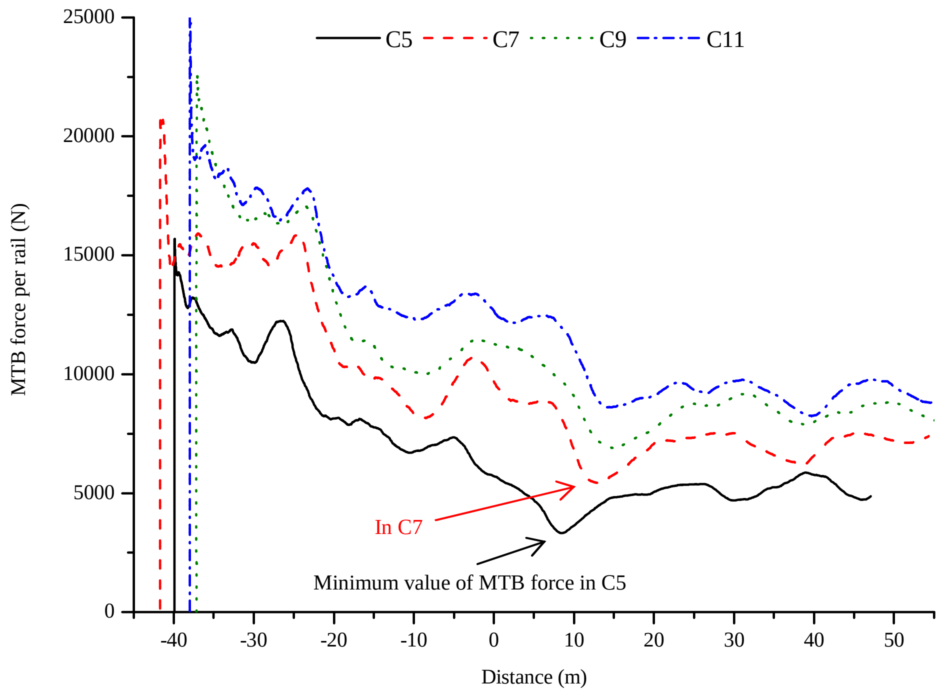

Fig. 4B.11. MTB force per rail along the distance in some wet runs of test C (initially contaminated section between 0 m and 25 m).

The minimum, average, and maximum values of the MTB force along the contaminated section in all runs of test C are displayed in Fig. 4B.12. A clear trend can be seen, in which the average and maximum values of the MTB force increased with the runs. The increasing slope was steeper in the wet runs (see Fig. 4B.12). On the other hand, the minimum MTB force was around the same value in all runs performed under dry conditions. Comparing the results in runs C4 and C5, it can be seen that the MTB force in run C5 was around 20% lower than in run C4. This indicates that the first application of water to the remaining leaf contamination reduced the friction level, in other words, wet leaf layers were more slippery than dry leaf layers. Furthermore, the average values of test C (Fig. 4B.12) were below the average value of test A in the range 22-27 km/h (Fig. 4B.5), reaching a maximum reduction of 61% in run C5 compared to the average value with “clean” rails.

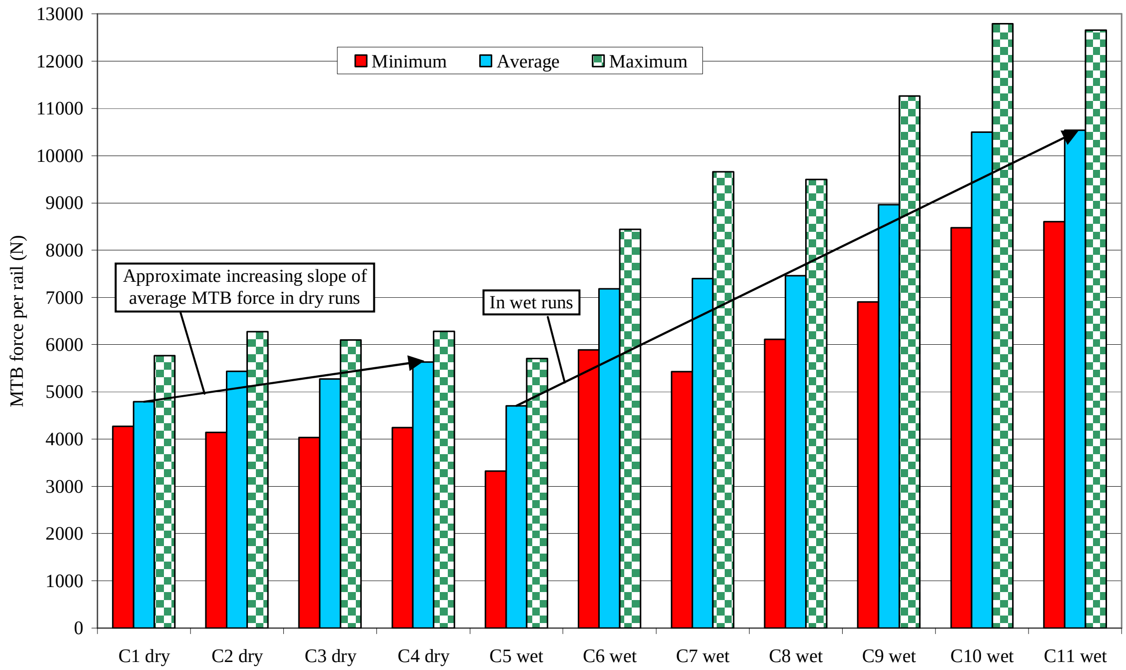

Fig. 4B.12. Minimum, average, and maximum values of the MTB force per rail along the contaminated section in the dry and wet runs of test C.

Fig. 4B.13 depicts the MTB force results of test G. In contrast with test C (Fig. 4B.12), the MTB force in test G did not follow any clear increasing trend in the dry runs. The first application of water in test G, i.e. run G9 in Fig. 4B.13, caused a decrease of around 10% in the minimum value of the MTB force compared to the value measured in G8. The average and maximum values only decreased a bit in run G9 compared to run G8. Under wet conditions, the MTB force increased with the runs but not continuously, as shown in Fig. 4B.13. This trend applied to minimum, average and maximum values of the MTB force. A comparison between the average values of test G (Fig. 4B.13) and the average value of test D in the range 22-27 km/h (Fig. 4B.5) points out that the maximum reduction of MTB force was 57% in run G2.

The results of test H are displayed in Fig. 4B.14. There existed a general but gentle trend of increasing values of the MTB force with the runs under both dry and wet conditions. Note that the value measured in H1 has not been included to draw the approximate slope of the increasing trend in Fig. 4B.14 because the increase between H1 and H2 was much larger. Comparing the MTB force measured in tests G and H, it can be said that the maximum and average values in runs of test H were somewhat lower than in test G under similar conditions.

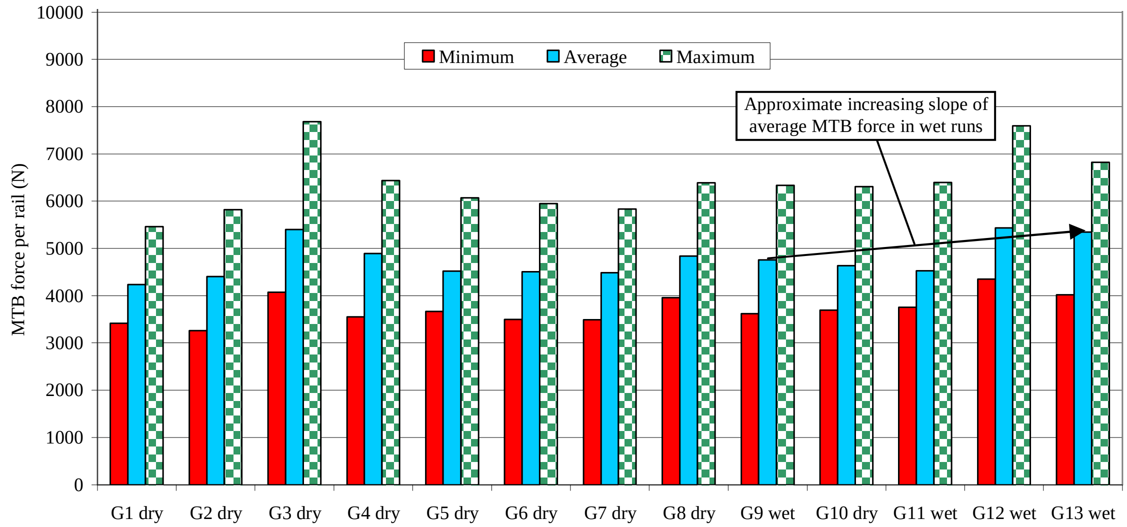

Fig. 4B.13. Minimum, average, and maximum values of the MTB force per rail along the contaminated section in the dry and wet runs of test G.

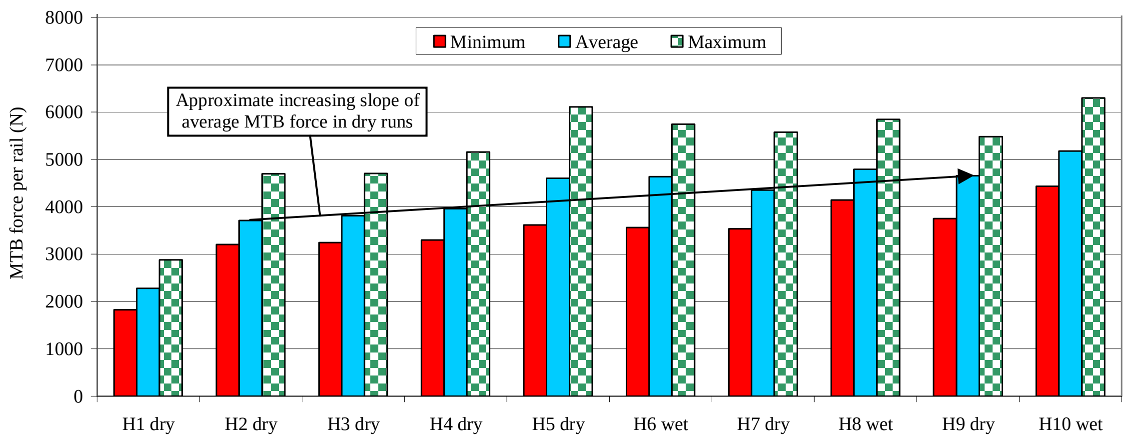

Fig. 4B.14. Minimum, average, and maximum values of the MTB force per rail along the contaminated section in the dry and wet runs of test H.

The MTB force results of the dry and wet runs in test N are given in Fig. 4B.15. It must be noted that test N was performed on a different test section than tests C, G and H (see Table 4B.1). The values of MTB force in test N were noticeably lower than those measured in the preceding leaf contaminated tests. This could have been due to surface changes in the brake shoes during the testing, as pointed out in Section 4B.3.1.1. The minimum, average and maximum values of the MTB force slightly increased with the runs under dry conditions. Under wet conditions, a similar but less continuous trend was obtained. The average values of MTB force in test N (Fig. 4B.15) were lower than the average value of test M in the range 22-27 km/h (Fig. 4B.5), reaching the maximum reduction in run N1 with 60% of the value with “clean” rails.

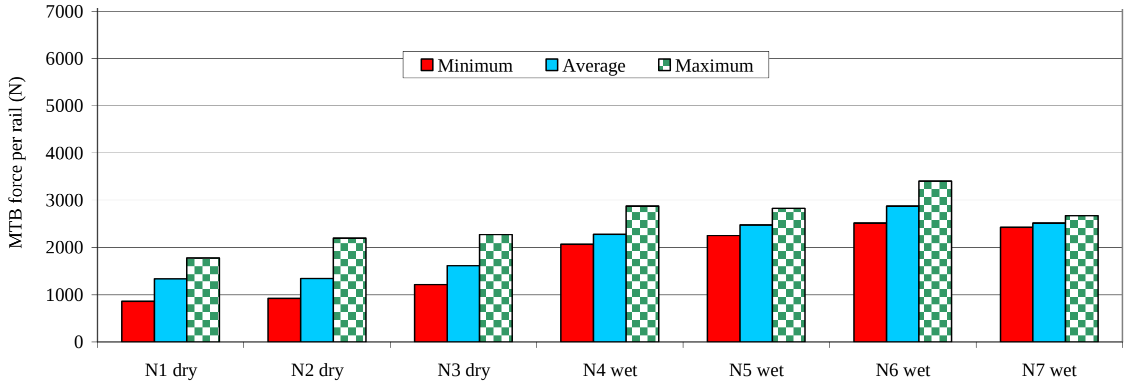

Fig. 4B.15. Minimum, average, and maximum values of the MTB force per rail along the contaminated section in the dry and wet runs of test N.

4B.3.1.3. Grease contaminated rails

The MTB force results of test O are shown in Figs. 4B.16-4B.17. In Fig. 4B.16, it can be observed that minimum and average values of the MTB force along the contaminated section tended to increase slightly with the runs. On the other hand, the maximum value of the MTB force did not follow the same trend, particularly in view of the large maximum values measured in runs O1 and O2. An explanation requires looking at Fig. 4B.17, in which the MTB force along the distance is given for some runs of test O. It can be seen that the largest MTB force before reaching the contaminated section mostly occurred in run O1. This could be attributed to two phenomena: the pick-up of grease by the MTB brake shoes with the increasing runs on the one hand, and the spread of grease along the rails by passing wheels on the other.

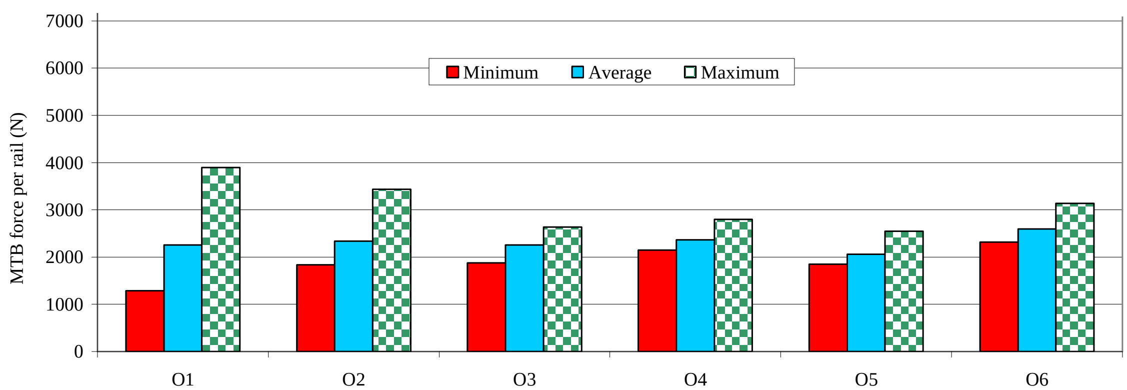

Fig. 4B.16. Minimum, average, and maximum values of the MTB force per rail along the contaminated section in the runs of test O.

Furthermore, an abrupt drop in the MTB force occurred in run O1 once the MTB entered the contaminated section, as shown in Fig. 4B.17. It can be understood that this drop could be due to the accumulation of grease in the contact between brake shoes and rails that led to a lower friction force. The lowest value of the MTB force along the contaminated section was reached at around 10 m. The drop in the MTB force was reduced with the passages, which explains the decreasing trend of the maximum value of MTB force in the first three runs (see Fig. 4B.16). In addition, the friction did not seem to increase in run O1 up to a distance of about 25 m, as shown in Fig. 4B.17. The length of track with low friction conditions in the contact between brake shoes and rails is in good agreement with the wheel-adhesion measurements in run O1, in which low adhesion conditions were observed between 5 m and 23 m of distance [4B.1]. A comparison of the MTB force values measured in test O (Fig. 4B.16) with the ones of test N (Fig. 4B.15) indicates that the MTB force was more reduced in the presence of dry leaf layers than grease on the rails.

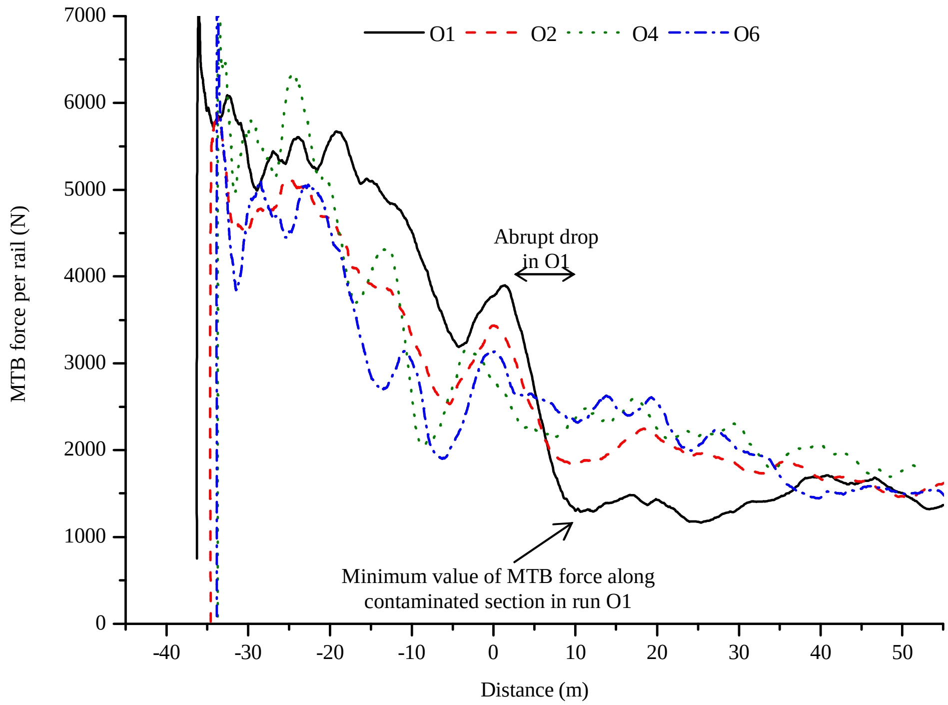

Fig. 4B.17. MTB force per rail along the distance in some runs of test O (initially contaminated section between 0 m and 15 m).

4B.3.2. Train braking performance

In the Netherlands, the Railway Regulations (*Reglement Keuring Spoorwegen*) demand that the braking distance on a descending slope of 5‰ at 140 km/h (maximum allowable line speed) should not exceed 1150 m [4B.17], which yields an average train deceleration of about 0.66 m/s^2. As outlined in [4B.1], insufficient decelerations can be obtained in the presence of (dry or wet) leaves or grease on the rails, compromising safe braking. The tests performed in these field investigations have aimed at measuring the adhesion improvement and braking force provided by one MTB, but in practice more MTBs of a train consist may be employed. In this Section, the measured data is extrapolated to cases with more active MTBs with a double aim. On one hand, some general formulae are provided, which can be used by train operating companies to calculate the braking performance of their rolling stock with the adhesion and MTB force results presented in these field investigations. On the other hand, the braking performance of the EMU employed in the tests is examined under the most adverse tested conditions.

Eq. 4B.1 displays the equation of motion of a train during braking, where BE is the total braking effort of the train, R_{tot} is the total train resistance, M is the mass of the train, and a is the train deceleration. In Eq. 4B.2 the two components of the train braking effort are given, where F_{Bi} is the braking force of the *i-th* wheel axle due to pneumatic (P) or electro-dynamic (ED) brakes, n is the number of braking wheel axles, F_{MTBi} is the MTB force measured in the *i-th* run of a test, and N is the number of active MTBs. The total braking force of the wheel axles is better expressed as function of N as indicated in Eq. 4B.3, where n_a is the number of braking wheel axles located ahead of the first MTB, μ_1 is the adhesion coefficient measured in the first run of a test, n_i is the number of braking wheel axles located between the *i-th* MTB and the *(i+1)-th* MTB, μ_{i+1} is the adhesion coefficient measured in the *(i+1)-th* run of a test, n_b is the number of braking wheel axles located behind the *N-th* MTB, μ_{N+1} is the adhesion coefficient measured in the *(N+1)-th* run of a test, g is the acceleration due to the gravity, n_T is the total number of wheel axles in the train. In the case of braking operation in P + ED mode, i.e. $N = 0$, the sum of n_a and n_b in Eq. 4B.3 is equal to n. Furthermore, it may happen that the measured adhesion coefficient in a test run (μ_i) is higher than the maximum adhesion possible in braking of the train under consideration (μ_{max}). This error can be avoided by simply applying Eq. 4B.4 in the calculation of Eq. 4B.3. Moreover, the components of the total train resistance are given in Eq. 4B.5, where R_{air} is the air resistance, $R_{running}$ is the running resistance, R_{curve} is the curve resistance, and $R_{gradient}$ is the gradient resistance.

$$BE + R_{tot} = M \cdot a \tag{4B.1}$$

$$BE = \sum_{i}^{n} F_{Bi} + \sum_{i}^{N} F_{MTBi} \tag{4B.2}$$

$$\sum_{i}^{n} F_{Bi} = (n_a \cdot \mu_1 + \sum_{i=1}^{N-1} n_i \cdot \mu_{i+1} + n_b \cdot \mu_{N+1}) \cdot g \cdot \frac{M}{n_T} \tag{4B.3}$$

$$\mu_i \leq \mu_{\max} \tag{4B.4}$$

$$R_{tot} = R_{air} + R_{running} + R_{curve} + R_{gradient} \tag{4B.5}$$

The braking performance of the EMU in the tests has been calculated in four braking modes: P + ED; P + ED + 1 MTB, with the first MTB being the one employed in the tests; P + ED + 2 MTBs with the second MTB being numbered 2 in Fig. 4B.1; P + ED + 3 MTBs with the third MTB being numbered 3 in Fig. 4B.1. Since an insufficient train deceleration can threaten the safety of railway transportation, the most critical case is chosen to be investigated in this Section, which is given by the minimum values of adhesion and MTB force measured along the contaminated section in the tests. In the tests only running and aerodynamic resistances were applicable as the track was straight and horizontal; however, they have been omitted in Eq. 4B.1 for the sake of simplicity. Note that this simplification was acceptable for the speed range of the tests. The formulae employed to calculate the minimum deceleration of the EMU in the four braking modes are shown in Table 4B.2. Note that for this EMU: M = 236.8 t (empty conditions), μ_{max} = 0.14, and n_T = 16.

Table 4B.2. Formulae to calculate the minimum deceleration of the EMU in different braking modes with data measured in the field tests.

Braking mode	Formulae
P + ED	$a_{\min} = \dfrac{16 \cdot \mu_{\min 1} \cdot g}{n_T}$
P + ED + 1MTB	$a_{\min} = \dfrac{F_{MTB\min 1}}{M} + \dfrac{(5 \cdot \mu_{\min 1} + 11 \cdot \mu_{\min 2}) \cdot g}{n_T}$
P + ED + 2MTBs	$a_{\min} = \dfrac{F_{MTB\min 1} + F_{MTB\min 2}}{M} + \dfrac{(5 \cdot \mu_{\min 1} + 4 \cdot \mu_{\min 2} + 7 \cdot \mu_{\min 3}) \cdot g}{n_T}$
P + ED + 3MTBs	$a_{\min} = \dfrac{F_{MTB\min 1} + F_{MTB\min 2} + F_{MTB\min 3}}{M} + \dfrac{(5 \cdot \mu_{\min 1} + 4 \cdot \mu_{\min 2} + 6 \cdot \mu_{\min 3} + 1 \cdot \mu_{\min 4}) \cdot g}{n_T}$

Fig. 4B.18 depicts the minimum deceleration of the EMU in the four braking modes. It can be seen that braking in P + ED mode led to a minimum deceleration below the required by the Dutch Railway Regulations in every test except test G-dry. Using one or more MTBs improved the deceleration compared to P + ED mode in every test (see Fig. 4B.18). This improvement was expected because of the MTB force and the improved adhesion conditions for wheels behind the MTBs. There was, however, one single exception to this trend in test G-dry for which using one MTB led to the lowest deceleration, which was due to the pick-up of leaf contamination by driven wheels before first MTB passage in test G-dry, as outlined in [4B.1]. Furthermore, the increase in the number of active MTBs led to an increase in the deceleration in most tests, as shown in Fig. 4B.18.

It can be seen in Fig. 4B.18 that the number of MTBs necessary to bring the train deceleration above the minimum requirement varied in the tests. In test C-wet, one active MTB was sufficient, while in tests H-wet, N-dry and N-wet, two MTBs were required. In test H-dry, three MTBs were needed. There were a few tests in which three MTBs did not bring the minimum train deceleration above requirements, namely tests C-dry, G-wet and O (see Fig. 4B.18). In these tests, the minimum deceleration was around 12% lower than the required value. Looking at Fig. 4B.18, it could be said that using two MTBs could increase the deceleration noticeably compared to one MTB, e.g. tests C-dry, N-dry and N-wet. Using three MTBs slightly increased the deceleration compared to two MTBs. This can mostly be attributed to the fact that only one wheel axle of the EMU benefits from the adhesion improvement after the third MTB passage (see Fig. 4B.1).

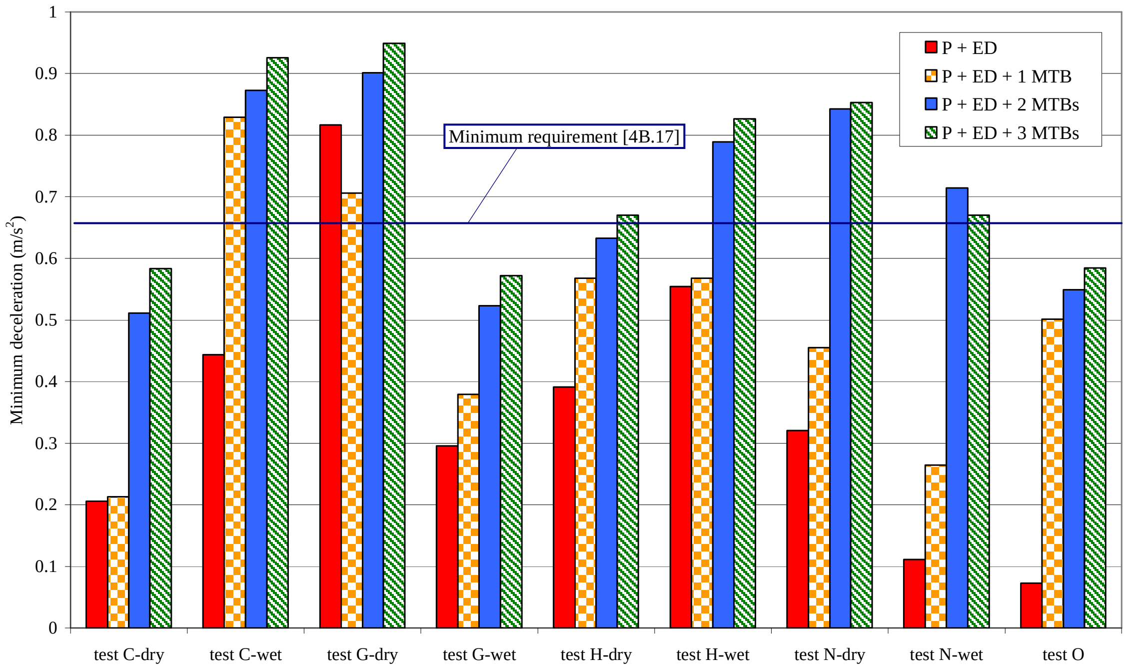

Fig. 4B.18. Calculated values of the minimum deceleration of the EMU in four different braking modes in the tests with leaf and grease contaminated rails.

4B.3.3. Examination of the brake shoes

The brake shoes of the two brake magnets were examined in the laboratory after the testing. Fig. 4B.19 shows a photograph of a set of brake shoes before and after being cleaned with acetone upon post-test examination. It can be seen in Fig. 4B.19a that some contamination layers remained on the surfaces of the brake shoes after the tests. The contamination layer could mostly be removed by rubbing with a cloth soaked in acetone, revealing more metallic surface, as pointed out in Fig. 4B.19b. Moreover, examinations on-site of the surfaces of the brake shoes indicated that contamination progressively accumulated throughout the testing. The accumulation of contamination in the course of the testing could have been responsible for the decreasing trend of the MTB force in tests with dry “clean” rails outlined in Section 4B.3.1.1. Furthermore, the surfaces of the brake shoes were examined in search for possible formation of welds. Welds have been reported to form on the surfaces of brake shoes under certain operating conditions for some pole shoe materials, reaching a thickness of up to a few millimeters and greatly diminishing the MTB force [4B.18]. During post-test examination no welds were found on the brake shoes, suggesting that this had not been the cause of the trend of decreasing MTB force in dry “clean” tests.

The surfaces of the brake shoes were also examined under a microscope. Fig. 4B.20 gives a micro-photograph of the surfaces of a pole shoe and an insulating strip after being cleaned with acetone. The surfaces of both brake shoes were characterized by numerous scratches and grooves, suggesting that abrasion had been taken place during sliding. In the pole shoes, a few particularly wide grooves were found with up to 0.46 mm in width, as shown in Fig. 4B.20a. These wide grooves could have been caused by entrapped sand particles, which perhaps remained after cleaning runs. In the insulating strips, fewer grooves were observed than in the pole shoes. Additionally, a few darker areas were present on the surfaces of the strips, which were presumably consequence of oxidation (see Fig. 4B.20). The average surface roughness of the brake shoes was measured after the tests, being 2.60 ± 0.16 µm for the pole shoes and 2.65 ± 0.75 µm for the insulating strips. Measurements before testing could not be undertaken.

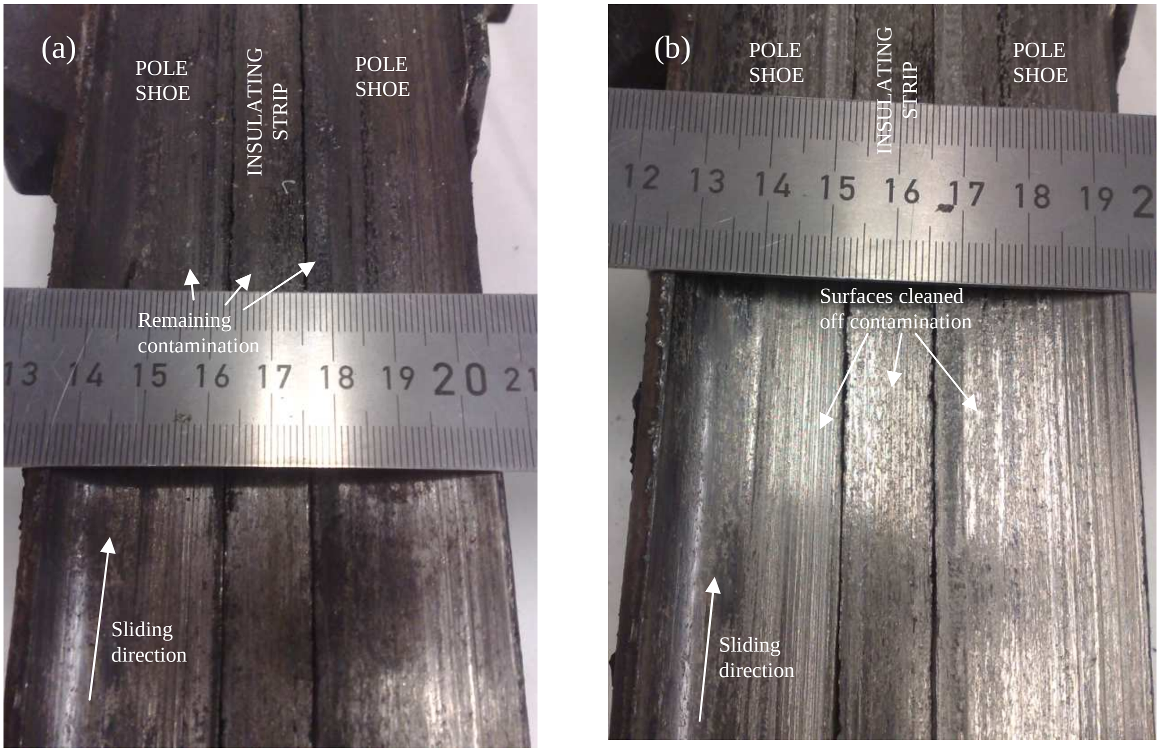

Fig. 4B.19. Brake shoes after testing: (a) before and (b) after cleaning the surface with acetone.

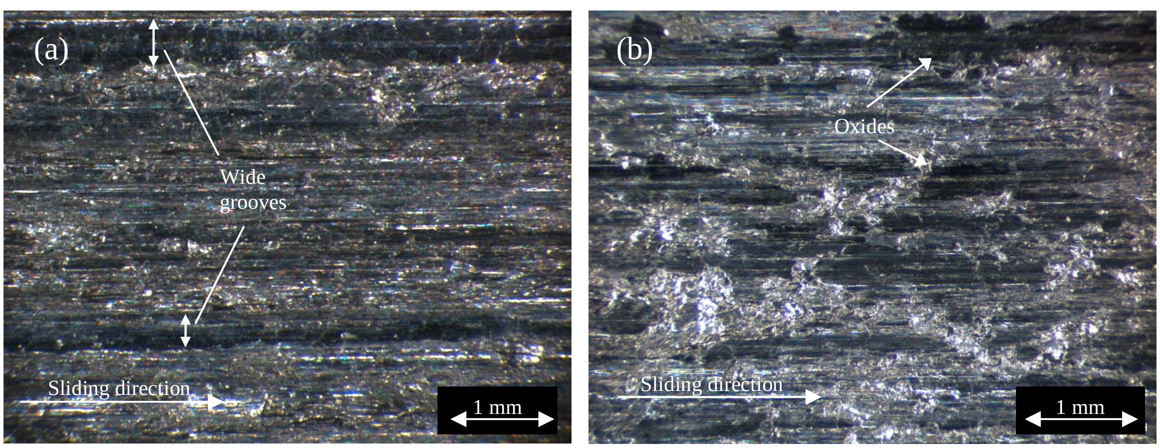

Fig. 4B.20. Micro-photographs of the brake shoes surfaces after testing and cleaning with acetone: a) pole shoe; b) insulating strip.

Figs. 4B.21-4B.22 display a photographed side view of an insulating strip and a pole shoe resting on the top of a rail after the tests. The high temperatures experienced during sliding in the tests seemed to have led to material transformation at the near-surface of the brake shoes. Particularly, a highly thermally affected zone could be seen in all insulating strips, reaching a depth of up to around 12 mm (see Fig. 4B.21). Moreover, most of the insulating strips had been deformed leading to a bend shape as schematically shown in Fig. 4B.23. Due to the bending, the contact area between the insulating strips and the rails had been reduced in the course of the testing. Hence, this may also have contributed to the decreasing trend of MTB force in the dry "clean" tests. Furthermore, the deformation at the surface of the pole shoes brought about the partial detachment of a few pieces of pole shoe from the bulk material, as shown in Fig. 4B.22.

Fig. 4B.21. Photograph of an insulating strip after testing and cleaning.

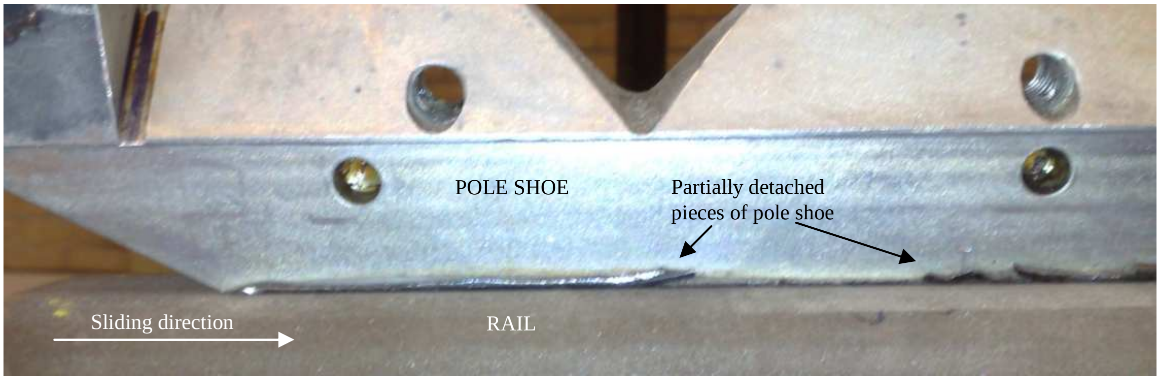

Fig. 4B.22. Photograph of a pole shoe after testing and cleaning.

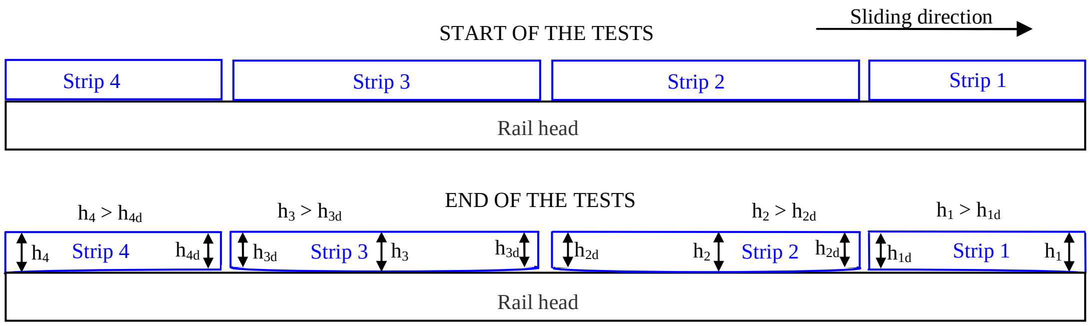

Fig. 4B.23. Schematic representation of the geometry change of the insulating strips in a brake magnet during the testing.

The hardness of the pole shoes and the insulating strips was measured in the laboratory after testing by means of Vickers indentation technique with a 20 kg load (see results in

Table 4B.3). Additionally, the bulk hardness of a piece of rail steel R260Mn, which is the standard used in the Dutch railways, was also measured. It can be seen in Table 4B.3 that the bulk hardness of both pole shoes and insulating strips, which can be considered equivalent to the hardness of new contact surfaces, was smaller than the bulk hardness of the rail. After the tests, the hardness of the contact surface of the brake shoes had increased. The pole shoes had been hardened more than the insulating strips, as shown in Table 4B.3.

Table 4B.3. Vickers macro-hardness (HV_{20kg}) measurements of the brake shoes and R260Mn rail in the laboratory.

HV_{20kg}	R260Mn Rail	Pole shoe	Insulating strip
Bulk	281	145	216
Post-test contact surface	n.a.	212	261

The mass loss of pole shoes and insulating strips of the two brake magnets was determined after the tests. Table 4B.4 displays the mean value of the total and specific mass loss of all brake shoes in a brake magnet. Note that the contact area between brake shoes and rail was estimated based on the appearance of the contact surfaces of brake shoes after the tests. It can be seen in Table 4B.4 that the pole shoes had a larger mass loss than insulating strips due to the larger contact area, while the specific mass loss was similar in both materials. According to data collected with the DGPS, the total slid distance of the MTB was about 16 km. Hence, it could be said that the wear rate of brake shoes in a brake magnet was 105.28 g/km on average in the tests.

Table 4B.4. Mean value and deviation of the mass loss measured in the pole shoes and insulating strips per brake magnet.

	Pole shoes	Insulating strip
Mass loss (g)	1321.54 ± 66.08	363.08 ± 1.77
Specific mass loss (g/m^2)	19060.42 ± 953.00	20536.20 ± 100.11

Since the MTB force and sliding speed were measured throughout the testing, an estimate of the wear rate in the tests can also be given as a function of the frictional dissipated energy. Integrating over time the frictional power (i.e. the product of the MTB force and the sliding speed) generated in each test run, the total dissipated energy in the whole testing accounted for 104.17 MJ per brake magnet. As it was not possible to separate the friction force contribution of pole shoes and insulating strips of a brake magnet, the estimated wear rate needs to be applied to all brake shoes of the brake magnet. Hence, the wear rate of the brake shoes in a brake magnet was 16.17 g/MJ on average in the tests.

4B.3.4. Examination of the rails

The rail profile was measured at six locations of the contaminated sections before and after the tests by means of MiniProf. No substantial change in the rail profile had been caused by the tests, which could be expected as only 49 MTB passages had taken place. The hardness of the running band of the rail was also measured on-site by means of

Equotip portable hardness tester at three positions of the contaminated section 1, namely at a distance of 0 m, 12 m, and 25 m. The measurements yielded an average value of 325 ± 20 HV. Note that this value was clearly higher than the bulk hardness of the rail material (see Table 4B.3). Furthermore, no significant difference in the surface hardness before and after testing could be appreciated in the measurements.

The surface roughness of the top of the rail was measured before and after the tests with a Hommel portable roughness tester at the same locations of the hardness measurements. Measurements were performed across the running band and on the top of the rail towards the field side and the gauge side, as schematically indicated in Fig. 4B.24. Each measurement was performed up to three times. In Fig. 4B.24 the maximum, average and minimum values of the measurements at the three locations are given for the left and right rails. It can be seen that the rail surface had mostly become rougher after the tests, with the exception of the location towards the field side. However, it must be noted that the increase in roughness of the running band may not be attributed only to the MTB because sand had also been applied to the contaminated section in the cleaning runs of the leaf tests. Laboratory investigations have shown that the application of sand to the wheel-rail contact can cause an increase in the surface roughness of the rail (and the wheel) [4B.19].

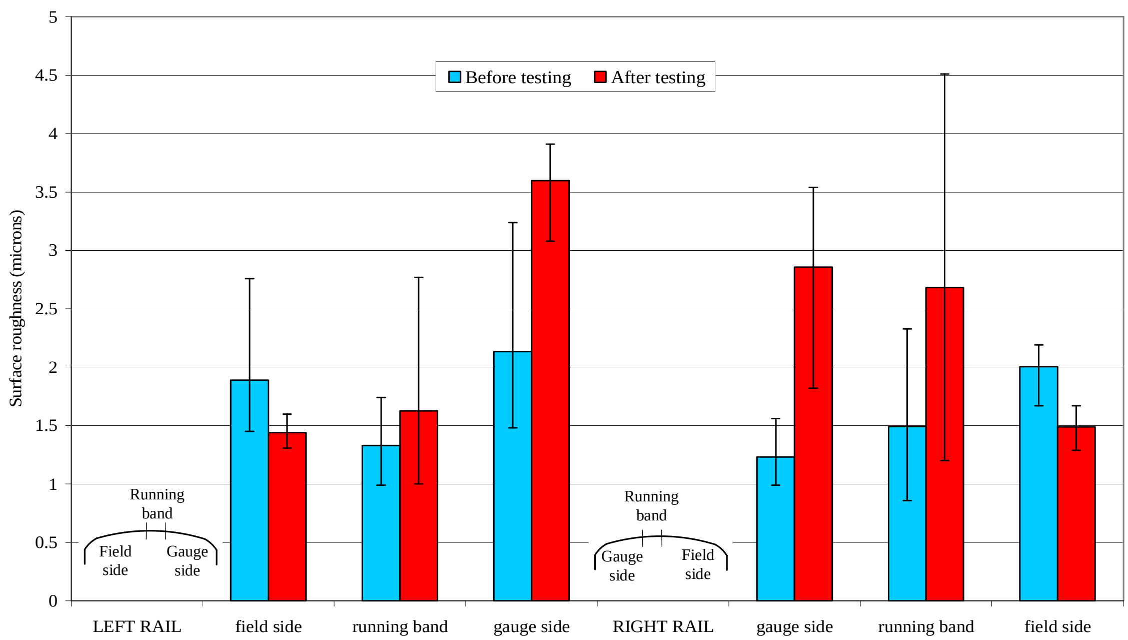

Fig. 4B.24. Maximum, average and minimum values of the surface roughness of the top of the rail at three locations before and after the testing.

4B.3.5. Examination of the insulated rail joint

In order to monitor the possible accumulation of debris at the IRJ, a video camera was installed next to the track. Among the videos taken of the different test runs, it appeared that the largest amount of debris depositing at the IRJ occurred in test run G4. Fig. 4B.25 displays photographs of the monitored IRJ during the different phases of G4. The top of the rail was free of debris at and around the IRJ before MTB passage (see Fig. 4B.25a). Due to the discontinuity in longitudinal profile between the insulating material of the IRJ and the adjacent rails, debris came off the brake shoes when the MTB exited its contact with the IRJ, as shown in Fig. 4B.25c. After the MTB passage, the debris has deposited at the IRJ and also some decimeters further (see Fig. 4B.25d). At some position in the transverse direction of the IRJ, the debris can be seen in Fig. 4B.25d to establish a bridge between the adjacent rails. In this situation, the electrical insulation provided by the IRJ could be compromised. Nevertheless, the debris was blown away from the top of the rail with each wheel passage due to the train's slipstream. After five wheel passages the bridge had disappeared (see Fig. 4B.25e), and after nine wheel passages most debris had been removed from the surroundings of the IRJ (see Fig. 4B.25f).

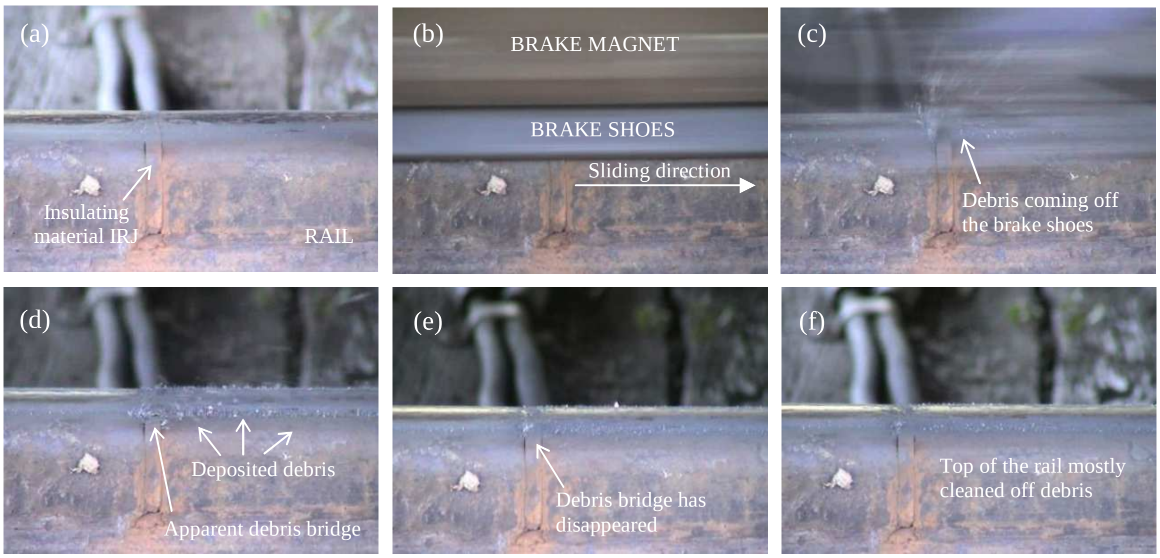

Fig. 4B.25. Photograph of the IRJ in test run G4: (a) before MTB passage; (b) upon MTB passage; (c) MTB leaving contact with the IRJ; (d) after MTB and one wheel passage; (e) after MTB and five wheel passages; (f) after MTB and nine wheel passages.

In addition to the visual inspection of debris, an IRJ tester (type RTL88 of NIEAF-SMITT BV) was employed in the tests to measure the electrical insulation between the adjacent rails after an EMU passage with MTB. Every measurement yielded a voltage higher than 45 V, while a minimum value of 8 V is demanded by ProRail. In order to have a reference in each measurement, the voltage between two points on the same rail was also measured, obtaining values below 1 V.

4B.4. Discussion

Rolling stock normally undergoes different types of maintenance that vary in frequency and extent. In the Netherlands, there is a short-term maintenance about every two days, in which important parts such as those related to the safety of a train are inspected, e.g. MTBs. In principle, unless breakage or mal-functioning is observed, the MTBs remain intact. Every 100 days or 77000 km, there is a long-term maintenance, where a more thorough maintenance is carried out. For example, brake shoes may be replaced or their surfaces may be cleaned. Thus, it is essential to examine the variation of the MTB performance with the use to determine the required maintenance frequency. Aiming at that goal, the brake shoes used in the tests were not cleaned or changed in the course of the testing, leading to changes in the surface conditions. Contamination could be seen on-site to adhere to the surfaces. During post-test examination, the surfaces were seen covered to a large extent with remaining contamination. Additionally, insulating strips adopted a bend shape that reduced their contact area with the rail. These changes could have resulted in the trend of decreasing MTB force in tests with dry “clean” rails, in which the average force in the range 0-40 km/h reduced up to 87% in the course of the testing. In the literature, MTB force reductions of up to 30% due to contamination on the brake shoes have also been reported [4B.20]. Since the reduction in the MTB force can affect its effectiveness against slippery tracks, and compromise safe braking distances, it is wise to investigate this phenomenon in future works. Monitoring of the MTB force in service may ultimately be necessary to establish the amount of variation that can be expected in actual operating conditions.

Another important aspect for the maintenance of the MTB brake shoes, which has been investigated in this work to some extent, is their wear. It can be understood that operational costs of using MTBs against slippery tracks may greatly be affected by the wear rates of brake shoes. In this work, the mass loss was measured after the entire testing, as it was not possible to undertake measurements in between tests or runs. Based on the measured mass loss, two estimates of the wear rate of the brake shoes in a brake magnet have been calculated: one as a function of the sliding distance (105.28 g/km) and the other as a function of the dissipated frictional power (16.17 g/MJ). According to specifications provided by the rolling stock maintenance company in the Netherlands, the maximum allowable height loss of the brake shoes is around 13 mm. If we assume that the profile evolution of pole shoes and insulating strips is uniform, the maximum allowable mass loss is estimated to be about 8031 g per brake magnet. Hence, a brake magnet could travel a maximum distance of around 76 km, or it could dissipate a maximum frictional power of around 497 MJ, before the brake shoes needed to be replaced under the tested conditions. Nevertheless, these values may not directly be extrapolated to practice due to several differences in operating conditions between the tests and actual conditions in service. In practice, the sliding speed and the duration of the braking application can differ from the tested conditions, with wear rates of cast iron in sliding contacts being strongly dependent on these two parameters [4B.21, 4B.22]. For the ideal use of MTBs against slippery tracks proposed by the authors, the brake shoes would mostly slide over contaminated rails; whereas, around 80% of the sliding distance in the tests was over “clean” rails. It could also be possible that different values of the surface hardness of brake shoes are present in actual conditions in service, which may have a great effect on the wear rates of sliding steel contacts [4B.23-4B.25]. Considering the importance of an accurate determination of the wear rate of brake shoes to determine the maintenance frequency of MTBs, future investigations should be performed taking these parameters into account.

Among the rail contamination conditions tested in this work, the MTB force was reduced the most in the presence of leaf layers, being as low as 40% on average of that measured with dry “clean” rails. The first application of water to the leaf contaminated rails mostly led to an additional reduction of the MTB force. This indicates that under the lowest adhesion conditions at the wheel-rail contact, the additional deceleration given by MTBs can also be at its lowest. However, water also seemed to help removing leaf contamination in most tests so that the MTB force increased in the next runs and the adhesion conditions for subsequent wheels was somewhat improved. In future works, it may be interesting to perform tests with leaf contaminated rails under wet conditions without preliminary runs under dry conditions to enable a direct comparison between dry and wet conditions of the rates of layer removal by MTBs.

The braking performance calculations have shown that using only pneumatic and electro-dynamic brakes led to decelerations of the EMU below the minimum requirements in eight out of the nine tested conditions due to the low adhesion conditions. Using up to three MTBs improved the braking performance above requirements for six of the tested conditions, while in the other three ones the deceleration was just 12% lower than required. Moreover, two MTBs have been found optimal for this EMU, but the optimal number of MTBs is clearly dependent on the type of train and it could be calculated with the formulae and data presented in this paper and in [4B.1]. It must be noted that possible improvement of adhesion conditions by slipping wheels has not been considered in the braking performance calculations, which may have led to calculated minimum decelerations somewhat lower than in actual conditions. Furthermore, the fourth MTB of the EMU has not been considered in the calculations because it was assumed that using MTBs against slippery tracks demands the active MTBs to be located behind the first braked wheels in the travelling direction. In this way, MTBs could be activated upon detection of wheel slide on those first wheels by the wheel slide protection (WSP) system, to minimize the sliding distance over uncontaminated rails. Nevertheless, it can be understood that in an emergency situation all available MTBs should be activated to maximize the braking effort of the train.

The tests presented in this work have been performed at a maximum train speed of 40 km/h partly due to the speed limitation of the stabling yard, while the maximum speed of passenger rolling stock is 140 km/h on conventional track in the Netherlands. It can be expected that some of the results presented in this paper may differ at higher speeds. The MTB force can clearly be affected by an increase in travelling speed, as shown in this paper. Hence, it is necessary to measure the MTB force at speeds up to 140 km/h in future investigations. The wear of the brake shoes and rails may also differ at higher sliding speeds, and it should also be investigated. On the other hand, there is no obvious reason to expect a more detrimental effect on the electrical insulation of an IRJ due to the increase of train speed, but perhaps the opposite effect, because debris could be removed faster as larger train's slipstream is generated at higher train speeds.

4B.5. Conclusions

Part B of the field investigations on the performance of MTB against slippery tracks has focused on the MTB force and possible side effects of frequent use of MTBs. Three types of contamination representative of slippery tracks (leaves, water, and grease) have been employed in the tests to analyze the MTB force under typical low adhesion conditions. Tests with dry "clean" rails have also been performed to investigate the influence on the MTB force of the train speed and the varying surface conditions of MTB brake shoes. The braking performance of the EMU has also been analyzed under the tested conditions. Furthermore, the surfaces of brake shoes and rails have been examined, and the wear of rails and brake shoes in the tests has been investigated. Moreover, the effect of MTB passage on the electrical insulation of an IRJ has been examined by means of electrical measurements and visual inspection. Based on the results obtained in this work, the following conclusions can be drawn:

a) Leaf contamination causes the largest reduction in the MTB force, closely followed by grease. The first application of water to leaf layers mostly leads to the lowest MTB force values, but subsequent applications promote leaf contamination removal by MTB leading to an increase of the MTB force.
b) The increase in train speed in the range 0-40 km/h leads to a decrease of the MTB force with dry “clean” rails. The amplitude of the decreasing slope is found to be strongly affected by variations in the surface conditions of the brake shoes.
c) The MTB force measured with dry “clean” rails decreased in the course of the testing up to 87% on average. This has been attributed to changes in the surface conditions of brake shoes, such as the accumulation of contamination and the reduction in contact area.
d) Braking performance calculations have shown that the deceleration capability of the EMU in slippery tracks may be below safety margins due to the low adhesion conditions. Using up to three MTBs in the EMU may mostly bring the braking performance to safe levels.
e) Using two MTBs under the tested conditions are found to yield an optimal braking performance for this EMU. Some general formulae have also been given to allow for the calculation of the optimal number of MTBs for other train configurations.
f) According to the wear rate calculations, around one fifth of the service life of the MTB brake shoes was consumed in the tests, while no significant rail wear was observed due to the small number of MTB passages in the tests.
g) Using MTBs does not necessarily affect the electrical insulation of an IRJ. When debris deposits at the gap between adjoining rails, it is mostly removed after several wheel passages due to the train’s slipstream.

References

[4B.1] O. Arias-Cuevas, Z. Li: Field Investigations on the Performance of Magnetic Track Brakes of an Electrical Multiple Unit against Slippery Tracks. Part I: Adhesion Recovery. Submitted for publication to Journal of Rail and Rapid Transit (2010).

[4B.2] J. Eleveld: Gladde Sporen, Oplossingsrichtingen voor Adhesieproblemen. Report published by the Dutch Railways Technical Research (NSTO) in Dutch (March 1999).

[4B.3] Managing Low Adhesion. Report published by the Adhesion Working Group, UK (September 2001).

[4B.4] C.W. Jenks: Improved Methods for Increasing Wheel/Rail Adhesion in the Presence of Natural Contaminants. Transit Cooperative Research Program Sponsored by the Federal Transit Administration, Transportation Research Board National Research Council (May 1997).

[4B.5] U. Olofsson, K. Sundvall: Influence of Leaf, Humidity and Applied Lubrication on Friction in the Wheel-Rail Contact: Pin-on-Disc Experiments. Journal of Rail and Rapid Transit 218 (2004) 235-242.

[4B.6] N. Tanabe, Y. Hirota, T. Omichi, J. Hirama, K. Nagase: Study on the Factors Which Cause the Wheel Skidding of JR Ltd. Express EMUs. JSME International Journal 47 (2004) 488-495.

[4B.7] W. Voges, P. Spiess: Optimising Services with EMU ET42x in Autumn 2004 and 2005. Proceedings of 7th World Congress on Railway Research, Canada (2006).
[4B.8] P-P. Mittertreiner: Magneetremtesten op wissels en puntstukken. Report produced by DeltaRail B.V. in Dutch (2010).
[4B.9] M. Cooijmans: Onderzoek ten Bate van Materiaal Specificatie Slijtdelen Trein Noodremsysteem. Report produced by Schielab B.V. in Dutch (September 2006).
[4B.10] O. Arias-Cuevas, Z. Li, R.I. Popovici, D.J. Schipper: Simulation of Curving Behavior under High Traction in Lubricated Wheel-Rail Contacts. In press, Journal of Vehicle System Dynamics (2010).
[4B.11] A. Savitzky, M.J.E. Golay: Smoothing and Differentiation of Data by Simplified Least Squares Procedures. Analytical Chemistry 36 (1964) 1627-1639.
[4B.12] OmniSTAR 8200HP User Manual, Issue 1.05 (April 2007).
[4B.13] N. Saka, A.M. Eleiche, N.P. Suh: Wear of Metals at High Sliding Speeds. Wear 44 (1977) 109-125.
[4B.14] K. Hirasata, K. Hayashi, Y. Inamoto: Friction and Wear of Several Kinds of Cast Irons under Severe Sliding Conditions. Wear 263 (2007) 790–800.
[4B.15] E.A. Gallardo-Hernandez, R. Lewis: Twin disc assessment of wheel/rail adhesion. Wear 265 (2008) 1309–1316.
[4B.16] C.R. Fulford: Review of low adhesion research. Report published by the Rail Safety and Standards Board, UK (2004).
[4B.17] Regeling Spoorverkeer, Article 8, Chapter 3: Maximumsnelheid Treinen. Available online in Dutch at http://wetten.overheid.nl/BWBR0017707 (accessed on February 3rd, 2010).
[4B.18] G. Gfatter, S. Haas, G. Vohla: Track Brakes. Knorr-Bremse Handbook (2004).
[4B.19] O. Arias-Cuevas, Z. Li, R. Lewis: A Laboratory Investigation on the Influence of the Particle Size and Slip During Sanding on the Adhesion and Wear in the Wheel-Rail Contact. In proceedings of the 8th International Conference on Contact Mechanics and Wear of Rail/Wheel Systems, Firenze, Italy, September 15-18 (2009).
[4B.20] L. Vermeulen: Beproeving van Elektromagnetische remmen en Microprocessorgestuurde Anti-blokkeerinstallatie van DH 3219 en DH 3113. Report produced by the Centre for Technical Research (CTO) of the Dutch Railways (1988) in Dutch.
[4B.21] Y. Zhang, Y. Chen, R. He, B. Shen: Investigation of tribological properties of brake shoe materials - phosphorous cast irons with different graphite morphologies. Wear 166 (1993) 179-186.
[4B.22] K. Hirasata, K. Hayashi, Y. Inamoto: Friction and wear of several kinds of cast irons under severe sliding conditions. Wear 263 (2007) 790–800.
[4B.23] T. Akagaki, D. A. Rigney: Sliding friction and wear of metals in vacuum. Wear 149 (1991) 353-374.
[4B.24] S. Bian, S. Maj, D.W. Borland: The unlubricated sliding wear of steels: the role of the hardness of the friction pair. Wear 166 (1993) l-5.
[4B.25] C.C. Viáfara, A. Sinatora: Influence of hardness of the harder body on wear regime transition in a sliding pair of steels. Wear 267 (2009) 425–432.

Chapter 5

Traction control

ABSTRACT

Chapter 5 presents numerical investigations that have been performed with a two-fold purpose: on one hand, the effectiveness of an existent TC algorithm is examined; on the other hand, the influence of the vehicle curving behaviour on the adhesion is analyzed. The chapter is divided in two parts. Part A introduces the vehicle model and its validation based on a wear pattern attributed to hunting. In Part B, two additional models, namely a TC model and a friction model, are presented and coupled to the vehicle model. Furthermore, the complete coupled model is employed in Part B to analyze a typical situation of low adhesion that occurs when the top of the high rail on a curve is undesirably contaminated with flange lubricant.

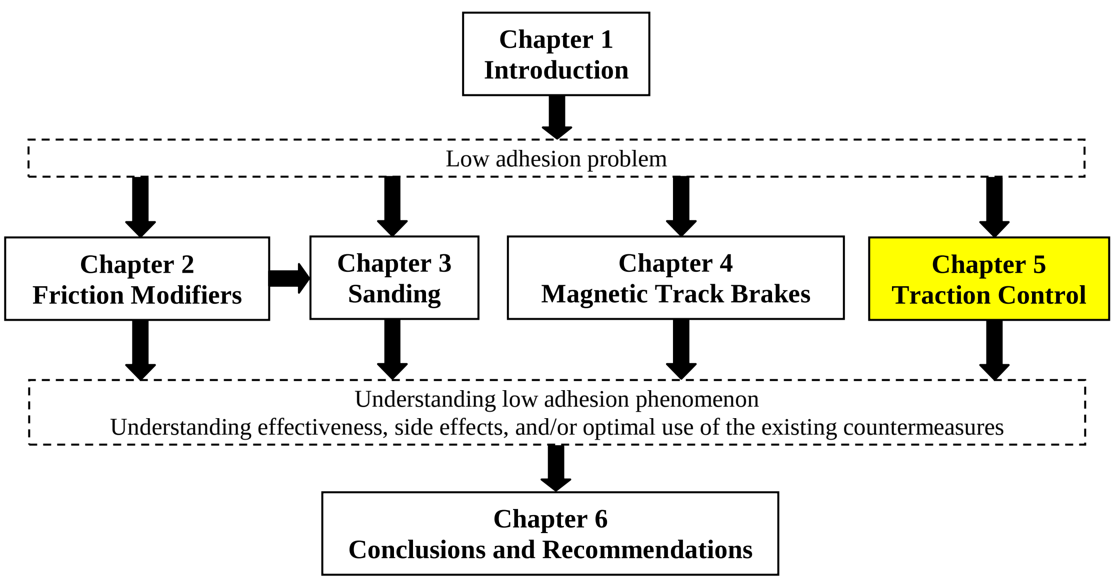

Chapter 5, Part A

Validation of vehicle model

ABSTRACT

A multi-body dynamics approach is adopted to build up a model with commercial software of the leading coach of an electrical multiple unit type VIRM of the Dutch railways. The model is validated by finding the correlation between the simulated bogie hunting motion and the oscillating rail gauge wear observed on several large-radius track sections of the Dutch network. In this paper, the influence of the vehicle suspension on bogie hunting on the measured track is also investigated.

5A.1. Introduction

A classical problem in the stability of railway vehicles with conventional solid axles and conical or profiled wheels is hunting, which is represented by coupled lateral and yaw oscillations of the vehicle, together with its wheelsets, following a disturbance in the vehicle-track interaction. The decaying rate of these oscillations is reduced with the increase in speed [5A.1]. At a certain speed, the so-called vehicle critical speed, the oscillations become sustained. When only the wheelsets and bogies are involved in the unstable movement, it is referred to as bogie instability or bogie hunting. When the wheel-rail contact conditions lead to low frequency, the carbody sometimes starts to move together with the bogies, and it is referred to as carbody instability or carbody hunting [5A.2]. The hunting phenomenon causes bad ride quality and, in the most severe case, even derailment. Furthermore, the wheelset displacements involved in hunting may make the wheel flange come into contact with the rail gauge corner or the rail gauge face, or both, depending on the rail and wheel profiles. Thus, flange contact forces are generated, which may cause, among other things, two negative effects on the track: wear in the rail gauge face and corner, and track irregularities in alignment and gauge.

Studies on hunting date as early as 1883, when Klingel gave the first mathematical formula of the linear purely kinematic oscillation of a single wheelset. After Klingel, many researchers such as Boedecker, Carter, Rocard and, Matsudaira, contributed to the study of railway vehicle stability. An extensive survey of the different approaches is presented in Knothe et al. [5A.3] and Gilchrist [5A.4]. In the last decades, developments in computer technology have allowed researchers to solve their mathematical models of the vehicle-track interaction in the time domain using numerical simulations. In their work, Bruni et al. [5A.5] presented a mathematical model that can simulate the lateral dynamics of a vehicle on straight track and curve. The model included a multi-body representation of the rail vehicle and a finite element schematization of the track. In their analysis they showed the positive effect of the anti-yaw dampers on the vehicle stability. The increase in the stability threshold by incorporating new wheel profiles was also shown. Sun et al. [5A.6] presented a three-dimensional mathematical model of a freight vehicle and the track, and used it to study the effect of detailed track modeling on hunting. They validated the model by comparing the simulated vehicle critical speed with the one observed in field. The results showed a discrepancy in the critical speed between the rigid and detailed track modeling, which was below 7 %. Lee et al. [5A.7, 5A.8] derived non-linear coupled equations of motion of a 10-DOF freight bogie system moving on both straight and curved tracks, and analyzed the influence of the suspension parameters on the vehicle critical speed. The primary longitudinal stiffness and secondary longitudinal dampers showed the strongest influence on straight track. They also demonstrated that worn wheel treads can enhance hunting. Special emphasis was put on the influence of the primary vertical stiffness and damping, normally neglected in hunting studies. The literature found by the authors has focused on the study of the sustained hunting, by analyzing the influence of different parameters on the vehicle critical speed. This paper presents a study on hunting that focuses on the non-sustained oscillations, whose negative consequences on track wear have been mentioned above and will be used to validate the model.

Rail wear measurements taken from several large-radius curves of the Dutch railways network by a track-monitoring vehicle have revealed an oscillating wear pattern of the rail gauge face and corner. This paper presents a multi-body dynamics model of the leading coach of train type that runs most frequently on one of the measured sections. In order to validate the model, the right values of the vehicle suspension parameters need to be identified from the nominal values. The model is validated by matching the wavelength of the simulated bogie hunting with the one observed in the rail wear measurements. The multi-body dynamics commercial software VI-Rail (formerly ADAMS/Rail) has been used in this work.

5A.2. Modeling description

A three-dimensional passenger vehicle model and its interaction with the track by a multi-body dynamics approach is presented in this paper. The vehicle model corresponds to the leading coach of an electrical multiple unit (EMU) type VIRM of the Dutch railways. Photographs of the EMU's leading coach and its corresponding vehicle model are given in Fig. 5A.1. The vehicle model is composed of four wheelsets, two bogies and a carbody, which are idealized as rigid bodies with their inertia and mass properties as input. The wheel profile in this vehicle is S1002, which can be introduced into the model as new or worn. The primary and secondary suspensions are modeled with springs and dampers, which include non-linear characteristics for some of the suspension elements. Special importance is given to the primary longitudinal suspension and the anti-yaw dampers of the secondary suspension. The anti-yaw and lateral dampers in the secondary suspension present higher damping than the ones of the primary suspension. On the other hand, the vehicle presents stiffer primary than secondary suspension, which is common on passenger vehicles for the sake of passenger comfort. This type of vehicle counts with two bumpstops that constrain the relative lateral displacement between bogie and carbody: a soft bumpstop with a 4 mm clearance and a stiff bumpstop with a 12 mm clearance. Moreover, the soft bumpstop has six times more stiffness than the secondary lateral suspension.

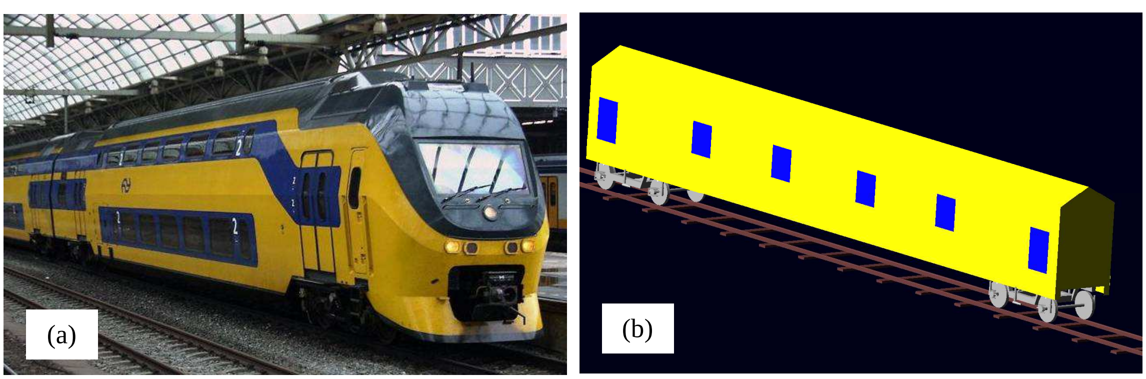

Fig. 5A.1. Leading coach of the EMU: (a) in reality; (b) in the model.

The track is modeled as rigid for the sake of simplicity, keeping in mind the considerations given in Sun et al. [5A.6]. In order to validate the model, the selected measured track section, hereafter called the reference section, is modeled (see Fig. 5A.2). Two types of irregularities are used to excite the system: a) measured lateral track irregularities from the reference section that were taken by a monitoring vehicle of the Dutch network, which are input along the whole section; b) an artificial lateral irregularity located in the constant-radius curve (250 m from the initial position), which consists of a half-cosine lateral deviation of the inner rail with 5 mm zero-to-peak amplitude and 10 m wavelength. The election of 10 m wavelength did not influence the inherent bogie hunting behavior. Simulations with artificial irregularities of 5, 10 and 20 m wavelength showed less than 5 % discrepancy in the wheelset hunting wavelength. In every simulation, the initial vehicle speed was 35 m/s, which corresponds to the observed speed of the vehicle on the reference track; hence, the influence of the speed on bogie hunting was not considered in this paper. Along the constant-radius curve there was a non-compensated acceleration of 0.64 m/s^2 due to cant deficiency.

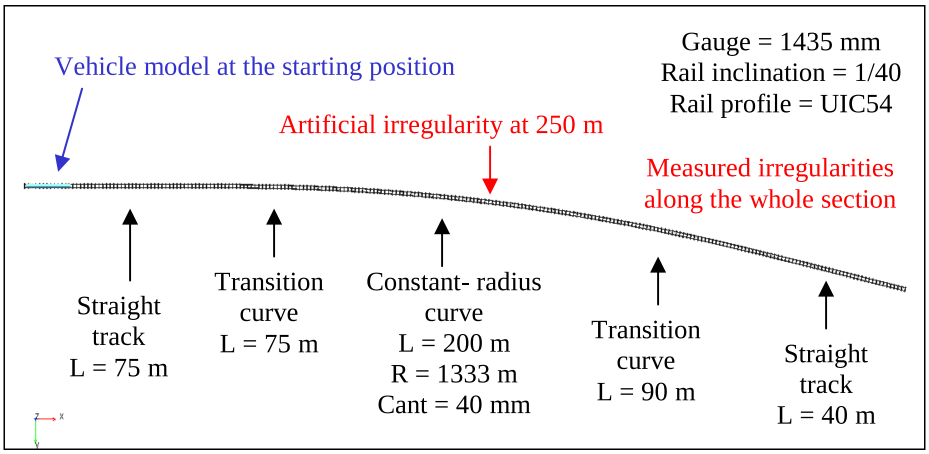

Fig. 5A.2. Modeling of the reference section.

5A.3. Results

Rail (and wheel) wear may be related to the dissipated energy at the wheel-rail contact point [5A.9]. The location of the contact point is determined by the lateral and yaw motions of the wheelset for a given combination of wheel and rail profiles. The validation consists, therefore, of relating the hunting wheelset's motions to the oscillating rail wear observed in the measurements. Since different rolling stock types normally run on a given track section, special emphasis was put to find a measured section in which a single type of vehicle was dominant. On the reference section, only two types of passenger vehicles were running, with the vehicle chosen accounting for 62.5 % of the traffic. The rail wear measurements of the reference track section model are shown in Fig. 5A.3. It must be noted that no rail wear measurements were taken between 274 m and 310 m, as indicated in Fig. 5A.3. Observation of the track layout and the rail wear measurements (see Fig. 5A.2 and Fig. 5A.3) shows a good correlation between the rail wear measurements and the expected location of the contact points. The wear in the gauge corner is the largest on the curve, while top-of-the-rail wear is dominant on the straight track section. For the purpose of validation, special attention was given to the wavelengths of the wear oscillations of the rail gauge corner and face, which were around 6 m and 9 m, as shown in Fig. 5A.3.

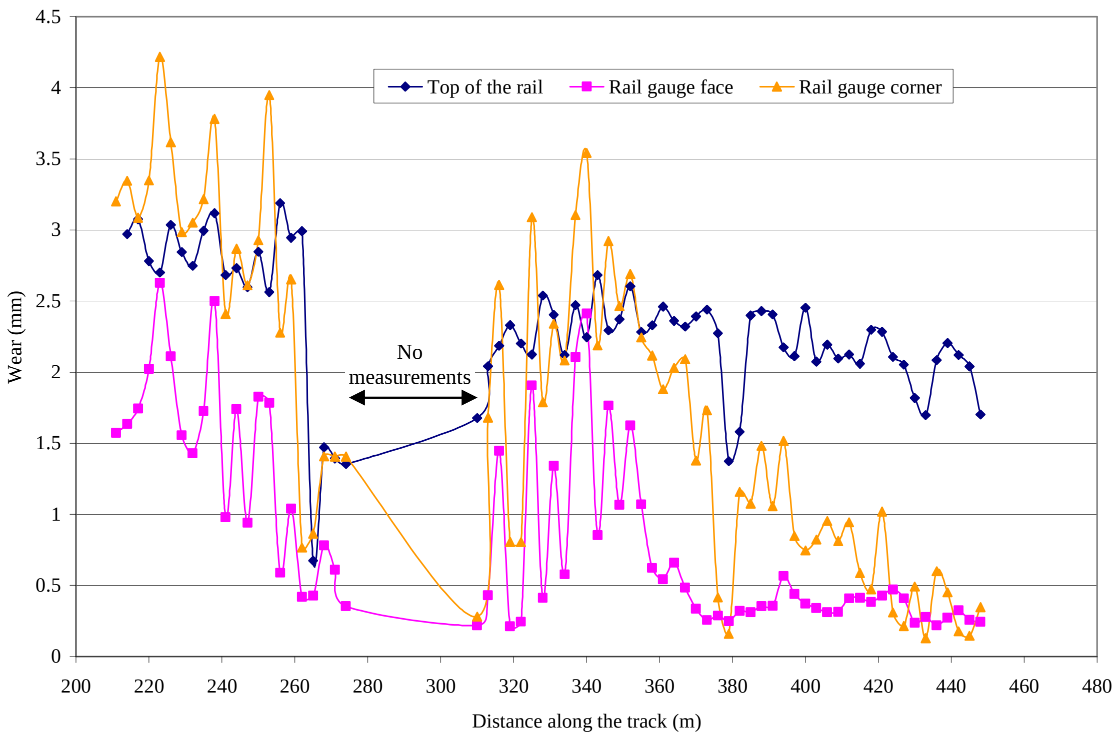

Fig. 5A.3. Rail wear measurements on the reference section.

In order to validate the vehicle model, simulations are performed on the reference track with the two types of irregularities abovementioned. The lateral displacement was found to establish the position of the first contact point, while the second contact point was influenced to a certain extent by the angle of attack (see Fig. 5A.4). When using new wheel and rail profiles, the second contact point was always located on the rail gauge corner at 25 mm from the origin of the rail reference system; therefore, no contact on the rail gauge face was observed. By computing the product between the creepages and the creep forces generated at the wheel-rail contact, a wear indication (so-called wear number in VI-Rail) was obtained.

The variation of wear showed a similar pattern with that of the location of the first contact point on the rail (see Fig. 5A.4). It must be mentioned that the software does not incorporate the wear caused by the second contact point. Furthermore, the wear peaks show that the wear is higher when the contact point is close to the rail gauge corner due to the increase in creepage, which agrees with the rail wear measurements. The model is finally validated by comparing the wavelength of the simulated bogie hunting with the one of the rail gauge corner wear. Since the trailing outer wheels had their first contact point on top of the rail relatively far from the gauge corner, only the leading wheelsets were considered for the validation purposes.

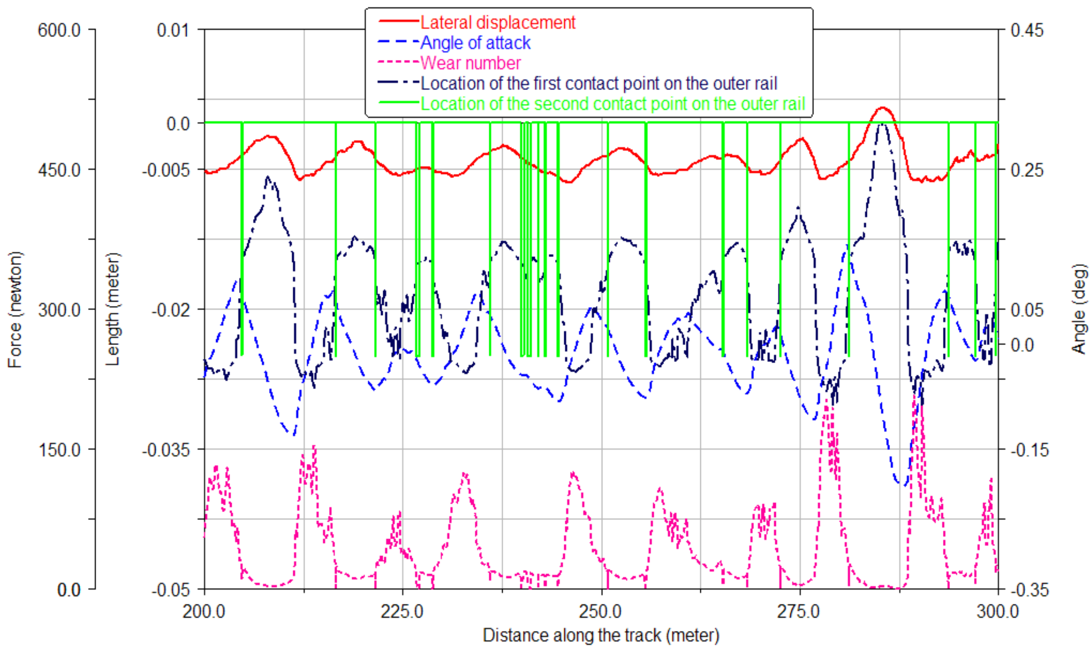

Fig. 5A.4. Representation of the hunting motions, the wear number, and the position of the first and second contact points on the outer rail for the first wheelset of the reference vehicle excited by measured irregularities.

The vehicle was initially modeled with the nominal values—herein called reference vehicle. Later, variations in the suspension parameters were carried out. Due to the forced behavior of the vehicle running on measured irregularities, only the section with artificial irregularities clearly represented the influence of the suspension parameters on bogie hunting. Observations of the wavelengths obtained in the simulations of the artificially excited vehicle led to the conclusion that a reduction of 30-40 % of longitudinal stiffness caused oscillations of the position of the first contact point of the first wheelset with similar wavelengths to those registered in the rail wear measurements around 9 m (see Fig. 5A.5). The oscillations of the third wheelset had a wavelength close to 12 m, as shown in Fig. 5A.6, which was larger due to the bumpstop in the secondary suspension and the different position of front and rear bogies on the curve. Therefore, by assuming that such a reduction in primary longitudinal stiffness is within real figures, the bogie hunting of the vehicle running with new wheel and rail profiles agrees with the rail wear measurements. Furthermore, a 50 % reduction in the stiffness of the soft bumpstop caused the vehicle to hunt with similar wavelengths with the rail wear measurements around 9 m for both first and third wheelsets, as shown in Figs. 5A.5-5A.6.

Besides the results presented here related to the validation of the vehicle model, a parametric study of the influence of vehicle suspension parameters on bogie hunting on both straight and curved track has also been carried out. In addition, the influence of the wheel and rail profiles on hunting behaviour of the vehicle running on a curved track has been studied. The results of these investigations are given in the Appendix.

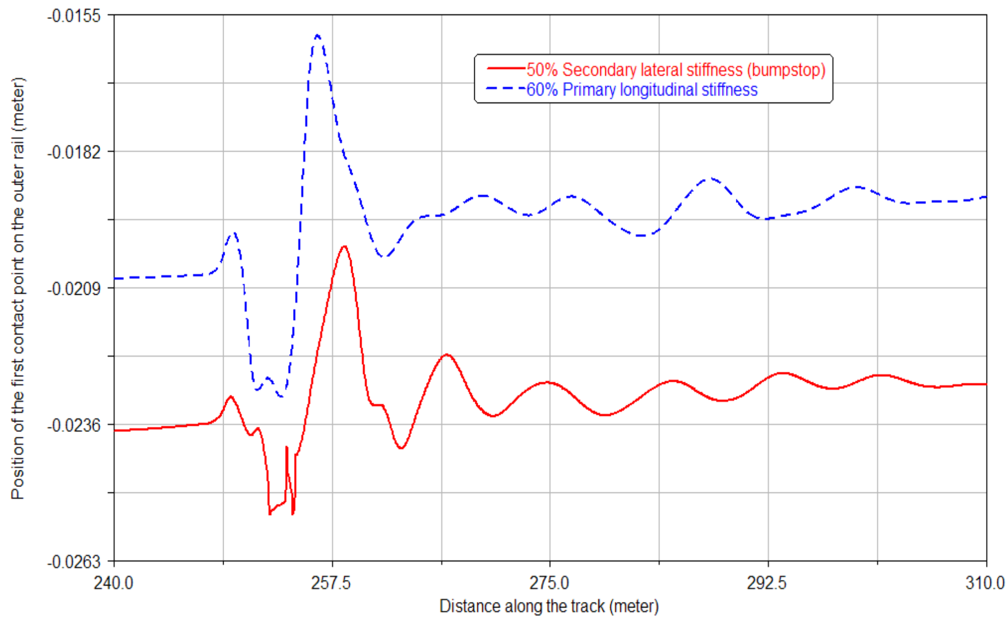

Fig. 5A.5. Variation of the position of the first contact point on the outer rail for the first wheelset for the vehicle running on curved track excited with an artificial irregularity.

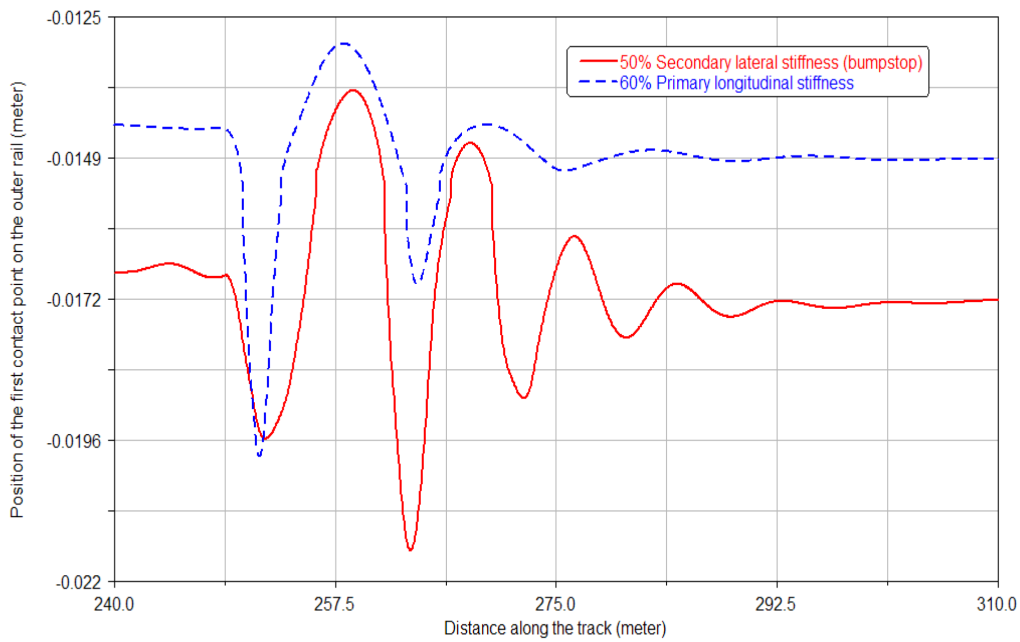

Fig. 5A.6. Variation of the position of the first contact point on the outer rail for the third wheelset for the vehicle running on curved track excited with an artificial irregularity.

5A.4. Conclusions

The multi-body dynamics model of the leading coach of an electrical multiple unit type VIRM of the Dutch railways is presented in this paper. The model has been validated with an oscillating rail wear pattern observed in several large-radius track sections of the Dutch network, which can be attributed to the wheelset hunting motions. The influence of the suspension on bogie hunting has been analyzed. Adjusting some values of the vehicle suspension, the hunting wavelength becomes similar to the one of the wear measurements.

References

[5A.1] A.H. Wickens. Fundamentals of rail vehicle dynamics. Swets & Zeitlinger B.V., Lisse, the Netherlands, 2003.
[5A.2] S. Iwnicki. Handbook of railway vehicle dynamics. Taylor & Francis Group, Boca Raton, 2006.
[5A.3] K. Knothe and F. Bohm. History of stability of railway and road vehicles. Vehicle Sys-tem Dynamics, 31, 283-323, 1999.
[5A.4] A.O. Gilchrist. The long road to solution of the railway hunting and curving problems. Journal of Rail and Rapid Transit, 212, 219-226, 1998.
[5A.5] S. Bruni, A. Collina, G. Diana and P. Vanolo. Lateral dynamics of a railway vehicle in tangent track and curve: tests and simulation. Vehicle System Dynamics, 33, 464-477, 1999.
[5A.6] Y.Q. Sun, M. Dhanasekar and D. Roach. A three-dimensional model for the lateral and vertical dynamics of wagon-track systems. Journal of Rail and Rapid Transit, 217, 31-45, 2003.
[5A.7] S.Y. Lee and Y.C. Cheng. Hunting stability analysis of high-speed railway vehicle trucks on tangent tracks. Journal of Sound and Vibration, 282, 881-898, 2005.
[5A.8] S.Y. Lee and Y.C. Cheng. Nonlinear analysis on hunting stability for high-speed rail-way vehicle trucks on curved tracks. Journal of Vibration and Acoustics, 127, 324-332, 2005.
[5A.9] F. Braghin, R. Lewis, R.S. Dwyer-Joyce, S. Bruni: A mathematical model to predict railway wheel profile evolution due to wear. Wear 261 (2006) 1253–1264.

Chapter 5, Part B

Curve behaviour in low adhesion[XIII]

ABSTRACT

Migration of the flange lubricant to the top of the high rail may compromise the traction of a rail vehicle and affect its curving behaviour. In order to simulate this possible situation, a lubrication model has been coupled to commercial multi-body dynamics software to describe the tangential formulation of the lubricated high-rail contact. Different friction levels have been adopted for the low rail to study their influence on the curving behaviour and traction. Since the creep force in the wheel-rail contact approaches saturation of the friction, the traction control unit of the rail vehicle under study has also been modelled to account for the reduction of the wheel axle torque in the presence of wheel macro-slip.

[XIII] This chapter has been published as:
O. Arias-Cuevas, Z. Li, R.I. Popovici, D.J. Schipper: Simulation of Curving Behaviour Under High Traction in Lubricated Wheel-Rail Contacts. In press, Vehicle System Dynamics (2010).

5B.1. Introduction

The curving behaviour of a rail vehicle is dependent on the yaw stiffness, track curvature, vehicle speed, traction/braking forces, the profiles of the wheel and rail, and the coefficient of friction (COF) at the wheel-rail interface [5B.1-5B.3]. In adverse conditions, excessive (micro-) slip and high contact stresses can occur in the contact patch of the high rail, which may lead to increased wear of the wheel flange and rail gauge corner/face, higher energy consumption, and occurrence of wheel flange noise. In order to reduce these negative effects, flange lubrication on curve has become an extensive practice in the majority of the railway networks around the world [5B.4-5B.6]. However, excessive application due to a malfunction of the applicator can result in migration of the lubricant to the top of the rail. This has been reported to be a cause of low adhesion in some countries [5B.7]. Locomotive sand has occasionally been observed at a lubrication site close to a station in the Netherlands, indicating that some driven wheels had experienced macro-slip.

When applying a wheel axle torque, the tangential force that the wheel can exert on the rail is limited by the COF and the normal load in the contact. Most of the lubricants can decrease the COF to values far below those required for normal traction and braking operation, depending on the lubrication regime. Nowadays, railway vehicles are fitted with traction control (TC) and wheel slide protection (WSP) systems, which adjust the traction and braking efforts, respectively, according to the friction available at the wheel-rail contact so that excessive macro-slip is diminished. Moreover, it is well-known that the friction required in the wheel-rail contact for traction can be as much as three times higher than that required for braking operation so that rail vehicles are more prone to experience low adhesion during traction operation. In order to analyze the impact of lubrication present on the top of the high rail, the curving behaviour of a rail vehicle under high traction is simulated in this paper considering different friction levels on the low rail.

In multi-body dynamics simulations the most widely used theory for the calculation of the creep forces is the non-linear simplified theory of Kalker implemented in his code FASTSIM [5B.8]. The major advantages of the code are the short computational time and reasonable accuracy for moderate values of spin creepage with respect to the exact theory of Kalker implemented in his code CONTACT [5B.8]. Alternative theories to FASTSIM that reduce the computational time are Shen-Hedrick-Elkins model [5B.9] and the code of Polach [5B.10]; however, their accuracy decreases with the spin. All the abovementioned theories consider the wheel-rail interface as a clean steel-on-steel contact. Furthermore, the COF was assumed to have a constant value so that the decrease of the COF with slip, which normally occurs at high slip in dry clean contacts, was ignored. In recent years, this shortcoming has been tackled by some researchers. Polach [5B.11] introduced a number of proportionality coefficients in his code to improve the approximation of his calculated traction curves to those measured under operating conditions on both dry and wet contacts. Giménez et al. [5B.12] modified the formulation of FASTSIM to allow for a kinetic and static COF for the slip and adhesion areas of the contact patch, respectively. Their model was used for curving simulations in order to study the occurrence of squeal noise on tight curves, for which the decreasing slope of the traction curve is responsible [5B.13]. Matsumoto et al. [5B.14] introduced the thin film lubrication theory into

FASTSIM to model the mixed lubrication contact in the presence of a friction modifier. The results of their model were validated against laboratory measurements undertaken with a twin-disc roller rig.

In this paper, a mixed lubrication model, which is developed by the co-authors and which has been validated against twin-disc laboratory measurements [5B.15], has been used to calculate the creep forces in the lubricated contact occurring on the high rail of the curve. In the lubrication model, the wheel-rail contact is assumed to be elliptical and flat. The model considers the rheological properties of the lubricant to generate the longitudinal and lateral friction forces for a given contact conditions (i.e. pressure and surface roughness, among others), speed and creepage. In order to reduce the computational time, an accurate curve fitting of the lubrication model is employed in the simulations. The lubricant selected for this work consists of a thin grease, which is currently applied trackside in many curved sections of the Dutch network [5B.16]. The vehicle dynamics have been simulated with the commercial multi-body dynamics software VI-Rail (formerly ADAMS/Rail), to which the lubrication model has been coupled for the creep forces calculation of the wheel-rail contacts on the high rail. Since the purpose of the paper is to examine the consequences of migration of the lubricant to the top of the rail, it has been assumed that the lubricant is present on the high rail not only on the gauge corner and gage face, but also on the top of the rail. The COF of the low rail has been varied according to some measured traction curves values incorporated in FASTSIM. In order to account for the torque regulation of the TC unit operating under low adhesion conditions, a TC model has been built up by means of MATLAB/Simulink. In this way, a co-simulation between both software packages is carried out with the module ADAMS/Controls to analyze the curving behaviour of tractive wheels close or at the limiting adhesion.

5B.2. Models description

5B.2.1. Vehicle model

In this work a model of the leading coach of an electrical multiple unit, which is used by the Dutch Railways, is employed in the simulations, see Fig. 5B.1 (a). The model was validated in previous work against a measured oscillating rail wear due to hunting observed on shallow curves [5B.17]. The vehicle model consists of 7 rigid bodies representing the carbody and the two bogies with two solid wheelsets, of which the axles of the rear bogie are driven. The linear and non-linear characteristics of the primary and secondary suspension are included in the model. New S1002 profile is considered for the wheels. The drive line, i.e., motor, gear box and so on, has not been modelled explicitly; instead, their mass and inertia have been included in the points of support of both bogie and wheelset.

To simulate the traction operation, a torque is applied on the inertia reference frame of the driven wheel axles. The maximum torque-speed characteristic of the motor, which is shown in Fig. 5B.1 (b), is included in the model to account for the limitation of the motor torque with speed. In practice, the actual torque requested by the driver may be lower than that shown in Fig. 5B.1 (b), but considering the scope of the paper it is assumed that the driver is requesting the maximum traction possible. In the model, it is assumed that the torque provided by each motor is the same. Although both motors are regulated by the same TC unit, this last assumption may not necessarily hold in all operating conditions as the motors may experience different loading conditions depending on their electrical coupling, which has not been considered in this work. The modelling of the regulation of the wheel torque according to the wheel slip is given in the next Section.

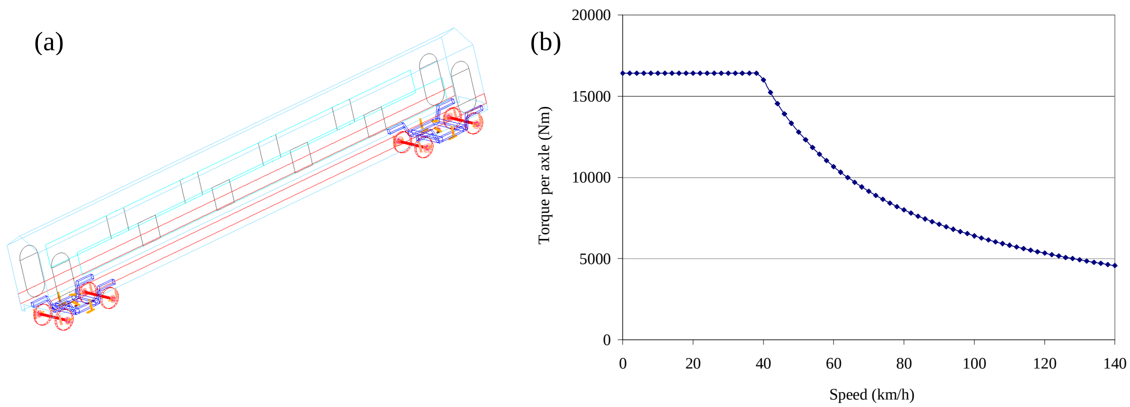

Fig. 5B.1. Representation of: (a) the vehicle model; (b) torque-speed characteristic of the motor.

5B.2.2. Traction control model

The TC unit has been modelled by means of MATLAB/Simulink. In the vehicle under consideration the slip threshold is determined with an estimated torque as reference of the applied torque on the axles according to Eq. 5B.1 and as depicted in Fig. 5B.2 (a). The parameters *A*, *B*, and *C* can be adjusted within a certain range, but in this work some default values are taken. At each time step of the co-simulation, the angular acceleration ($\ddot{\alpha}$) and estimated wheel axle torque (T_{est}) of each wheelset are evaluated. If the angular acceleration of any wheelset surpasses the calculated critical threshold ($\ddot{\alpha}_{crit}$) as given in Eq. 5B.1, macro-slip is detected and the TC unit takes control of the wheel axle torque over the driver.

$$\ddot{\alpha}_{crit} = A - \frac{(B-A)}{C} T_{est} \tag{5B.1}$$

Fig. 5B.2 (b) shows a simplified example of the actual torque regulation once the wheels experience macro-slip due to, for instance, the presence of some contamination on the track. If the available friction (given by the red dashed line in Fig. 5B.2 (b)) is higher than the adhesion requirements of the torque requested by the driver, T_{ref} (represented by the green dash-dot line), no macro-slip is detected and the output of the TC unit, T_{out} (given with the blue solid line), equals T_{ref}. Once the friction level falls below the adhesion required, e.g. due to the presence of some grease on the rail surface, the driven wheels accelerate above $\ddot{\alpha}_{crit}$ and macro-slip is detected by the TC unit. Accordingly, T_{out} is reduced with a slope K_1 until no macro-slip has been detected in a period t_1 (see Fig. 5B.2 (b)). Then, T_{out} is maintained (K_2 = 0) for a period t_2, followed by two increases with slopes and periods (K_3, t_3) and (K_4, t_4), until T_{out} equals T_{ref}. This forms a complete cycle of the TC. Although it is not explicitly indicated in Fig. 5B.2 (b), it can be understood that if macro-slip is detected again while increasing the torque towards the driver's request, T_{out} is immediately decreased with K_1 and a complete TC cycle starts again. The slopes and periods of the torque regulation can be adjusted in the control unit within a certain range; however, only some default values have been used on this paper. The MATLAB/Stateflow application has been used to model the torque regulation algorithm represented in Fig. 5B.2 (b), in which slip, T_{ref}, and simulation time are taken as inputs to produce the T_{out} as output.

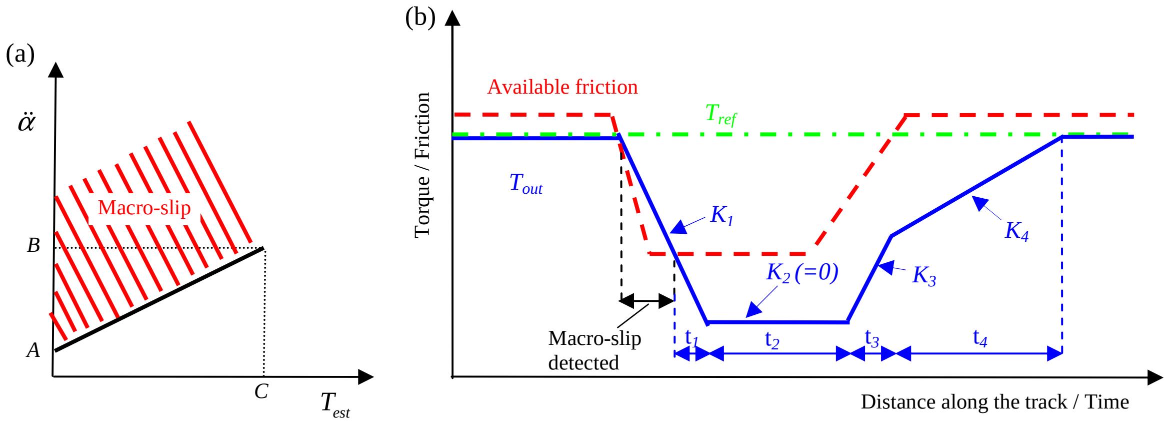

Fig. 5B.2. Representation of: a) slip calculation model; b) torque regulation in low adhesion conditions.

5B.2.3. Lubrication model

The slip, or creepage (S), generated during the rolling-sliding motion of a tractive wheel over a rail can be expressed by the quotient between the relative velocity (v^{rel}) and the sum velocity (v^{+}), as shown in Eq. 5B.2. Where, v_w and v_r are the velocities of an underformed material particle belonging to the wheel and the rail surfaces in contact, respectively.

$$S = \frac{v^{rel}}{0.5 \cdot v^{+}} = \frac{(v_w - v_r)}{0.5 \cdot (v_w + v_r)} \tag{5B.2}$$

In the presence of lubrication in the contact, three regimes can be distinguished: 1) the boundary lubrication (BL) regime, in which the sum velocity of the wheel is low and the load is carried solely by interacting asperities of the opposing surfaces; 2) the elasto-hydrodynamic lubrication (EHL) regime, which occurs at high sum velocities when the load is carried by the pressure generated in the lubricant so that the friction is controlled by the shearing of the lubricant; 3) the mixed lubrication (ML) regime, which is the transition between the two former regimes, at which the load is carried by the asperities as well as by the pressure generated in the lubricant. The transition between these regimes in the sum velocity range is given by the so-called Stribeck curve [5B.18]. In general, it can be said that the shape and values of the Stribeck curve mostly depend on the rheological properties of the lubricant under consideration and on the contact conditions, such as the slip, the contact pressure and the surface roughness (among others) [5B.15]. A generalized example of the Stribeck curve is shown in Fig. 5B.3, in which a schematic representation of the interacting wheel and rail surfaces under the different regimes is also given.

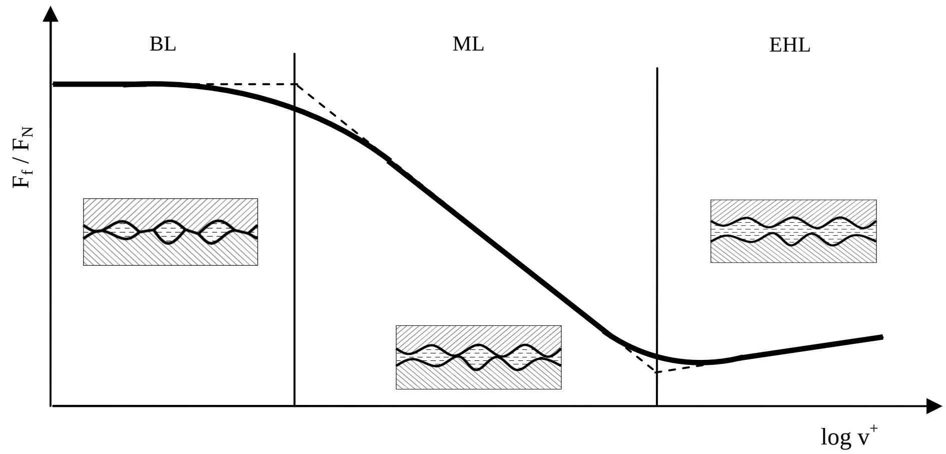

Fig. 5B.3. Generalized Stribeck curve representing the different regimes of lubrication.

The lubrication model used in this work considers the BL and EHL components of the friction force as well as its transition in the ML regime; therefore, it is referred herein as mixed lubrication model. In the model the wheel-rail contact is assumed to be a flat elliptical area, in which the total creepage (*S)* is computed according to Eq. 5B.3 for a given longitudinal and lateral creepage (S_x, S_y). It must be mentioned that the slip is used in the whole paper in its non-dimensional form, unless a percentage symbol is explicitly indicated. When the angle of attack of the wheelset is below 45 mrad, the sum velocity can be approximated as shown in Eq. 5B.4 [5B.15]. Where, w_w is the rotational velocity of the wheel (in rad/s), r_w is the rolling radius of the wheel at the contact point (in m), and V is the train forward velocity (in m/s).

$$S = \sqrt{S_x^{\ 2} + S_y^{\ 2}} = \frac{\sqrt{\left(v_x^{\ rel}\right)^2 + \left(v_y^{\ rel}\right)^2}}{0.5 \cdot v^+} \tag{5B.3}$$

$$v^+ \approx V + w_w \cdot r_w \tag{5B.4}$$

5B.2.3.1. Boundary component

The friction force generated at the asperity level is calculated assuming that the friction between asperities is of the Coulomb type with a coefficient of friction (f_C) constant for all asperities. According to [5B.15], the friction force in the BL regime can be expressed as given in Eq. 5B.5, where f_C is the coefficient of friction in BL regime and S_{ep} is the slip at which the elastic to plastic transition of the boundary layer is observed in the traction curve. Both parameters, f_C and S_{ep}, need to be determined experimentally for the lubricant under consideration. The so-called surface force apparatus is used to determine f_C by pressing and sliding a ball shaped specimen (representing the wheel tread) against the top of a rail. In order to obtain S_{ep}, twin-disc tests have to be carried out at very low rolling speeds. Furthermore, the load carried by asperities, F_C, is calculated considering the wheel as a rigid flat surface and the rail as a rough surface [5B.15]. In this work a rail roughness of R_a = 1 μm is considered, which corresponds to representative values measured on the top of rails during some field tests. Although not shown in this work, it can be understood that rougher wheel and rail surfaces in contact normally lead to a wider speed range of BL regime.

$$F_{f,BL} = f_C F_C \frac{2}{\pi} \arctan\left(\frac{\pi}{2}\frac{S}{S_{ep}}\right) \tag{5B.5}$$

5B.2.3.2. Hydrodynamic component

The friction force in the EHL regime is considered to be generated by shearing the lubricant between the contacting bodies according to the Eyring model [5B.19] as indicated in Eq. 5B.6. Where, τ_0 is the Eyring shear stress (in Pa), A_H is the hydrodynamic area (in m^2), h_c is the central film thickness (in m), η is the lubricant viscosity (in Pa·s), and v^+ is the sum velocity (in m/s) as given in Eq. 5B.4. The Eyring shear stress is a rheological property of the lubricant that needs to be determined experimentally [5B.16]. The central film thickness and hydrodynamic area are determined by solving the typical system of three equations, i.e. Reynolds, film shape, and load balance [5B.15, 5B.16].

$$F_{f,EHL} = \tau_0 A_H \operatorname{arcsinh}\left(\frac{\eta S v^+}{2\tau_0 h_c}\right) \tag{5B.6}$$

The viscosity of the lubricant (η) is considered to vary with pressure, p (in Pa) as given in Eq. 5B.7, according to the equation of Roelands [5B.20]. Where, η_0 is the viscosity (in Pa·s) at ambient pressure and z is the viscosity-pressure index (non-dimensional). These two rheological properties of the lubricant need to be determined experimentally [5B.16].

$$\eta(p) = 6.315\cdot 10^{-5} \exp\left\{\left[\left(1+\frac{p}{1.962\cdot 10^{8}}\right)^{z} - 1\right]\ln\left(\frac{\eta_0}{6.315\cdot 10^{-5}}\right)\right\} \tag{5B.7}$$

5B.2.3.3. Mixed lubrication model

The friction force in the mixed lubrication model takes into account the summation of the boundary and the hydrodynamic components as shown in Eq. 5B.8. Moreover, this total friction force is decomposed into the longitudinal and lateral directions according to Eqs. 5B.9-10, where the negative sign indicates that the force acts in the opposite direction of the slip.

$$F_f = F_{f,BL} + F_{f,EHL} = \left[f_C F_C \frac{2}{\pi} \arctan\left(\frac{\pi}{2}\frac{S}{S_{ep}}\right) + \tau_0 A_H \operatorname{arcsinh}\left(\frac{\eta S v^+}{2\tau_0 h_c}\right)\right] \tag{5B.8}$$

$$F_{fx} = \frac{-S_x}{S}\cdot F_f \tag{5B.9}$$

$$F_{fy} = \frac{-S_y}{S} \cdot F_f \qquad (5B.10)$$

Some results of the non-dimensional friction force for different ranges of sum velocity and slip are given in Fig. 5B.4. It can be seen from the Stribeck curves that the transition to EHL occurs at around 1 m/s with the lubricant considered in this work. Looking at each of the traction curves given in Fig. 5B.4 (b) it can be observed that the non-dimensional tangential force always increases with the slip, firstly with an abrupt slope at low values of slip and then followed by a gentler positive slope.

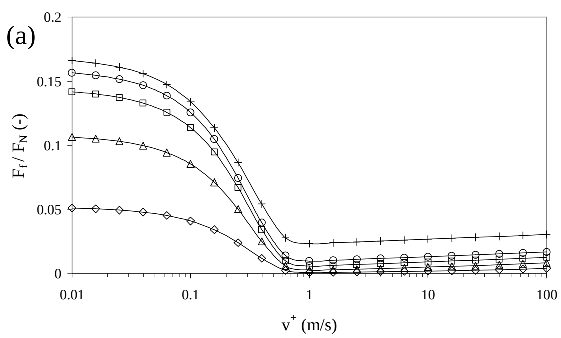

Fig. 5B.4. (a) Stribeck curve for different input slip values: ◊ 0.005, Δ 0.015, □ 0.04, ○ 0.1 and + 2; (b) traction curve for different input sum velocities: ◊ 0.01, Δ 0.1, □ 0.3, ○ 0.8 and + 10 m/s.

5B.2.3.4. Approximation of the mixed lubrication model

Due to the complexity of the mixed lubrication model and the associated long computational time required for each calculation step, a direct coupling to the multi-body dynamics software is impractical. Hence, an approximation of the mixed lubrication model was found with an empirical fit function, which takes as inputs the sum velocity and the slip, as shown in Eq. 5B.11.

$$F_f\left(v^+, S\right) = \left[\left(0.027 + \frac{0.2166}{1+10^{2.822 \cdot v^+ - 0.2979}}\right) \cdot \exp\left\{\frac{-\left[\ln\left(S \cdot 100\right) - 6.8837\right]^2}{25.6209}\right\}\right] F_N \qquad (5B.11)$$

In Fig. 5B.5 results obtained with both approaches are plotted. It can be seen that there exists a very good agreement between the mixed lubrication model and its approximation with an average relative error for the Stribeck curve of 5% and for the traction curve of only 2%. One source of error of the approximation comes from the variations in the contact pressure and the ellipse shape of the contact area that can occur as a wheelset negotiates curves, which may influence the viscosity of the considered lubricant (see Eq. 5B.5) and the shear rate through the film thickness. However, these changes are found to have a negligible influence in the EHL regime, as shown in Fig. 5B.6 for a range of lateral displacements of the wheelset on the track. Since the vehicle speed of the simulations carried out in this work are to be considerably larger than 1 m/s, which has been observed to be the transition velocity to EHL regime for the lubricant under consideration, the approximation remains a valid approach for this study.

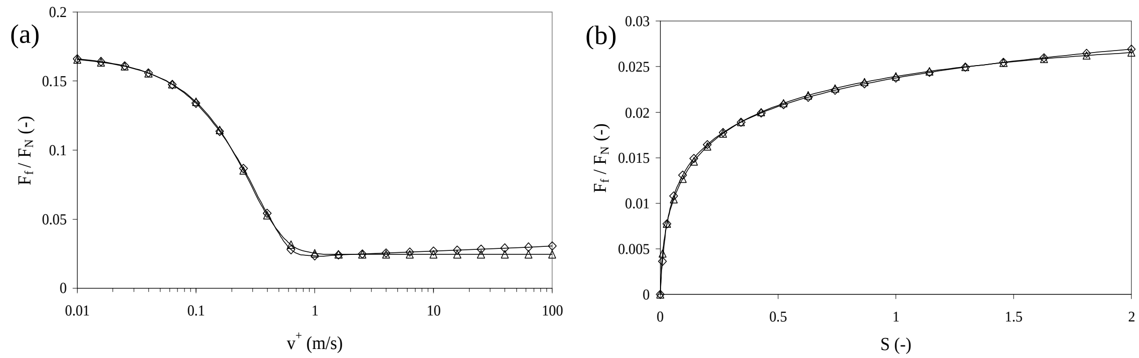

Fig. 5B.5. (a) Stribeck curve (for S = 2) predicted with the exact model (◊) and approximation (Δ); (b) traction curve (for v^+ = 10 m/s) predicted with the exact model (◊) and approximation (Δ).

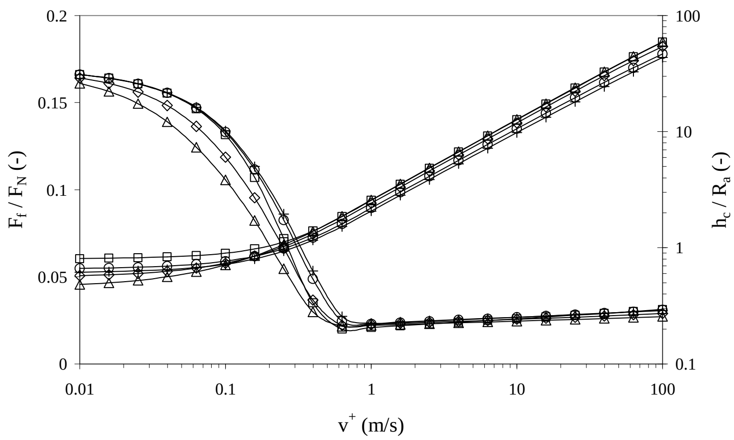

Fig. 5B.6. Stribeck curve and film thickness-roughness ratio for different lateral positions of the wheelset on the track: ◊ -5 mm, Δ -3 mm, □ 0 mm, ○ +3 mm, and + +5 mm (S1002 and UIC54 are the wheel and rail profiles).

5B.2.4. Coupling between models

The vehicle together with the track on which it runs, is modelled and simulated in VI-Rail. In the co-simulation between VI-Rail and MATLAB/Simulink, the programs exchange a flow of data as indicated in Fig. 5B.7. The frequency of data exchange is fixed according to the sampling rate of the TC unit. The typical cycles taken in the calculation of each simulation step in the ADAMS/VI-Rail subsystem are given in Fig. 5B.8. Moreover, the lubrication model used for the tangential formulation for the high-rail contact points is coupled to VI-Rail by means of a custom dynamic library, taking creepages and vehicle speed as inputs to calculate Eqs. 5B.7-9.

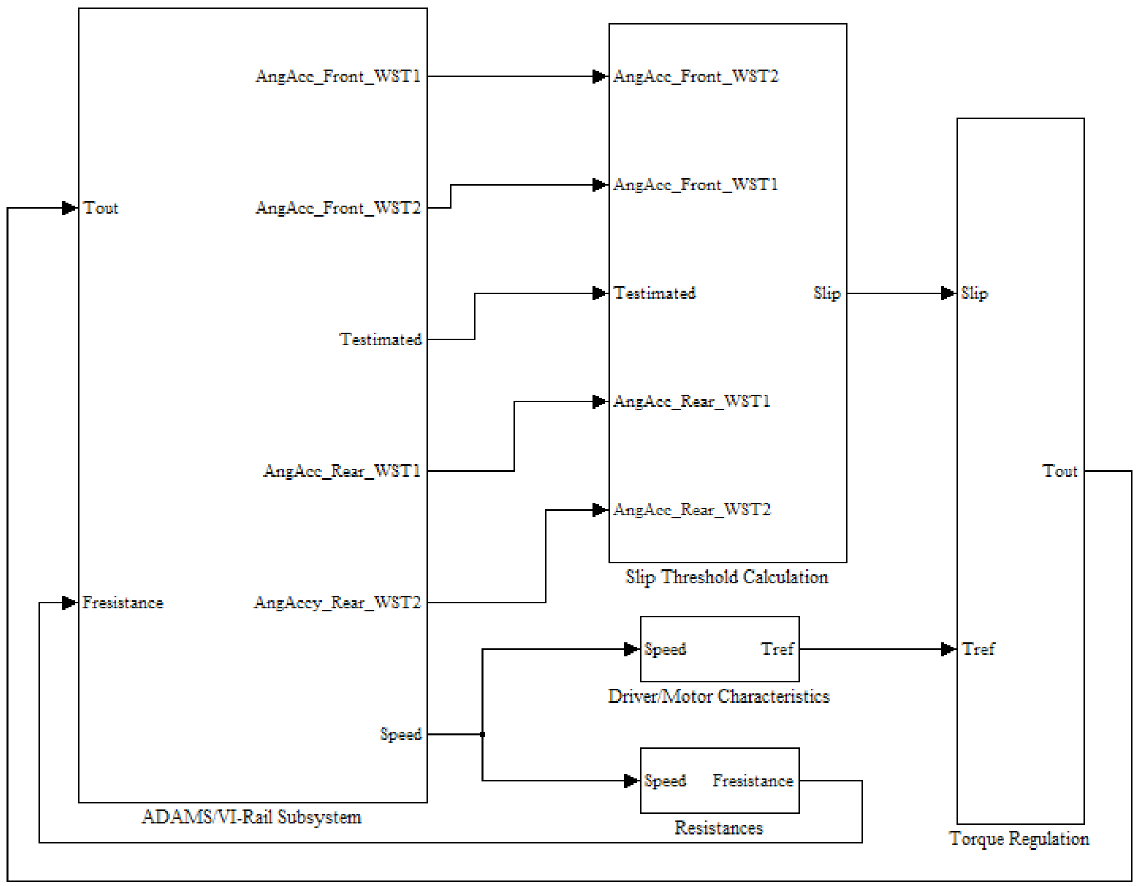

Fig. 5B.7. Co-simulation chart of the information exchange between ADAMS/VI-Rail and MATLAB/Simulink.

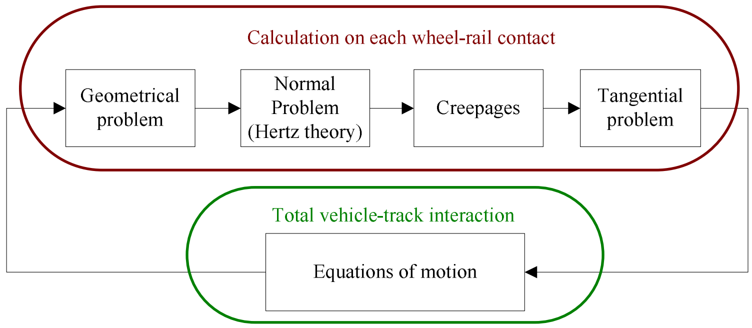

Fig. 5B.8. Simplified diagram of the calculation cycles undertaken in the ADAMS/VI-Rail subsystem.

5B.3. Results

The simulations have been run on a curve of 500 m radius with new UIC54 rail profile. Prior to the constant-radius curve, the vehicle travels through a small section of straight track followed by a transition curve. Once entering the constant-radius curve, steady state curving is reached. In the results presented in this paper, the initial condition is considered to be after reaching the steady state along the constant-radius curve. In these defined initial conditions the vehicle speed is around 10 m/s (see Fig. 5B.11), increasing further in time as a consequence of the applied traction. Two values for the track cant have been modelled, namely 5 and 20 mrad, which yield a balance speed of 5 and 10 m/s, respectively. In this way, the influence of the balance speed could also be investigated. In the defined initial conditions, the driving torque applied on the wheel axle is slightly above 4300 Nm, as will be shown in Fig. 5B.10. The torque increases in time according to the driver and motor characteristics explained in Section 5B.2.1, unless macro-slip is detected and, therefore, the wheel axle torque is controlled by the TC unit.

Different solution methods for the tangential problem have been used for the contact patches of right and left wheels to account for the different friction conditions. In the simulations, the lubricant is assumed to be present not only on the gauge face/corner, but also on the top of the (high) rail. The lubrication model has been used to obtain the friction forces of all wheel-rail contacts on the high rail. Note that the left wheels are in contact with the high rail in all simulations carried out. It must be noted that for the wheel-rail profile combination used in the simulation conditions, only one contact point was observed on the high rail for each wheel, which was either on the rail gauge corner or on the top of the rail, depending on the lateral displacement and angle of attack of the wheelset.

For the low rail, measured traction curves have been incorporated into FASTSIM to model actual traction conditions. These input traction curves, which are depicted in Fig. 5B.9 (a), represent typical values of those measured with a trainborne tribometer on the Dutch railway network in autumn 2008 [5B.15]. Since these measurements were restricted to a 15% slip, the traction coefficient has been assumed to remain constant for higher slip (see Fig. 5B.9 (a)). It must be noted that this approximation may not necessarily be very accurate due to the thermal effects occurring at higher slip. Moreover, the notation dry, which has been used to denominate the measured traction curves, does not mean that the contact was not contaminated during the measurements. It has been shown in the laboratory that clean dry steel-on-steel contact yields a COF around 0.6 [5B.21]. It must be noted that the color and line convention used in Fig. 5B.9 (a) will be followed to present the results obtained with friction conditions adopted for the low rail. In addition, Fig. 5B.9 (b) depicts the absolute value of the decreasing slope of the traction curves given in Fig. 5B.9 (a). This decreasing slope starts from the maximum in the traction coefficient, which occurs at around 2.5% of longitudinal creepage for the measured curves.

5B.3.1. Traction

The wheel axle torque during curve negotiation is given in Fig. 5B.10 for all simulated friction conditions in both cases of initially balanced and unbalance speed. Note that the same wheel axle torque is applied to both driven axles, as explained in Section 5B.2.1. In Fig. 5B.10 it can be seen that initially the torque increases linearly according to the driver's requirements until either the motor's speed limits are reached (e.g., dry0.40 and dry0.45) or macro-slip is detected by the TC unit (e.g., dry0.35, dry0.30 and dry0.20). The increase in torque has to be sustained by the tangential forces occurring at the wheel-rail contacts, but the low friction available on the lubricated high rail enforces the low rail to bear most of the traction force. The simulation results show that no macro-slip is detected by the TC unit when the COF on the low rail is equal or higher than 0.40. Correspondingly, the curves of Tout and vehicle speed for the cases dry0.40 and dry0.45 overlap in Figs. 5B.10-5B.11. On the other hand, lowering the COF of the low rail leads to a faster occurrence (and detection) of macro-slip, as expected. This results in an earlier decrease of the wheel axle torque by the TC unit (see Fig. 5B.10).

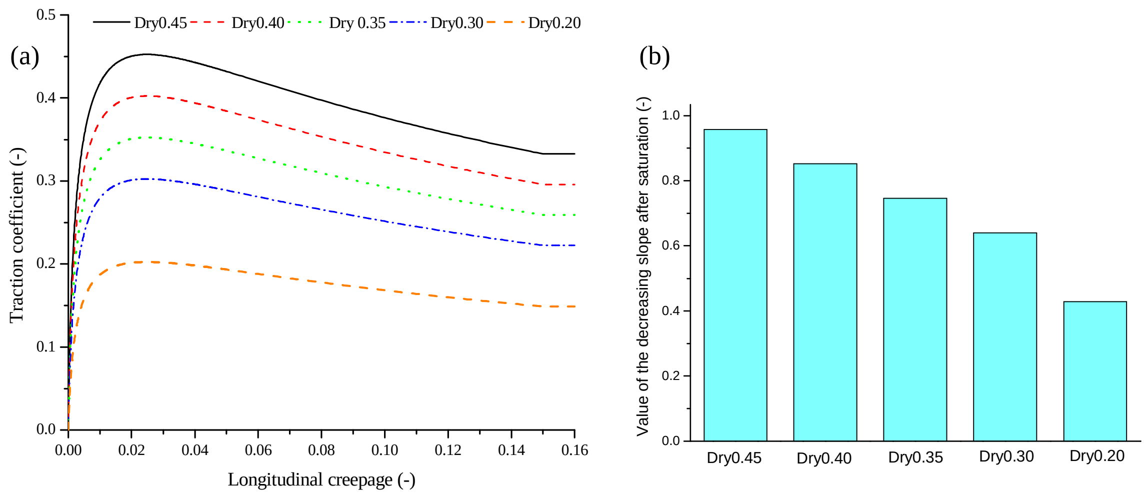

Fig. 5B.9. (a) Measured traction curves used as input to FASTSIM to calculate creep forces on the low rail; (b) value of the decreasing slope of the traction curves.

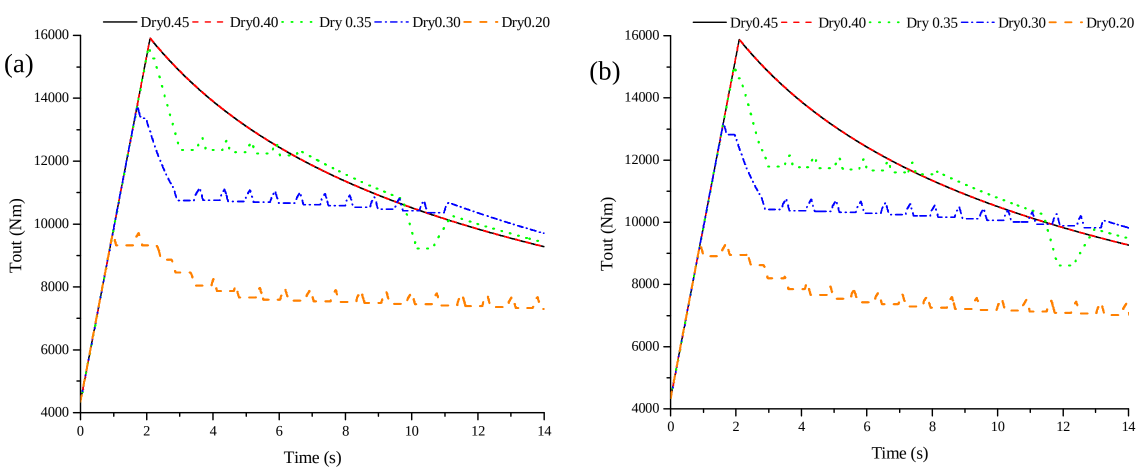

Fig. 5B.10. Wheel axle torque for cases with: (a) initially balanced speed; (b) initially unbalanced speed.

It is worthwhile to mention that the decrease in torque observed at around 10 s for the dry0.35 simulation in Fig. 5B.10 (a) is due to the transition from full sliding conditions (or macro-slip) to micro-slip, as it will be shown in Figs. 5B.12-5B.15. It can also be seen in Fig. 5B.10 that a sequence of cycles of torque regulation occurs in the cases dry0.35, dry0.30 and dry0.20. In comparison with the simplified example given in Fig. 5B.2b, the cycle shown in Fig. 5B.10 is constantly interrupted during the torque increase, i.e. Tout does not reach Tref, because wheel macro-slip is again detected by the TC unit. This is due to the low (constant) friction level of the simulated case, which is insufficient for the traction effort requested by the driver. In the dry0.35 case, Tout reaches Tref at around 7 s of simulation after five cycles of torque regulation, as shown in Fig. 5B.10 (a). On the other hand, Tout never reaches Tref in the dry0.20 case because the friction level is still insufficient. Due to the reduced torque on the wheel axle, lower final vehicle speeds are reached when having lower COF on the low rail, as shown in Fig. 5B.11.

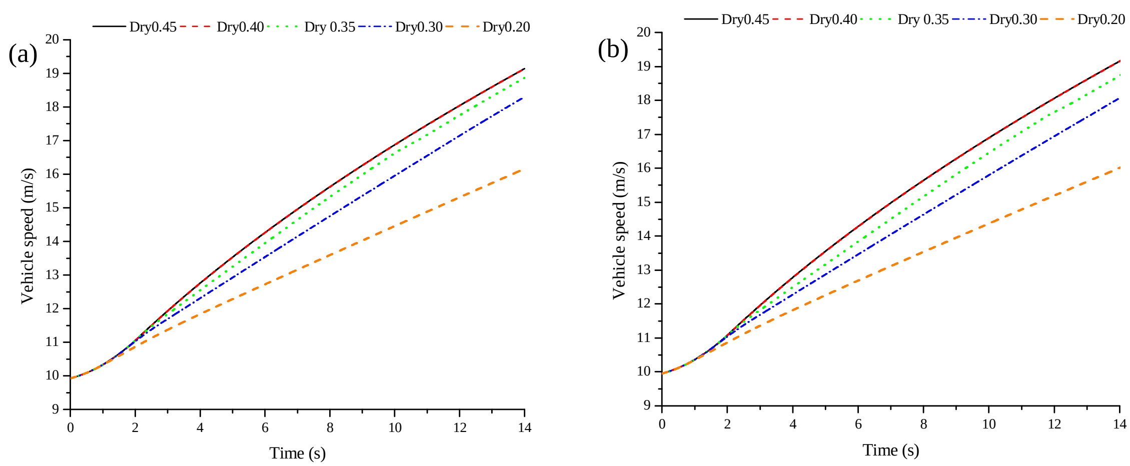

Fig. 5B.11. Vehicle speed for cases with: (a) initially balanced speed; (b) initially unbalanced speed.

Comparing Figs. 5B.10 (a) and (b), it is observed that the initially unbalanced speed causes a faster detection of macro-slip, which leads to an earlier reduction of the wheel axle torque for the three cases dry0.35, dry0.30 and dry0.20. This is a consequence of the different position and orientation of the wheelsets on the track during curve negotiation, which leads to different longitudinal creepage and, therefore, occurrence (and detection) of macro-slip.

In Figs. 5B.12-5B.15 the longitudinal creepage of the left (a) and right (b) wheels of the motorized bogie are given for both initially balanced and unbalanced speed cases. Note that the sign convention is that it is positive in the rolling direction. Macro-slip is observed to occur in all simulated cases where COF of the low rail is below 0.40. Although for each friction case the torque applied to the two driven axles is the same, only the first driven axle experiences macro-slip. The maximum longitudinal creepage reached in the wheel-rail contact is around 30% for the first driven axle, and a bit less than 2% for the second driven axle. The different creepage evolution between the two axles is due to the curving properties of the motorized bogie, which will be explained in Section 5B.3.2.

Despite the fact that decreasing the COF on the low rail leads to a faster occurrence of macro-slip, the longitudinal creepage reaches its maximum earlier for the case dry0.35 than dry0.20, as shown in Figs. 5B.12 and 5B.14. This can be understood by examining both the traction curves presented in Fig. 5B.9 and the functioning of the TC unit. On one hand, traction curves with higher COF have a steeper decreasing slope after reaching saturation, as shown in Fig. 5B.9 (b). This means that for the same torque increase more macro-slip arises. On the other hand, the TC unit monitors the accelerations of the driven axles for the possible occurrence of macro-slip in a fixed time interval during the application of traction. Therefore, when the tangential forces are close to saturation an increase in the motor torque can lead to a more rapid increase in the longitudinal creepage for friction conditions of steeper decreasing slope. This can be observed by looking at the increasing slope of the longitudinal creepage in the cases with macro-slip in Figs. 5B.12 and 5B.14, which is steeper for cases with higher COF (e.g. dry0.35 is the steepest). Moreover, it can be understood that this increasing slope of the longitudinal creepage upon full sliding conditions would be minimum if one uses the original formulation of FASTSIM, in which the decreasing slope of the traction curve is ignored.

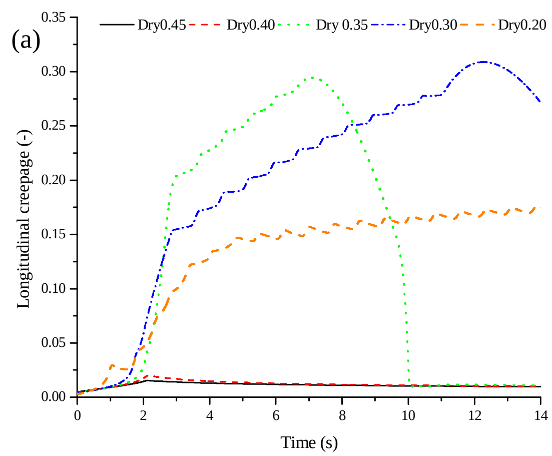

Fig. 5B.12. Longitudinal creepage of the left (a) and right (b) wheels of the first driven axle for the initially balanced speed case.

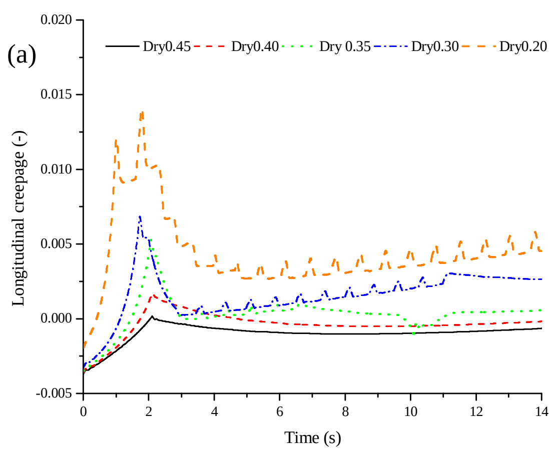

Fig. 5B.13. Longitudinal creepage of the left (a) and right (b) wheels of the second driven axle for the initially balanced speed case.

By looking at the longitudinal creepage in the contact patches where the friction force did not reach saturation, one can see that the left wheel experiences higher positive longitudinal creepage than the right one in the first driven axle, as shown in Figs. 5B.12

and 5B.14 for cases dry0.40 and dry0.45. On the contrary, higher positive longitudinal creepage was observed on the right wheel of the second driven axle for all simulated friction cases (see Figs. 5B.13 and 5B.15). In order to understand these results, one has to examine the curving behaviour of the bogie (given in the Section 5B.3.2).

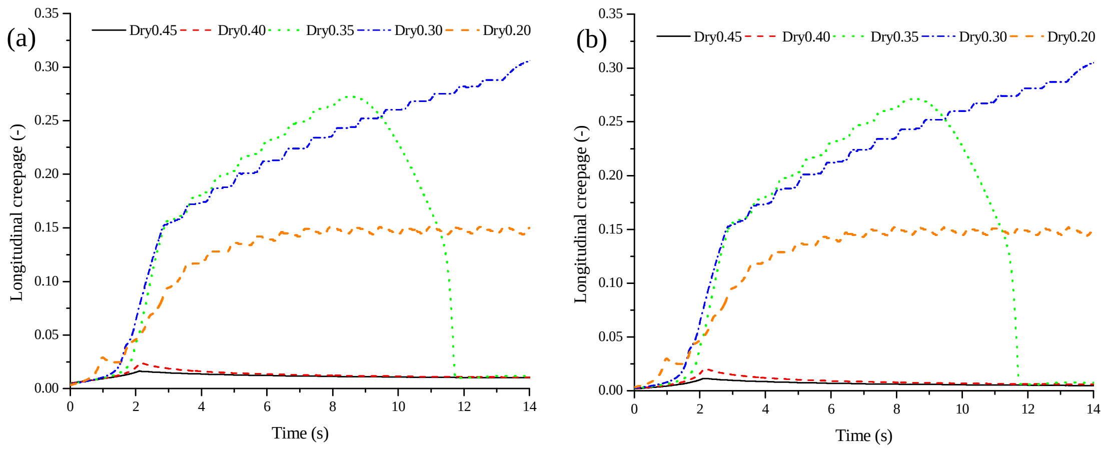

Fig. 5B.14. Longitudinal creepage of the left (a) and right (b) wheels of the first driven axle for the initially unbalanced speed case.

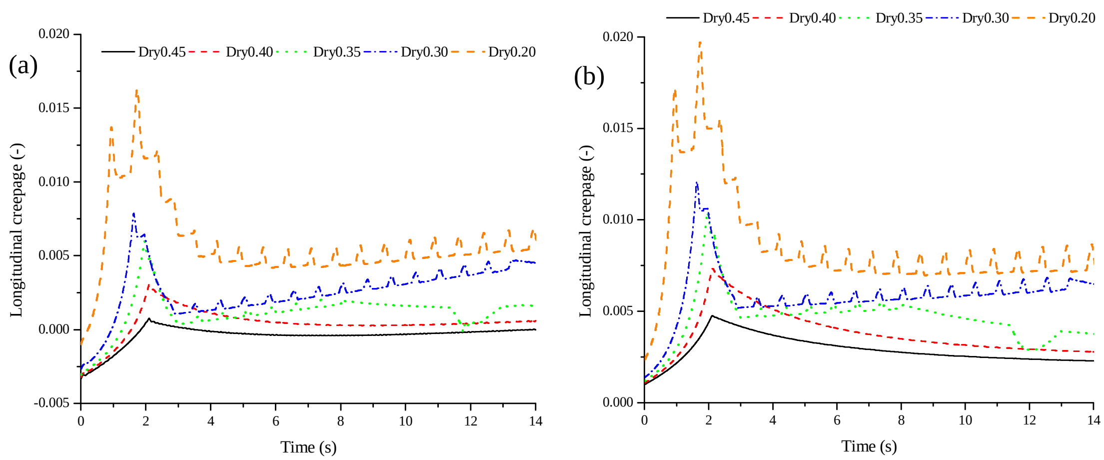

Fig. 5B.15. Longitudinal creepage of the left (a) and right (b) wheels of the second driven axle for the initially unbalanced speed case.

5B.3.2. Curving

The angle of attack (AoA) of the driven axles is given in Figs. 5B.16-5B.17 for all the simulated friction conditions in both cases of initially balanced and unbalance speed. Note that a positive sign of AoA indicates that the outer wheel is running into the rail. It can be seen that the first driven axle has a larger AoA than the second driven axle. The AoA is found to be dependent on the traction and the friction conditions. The increase of traction torque causes an increase in the AoA of the driven wheel axles. An example is the dry0.45 case, for which the AoA, which is shown in Figs. 5B.16-5B.17, clearly follows the evolution of the wheel axle torque depicted in Fig. 5B.10. This is a consequence of two facts. On one hand, the reduced friction of the lubricated high rail fails to provide enough longitudinal creep force to assist steering. On the other hand, the increase in the wheel axle torque leads to a longitudinal creep force acting on the low rail that opposes the steering force given by the rolling radius difference. Observations on the degraded steering behaviour of a motorized bogie have also been pointed out by other authors [5B.2, 5B.3].

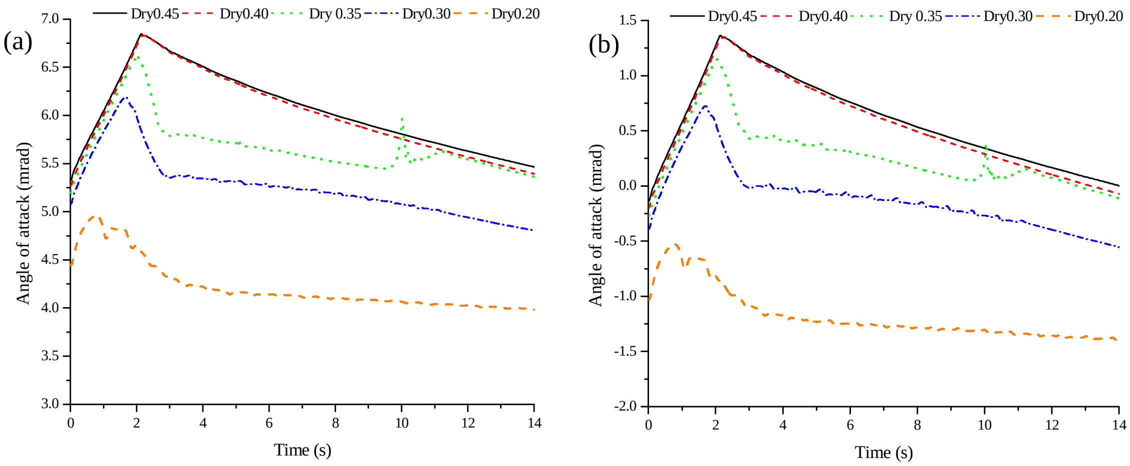

Fig. 5B.16. Angle of attack of the first (a) and second (b) driven axles for the initially balanced speed case.

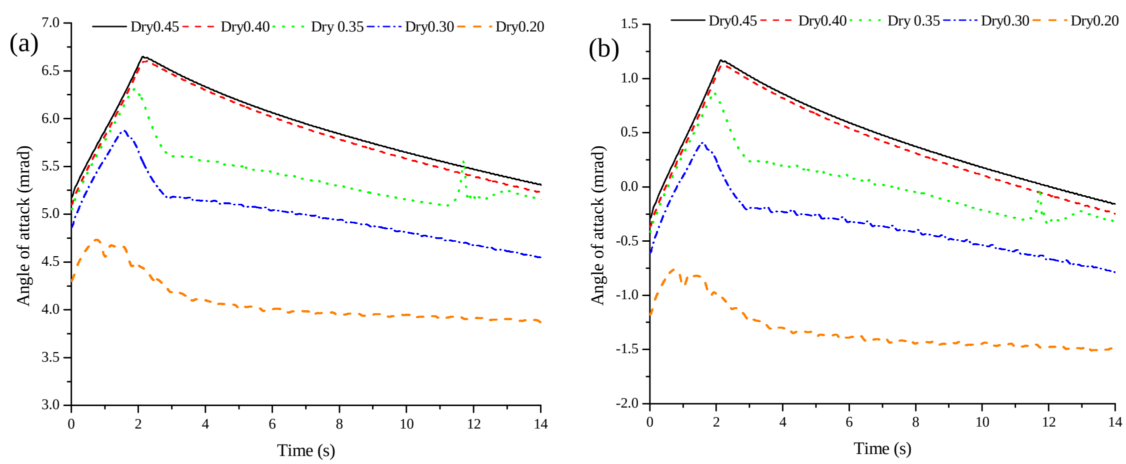

Fig. 5B.17. Angle of attack of the first (a) and second (b) driven axles for the initially unbalanced speed case.

Furthermore, the different friction conditions of the low rail also exert an influence on the AoA, leading to larger AoA for higher COF of the low rail. In order to observe this effect separately from the additional influence of the traction, one can refer to the cases dry0.45 and dry0.40, for which the wheel axle torque remains the same (see Fig. 5B.10). In Figs. 5B.16-5B.17 it can be seen that the AoA of dry0.45 case is larger than the one of dry0.40. In addition, comparing Figs. 5B.16-5B.17 it can be seen that an initially unbalanced vehicle speed decreases the AoA compared to the case of initially balanced speed. This is a result of the increase in the outwards lateral displacement of the driven wheelsets that is caused by the uncompensated centrifugal force, as observed by comparison of Figs. 5B.18-5B.19. This is in agreement with previous results on curving presented by other authors [5B.13].

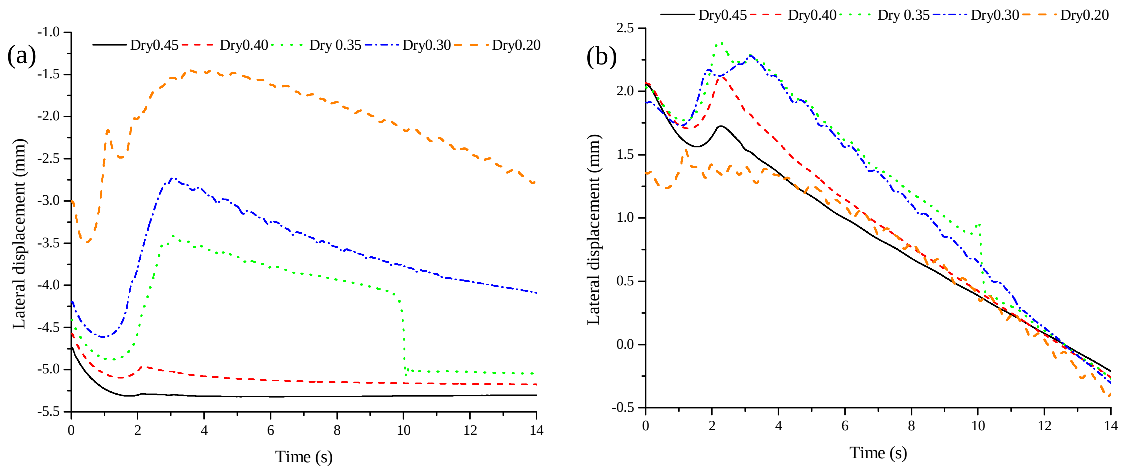

Fig. 5B.18. Lateral displacement from the track centreline of the first (a) and the second (b) driven axles for the initially balanced speed case.

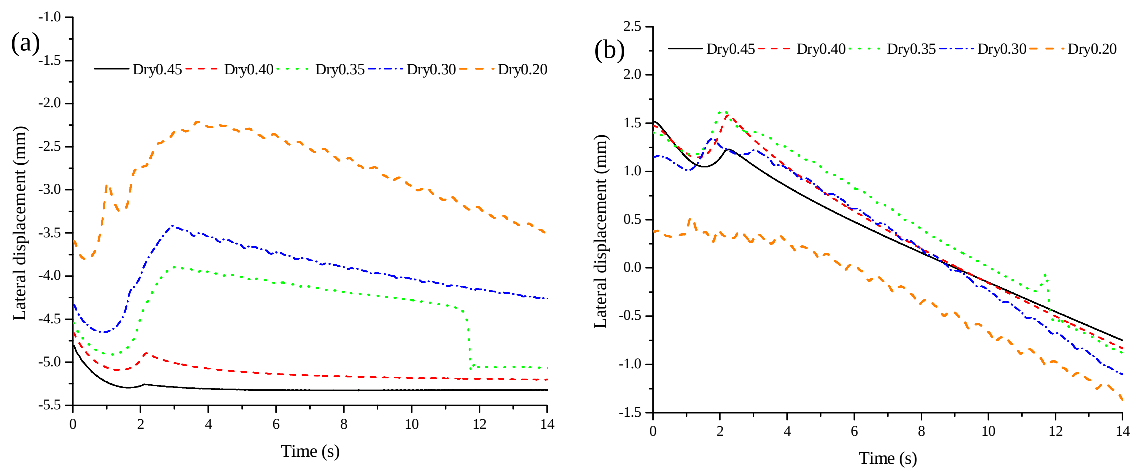

Fig. 5B.19. Lateral displacement from the track centerline of the first (a) and the second (b) driven axles for the initially unbalanced speed case.

Figs. 5B.18-5B.19 depict the lateral displacement of both driven axles from the track centerline for both cases of initially balanced and unbalance speed. Note that a negative sign indicates an outward displacement. It is found that the lateral displacement is influenced by both the traction and the friction conditions. An increase in the traction causes both driven wheelsets to be displaced to the outside of the track. On the first driven axle, this lateral displacement adds to the initial lateral displacement consequence of the curve negotiation. The second driven axle is initially closer to the centered position on the track, but with a tendency to move outwards with the increase in wheel axle torque. The influence of the COF on the lateral displacement is clearly observed in the first driven wheelset, which displaces more to the outside of the track for higher COF of the low rail. Additionally, it can be observed in Figs. 5B.18-5B.19 that both driven wheelsets tend to move outwards as the speed of the vehicle increases as result of the increase in uncompensated lateral acceleration.

Sudden fluctuations in both AoA and lateral displacement are observed in the cases where the friction became saturated, as clearly seen for the dry0.35 case in Figs. 5B.16 and 5B.18 at around 10 s of simulation and at around 11.5 s in Figs. 5B.17 and 5B.19. This fluctuation is attributed to the transition from full sliding conditions to micro-slip in the contact patch, which was shown in Figs. 5B.12 and 5B.14. Similarly, the saturation of the friction force caused a large decrease in the AoA, which can be seen for the case dry0.35 to occur at around 2 s of simulation in Figs. 5B.16-5B.17, and in the lateral displacement of the first driven wheelset as shown in Figs. 5B.18 (a) and 5B.19 (a) for the same friction case and simulation time.

5B.4. Discussion

In the simulations of this work it is shown that, if the contact points located on the high rail of the curve become lubricated, traction operation cannot be at the maximum possible performance, which is given by the torque-speed characteristic of the motor, unless the COF of the low rail is sufficiently high. According to the vehicle and operating conditions investigated, only a COF of at least 0.40 could avoid the occurrence of macro-slip. In practice, curving lubrication is mostly carried out throughout the year. During some periods of the year, natural contamination (e.g. water, leaves, etc.) may be present at the wheel-rail contacts of the low rail, reducing the COF to values considerably below 0.40 [5B.21, 5B.22]. Hence, malfunction of the applicators mainly becomes detrimental on days susceptible to have contamination affecting the friction level of the low rail.

In the past years, statistical analysis of low adhesion incidents in the Netherlands identified that curves are one of the hot spots [5B.23]. When a motorized bogie negotiates a curve, the adhesion is reduced as some part of the available friction is utilized to steer the wheelset, as pointed out in the literature [5B.3]. Hence, low adhesion incidents can be expected to be more likely to occur on a curve than on a straight track under the same contact conditions. In this work, the increase of the balance speed has shown to cause an earlier saturation of the available friction. It has also been pointed out that friction is saturated first on the first wheelset due to the curving behaviour of the motorized bogie. Therefore, it is interesting to look at the running dynamics of motorized bogies during curve negotiation under various lubrication/contamination conditions in investigations dealing with their traction performance.

Laboratory measurements have indicated that the maximum of the traction curve lies around 2-3% of creepage on dry clean contacts [5B.21], which is close to values measured in field [5B.15]. In most multi-body dynamics packages FASTSIM is often used for the tangential problem, predicting the maximum of the traction curve in dry clean contacts at around 1% of creepage. This may lead to premature saturation of the friction in some studies under dry friction. Hence, appropriate modeling of the tangential formulation is essential to obtain realistic results on curving studies. In addition, the decreasing slope of the traction curve, which is observed under some contact conditions after saturation of the friction force, has been shown in this work to influence the evolution of the creepage during full-sliding conditions. Therefore, accurate decreasing slopes representative of typical types of contamination need to be considered in the tangential formulation for investigations of traction/braking control.

In this paper, we have considered the most critical case of undesired lubrication, in which no starvation has occurred. In another work, the co-authors have also introduced the starvation conditions into the lubrication model [5B.15], which can be used to investigate the variation of the friction conditions as the thickness of the lubricant layers is progressively decreased by passing wheels. It can be said that in starvation conditions the Stribeck curve, which is depicted in Fig. 5B.3, tends to become a straight line with a friction level corresponding to that of BL regime, independently of the sum velocity. Hence, it can be expected that the first driven axles of a train are more affected by the undesired lubrication than the subsequent ones. In future works, it may be interesting to investigate the amount of axle passages that are necessary to bring the friction to suitable levels for traction and braking on lubricated curves.

5B.5. Conclusions

In this paper, a mixed lubrication model has been coupled to a commercial multi-body dynamics software package to simulate the curving vehicle behaviour under high traction with high rail lubrication. Particularly, the undesired case of the migration of the lubricant to the top of the high rail has been examined. Different friction conditions have been assumed for the low rail based on measured traction curves. The simulation results show that:

a) Due to the existence of lubricant on the high rail only a COF equal or higher than 0.40 on the low rail is able to bear the applied traction torque on the driven wheel axles without the occurrence of macro-slip. If macro-slip occurs, the torque is correspondingly reduced by the TC unit, which has an important impact on the final vehicle speed.
b) The first driven axle of the motorized bogie is shown to experience considerably larger slip than the second axle for cases with COF below 0.40 on the low rail, which is attributed to the curving behaviour of the bogie. In fact, macro-slip is only experienced by the first driven axle.
c) The occurrence of macro-slip is accentuated when the vehicle runs on the curve with an initially unbalanced speed.
d) The curving behaviour is found to be influenced by the traction, the friction conditions, and the balance speed.
    a. The increase in wheel axle torque causes an increase in the AoA of the wheelsets, with considerably larger AoA in the first driven axle.
    b. There exists a tendency of the wheelset to be displaced outwards with the increase of wheel axle torque.
    c. Higher COF on the low rail leads to larger AoA and outwards lateral displacement of the driven wheelsets.
e) The existence of an initially unbalanced speed leads to an increase in the wheelset lateral displacement and a decrease in the AoA for a given wheel axle torque.

References

[5B.1] A.H. Wickens: Fundamentals of rail vehicle dynamics. Swets & Zeitlinger B.V., Lisse, the Netherlands (2003).

[5B.2] W. Kik, R. Menssen, J. Piotrowski: On the Impact of the Contact Model on Predicted Traction Forces Developed by Wheels of a Locomotive on Curve. Vehicle System Dynamics Supplement 29 (1998) 380-389.

[5B.3] S.L. Grassie, J.A. Elkins: Tractive Effort, Curving and Surface Damage of Rails, Part 1, Forces Exerted on the Rails. Wear 258 (2005) 1235-1244.

[5B.4] P. Scroba, M. Roney, R. Dashko, E. Magel: Canadian Pacific Railway's 100% Effective Lubrication Initiative. AREMA 2001, Conference and Exhibition, Chicago, Illinois (2001).

[5B.5] U. Olofsson, R. Lewis: Tribology of the Wheel-Rail Contact in Handbook of Railway Vehicle Dynamics. Taylor & Francis Group, Boca Raton (2006).

[5B.6] R. Fröhling, J. de Koker, M. Amade: Rail Lubrication and its Impact on the Wheel/Rail System. Proc. Inst. Mech. Eng. Part F: Journal of Rail and Rapid Transit 223 (2009) 173.

[5B.7] Managing Low Adhesion. Report published by the Adhesion Working Group (2001), website: http://www.awg-rail.co.uk/.

[5B.8] J.J. Kalker: Three-Dimensional Elastic Bodies in Rolling Contact. Kluwer Academic Publishers, Dordrecht, the Netherlands (1990).

[5B.9] Z.Y. Shen, J.K. Hedrick, J.A. Elkins: A comparison of alternative creep-force model for rail vehicle dynamic analysis. In the proceedings of 8th IAVSD Symposium, MIT, Cambridge, MA (1984).

[5B.10] O. Polach: A Fast Wheel-Rail Forces Calculation Computer Code. Vehicle System Dynamics Supplement 33 (1999) 728-739.

[5B.11] O. Polach: Creep Forces in Simulations of Traction Vehicle Running on Adhesion Limit. Wear 258 (2005) 992-1000.

[5B.12] J.G. Giménez, A. Alonso, E. Gómez: Introduction of a Friction Coefficient Dependent on the Slip in the FASTSIM Algorithm. Vehicle System Dynamics 43 (2005) 233-244.

[5B.13] G. Xie, P.D. Allen, S.D. Iwnicki, A. Alonso, D.J. Thompson, C.J.C. Jones, Z.Y. Huang: Introduction of Falling Friction Coefficients into Curving Calculations for Studying Curve Squeal Noise. Vehicle System Dynamics Supplement 44 (2006) 261-271.

[5B.14] K. Matsumoto, Y. Suda, H. Komine, T. Nakai, M. Tomeoka, K. Shimizu, M. Tanimoto, Y. Kishimoto, T. Fujii: A Proposal of Wheel/Rail Contact Model for Friction Control. Journal of Mechanical Science and Technology 19 (2005) 437-443.

[5B.15] R.I. Popovici: Friction in the Wheel-Rail Contacts. PhD Thesis, University of Twente, Enschede, the Netherlands (2010) http://dx.doi.org/10.3990/1.9789036529570.

[5B.16] R.I. Popovici, D.J. Schipper: Modeling Contact Phenomena and Those Influenced by Greases. Eurogrease 2009-1 (2009) 17-26.

[5B.17] O. Arias-Cuevas, Z. Li, C. Esveld: Simulation of the Lateral Dynamics of a Railway Vehicle and its Validation Based on Rail Wear Measurements. In the proceedings of the ECCOMAS Thematic Conference on Multibody Dynamics, Politecnico di Milano (2007).

[5B.18] R. Stribeck: Die wesentlichen Eigenschaften der Gleit- und Rollenlager. VDI-Zeitschrift 46 (1902) 1341-1348, 1432-1438 and 1463-1470.

[5B.19] H. Eyring: Viscosity, Plasticity, and Diffusion as Examples of Absolute Reaction Rates. Journal of Chemical Physics 4 (1936) 283–287.

[5B.20] C.J.A. Roelands: Correlation aspects of the viscosity-temperature-pressure relationship of lubricated oils. PhD thesis, Technische Hogeschool Delft, the Netherlands (1966).

[5B.21] O. Arias-Cuevas, Z. Li, R. Lewis, E.A. Gallardo-Hernandez: Rolling-Sliding Laboratory Tests of Friction Modifiers in Dry and Wet Wheel-Rail Contacts. Wear 268 (2010) 543–551, doi:10.1016/j.wear.2009.09.015.

[5B.22] Z. Li, O. Arias-Cuevas, R. Lewis, E.A. Gallardo-Hernandez: Rolling-Sliding Laboratory Tests of Friction Modifiers in Leaf Contaminated Wheel-Rail Contacts. Tribology Letters 33 (2009) 97–109, doi:10.1007/s11249-008-9393-3.

[5B.23] J. Eleveld: Gladde Sporen, Oplossingsrichtingen voor Adhesieproblemen. Report published by the Dutch Railways Technical Research Department (NSTO) in Dutch (March 1999).

Chapter 6

Conclusions and Recommendations

ABSTRACT

In this chapter, the conclusions and recommendations of the research are presented. In comparison with the more detailed conclusions given in Chapters 2-5, the conclusions of this chapter are rather general in an attempt to answer the questions presented in the research motivation. The recommendations outline interesting lines of scientific research on the one hand, and possible prosperous investments for rolling stock operators and railway network managers dealing with low adhesion problems on the other.

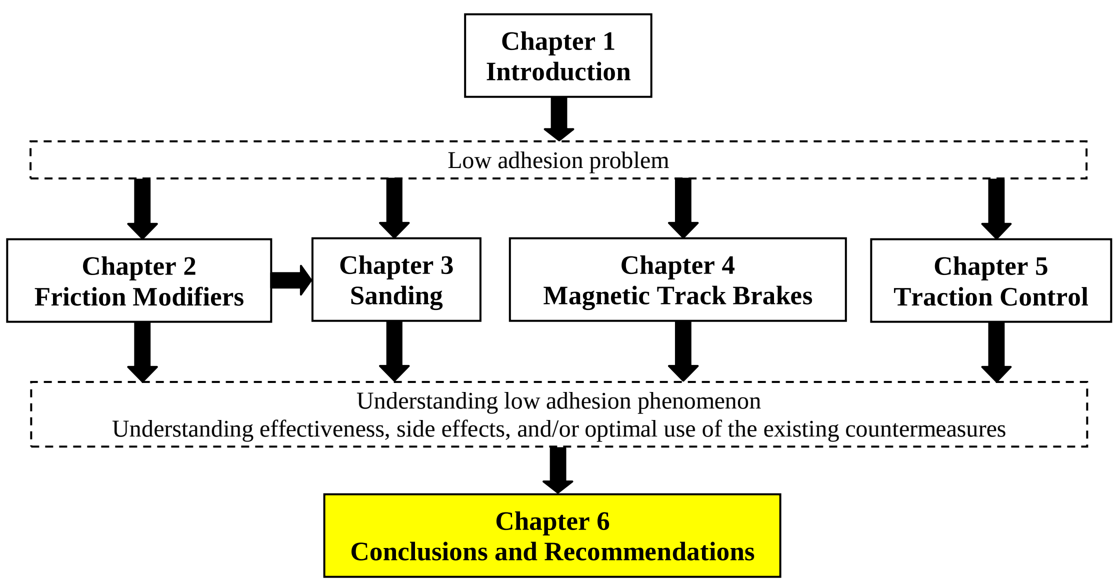

6.1. Conclusions

Low adhesion phenomenon

1. The reduction of adhesion in wheel-rail contaminated contacts and its effect on the railway transportation depends on the type of contamination.
   a. Water in clean contacts may mostly cause low adhesion problems in traction operation, as found out in lab and field tests.
   b. Grease contamination can affect both traction and braking operations when it is present on both rails. Furthermore, numerical simulations have shown that when grease is only present on one rail (e.g. malfunction of a flange lubricator on a curve), low adhesion incidents may not occur if the contact conditions on the other rail are adequate to bear most of the tractive/braking effort.
   c. Leaf layers, especially in combination with moisture, have been found in field tests to be the most important adhesion reducers of the typical known contaminants in railway transportation. Under dry conditions, leaf layers reduce the adhesion to insufficient values for traction operation, whereas they may not compromise safe braking for long trains. In wet conditions, leaf layers can affect both traction and braking operations.
2. Contamination that has deposited on rails can be highly mobile by passing wheels, leading to low adhesion incidents away from the original source of contamination.
   a. Grease has been found to be the most mobile contamination, for which the low adhesion section can reach 400 % of the initially contaminated length. This needs special consideration by infrastructure managers when installing trackside flange lubricators close to stations, signals or level crossings.
   b. Leaves resting on rails can adhere to passing wheels, being deposited up to several tens of meters away. On the other hand, once the leaf layers are formed on the top of the rails they may only be displaced (or removed) by tractive/braking wheels.
3. The wheel slip can contribute to the removal of contamination from the wheel-rail contact, giving explanation to the practical observation that longer trains are less affected by low adhesion than shorter ones. Experimental investigations in the laboratory under controlled conditions have shown that:
   a. in wet clean contacts, the increase in wheel slip in the range 0.5-2 % shortens the adhesion recovery by a factor of 3;
   b. in leaf contaminated contacts, the increase in wheel slip in the range 0.5-10 % leads to a clear adhesion improvement, but slips of at least 15 % are necessary to break up the leaf layers effectively.
4. When a motorized bogie negotiates a curve, the adhesion is reduced as some part of the available friction is utilized to steer the wheelsets. Hence, low adhesion incidents can be expected to be more likely to occur on a curve than on a straight track under the same contact conditions; this agrees with statistical analysis of some hot spots of low adhesion in the Netherlands. Numerical simulations have shown that the chance

of experiencing low adhesion is accentuated when the vehicle runs on the curve with an initially unbalanced speed.

Friction modifiers

5. Under dry conditions, FMA seems to form a durable third body layer that yields moderate adhesion coefficients, reducing wear and strain accumulation in the near-surface region compared to the baseline (i.e. untreated situation). FMB leads to similar wear rates and strain accumulation as the baseline.
6. FMA has a longer lasting effect than FMB, which could be attributed to its stronger matrix of solid particles and polymeric components. Furthermore, the application of water reduces the lasting effect of FMB, but it does not appear to affect FMA. In addition, increasing the slip reduces the lasting effect of both FMs.
7. The adhesion improvement given by the investigated FMs differs in the wet and leaf contaminated contacts.
   a. In wet contacts, FMA yields a more rapid adhesion recovery than the baseline, but its moderate adhesion characteristics may lead to adhesion problems in wet contacts for traction operation of most rail vehicles. For slips higher than 0.5 % slip there appears to be no added value of using FMB because it is rapidly removed from the disks surfaces.
   b. In leaf contaminated contacts, FMA only shows some improvement compared to the baseline at 0.5% slip, leading to lower adhesion for higher slips. On the contrary, FMB leads to a clear improvement of the wheel-rail adhesion for all slips investigated. Hence, the larger and harder solid particles of FMB are more effective to remove the leaf layer than the particles of FMA.
8. None of the investigated FMs is found to be optimal under the tested conditions, suggesting that some benefit could be obtained by modifying some of their design parameters. In particular, three FM parameters have been identified to be of prime importance: additives in the mix, size and hardness of the solid particles.

Sanding

9. In a dry wheel-rail contact an optimal adhesion coefficient may be achieved with a suitable combination of particle size, feed rate and wheel slip. Lab tests have shown that a higher adhesion coefficient in dry contacts may be obtained by using larger sized sand, increasing the wheel slip, or decreasing the feed rate.
10. The electrical insulation caused by sanding may be reduced by suitable selection of the sanding parameters, such as using a larger particle size or reducing the feed rate. Furthermore, in leaf contaminated contacts, the application of sand may help improving the train detection as it promotes the leaf layer removal.
11. The wear rates of wheels and rails during sanding may be increased with the wheel slip independent of the particle size, as shown in lab tests. On the other hand, the effect of the particle size on the wear rates has been found to be dependent on the slip: at 10 % slip wear rates may roughly be higher for larger particles, while the opposite

may occur at 1 % slip. Furthermore, large particle sizes and high slips may lead to more strain accumulation in the near-surface region of wheels and rails.

12. Sanding is found effective in improving the wheel-rail adhesion in the presence of dry and wet leaf layers not only for the wheels of sanding axles, but also for the subsequent wheels. However, the amount of adhesion improvement is strongly dependent on the particle size, the wheel slip, and the number of sanding axles.
    a. Using a smaller sand can double the adhesion improvement compared to the larger sand due to a more effective particle entrapment. In both laboratory and field tests the optimum particle size distribution for adhesion improvement has been found to be in the range 0.2-0.6 mm with a peak at around 0.4 mm. However, attention has to be paid to ensuring adequate train detection by selecting adequate feed rates.
    b. Increasing the wheel slip in the range 1-10 % promotes adhesion improvement, as well as the break-up of leaf layers. However, considering the increase of wear rates with wheel slip observed in the laboratory tests 5 % slip may be proposed as the optimum for most sand sizes.
    c. Increasing the number of sanding axles considerably promotes a faster adhesion recovery for the same slip and particle size. The optimal number should be chosen towards a balance between adhesion requirements and operational costs. For the optimal sand size proposed above, one sander against dry leaf layers and three sanders against wet leaf layers have been found to guarantee an adequate traction and braking performance. For other sand sizes, data has been made available to calculate the number of sanders necessary for a given adhesion requirement.

Magnetic track brakes

13. With leaf, water and grease contaminated rails a continuous adhesion improvement is obtained with the MTB passages. It has been shown that using two MTBs brings the adhesion level above safety requirements for most typical contamination conditions, except for wet leaf layers for which more than three MTBs can be necessary.
14. The braking force of the MTB is reduced the largest by leaf contamination, closely followed by grease. In addition, the first application of water to leaf layers mostly leads to the lowest braking force, but subsequent water applications promote leaf contamination removal by the MTB leading to an increase of the force.
15. The braking performance of the VIRM train can be brought above, or close to, safe levels of deceleration in typically contaminated conditions by using three MTBs. From the point of view of a cost-benefit analysis, two MTBs may be proposed to be optimal for the VIRM train. Furthermore, a general formula has been given to determine the optimal number of MTBs for a certain deceleration in other train types in typically contaminated contacts based on the data collected in the field tests.
16. The maintenance of the brake shoes is found to be critical in the MTB performance, as field tests have shown that variations in the surface conditions of the brake shoes can greatly reduce the MTB force. In addition, two estimates of the wear rate of the

brake shoes as function of the sliding distance (105.28 g/km) and the dissipated frictional power (16.17 g/MJ) have been obtained in the tests in a first attempt to determine the required maintenance period of the MTBs.

17. Using MTBs does not necessarily affect the electrical insulation of an IRJ. When debris deposits at the gap between adjacent rails, it is mostly removed after several wheel passages due to the train slipstream.

Traction control

18. The existing traction control algorithm can lead to levels of wheel slip up to 35 % in typically contaminated contacts, as shown in field tests and simulations. The developed coupled numerical models may be used as a first step for possible optimization of the TC algorithm for operation under typical low adhesion conditions.

6.2. Recommendations

The investigations performed in this dissertation have led to a number of ideas for further work, some of them are related to more fundamental aspects, while others are more practical intended for the TOCs and railway infrastructure managers that still struggle with the low adhesion problem.

Fundamental aspects

1. In many investigations on the wheel-rail contact in general, and low adhesion in particular, scaled laboratory tests are preferred due to their lower costs and controlled conditions in comparison with field tests. Twin-disk and pin-on-disk machines are often employed to simulate the actual wheel-rail contact; however, there still exists some doubts about the quantitative relevance of the results. In this dissertation, some agreement has been found between results obtained in field and laboratory tests under similar operating conditions. In future investigations, it is recommended to pursue a better understanding on the factors that affect the quantitative relationship between the two scales so that laboratory results may directly be extrapolated to actual conditions.

2. Neither the laboratory investigations of this dissertation nor previous works in the literature have examined the influence that contact pressure, surface roughness and rolling velocity can exert on the wheel-rail adhesion in leaf contaminated contacts and on the effectiveness of sanding and FMs. Although some representative values have been considered in this dissertation, they could clearly vary to some extent in practice due to numerous factors. Future investigations on these parameters are recommended for the following reasons. The influence of the contact pressure could lead to the design of a particular wheel-rail profile combination beneficial for adhesion, and perhaps derive into a re-profiling guideline suitable for specific periods of the year. The surface roughness can influence the actual metallic contact area between wheels and rails in the presence of leaf contamination, affecting not only the adhesion but also the train detection. The investigations on the surface roughness could be encouraged by grinding companies interested in offering their services to effectively overcome the low adhesion problem. The influence of the rolling velocity is of special importance because the adhesion requirements vary with the rolling velocity.

In addition, optimal application rates of sand or FMs may clearly vary with the rolling velocity.

3. In this dissertation, friction management for adhesion improvement in contaminated wheel-rail contacts has been investigated. The additives, the particle size and the hardness of the solid particles in an FM have been shown to affect its effectiveness and side effects. Considering recent developments of the industry towards an extensive friction management practice in some railways, several recommendations can be made as a result of the research described in this dissertation. Further work on the selection of adequate additives should promote the lasting effect and water repellency of the FM. The influence of the size of the solid particles has been investigated in detail in this dissertation taking sand as the reference material, and an optimal particle size has been proposed. Clearly other particle sizes may be optimal for different materials, and this should be considered in the design stage of an FM. Limitations in budget and time available during the realization of this dissertation have impeded investigations on the influence of the particle hardness and toughness. Such investigations are recommended in future works, not only motivated by the different results obtained between FMA and FMB as described in this dissertation, but also by the early work of Andrews[XIV] with different mineral powders published in the 60s.

4. The increasing adhesion improvement in the slip range 0.5-15 % observed in the baseline laboratory tests may encourage further work towards leaf layer removal by thermal mechanisms. In particular, efforts should be put to establish the thermal energy required to burn off the leaf layers. It may be possible to use some wheel axles of a train to remove the contamination by adjustment of the slip threshold in their correspondent TC/WSP systems. In this line of research, it could also be interesting to investigate the influence of the normal load and sliding velocity of the MTB on the layer removal. This is especially interesting for TOCs that have electro-MTBs, in which the attractive (contact) load could be adjusted to an optimum value for layer removal as a function of the train velocity.

5. In future works, investigations on the possible optimization of the TC algorithm employed in the VIRM train are recommended. This can be achieved by means of simulations with the developed coupled numerical models, and using adhesion data collected in autumn from the Dutch network in the frame of the AdRem project. With an adequate understanding on optimal parameters for the TC algorithm, field tests could be carried out in typically contaminated contacts to corroborate the simulation findings for implementation.

6. Although outside of the scope of this dissertation, investigations available in the literature about chemical methods to improve the adhesion suggest that some further work in this area may have some benefit, perhaps in combination with existent mechanical (e.g. sanding) and thermal (e.g. MTBs) methods. In particular, the early

[XIV] H.I. Andrews: Chemical Methods of Improving Rail Adhesion. Proceedings Institute of Mechanical Engineers 178 (1963-64) 172-184.

work of Andrews[I] and the recent work of Hyde et al.[XV] represent some examples of promising lines of investigation.

Practical aspects

7. The adhesion values measured in laboratory and field investigations of this dissertation, together with adhesion data collected from the Dutch network in the frame of the AdRem project, show that low adhesion incidents can occur in autumn because of insufficient adhesion available to satisfy the timetable requirements. If a train is delayed, the following trains on the same line may also be delayed. Additionally, damage to wheels and rails may also reduce the transportation capacity. Hence, it is recommended to analyze whether adopting an autumn timetable may become beneficial in practice.
8. In case of malfunction, (trackside) flange lubricators may undesirably bring the lubricant to the top of the high rail, affecting traction and braking performance if the other rail is not dry and clean. Hence, lubrication sites close to critical stopping points, such as stations and level crossings, need to be given special attention in typical humid or autumn days.
9. In addition to the recommendations made for the more fundamental aspects about friction management, some practical advices can be given to railways that make broad use of FMB. The investigations in this dissertation have shown that FMB is effective against leaf contamination, but its lasting effect is rather poor. This may encourage railways to revise the frequency of FMB application in field especially in humid or rainy days, or to request the supplier for a modified version of FMB with additives that can yield a similar lasting effect as the one observed with FMA. In addition, the particle size of the sand of FMB is also slightly larger than the optimal value found in this dissertation.
10. The investigations on sanding have shown that some parameters, such as the particle size and the feed rate, can exert a strong influence on the effectiveness and side effects of sanding. Regarding the particle size, changes can already be recommended for some railways, like in the UK, where the size of the sand employed is much larger than the optimal value found in this dissertation. The optimal feed rate still needs to be investigated for a selected particle size, bearing in mind that excessive feed rates may affect train detection. Clearly, it can be said that the optimal feed rate should be train velocity dependent, and perhaps not linear in the entire velocity range. In addition, TOCs could make use of the results presented in this dissertation about the number of sanding axles to establish the optimal number of sanders for adhesion improvement in leaf contaminated contacts. Moreover, the increasing adhesion improvement of sanding with wheel slip observed in this dissertation may encourage TOCs to consider adjusting the slip threshold of the TC/WSP systems in the sanding axles to a high value that does not compromise acceptable wear rates of wheels and rails.

[XV] P. Hyde, D. Fletcher, A. Kapoor, S. Richardson: Full Scale Testing to Investigate the Effect of Rail Head Treatments of Differing pH on Railway Rail Leaf Films. Proceedings of 7th WCRR, Canada (2006).

11. A comparison between MTBs, sanding and FMs indicates that MTBs, although leading to certain adhesion improvement, are not the most effective method to combat the low adhesion problem caused by leaf contamination in speed range 0-40 km/h. However, any further recommendation about MTBs needs to consider the particular situation of each railway.

    a) In countries like the UK, where the rolling stock is not fitted with MTBs but sanders, it can be recommended to invest on the optimization of the current sanding practice rather than on retro-fitting the fleet with MTBs.

    b) In countries like the Netherlands, where almost half of the fleet is fitted with MTBs and sanders are only available on locomotives, more investigations can be recommended towards the frequent use of MTBs against low adhesion conditions. In particular, two main aspects need to be examined, namely the wear rates of the brake shoes in the complete operational speed range and the adhesion improvement and braking force in the range 40-140 km/h.

12. As a continuation of the laboratory work presented in this dissertation, investments to investigate the optimal wheel slip for contamination removal are recommended to the railway industry. In this line of work, an optimization of the TC/WSP algorithms suitable for actual low adhesion conditions is also recommended to the TOCs for three basic reasons: the use of available adhesion may be maximized, the damage of wheels and rails may be minimized, and there are no significant operational or maintenance costs after implementation of this countermeasure.

.

Appendix

A.1. Influence on bogie hunting of the suspension parameters of the vehicle model running on straight track

The vehicle model presented in Section 5A.1 was simulated on straight track with the lateral artificial irregularity used as the excitation source. The bogie hunting behavior was represented by lateral and yaw oscillations of the wheelset around its centered position on the track. Parameter variation indicated that the lateral and longitudinal stiffnesses were the most influencing parameters of the primary suspension on bogie hunting. The influence of the primary vertical suspension was not shown because the variation of the contact point position was within the low conicity part of the wheel profile. The primary longitudinal and lateral dampers did not show any appreciable influence on bogie hunting because their contribution in terms of force was less than 1 % of the total primary suspension due to their low damping. Furthermore, the bogie hunting hindering mechanism was found in the secondary suspension by the lateral and the anti-yaw dampers. If both dampers were reduced to 1 % of their nominal value, very small sustained oscillations remained near the equilibrium position. On straight track, the influence of the bumpstops could not be studied because the clearance was not reached.

Reductions in the primary longitudinal and lateral stiffnesses increased the number of oscillations of the bogie hunting and, therefore, the tendency to sustained oscillations. This was attributed to the decrease in the constraint of the wheelset to the bogie, which hinders the effect of the secondary dampers. The primary longitudinal stiffness showed a more important role in bogie hunting stability. The first observation of sustained hunting oscillations corresponded to a reduction of 90 % in the primary longitudinal stiffness; however, 99 % reduction was required in the primary lateral stiffness to obtain sustained hunting oscillations. Furthermore, a reduction in these stiffnesses reduced the wavelength of the bogie hunting oscillations, as shown in Fig. A.1 and Fig. A.2. This agrees with the literature [5A.2] because the increase in freedom of the wheelset with respect to the bogie and, therefore, to the carbody, lets the wheelset hunt at higher frequency.

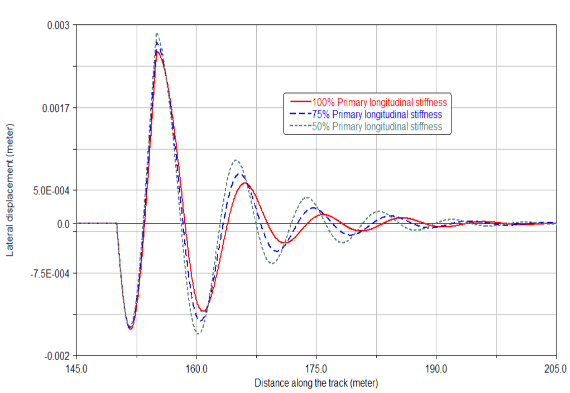

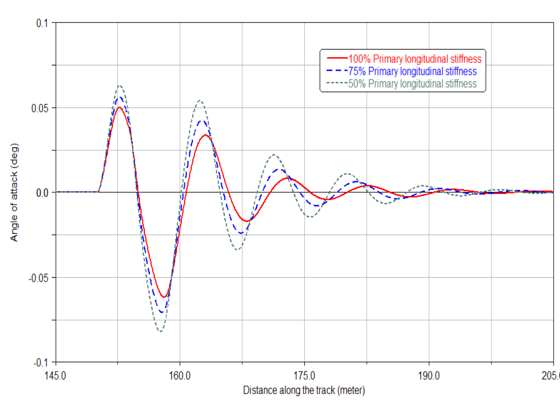

Fig. A.1. Variation of the contact point location on the outer rail for the first (left) and the third (right) wheelsets for the vehicle running on curved track excited with an artificial irregularity.

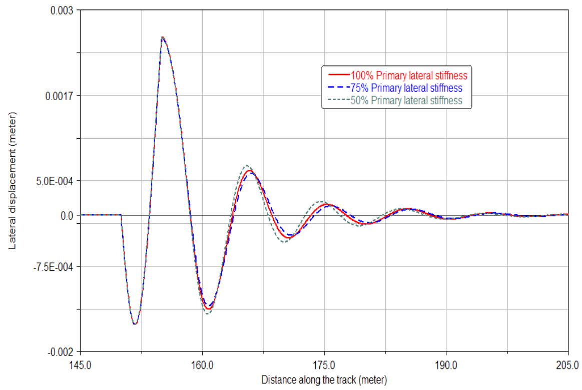

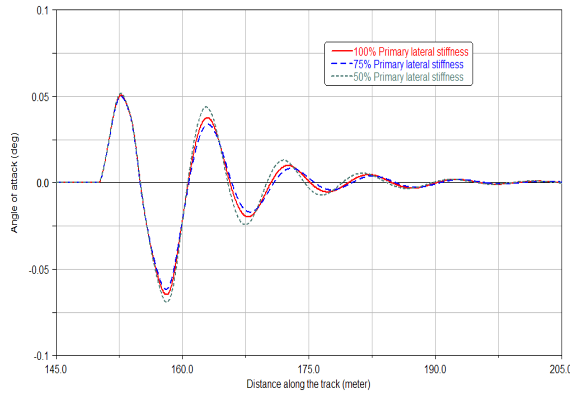

Fig. A.2. Lateral (left) and yaw (right) motions of the first wheelset for different lateral stiffnesses, when the vehicle running on straight track is excited.

A.2. Influence on bogie hunting of the suspension parameters of the vehicle model running on curved track

The vehicle model was simulated on the reference section with the lateral artificial irregularity used as excitation source (see Section 5A.1). Due to the suspension properties of the vehicle, the primary dampers exerted less than 2 % of the total primary suspension forces, showing no visible influence on the bogie hunting results. In addition, a decrease of 50 % in the vertical stiffness showed slight influence on the amplitudes of the bogie hunting oscillations, but no appreciable influence on the pattern and wavelength. Moreover, the lateral and longitudinal stiffnesses were the most influencing parameters of the primary suspension. Their influence on the position of the first contact point on the rail reference system is shown in Table A.1. It can be observed that the higher the longitudinal stiffness, the closer the first contact point to the rail corner, which is due to less freedom given to the wheelsets to take up radial attitude on the curve. On the other hand, a reduction in the lateral stiffness gave more lateral freedom to the wheelsets to adopt their desired position on the curve considering their restrictions in yaw motion by the longitudinal stiffness.

Table A.1. Position of the first contact point on the outer rail for different longitudinal and lateral primary stiffness.

k_x	1st Wheelset	2nd Wheelset	3rd Wheelset	4th Wheelset
100 %	23.1 mm	12.1 mm	17.0 mm	11.0 mm
75 %	21.2 mm	11.7 mm	15.1 mm	10.8 mm
50 %	18.1 mm	11.3 mm	14.3 mm	10.5 mm
k_y	1st Wheelset	2nd Wheelset	3rd Wheelset	4th Wheelset
100 %	23.1 mm	12.1 mm	17.0 mm	11.0 mm
75 %	23.2 mm	11.5 mm	17.1 mm	10.1 mm
50 %	23.5 mm	10.2 mm	17.1 mm	8.7 mm

Furthermore, the influence of the primary longitudinal stiffness on the occurrence of second point contact was also observed. The second contact point after encountering the irregularity was observed on the third but not on the first wheelset for values up to 50 %

of the nominal longitudinal stiffness, which was attributed to the larger angle of attack of the third wheelset. Further reductions in the longitudinal stiffness led to larger amplitudes in the yaw oscillations on the first wheelset, which caused the second contact point for the first two oscillations.

The influence of the secondary suspension was also investigated. The lateral and anti-yaw dampers were again recognized as major elements hindering the hunting. Sustained hunting oscillations for the model with a decrease to 1 % in the lateral and anti-yaw dampings were observed. Furthermore, the clearance of the soft bumpstop was reached on the curve, allowing its influence to be studied. Reductions up to 50 % in the soft bumpstop stiffness caused more bogie hunting oscillations and at shorter wavelength due to the decoupling between bogies and carbody. The clearance of the stiff bumpstop was not reached in any of the simulations carried out.

A.3. Influence on bogie hunting of the wheel and rail profiles

In order to study the influence of the wheel and rail profiles on bogie hunting, four combinations of wheel and rail profiles were used to simulate the bogie hunting behavior of the vehicle model with 60 % nominal longitudinal primary stiffness running on the reference track and excited by the artificial irregularity (see Section 5A.1). Severe worn S1002 and UIC54 profiles for wheels and rails, respectively, were taken from the reference section and included in the model. The hunting motions of the first wheelset are shown in Fig. A.3. The pattern and wavelength of the bogie hunting oscillations for new and worn wheel profiles running on worn rails were very similar, with small variations in the contact point position. Furthermore, the introduction of worn rail profiles provoked contact of the outer wheel on the rail gauge corner and face for every wheelset. In addition, no second point contact in any wheelset was observed for new and worn wheel when the worn rail profile was utilized, which could be attributed to the conformity between wheel and rail profiles. On the other hand, it was observed that worn wheel profile running on new rails caused second point contact in every wheelset. Furthermore, the position of the first contact point was also modified with respect to the one obtained with new wheel profiles.

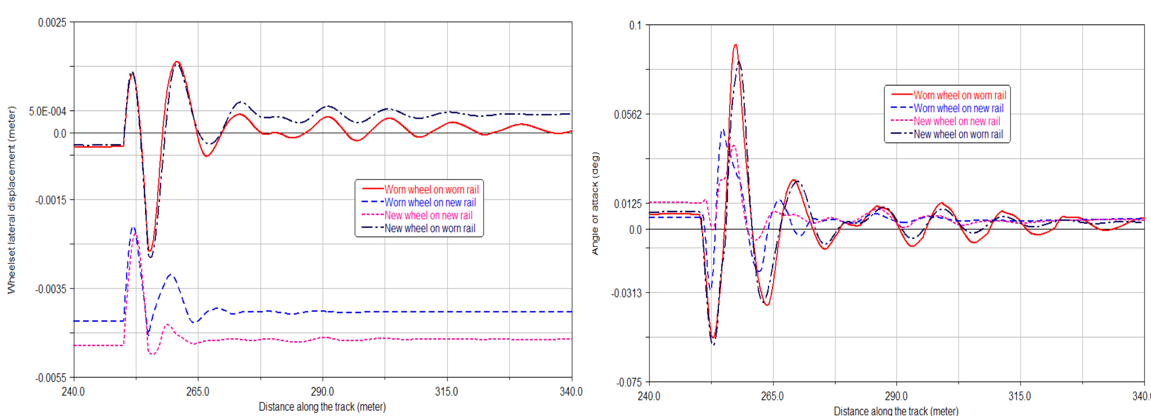

Fig. A.3. Lateral (left) and yaw (right) motions of the first wheelset of the vehicle with 60 % nominal primary longitudinal stiffness for different combinations of new and worn wheel and rail profiles.

Curriculum vitae

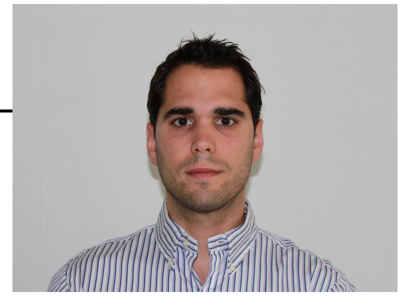

Personal:

Oscar Arias-Cuevas
September 3, 1982
Madrid (Spain)

Education:

2006 - Now	**PhD**, Delft University of Technology
2000 - 2006	**Mechanical Engineering (Ing. Sup. Industrial)**, Universidad Carlos III de Madrid

Work experience:

2006 - Now	**Research Assistant,** Section of Road and Railway Engineering, Faculty of Civil Engineering and Geosciences, Delft University of Technology
2006 - 2010	**Researcher,** project AdRem for ProRail and NS, in collaboration with DeltaRail, LRRE, Wageningen University and University of Twente
2005 - 2006	**Trainee**, TNO Defensie en Veiligheid, Rijswijk (the Netherlands)

Papers in internationally refereed journals:

(1) O. Arias-Cuevas, Z. Li, R. Lewis, E.A. Gallardo-Hernandez: Rolling-Sliding Laboratory Tests of Friction Modifiers in Dry and Wet Wheel-Rail Contacts. **Wear** 268 (2010) 543-551.

(2) Z. Li, O. Arias-Cuevas, R. Lewis, E.A. Gallardo-Hernandez: Rolling-sliding Laboratory Tests of Friction Modifiers in Leaf Contaminated Wheel-Rail Contacts. **Tribology Letters** 33 (2009) 97-109.

(3) O. Arias-Cuevas, Z. Li, R. Lewis: A Laboratory Investigation on the Influence of the Particle Size and Slip During Sanding on the Adhesion and Wear in the Wheel-Rail Contact. **Wear**, in review.

(4) O. Arias-Cuevas, Z. Li, R. Lewis: Investigating the Lubricity and Electrical Insulation Caused by Sanding in Dry Wheel-Rail Contacts. **Tribology Letters** 37 (2010) 623–635.

(5) O. Arias-Cuevas, Z. Li, R. Lewis, E.A. Gallardo-Hernandez: Investigation of some Sanding Parameters to Improve the Adhesion in Leaf Contaminated Wheel-Rail Contacts. **Proc. IMechE, Part F: J. Rail and Rapid Transit** 224 (2010) 139-157.

(6) O. Arias-Cuevas, Z. Li, R.I. Popovici, D.J. Schipper: Simulation of Curving Behavior under High Traction in Lubricated Wheel-Rail Contacts. **Vehicle System Dynamics**, in press.

(7) O. Arias-Cuevas, Z. Li: Field Investigations on the Adhesion Recovery in Leaf Contaminated Wheel-Rail Contacts with Locomotive Sanders. **Proc. IMechE, Part F: J. Rail and Rapid Transit**, submitted in 2010.

(8) O. Arias-Cuevas, Z. Li: Field Investigations on the Performance of Magnetic Track Brakes of an Electrical Multiple Unit against Slippery Tracks. Part I: Adhesion Improvement. **Proc. IMechE, Part F: J. Rail and Rapid Transit**, submitted in 2010.

(9) O. Arias-Cuevas, Z. Li: Field Investigations on the Performance of Magnetic Track Brakes of an Electrical Multiple Unit against Slippery Tracks. Part II: Braking Force and Side Effects. **Proc. IMechE, Part F: J. Rail and Rapid Transit**, submitted in 2010.

Papers in (international) conferences:

(1) O. Arias-Cuevas, Z. Li, C. Esveld: Simulation of the Lateral Dynamics of a Railway Vehicle and its Validation Based on Rail Wear Measurements. **ECCOMAS Thematic Conference on Multibody Dynamics**, June 25-28, 2007, Politecnico di Milano, Italy.

(2) O. Arias-Cuevas, Z. Li: Low Adhesion in the Contact between Wheel and Rail. **CROW Infradagen**, June 25-26, 2008, Delft the Netherlands.

(3) O. Arias-Cuevas, Z. Li, R. Lewis, E.A. Gallardo-Hernandez: Rolling-sliding Laboratory Tests of Friction Modifiers in Leaf Contaminated Wheel-Rail Contacts. **STLE/ASME International Joint Tribology Conference**, October 20-22, 2008, Miami, Florida, USA.

(4) O. Arias-Cuevas, Z. Li, R.I. Popovici, D.J. Schipper: Simulation of Curving Behavior under High Traction in Lubricated Wheel-Rail Contacts. **21st International Symposium on Dynamics of Vehicles on Roads and Tracks**, August 17-21, 2009, Stockholm, Sweden.

(5) O. Arias-Cuevas, Z. Li, R.I. Popovici, D.J. Schipper: Simulation of Curving Behavior under High Traction in Lubricated Wheel-Rail Contacts. **21st International Symposium on Dynamics of Vehicles on Roads and Tracks**, August 17-21, 2009, Stockholm, Sweden.

(6) O. Arias-Cuevas, Z. Li, R. Lewis: A Laboratory Investigation on the Influence of the Particle Size and Slip During Sanding on the Adhesion and Wear in the Wheel-Rail Contact. **8th International Conference on Contact Mechanics and Wear of Rail/Wheel Systems**, September 15-18, 2009, Firenze, Italy.

(7) O. Arias-Cuevas, Z. Li: Field Investigations on Rolling Stock Components Designed to Overcome Low Adhesion Related Problems. **2010 Joint Rail Conference**, April 27-29, 2010, Urbana-Champaign, Illinois, USA.

(8) O. Arias-Cuevas, Z. Li: Investigaciones sobre la problemática de la baja adherencia en el transporte ferroviario. **IX Congreso de Ingeniería del Transporte**, July 7-9, 2010, Madrid, Spain.

(Space for notes)